

AD-A128 789

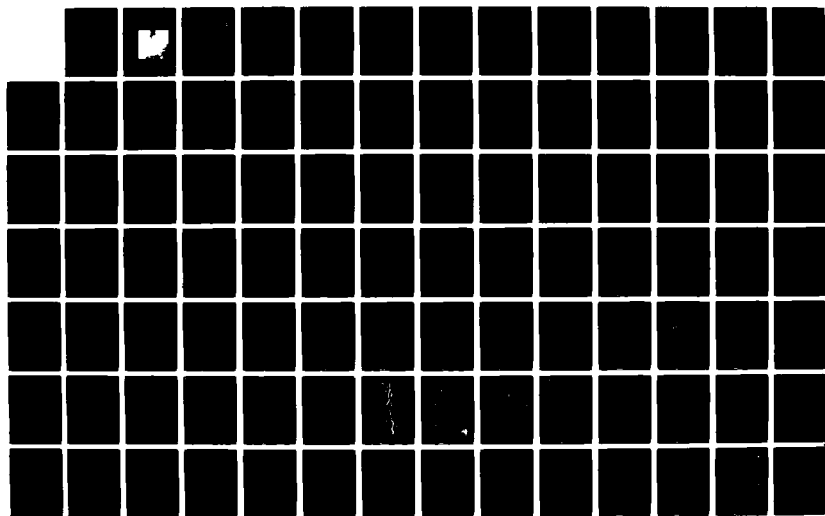
PROCEEDINGS OF THE WORKSHOP ON GULF STREAM STRUCTURE
AND VARIABILITY HELD..(U) NORTH CAROLINA UNIV AT CHAPEL
HILL APR 82 N00014-82-G-0059

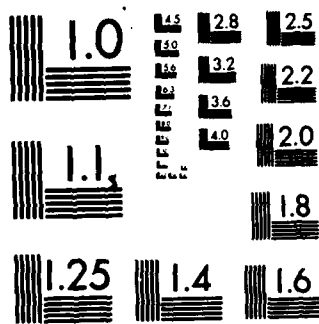
1/5

UNCLASSIFIED

F/G 8/3

NL





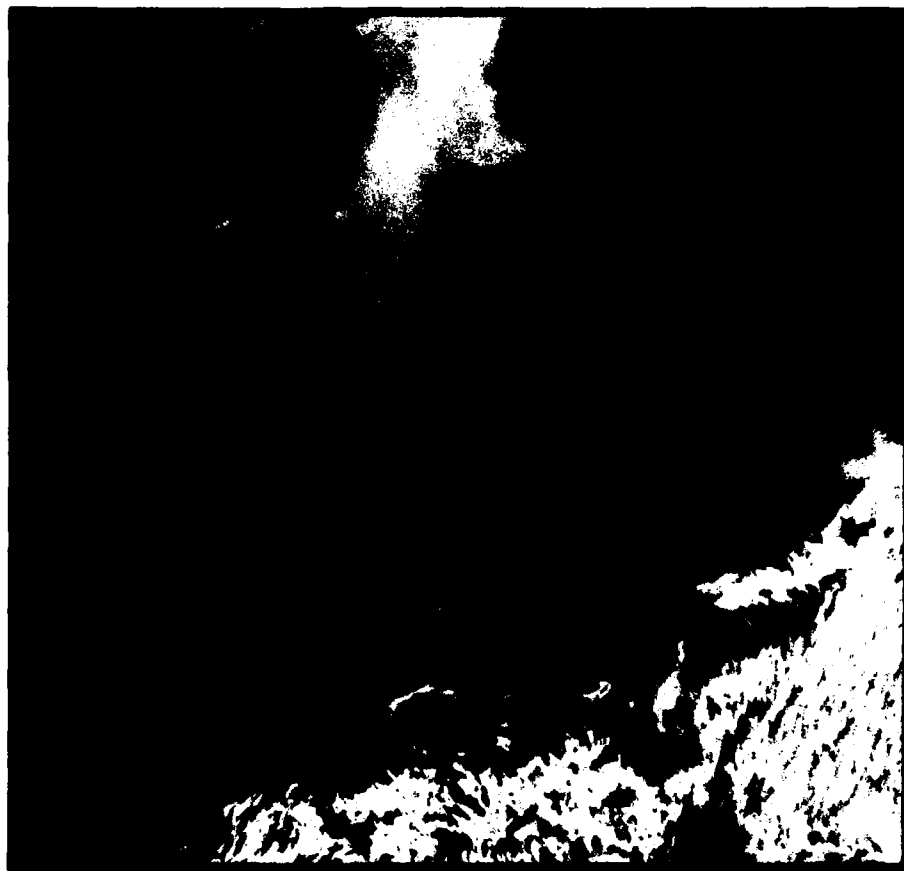
MICROCOPY RESOLUTION TEST CHART
NATIONAL BUREAU OF STANDARDS-1963-A

13

AD A 128 789

WORKSHOP ON GULF STREAM STRUCTURE AND VARIABILITY

PROCEEDINGS



DTIC FILE COPY

GOVERNOR'S INN
RESEARCH TRIANGLE PARK, NORTH CAROLINA
1-2 APRIL 1982

Host: University of North Carolina at Chapel Hill

Sponsor: U.S. Office of Naval Research

Convenor: John M. Bane, Jr.

This document has been approved
for public release and sale; its
distribution is unlimited.

83 04 29 004

DTIC
ELECTE

MAY 2 1983

A

COMPONENT PART NOTICE

THIS PAPER IS A COMPONENT PART OF THE FOLLOWING COMPILATION REPORT:

(TITLE): Proceedings of the Workshop on Gulf Stream Structure and Variability
Held at Research Triangle Park, North Carolina on 1-2 April 1982.

(SOURCE): North Carolina Univ. at Chapel Hill.

DTIC

JUN 6 1983

TO ORDER THE COMPLETE COMPILATION REPORT USE AD-A128 789.

A

THE COMPONENT PART IS PROVIDED HERE TO ALLOW USERS ACCESS TO INDIVIDUALLY AUTHORED SECTIONS OF PROCEEDINGS, ANNALS, SYMPOSIA, ETC. HOWEVER, THE COMPONENT SHOULD BE CONSIDERED WITHIN THE CONTEXT OF THE OVERALL COMPILATION REPORT AND NOT AS A STAND-ALONE TECHNICAL REPORT.

THE FOLLOWING COMPONENT PART NUMBERS COMPRISE THE COMPILATION REPORT:

AD#:	P001 039	TITLE:	Gulf Stream Fluctuations and Their Relation to the Winds off North Carolina.
	P001 040		A Seasonal Comparison of Gulf Stream Fluctuations off North Carolina.
	P001 041		Review of Gulf Stream Measurements in the Region South of New England.
	P001 042		A Truncated Model of the Long-Period Gulf-Stream Fluctuations and Their Feedback to the Atmosphere.
	P001 043		The Propagation of a Cold-Dome Meander: A Conceptual Model.
	P001 044		The Gulf Stream's Western Surface Front in the South Atlantic Bight, 1976-78: Preliminary Results from an Empirical Orthogonal Function Analysis.
	P001 045		Energy and Mass Flux in the Gulf Stream.
	P001 046		Models of Gulf Stream Variability -- An Overly Brief Review.
	P001 047		Simulation of North Atlantic Variability.
	P001 048		The Behavior of an Individual Current Meander in Different Dynamical Regimes.
	P001 049		An Analysis of the Potential Vorticity Distribution Across the Gulf Stream.
	P001 050		Observations on the Vertical Coherence of Gulf Stream Meanders.
	P001 051		Preliminary Results on Normalization of Hydrographic Sections of the Gulf Stream.
	P001 052		On Gulf Stream Frontal Eddies Along the Southeast U.S. (United States) Outer Continental Shelf.
	P001 053		On Gulf Stream Variability at 30 N.
	P001 054		Spatially Unstable Waves in the Gulf Stream over the Carolina Continental Slope.
	P001 055		Gulf Stream Frontal Statistics from Florida Straits to Cape Hatteras Derived from Satellite and Historical Data.
	P001 056		The Pegasus Program East of Cape Hatteras.
	P001 057		Variability of the Florida and Antilles Current.

This document has been approved
for public release and sale; its
distribution is unlimited.

COMPONENT PART NOTICE (CON'T)

AD#: P001 058 TITLE: Synoptic Measurements of Sea Surface Temperatures
in Gulf Stream Frontal Zone between Savannah,
Georgia and Cape Hatteras, North Carolina.
P001 059 A Numerical Study of the Influence of the New
England Seamount Chain on the Gulf Stream:
Preliminary Results.
P001 060 Preliminary Estimates of Surface Vorticity and
Divergence in Gulf Stream Western Boundary
Perturbations Using Satellite and Buoy Data.
P001 061 Observations on Propagation and Growth of Gulf
Stream Meanders.

Accession No.	
NTIS GRA&I	8
DTIC TAB	
Unannounced	
Justification	
By	
Distribution	
Availability Codes	
Dist	Avail. or
A	Not avail.

PROCEEDINGS OF THE
WORKSHOP ON GULF STREAM
STRUCTURE AND VARIABILITY

Research Triangle Park, NC

April 1982

Sponsored by
THE OFFICE OF NAVAL RESEARCH

PREFACE

During the 1970's observational and theoretical studies greatly increased our knowledge of the structure and dynamics of the Gulf Stream. As we enter the next decade there are expected to be several large, intensive studies of the current system, promising to add new understanding. The number of research oceanographers actively working on the Gulf Stream and related phenomena is probably higher now than ever before. Many new observational tools are being employed in this research, including free drop current profilers, acoustic soundings of the Stream's thermal structure, aircraft-deployed sensors, and long-term instrument moorings.

Recognizing the desirability of having good communication about recent and on-going Gulf Stream research among the participating scientists and other interested parties from industry and government, several of my colleagues and I discussed the possibility of having a Gulf Stream workshop. We felt that a workshop forum would provide an open, congenial atmosphere within which discussions could focus upon ongoing research, and hopefully inspire some new plans and goals for the future.

Under the sponsorship of the Office of Naval Research, and with the above aims in mind, the University of North Carolina hosted the Workshop on Gulf Stream Structure and Variability, on April 1 and 2, 1982. The papers contained in this volume are written versions of presentations made at the Workshop. These papers represent a cross-section of modern Gulf Stream physical oceanographic research. They are by no means exhaustive. This Proceedings Volume is distributed with the hope that it may serve as a source book for determining "who is doing what" in Gulf Stream research.

The value of this meeting was primarily in increasing the communication among investigators. The major Gulf Stream research projects in the past few years have evolved rapidly, with funding from several sources, and with each project being an almost self-contained study of some identifiable aspect of the Stream. This evolution of scientific study is, of course, a natural one. The progression of scientific studies into addressing questions of large scope - ones which would by their nature require a larger, more systematic approach than has been used in most Gulf Stream research in the past - seems to be the stage in which we Gulf Stream researchers find ourselves. The Warm Core Rings Study is perhaps the first example of such a large, coordinated study on a portion of the Stream. Because of the feeling which I have in coming away from the Workshop, I anticipate seeing an increasing "internal" coordination among Gulf Stream oceanographers. The study of large-scale processes such as vorticity homogenization in the recirculation region, low frequency transport variations in the Stream and the recirculation system, fluxes of energy, momentum and heat through the North Atlantic, the instability processes which contribute to the Stream's short-term variability, and Lagrangian movement of water parcels in the Stream demand scientific investigation over large space and time scales. The continued identification of well-defined, large-scale problems will occur, and the scientific teams required to tackle these problems will form.

Theoretical and numerical studies of Gulf Stream dynamics have recently focused on the processes which produce the short-term variability in the Stream, such as Gulf Stream meanders and rings. Large-scale, eddy resolving circulation models are making significant progress in simulating and providing an understanding of Gulf Stream variability. The capabilities exist to investigate further the fluctuation dynamics in the regions where the Gulf Stream's variability increases dramatically. The region between the Florida Straits and Cape Hatteras is one portion of the current system which is ripe for receiving such attention. The ring producing area near the New England seamount chain is another.

Remote sensing techniques, especially sea surface temperature mapping, have provided insight into Gulf Stream structure, and have also guided the design and execution of more traditional observational studies. The increasing use of microwave radiometers, synthetic aperture radars, and laser altimeters should add to existing knowledge of the statistical properties of Gulf Stream variability by providing data during longer periods than do the infrared radiometers, which are affected by cloud cover and the loss of surface temperature contrast during periods of upper layer warming.

With these several approaches being applied to the study of the current system, efficient communication of ongoing and newly developing research activities is essential. I believe the Workshop on Gulf Stream Structure and Variability contributed to that objective. The feedback which I have received since the Workshop has been quite favorable. As do others, I feel that a Gulf Stream Workshop II will be appropriate in the near future.

John M. Bane, Jr.
December, 1982

A

TABLE OF CONTENTS

Preface	i
Acknowledgements	iii
Table of Contents	iv
GULF STREAM FLUCTUATIONS AND THEIR RELATION TO THE WINDS OFF NORTH CAROLINA	1
David A. Brooks (TAMU)	
A SEASONAL COMPARISON OF GULF STREAM FLUCTUATIONS OFF NORTH CAROLINA	17
David A. Brooks (TAMU) and John M. Bane, Jr. (UNC)	
REVIEW OF GULF STREAM MEASUREMENTS IN THE REGIONS SOUTH OF NEW ENGLAND	48
Harry S. Bryden (UW)	
A TRUNCATED SPECTRAL MODEL OF THE LONG-PERIOD GULF-STREAM FLUCTUATIONS AND THEIR FEEDBACK TO THE ATMOSPHERE	60
Shenn-Yu Chao (NOVA)	
THE PROPAGATION OF A COLD-DOME MEANDER: A CONCEPTUAL MODEL	63
Frank Chew (NOAA/AOML), John M. Bane, Jr. (UNC), and David A. Brooks (TAMU)	
THE GULF STREAM'S WESTERN SURFACE FRONT IN THE SOUTH ATLANTIC BIGHT, 1976-1978: PRELIMINARY RESULTS FROM AN EMPIRICAL ORTHOGONAL FUNCTION ANALYSIS	69
Leonidas S. Cordova (UNC)	
ENERGY AND MASS FLUX IN THE GULF STREAM	91
Nicholas P. Fofonoff (WHOI)	
MODELS OF GULF STREAM VARIABILITY -- AN OVERLY BRIEF REVIEW	98
Dale B. Haidvogel (WHOI)	
SIMULATION OF NORTH ATLANTIC VARIABILITY	114
William R. Holland (NCAR)	
THE BEHAVIOR OF AN INDIVIDUAL CURRENT METER IN DIFFERENT DYNAMICAL REGIMES	127
Harley E. Hurlburt (NORDA) and J. Dana Thompson (NCSU)	
AN ANALYSIS OF THE POTENTIAL VORTICITY DISTRIBUTION ACROSS THE GULF STREAM	153
Elizabeth M. Johns and D. Randolph Watts (URI)	
OBSERVATIONS ON THE VERTICAL COHERENCE OF GULF STREAM MEANDERS	164
William E. Johns (URI)	

PRELIMINARY RESULTS ON NORMALIZATION OF HYDROGRAPHIC SECTIONS OF THE GULF STREAM	180
Timothy W. Kao (CUA)	
ON GULF STREAM FRONTAL EDDIES ALONG THE SOUTHEAST U.S. OUTER CONTINENTAL SHELF	186
Thomas N. Lee (RSMAS) and Larry P. Atkinson (SKIO)	
ON GULF STREAM VARIABILITY AT 30°N	223
Thomas N. Lee (RSMAS) and Evans Waddell (SAI)	
SPATIALLY UNSTABLE WAVES IN THE GULF STREAM OVER THE CAROLINA CONTINENTAL SLOPE	254
Mark E. Luther (FSU)	
GULF STREAM FRONTAL STATISTICS FROM FLORIDA STRAITS TO CAPE HATTERAS DERIVED FROM SATELLITE AND HISTORICAL DATA ...	278
Donald B. Olson, Otis B. Brown, and Steven R. Emmerson (RSMAS)	
THE PEGASUS PROGRAM EAST OF CAPE HATTERAS	302
H. Thomas Rossby and Daniel Halkin (URI)	
VARIABILITY OF THE FLORIDA AND ANTILLES CURRENT	309
Freidrich Schott (RSMAS)	
SYNOPTIC MEASUREMENTS OF SEA SURFACE TEMPERATURES IN THE GULF STREAM FRONTAL ZONE BETWEEN SAVANNAH, GA AND CAPE HATTERAS, NC	331
Cynthia M. Seay (JAYCOR)	
TRAPPED AND RADIATING INSTABILITIES OF A TWO-LAYER JET, APPLIED TO THE GULF STREAM	343
Lynn Talley (WHOI)	
EIGHTEEN DEGREE WATER VARIABILITY	344
Lynn Talley (WHOI)	
A NUMERICAL STUDY OF THE INFLUENCE OF THE NEW ENGLAND SEAMOUNT CHAIN ON THE GULF STREAM: PRELIMINARY RESULTS	346
J. Dana Thompson (NCSU) AND Harley E. Hurlburt (NORDA)	
PRELIMINARY ESTIMATES OF SURFACE VORTICITY AND DIVERGENCE IN GULF STREAM WESTERN BOUNDARY PERTURBATIONS USING SATELLITE AND BUOY DATA	363
Fred M. Vukovich (RTI) and George A. Maul (NOAA/AOML)	
OBSERVATION ON PROPAGATION AND GROWTH OF GULF STREAM MEANDERS	373
D. Randolph Watts and William E. Johns (URI)	
List of Participants	392

AD P001039

GULF STREAM FLUCTUATIONS AND THEIR RELATION
TO THE WINDS OFF NORTH CAROLINA

By

David A. Brooks
Department of Oceanography
Texas A&M University
College Station, TX 77843

ABSTRACT

The Gulf Stream Meanders Experiment (GSME) produced two 4-month data sets of current fluctuations in the Gulf Stream over the continental slope off North Carolina. Wind speed and direction data were simultaneously collected at two offshore-moored data buoys and at Cape Hatteras. The location of the wind stations permitted calculation of the wind stress curl and divergence over the GSME area. Summary analysis results are presented here which show that there was no significant coherence between the wind or its curl or divergence and the weekly-scale current fluctuations typical of Gulf Stream meanders. There was marginally significant coherence between the wind and current fluctuations for 3- to 4-day periods. The calculated rate at which the fluctuating winds worked on the currents was insignificant compared to kinetic energy redistribution within the Stream. The direct action of the wind appears to be ruled out as an important energy source for subtidal Gulf Stream fluctuations in the GSME area.

1. Background and Introduction

The wind is a natural candidate forcing mechanism for low frequency Gulf Stream fluctuations. Early investigators associated Gulf Stream variations with atmospheric phenomena. In his pioneering study of the

Florida Current-Gulf Stream system, Pillsbury (1891) described the passage of an atmospheric cold front over the eastern United States, which he said caused Florida Current surface velocities which were ". . . decidedly too high." Variable winds have been related to current fluctuations in coastal waters adjacent to Florida, Georgia, and North Carolina (Lee and Mayer, 1977; Lee and Brooks, 1979; Janowitz and Pietrafesa, 1980; Hofmann *et al.*, 1981). Direct correlations between atmospheric parameters and velocity fluctuations have been found in the Florida Current (Duing, *et al.*), but farther north, where the Florida continental shelf widens and the Current is located farther offshore, there is a distinct drop in this correlation seaward of the shelf "break" (Lee and Brooks, 1979). This suggests that the influence of the local wind is confined to the coastal margin, where the coastal boundary can produce an effective divergence of wind-driven Ekman flux in the surface layer.

There are, however, ways in which the wind may be directly coupled to water motions in the absence of a coastal boundary. The vorticity equation shows that the wind stress curl, which introduces local divergences or convergences in the surface layer, may be an effective forcing function for water motions (e.g., Pedlosky, 1979). Likewise, the wind stress divergence may be important.

Webster's (1961a) description of Gulf Stream meanders off North Carolina is especially provocative concerning wind forcing. Trying to identify a source mechanism for the dominant weekly time-scale meanders, he compared the offshore position of the Gulf Stream front with the difference between the atmospheric pressure at Cape Hatteras and Charleston (Fig. 1). He found a good visual correlation between the pressure difference, presumed to be proportional to the offshore geostrophic winds,

and the offshore position of the front. However, a calculation showed that the energy that the wind could be expected to contribute to the meanders was much less than the kinetic energy redistributions within the Stream (Webster, 1961b), and it was therefore concluded that the apparent connection between the winds and meanders might have been coincidental.

In 1979, the Gulf Stream Meanders Experiment (GSME) was conducted off North Carolina in the area shown by the boxed inset of Fig. 1. During the experiment, 10 Aanderaa current meters were deployed on four moorings in the Gulf Stream for two 4-month periods, one each in the winter and the summer. An overview of the GSME and a seasonal comparison of the subtidal fluctuations is given in this issue by Brooks and Bane (1982; referred to herein as BB82). During both GSME periods, atmospheric data were collected at Cape Hatteras and at two National Data Buoy Office (NDBO) offshore-moored data buoys (NDBO-2 and NDBO-4, Fig. 1). These three stations were approximately located at the vertices of a right triangle, which facilitates finite-difference computation of the wind stress curl and divergence terms in the enclosed area. The Cape Hatteras Observation station is remotely located on the coastal barrier strip between Pamlico Sound and the Atlantic Ocean, which assures that all the meteorological data were relatively free of the effects of land influences.

The effectiveness of atmospheric forcing of subtidal Gulf Stream fluctuations during the GSME is summarized in this paper. For representative examples, a direct comparison of currents and winds is given, and the the wind stress curl and divergence are compared to the current fluctuations and their associated relative vorticity. It is concluded that the fluctuations

observed during the GSME were not effectively forced by the wind, although some suggestion of shorter-period (several days) coupling is apparent. The wind stress curl and divergence likewise were only weakly and inconsistently correlated with the current and its relative vorticity fluctuations. These results support and extend Webster's (1961a,b) conclusion that the atmosphere is not the primary energy source of low-frequency Gulf Stream fluctuations off North Carolina.

2. Data Methods and Statistical Summary

The GSME data set has been extensively documented (see BB82 for data reports available). The locations of the four moorings are shown in Fig.

1. Each mooring supported two or three current meters in the lower half of the water column. The mean surface Gulf Stream axis approximately overlies the 400 m isobath in the GSME area. The instruments were supported at nominal depths of 100 and 180 m over the 200 m isobath, and at 260, 320 and 380 m over the 400 m isobath. The low-frequency (subtidal) fluctuations were dominated by the effects of the meandering Stream, which occurred on approximately a 7- to 10-day time scale in the winter and a 5- to 7-day time scale in the summer. A seasonal description of the meanders is given in BB82.

The raw atmospheric data consisted of hourly values of surface wind speed and direction, atmospheric pressure and air temperature. The NDBO buoys also provided sea-surface temperature. Hourly values of the wind stress vector, $\vec{\tau}$, were computed as

$$\vec{\tau} = \rho_a C_D |W| (\hat{i}W_u + \hat{j}W_v),$$

where the air density at the surface was taken to be $\rho_a = 1.2 \times 10^{-3} \text{ gm cm}^{-3}$, the drag coefficient $C_D = 1.5 \times 10^{-3}$, and the wind vector, \vec{W} , has magnitude $|\vec{W}|$ and components (W_u, W_v) in the (\hat{i}, \hat{j}) coordinate directions. The vector horizontal coordinate frame (\hat{i}, \hat{j}) was rotated 34° clockwise to conform with the local orientation of the 400 m isobath, such that the u-component of $\vec{\tau}$ and \vec{W} is offshore and the v-component of $\vec{\tau}$ and \vec{W} is in the downstream direction of the Stream. In a separate calculation, the vector components of $\vec{\tau}$ were computed in a non-rotated frame. The non-rotated components were used in the calculation of $\nabla \times \vec{\tau}$ and $\nabla \cdot \vec{\tau}$, because the meteorological stations were approximately oriented along east-west and north-south lines (Fig. 1). All of the atmospheric time-series were then smoothed with a forty-hour low-pass (40 HRLP) filter, which removes the variance with periods shorter than 40 hrs.

The vertical component of the wind stress curl and the wind stress divergence were computed from the non-rotated wind stress vector components as follows:

$$\nabla \times \vec{\tau} = \frac{\partial \tau}{\partial x}(y) - \frac{\partial \tau}{\partial y}(x) = (\tau_2(y) - \tau_4(y))\Delta x^{-1} - (\tau_H(x) - \tau_2(x))\Delta y^{-1} \quad (2a)$$

$$\nabla \cdot \vec{\tau} = \frac{\partial \tau}{\partial x}(x) + \frac{\partial \tau}{\partial y}(y) = (\tau_2(x) - \tau_4(x))\Delta x^{-1} + (\tau_H(y) - \tau_2(y))\Delta y^{-1} \quad (2b)$$

In this notation, the subscripts 2,4,H refer to atmospheric stations NDBO-2, NDBO-4, and Cape Hatteras, respectively (Fig. 1); the east-west separation between NDBO-2 and NDBO-4 is $\Delta x = 322 \text{ km}$, and the north-south separation between NDBO-2 and Cape Hatteras is $\Delta y = 328 \text{ km}$.

First-order statistics for the low-pass filtered wind stress and its curl and divergence are shown in Table 1, for both mooring periods. An analogous table for current statistics is given in BB82. In both seasons,

the mean wind stress at the offshore buoy was essentially in the downstream direction. The wind stress curl and divergence fluctuated about near-zero means. The maximum wind stress of $4.3 \text{ dynes cm}^{-2}$ (downstream) occurred in the winter, and it corresponds to a wind speed of about 20 m s^{-1} sustained for several days at the offshore NDBO buoy. The maximum values of the quantities in Table 1 are consistent with those expected for a typical extratropical cyclone northeast of Cape Hatteras (Mooers *et al.*, 1976).

3. Atmospheric Influences on Gulf Stream Fluctuations

The downstream (v) current fluctuations over the 200 m isobath are compared with atmospheric variables in Fig. 2. The first 30 days of the 40-hr low-pass filtered data are shown for winter and summer GSME periods. These periods were characterized by active meandering of the Stream, manifested by large weekly time-scale v -component oscillations. The components of the vertical relative vorticity, $\partial v / \partial x - \partial u / \partial y$, are also shown for each season. The $\partial v / \partial x$ term was calculated from the mid-depth current meters on the A and B moorings, and the $-\partial u / \partial y$ term was calculated from the mid-depth current meters on the C and D moorings. The $-\partial u / \partial y$ term was given an artificial time lead of (39,38) hrs in the (winter, summer) to account for the mean downstream propagation speed of the meanders. The resulting time series of relative vorticity components can be viewed as mid-depth estimates in a $15 \text{ km} \times 15 \text{ km}$ box centered between the A and B moorings.

In each season, there is a similarity between the wind and the current fluctuations with time scales of 3- to 4 days (Fig. 2). The relationship is more evident in the winter, when the clockwise-polarized downstream (W_v) and offshore (W_u) wind components are typically associated with the passage of atmospheric fronts. The wind component fluctuations

with 3- to 4-day periods lead the v-component current fluctuations by less than one day in each season.

In contrast, there is little connection evident between the wind and the meander-related v-component peaks which occurred on 26 January and 5 and 11 February in the winter, and on 11, 18 and 26 August and 8 September in the summer (Fig. 2). The fluctuations associated with the meandering are distinct from the smaller-amplitude, 3- to 4-day period fluctuations.

There is also no obvious connection between the wind stress curl or divergence and the v-component of the current or the relative vorticity fluctuations, in either season (Fig. 2). It is evident that positive (cyclonic) relative vorticity peaks sometimes occur in association with large-amplitude, v-component meander signatures. The vorticity peaks usually occur ~ 0.5 day later than the v-peak, or shortly after the passage of the meander crest (the shoreward-most excursion of the Gulf Stream front). The vorticity peaks are an indication of the bulk cyclonic rotation of the water that usually occurs a few km upstream of meander crests (BB82).

The visual relationships between wind and current fluctuations during the 30-d intervals in Fig. 2 are representative of the full 4-month records. A spectral summary of the full-record relationships is shown for a representative winter case in Figs. 3 and 4. The spectrum density distribution of the current fluctuations changed seasonally (BB82), but the coherence between the meandering currents and the wind stress was insignificant in both seasons. The spectrum density of the wind stress components bears little resemblance to the A_T -v spectrum density (Fig. 3a), and there is a pronounced coherence "gap" between the wind stress and the current

fluctuations for 7- to 10-day period meanders (Fig. 3b). There was, however, marginally significant coherence between the v-current component and the wind stress for 3- to 4-day periods in the winter, and for 2- to 3-day periods in the summer (not shown), consistent with the discussion concerning Fig. 2. Examination of many other combinations of wind stress and current components from the GSME data set has confirmed the lack of consistent coherence for period ranges associated with meanders in both seasons (Cohen, 1981).

The wind stress curl and divergence were marginally coherent with the current fluctuations only in the 3- to 4-day period band (Fig. 4). In contrast with the wind stress, the spectrum of the wind stress curl has a peak that corresponds with the A_T -v peak at a period of ~ 9 days, but there is only a suggestion of enhanced coherence between the fluctuating currents and the differential wind stress in the 7- to 10-day period band. Examination of other combinations of variables suggests that the differential wind stress forcing mechanism was more effective than the direct action of the wind stress, as expected for the GSME area, but a consistent and statistically convincing relationship between fluctuations of the current and the differential wind stress was not found (Cohen, 1981).

The essential independence of the wind and current fluctuations off North Carolina can be demonstrated from the rate of working of the wind stress on the currents. Ideally, an estimate of this quantity would require the measurement of surface currents, which are not available in the present case. However, the high vertical coherence and in-phase nature of the fluctuations (BB82) can be exploited, allowing the rate of working to be calculated using a mid-depth current record. The result, which can

be interpreted as a column-averaged estimate of the downstream rate-of-working in each frequency band, is the co-spectrum between the v-component of the wind stress and the v-component of the current fluctuations. A winter example is shown in Fig. 5 for the A mooring. Positive values in period bands of significant coherence indicate work being done on the current by the wind. This occurred only in the downstream direction, and only for the 3- to 4-day period band in the winter. The cross-stream rate of working was insignificant.

The peak value of the coherent downstream co-spectrum occurs at a period of 4 days in Fig. 5. Multiplying the peak value by the peak bandwidth (~ 0.05 CPD) yields $\sim 1.5 \text{ erg cm}^{-2} \text{ s}^{-1}$ as the average rate of working on the column by the wind, per unit surface area, or $4.5 \times 10^6 \text{ erg cm}^{-1} \text{ s}^{-1}$ as the average rate in a 30 km-wide cross-shelf scale width. For a mean Stream velocity of 0.5 m s^{-1} in the top 100 m of the 30 km-wide strip, the mean kinetic energy density is $7.5 \times 10^{13} \text{ erg cm}^{-1}$, which implies a wind-driven mean kinetic energy doubling time of ~ 0.5 yr. For comparison, doubling times of a few weeks are indicated by the calculated rate of kinetic energy eddy transfer from the fluctuating currents to the mean Stream in the GSME area (Webster, 1961b; BB82). The marginal coherence between the wind and the 3- to 4-day period current fluctuations (Fig. 3) is therefore probably not a direct result of wind forcing; rather, it may be a vestigial indication that the wind forcing was effective in the near-shore zone, shoreward of the GSME moorings. The cross-shelf scale within which the coastal wind forcing mechanism is effective in the GSME area is ~ 30 km (Chao and Pietrafesa, 1980). The A mooring was several times this distance from the coast.

4. Summary

There was no direct, consistent correlation evident between atmospheric and Gulf Stream fluctuations with periods longer than 2 days during the Gulf Stream Meanders Experiment (GSME). This result extends Webster's (1961a,b) conclusion based on a theoretical estimate of the energy transfer from the winds to the currents. His estimate of this transfer rate for the surface layer, applied to a water column 100 m deep, is $1 \text{ erg cm}^{-2} \text{ s}^{-1}$, which compares well with the present estimate of $1.5 \text{ erg cm}^{-2} \text{ s}^{-1}$, calculated from the winter GSME observations in the same area. The rate of kinetic energy transfer from the fluctuations to the mean Stream by turbulent Reynolds' stresses has been shown to be several orders of magnitude larger than this (Webster, 1961b; BB82), which effectively rules out the wind as an important direct forcing mechanism for subtidal Gulf Stream fluctuations over the continental slope off North Carolina. The GSME data suggest, however, that the wind may provide an effective forcing mechanism for near-shore water motions, consistent with observations in relatively shallow water shoreward of the GSME area (e.g., Hofmann *et al.*, 1981).

Theoretical considerations suggest that the curl and divergence of the wind stress may provide direct forcing of water motions, independent of coastal boundaries. However, there was no consistent pattern of correlation between the curl and divergence of the wind stress and the current fluctuations during the GSME, although hints of a frequency-selective and seasonally-varying coupling process were evident.

ACKNOWLEDGEMENTS

The Gulf Stream Meanders Experiment (GSME) was supported by the National Science Foundation, grant numbers OCE 77-25682 and OCE 79-06710. The latter grant also supported Mr. Cohen's master's thesis, from which the information in Table 1 was condensed. Mr. Cohen assisted in several GSME cruises and organized most of the meteorological data sets.

Table 1. First-order statistics for (offshore, longshore) wind stress components from NDBO offshore buoy 41002 (τ_u, τ_v ; dynes cm^{-2}), wind stress curl ($\nabla \times \tau$; dynes $\text{cm}^{-3} \times 10^6$) and wind stress divergence ($\nabla \cdot \vec{\tau}$; dynes $\text{cm}^{-3} \times 10^6$). Values are compared for the winter/summer mooring periods. All data were first smoothed by a 40-hr low-pass filter (from Cohen, 1981).

	Minimum	Maximum	Mean	Standard deviation
τ_u	-2.9/-2.7	3.4/3.7	.01/-0.11	0.85/0.74
τ_v	-2.5/-3.1	4.3/3.3	.25/.18	0.85/0.85
$\nabla \times \vec{\tau}$	-.07/- .05	.07/.07	.02/.03	.04/.04
$\nabla \cdot \vec{\tau}$	-.08/- .07	.06/,05	-.01/- .01	.03/.02

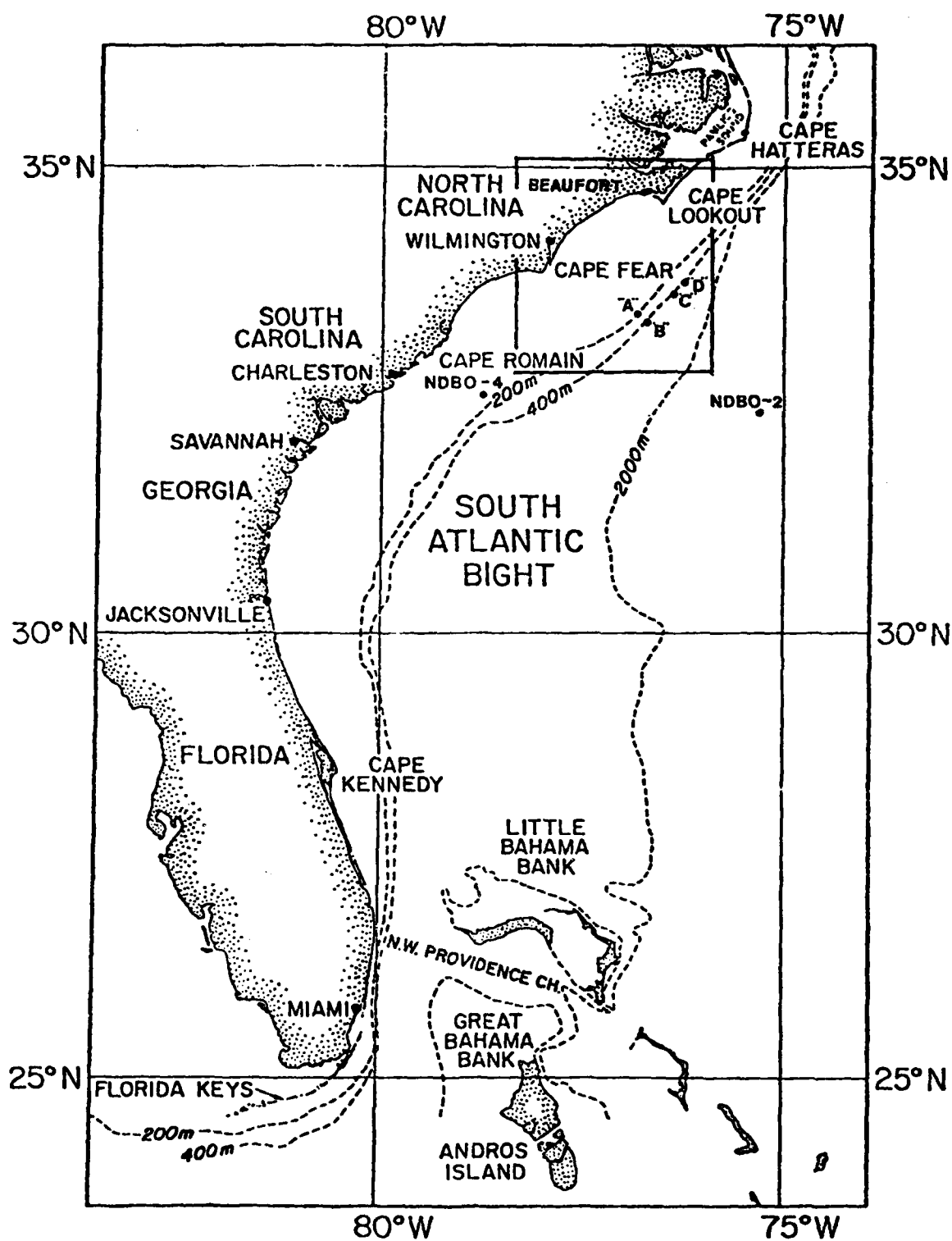


Fig. 1. Map of the South Atlantic Bight, showing the GSME study area (boxed inset). The four moorings were located at the points labelled "A" through "D." Moored meteorological observation platforms were maintained at sites "NDBO-2" and "NDBO-4" by the National Data Buoy Office and meteorological observations were also obtained from Cape Hatteras.

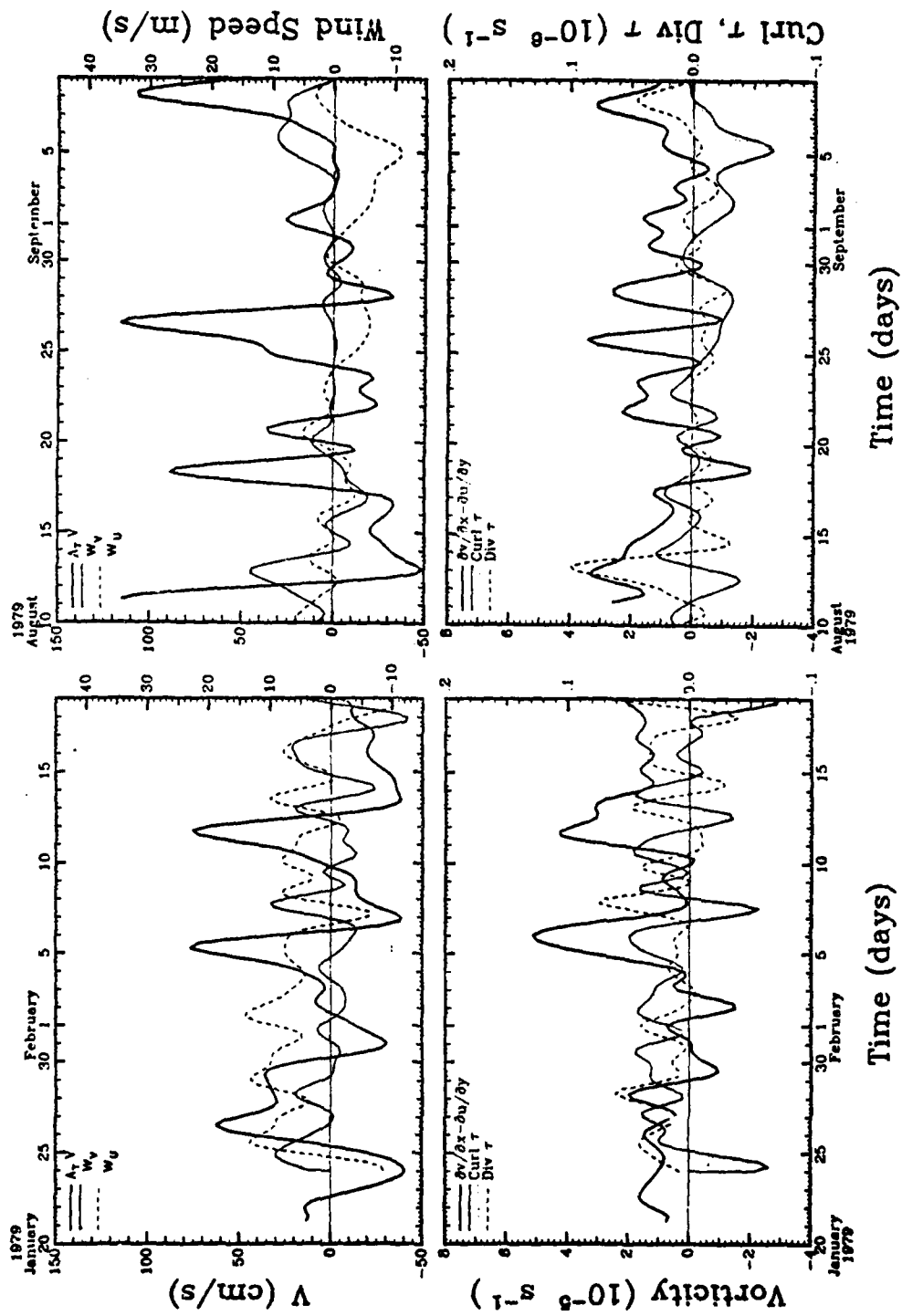


Fig. 2a A comparison of the v-velocity component at the top instrument of the A mooring with the (offshore, downstream) wind component (w_u, w_v), the relative vorticity, $\zeta = \partial v / \partial x - \partial u / \partial y$, and the curl and divergence of the wind stress, τ , for the first 30 days of the winter period. All data have been 40-hr low-pass filtered.

Fig. 2b A comparison of the v-velocity component at the top instrument of the A mooring with the (offshore, downstream) wind component (w_u, w_v), the relative vorticity, $\zeta = \partial v / \partial x - \partial u / \partial y$, and the curl and divergence of the wind stress, τ , for the first 30 days of the summer period. All data have been 40-hr low-pass filtered.

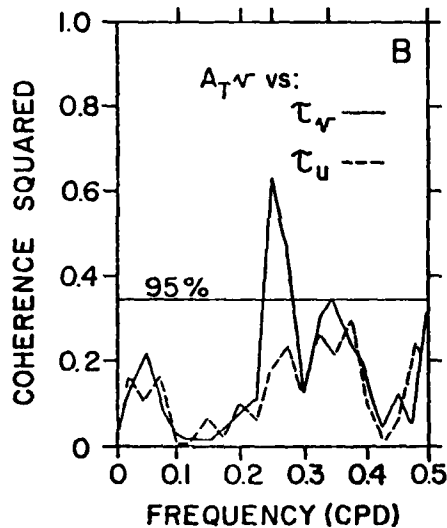
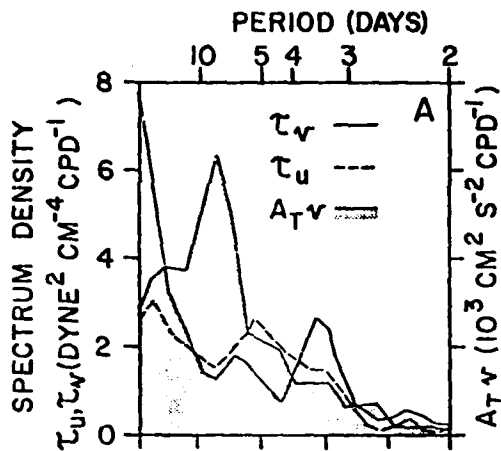


Fig. 3

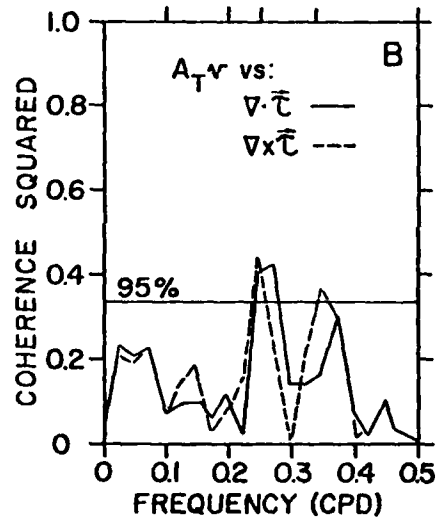
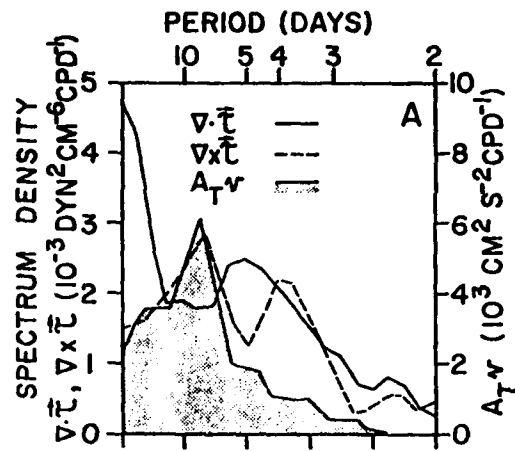


Fig. 4

Fig. 3. (A) Spectrum density of wind stress components (τ_v, τ_u) at the offshore buoy NDBO-2 and the v-component of the current at the A-top instrument.

(B) Coherence between the wind stress components and the A-top v-component of current. The 95% null hypothesis level is shown by the horizontal line. All spectrum estimates carry about 15 degrees of freedom.

Fig. 4 As in Fig. 3, except comparing the wind stress divergence and curl with the A-top v current component.

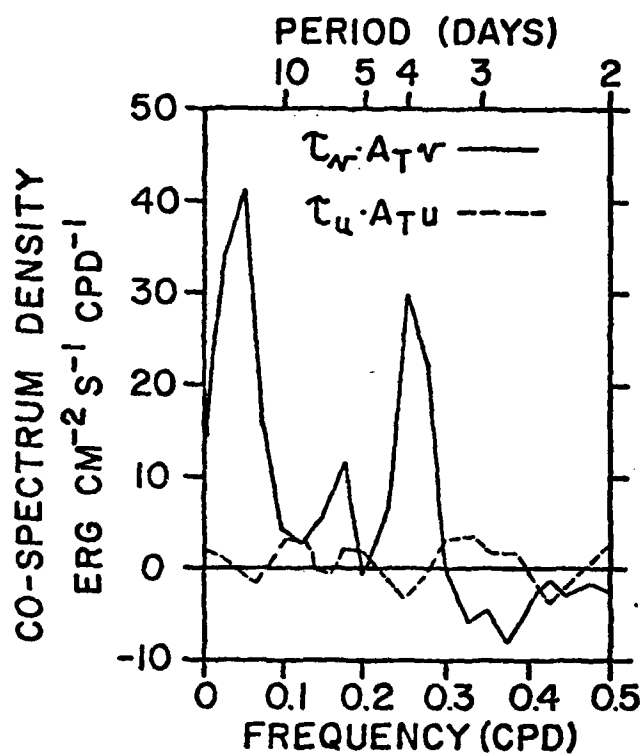


Fig. 5. Co-spectrum density between the wind stress components at offshore buoy NDBO-2 and the corresponding A-top current components. Positive values indicate that the fluctuating wind is doing work on the water column.

REFERENCES

- Brooks, D. A. and J. M. Bane, Jr., A seasonal comparison of Gulf Stream fluctuations off North Carolina. Submitted to *J. Geophys. Res.*, 1982.
- Chao, S.-Y. and L. J. Pietrafesa, The subtidal response of sea level to atmospheric forcing in the Carolina Capes. *J. Phys. Oceanogr.*, 10, 1246-1255, 1980.
- Cohen, R. L., Atmospheric influences on Gulf Stream fluctuations off Onslow Bay, North Carolina. M.S. thesis, 51 pp., Texas A&M University, 1981.
- Düing, W. O., C. N. K. Mooers, and T. N. Lee, Low-frequency variability in the Florida Current and relations to atmospheric forcing from 1972 to 1974. *J. Mar. Res.*, 35, 129-161, 1977.
- Hofmann, E. E., L. J. Pietrafesa, and L. P. Atkinson, A bottom water intrusion in Onslow Bay, North Carolina. *Deep-Sea Res.*, 28A, 329-345, 1981.
- Janowitz, G. S. and L. J. Pietrafesa, A model and observations of time dependent upwelling over the mid-shelf and slope. *J. Phys. Oceanogr.*, 10, 1574-1583, 1980.
- Lee, T. N. and D. A. Brooks, Initial observations of current, temperature and coastal sea level response to atmospheric and Gulf Stream forcing on the Georgia shelf. *Geophys. Res. Lett.*, 6, 321-324, 1979.
- Lee, T. N. and D. A. Mayer, Low-frequency current variability and spin-off eddies along the shelf off southeast Florida. *J. Mar. Res.*, 35, 193-220, 1977.
- Mooers, C. N. K., J. Fernandez-Partagas, and J. F. Price, Meteorological forcing fields of the New York Bight (First Year). *Tech. Rep. TR76-8*, Marine Studies Center, University of Delaware, 1976.
- Pedlosky, J., *Geophysical Fluid Dynamics*. Springer-Verlag, New York, 1979.
- Pillsbury, J. E., The Gulf Stream . . . Rept. Supt., U.S. Coast and Geod. Surv., for year ending June, 1890. (Appen. 10).
- Webster, F., A description of Gulf Stream meanders off Onslow Bay. *Deep-Sea Res.*, 9, 130-143, 1961a.
- Webster, F., The effect of meanders on the kinetic energy balance of the Gulf Stream. *Tellus*, 13, 392-401.

AD P001040

17

A SEASONAL COMPARISON OF GULF STREAM FLUCTUATIONS
OFF NORTH CAROLINA

By

David A. Brooks
Department of Oceanography
Texas A&M University
College Station, TX 77843

and

John M. Bane, Jr
Curriculum in Marine Sciences
The University of North Carolina at Chapel Hill
Chapel Hill, NC 27514

ABSTRACT

The Gulf Stream Meanders Experiment (GSME) was conducted off North Carolina in 1979. Instruments were moored in the Stream over the 200 m and 400 m isobaths on the continental slope for two 4-month periods, one in the winter and one in the summer. In both seasons, the downstream current speed typically fluctuated between -50 cm/s and $+100 \text{ cm/s}$ about a 30 cm/s mean. The velocity, temperature, and salinity fluctuations had a prominent 7- to 10-day period in the winter, and a less prominent 5- to 7-day period in the summer. The fluctuations, which were nearly in-phase vertically and propagated down-stream at $\sim 40 \text{ km/d}$, apparently resulted from lateral, wavelike excursions or meanders of the Gulf Stream front, as first described by Webster (1961a). The observed structure is complicated along the shoreward edge of the Stream, where shallow surface filaments of warm water often trail southwestward from meander crests. The warm filaments are usually separated from the Stream by a band of cool surface water, which is a manifestation of deeper uplifting or upwelling associated with the meander process. Strong cyclonic circulation around the uplifted cool water "pool" is a characteristic feature of meanders. In both seasons, the leading term in the energy equation indicated that part of the fluctuation kinetic energy was converted to mean Stream kinetic energy, with an implied doubling time of a few weeks. Direct forcing by the wind was found to be ineffective during the GSME. The seasonal persistence of meanders in the GSME area thus indicates an upstream source of their kinetic energy.

1. Historical Setting

It is remarkable that the variability of the Gulf Stream was appreciated soon after the Stream's discovery in 1513 by Ponce de Leon. One can share Ponce de Leon's amazement as his ships were swept northward along the southeastern Florida coast (Fig. 1) by a "current which was more powerful than the wind" (Herrera, 1601; also see Scisco, 1913, for a detailed description of Ponce de Leon's track and Herrera's paraphrase of the expedition). The explorers initially encountered the current near what is now Jupiter Inlet and again near Lake Worth; on both occasions they were compelled to seek anchorages under the lee of coastal capes because they could not stem the current offshore. Scisco suggested that the vessels "waited for the [tidal] current to abate," supposing that they were too near the land to be directly influenced by the Gulf Stream. However, more recent information indicates that the Stream meanders laterally, at times bringing strong northward currents within a few km of the southeastern Florida coast. It is unlikely that Ponce de Leon was waiting for a favorable tide, because the expedition remained at each anchorage for many days while occupied with other matters. When they did leave, in each case they were able to continue their southward progress. It is conceivable that the Gulf Stream's discoverer was also the first to exploit its meandering nature.

By the latter half of the 16th century, a working knowledge of Gulf Stream eddies in the South Atlantic Bight (Fig. 1) was available. John White's casual remark in 1590 about southward-setting eddy currents along the Carolina coasts suggests the familiar nature of this information (see Quinn (1952) for the context in which White's remark was made). It is not surprising that such practical advice quickly spread among mariners, since their lives often depended on its successful application. During the next two centuries, many observations

were made in the Gulf Stream, and a number of theories were offered to explain its existence (cf Stommel, 1966). Benjamin Franklin and William De Brahm have been credited with producing the first realistic charts of the Gulf Stream (DeVorse, 1976), and copies of Franklin's original 1769 chart have only recently been re-discovered (Richardson, 1980). Franklin's grand-nephew, Jonathan Williams (1793), applied his uncle's ideas about thermometric navigation while sailing from Halifax to New York, and gave what may be the first description of a Gulf Stream ring.

Nineteenth century surveys in the South Atlantic Bight lead to Bache's discovery in 1860 of cold water bands interleaved within the Stream (Pillsbury, 1890; Stommel, 1966). Pillsbury (1890) showed that the interleaving was variable in time and position, and he attempted to relate Gulf Stream fluctuations to atmospheric and lunar effects. More recent studies (e.g., Webster, 1961a) show that the interleaving process is associated with meandering, which produces warm filaments of surface water extruded from the inshore edge of the Gulf Stream and separated from it by a cold water band. Webster (1961a) provided a detailed description of the upper-layer meandering process in the boxed region of Fig. 1, based on temperature measurements from consecutive crossings of the Stream. He described the meanders as skewed, wavelike, lateral excursions of the mean Stream. These features were observed to travel downstream, such that the temperature fluctuations at a fixed observation site had a prominent weekly time scale.

2. The Gulf Stream Meanders Experiment (GSME)

To continue the study of meanders, in 1979 we conducted a field experiment in the boxed region shown in Fig. 1. Subsurface moorings supporting two or three Aanderaa current meters each were maintained at sites A through D for two 4-month periods, one in the winter and one in the summer. The

instruments were deployed in the Gulf Stream over the 200 m and 400 m isobaths, at nominal depths of 100 and 180 m at mooring A and at depths of 250, 320, and 380 m at the other moorings. The winter observations have been summarized by Brooks and Bane (1981; referred to herein as BB81), who give more information about the mooring array design and the basic data processing techniques that were used. The full set of observations, including those from four hydrographic cruises and 16 aircraft air-dropped expendable bathythermograph (AXBT) surveys, are given in a set of data reports listed in the references. The primary objective of the GSME was to directly measure the meandering Gulf Stream currents and to provide a quasi-synoptic, hydrographic description of meanders.

In this paper we present a seasonal comparison of Gulf Stream fluctuations and meanders observed over the continental slope between Charleston and Cape Hatteras (Fig. 1). Previous direct observations of the Gulf Stream in this area (Webster, 1961a; Richardson, et al., 1969) have not permitted this comparison because of their relatively short duration. The seasonal perspective available from the GSME data set may help address some of the fundamental questions about the meander mechanism.

A basic statistical comparison of the winter and summer data sets is given in the next section, followed by a more detailed discussion of the fluctuations and the structure of meanders. In this context, "winter" refers to the period 16 January to 14 May 1979, and "summer" refers to the period 1 August to 17 November 1979. Direct comparisons between seasons are shown when warranted, but in some cases reference is made to BB81 for winter cases.

TABLE 1. Seasonal comparisons (winter/summer) of 3-hour lowpass-filtered current components (u,v; cm s^{-1}) and temperature (T; $^{\circ}\text{C}$) for each moored instrument. "Winter" means 16 Jan-14 May 1979, and "summer" means 1 Aug-17 Nov 1979. The water depth was nominally 200 m at the "A" mooring and 400 m at the others.

Instrument					
Depth (m)	Parameter	Minimum	Maximum	Mean	Standard Deviation
<u>A-top</u> (98/100)	u	-39/-37	49/50	0/2	10/13
	v	-71/-86	117/126	7/5	34/44
	T	13/12	24/24	17/18	2/2
<u>A-bot</u> (178/180)	u	-32/-51	44/31	-3/-8	9/10
	v	-59/-66	75/76	4/2	21/20
	T	4/*	20/*	12/*	3/*
<u>B-top</u> (250/270)	u	-56/-59	64/48	1/-1	16/16
	v	-50/-41	134/126	25/26	29/30
	T	9/9	19/17	13/12	3/2
<u>B-bot</u> (370/390)	u	-34/-36	40/41	2/1	11/10
	v	-63/-41	53/67	5/6	17/10
	T	6/6	14/12	9/8	2/1
<u>C-top</u> (245/260)	u	-33/-38	54/36	4/1	12/10
	v	-44/-57	135/139	32/25	34/34
	T	9/9	18/17	13/12	2/2
<u>C-mid</u> (305/320)	u	-99/-30	83/37	0/0	16/9
	v	-46/-56	113/113	23/17	27/27
	T	3/8	30/16	11/11	2/2
<u>C-bot</u> (365/380)	u	-33/-24	48/29	-1/-1	10/8
	v	-40/-50	74/63	9/8	20/19
	T	7/6	14/13	9/9	1/1
<u>D-top</u> (236/250)	u	-28/-41	48/39	4/1	10/10
	v	-35/-48	122/142	32/24	29/34
	T	9/9	19/17	13/12	2/2
<u>D-mid</u> (296/310)	u	-30/*	42/*	-1/*	9/*
	v	-46/*	116/*	24/*	29/*
	T	8/*	19/*	11/*	2/*
<u>D-bot</u> (356/370)	u	-27/*	35/*	0/*	8/*
	v	-38/*	55/*	8/*	17/*
	T	7/*	14/*	9/*	1/*

* No data.

3. Basic Statistics of the Winter and Summer Observations

The mooring locations and the mean 3 HRLP¹ current vectors for the summer case are shown in Fig. 2. The analogous mean winter currents are shown in BB81. The moorings were deployed in approximately the same location on the continental slope in both seasons. The current meter spacing provided measurements on scales of 64 and 75 km in the downstream direction, 18 km cross-stream, and 60-120 m vertically. The velocity components and vectors are presented in a coordinate frame rotated 34° clockwise from true north to align with the local topography, such that the v-component of the velocity vector is positive in the downstream direction and the u-component is positive offshore. A seasonal comparison of first-order statistics of the velocity components and water temperature at each instrument is given in Table 1.

In both seasons, the mean flow was essentially in the downstream direction at all instruments, except for the near-bottom instrument on mooring A ("A-bot"; we use appended abbreviations to identify the instruments). The shoreward component of the mean flow at A-bot was stronger in summer (-8 cm s^{-1}) than in the winter (-3 cm s^{-1}), and the vector rotation sense was consistent with that expected in a bottom Ekman boundary layer. The mean velocity components and mean temperatures were seasonally similar at the upstream instruments (moorings A and B), but the summer mean velocity components were about 20% larger than in the winter at most of the downstream instruments (moorings C and D). In

¹

The basic sampling rate was $\Delta t = 20 \text{ min}$ for all instruments. The edited data were smoothed with a 3-hour low pass (3 HRLP) filtered to reduce sampling noise. A 40-hour low pass (40 HRLP) filter was then used to separate the fluctuations with periods longer than 40 hrs from those of shorter periods (cf BB81). A Lanczos taper was used for both filters.

most cases, the range of the velocity component fluctuations was much larger than the corresponding means, the extreme example being the summertime v-component range of -86 to 126 cm s^{-1} relative to a mean of 5 cm s^{-1} at A-top. The standard deviations of the velocity components at a particular instrument show little seasonal difference, and the spatial distribution of horizontal kinetic energy was similar in the two seasons.

The frequency distribution of the kinetic energy differed substantially between winter and summer, however. Figure 3 shows summary velocity-component variance spectra for the two seasons. For each season, the mean variance estimate for all the instruments in each frequency band is shown by the heavy lines. The thin lines show the extrema, and the shaded area covers one standard deviation relative to the means. In the winter, velocity component fluctuations with 7- to 10-day and 3- to 4-day time scales were prominent in the variance spectrum. The winter spectrum in Fig. 3 is typical of Gulf Stream meanders as discussed by Webster (1961a). In the summer, the velocity component fluctuations had less prominent time scales of 5-to-7 days and 3-to-4 days, superimposed on a background of motions with very long periods (> 2 weeks). In both seasons, the mean subtidal u-component variance was about one-fifth of the v-component variance. The tidal fluctuations in both seasons were primarily semi-diurnal, and they were about twice as energetic in the u-component as in the v-component. The inertial period at the experiment latitude ($\sim 33^{\circ}40'N$) is 21.7 hrs, but there is only inconclusive evidence of an inertial peak in the mean variance spectra in either season.

Temperature-salinity (T-S) correlations from data collected during cruises conducted before, between, and after the mooring periods are shown in Fig. 4. The curves are polynomials that have been spline-fitted to the T-S data points, after removing obviously bad points and points clearly indicating coastal water

influences. The mean T-S correlations clearly show the Subtropical Underwater salinity maximum, which occurs at depths of about 150 m and is a defining characteristic of Gulf Stream waters (Iselin, 1936). A seasonal warming cycle is evident in the upper layers, but the T-S relationship of the waters below the salinity maximum was remarkably uniform throughout the experiment.

The cruises primarily surveyed the boxed area in Fig. 1, permitting the construction of cross-stream section views of the parameter fields, but the time required for each ship survey precluded the construction of synoptic horizontal maps of the meandering Stream. The aircraft surveys (discussed later) gave nearly synoptic coverage of the temperature fields, however.

4. Subtidal Fluctuations

Seasonal differences in the subtidal fluctuation time scales are quite apparent in the full-length 40 HRLP records, shown for the B-top instrument in Fig. 5. The 7- to 10-day time scale is prominent in the winter velocity, temperature and salinity, especially during the first and last thirds of the record. In the summer, the band of energetic fluctuations extended to noticeably shorter periods of 3 or 4 days, which is consistent with the mean variance distribution for the entire array (Fig. 3). Following Webster (1961a), we refer to the dominant subtidal fluctuations as "meanders."

The meandering at B-top abated in late February and did not resume until 29 March (Fig. 5a). The absence of the v-component reversals associated with the weekly meandering time scale makes this quiescent period stand out in the winter velocity-vector time series. The 3- to 4-day period fluctuations are relatively more noticeable during the quiescent period. The velocity, temperature and salinity decreased slowly during March, perhaps as the Stream gradually moved offshore of the array area. A satellite image (not shown) of the surface

temperature structure from the week prior to the 29 March meander indicates that the Stream, or at least its surface manifestation, was located unusually far offshore during late March. The 29 March meander, which ended the quiescent period, produced the largest downstream current speed of either season at B-top.

A period of relatively low activity also occurred during the summer (mid-September to mid-October, Fig. 5b). However, this period is distinguished mainly by a reduction in the amplitude of the fluctuations, and not by an absence of v-component reversals or decreasing temperature and salinity, as occurred in the winter.

In both seasons, the v-component of velocity, temperature, salinity, and the horizontal velocity shear term, $\partial v / \partial x$, fluctuated nearly in-phase (Fig. 5). The cyclonic rotation of the velocity vectors (leading phase of u with respect to v at a single instrument), and the positive peaks in $\partial v / \partial x$ appear to be characteristic features of meanders. These characteristics have been discussed by BB81 for the large winter meander which occurred on 29 March, and by Bane, Brooks and Lorenson (1981; herein BBL) for the meanders which occurred on 5 and 11 February. In both seasons, the magnitude of the shear term $\partial v / \partial x$ often approached the local value of the Coriolis parameter (f), which is equal to $8.2 \times 10^{-5} \text{ s}^{-1}$ at 34° latitude. During most of the meanders, the $-\partial u / \partial y$ term was smaller than and tended to be out-of-phase with the $\partial v / \partial x$ term, but an exception occurred during the 29 March meander. During that event, the terms in the relative vorticity, $\zeta = \partial v / \partial x - \partial u / \partial y$, were of about equal magnitude and they had the same sign, leading to the largest value of ζ for the entire GSME period. As noted in BB81, the 29 March meander occurred as the Stream moved shoreward over the moorings, ending a month-long period of unusually low meandering activity. The relatively large positive values of $-\partial u / \partial y$ during the 29 March meander may be an indication of the onshore orientation of the mean Stream at

the end of the quiescent period.

The effects of several large meanders are evident in Fig. 5b during the first few weeks of the summer B-top records. These meanders were also responsible for large-amplitude fluctuations at the A-top instrument during the first 30 days of the summer mooring period (Fig. 6). This figure can be directly compared with Fig. 2 in BB81, which shows the same information for the first 30 days of the winter mooring period. In both seasons, the v , T and S increases were almost in-phase, and the u -increases lead the v -increases by less than one-quarter of a meander period. These phase relationships imply an offshore flux of heat and momentum. It can also be seen in Fig. 6 that increases in v , which occur during the approaching phase of a meander crest², last longer than the decreases in v , which occur after the crest passes. This asymmetry was pointed out by BB81 for the winter case, and it appears to be a fundamental meander characteristic which is independent of season. The sense of the observed meander skewness (a relatively gentle approach of the Gulf Stream front, followed by an abrupt offshore displacement of the front after the crest passes) is consistent with Webster's (1961a) description of the temperature field skewness that he observed in the upper 200 m. The skewness sense and our computed momentum fluxes are also consistent with a local conversion of meander kinetic energy to mean Stream kinetic energy, a surprising result first noted for the surface layer by Webster (1961b).

The three large v -component peaks at A-top (Fig. 6) associated with the meanders that occurred on 11, 18, and 26 August appeared 36, 30 and 33 hrs

² A crest is the local, shoreward-most deflection of the Gulf Stream front.

later, respectively, at the C-top instrument (Fig. 7). Over the 64 km separating the downstream C-mooring from the A-to-B line, the time delays give phase propagation speeds of 43, 51, and 47 km d⁻¹, respectively. These estimates of the summer phase speed can be compared with a mean wintertime estimate of 40 km d⁻¹ deduced from satellite images of the Stream's surface thermal front (Legeckis, 1979), and with estimates ranging from 30 to 45 km d⁻¹ for individual winter meanders (BB81, BBL). Averaged over the full record lengths, lagged correlations between the v-components at B-top and C-top (Ignaszewski, 1982) lead to estimates of the mean downstream phase speed of 40 and 42 km d⁻¹ for winter and summer cases, respectively.

The subtidal fluctuations were highly correlated and vertically in-phase during the summer at mooring C, as shown in Fig. 7 for the first 30 days of the record. A similar situation existed in the winter (BB81), when satellite images of the surface temperature structure showed that the deep velocity fluctuations were also highly correlated with the Stream's meandering surface thermal front. In both seasons, the high vertical coherence and the in-phase nature of the fluctuations are consistent with a simple oscillatory lateral translation of the subsurface Gulf Stream front over the array site, as Webster (1961a) originally suggested. Detailed AXBT surveys of meanders passing through the array area support this zero-order kinematic interpretation, although a more complicated vertical structure is apparent along the inshore edge of the Stream and upstream of the GSME area (BBL).

Periods of upstream flow, or countercurrents, have been shown (BB81, BBL) to be correlated with the passage over the array of warm filaments found along the inshore edge of the Stream. The filaments usually appear to be elongated bands of Gulf Stream water that trail southwestward from meander crests. The warmth of filaments is primarily a surface feature, confined

to the upper few tens of meters, but the countercurrents associated with them are deeper features associated with upwarping of the Gulf Stream front during the onshore phase of a meander. Thus, at the 100 m depth over the 200 m isobath, for example, the countercurrents following the passages of meander crests are associated with decreasing temperature and salinity (Fig. 6).

Figure 8 shows a winter example of a temperature section through a warm filament on the inshore edge of the Stream. The cold surface water separating the filament from the main Stream is clearly evident. The cold water bands noted by Bache and Pillsbury (Pillsbury, 1890) were probably features of this type, and the southward-setting "eddy currents" mentioned by John White in 1590 may have been countercurrents associated with the meandering process.

Much of the information about subtidal fluctuations can be conveniently summarized in a spectral representation. A seasonal comparison of spectra, coherence and phase results keyed on the B-top instrument is given in Fig. 9. The top panels (A) show selected autospectra for v at instruments separated in the cross-stream and downstream directions, the middle panels (B) show the coherence and phase relations between v at instruments separated 64 km in the downstream direction, and the bottom panels (C) show the coherence, phase and momentum flux relations between u and v at a single instrument. The spectrum estimates were computed with 15 degrees of freedom, and the effective bandwidth is 0.033 CPD.

The seasonal change in the distribution of variance noted earlier (Figs. 3 and 5) is very evident in the v -autospectra (Fig. 9, panels A). In the winter, the dominance of the 7- to 10-day period band is emphasized by the relative lack of kinetic energy of motions with very long periods (> 2 weeks)³.

³

The spectrum density estimates in Fig. 9 are not artificially whitened, as they are in the variance-conserving format of Fig. 3. Mean values were removed from the 40 HRLP data before calculating the spectrum densities, but no further filtering or spectrum weighting was performed.

In the summer, on the other hand, the spectrum densities generally increase for very long periods, which tends to mask the peak in the 7- to 10-day period band, especially for the C-top v-component. The summertime spectrum redness is also apparent for the B-top and B-bot v-components, which can be visually verified for B-top in Fig. 5b. The general organization of the fluctuations into two period bands, roughly 3-to-4 days and 7-to-10 days, was first pointed out by Webster (1961a) for the near-surface layer. A similar organization is evident in Fig. 9 for the near-bottom and mid-depth current fluctuations, although the relative spectrum density in the two bands depends on season and instrument location.

The fluctuations were coherent over the downstream scale of the array (64 km) for the period range of about 2-to-10 days, in both seasons (Fig. 9, panels B). In this range, the summer coherence values were generally lower band-for-band than in the winter, except for the 3- to 4-day period band, which also stands out in the summer time-series of v at B-top (Fig. 5b). The summer increase in variance at very long periods (> 2 weeks) is reflected in increasing downstream coherence at very long periods. The downstream phase propagation noted for the individual meanders in Fig. 6 is a general feature of the coherent subtidal fluctuations. This is clearly evident in the sloping phase-vs-frequency graphs in Panels B. The mean slopes of the phase graphs are very similar, indicating a downstream phase speed of 43 km d^{-1} in each season for the coherent subtidal spectrum of fluctuations. Small differences in the structure of the two graphs may imply that the phase speeds were period-dependent and seasonally dissimilar, but the statistical confidence in the phase estimates does not permit such a detailed comparison.⁴

⁴ The 95% confidence interval on the phase estimate is about $\pm (3, 12, 18)$ degrees in a frequency band with a coherence squared estimate of (0.9, 0.8, 0.7).

5. Meander Structure

Conventional hydrographic surveys from a single vessel are too slow to adequately resolve the three-dimensional structure of Gulf Stream meanders off North Carolina. For this reason, two sequences of 8 aircraft flights each were made along the continental margin between Cape Hatteras and Charleston (Fig. 1). During each flight, AXBT's were dropped on a grid which included the GSME moored instruments, giving a quasi-synoptic, three-dimensional picture of the temperature field in the upper 400 m. Station spacing was nominally 12.5 km in the cross-stream direction and 50 km in the along-stream direction. Each AXBT survey required about 4 hours to complete, during which time the thermal expression of a Stream meander could be expected to move downstream under the survey by about 6.5 km. Further details concerning the survey technique and AXBT drop stations are given in BBL and in the sequence of GSME data reports listed in the References.

Examples of the AXBT views of the temperature field are given in Fig. 10 for surveys performed on 11 February and 27 November. The February flight sequence occurred as two large meanders were propagating through the area. The v-component signatures of these meanders are evident in Fig. 5a on 5 and 11 February, and their relation to the AXBT temperature field has been discussed in detail by BBL. The A-to-B mooring line corresponds to about the 50 km downstream coordinate distance in Fig. 10, indicating that the upstream meander crest was just passing over the B mooring at the time of the survey. Both of the meanders in the 11 February view were trailing warm filaments, and the shallowness (~ 30 m) of their filament thermal structure is apparent on the upstream face of the view. In contrast, the cool surface water separating the filament from the main Stream is indicative of isotherm-uplifting that defines a cool core of water extending to greater than the 400 m depth of the survey. The positive vorticity peaks noted earlier (Fig. 5) occur just after the passage of meander crests, at the

times when cool cores such as those shown in Figs. 8 and 10 pass over the moored array. The cyclonic circulation is consistent with that expected around a dome-like structure of uplifted cool water.

The 27 November AXBT survey was completed several days after the end of the summer mooring period. However, the onshore phase of a meander had just begun on 25 November, when the instruments were retrieved. This is indicated in the 3 HRLP data (not shown here, see data reports) by increasing v and T at the B-top instrument. Two days later, at the time of the AXBT view in Fig. 10, the meander crest appeared to be 50-60 km downstream of the B-mooring, and the characteristic interleaving of warm and cool surface waters "behind" the meander crest is apparent near the upstream end of the view. The surface temperature contrast between these features is much smaller than it was in the winter case, because of summer warming of the coastal and shelf waters which abut the Stream. The subsurface (> 100 m) structure, however, was similar in both seasons. The cool core of water upstream of the meander crest is clearly evident below 100 m in the summer view, and this subsurface similarity is also reflected in the seasonal T-S characteristics (Fig. 4).

The skewness of the meandering process, mentioned earlier, is readily apparent in the 11 February AXBT view (Fig. 10). It is manifested in the surface temperature, for example, by the horizontal slope of the 20°C isotherm, which is smaller downstream of the meander crest than upstream of it. The skewness is also reflected in the vertical slopes of isotherms along the downstream face of the views; *viz.*, the isotherms move slowly downward as a crest approaches, then rapidly rise in the cool core upstream of the crest. The subsurface skewness is clear in the late summer case (the 27 November

view, even though much of the surface temperature structure was obliterated.

The u - and v -components of velocity at the B-top instrument were mutually coherent over the period range of 2- to 10 days in both seasons (Fig. 9, panels C). They were also in near-quadrature over this range, with u leading v by 45 - 90° , consistent with the cyclonic rotation of the velocity vector at B-top (Fig. 5). The sense of the meander skewness is consistent with u leading v by less than a quarter-period, which implies an offshore eddy-transfer of momentum. In the summer, the Reynolds' stress momentum flux term $\overline{pu'v'}$ was concentrated in the 3- to 5-day period range, while in the winter it was concentrated at periods greater than about 5 days, reflecting the general seasonal differences already mentioned. The average subtidal value of $\overline{u'v'}$, determined from Fig. 9, is about $100 \text{ cm}^2 \text{ s}^{-2}$ offshore in each season. This compares well with the winter estimate of $(119 \pm 23) \text{ cm}^2 \text{ s}^{-2}$ at B-top, calculated from the full record by direct correlation (BB81). The analogous calculation for the summer case yields $(101 \pm 23) \text{ cm}^2 \text{ s}^{-2}$ at B-top. In both seasons, the offshore momentum flux was larger at B-top than at A-top, and the resulting divergence indicates retardation of the inshore edge of the mean stream. Although the average momentum flux was similar in each season, the associated eddy transfer process had shorter periods in the summer than in the winter (3- to 5-days vs > 5 days, Fig. 9C).

In the cyclonic shear zone of the mean Stream, offshore momentum flux results in a transfer of kinetic energy from the fluctuations to the mean Stream, via the $\overline{pu'v'} \partial \bar{v} / \partial x$ term in the energy equation (e.g., Webster, 1961b). The shear of the mean Stream during the GSME, calculated as $(v_{\text{B-top}} - v_{\text{A-top}}) \Delta x^{-1}$, where $\Delta x = 18 \text{ km}$ is the mooring separation distance, was $1.05 \times 10^{-5} \text{ s}^{-1}$ in

the winter and $1.18 \times 10^{-5} \text{ s}^{-1}$ in the summer⁵. The corresponding energy fluxes for the full record lengths were $(125 \pm 24.3) \times 10^{-5} \text{ ergs cm}^{-3} \text{ s}^{-1}$ in the winter and $(120 \pm 27) \times 10^{-5} \text{ ergs cm}^{-3} \text{ s}^{-1}$ in the summer, insignificantly different. For a column-averaged mean downstream current speed of 50 cm s^{-1} , the mean Stream kinetic energy density is $1.25 \times 10^3 \text{ ergs cm}^{-3}$, which implies a mean Stream kinetic energy doubling time of a few weeks due to the eddy conversion process. This surprisingly rapid conversion of kinetic energy from the fluctuations to the mean Stream in the GSME area, first noted by Webster (1961b) for the surface layer, implies an upstream or external energy source for the meanders. Direct forcing by the wind appears to be ruled out as a significant meander energy source, as shown by theoretical arguments (Webster, 1961b) and by calculation of the rate-of-working of the wind on the ocean during the GSME periods (Brooks, 1982, this issue). The possibility of an energy source for meander growth upstream of the GSME area has been discussed by BB81 and BBL.

In terms of a fluctuation streamfunction, ψ , the previously discussed term in the rate of energy transfer from the meanders to the mean Stream can be written

$$\overline{\rho u'v'} \frac{\partial \bar{v}}{\partial x} = -\rho \overline{\frac{\partial \psi}{\partial y} \frac{\partial \psi}{\partial x}} \frac{\partial \bar{v}}{\partial x}.$$

Since

$$-\frac{\partial \psi}{\partial y} \frac{\partial \psi}{\partial x} = \frac{\partial y}{\partial x} \bigg|_{\text{const } \psi} \left(\frac{\partial \psi}{\partial y} \right)^2,$$

a positive average streamline slope in regions where $\frac{\partial \bar{v}}{\partial x} > 0$ indicates energy transfer from the fluctuations to the mean flow. In order for the streamline

5

The A-top current meter was about 150 m shallower than the B-top current meter, so the calculated mean shear is not exactly in a horizontal plane. The bottom current meter on the A mooring was not used in this calculation because of possible bottom boundary layer influences.

slope to be positive when averaged over a wave period, the fluctuation velocity hodograph must be elliptical, with a positive major axis slope. Two schematics of a skewed, meandering front are shown in Fig. 11. In case A, the elliptical orbits of the fluctuation streamfunction are elongated with a positive average slope, and in case B they have a negative average slope. The observed asymmetry of the meandering Gulf Stream front in the GSME area resembles case A but not case B, which is consistent with the calculated offshore energy flux.

6. Summary and Conclusions

Gulf Stream meanders were prominent during most of the 4-month winter and summer mooring periods of the Gulf Stream Meanders Experiment (GSME). In both seasons, the mid-depth current speeds over the 400 m isobath typically fluctuated between -50 cm s^{-1} and $+100 \text{ cm s}^{-1}$ relative to a mean value of 30 cm s^{-1} in the downstream direction. In the winter (January to May), the velocity, temperature and salinity fluctuations had a prominent period of 7-to-10 days and a less prominent period of 3-to-4 days. In the summer (July to November), the fluctuations had identifiable periods of 5-to-7-days and 3-to-4-days, but they were less distinctly defined than in the winter case. The subtidal velocity fluctuations were highly coherent and nearly in-phase vertically throughout the lower half of the water column. They were also coherent over the downstream scale of the array (64 km), with an indicated downstream propagation speed of $\sim 40 \text{ km d}^{-1}$ in both seasons.

The GSME observations show that the fluctuations of the Stream known as meanders extend to near-bottom in both seasons. Webster (1961a) first described the meanders in the upper 200 m as lateral, wavelike, downstream-propagating excursions of the Gulf Stream front having a prominent weekly time scale.

Detailed GSME surveys of the thermal structure of meanders support this description, although the structure is complicated along the shoreward edge of the Stream, where shallow surface filaments of warm water often trail southwestward from meander crests. Strong cyclonic rotation of the velocity vectors at individual instruments and also of the bulk water column is characteristically observed just after the passage of a meander crest. The cyclonic rotation is associated with deep uplifting or upwelling of cool water from within the Stream upstream of the meander crest. The intensity of this aspect of the meander process is often sufficient to bring cool water to the surface, producing longshore bands or streaks of cool water separating the warm filaments from the Stream farther offshore. The cyclonic circulation around the resulting dome of cool water is often strong enough to produce surface countercurrents (i.e., upstream or southwestward flow) of 50 cm s^{-1} in the warm filaments. It is most likely that similar countercurrents prompted White's cautionary remark in 1590 about Gulf Stream eddies off the Carolinas.

Some fundamental aspects of the meander mechanism are not yet apparent. Meandering occurred in both GSME seasons, but there were significant seasonal differences in the frequency distribution of the variance. The leading term in the energy equation, when evaluated for the two GSME data periods, clearly indicated a conversion of fluctuation kinetic energy to mean Stream kinetic energy, with a surprisingly small doubling time of a few weeks -- several meander periods -- for the mean Stream. This conversion process is associated with the lateral asymmetry or skewness of the meanders, which is a feature commonly observed in the surface and subsurface thermal structure of the Stream. The Reynolds' stress term responsible for the conversion, $\overline{\rho u'v'}$, had about the same subtidal average value in each season, but its frequency distribution reflected the tendency toward shorter periods of meandering in the summer.

The persistence of the meanders off North Carolina thus implies an upstream or external source of their kinetic energy. Direct forcing by the wind was found to be ineffective during the GSME periods. This suggests that the rapid amplification of meanders which has been observed in the region off Charleston, South Carolina is an intensive, local process that takes place over a downstream distance of about one meander wavelength (a few hundred km). The seasonal variability of the meandering observed in the GSME area may have resulted from seasonal differences in the factors controlling the meander amplification process farther upstream.

ACKNOWLEDGMENTS

The major results from the Gulf Stream Meanders Experiment (GSME) are summarized in this paper. We are pleased to acknowledge the joint project support of the National Science Foundation, grant numbers OCE 77-25682 and OCE 79-06710, and the Office of Naval Research, contract N-00014-77-C-0354. Since the inception of the GSME in 1976, many individuals, too numerous to mention here but acknowledged in previous papers, have made valuable contributions of time, labor, and thought. We are especially indebted to Mr. Paul Blankinship, of North Carolina State University, for his meticulous preparation of instruments. The high percentage of data returned without the loss of a single instrument attests to his carefulness. We also thank Captain Herb Bennett and the crew of R/V Endeavor for contributing to four successful and enjoyable cruises in the Gulf Stream in 1979.

In retrospect, it appears that more questions have been raised than answered concerning Gulf Stream meanders off North Carolina. We hope that the GSME data sets will provide a provocative incentive for continuing study of the Stream.

REFERENCES

- Bane, J. M., Jr., D. A. Brooks and K. R. Lorenson, Synoptic observations of the three-dimensional structure and propagation of Gulf Stream meanders along the Carolina continental margin. *J. Geophys. Res.*, 86, No. C7, 6411-6425, 1981.
- Brooks, D. A., and J. M. Bane, Jr., Gulf Stream fluctuations and meanders over the Onslow Bay upper continental slope. *J. Phys. Oceanogr.*, 11, 247-256, 1981.
- Brooks, D. A., J. M. Bane, R. L. Cohen, and P. Blankinship. The Gulf Stream Meanders Experiment: Current meter and atmospheric data report for the August to November, 1979 mooring period. Texas A&M University, Rep. 81-3-T, 1981. Note: This report contains a complete listing of the six GSME data reports.
- Brooks, D. A., Gulf Stream fluctuations and their relation to the winds off North Carolina, *J. Geophys. Res.* (submitted). 1982.
- DeVorse, L., Pioneer charting of the Gulf Stream: The contributions of Benjamin Franklin and William Gerard de Brahm. *Imago Mundi*, 28(2), 105-120, 1976.
- Herrera y Tordesillas, Antonio de, Historia general de los hechos de los Castellanos en las islas i tierra firme del Mar Oceano. Madrid: Empronta real, por Iuan Flamenco. 5 vols. in 2. 1601.
- Ignaszewski, M., The vorticity balance of Gulf Stream meanders off North Carolina. M.S. thesis, Texas A&M University (in preparation), 1982.
- Iselin, C. O'D., A study of the circulation of the western North Atlantic. *Pap. Phys. Oceanogr. and Meteor.*, 4(4), 101 pp. 1936.
- Lee, T. N., L. P. Atkinson, and R. Legeckis, Detailed observations of a Gulf Stream frontal eddy on the Georgia continental shelf, April 1977. *Deep Sea Res.*, 28A(4), 347-375, 1981.
- Legeckis, R. V., Satellite observations of the influence of bottom topography on the seaward deflection of the Gulf Stream off Charleston, South Carolina. *J. Phys. Oceanogr.*, 9, 483-497, 1979.
- Pillsbury, J. E., The Gulf Stream . . . Rept. Supt., U.S. Coast and Geod. Surv., for year ending June, 1890, pp. 459-620 (- Appen. 10).
- Quinn, D. (Ed.), *The Roanoke Voyages*, Vol. 2, The Hakluyt Society, London (see p. 608). 1952.
- Richardson, P. L., Benjamin Franklin and Timothy Folger's First Printed Chart of the Gulf Stream. *Science*, 207, 643-645. 1980.

- Richardson, W. S., W. J. Schmitz, and P. P. Niiler, The velocity structure of the Florida Current from the Straits of Florida to Cape Fear. *Deep Sea Res.*, 16, 225-231. 1969.
- Scisco, L. D., The track of Ponce de Leon in 1513. *Bull. Am. Geog. Soc. XLV(10)*, 721-735. 1913.
- Stommel, H., *The Gulf Stream*. Univ. of California Press, Berkeley , 248 pp. 1966.
- Webster, F., A description of Gulf Stream meanders off Onslow Bay. *Deep Sea Res.*, 9, 130-143. 1961a.
- Webster, F., The effect of meanders on the kinetic energy balance of the Gulf Stream. *Tellus*, 13, 392-401. 1961b.
- Williams, J., On the use of the thermometer in discovering banks, soundings, etc. *Trans. Am. Philo Soc.*, III, 82-89. 1783.

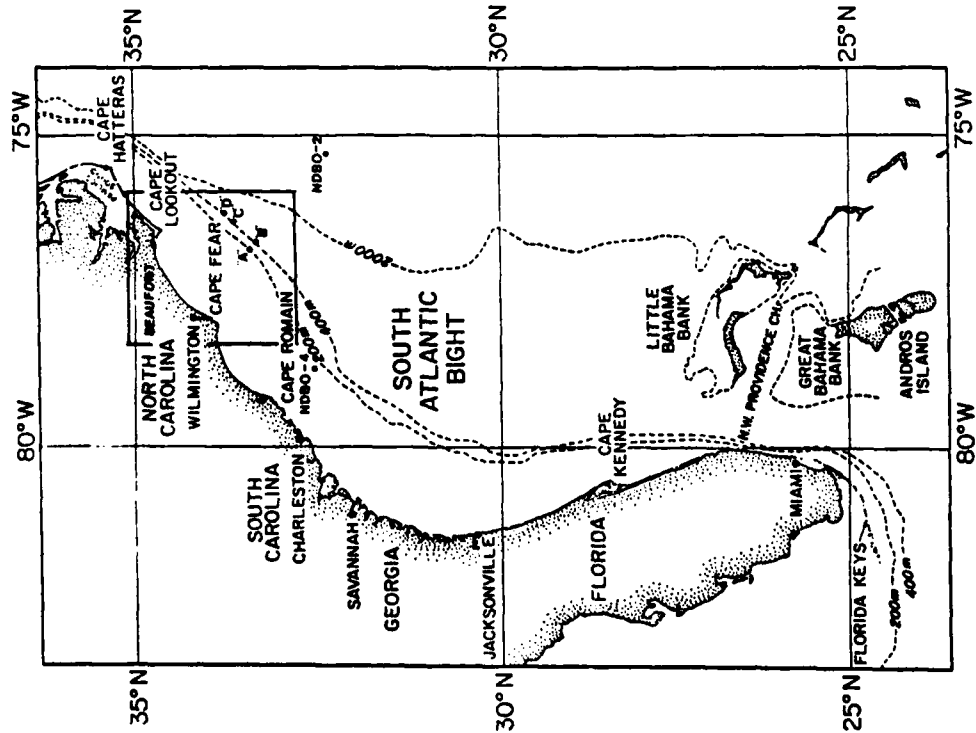


Fig. 1. Map of the South Atlantic Bight, showing the study area (boxed inset). The locations of the four moorings are labelled "A" through "D." Meteorological observations were obtained at the National Data Buoy Office offshore stations marked ND80-4 and ND80-2, and also at Cape Hatteras.

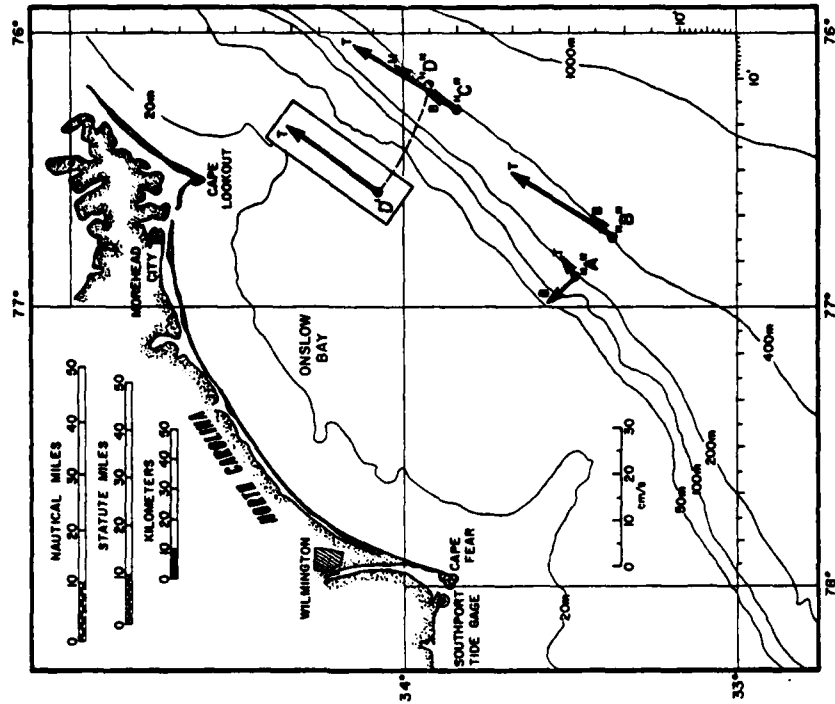


Fig. 2. Map of study area, showing mean current vectors for each instrument for the 4-month summer period. The vector for mooring D is displaced for clarity (inset box). The letters at the arrowheads identify top (T), middle (M), and bottom (B) instruments (see table 1 for depths). The analogous winter mean vectors are given by B581.

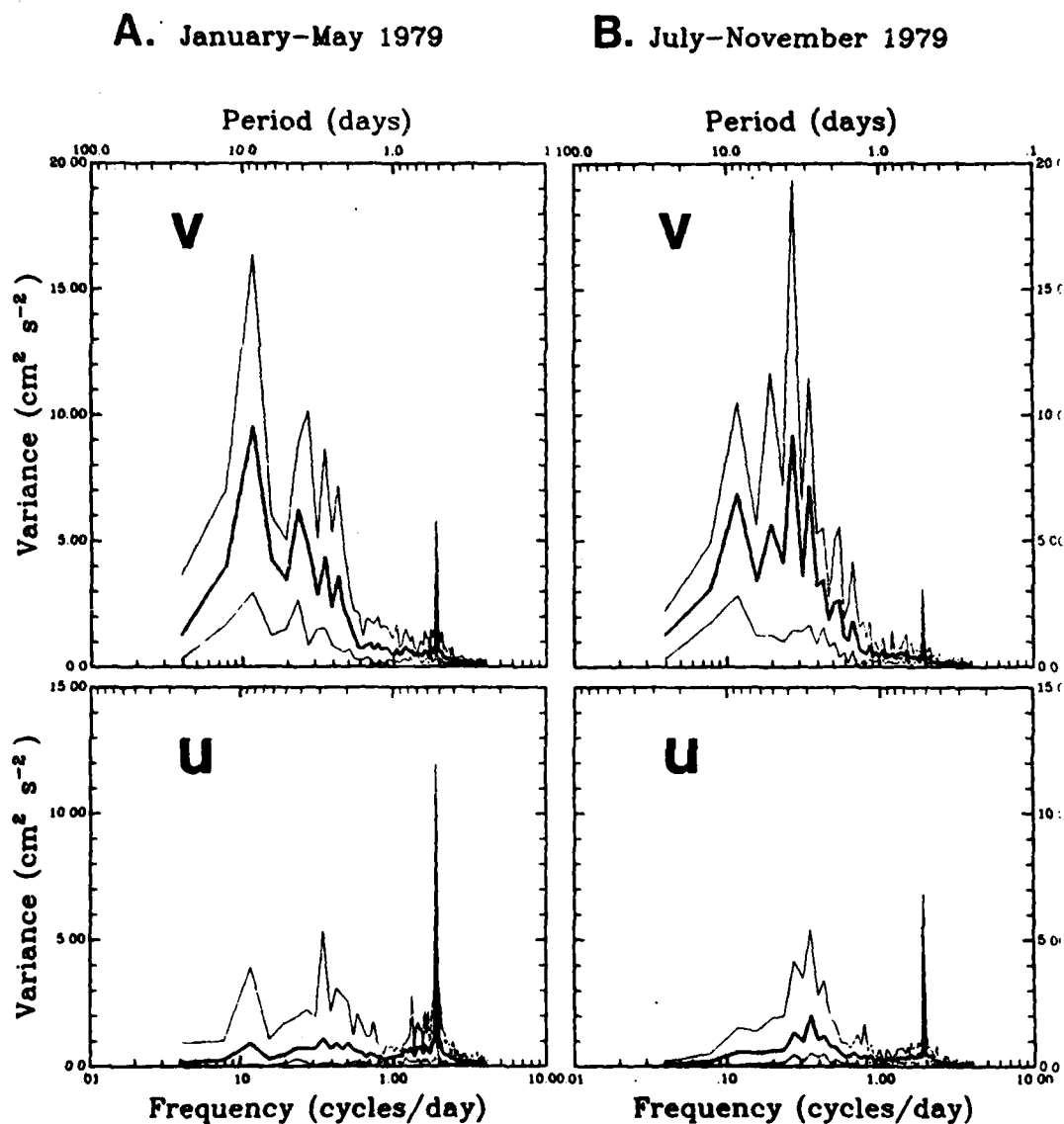


Fig. 3 Frequency distribution of the current-component variance, for the winter (A) and summer (B) periods. The downstream component (v) is aligned with the local bottom topography (34°T), and the u-component is offshore. The heavy lines show the mean variance estimate in each frequency band for all the instruments. The thin lines show the corresponding maxima and minima, and the shaded area covers one standard deviation in each band. The mean variance estimates have about 20 degrees of freedom in each band.

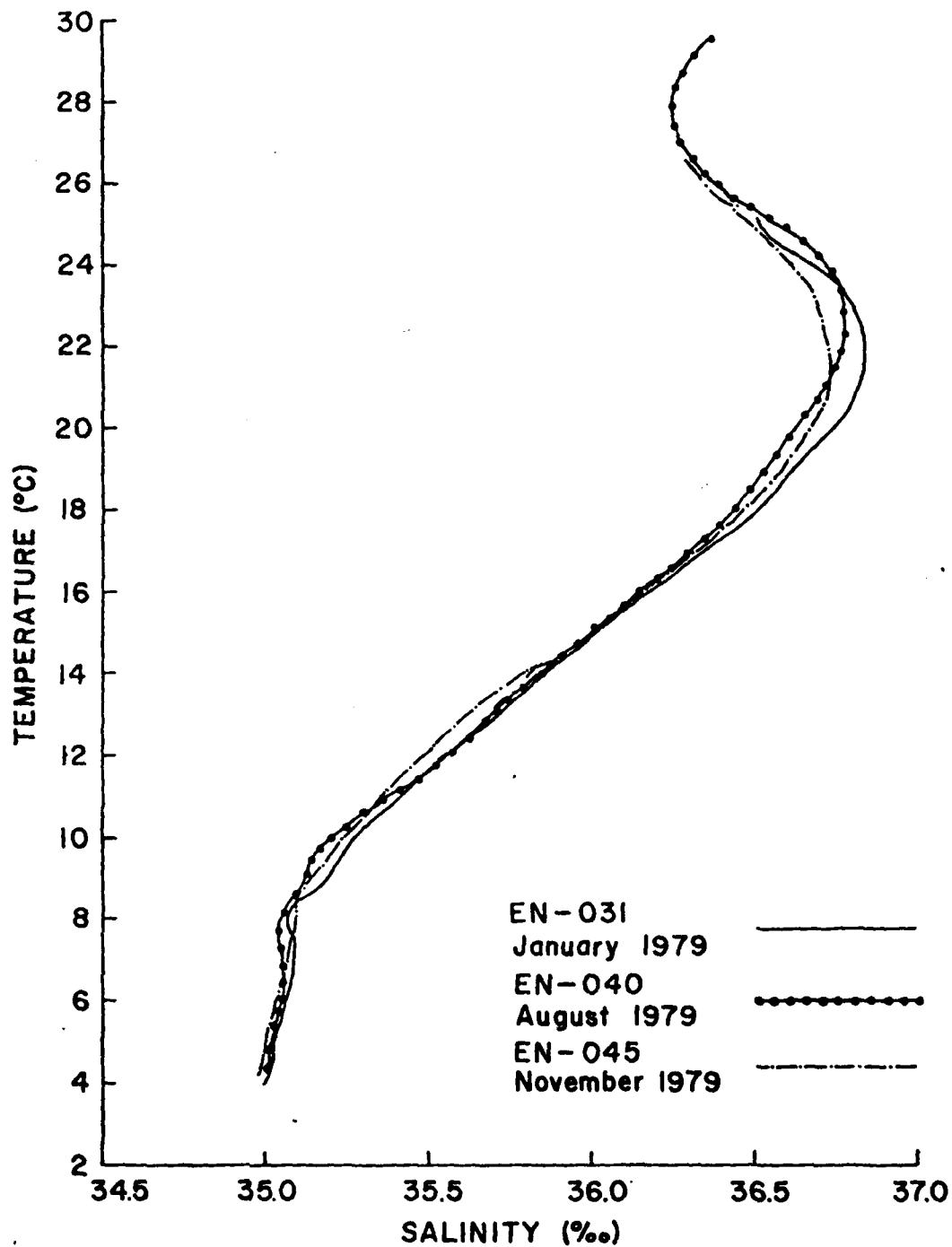


Fig. 4. Temperature-salinity correlations from winter, summer, and late fall cruises in the Gulf Stream during the GSME. The subsurface salinity maximum occurs in the depth range 100-200 m and is characteristic of Gulf Stream waters.

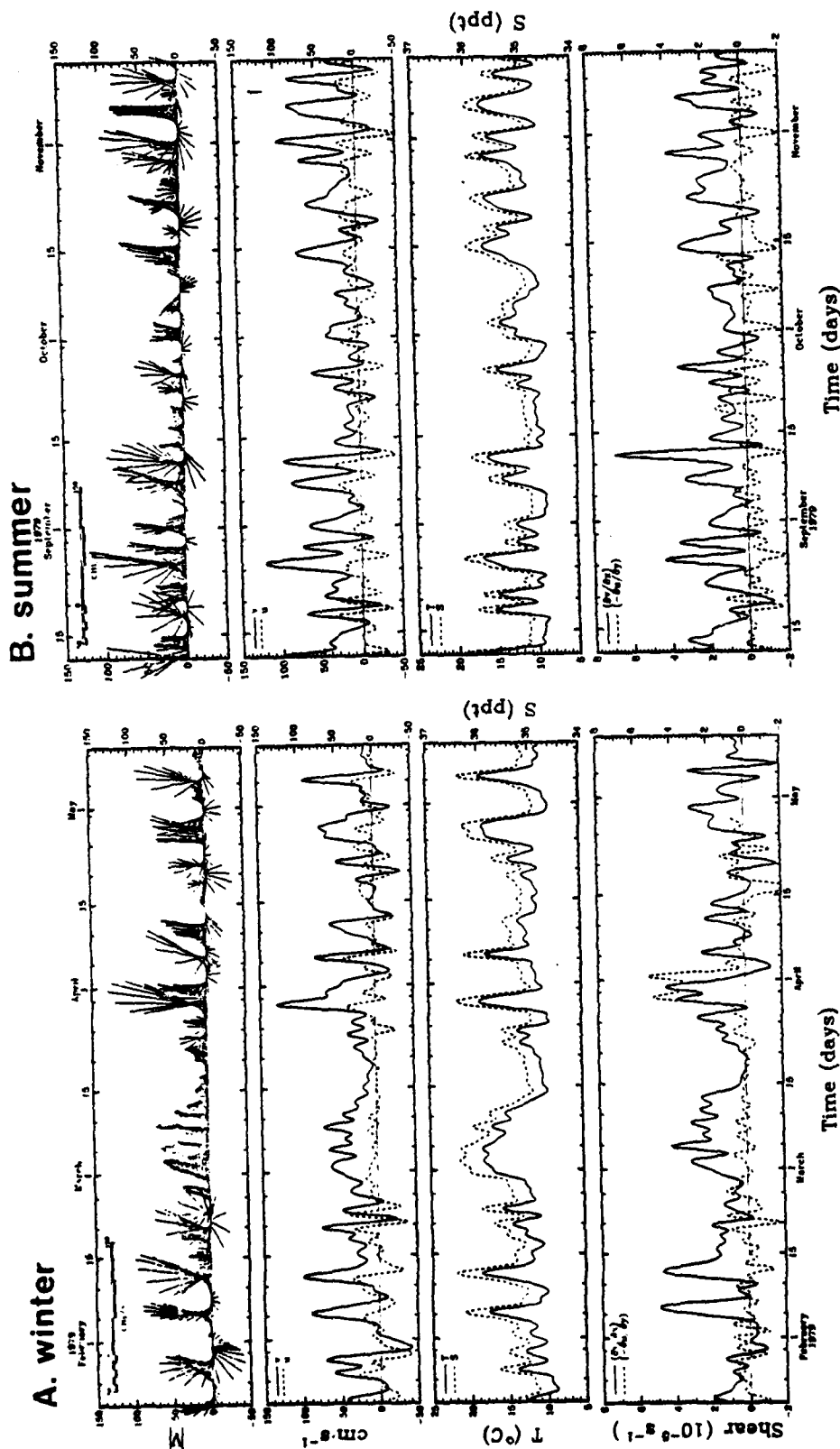


Fig. 5a Full length, 40-hr low-pass filtered records of velocity vectors and components (v, u), temperature (T), and salinity (S) from the B-top instrument during winter. Velocity vectors (top panel) pointing toward the top of the figure correspond to downstream flow. The bottom panel shows the relative-vorticity components due to horizontal velocity shear, estimated from the moored array (see text). The $-\partial u / \partial y$ term has been shifted to the left by 39 hours to account for the mean downstream propagation speed of the fluctuations. Prominent oscillations occurred in the winter with 7-to-10 day periods.

Fig. 5b Full length, 40-hr low-pass filtered records of velocity vectors and components (v, u), temperature (T), and salinity (S) from the B-top instrument during summer. Velocity vectors (top panel) pointing toward the top of the figure correspond to downstream flow. The bottom panel shows the relative-vorticity components due to horizontal velocity shear, estimated from the moored array (see text). The $-\partial u / \partial y$ term has been shifted to the left by 38 hours to account for the mean downstream propagation speed of the fluctuations.

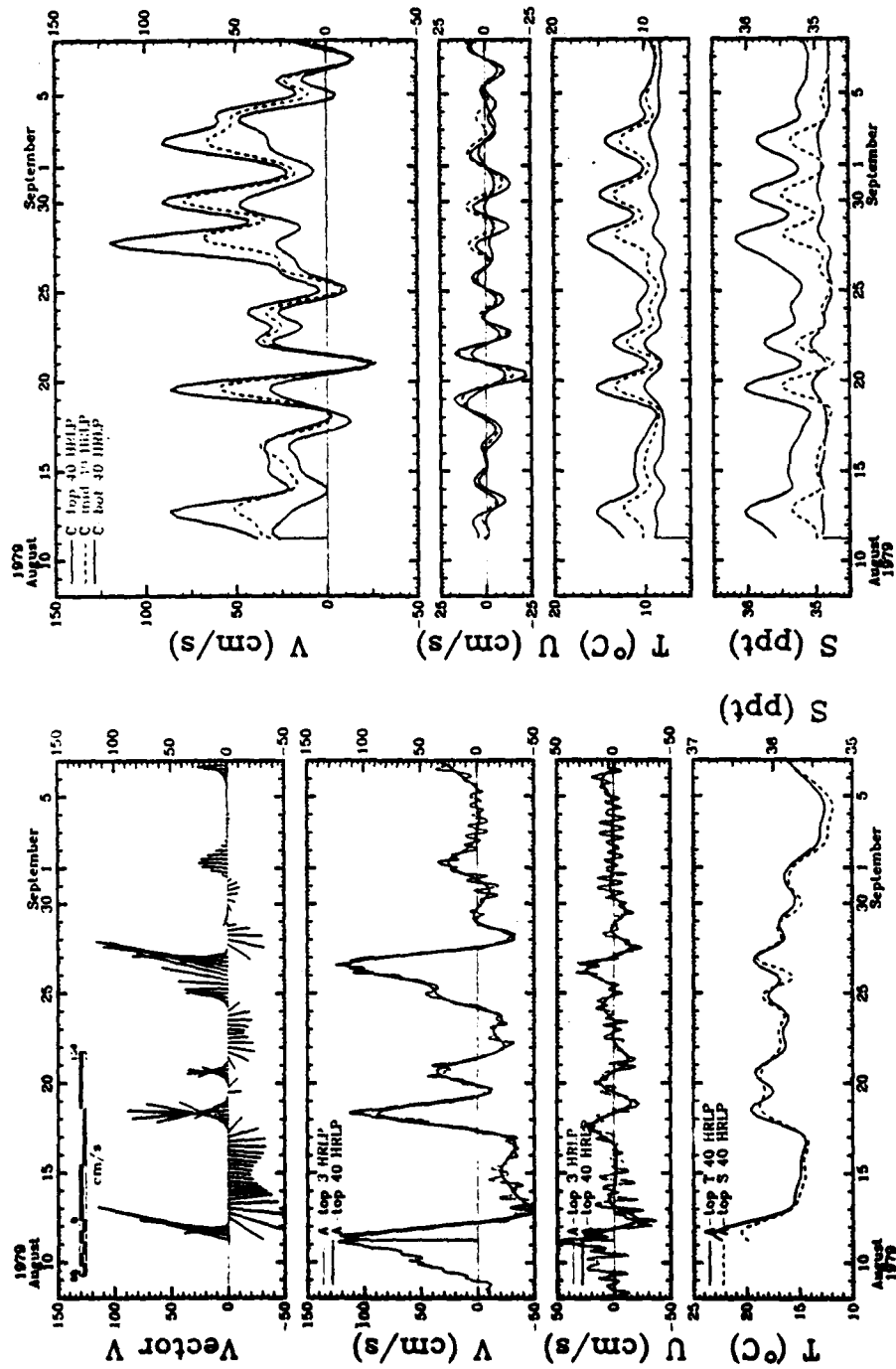


Fig. 6 Velocity vectors and velocity components (v, u), temperature (T), and salinity (S) from the A-top instrument during the first 30 days of the summer experiment. The effects of three meanders are prominent. This figure can be directly compared with Fig. 2 in BBS for the winter case. The vector convention is the same as Fig. 5. Thin lines show 3-hr low-pass filtered data, and heavy lines (solid and broken) show 40-hr low-pass filtered data.

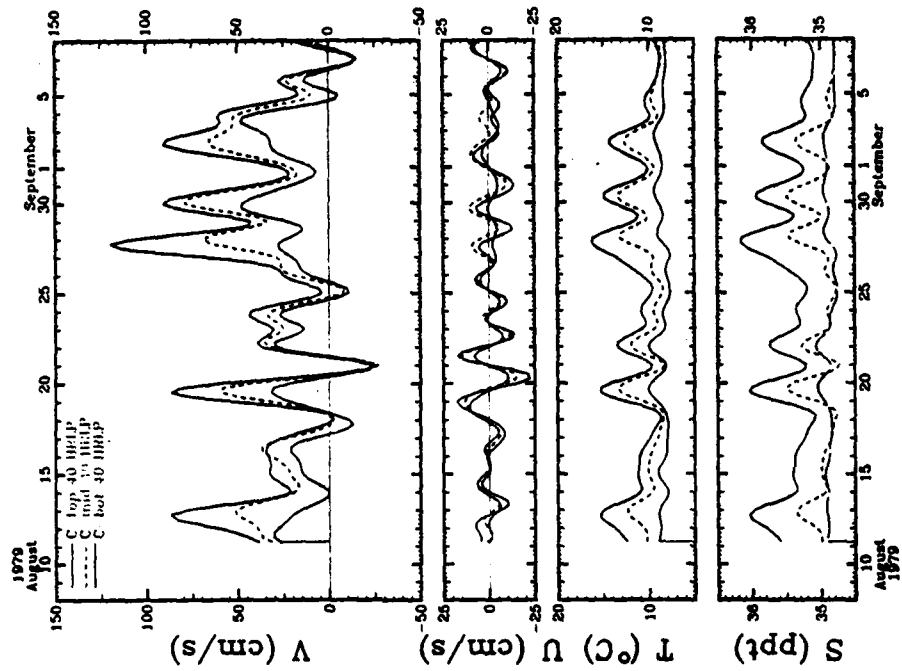


Fig. 7 Velocity components (v, u), temperature (T), and salinity (S) from the top, middle, and bottom instruments on mooring "C" during the first 30 days of the summer experiment. The high vertical coherence of the meandering currents is apparent in this figure.

Date/Time

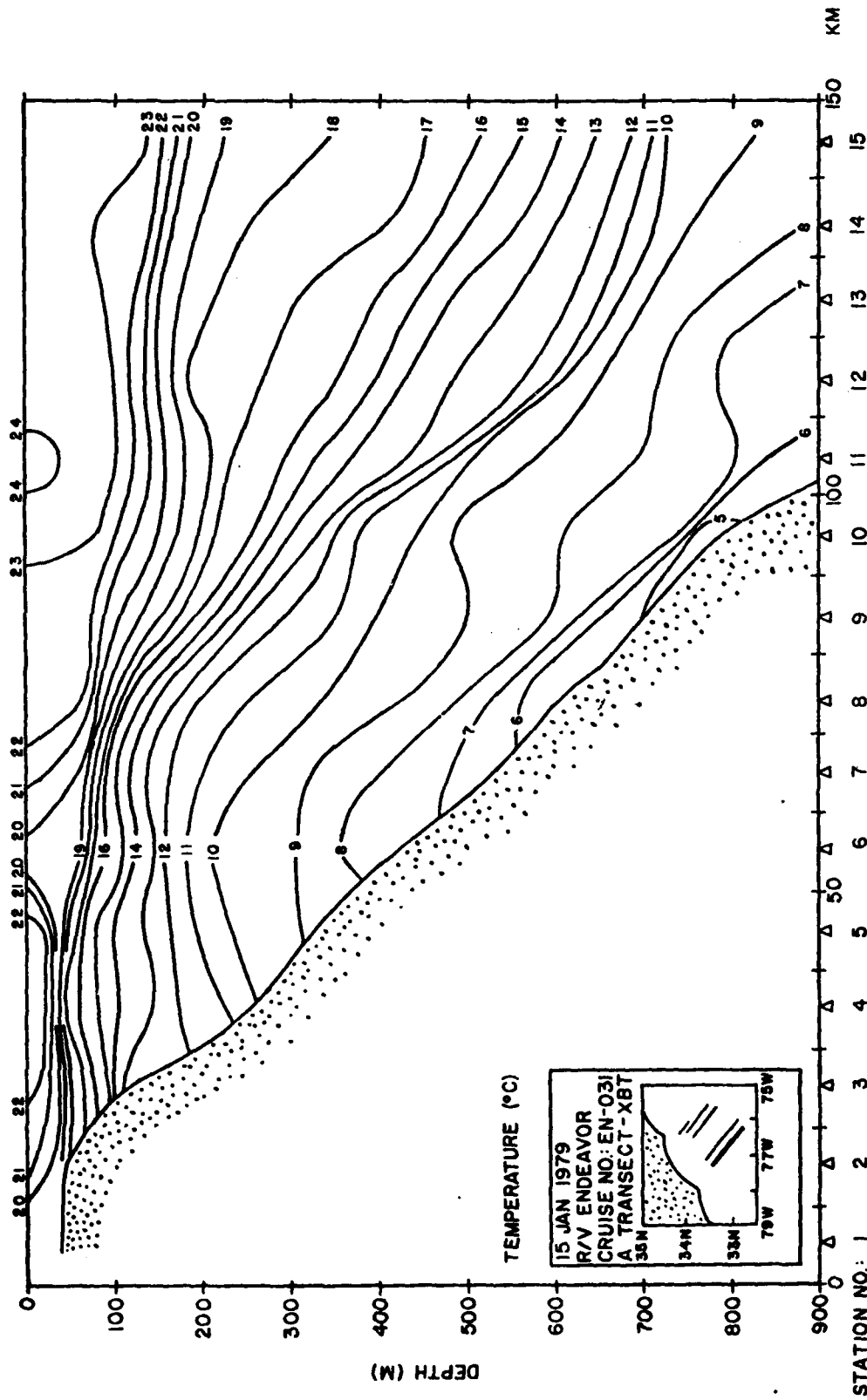


Fig. 8. A temperature section across the Stream, approximately along the line between the A and B moorings (inset). This winter example clearly shows the shallowness of a "warm filament" on the inshore edge of the main Gulf Stream front, and the relatively cold water separating them at the surface. The upward warping of isotherms under the cold surface water is associated with cyclonic rotation of the water after the meander crest passes over a fixed location. This section was taken about 20 km upstream of a meander crest.

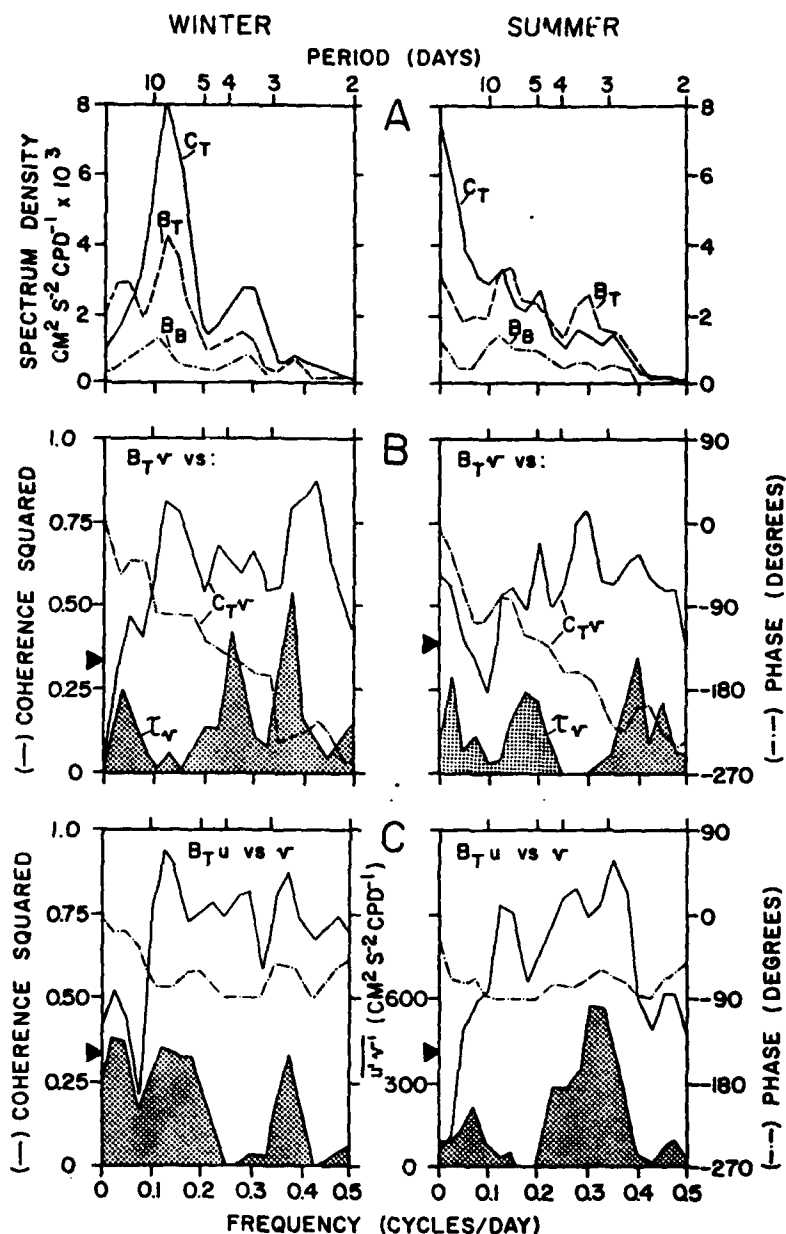


Fig. 9 Summary spectrum calculations keyed on the B-top current meter, for the winter and summer cases. The top panels (A) show auto-spectra of the v -velocity components from selected instruments, permitting a vertical and a downstream comparison of the frequency structure of the fluctuations in each season. The middle panels (B) show the coherence and phase difference of the v -component between the B-top and C-top instruments, and an example of the low coherence between the currents and the downstream wind stress (τ_v) at offshore buoy NDBO-2 (shaded area). The bottom panels (C) show high coherence and near-quadrature phase of the velocity components at B-top, and the positive co-spectrum values ($u'v'$, shaded) indicate an offshore momentum flux. The spectrum density estimates carry 15 degrees of freedom, and the 95% significance level for coherence squared is shown by the horizontal arrowheads.

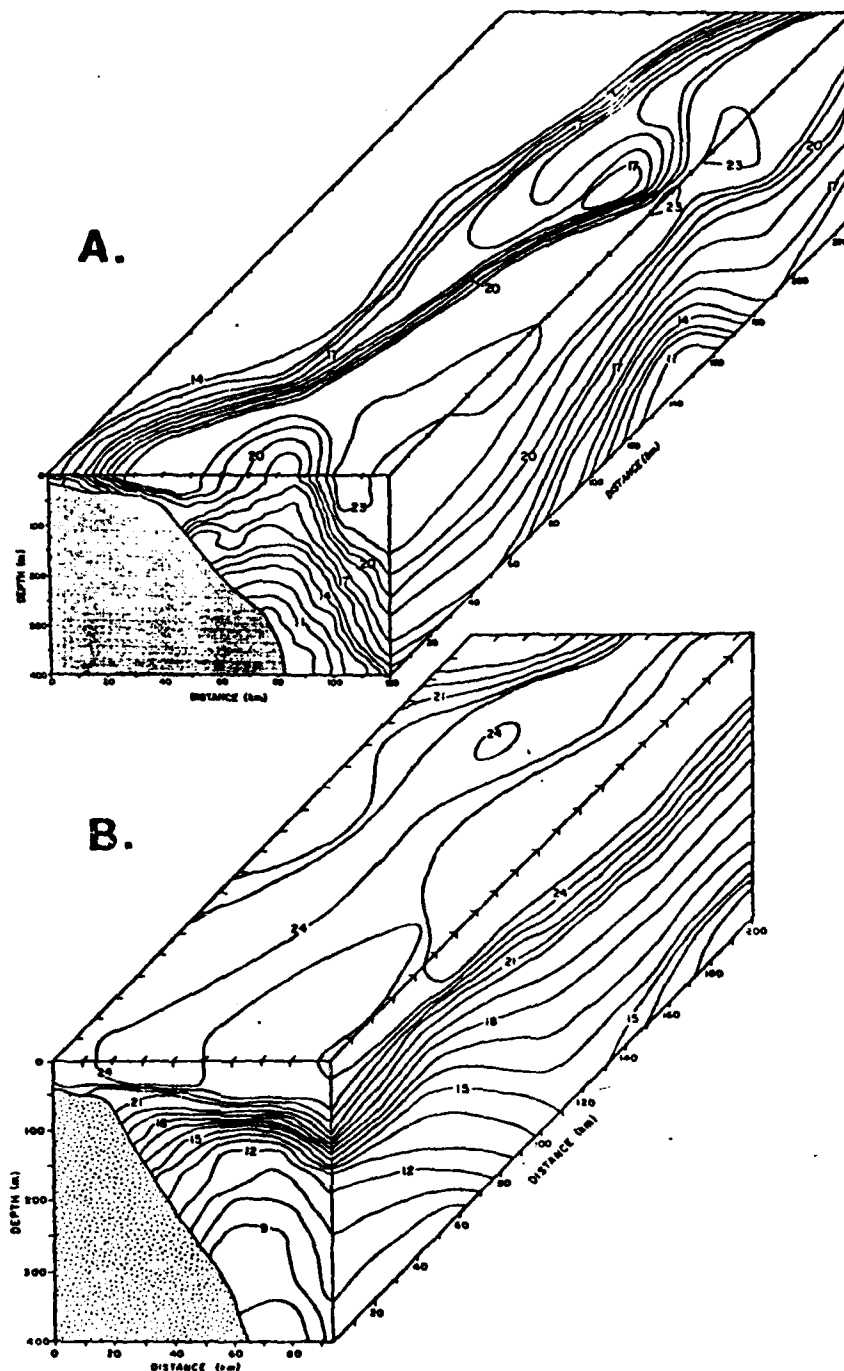


Fig. 10 Oblique views of the thermal field of the meandering Stream on 11 February 79 (A) and 27 November 79 (B), obtained in the GSME area by air-dropped expendable bathythermograph (AXBT) surveys. The 11 February case is from BBL, who give details of the survey technique and station locations. The A-to-B line in Fig. 1 corresponds to the 50 km position along the downstream coordinate in this figure. The AXBT survey resolution was about 12.5 km in the off-shore direction and 50 km in the downstream direction. In both views, warm filaments and cold bands are evident at the surface, adjacent to the main Stream, and the uplifting of isotherms upstream of meander crests is apparent. The temperature field asymmetry in the horizontal and vertical planes is related to an offshore flux of energy (see text).

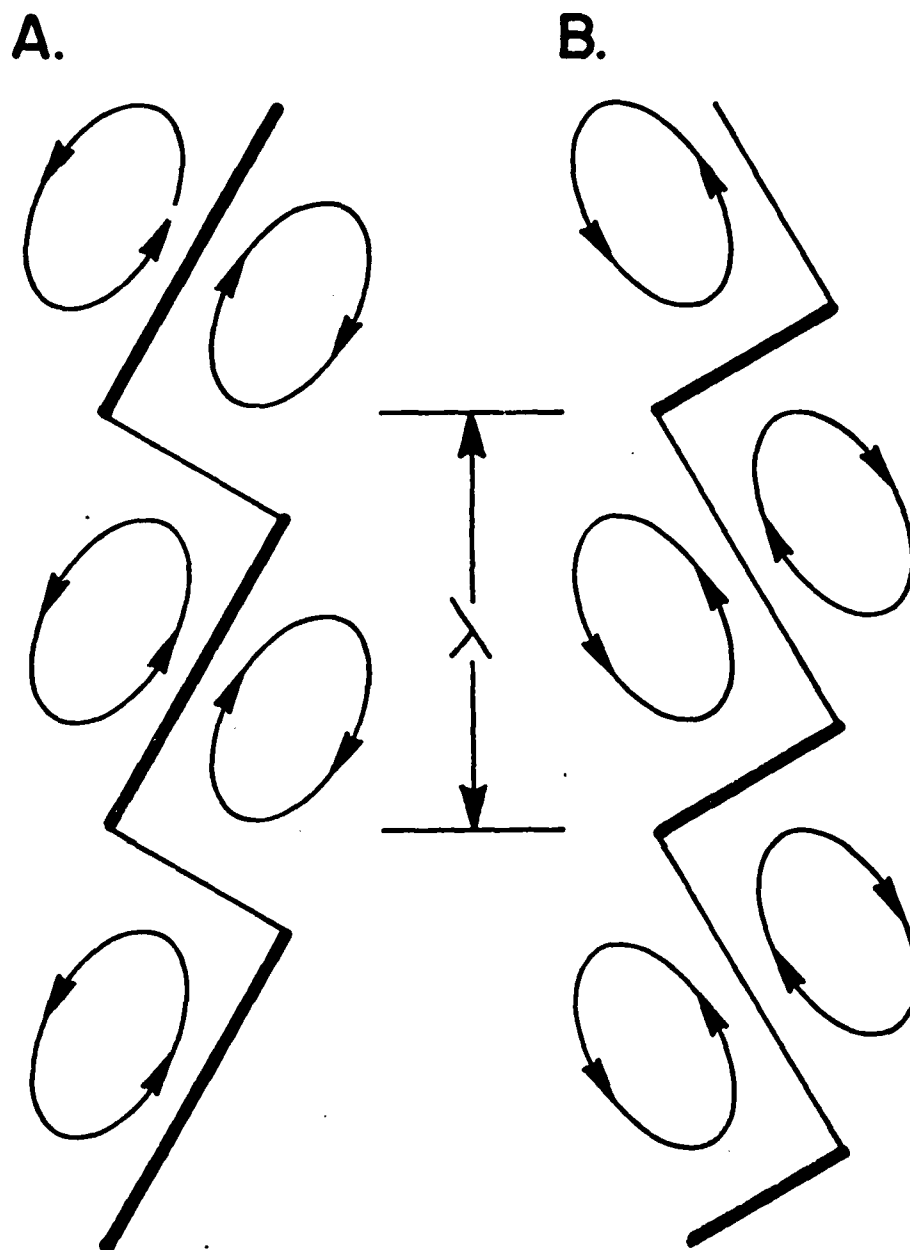


Fig. 11 Schematic perturbation streamlines showing the flow directions for two meandering fronts having the same wavelength (λ) but opposite skewness sense. The fronts propagate toward the top of the figure. Case "A" (positive skewness) better conforms with the observed features of Gulf Stream meanders, in which strong surface thermal fronts (bold lines) form at an offshore location, move shoreward locally as the pattern travels downstream, and then become diffuse or reform offshore. The positive skewness of the Case A pattern results in eddy energy transfer from the meander to the mean flow, and conversely for Case B. A symmetric pattern would have circular streamlines and no eddy energy transfer.

AD P001041

REVIEW OF GULF STREAM MEASUREMENTS IN THE REGION SOUTH OF NEW ENGLAND

Harry L. Bryden
The Joint Institute for the Study of the Atmosphere and Ocean
School of Oceanography, WB-10
University of Washington
Seattle, WA 98195

Investigations of the Gulf Stream have been central to the development of physical understanding of the ocean. Stommel (1950, 1965) has described attempts to explain the cause of the Gulf Stream from the time of its discovery by Ponce de Leon in 1513 through the modern wind-driven and inertial theories which provide the framework of our understanding of ocean circulation. Fofonoff (1980) and Watts (1982) have reviewed efforts of the last 20 years to make measurements in the Gulf Stream. Despite these measurements and recent attempts to synthesize them into a unified description by Worthington (1976) and Wunsch (1978), there remains a controversy over the structure of the Gulf Stream and the magnitude of its transport after it flows past Cape Hatteras, and the origin of fluctuations in the Gulf Stream east of Cape Hatteras and their effects on the circulation are not understood.

Descriptions of the structure of the Gulf Stream before it reaches Cape Hatteras are in general agreement. After it flows past Hatteras and leaves the continental slope, there is a controversy as to whether the Gulf Stream penetrates to the bottom. In their classic descriptions of the Gulf Stream, Iselin (1936), Sverdrup, Johnson and Fleming (1942), and Stommel (1965) all assumed a level of no motion near 2000 m depth. Gulf Stream '60 measurements (Fuglister, 1963), however, indicated that the Gulf Stream extended to the bottom. Hydrographic sections (Figure 1, for example) showed that the large isotherm slopes associated with the Gulf

Stream are present in the deep water as well as the thermocline. And, deep velocity measurements by neutrally buoyant floats suggested a deep flow in the same direction as the thermocline Gulf Stream. These measurements led Worthington (1976) to use the bottom as a reference level, and he then estimated a maximum Gulf Stream transport of $149 \times 10^6 \text{ m}^3 \text{ s}^{-1}$, more than twice as large as Iselin, Sverdrup, or Stommel had estimated.

More recent velocity measurements in the region east of Cape Hatteras are ambiguous as to whether the Gulf Stream penetrates to the bottom. Float measurements (Warren and Volkmann, 1969; Schmitz, Price, Richardson, Owens, Webb, Cheney, and Rossby, 1981) suggest a deep flow in the same direction as the surface Gulf Stream. Vertical profiles of velocity, on the other hand, suggest a level of no motion at about 2200 m with a deep flow counter to the surface Gulf Stream (Spencer, 1979; Figure 2). Each of these measurements in the Gulf Stream is of relatively short duration. Two-month moored current meter records in the deep water along 70°W showed a deep flow in the same direction as the surface Gulf Stream (Schmitz, Robinson, and Fuglister, 1970), but eight-month records from the same region exhibited such large temporal variability and such short horizontal scale variability that no conclusions as to the direction of the deep flow seemed possible (Luyten, 1977). Deep records of short duration near 50°W suggested penetration of the Gulf Stream to the bottom in 1970 (Clarke and Reiniger, 1973) but not in 1972 (Clarke, Hill, Reiniger, and Warren, 1980), and records of more than a year's duration near 55°W showed a deep counterflow under the mean position of the Gulf Stream (Schmitz, 1977; Hendry, 1982). Schmitz (1977), however, suggested that there is a deep flow in the same direction as the surface Gulf Stream along 55°W but that it is displaced southward relative to the surface flow.

In an attempt to determine objectively whether the Gulf Stream penetrates to the bottom or has a level of no motion near 2000 m with a deep counterflow, Wunsch (1978) applied the inverse technique to hydrographic measurements first with a reference level at the bottom to resemble Worthington's circulation and secondly with a reference level at 2000 m to resemble the Iselin, Sverdrup and Stommel circulations. The two solutions (Figure 3) differ most notably in the maximum transport of the Gulf Stream ($124 \times 10^6 \text{ m}^3 \text{ s}^{-1}$ for the first solution and $80 \times 10^6 \text{ m}^3 \text{ s}^{-1}$ for the second) and in the sense of the deep water circulation (clockwise in the region east of Hatteras in the first and counterclockwise in the second). Despite these large differences, Wunsch (1978) was unable to choose between the two solutions except on subjective grounds. Thus, existing hydrographic and current measurements are not sufficient to determine whether the Gulf Stream penetrates to the bottom.

There are two problems with previous current measurements. First, there is no statistical reliability in short period current measurements made in conjunction with hydrographic measurements so that the measured currents are assumed to be under the surface Gulf Stream. Second, long-term measurements have not been made simultaneously in the deep water and in the upper water column; therefore, it has not been possible to determine whether the measured deep velocities are related to the Gulf Stream flow in the upper water. It appears, then, that long time series of direct current measurements extending from the ocean bottom up into the thermocline of the Gulf Stream are needed to resolve the vertical structure of the Gulf Stream and to define the magnitude of the Gulf Stream transport and related circulation in this region.

The origin of temporal fluctuations in the Gulf Stream east of Cape Hatteras (Figure 4) and their effects on the circulation are questions which have intrigued oceanographers for 30 years since they were described by Fuglister and Worthington (1951). Such temporal fluctuations are usually referred to as meanders or rings by oceanographers who make measurements of the Gulf Stream and as eddies by oceanographers who analyze composite historical measurements or numerical models. Initial models of these meanders were path models in which the Gulf Stream develops meanders in response to changes in inlet conditions such as transport, orientation, or bottom velocity at Cape Hatteras (Warren, 1963; Niiler and Robinson, 1967). Recent numerical models indicate that the Gulf Stream in this region is unstable so that meanders or eddies grow spontaneously by converting energy contained in the mean field (Holland, 1978; Robinson, Harrison, Mintz, and Semtner, 1977). These two numerical models differ, however, in their energy sources: in the Holland (1978) model, the eddies appear to grow by converting available potential energy in a baroclinic instability process; while in the Robinson *et al.* (1977) model, the eddies grow by converting mean kinetic energy in a barotropic instability process. Thus, a major difference between models of temporal fluctuations of the Gulf Stream in the region downstream of Cape Hatteras is the energy source for the fluctuations: the Holland (1978) model predicts down-gradient eddy heat flux to convert available potential energy into eddy potential energy; and the Robinson *et al.* (1977) model predicts down-gradient momentum flux to convert mean kinetic energy into eddy kinetic energy. It appears, then, that array measurements are needed to provide estimates of eddy heat and momentum fluxes and of mean horizontal gradients of temperature

and velocity in the thermocline so that the generation mechanism for these fluctuations can be identified by estimating energy conversions between mean and eddy, kinetic and potential energies as Bryden (1982) has done for the Polymode Local Dynamics Experiment measurements.

In the deep water where current measurements have been made in this region, the fluctuations have been shown to be topographic Rossby waves (Thompson and Luyten, 1976; Thompson, 1977; Hogg, 1981). These waves appear to transport eastward momentum toward the latitude of the mean Gulf Stream, thereby helping to drive a deep circulation in the same direction as the surface Gulf Stream (Schmitz, 1977, Thompson, 1977). Thompson (1971) hypothesized that these waves are generated by fluctuations of the Gulf Stream, but Luyten (1977), could detect no relationship between the deep fluctuations and the surface Gulf Stream. Hogg (1981) traced the origin of waves observed near 70°W back to a generation region near 38°N, 68°W.

The problems then in understanding the deep fluctuations are to determine the mechanism of their generation and to quantify their effect in driving a deep mean circulation. How are the deep fluctuations related to fluctuations in the thermocline Gulf Stream? Is there local conversion from either mean kinetic or potential energies into eddy energy in the deep water near 38°N, 68°W? Or does the conversion from mean to eddy energy occur only in the thermocline and then eddy energy is transported down to generate the deep fluctuations? To quantify the effect of these deep fluctuations on the mean circulation, it is necessary to estimate how much kinetic energy the fluctuations transfer to the mean flow. As for the thermocline fluctuations, these questions would be most effectively addressed by making array measurements from which energy conversions could

be estimated.

Thus, despite much past work, there remains a need for new measurements in the Gulf Stream as it flows eastward in the region south of New England to determine ^{its} ~~the~~ structure of the Gulf Stream and understand its variability. In particular, time series of direct current measurements extending from the ocean bottom up into the Gulf Stream thermocline are needed to determine whether the Gulf Stream penetrates to the bottom and to define ~~the~~ transport of the Gulf Stream. Also, array measurements of current and temperature are needed both in the thermocline and in the deep water to understand the origin of fluctuations in the Gulf Stream and their effects on the mean circulation. Such measurements are now being planned as part of the Gulf Stream Observations (GUSTO) program.

References

- Bryden, H. L., Sources of eddy energy in the Gulf Stream recirculation region, Journal of Marine Research, submitted
- Clarke, R. A., H. W. Hill, R. F. Reiniger, and B. A. Warren, Current system south and east of the Grand Banks of Newfoundland, Journal of Physical Oceanography, 10, 25-65, 1980.
- Clarke, R. A., and R. F. Reiniger, The Gulf Stream at 49° 30'W, Deep-Sea Research, 20, 627-641, 1973.
- Fofonoff, N. P., The Gulf Stream system, Evolution of Physical Oceanography, Scientific Surveys in Honor of Henry Stommel, B. A. Warren and C. Wunsch, editors, The MIT Press, Cambridge, Massachusetts, 112-139, 1980.
- Fuglister, F. C., Gulf Stream '60, Progress in Oceanography, M. Sears, editor, 1, chapter 5, 265-373, 1963.
- Fuglister, F. C., and L. V. Worthington, Some results of a multiple ship survey of the Gulf Stream, Tellus, 3, 1-14, 1951.
- Hendry, R. M., On the structure of the deep Gulf Stream, Journal of Marine Research, 40, 119-142, 1982.
- Hogg, N. G., Topographic waves along 70°W on the continental rise, Journal of Marine Research, 39, 627-649, 1981.
- Holland, W. R., The role of mesoscale eddies in the general circulation of the ocean -- Numerical experiments using a wind-driven quasi-geostrophic model. Journal of Physical Oceanography, 8, 363-392, 1978.
- Iselin, C. O'D., A study of the circulation of the western North Atlantic, Papers in Physical Oceanography and Meteorology, 4, (4), 101 p., 1936.

Luyten, J. R., Scales of motion in the deep Gulf Stream and across the continental rise, Journal of Marine Research, 35, 49-74, 1977.

Niiler, P. P., and A. R. Robinson, The theory of free inertial jets.

II: A numerical experiment for the path of the Gulf Stream, Tellus, 19, 601-619, 1967.

Robinson, A. R., D. E. Harrison, Y. Mintz, and A. J. Semtner, Eddies and the General Circulation of an idealized oceanic gyre: A wind and thermally driven primitive equation numerical experiment, Journal of Physical Oceanography, 7, 182-207, 1977.

Schmitz, W. J., Jr., On the deep general circulation in the western North Atlantic, Journal of Marine Research, 35, 21-28, 1977.

Schmitz, W. J., Jr., J. F. Price, P. L. Richardson, W. B. Owens, D. C. Webb, R. E. Cheney, and H. T. Rossby, A preliminary exploration of the Gulf Stream system with SOFAR Floats, Journal of Physical Oceanography, 11, 1194-1204, 1981.

Schmitz, W. J., Jr., A. R. Robinson, and F. C. Fuglister, Bottom velocity observations directly under the Gulf Stream, Science, 170, 1192-1194, 1970.

Spencer, A., A compilation of moored current meter data, Whitehorse profiles and associated oceanographic observations, Volume XX (Rise Array, 1974), Woods Hole Oceanographic Institution Technical Report WHOI-79-56, 59 pp., 1979.

Stommel, H., The Gulf Stream, a brief history of the ideas concerning its cause, The Scientific Monthly, 70, 242-253, 1950.

Stommel, H., The Gulf Stream, University of California Press, Berkeley, 248 pp., 1965.

- Sverdrup, H. U., M. W. Johnson, and R. H. Fleming, The Oceans: Their Physics, Chemistry, and General Biology, Prentice-Hall, Englewood Cliffs, New Jersey, 1087 pp., 1942.
- Thompson, R. O. R. Y., Topographic Rossby waves at a site north of the Gulf Stream, Deep-Sea Research, 18, 1-19, 1971.
- Thompson, R. O. R. Y., Observations of Rossby waves near Site D, Progress in Oceanography, 7, 135-162, 1977
- Thompson, R. O. R. Y., and J. R. Luyten, Evidence for bottom-trapped topographic Rossby waves from single moorings, Deep-Sea Research, 23, 629-635, 1976.
- Warren, B. A., Topographic influences on the path of the Gulf Stream, Tellus, 15, 167-183, 1963.
- Warren, B. A., and G. H. Volkmann, Measurement of volume transport of the Gulf Stream south of New England, Journal of Marine Research, 26, 110-126, 1968.
- Watts, D. R., Western North Atlantic Gulf Stream variability, Eddies in Marine Science, A. R. Robinson, editor, Springer-Verlag, New York, 1982.
- Worthington, L. V., On the North Atlantic Circulation, the Johns Hopkins University Press, Baltimore, 110 pp., 1976.
- Wunsch, C., The North Atlantic general circulation west of 50°W determined by inverse methods, Reviews of Geophysics and Space Physics, 16, 583-620, 1978.

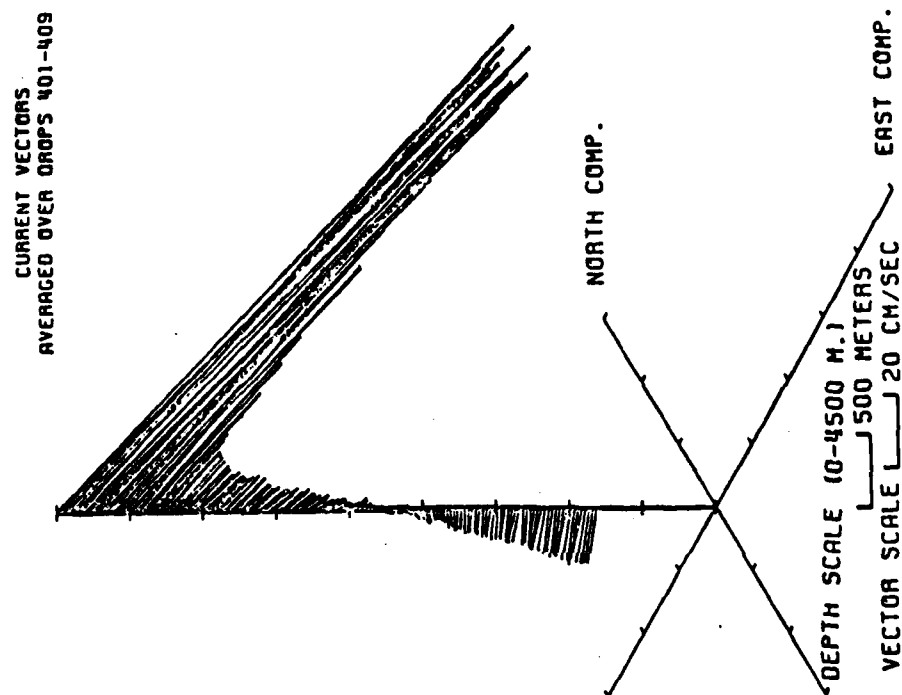


Fig. 2. Vertical profile of horizontal current in the Gulf Stream near $38^{\circ}\text{N}, 70^{\circ}\text{W}$ (Spencer, 1979). This profile is average of nine Whitehorse profiles taken during a four-day period. Note the reversal in current direction at about 2200m suggesting an intermediate level of no motion under the Gulf Stream.

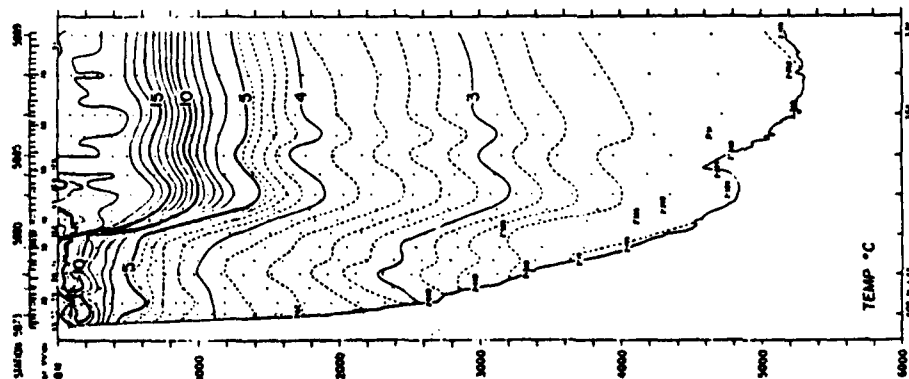
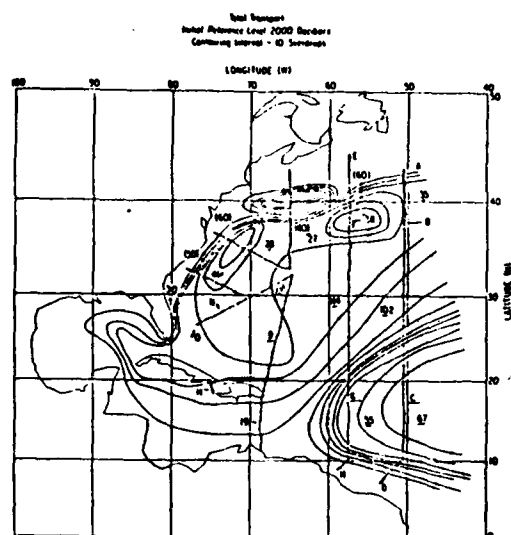
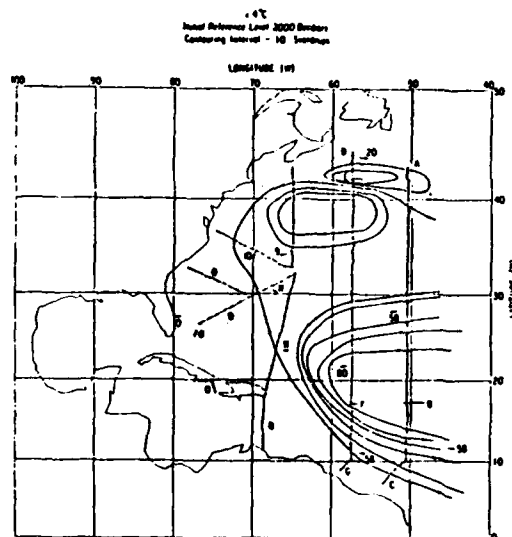


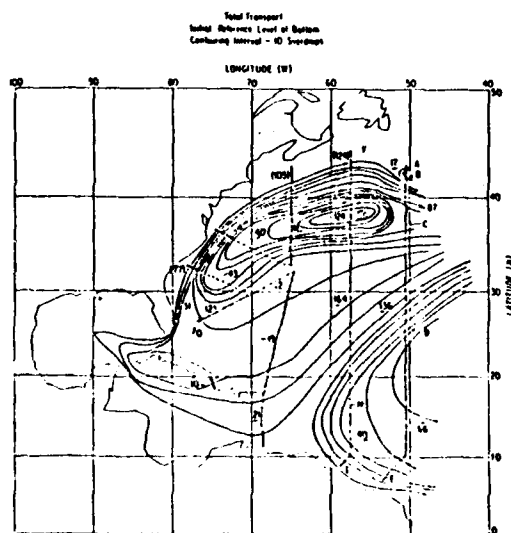
Fig. 1. Temperature section across the Gulf Stream along $68^{\circ}30'\text{W}$ (Fuglister, 1963). Note the presence of sharp slopes of isotherms associated with the Gulf Stream extending throughout the water column which suggests that the Gulf Stream penetrates to the bottom.



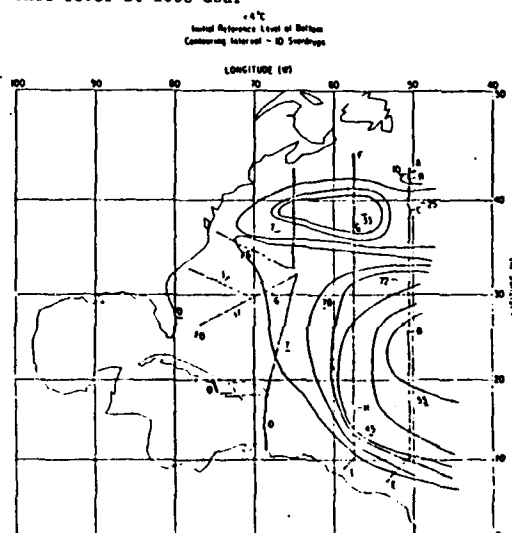
(a) total transport with the initial reference level chosen to be at 2000 dbar.



(c) circulation of deep water with potential temperature less than 4°C with initial reference level at 2000 dbar



(b) total transport with initial reference level at the bottom



(d) circulation of deep water with initial reference level at bottom

Fig. 3(a)-(d)

North Atlantic circulation determined by inverse method (Wunsch, 1978)

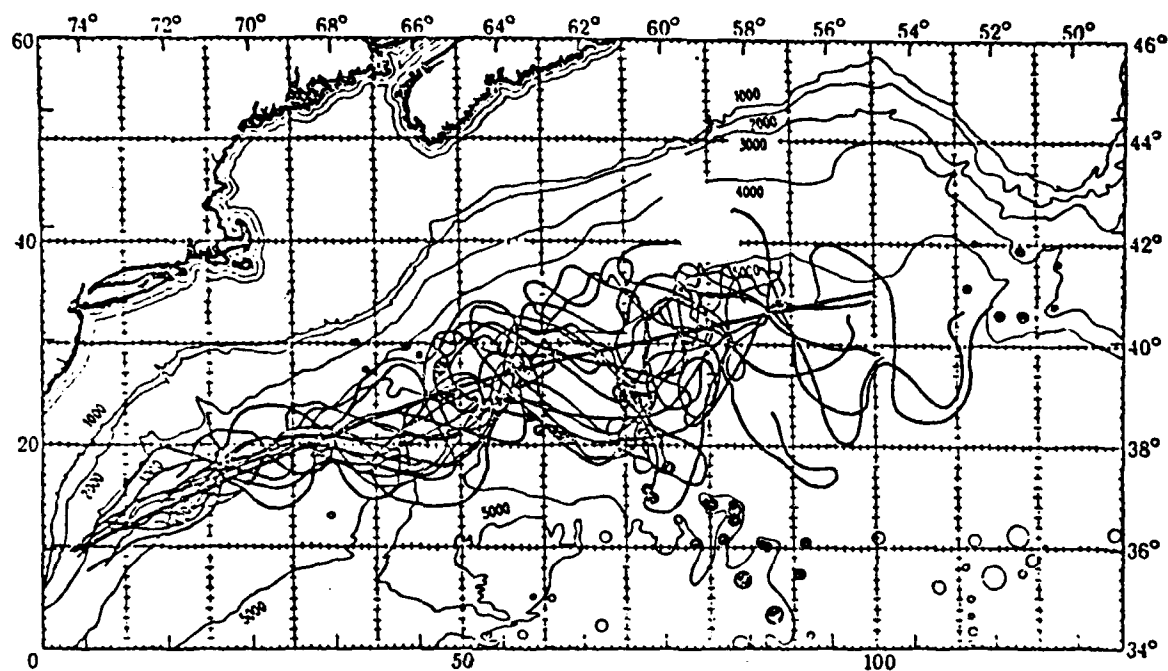


Figure 4. Composite of all available Gulf Stream paths through May 1966 (Niiler and Robinson, 1967).



A TRUNCATED SPECTRAL MODEL OF THE LONG-PERIOD GULF-STREAM FLUCTUATIONS AND
THEIR FEEDBACK TO THE ATMOSPHERE

Shenn-Yu Chao
Nova University Oceanographic Center
8000 North Ocean Drive
Dania, Florida 33004

The spectra of the atmospheric fluctuations are remarkably rich in temporal variations with periods from hours to years (Ward and Shapiro, 1961). Interannual fluctuations, although not as clearly observed as exact periodicities, do exist in the atmosphere. For example, the southern oscillation is dominated by periods from three to six years (Wright, 1977). On the other hand, the dynamics of the atmosphere are characterized by their short time span; the time required for a small-scale perturbation in the flow to reach global scales of motions via the nonlinear terms in the Navier-Stokes equations ranges between 1 week and 3 weeks. Therefore, the presence of interannual fluctuations in the atmosphere may be an indication that the ocean circulation dynamics play an important role in the long-period variability of the atmosphere, since the dominant time scale for the oceanic variability is at least one order of magnitude longer than that of the atmosphere.

In this work we address the questions of how the ocean feedback to the atmosphere affects the lower atmosphere, and what time and spatial scales dominate the coupled ocean-atmosphere system. We do so by analyzing a simple model of a barotropic atmosphere overlying a piece of land and a piece of $1\frac{1}{2}$ layer ocean, that is, a two-layer ocean having the lower layer inert. This model is applied to the extratropical region where both the atmosphere and the ocean are assumed quasi-geostrophic. The barotropic atmosphere is externally forced by some vorticity sources representing the solar radiation field. The upper ocean is driven by a

wind stress which is linearly proportional to the wind speed. On a longer time scale, the ocean feeds back its energy to the atmosphere through a vorticity source representing a heat flux induced by the ocean circulation gyre, forcing the atmosphere to vary on an interannual time scale. The model is highly truncated by retaining only the lowest few Fourier components (Lorentz, 1963). Such a severe truncation, although somewhat heuristic, drastically cuts down computer costs so that an extensive parametric study can be made.

Details about the model formulation and the numerical results can be found in Chao (1982). Important conclusions are the following. The effect of ocean feedback increases the strength of the circulations, both in the atmosphere and in the ocean, thus making the coupled system a better heat engine with respect to an atmosphere without the ocean feedback. This coupled heat engine is made particularly effective in the case of resonance, in which the global-scale forcing to the atmosphere greatly enhances the strength of the atmospheric and the oceanic circulations.

The ocean circulation favors an interannual time scale, T_R , which is the time required for the first baroclinic Rossby wave to travel westward across the ocean basin. This interannual time scale is both the spin-up time and the natural oscillation period of the ocean. In the tropical region T_R is on the order of several months; it increases poleward as the square of the latitude, becoming an interannual time scale in the extratropical region. The ocean oscillating at T_R affects the long-period, large-scale variability of the atmosphere. Therefore, one would expect that the dominant time scale for our climate increases from equator to poles. The interannual time scales for the Kuroshio and the Gulf Stream should also be dominated by T_R .

In the cases of super-resonance and sub-resonance, the oceanic oscillations at T_R triggers a strong westward propagation and a weak eastward propagation of forced Rossby waves at the same period. In the case of near-resonance, short-period pulsation

of the atmosphere with a period of several days can be triggered by the ocean. These short-period oscillations are related to the barotropic instability of Rayleigh type, dissipating a portion of the excess amount of energy generated by the resonance.

REFERENCES

- Chao, S.-Y., 1982: An extratropical model of ocean-atmosphere coupling. Submitted to J. Atmos. Sci.
- Lorentz, E.N., 1963: The mechanics of vacillation. J. Atmos. Sci., 20, 448-464.
- Ward, F., and R. Shapiro, 1961: Meteorological Periodicities. J. Meteorology, 18, 635-656.
- Wright, P.B., 1977: The southern oscillation patterns and mechanisms of the teleconnections and the persistence. Hawaii Institute of Geophysics. Tech. Rep. HIG-77-13, 107pp.

THE PROPAGATION OF A COLD-DOME MEANDER: A CONCEPTUAL MODEL

Frank Chew
NOAA/AOML
Miami, FL 33149

John M. Bane, Jr.
Curriculum in Marine Sciences
The University of North Carolina at Chapel Hill
Chapel Hill, NC 27514

David A. Brooks
Department of Oceanography
Texas A&M University
College Station, TX 77843

Gulf Stream meanders are a dominant transient in the South Atlantic Bight. The meanders have two common characteristics: the presence of an underlying cold dome in the meander, and their joint propagation downstream. Our synoptic observations off Beaufort, N.C., on February 11, 1979 show the thermal structure clearly: Fig. 1 and 2 are plan views of the temperature fields at the 1 m and 350 m depths respectively, and Fig. 3 and 4 are vertical temperature transects across and along the meander respectively.

Kinematically there is strong evidence for an upwelling, cyclonic circulation inside the dome on whose offshore side the high speed warm flow is known to meander by.

THE MODEL *makes*

There are two assumptions. First we assume the cold water giving form to the dome is not trapped within the dome. We envisage a systematic vertical mass exchange: upwelling mass in the forward region replacing downwelling mass in the rear. Second, to attain the observed vertical coherence of the meander we assume the warm water overlying the dome to shrink or stretch in direct opposition to the stretching or shrinking within the dome.

< [faded]

For an adiabatic system of two moving layers Fig. 5 illustrates the postulated vertical motion. The cold dome has three parts: a dome proper of already upwelled water, an active upwelling part in front, and an active downwelling part in the rear. In each active column, vertical motion of the same sign extends from the flat bottom into the sea surface and varies in magnitude to reach a maximum speed at the interface between the slower, cold layer below and the faster, warm stream above. Thus, in an upwelling column up front, convergence within the dome increases its thickness while within the upper layer there is sufficient mass divergence to result in a negative pressure tendency at the sea bottom. And in the subsiding water in the rear, the weight gain in the stretching warm columns above more than offsets the weight loss in the shrinking cold columns below.

DIVERGENCE AND TEMPERATURE GRADIENT

By shrinking a stratified column and thereby reducing the vertical distance in between, divergence strengthens the vertical rate of temperature increase. And by stretching the column, convergence weakens that rate. While there are other factors, these changes appear to be the dominant ones in Fig. 4. By identifying the break in vertical temperature change near the 175 m depth at station 133 with the level of non-divergence in the model up front, we see a faster temperature increase with height in the upwelling divergence in the layer above than in the upwelling convergence in the cold dome below. Similarly, by identifying the break in the temperature change near the 275 m depth at station 114 with the level of non-divergence in the model in the rear, we see the required reversal in temperature pattern, as the convergent layer now overlies the divergent layer. This fore-and-aft asymmetry of the cold

dome is clear evidence of the convergent stretching and divergent shrinking in the meander columns.

Divergence also changes the horizontal temperature gradient. By spreading the water out laterally divergence weakens the gradient; while the reverse holds for convergence. Again these changes appear to be the dominant ones in Fig. 1 and 2. At the 1 m depth the lateral gradient is strong from line I to line E, while it is weak from line E to line C. At the 350 m depth the reverse pattern holds. In sum, a divergence pattern and thus, by implication, a vertical motion field consistent with Fig. 5 are suggested.

FILAMENT FORMATION

The active upwelling in our model is a potentially effective mechanism in the formation of the warm, thin filament in Fig. 1. If the warm, inshore flank of the Gulf Stream overlies the rising dome, in reaching the sea surface the dome will also split apart the flank, and so form a filament of warm surface water as the dome moves downstream.

CONCLUSION

The model provides a new perspective, and the encouraging agreement found suggests that further study of the model could yield new insights into the dynamics of meandering.

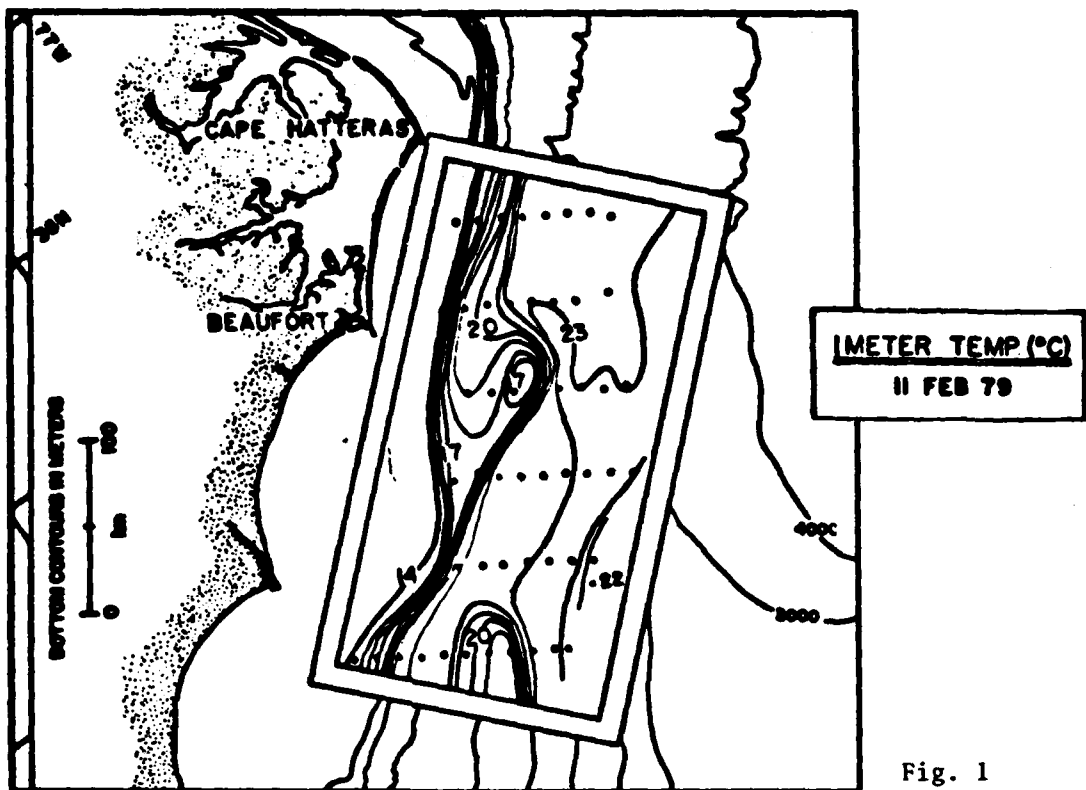


Fig. 1

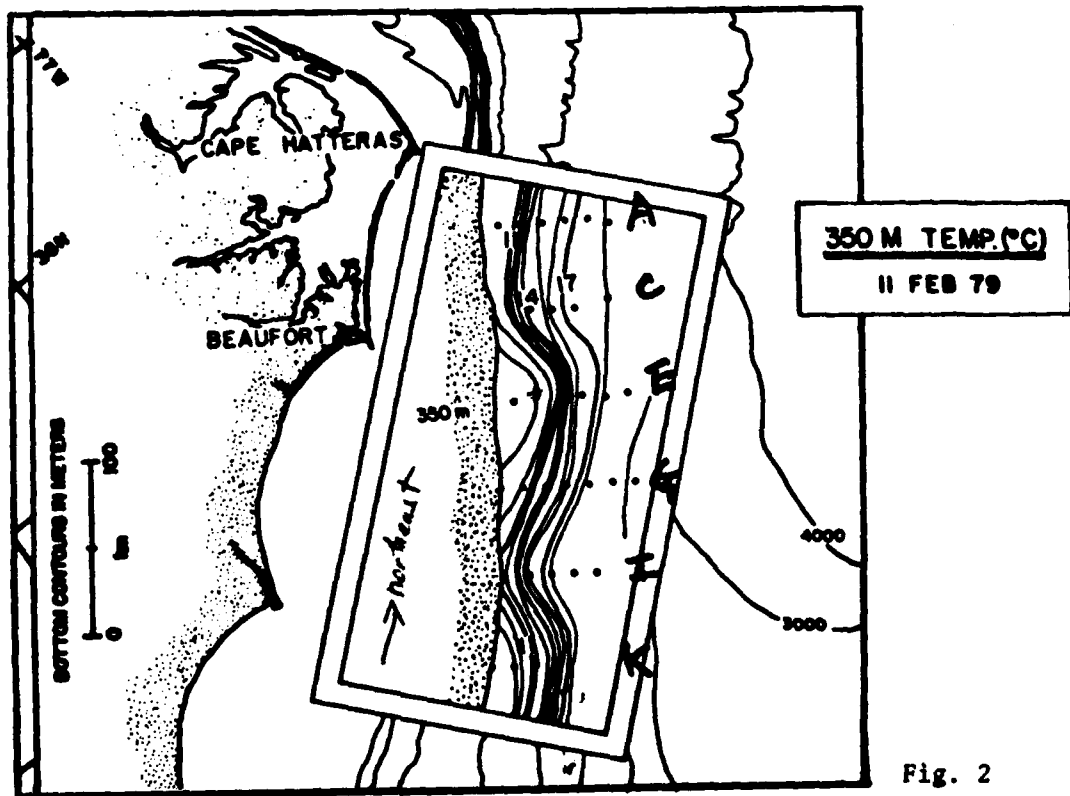


Fig. 2

LINE E
TEMPERATURE
(°C)
11 FEB 79

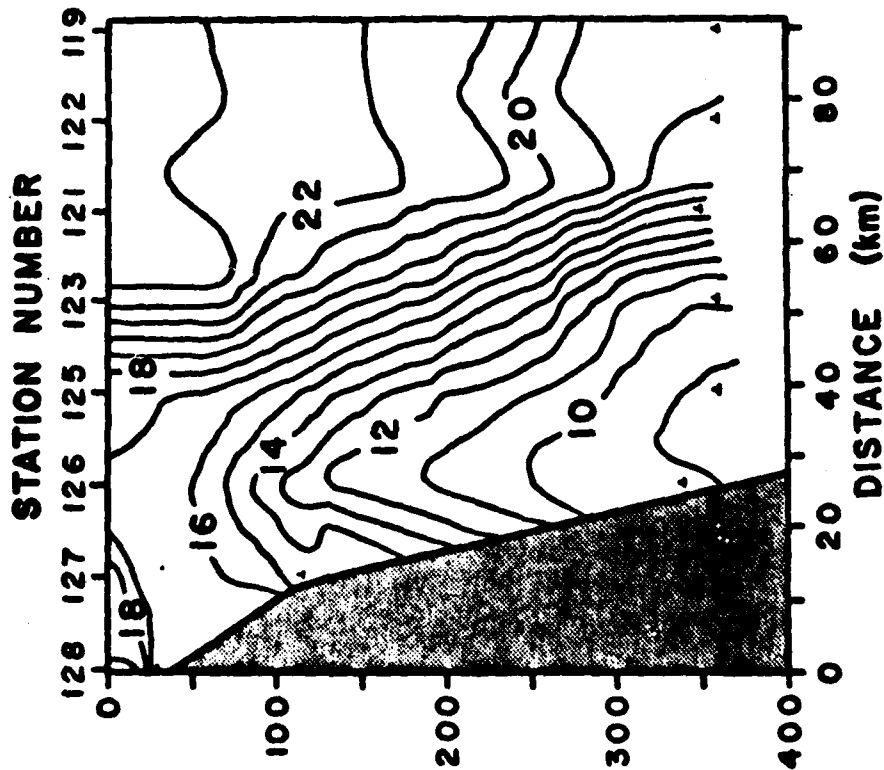


Fig. 3

ALONGSHORE
TEMPERATURE
(°C)
11 FEB 79

direction of meander movement →

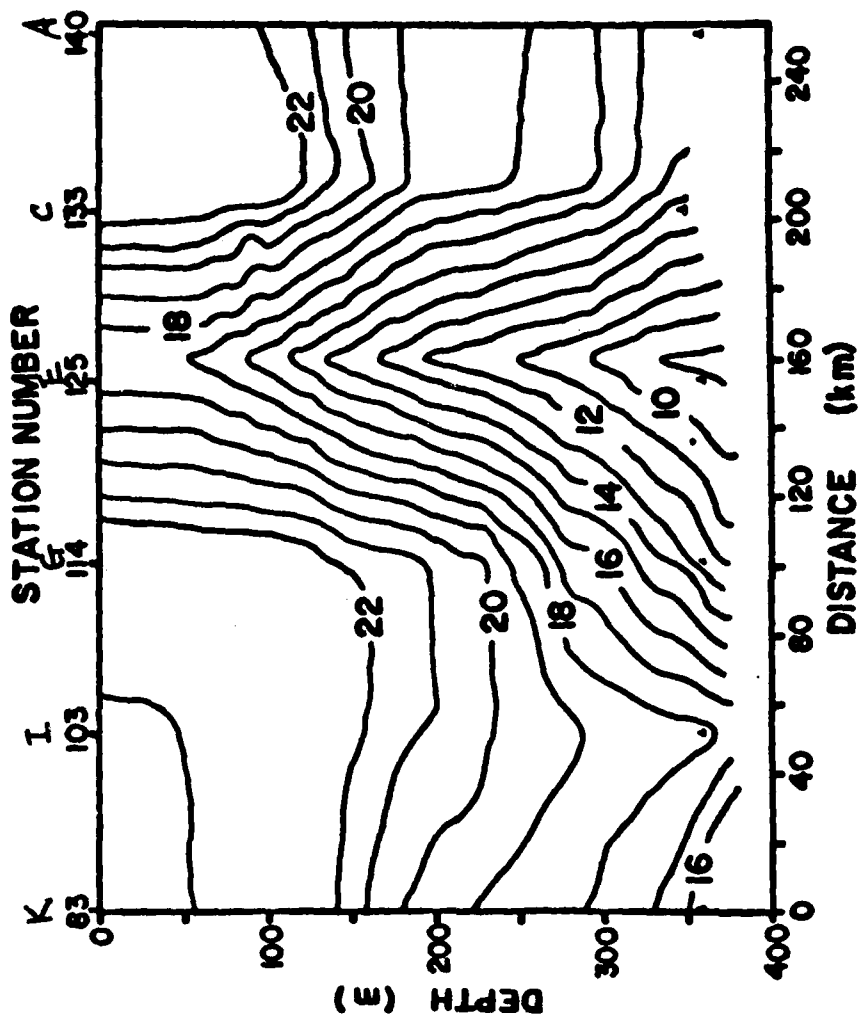


Fig. 4

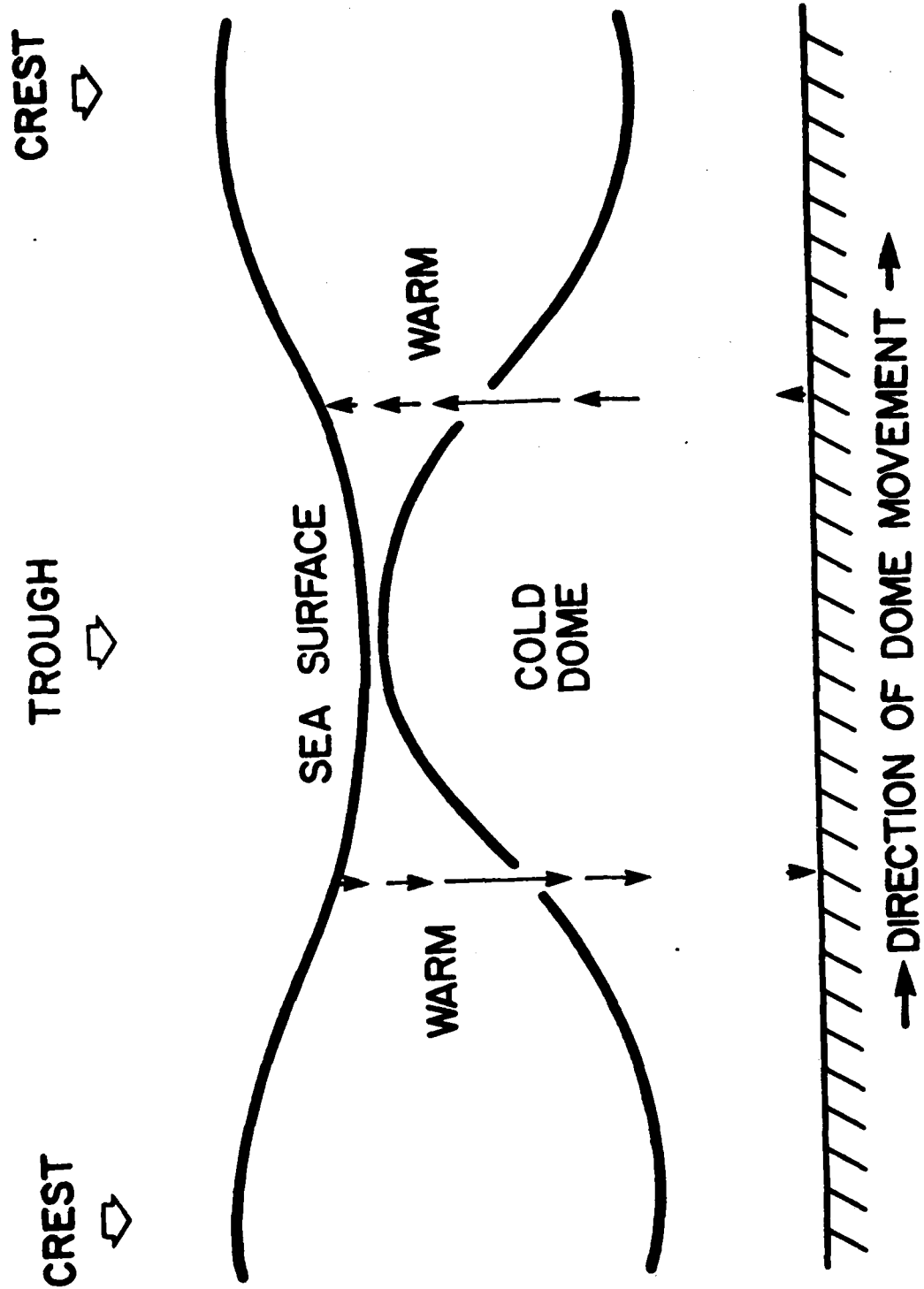


Fig. 5

AD P001044

THE GULF STREAM'S WESTERN SURFACE FRONT IN THE
SOUTH ATLANTIC BIGHT, 1976-78: PRELIMINARY RESULTS FROM AN
EMPIRICAL ORTHOGONAL FUNCTION ANALYSIS

Leonidas S. Cordova

Curriculum in Marine Sciences

University of North Carolina, Chapel Hill, NC 27514

ABSTRACT

Preliminary results from a study of 105 weekly Experimental Ocean Frontal Analysis Charts, produced by the U.S. Naval Oceanographic Office between 2 June 1976 and 31 May 1978, are reported. Basic statistics of the excursions of the front (as measured from a 64-week mean axis extending from Cape Canaveral to Cape Hatteras) show appreciable changes between year-long subsets of the data. Estimates of standard deviations as well as extrema of the frontal amplitudes are presented. Empirical Orthogonal Function Analysis has provided 6 components of the front which account for 85% of the original variance. Their associated eigenvectors offer a more compact assessment of the spatial variability and are used to generate time series whose spectra contain significant peaks in frequency bands centered near periods of 2.3, 3.2, 4.4, 6.0 and 17 weeks. A yearly band seems also present in the first five principal components.

INTRODUCTION

In the region between the Straits of Florida and Cape Hatteras, the Gulf Stream exhibits lateral displacements of a wavelike appearance which seem evidently constrained by the presence of these two topographical features. Between these near-nodal areas, large lateral oscillations of the Stream have been observed, as defined by the surface temperature gradients appearing in infrared imagery from satellites, in subsurface in situ measurements using moored arrays of recording instruments and in direct observations by research vessels and aircraft. These recent advances in data acquisition procedures have generated consistent, synoptic three-dimensional pictures of the temperature fields at given times in the Gulf Stream and have revealed the existence of other similar large-scale features of ocean circulation (Legeckis, 1975; 1978). In particular, the meandering patterns of the Stream and their effects on shelf circulation have been documented since the early 1950's (Fofonoff, 1981).

Information on the spatial and temporal scales of the meanderings in the region has existed at least since the early 1960's. Lateral amplitudes of 10 km and periods of 4 and 10 days are described as dominant by Webster (1961) at the continental shelf break off Onslow Bay, North Carolina. In the Straits of Florida, results of the SYNOPS 71 observational program suggested characteristic periods of 4 to 6 days as time scales for crosstream velocity components which appeared to be propagating northward at about 40 km per day. The associated wavelengths ranged from 160 to 240 km (Duing, 1975). Subinertial motions in the bands of 2-3 days, 4-5 days, and 8-25 days are reported for the same area in 1972-1974 by Duing, Mooers, and Lee (1977). These authors also point out the existence of an annual cycle in the meridional velocity component. For the continental shelf off Miami,

Florida, Lee and Mayer (1977) describe currents events spatially coherent in a scale of at least 10 km along the shelf with periods in a band of 2 days to 2 weeks. They observed cyclonic eddies, characterized as having mean diameters between 10 and 30 km and a lifespan of 1 to 3 weeks. In their two-year study of the Gulf Stream system front (1976-1978), Maul et al. (1978) have found periods of 5-8 days to be typical off Onslow Bay, North Carolina. They have reported low-frequency variability in the band of 22-36 days as well. Legeckis (1979) has used satellite data to isolate waves progressing along the surface temperature front at speeds of near 40 km/day, with peak-to-peak maxima of less than 100 km. Periods for these waves are about 4-5 days. From a series of observations begun in 1979 off the coast of the Carolinas, Bane and Brooks (1979), Brooks and Bane (1981), and Bane et al. (1981), have presented detailed accounts of meander motion and evolution. Their data have confirmed the wavelengths of about 200 km for the frontal disturbances travelling downstream in the area, with periods of about 5-7 days.

Indications of longer time scales, seasonal and yearly, perhaps influencing the motions of the Gulf Stream, have been found in transport studies by Schmitz and Richardson (1968), Niiler and Richardson (1973), and Duing (1977) in measurements across the Florida Straits. Brooks and Bane (1982) have recently presented evidence of seasonal changes in the meanders off North Carolina.

This paper reports current work anticipated to contribute data in the very-low-frequency end of the Stream's western front variability, comprising periods of two weeks to a few months. The study aims at the characterization of a frontal strip extending from 27.5 to 35.3 degrees of latitude North, along the mean location of its surface signature. It follows in part the approach taken by Halliwell and Mooers (1979), in their analyses of the Gulf Stream front and its interactions with the shelf between Virginia and Nova Scotia.

INFORMATION AND DATA PROCESSING

The original information was contained in the Experimental Ocean Frontal Analysis Charts (hereafter referred to as EOFAC's), generated on a weekly basis by the U.S. Naval Oceanographic Office. A set of 105 charts, dated from 02 June 1976 to 31 May 1978 was used as a source of data for this study. After the latter date the format of the charts was substantially changed. This product was discontinued as such at the beginning of 1980 as it became a standard part of the navigational aids disseminated daily by the Navy for its own uses.

A good discussion of the sources of data for the generation of EOFAC's and their inherent errors can be found in Halliwell and Mooers (1979). In essence these charts display the positions of the western and eastern surface thermal fronts of the Gulf Stream. Eddies spinning off from the Stream are indicated and labelled. Numeric values are plotted at various points to give an estimation of the gradients defining the fronts. In addition, indications concerning the conditions under which the curves were drawn are given. Comments are sometimes present about trends or particular features. A copy of one chart is shown in Figure 1a.

Preparation of the sampling grid.

Western frontal shapes were first extracted from the original EOFAC's by tracing them on transparent sheets with appropriate register marks. This step was necessary since the "original" set of charts had been written over and photocopies of them showed poor contrast due to the writings. The tracings procedure also revealed small but significant differences in the scales as a result of either: a) a change in the scale of the master map used to draw the charts at the originating Navy office, or; b) most likely, use of different duplicating machines at that location. Whatever

the case, the existence of these differences was realized and taken into consideration in the definition of the measuring grid.

A sampling grid was available from previous work which utilized a 64-week subset of the 105 charts considered in this study (Bane and Brooks, 1979). It consisted of the mean-line of 14 sections drawn between Cape Canaveral and Cape Hatteras, the origin of each section being the 200-meter isobath. It was decided to redefine the sections so that they would be separated by 50 km on the meanline. This redefinition needed as a previous step the determination of a segment representing that distance on the EOFAC's. A weighted average of the chart's 5-degree latitude and longitude intervals was used to this effect. Thus, 22 points were obtained on the mean line and perpendiculars to the local tangents traced at each of them. On the normals 1 mm marks were made, defining the new sections and therefore the grid. The resolution nominally obtained with the procedure just described is about 3 km, or one-half of the minimum division on each section, which corresponds to about 6 km on the charts. The sections were numbered from south to north.

The grid as defined above constitutes a quasi-natural coordinate system for the frontal excursions, in the sense that it contains the average of 64 realizations of the 105 used in this study, along which the sections have been positioned and from which the lateral displacements of the front are measured. Figure 1b contains the grid superimposed on a map of the region of interest, with the 200 m isobath as a reference.

Data generation

Digitization of the frontal shapes was performed manually. Whenever possible three measurements were made at each section:

- a. the maximum value of the frontal amplitude,
- b. the minimum value, and

- c. a "smoothed" value where filaments or circumvolutions of the front are present. This last value is naturally subjective, and follows the idea of joining the frontal positions before and after a filament with an arc that preserves the direction of the tangents and matches the curvatures at the "end" of each feature. The "middle" value in an S-shaped feature was sometimes read off if considered appropriate.

Use of the above procedure generated two basic, different datasets:

a) MINARRAY, containing the minimum values of the amplitudes at each section as seen from the current axis, and b) MAXARRAY, containing the maximum values of the same. These datasets also incorporated date, section number (=1-22), week number (1-105), a year variable (=1,2), and a season variable (=1-8), all in a matrix format designed expressly for the ensuing array processing.

In both datasets, a missing value was replaced by the smoothed value of that section. If the latter was missing, the only existing value was entered. In essence, MINARRAY is a version of the frontal shape where all multivalued features have been eliminated by assignment of the smallest value as seen from the center of the stream. On the other hand, MAXARRAY keeps all of the filaments and other multivalued features of the front.

Data processing

Array processing has produced basic statistics (mean, standard error of the mean, standard deviation, extremal values, variance and higher moments) for each season, each year, and for the entire datasets. The complete set of these results is available in Cordova (1982).

Empirical Orthogonal Functions (EOF's) were computed for year 1, year 2 and both years. EOF analysis is a powerful tool in reduction of certain large data bases and as such has encountered wide applicability in the fields

of meteorology and oceanography (see below for references). The method is known in multivariate statistics under the names of factor analysis or principal component analysis, depending on whether a correlation matrix or a variance-covariance matrix is the starting point for the procedure. The choice of matrix is essentially dictated by the nature of the problem. A good introduction to both branches can be found in Morrison (1976).

In this case, as explained in the Results section, the variance-covariance matrix was used. The dimension of the matrix is N -squared where N is the (fixed) number of locations in space where the amplitudes of the front are sampled. An averaging process is done over the time variable to obtain it. The EOF's are the eigenvectors of the matrix, that is, they are timeaveraged spatial shapes that are uncorrelated between themselves. These shapes are subject to no other requirement and are generated by a well-defined, standard diagonalization process of a real symmetric matrix; the eigenvalues (always real in the case of a Hermitean matrix) are used to label the eigenvectors, beginning with the largest, in descending order.

The original amplitude time series are then expressed as a linear combination of the EOF's (the purely spatial part) through coefficients known as the principal components, time series themselves, with norms equal to the eigenvalues. For the mathematical details, see Jaspersen (1971) or Morrison (1976).

Published examples of the use of EOF's show that the first five modes usually account for 80-90% of the total observed variance (Jaspersen, 1971; Kundu et al. 1975; Davis, 1976; Weare et al. 1976; Halliwell and Mooers, 1979; Smith and Petrie, 1982). Thus the variance of the observations can be expressed by just a few components, reducing the description considerably. The components contain, in the present example, the temporal variability.

Fourier-transforming the components to the frequency domain is the next step. The periodograms thus obtained are then smoothed using a spectral window of appropriate shape and width. The final results, displaying spectral density versus frequency for each component, are more conveniently presented in semilog form, as suggested by Jenkins and Watts (1968).

A note on the nomenclature seems in order here. In the applications of Factor Analysis or Principal Components Analysis to geophysical data, where it is known as Empirical Orthogonal Function Analysis, there is no uniform terminology to designate the eigenvectors or the time series generated from the expansion of the original data in terms of them. Even the conception of these "modal" analyses is slightly different between statisticians and geophysicists. In this article, to be consistent with the statistical and geophysical literature, the eigenvectors will be called the "modes" (usually known as the empirical orthogonal functions or EOF's in oceanography) and their associated time-series will be referred to as the "principal components" or simply the "components".

RESULTS

Only the results concerning the array of minimum displacements from the Gulf Stream's axis (MINARRAY) will be presented here.

Basic Statistics

The basic statistics for years 1, 2, and both years combined are contained in Figures 2a, 2b and 2c, respectively. In these illustrations, the center line is the 2-year mean. The envelopes are defined by the extremal (smallest, largest) values of the front at each section. Between the envelopes, which are not necessarily symmetric about the mean, a broken line on either side of the mean marks intervals equal to minus or plus one standard deviation centered on the mean. The 200 m isobath is also present.

A superposition of the mean lines for years 1 and 2 (Figure 2d) shows that there is a clear, mostly seaward, interannual shift, most pronounced at section 13, off Cape Romain, where it reaches about 24 km. The minimum changes occur at sections 1, 8, and 20, where they are below the resolution of the grid (less than 0.05 of 1 division, or less than 150 m). Note that at sections 21 and 22 the change is shoreward. The standard deviation increases 20% between sections 14-15 in year 1, and sections 15-18 in year 2 (maximal variability bands). Another measure of the interannual variability is the range of the frontal displacements, which is considerably increased in year 2. So, not only did the mean shift, but in addition, the activity of the front increased, in this case.

Additional evidence for the seaward trend is contained in Figures 3a and 3b, where the original time series at sections 11 and 16 are displayed. These sections were chosen to illustrate a very low-frequency oscillation

riding on the trend (Figure 3a) whose period seems to be 14 months or so. (This period could not be resolved in this study, although a broad near-annual cycle is apparent in the spectra.)

It is interesting to note that of the 3 largest positive events in section 11, the first occurs simultaneously at section 16 (end 1976) but the other two are delayed one or two weeks (week 64, March 1977 and week 98, April 1978). Note also that a positive change means a seaward motion. The downward (negative) spikes are possibly indications of the passage of a filament.

EOF's and Spectral Analysis

In view of the homogeneity of the variables and the use of a common scale in measuring their changes, the variance-covariance matrix was considered to be the proper choice for the empirical orthogonal function analysis. The following are essentially the findings concerning the two-year, minimal data.

Eigenvalues for the covariance matrix were computed using two procedures and found in agreement within round-off errors. It is well-known that eigenvectors can be determined only up to an arbitrary scale factor (positive or negative). The computing routines often remove part of the ambiguity by imposing the extra condition that the norm of the eigenvectors be equal to one. Still the matter of choice of sign remains. These facts only reflect the notion that the eigenvalue problem defines invariant orientations in space, but not a direction or a scale along them. In this application, since it was known that the original time series contained a positive trend, the choice was made such that the modes also contained positive trends.

Following the procedure outlined in section 2, the 6 most significant eigenvectors and the spectral composition of their associated components were found (Figures 4a, 4f). Note that the eigenvector coordinates have

been multiplied by a factor of 10 to show their values more clearly. They are drawn on a system of coordinates that has the same orientation as that in Figure 1b, but those origins have been shifted to coincide with the 2-year mean line. This has been done since the data is centered before computing covariances and components.

Eigenvector 1 offers as a main feature what resembles a smooth version of the standard deviation distribution along the mean. It follows the mean line very closely up to section 8 and then separates seaward. In so doing it mimics a turn of the stream which has frequently been observed at about the latitude of the Charleston bump (Brooks and Bane, 1978; Pietrafesa et al., 1978; Legeckis, 1979). Its component spectrum exhibits an essentially reddish composition, the largest spectral density in a band suggesting a yearly cycle.

Eigenvector 2 follows the mean up to section 9, where it separates shoreward. It has essentially one zero crossing between sections 15 and 16, off Cape Fear. It looks like a very long, attenuated wave, since the amplitude of its second half-cycle decays progressively towards zero off Hatteras. There is no single peak in the component 2 spectrum. The signal-to-noise ratio seems best towards the high frequency end. There is a hint of a yearly band and of a broad 17-week component.

Separation from the mean occurs at section 7 for vector 3, crossing over zero between 13 and 14, and also between 18 and 19. Again, there is a damped-wave look to it. The wavelength for this shape would be about 350 km.

There is an unexpected similarity in shape between EOF's 4 and 3, particularly downstream from the Charleston bump area. This likeness extends into the time domain and the relative variance contributions of each of

its components. Both seem to contain significant power in a band around 2.5 cycles per week (or period of about a month).

In Mode 5 there is once more indications of a wave pattern that decreases in amplitude towards Hatteras. The wavelength appears to be about 400 km. A most significant frequency band in its component lies about .9 cpw (or 11-week period).

Mode 6, finally, exhibits a sharp turn seaward in the vicinity of the bump, followed by undulations of a nearly 400 km repeat. In the frequency domain, there are peaks at periods of nearly 2.5 weeks and 1 month. The upward, red end shape of the associated spectrum displayed by the first five components is not present here.

ACKNOWLEDGEMENTS

I thank R. Ault for help in computer work, J. Bane for proposing this work, for advice and discussions, S. Fisher and K. Berleman for typing, S. Cambanis for help in statistics, T. Curtin for EOFAC's, and C. Lucaveche for help in darkroom and digitization work. Supported in part by ONR Contract N00014-77-C-0354.

REFERENCES

- Bane, J.M. and D.A. Brooks, 1979. Gulf Stream Meanders Along the Continental Margin From the Florida Straits to Cape Hatteras. Geophys. Res. Lett., 6, 4:280-282.
- Bane, J.M., D.A. Brooks and K.R. Lorenson. 1981. Synoptic Observations of Three-Dimensional Structure, Propagation and Evolution of Gulf Stream Meanders Along the Carolina Continental Margin. J. Geophys. Res., (C7):6411-6425.
- Brooks, D.A. and J. M. Bane. 1978. Gulf Stream Deflection by a Bottom Feature Off Charleston, South Carolina. Science, 201:1225-1226.
- Brooks, D.A. and Bane, J.M., Jr. 1982. Gulf Stream Meanders off North Carolina: A Seasonal Comparison of Their Observed Characteristics. EOS 63 (18):362.
- Chao, S.-Y. and L. J. Pietrafesa. 1980. The Subtidal Response of Sea Level to Atmospheric Forcing on the Carolina Capes. J. Phys. Oceanogr. 10, 8:1246-1255.
- Cordova, L., 1982. The Gulf Stream's Western Surface Temperature Front in the South Atlantic Bight, 1976-78: II. Basic Statistical, Spectral and Component Analysis Results (in preparation).
- Davis, R.E. 1976. Predictability of Sea Surface Temperature and Sea Level Pressure Anomalies Over the North Pacific Ocean. J. Phys. Oceanogr. 6, 3:249-266.
- Duing, W. 1975. Synoptic Studies of Transients in the Florida Current. J. Mar. Res., 33, 1:53.
- Duing, W. 1978. Spatial and Temporal Variability of Major Ocean Currents and Mesoscale Eddies. Boundary-Layer Meteorology, 13:7-22.

- Duing, W., Mooers, C.N.K. and Lee, T. 1977. Low-frequency variability in the Florida Current and relations to atmospheric forcing from 1972 to 1974. J. Mar. Res. 35, 2:129-161.
- Fofonoff, N.P. 1981. The Gulf Stream System, In: Evolution of Physical Oceanography, B.A. Warren and C. Wousch, eds. MIT Press.
- Halliwel, G.R. and C.N.K. Mooers. 1979. The Space-Time Structure and Variability of the Shelf Water/Slope Water and Gulf Stream Surface Temperature Fronts and Associated Warm-Core Eddies. J. Geophys. Res. 84, C12:7707-7725.
- Jaspersen, W. 1971. Representation of Meteorological Variables by Empirical Orthogonal Functions. In: Statistical Methods and Instrumentation in Geophysics. A.G. Kjelaas, ed. Teknologisk Forlag, Oslo.
- Kundu, P.K., J.S. Aleen and R.L. Smith. 1975. Modal Decomposition of the Velocity Field Near the Oregon Coast. J. Phys. Oceanogr., 5:683-704.
- Lee, T.N. and D.A. Mayer. 1977. Low-Frequency Current Variability and Spin-Off Eddies Along the Shelf Off Southeast Florida. J. Mar. Res. 35, 1:193-220.
- Legeckis, R.V. 1975. Application of Synchronous Meteorological Satellite Data to the Study of Time Dependent Sea Surface Temperature Changes Along the Boundary of the Gulf Stream. Geophys. Res. Lett., 2:435-438.
- Legeckis, R.V. 1978. A Survey of Worldwide Sea Surface Temperature Fronts Detected by Environmental Satellites. J. Geophys. Res. 83, C9:4501.
- Legeckis, R.V. 1979. Satellite Observations of the Influence of Bottom Topography on the Seaward Deflection of the Gulf Stream off Charleston, South Carolina. J. Phys. Oceanogr., 9:483-497.
- Maul, G.A., P.W. DeWitt, A. Yanway and S.R. Baig. 1978. Geostationary Satellite Observations of Gulf Stream Meanders: Infrared Measurements and Time Series Analysis. J. Geophys. Res. 83, C12:6123-6135.

- Niiler, P.P. and W.S. Richardson. 1973. Seasonal Variability of the Florida Current. J. Mar. Res. 31, 3:144-167.
- Pietrafesa, L.J., J.O. Blanton and L.P. Atkinson. 1978. Evidence for Deflection of the Gulf Stream at the Charleston Rise. Gulfstream 4, 11:2-4.
- Schmitz, W.J. and W.S. Richardson. 1968. On the Transport of the Florida Current. Deep-Sea Res., 15:679-693.
- Smith, P.C. and Petrie, B.D. 1982. Low-frequency Circulation at the Edge of the Scotian Shelf. J. Phys. Oceanogr. 12, 1:28-46.
- Weare, B.C., A.R. Navato and R.E. Newll. 1976. Empirical Othogonal Analysis of Pacific Sea Surface Temperatures. J. Phys. Oceanogr., 6:671-678.
- Webster, F. 1961a. A Description of Gulf Stream Meanders off Oslo Bay. Deep-Sea Res., 8:130-143.
- Wunsch, C., D.V. Hansen and B.D. Zettler. 1969. Fluctuations in the Florida Current Inferred from Sea Level Records. Deep-Sea Res. Suppl. to vol. 16:447-470.

FIGURE LEGENDS

Figures 2a,b,c. Basic frontal statistics for year 1, year 2 and both years, respectively. The center line joins the mean values at each section for each period. The dotted lines to each side of the mean represent 1 standard deviation estimate. The envelopes mark the extremal values of the front excursions during that time.

Figure 2d. An overlay of the means of years 1 and 2 shows a clear seaward shift, with the exception of the end at Hatteras (last two sections). The standard error of the means is about the same as the resolution of the grid (one-half of a division).

Figures 3a,b. Section 11 and Section 16 raw data vs. time. In 3a, a long-period (approximately 14 months) oscillation can be discerned about an upward trend, the latter more clearly seen in 3b. Weeks 32 and 84 mark the beginnings of 1977 and 1978.

Figures 4a-f. Eigenvectors of the covariance matrix (EOF's) and the spectral densities of their associated principal components. The percentage of the total original variance explained by each component is indicated. The system of coordinates is now centered on the two-year mean, the orientation of the sections remains unchanged. The eigenvector structures are displayed at a lateral magnification of 10x, for clarity. The bars in 4a are the bandwidth (along abscissa) and the confidence interval (along ordinate), common to all six graphs.

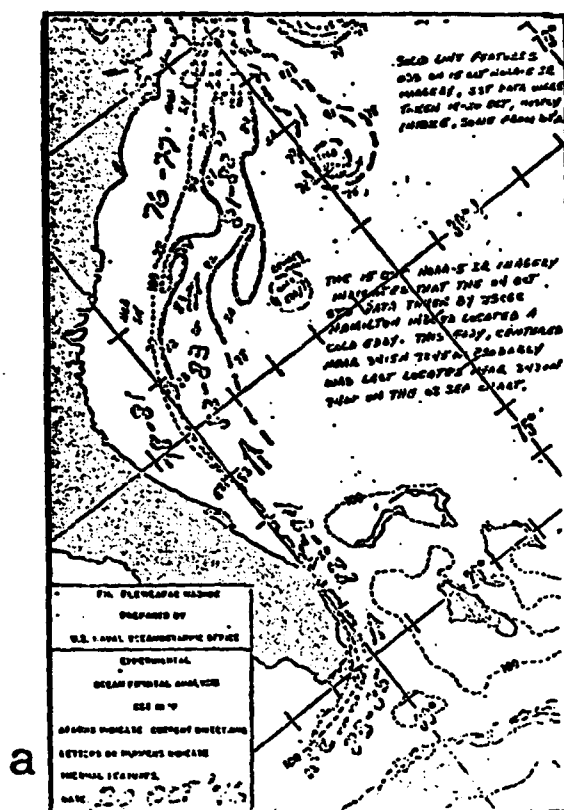


Fig. 1.a.

Sampling grid, consisting of 22 sections at a mean interval of 50 km, positioned along a 64-week mean (solid) line, starting at 27.5 N. The total length covered is 1050 km. The 200-m isobath is included. Each section is normal to the local tangent. The fine marks on the sections are 1 mm apart in the original (about 6 km on charts.)

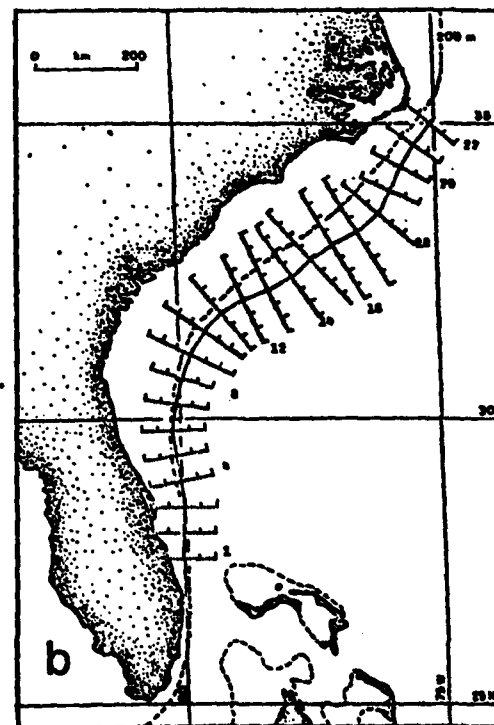
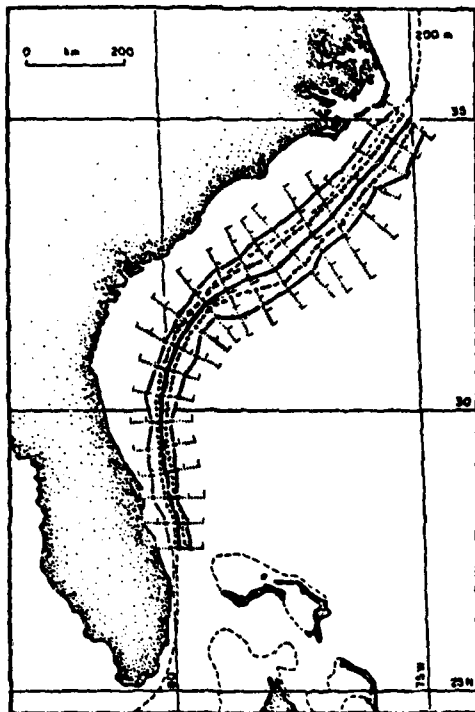
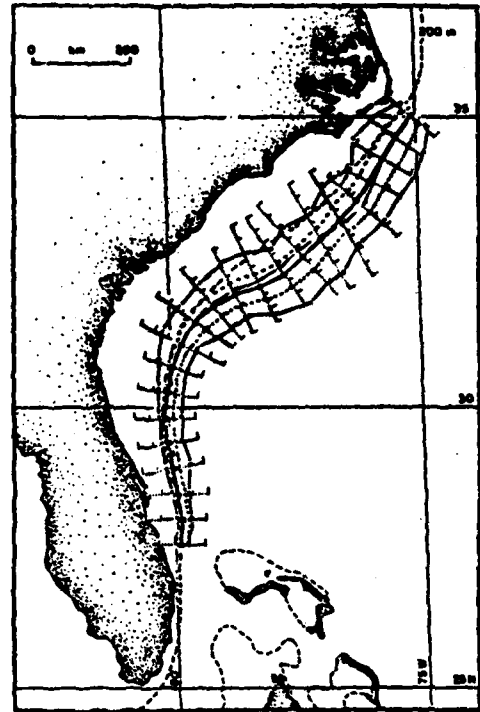


Fig. 1.b.

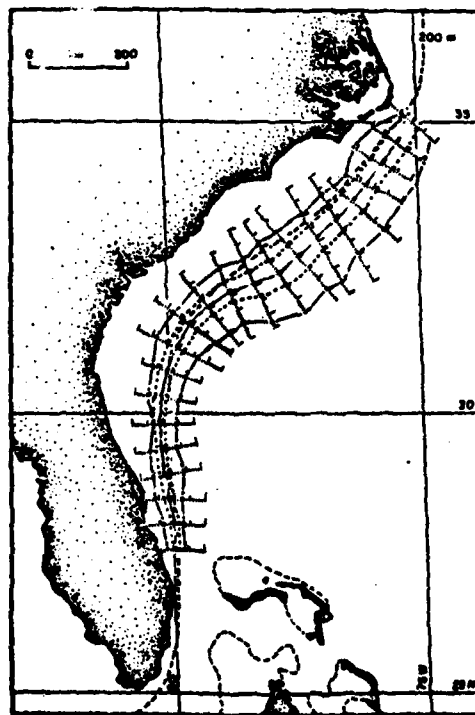
Facsimile of EOFAC dated 20 October 1976. The product used to obtain data for this study was page 1, shown here. The reference bottom topography line is 100 fathoms. The western surface front was extracted by tracing it onto transparent sheets, from 27.5 N to its intersection with 75 W off Cape Hatteras.



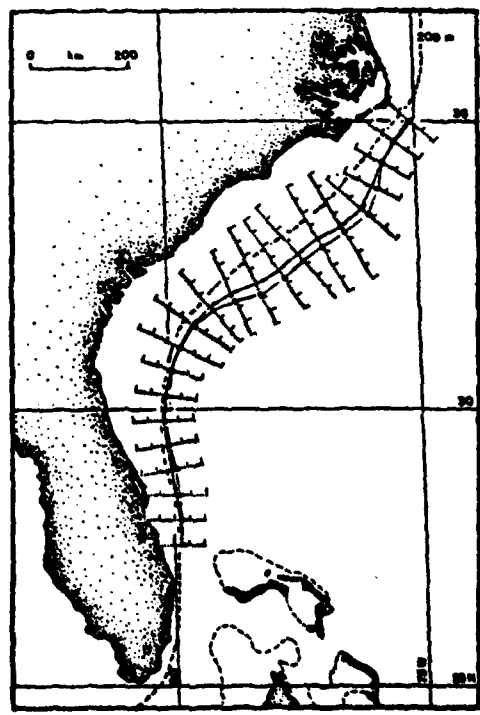
2a



2b



2c



2d

Fig. 2.a-d.

MINARRAY BOTH YEARS:SECTION DATA/TIME

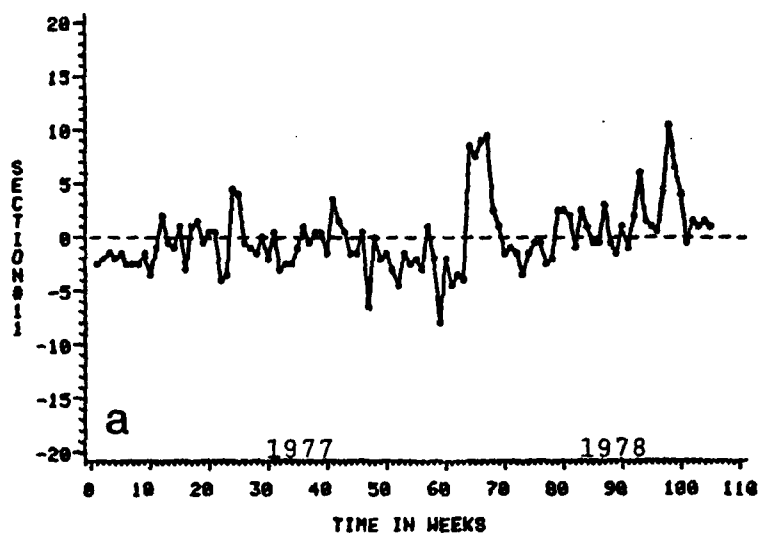


Fig. 3.a.

MINARRAY BOTH YEARS:SECTION DATA/TIME

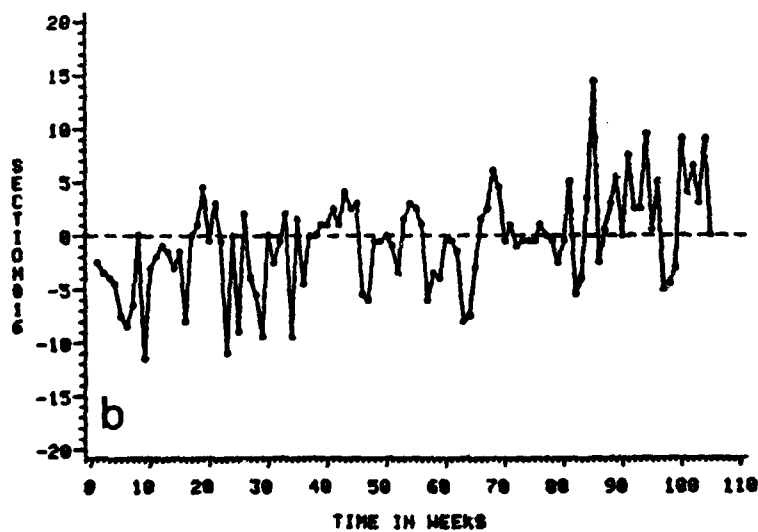


Fig. 3.b.

AD-A128 789

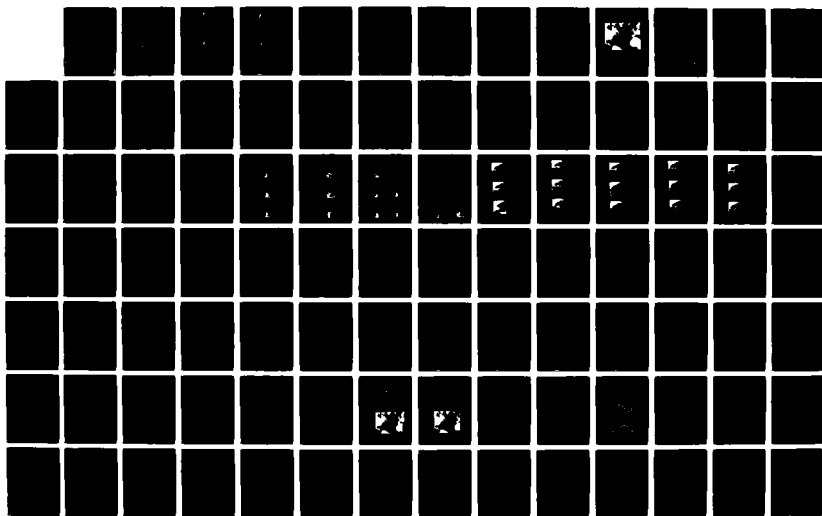
PROCEEDINGS OF THE WORKSHOP ON GULF STREAM STRUCTURE
AND VARIABILITY HELD... (U) NORTH CAROLINA UNIV AT CHAPEL
HILL APR 82 N00014-82-G-0059

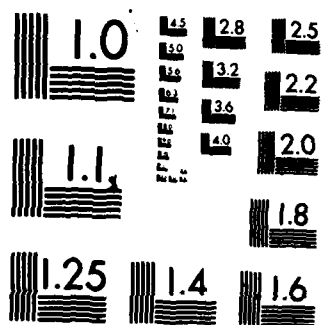
2/5

UNCLASSIFIED

F/G 8/3

NL





MICROCOPY RESOLUTION TEST CHART
NATIONAL BUREAU OF STANDARDS-1963-A

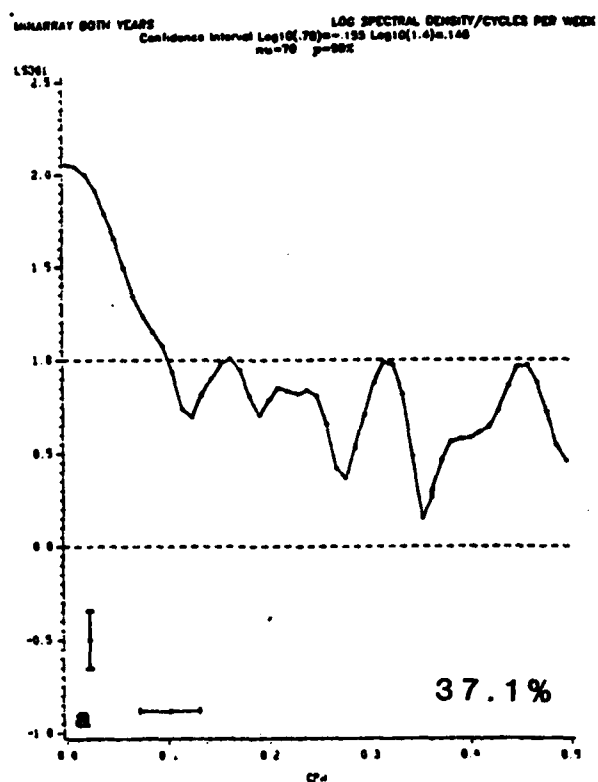
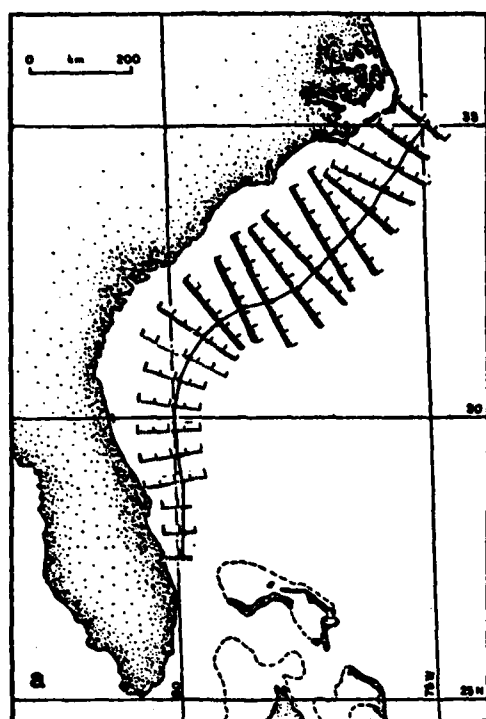


Fig. 4.a.

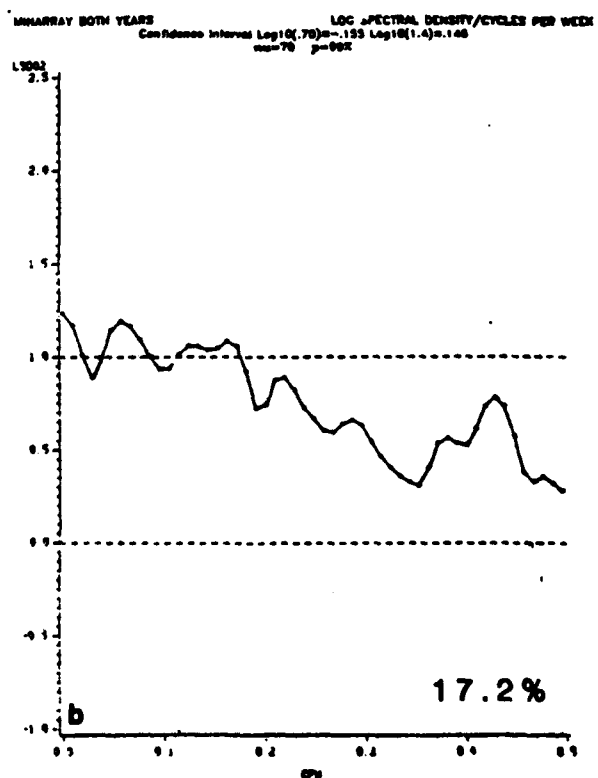
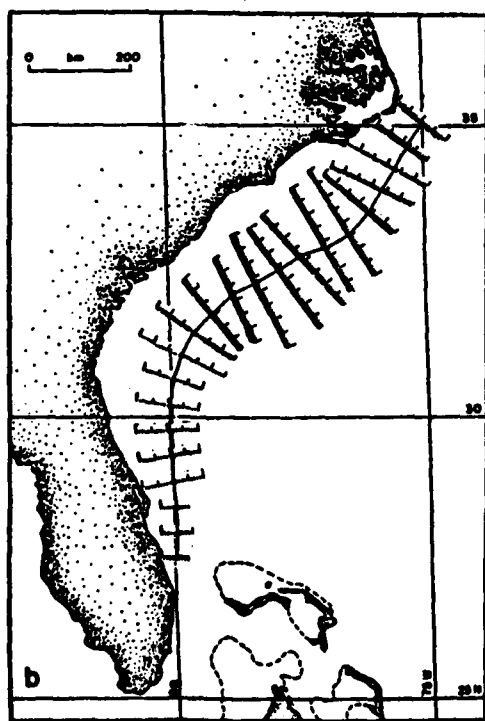


Fig. 4.b.

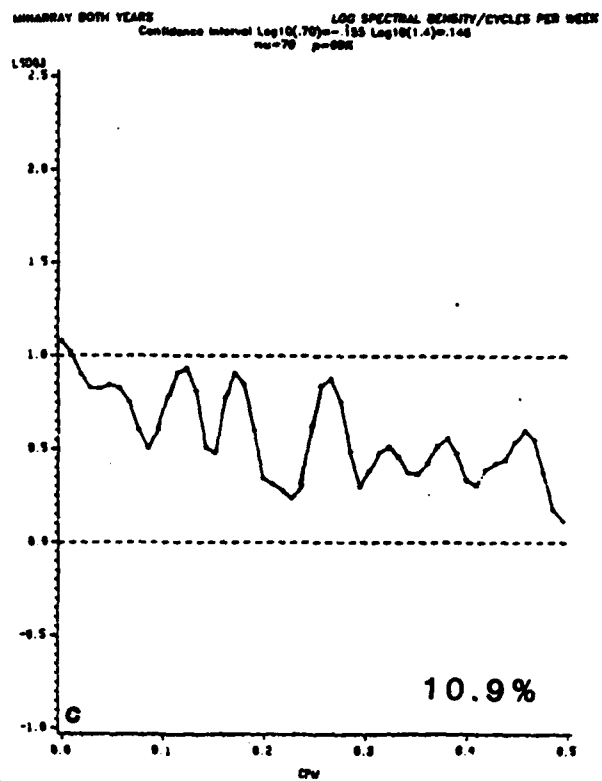
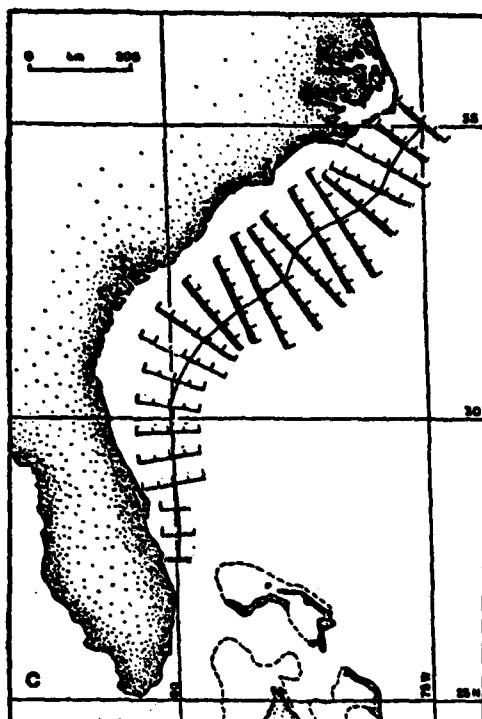


Fig. 4.c.

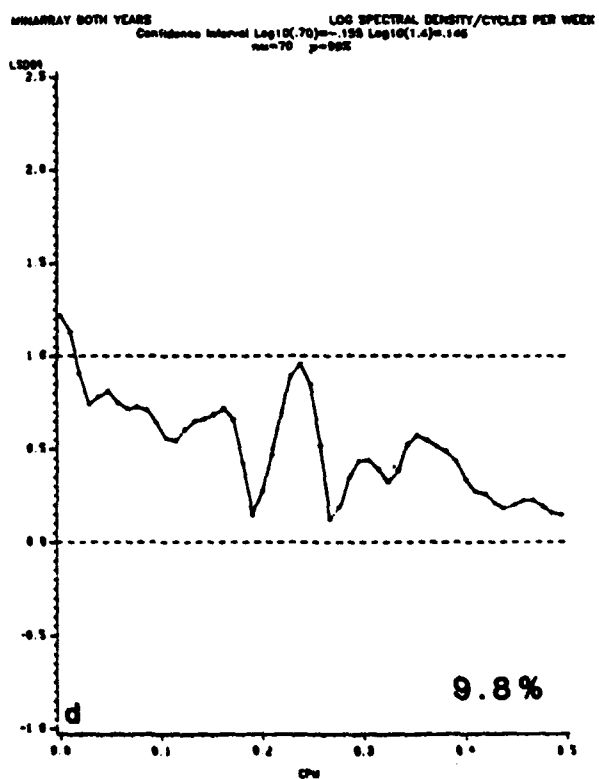
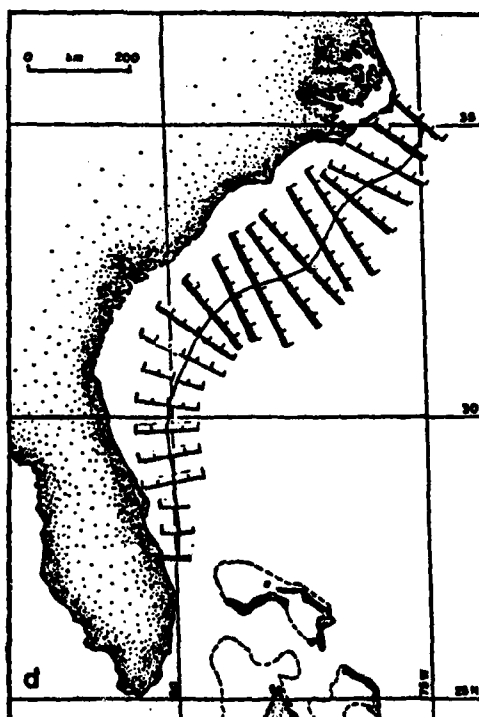


Fig. 4.d.

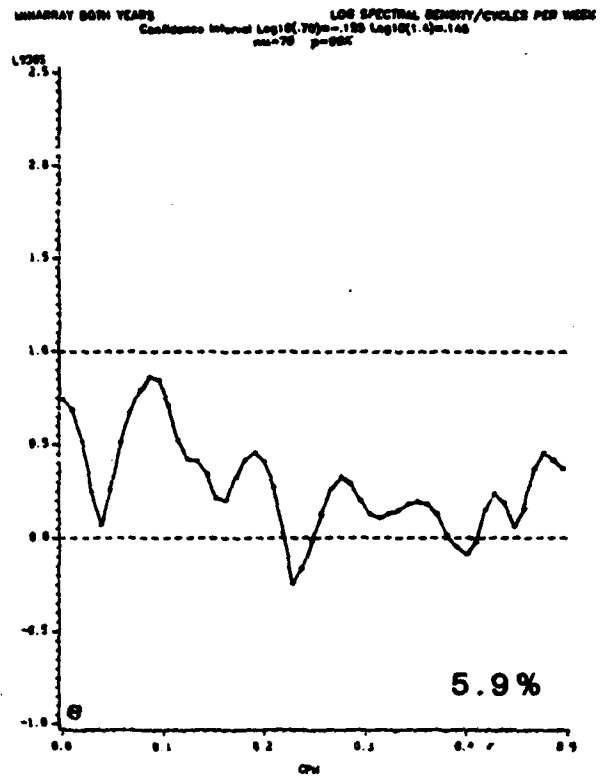
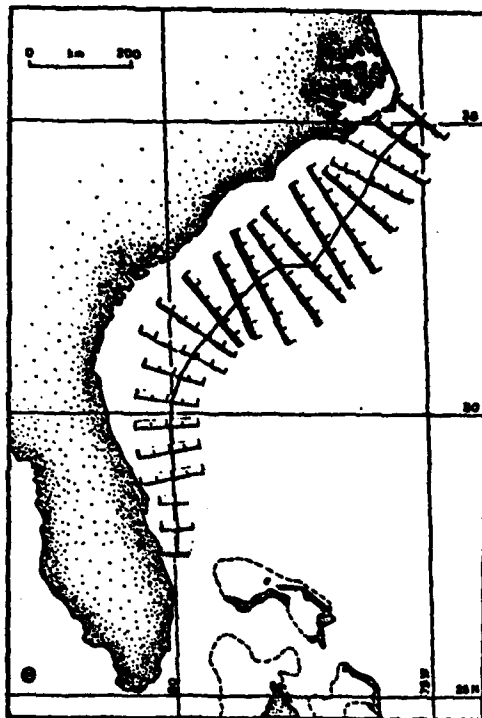


Fig. 4.e.

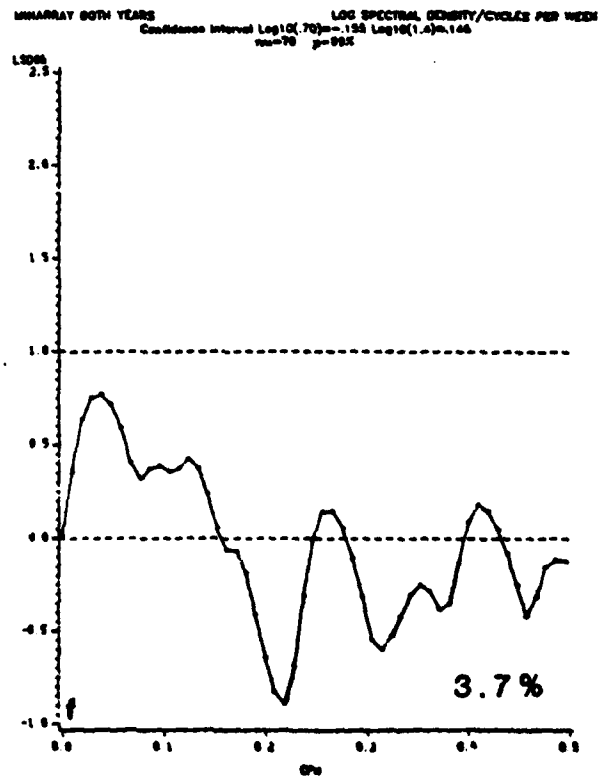
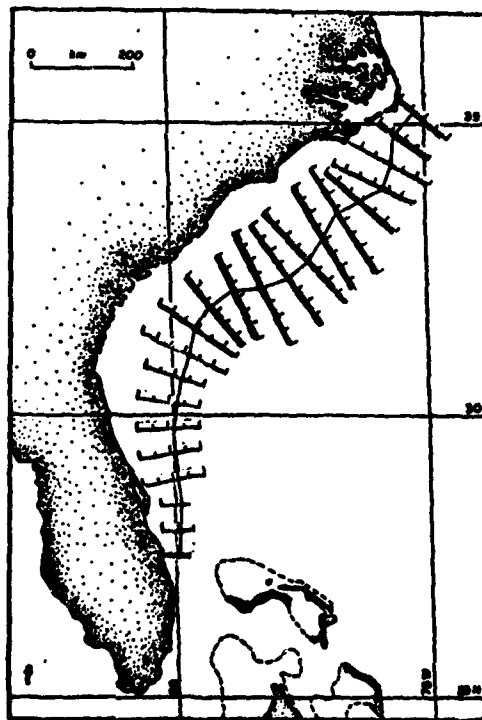
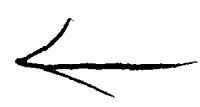


Fig. 4.f.



Energy and Mass Flux in the Gulf Stream

N. P. Fofonoff

Woods Hole Oceanographic Institution

Abstract

Estimates of the kinetic energy and momentum fluxes of the Gulf Stream are obtained from the meridional hydrographic sections taken during the Gulf Stream '60 surveys (Fuglister, 1963). The kinetic energy flux appears to be higher than the input of potential energy by wind stress requiring recycling of energy in the Worthington recirculation gyre. The momentum flux divergence is sufficiently large to account for a major fraction of the east-west pressure difference in the North Atlantic at Gulf Stream latitudes. The effects of ageostrophic fluxes cannot be ignored in Gulf Stream dynamics. - 10 p. 1045

It is surprising to me that despite a substantial literature on the Gulf Stream and its dynamics, there is comparatively little discussion or estimation of the energy fluxes that must accompany the mass flux. It seemed, therefore, appropriate to devote some effort to examining the energy sources, sinks and fluxes at this workshop on Gulf Stream structure and variability. I hope that a description of some of the outstanding problems will encourage new looks at the energetics of the Stream.

On examining the Gulf Stream recirculation gyre postulated by Worthington (1972, 1976), shown in Fig. 1, one is struck by the continued acceleration and intensification of the Stream well past Cape Hatteras. What is the mechanism that concentrates the flow and generates the kinetic energy that is fluxed seaward of the Cape? East of 60°W, the Stream is depicted as losing mass flux almost uniformly to the westward recirculation in the Sargasso. Is Worthington's schematic portrayal of the recirculation energetically consistent? How does the westward flow regain its energy to reform the Stream? Clearly, the energy must be recycled as well as the mass.

A brief examination of the energy cycle in ocean circulation may be helpful. In my simplified look, the major source of energy is assumed to be the work done on the ocean surface by wind stress. If the surface velocity in the ocean is separated into an Ekman component v_e and a geostrophic component v_g , the total work per

unit area is given by

$$W_t = \tau \cdot (\underline{v}_e + \underline{v}_g)$$

where τ is wind stress. As the Ekman layer is steady on the average and is not accumulating energy, dissipation must balance the energy input. Thus, the portion $\tau \cdot \underline{v}_e$ must be dissipated entirely in the Ekman layer and is not available to drive the mean circulation. The remaining portion $\tau \cdot \underline{v}_g$ is the energy supply for the mean flow. It is easy to show that this term represents a contribution to potential energy and not to kinetic energy.

The geostrophic velocity at the ocean surface is given in terms of the pressure gradient by

$$\underline{v}_g = (\underline{k} \times \nabla p) / \rho f = (\underline{k} \times g \nabla \eta) / f$$

where \underline{k} is a unit vector, p is pressure, ρ density, f Coriolis parameter, g gravity and η the free surface measured relative to a geopotential surface. The work can be written

$$\begin{aligned} W &= \tau \cdot \underline{v}_g = \tau \cdot (\underline{k} \times g \nabla \eta) / f \\ &= -g \nabla \eta \cdot (\underline{k} \times \tau) / f = \underline{v}_e \cdot g \nabla \eta \end{aligned}$$

where \underline{v}_e is Ekman transport. Thus, the work done by the wind stress is simply the Ekman mass transport driven up or down the slope induced by the surface geostrophic current. As this term represents a flux of mass across geopotential surfaces, it is a contribution to potential energy.

Potential energy is determined by the mass distribution relative to geopotential surfaces and is a function of position. Consequently, there cannot be a flux of potential energy. Rather, energy is transferred as pressure work or kinetic energy flux and accumulated as potential energy.

Energy input by wind stress depends on the distribution of surface geostrophic currents, or, more directly, on surface slopes. Thus, although the total mass transport is fixed by the vorticity constraint of the Sverdrup equation, the energy input is not. For a fixed total transport, the work done by wind stress will depend on the velocity profile. Fofonoff (1981) estimated the energy input by wind stress over the North Atlantic subtropical gyre to be 20×10^9 watts, using values of mean wind stress of $.05 \text{ N m}^{-2}$ and surface geostrophic current speeds of 0.04 m s^{-1} over an area of 10^{13} m^2 ($2000 \times 5000 \text{ km}$). The estimate is very rough and should be computed more accurately. This energy is accumulated as potential energy by Ekman flux into the anticyclonic region of the circulation. Conversion to kinetic energy occurs, most likely, as flow down a pressure gradient within the Gulf Stream. If the flow were simply accelerating down the pressure gradient with no dissipation, the Bernoulli function would be constant along streamlines indicating conversion from pressure work $p \nabla \cdot \mathbf{v}$ to kinetic energy flux $\frac{1}{2} \rho (\mathbf{v} \cdot \mathbf{v}) \mathbf{v}$.

Does this simple interpretation fit the Gulf Stream? Estimates of the kinetic energy flux in the Gulf Stream are rare. In Fig. 2 values obtained using geostrophic calculations from the meridional Gulf Stream '60 hydrographic stations (Fuglister, 1963) are compared with an inertial two-layer model (Fofonoff, 1962) having the same dimensions and mass transport. In the model, 86% of the kinetic energy flux and 69% of the momentum flux take place within one Rossby radius of deformation (40 km) of the jet edge, while only 40% of the mass transport is contained within this width.

The fluxes are sensitive to station spacing and positioning relative to the Stream edge, but not very sensitive to choice of reference levels deeper than 2000 decibars. The range of variation is about 20% for reference levels between 2000 and 4000 decibars. In Section 1, near the point of maximum intensity of the Stream, the momentum and kinetic energy fluxes exceed the model fluxes but drop quickly below the model downstream. The maximum kinetic energy flux is several times the energy input by wind stress, indicating that energy is being recycled in the recirculation gyre if the estimates are to be believed.

If the energy is recycled, an opposing pressure gradient must act to convert kinetic to potential energy. As the Stream is a free jet, the opposing gradient has to extend into the Slope Water region to the north resulting in a geostrophically balanced outflow to the Slope Water. An analogous argument leads to the conclusion that the accelerating Stream past Cape Hatteras requires a dropping pressure and an inflow or entrainment of Slope Water if the Stream is detached from the coastal boundary.

If the kinetic energy is not fully recovered along a streamline and is not replaced from another source, the Stream line cannot join the recirculation region and must depart to rejoin the larger scale Sverdrup interior flow.

The estimates presented here indicate that the kinetic energy flux in the Stream is several times the energy input by wind stress requiring the recirculation gyre to recycle most of its energy. The estimate for wind stress work is very shaky and may be considerably larger than given. There are also other sources such as heating that can contribute to the potential energy. The contributions have not been examined. Because the kinetic energy flux is confined primarily to the highest velocity core of the Stream, it is possible that the recirculation gyre contains a smaller fraction of the total energy flux. In the inertial jet, 60% of the mass flux contains only 14% of the kinetic energy flux.

The momentum flux decreases from about 100 Newtons at Section I to 40 Newtons at Section IX. This flux divergence is equivalent to a force acting downstream over the width of the Stream. As most of the flux is confined to the high speed core, an estimate of the total force is the flux divergence divided by the Rossby radius of deformation, i.e., $\Delta MF/R$. For a radius of deformation of 40 km, the downstream force attributable to the momentum flux divergence is equivalent to the Coriolis force acting on a meridional transport of 15 Sverdrups (15×10^9 kg/s). Thus, a major fraction of the east-west pressure differences across the North Atlantic at Gulf Stream latitudes can be balanced by the ageostrophic flux divergence in the Stream without

invoking unreasonably large meridional transports.

In summary, the kinetic energy and momentum fluxes are sufficiently large that their effects cannot be ignored in describing the dynamical balances of the Gulf Stream.

References

- Fofonoff, N. P., 1962. Dynamics of ocean currents. In: The Sea: Ideas and observations on Progress in the Study of the Seas, 1: Physical Oceanography, M. N. Hill, Editor, Wiley, Interscience, New York, pp. 323-395.
- Fofonoff, N. P., 1981. The Gulf Stream System. In: Evolution of Physical Oceanography, B. A. Warren and C. Wunsch, Editors, The M.I.T. Press, Cambridge, Mass., pp. 113-139.
- Fuglister, F. C., 1963. Gulf Stream '60. Progress in Oceanography 1: 265-373.
- Worthington, L. V., 1962. Evidence for a two-gyre circulation system in the North Atlantic. Deep-Sea Research, 9, 51-67.
- Worthington, L. V., 1976. On the North Atlantic Circulation. The Johns Hopkins Oceanographic Studies, Number 6. The Johns Hopkins University Press, Baltimore MD, 110 pp.

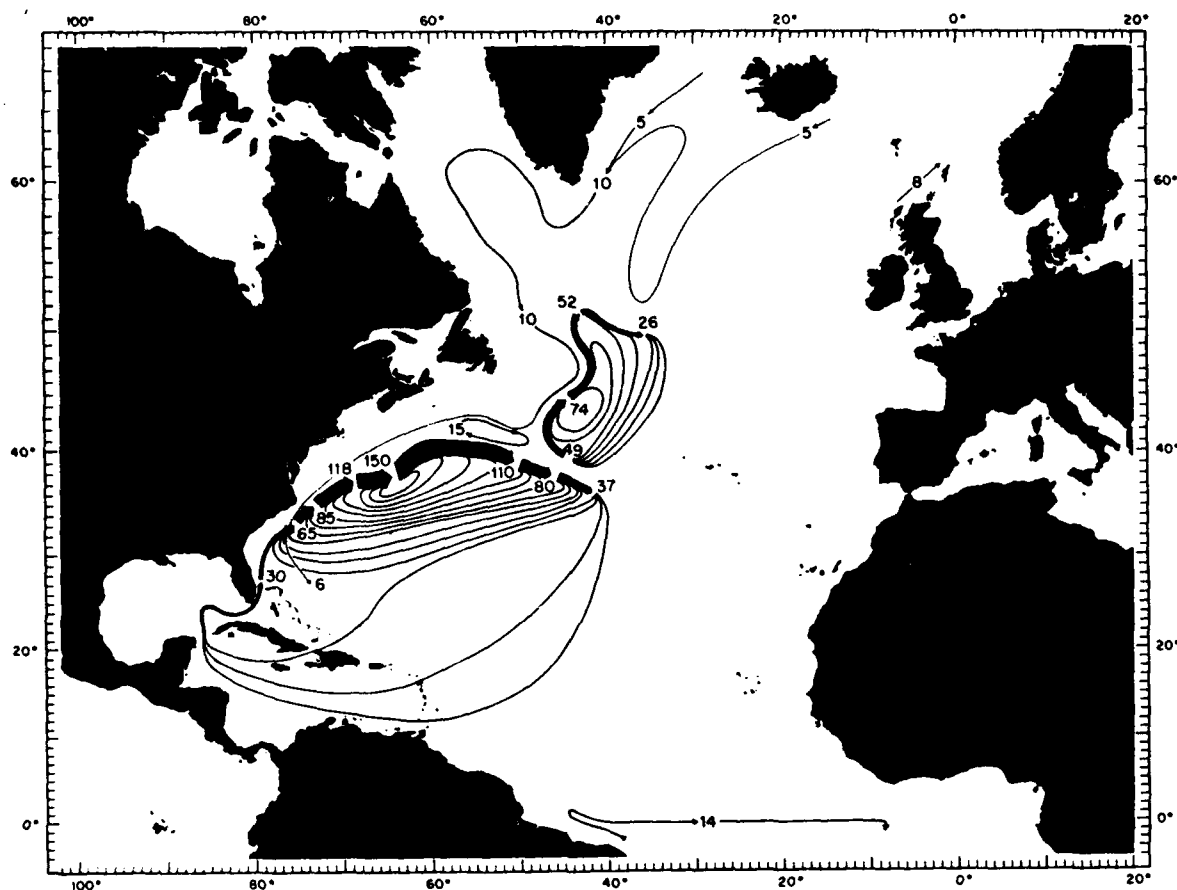
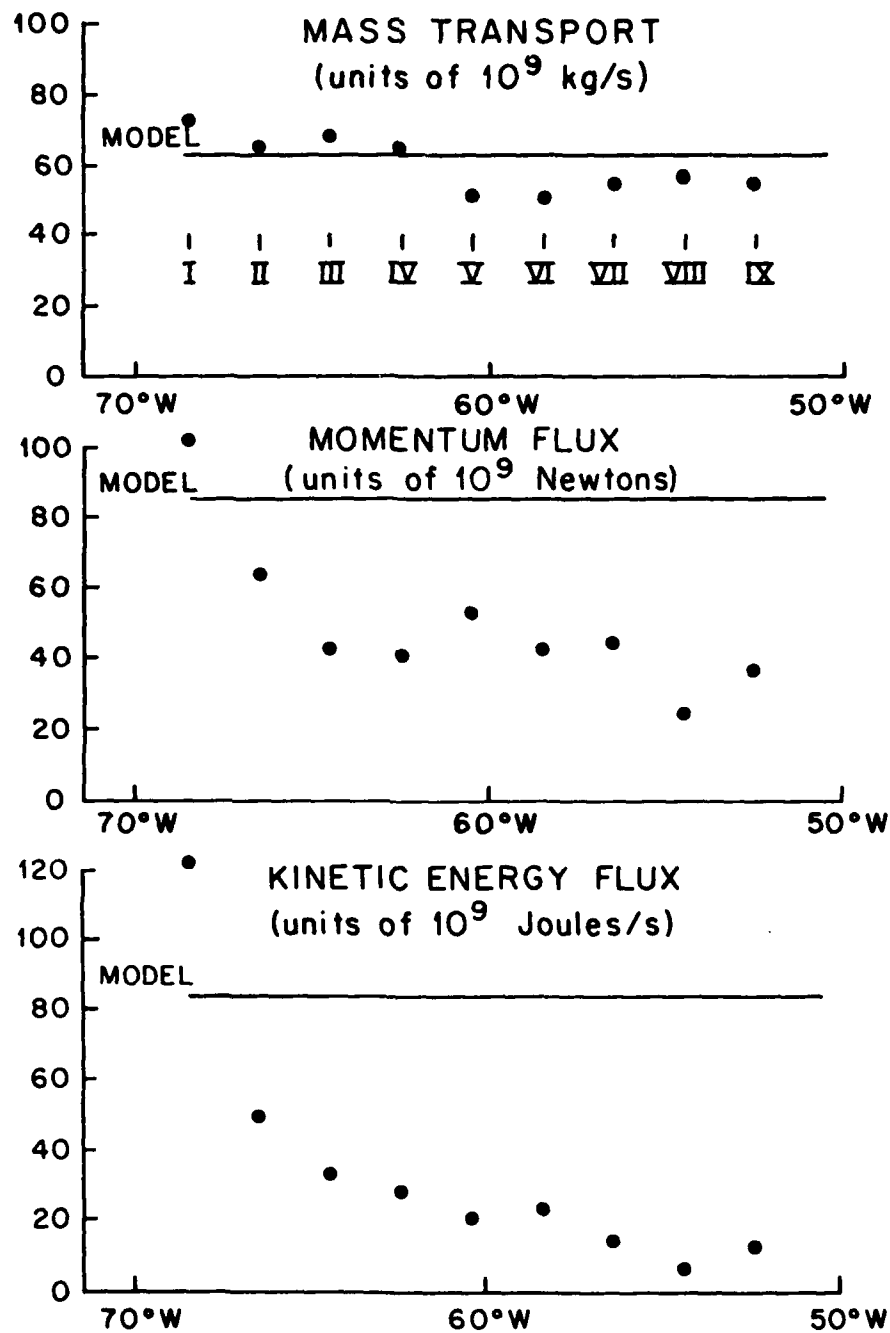


Figure 1. The Gulf Stream recirculation gyre proposed by Worthington
The contour interval is approximately 10×10^9 kg/s.

GULF STREAM '60 SECTIONS



W.H.O.I.
FOFONOFF

Figure 2. Estimates of mass, momentum and kinetic energy fluxes obtained from Gulf Stream '60 meridional hydrographic sections compared with a two-layer inertial jet having the same mass transport.

MODELS OF GULF STREAM VARIABILITY -- AN OVERLY BRIEF REVIEW

Dale B. Haidvogel

Department of Physical Oceanography
Woods Hole Oceanographic Institution
Woods Hole, Massachusetts 02543

1. Introduction

As the title suggests, it will be possible here to briefly touch on a few of the theoretical and numerical models which have been advanced to account for Gulf Stream variability. In particular, a limited number of the relevant research papers will be explicitly mentioned. Fortunately, more extensive reviews have recently been provided by Fofonoff (1981) and Watts (1982). These reviews, and the papers referred to herein, may be sought for further detail.

As observations have increased in availability and coverage, it has become clear that the Gulf Stream System -- from its origin at the Florida Straits until its eventual disappearance (somewhere) downstream of Cape Hatteras -- is dynamically complex, and potentially composed of several distinct dynamical regimes. It is not surprising then that, although a variety of theoretical explanations have been examined, no single model available today offers a complete dynamical account of the space/time variability of the Gulf Stream, nor seems to apply over more than a fraction of the length of the Stream. Before examining some of the existing models, we review some of the known features of Gulf Stream variability for which theoretical explanations have been sought.

1.1 Kinematic properties

Many studies of Gulf Stream meanders have been made, both between the Straits of Florida and Cape Hatteras (e.g., Maul et al., 1978) and between Cape Hatteras and the Grand Banks (Hansen, 1970; Robinson, Luyten, and Fuglister, 1974). These studies incorporate data from a wide variety of sources: hydrographic and XBT surveys, moored and free-fall current meter measurements, and surface temperature obtained from airborne and satellite surveys. On the basis of these results, a statistical picture is beginning to emerge which indicates Gulf Stream variability on a broad range of scales.

South of Cape Hatteras at Onslow Bay, the dominant contribution to meandering activity is made by motions having periods of 4-6 and (about) 30 days (Maul et al., 1978). The former motions are presumably related to atmospheric forcing at these frequencies [e.g., Brooks (1978)]; however, the origin of the latter band of variance is uncertain. Fluctuations in the transport through the Straits of Florida occur on 1-10 day time-scales, with variability also at lower frequencies [including an ill-defined seasonal cycle (Niiler, 1975)].

Downstream of Cape Hatteras, the Gulf Stream gradually separates from the coast and moves across the continental rise into deeper water. No longer constrained by the presence of the continental boundary, the Gulf Stream undergoes meandering on a wide variety of scales. According to Hansen's (1970) study of meandering between Cape Hatteras and the Grand Banks, motion of the Gulf Stream axis can be adequately characterized as quasi-geostrophic wave patterns with a wavelength of 200-400 km and an

eastward propagation of phase at 5-10 cm/sec. On the basis of aerial surveys, near-bottom current meters, BTs, and near surface drogues, Robinson, Luyten, and Fuglister (1974) tentatively identified three regimes of Gulf Stream variability -- secular, large-scale, and small-scale -- with the associated length and time scales spanning the ranges (250-20) km and (15-2) days. The deep current measurements made by Luyten (1977) beneath the Gulf Stream near 70°W show a more chaotic picture than the near-surface surveys would indicate. Luyten finds burst-dominated near-bottom motions at depths greater than 4000 m, characterized by large (~ 150 km) meridional scales but very short (< 50 km) zonal scales. Phase propagation to the south at 8-15 cm sec⁻¹ was observed.

In summary form, Figure 1 shows mean Gulf Stream displacement as a function of distance along its mean path. Local maxima occur in association with the seaward deflection of the Stream near the Charleston Bump (Bane and Brooks, 1979) and downstream of Cape Hatteras, where expected meander amplitudes approach 100 km. Despite this nearly monotonic downstream increase in meander amplitude, however, the time scales on which meandering occurs show substantial along-path variability (Figure 2). Strong temporal intermittency of meander properties is also suggested [e.g., Legeckis (1979)]. Table 1, taken from Watts' (1982) review, gives a general picture of the observed time and space scale of Gulf Stream path variability.

1.2 Dynamical/energetic properties

In the surface layers of the Florida Current, energy transfer measurements indicate that the time-mean current systematically derives

kinetic energy from the fluctuating field of motions in the onshore region of cyclonic shear (Brooks and Niiler, 1977). Systematic local transfers of potential energy between the mean and fluctuating motions also appear to be taking place. However, although strong local conversions of eddy energy to mean flow energy apparently occur, the total cross-stream transfer of energy from transient to mean motions is small, and not reliably known. Strong depth dependence of these energy conversions has also been observed (Brooks and Niiler, 1977). Similar energetic behavior has been observed at other locations between the Florida Straits and Cape Hatteras -- for instance, off Onslow Bay, North Carolina (Brooks and Bane, 1981).

Few direct measurements of energy transfer between the time-mean and fluctuating current have been made downstream of Cape Hatteras. Array measurements of current and temperature in the Gulf Stream recirculation (31°N , $69^{\circ}31'\text{W}$) indicate a strong net conversion of available potential energy from the mean circulation to the eddies (Bryden, 1982). Although the eddies appear to lose kinetic energy in their interaction with the mean, there is no clear associated local production of mean kinetic energy; that is, the eddies do not seem to drive the mean flow in this region. Across the Continental Rise near 70°W , Luyten (1977) finds strong eddy to mean conversions of kinetic energy in the deep Gulf Stream. By comparison, energetic calculations from four current meter records in deep waters under the Gulf Stream off Cape Hatteras indicate a flux of kinetic energy from the mean flow to the fluctuations, with little net transfer of potential energy (Watts and Johns, 1982).

2. Theoretical and Numerical Studies

2.1 Local dynamical models

Two early theoretical approaches were used to provide local dynamical descriptions of the observed statistics of Gulf Stream path variations. These local theories typically use estimates of the integral properties of the Gulf Stream (mean transport, bottom velocity, and so on) to predict higher order statistical properties of the Gulf Stream including the time and space scales characterizing the motion of its path, and the energy transfers occurring between the time-mean and fluctuating components of motion.

Assuming that Gulf Stream current paths are associated with conservation of potential vorticity and that topographic effects dominate, Warren (1963) first showed how the free current path of the Gulf Stream could be obtained from a simple integro-differential path equation, once the cross-sectional integral properties of the Stream were known. Under this theory, the variety of observed meander patterns was attributed to fluctuations in the inlet conditions -- mean transport, bottom speed, direction of flow, etc. -- at Cape Hatteras. Niiler and Robinson (1967) constructed a more elaborate steady-state theory for free inertial currents above topography. This theoretical model pictures a narrow current of high velocity and high relative vorticity ($\zeta = f$) embedded in a slow geostrophic flow ($\zeta \ll f$). Using the inviscid, Boussinesq, β -plane equations and neglecting cross-stream variations in f , bottom topography and flow curvature, they were able to derive an equilibrium path equation valid for paths of small curvature ($\kappa \ll$ stream width). A

statistical comparison of model-predicted position and wavelength information with the Warren (1963) data set showed that the steady-state inertial jet model was capable of reproducing the observed mean control path of the Gulf Stream; however, predicted meander wavelengths were too long. Further, Niiler and Robinson concluded that steady-state non-divergent theories such as theirs and Warren's cannot account for the details of individual Gulf Stream paths. A time-dependent meandering model for a thin baroclinic jet moving over bottom topography has been developed and elaborated by Robinson, Luyten, and Flierl (1975), and Robinson and Flierl (1982).

The properties of unstable quasi-geostrophic wave disturbances which increase their amplitude through interaction with the basic state current have been examined many times as prototype mechanisms for the origin of Gulf Stream variability. Lipps (1963) studied the properties of barotropically unstable disturbances in a divergent finite-depth ocean. For a fixed (sech^2) jet structure of 30 km half-width (L_5) and maximum velocity (V_m) of 150 cm sec^{-1} in a layer of 550 m in thickness, the maximally unstable disturbances have a wavelength of 180 km, a four-day e-folding growth time, and an eastward-directed phase speed of 50 cm sec^{-1} . The source of energy for these growing perturbations is the kinetic energy of the basic state current.

With the addition of vertical shear to the mean currents, growth of waves at the expense of the field of mean potential energy is also possible. Orlandi (1969) has studied the influence of underlying topography on the baroclinic instability problem for the Gulf Stream.

With assumed exponential profiles for the basic state velocity ($V_m = 150 \text{ cm sec}^{-1}$, $L_S = 50 \text{ km}$) and a bottom topography profile reminiscent of shelf-slope conditions, Orlanski predicts a maximally unstable disturbance wavelength (365 km) and phase speed (7 cm sec^{-1}) close to those observed by Hansen (1970). As in the case of the pure barotropic instability studies, however, the predicted linear growth time (~ 3 days) is too short for favorable comparison with observations of Gulf Stream meander evolution. In Orlanski's model, the transient disturbances derive their energy from the potential energy of the mean field; simultaneously, energy is transferred from eddy to mean kinetic energy, a direction of energy transfer in accord with the direct measurements made by Webster (1965) and Luyten (1977).

The mixed stability analysis for a representative Gulf Stream current distribution has been studied in the two-layer quasi-geostrophic limit by Holland and Haidvogel (1980). For Flierl's (1975) equivalent two-layer Gulf Stream model (derived from data taken in the neighborhood of the Stream), the resulting mixed stability analysis yields a maximally unstable mode with a wavelength of 308 km, an eastward propagation speed of 19 cm sec^{-1} , a period of 18.6 days, and an e-folding time of 6.0 days. These kinematic features roughly coincide with those assigned by Robinson et al. (1974) to the Gulf Stream "large-scale" space-time variability. In this mixed instability, the unstable waves obtain 90 percent (10 percent) of their energy from the mean potential (kinetic) energy of the basic state current. Similar mixed stability results are obtained if actual observed Gulf Stream velocity profiles are used to construct the basic

state current demanded by the linear theory; however, the theoretical justification for using synoptic velocity data in this way is meagre.

Although linearized stability theories do appear to predict time and space scales of Gulf Stream variability near to those observed, their dependence on the assumption of linearity is troubling, particularly in view of the inarguable finite-amplitude character of the Gulf Stream meandering process. As has been seen to be true in studies of quasi-geostrophic turbulence [e.g., Haidvogel and Held (1980)], however, some aspects of the linear dynamics of the unstable waves may indeed survive into the finite-amplitude meandering state. The extent to which this is the case awaits further simulation of the finite-amplitude meandering problem [e.g., Ikeda (1981), Thompson and Hurlburt (this volume), and Haidvogel and Killworth (1982) -- see also Figure 3].

2.2 Eddy-resolving numerical models of the Gulf Stream

In recent years, a new class of ocean general circulation models which include explicit fine-scale spatial resolution of mesoscale eddy effects has been developed (Holland, 1978). These EGCMs, or eddy-resolving general circulation models, allow explicit examination of direct energy transfers between the large-scale oceanic circulation (of which the Gulf Stream is a prominent component) and motion on smaller (50-200 km) scales. A review of these recent modeling efforts has been given by Robinson, Harrison, and Haidvogel (1979). These dissipative, fully nonlinear models can take explicit account of complex topographic and inertial effects (which seem to determine, at least in a statistical

sense, the path of the Gulf Stream) and finite-amplitude eddy-mean field interactive effects. As they are applied in increasingly realistic situations, they promise estimates of Gulf Stream space-time variability and energetic properties of increasing sophistication. Comparisons of model-derived eddy energy and Reynolds stress distributions with deep moored current meter data are underway (Schmitz and Holland, 1982; see also Holland's review in this issue). Further predictions of local vorticity, energetic, and thermodynamic balances within the Gulf Stream region can be expected in the near future from these, and other, dynamical models. [For instance, local simulations of the mean Gulf Stream frontal structure, and comparison with satellite-derived altimeter observations are underway (e.g., Kao, 1979).]

3. Discussion and Future Prospects

Many questions concerning the dynamic origins and implications of Gulf Stream variability remain. Nonetheless, observations and models are now developed to the point where significant interaction between them is possible in the near future. For instance, the numerical tools presently exist for a non-linear simulation of Gulf Stream variability between the Florida Strait and Cape Hatteras, including the important effects of bottom topography (e.g., the Charleston bump). Because meanders are observed to decay downstream from Charleston, a satisfactory numerical model for this region could probably be formulated within a periodic channel geometry (oriented along-coast).

Beyond Cape Hatteras, meanders grow systematically downstream; therefore, the formulation of an appropriate initial-boundary value

problem for Gulf Stream variability in this local region will be difficult. Of particular import here is whether meander evolution is dictated by the imposed "inlet" conditions, or by internal physics (e.g., hydrodynamic instability). If predominantly the former, then a purely statistical forecast of meander evolution (or some applicable form of deterministic path model) may be all that is needed to "predict" meander evolution. If internal effects, such as local energy transfers, are also important, more complicated dynamical models may be necessary. Both regional models of the Gulf Stream System, and global eddy-resolving models of the entire North Atlantic circulation including the Gulf Stream need to be pursued.

New observations aimed at providing critical tests of model predictions will also be needed. For example, intensive local experiments in the Gulf Stream should be considered to provide enhanced deterministic and statistical information on the kinematics (space/time properties) of meander evolution. Reliable measurements of the energetic/dynamic balances within various regimes of the Gulf Stream System will also be particularly valuable in validating the meandering and eddy shedding mechanisms operative in mesoscale resolution ocean circulation models.

4. Acknowledgements

The author's work on models of the Gulf Stream is supported by the Office of Naval Research under contract N00014-C-0019, NR083-004 to the Woods Hole Oceanographic Institution.

5. References

- Bane, J. M. and D. A. Brooks (1979). Geophysical Research Letters, 6, 280.
- Brooks, D. A. (1978). Journal of Physical Oceanography, 8, 481.
- Brooks, D. A. and J. M. Bane (1981). Journal of Physical Oceanography, 11, 247.
- Brooks, I. H. and P. P. Niiler (1977). Journal of Marine Research, 35, 163.
- Bryden, H. L. (1982). Submitted for publication.
- Flierl, G. (1975). Ph.D. dissertation, Harvard University.
- Fofonoff, N. P. (1981). Evolution of Physical Oceanography, pp. 112.
- Haidvogel, D. B. and P. B. Killworth (1982). In preparation.
- Haidvogel, D. B. and I. M. Held (1980). Journal of the Atmospheric Sciences, 37, 2644.
- Hansen, D. V. (1970). Deep-Sea Research, 17, 495.
- Holland, W. R. (1978). Journal of Physical Oceanography, 8, 363.
- Holland, W. R. and D. B. Haidvogel (1980). Dynamics of Atmospheres and Oceans, 4, 185.
- Ikeda, M. (1981). Journal of Physical Oceanography, 11, 526.
- Kao, T. W. (1979). NASA Technical Memorandum 80335.
- Legeckis, R. V. (1979). Journal of Physical Oceanography, 9, 483.
- Lipps, F. B. (1963). Journal of the Atmospheric Sciences, 20, 120.
- Luyten, J. R. (1977). Journal of Marine Research, 35, 49.
- Maul, G. A., P. W. DeWitt, A. Yanaway, and S. R. Baig (1978). Journal of Geophysical Research, 83, 6123.

- Niiler, P. P. (1975). In: Numerical Models of Ocean Circulation, National Academy of Sciences, pp. 216-236.
- Niiler, P. P. and A. R. Robinson (1967). Tellus, 19, 601.
- Orlanski, I. (1969). Journal of the Atmospheric Sciences, 26, 1216.
- Robinson, A. R. and G. R. Flierl (1982). In preparation.
- Robinson, A. R., D. E. Harrison, and D. B. Haidvogel (1979). Dynamics of Atmospheres and Oceans, 3, 143.
- Robinson, A. R., J. R. Luyten, and G. Flierl (1975). Geophysical Fluid Dynamics, 6, 211.
- Robinson, A. R., J. R. Luyten, and F. C. Fuglister (1974). Journal of Physical Oceanography, 4, 237.
- Schmitz, W. J. and W. R. Holland (1982). Journal of Marine Research, 40, 75.
- Warren, B. A. (1963). Tellus, 15, 167.
- Watts, D. R. (1982). To appear in: Eddies in Marine Science; A. R. Robinson, editor.
- Watts, D. R. and W. E. Johns (1982). Journal of Geophysical Research, submitted.
- Webster, F. (1965). Tellus, 17, 239.

Table 1. Gulf Stream Path Variability
From Watts (1982)

	Florida Straits	Carolina Capes	Cape Hatteras 73°-75°W	~ 65° - 70°W
Periodicities (days)	9-12 (d) 10-13 (k) 7-14 (c)	3 - 8 (b) 4 - 7 (m) 30 -36 (l)	2 - 60 (l)	50 - 60 (f) 45 (i) 12 - 25 (j) ~ 6 (j)
Wavelengths (km)	170 (j) 1000 (c)	200-250 (b) 90-260 (h)	150- 600 (l)	320 -360 (f) 130 -190 (j) ~250 (j) 200 -400 (g)
Propagation Speeds (km day ⁻¹)	17S (k) 100S (c)	30- 45N(b) 40N(h)	18 -36NE(l)	6 - 7E (f) 5 - 8E (j) ~22E (i) 5 -10E (g) ~17E (e)
Amplitude rms (km)	5 (a)	10- 25 (a) 10 (m)	15 -30 (l)	50 -80 (f)
Growth and Decay Characteristics	Slow growth	Perturbation at "Charleston Bump" and decay downstream	Rapid growth	Moderate growth
Comments	Seasonal variation in transport			Wavelength decreases as amplitude increases downstream (f) interannual shifts >50 km (f)

- (a) Bane and Brooks (1979)
 (b) Brooks and Bane (1981)
 (c) Brooks and Mooers (1977)
 (d) Düling et al. (1977)
 (e) Fuglister and Worthington (1951)
 (f) Halliwell and Mooers (1979)
 (g) Hansen (1970)

- (h) Legeckis (1979)
 (i) Maul et al. (1980)
 (j) Robinson et al. (1974)
 (k) Schott and Düling (1976)
 (l) Watts and Johns (1982)
 (m) Webster (1961)

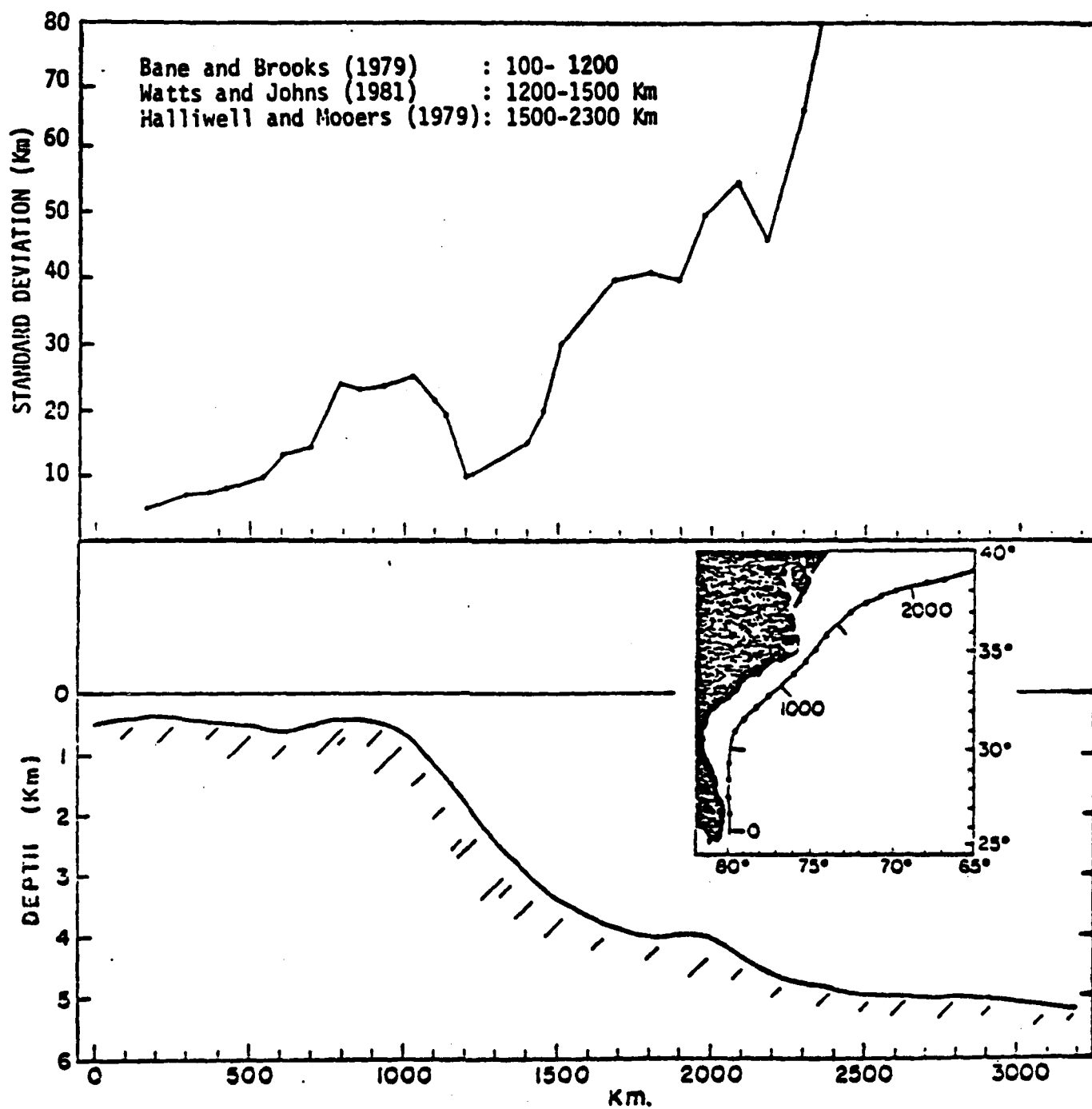
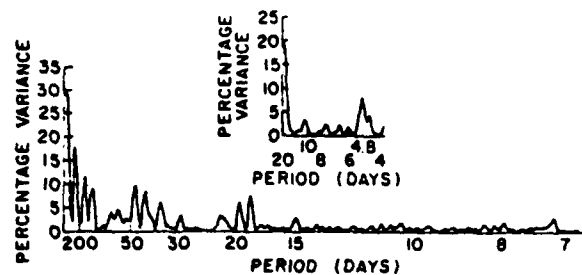


Figure 1. RMS displacement of the Gulf Stream path as a function of downstream distance. From Watts (1982).

70°W



ONslow BAY, N.C.

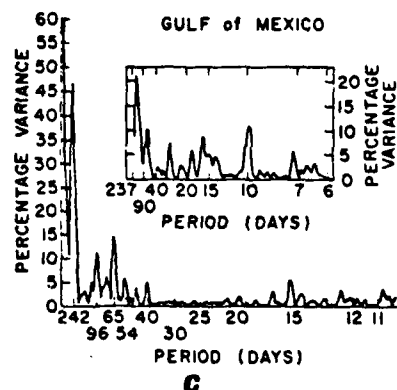
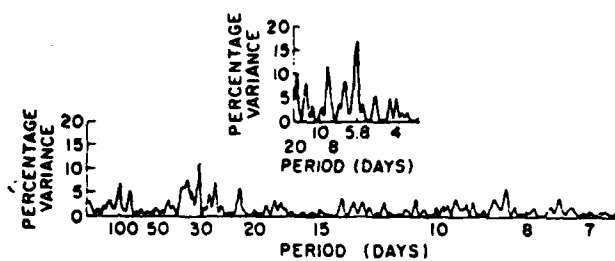


Figure 2. Least squares analyzed spectra of Gulf Stream meanders at three locations: (a) South of Cape Cod along 70°W longitude; inset is 70° spectrum for days 420-522 only; (b) along a line orthogonal to the coast in the offing of Onslow Bay; inset is Onslow Bay spectrum for days 402-504 only; (c) along 86°W longitude in the eastern Gulf of Mexico; inset is Gulf of Mexico spectrum for days 277-514 only. From Maul et al. (1978).

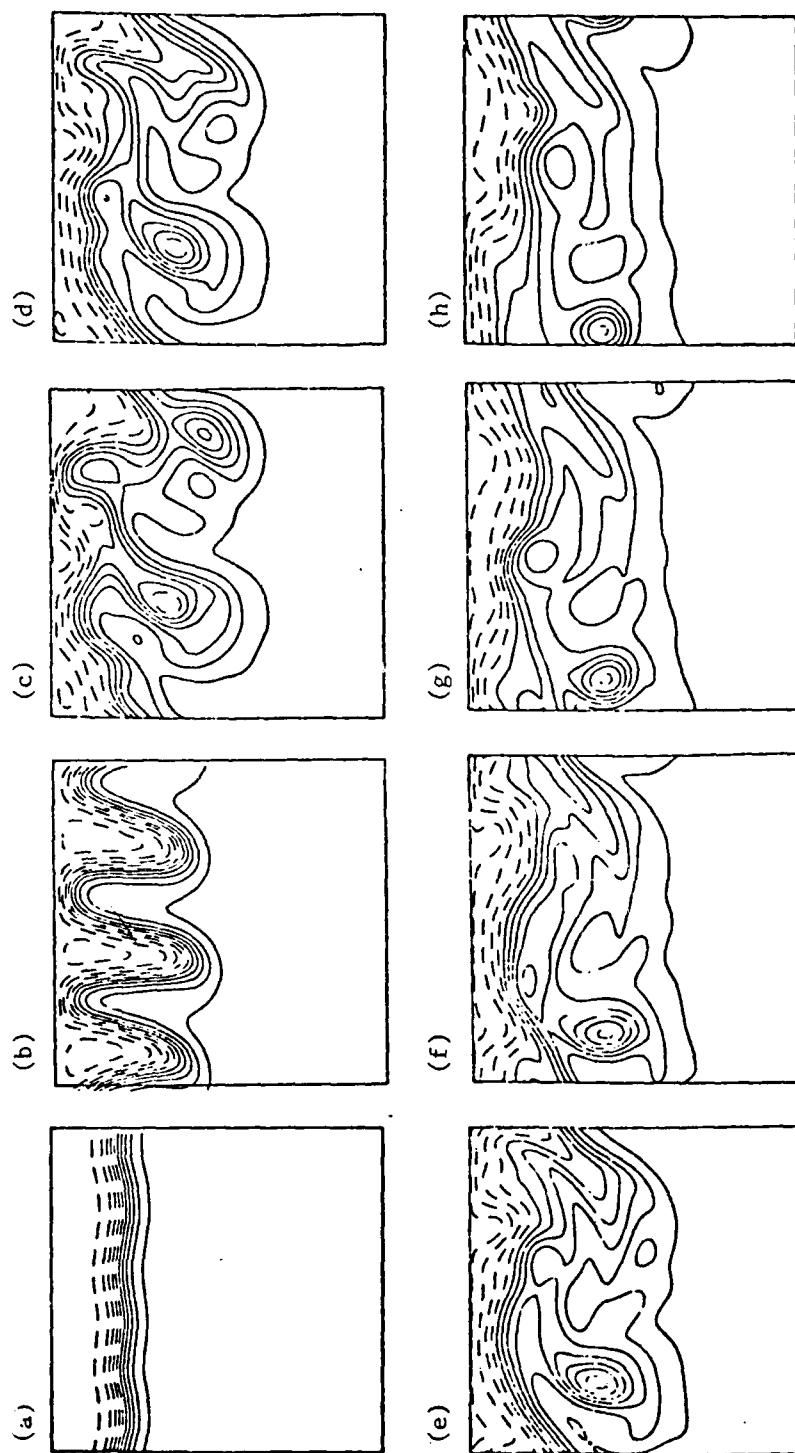


Figure 3. The non-linear evolution of a baroclinic Gulf-Stream-like jet in an x-periodic channel 1000 km on a side. The initial ($t=0$) jet profile is $\text{sech}^2(y)$ with a jet width $(l/a) = 50$ km. The amplitude of the barotropic mode -- see Figure 2 -- is chosen such that the total jet transport equals $100 \times 10^6 \text{ m}^3/\text{sec}$. The amplitude of the baroclinic mode is 0.9 times the amplitude of the barotropic mode (as suggested by observations). (a) $t = 30$ days, the most unstable linear perturbation begins to reach a perceptible amplitude; (b) $t = 60$ days, well-ordered finite-amplitude meanders result from the linear stability process; and (c) - (h), $108 \leq t \leq 138$ days at intervals of 6 days, the jet eventually goes turbulent and, as shown here, sheds small-scale rings which propagate away from the source region. The process of eddy shedding, and its implications for the energetics of the mid-ocean, are presently under examination.

SIMULATION OF NORTH ATLANTIC VARIABILITY

by William R. Holland
National Center for Atmospheric Research
Boulder, CO

Studies using idealized eddy resolved models of ocean circulation continue to be useful in unravelling the mechanisms by which the large-scale wind-driven midlatitude gyres reach a statistical equilibrium. It is now apparent that instabilities in the Gulf Stream downstream from Hatteras, in the recirculation region, and on the southern flank of the subtropical gyre itself all lead to mesoscale eddy production with important heat, vorticity and momentum fluxes occurring locally.

The various regions of eddy production, radiation, and decay define an interesting problem: how do we measure, describe, and understand the geography of variability throughout the subtropical gyre? That is, what is the general circulation in this region? By this we mean not only what is the mean flow but what are other statistical properties as well, what is their vertical structure and how do they vary geographically?

In a recent paper, Schmitz and Holland (1982) made a first comprehensive attempt to compare a number of simple quasigeostrophic numerical experiments with observations. For the first time it became clear that the first order problem was to be able to simulate the geographic distributions of variability as measured for example by eddy kinetic energy patterns and to associate these with the large-scale patterns of mean flow. Moreover, it seemed necessary to do this from the near Gulf Stream region to the North Equatorial Current, from the ocean surface to abyssal depths, and from the western boundary to the

eastern basins. While the data are and will continue to be very "broad brush" (i.e., sparse in space and time), the combination of analyses of older data, the collection of new data from a few critical areas, and the development and exploration of realistic numerical models should lead to a much better synthesis of our understanding of the system.

Since the Schmitz and Holland study, EGCM development has proceeded in two ways: (i) simple, steadily forced, wind-driven oceans with rectangular domain and three layers in the vertical, and (ii) a model of the North Atlantic basin with realistic geometry and wind-forcing. I would like to show you a few results from both kinds of models.

Figures 1 and 2 show the mean (time averaged over 5 years) and instantaneous quasigeostrophic streamfunctions for a three-layer ocean in a 4000 km square domain with a single wind gyre of forcing. The friction in the model is a combination of ordinary lateral friction with no-slip boundary conditions ($A = 200 \text{ m}^2/\text{s}$) and bottom friction ($c = 1 \times 10^{-7} \text{ s}^{-1}$). See Holland (1978) for a full discussion of the two-layer version of this model.

Three important regions of eddy generation show up in this calculation: the Gulf Stream (a mixed instability), the recirculation regime (mainly a baroclinic instability), and the shallow Sverdrup flow on the southern flank of the subtropical gyre (completely a baroclinic instability). In all of these regions the eddy energy propagates

mainly westward, filling out the ocean zonally from the region of origin. Figure 3 shows the eddy kinetic energy and eddy potential energy patterns associated with these multiple sources of eddy energy. As in earlier work (Holland, 1978) the deep sea is filled with eddy energy and deep mean gyres are forced by the eddy field.

Three layers allow a better sense of the vertical structure of the circulation and thermocline than earlier two-layer models. In particular, in the far reaches of the gyre (in the Sverdrup region) the flow is mostly confined to the upper layer; i.e., it is a shallow circulation. As one moves into the middle of the gyre, where eddy effects from the recirculation regime begin to be important, the circulation deepens and the second layer begins to take part in the gyral circulation. The deep ocean, however, has important mean flows only very near to (and under) the Gulf Stream. Thus the depth of penetration of the gyre slopes poleward--shallow in the south, thermocline depth in mid-gyre, to the bottom at the Gulf Stream.

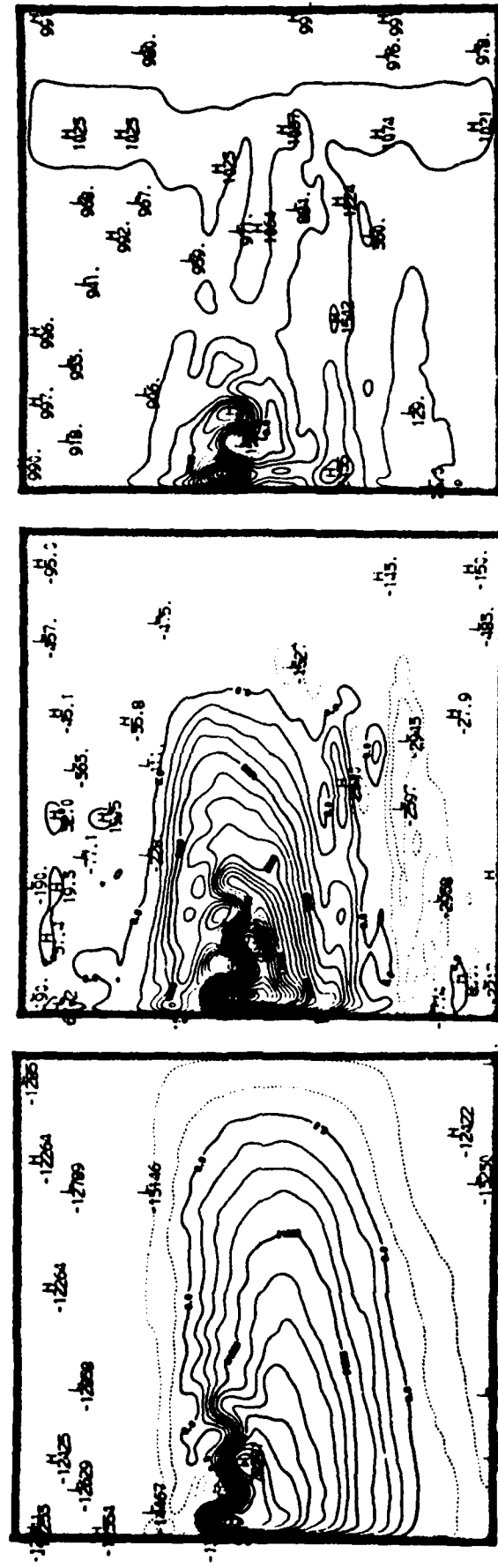
Two discoveries of potential importance were made with the development of these 3-layer models : (i) the southern flank instability produces eddies near the latitudes of the North Equatorial Current (these eddies also drive deep weak mean flows that are like thin zonal jets with velocities of a cm/s or so; see Fig. 1c); (ii) the potential vorticity of the interior of the subtropical gyre (i.e., in the middle layer) becomes homogenized over very large areas. Figure 4 shows maps of mean as well as instantaneous potential vorticity fields in the basin. Note the well-mixed region in the middle layer near the Gulf Stream region.

This finding has led to new theories and observational analyses that suggest the importance of this effect.

I would like to turn now to recent efforts to collect together the best ideas we have developed (in terms of modeling techniques) and put them together into a North Atlantic model. For the case shown, the horizontal resolution is $1/4^\circ$ of latitude and longitude. The depth is constant. Figure 5 shows the mean $\bar{\psi}_i$ for a three-layer model driven by the mean annual Bunker wind stress. Figure 6 shows the patterns of eddy kinetic energy; Fig. 7 shows the patterns of eddy potential energy; and Fig. 8 shows the time averaged potential vorticity in the middle layer. Finally, Fig. 9 shows a time sequence of instantaneous upper layer streamfunction to show something of the time dependence.

These experiments have a realistic flavor to them. Gulf Stream meandering produces warm and cold core Rings, mesoscale eddy energy has about the right amplitude and structure, and the mean flows have about the right strength. Careful and thorough comparisons with observations have yet to be made but we are on the verge of having a true general circulation model of the North Atlantic basin in which we can test our ideas about realistic oceanic flows.

About a half dozen such experiments have now been carried out and we are beginning to home in on an experiment for which a Schmitz and Holland (1982) type observational comparison can best be done. We will then have a solid idea about how well we are doing in simulating the geographical variability (as well as the mean circulation) in a realistic ocean basin.



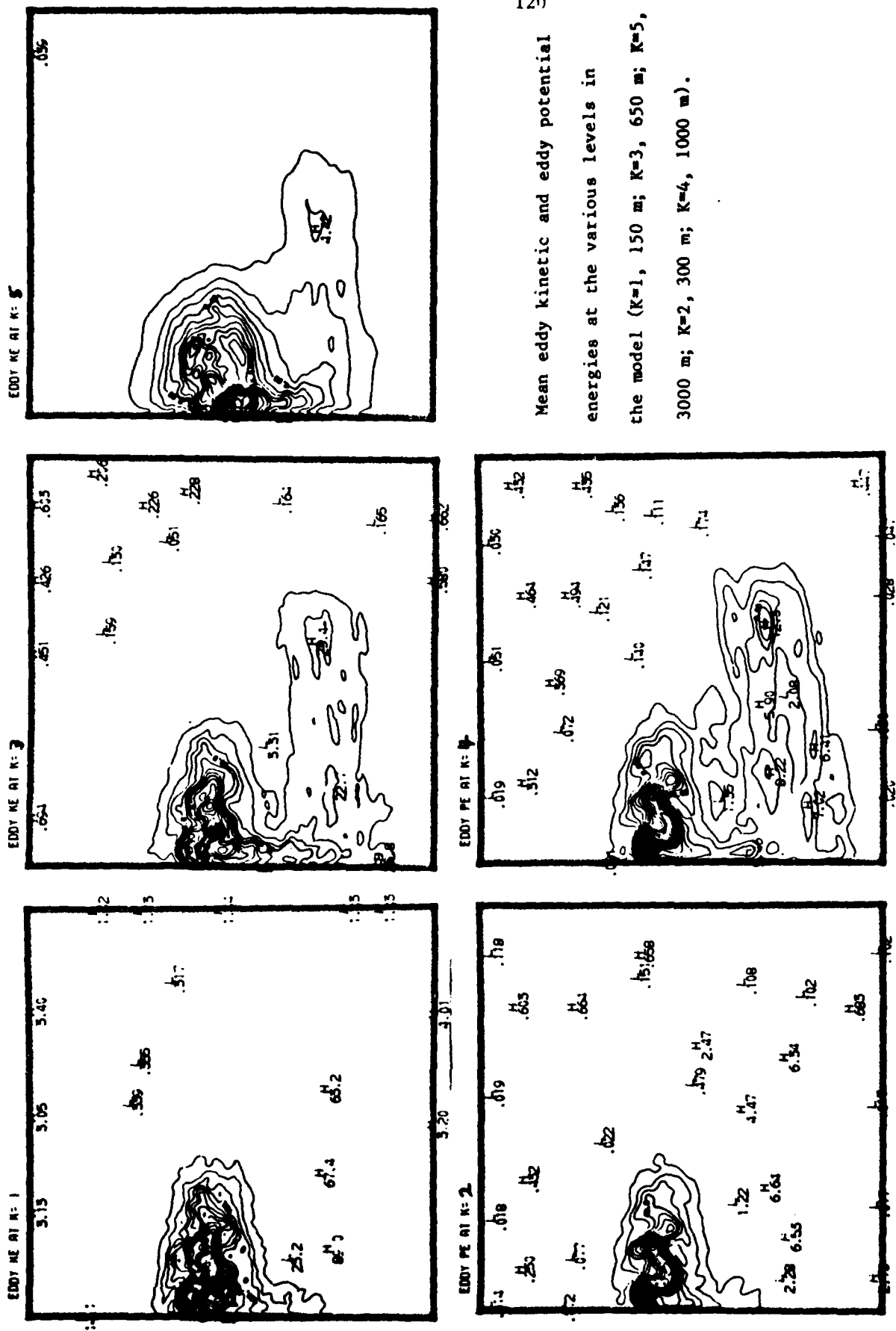
Mean quasigeostrophic streamfunctions at the three levels 150 m,
650 m, and 3000 m.

Fig. 1.



Instantaneous quasigeostrophic streamfunctions at the three levels.

Fig. 2



Mean eddy kinetic and eddy potential energies at the various levels in the model ($K=1$, 150 m; $K=3$, 650 m; $K=5$, 3000 m; $K=2$, 300 m; $K=4$, 1000 m).

Fig. 3.

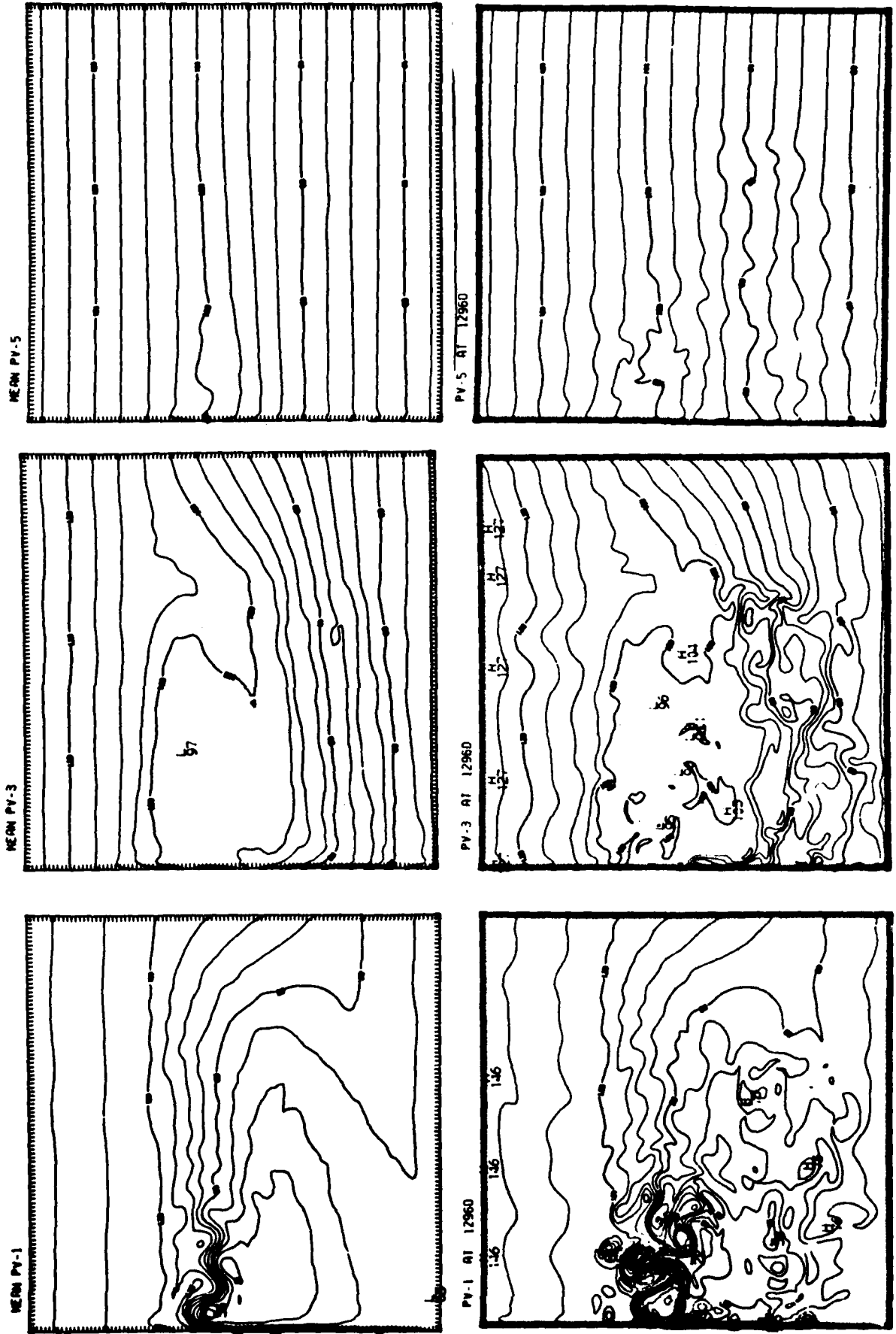
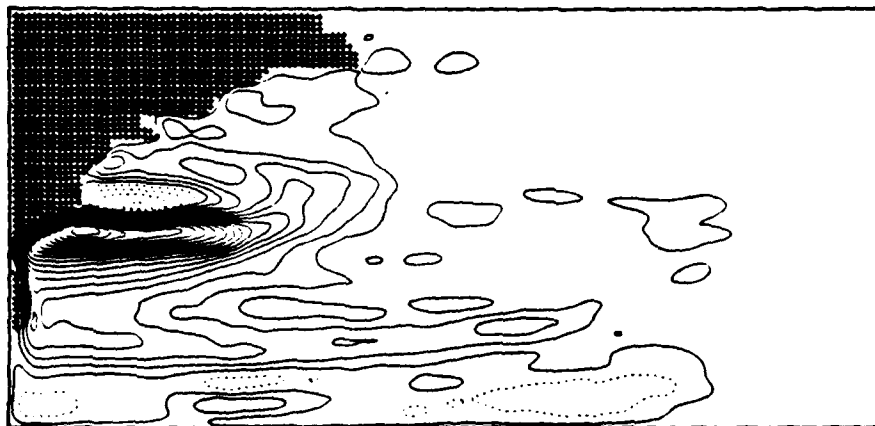


Fig. 4. Mean and instantaneous maps of potential vorticity at three levels in the model.

MEAN PSI 1 CASE 6



MEAN PSI 3 CASE 6

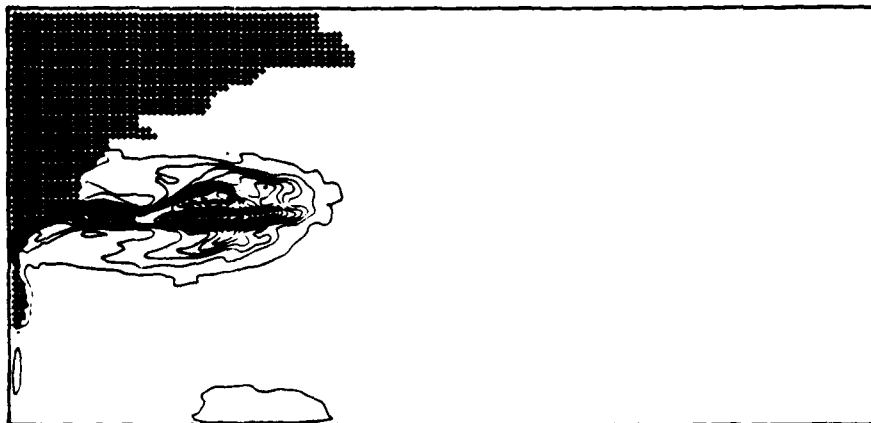


MEAN PSI 5 CASE 6

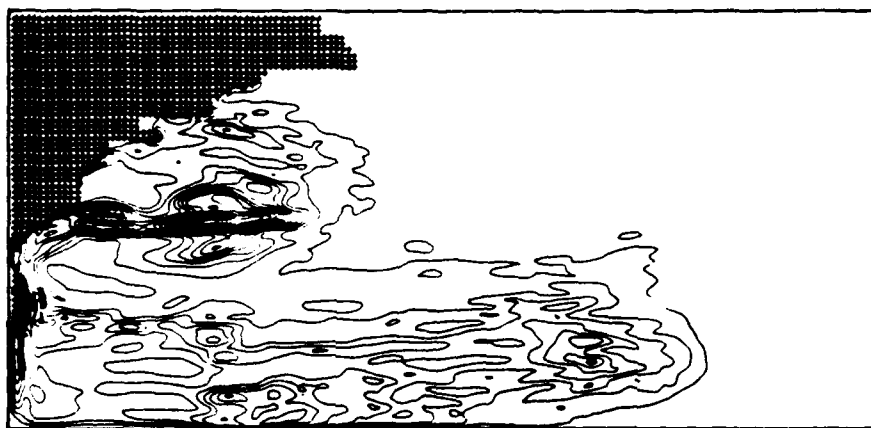


Fig. 5. Mean quasigeostrophic streamfunctions at the three levels in the North Atlantic basin, 150 m, 650 m, and 3000 m.

MEAN EDDY KE 1 CASE 6



MEAN EDDY KE 3 CASE 6



MEAN EDDY KE 5 CASE 6

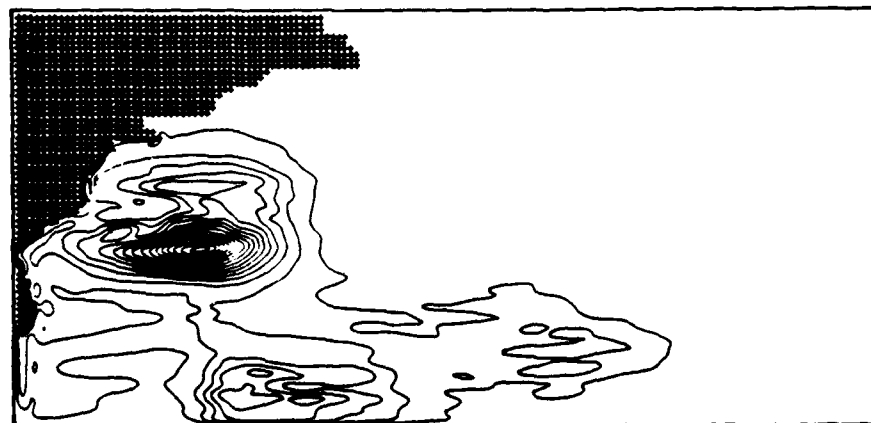
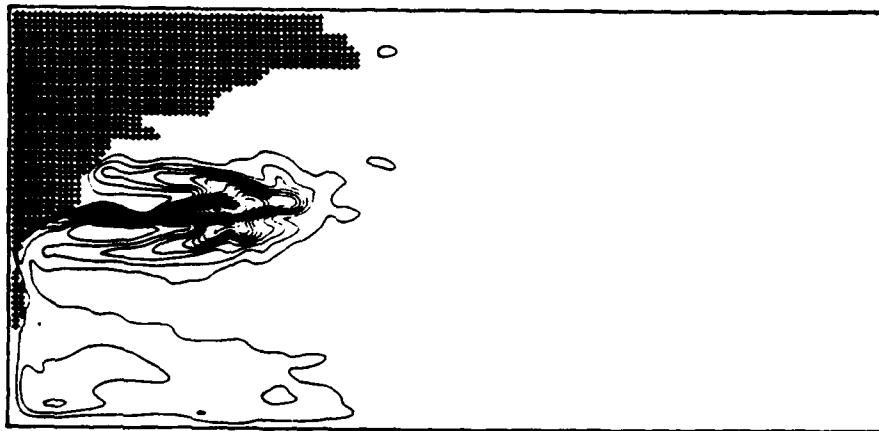


Fig. 6. Mean eddy kinetic energy at three levels in the North Atlantic basin, 150m, 650 m, and 3000 m.

MEAN EDDY PE 2 CASE 6



MEAN EDDY PE 4 CASE 6



Fig. 7. Mean eddy potential energy at two levels in the North Atlantic basin, 300 m and 1000 m.

MEAN Q 3 CASE 6

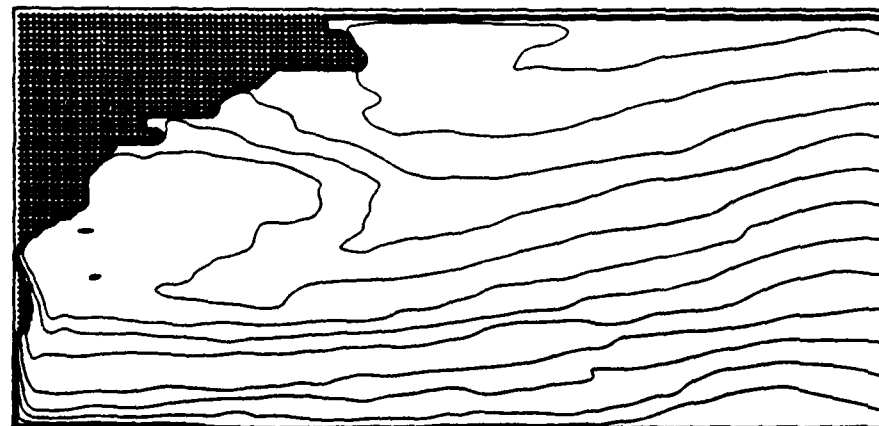


Fig. 8. Mean potential vorticity in the middle layer (at 650 m) of the North Atlantic basin.

S-1 DAY=2680.0 CASE= 6



S-1 DAY=2720.0 CASE= 6



S-1 DAY=2760.0 CASE= 6



Fig. 9a. Instantaneous maps of upper layer quasigeostrophic streamfunction at intervals of 40 days.

S-1 DAY=2800.0 CASE= 6



S-1 DAY=2840.0 CASE= 6



S-1 DAY=2880.0 CASE= 6



Fig. 9b.



The Behavior of an Individual Current Meander in Different Dynamical Regimes

Harley E. Hurlburt
J. Dana Thompson, Jr.¹
NORDA Code 320
NSTL Station, MS 39529

ABSTRACT

This study represents a middle ground between investigations of mesoscale isolated vortices and studies of unstable currents with such large populations of eddies that the basic evolution of individual current meanders tends to be obscured. Here, the behavior of individual current meanders in different dynamical regimes is examined using a two-layer primitive-equation model and schematic geometry of the Gulf of Mexico, a geometry useful in studying a single current meander. The dynamical regimes include horizontal shear instability of the first internal mode, baroclinic instability, and mixed instability. In most cases the flow is driven entirely by currents through the boundary in the upper layer. In each case the evolution of three links in the dynamical chain are examined: (1) the formation and detachment of eddies from a large amplitude meander, (2) the flow driven in the lower layer by features in the upper layer, and (3) the significant back interaction from the deep flow to the upper layer. The influence of large amplitude topography is important.

In all of the regimes there is a tendency for eddies in the upper layer to drive a modon² in the lower layer. The upper and lower layer phase relations are quite similar for both barotropic and baroclinic instability, although there is some southward shift of the lower layer eddies toward the more westward branch of the meander when baroclinic instability is present. The westward propagation speed of the upper layer vortex/modon system associated with baroclinic instability is 2 to 3 times faster than that associated with barotropic. When the large amplitude topography is present, baroclinic instability is suppressed and the modons tend to be confined to the abyssal plain. The topography also demonstrates some ability to steer eddies in the upper ocean through back interaction from eddies in the lower layer.

¹Current affiliation: Dept. of Marine, Earth and Atmospheric Sciences, North Carolina State University, Raleigh, N.C. 27650

²For convenience and in the spirit of Stern's (1975) application to observations we have generalized the term "modon" to refer to any counter-rotating vortex pair in the lower layer generated by a single vortex in the upper layer.

1. INTRODUCTION

This contribution to the Gulf Stream Workshop was prompted by the resemblance between the eddy-shedding by the Loop Current in the Gulf of Mexico and certain aspects of the eddy-shedding by Gulf Stream meanders. The schematic geometry of the Gulf of Mexico provides an attractive opportunity to study the evolution of an individual meander in isolation (Fig. 1). Thus, we have found a middle ground between 1) studies of isolated vortices and 2) investigations of meandering currents where the population of eddies and meanders is large. In the first case the eddy formation process and the subsequent effects of this process are ignored. In the second case the population of eddies and meanders is so large that it is difficult to separate the basic evolution of an individual meander from the complex interaction of multiple eddies and meanders. For the purposes of this study we will consider these interactions to be statistical noise which tends to obscure the basic evolution of the meander.

Two limitations of this application to the Gulf Stream should be noted: 1) the small amplitude development of the meander is quite different, and 2) the geometry prevents propagation of the meander. Despite the limitations of the application to the Gulf Stream, the large amplitude meander development and eddy-shedding seem to bear a striking resemblance to certain aspects of the large amplitude development and eddy-shedding of Gulf Stream meanders. The large amplitude development and eddy-shedding are the focus of this study.

A two-layer primitive equation model integrated to statistical equilibrium is used to investigate the behavior of individual current meanders in different dynamical regimes; including barotropic, baroclinic, and mixed instability. The evolution of three links in the dynamical chain are considered: (1) the formation and detachment of eddies from a large amplitude meander, (2) the deep flow patterns driven by features in the upper ocean, and (3) the back interaction from the deep flow to the upper ocean. The influence of large amplitude topography is considered for each link in the dynamical chain.

The model design and parameters are discussed in Section 2. In Section 3 we illustrate an eddy-shedding cycle and discuss some basic dynamical results gleaned from reduced gravity models. In Section 4 we present the eddy-mean energetics for experiments in different dynamical regimes, including paired experiments with and without large amplitude topography. Section 5 presents the signatures of the different regimes in terms of kinetic energy vs. time. In Sections 6, 7, and 8 we illustrate some characteristic features of the different regimes using synoptic

maps of upper and lower layer pressure. The effects of large amplitude topography are included among the illustrations. Much of Sections 4-8 has been excerpted from Section 8 of Hurlburt and Thompson (1982).

2. MODEL DESIGN AND PARAMETERS.

The models are primitive equation on a β -plane and retain a free surface. All but one of the experiments discussed here use a model with two active layers, the minimum to allow baroclinic instability and the coexistence of topography and the pycnocline. One experiment uses a reduced gravity model with an active upper layer and a lower layer which is infinitely deep and at rest. The pycnocline is represented by an immiscible interface between two layers with a prescribed density contrast.

Using common approximations the two-layer model equations are

$$\frac{\partial \vec{V}_i}{\partial t} + (\nabla \cdot \vec{V}_i + \vec{V}_i \cdot \nabla) \vec{V}_i + \hat{k} \times f \vec{V}_i = -h_i \nabla p_i + (\vec{\tau}_i + \vec{\tau}_{i+1})/\rho + A \nabla^2 \vec{V}_i$$

where $i=1$ for the upper and 2 for the lower layer and

$$\nabla = \frac{\partial}{\partial x} \hat{i} + \frac{\partial}{\partial y} \hat{j}$$

$$g' = g(\rho_2 - \rho_1)/\rho$$

$$p_1 = g\eta_1$$

$$f = f_0 + \beta(y - y_0)$$

$$p_2 = p_1 - g'(h_1 - H_1)$$

$$\vec{\tau}_i = \tau_i^x \hat{i} + \tau_i^y \hat{j}$$

$$\vec{V}_i = h_i \vec{v}_i = h_i (u_i \hat{i} + v_i \hat{j})$$

Symbol definitions are common in oceanography and are listed in the Appendix. In the reduced gravity model the lower layer momentum equation is $g \nabla \eta_1 = g' \nabla h_1$.

About 200 numerical experiments have been driven from rest by prescribed inflow through a port in the southern boundary compensated by outflow through a port in the eastern boundary. Except at the ports the boundaries are rigid and the no-slip condition is used. \vec{V}_i is prescribed at the southern (inflow) port using a parabolic inflow profile. At the eastern (outflow) port the flow is normal to the boundary and is self determined. See Hurlburt and Thompson (1980) for details on this.

The model equations were integrated using a semi-implicit numerical scheme where the external and internal gravity waves were treated implicitly in a manner patterned after Kwizak and Robert (1971). This allows a time step much larger than possible in the corresponding explicit free-surface model and substantially longer than possible in a primitive-equation rigid-lid model. The time step limitation is more stringent than that for a quasi-geostrophic model only by a $1/|f|$ stability criterion imposed by the numerical scheme for the Coriolis force. Hurlburt and Thompson (1980) discuss the numerical formulation of the models in detail. To the best of our knowledge the investigations of the Gulf of Mexico by Hurlburt and Thompson (1980, 1982) represent the first application of the "semi-implicit method" to long-term oceanographic integrations.

Table 1 presents the standard parameters for the reduced gravity and two-active-layer models. These parameters imply a maximum upper layer inflow velocity of 70-75 cm/s and an internal radius of deformation of $\lambda = c/f = 45$ km, where c is the internal gravity wave speed.

TABLE 1
Model parameters for standard case

A	$10^7 \text{ cm}^2 \text{ sec}^{-1}$	β	$2 \times 10^{-13} \text{ cm}^{-1} \text{ sec}^{-1}$
f_0	$5 \times 10^{-5} \text{ sec}^{-1}$	ρ	1 gm cm^{-3}
g	980 cm sec^{-2}	τ_i	0
g'	3 cm sec^{-2}	Δx	20 km*
H_1	200 m	Δy	18.75 km*
H_2	2800 m	Δt	1.5 hr
Domain Size, x_L by y_L			1600 x 900 km
Southern Port Width, L_{pw}			160 km
Eastern Port Width, L_e			150 km
Center of southern port at x_p			1200 km
Center of eastern port at y_p			75 km
Upper Layer Inflow Transport**			$20 \times 10^6 \text{ m}^3 \text{ sec}^{-1}$ (20 Sv)
Lower Layer Inflow Transport			$10 \times 10^6 \text{ m}^3 \text{ sec}^{-1}$ (10 Sv)
Angle of inflow from x-axis, θ_I			90°
Inflow spin-up time constant			30 days

* for a given variable

** also for the standard reduced gravity model

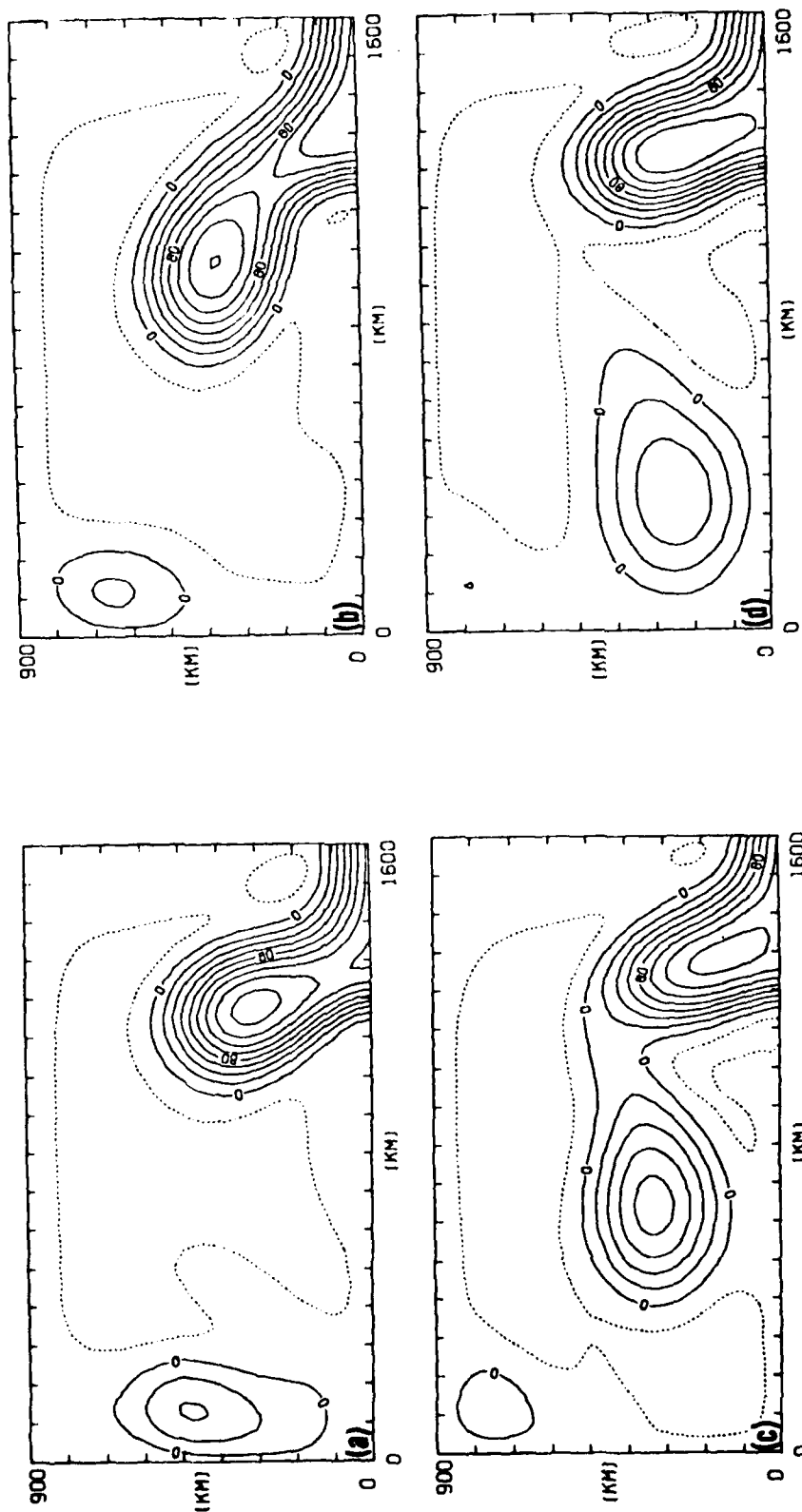


Fig. 1. Sequence of synoptic maps of PA at 70-day intervals showing the life cycle of an eddy starting at day 2210. The contour interval is 20 m. In all the figures dashed contours are negative. PA is positive downward. The case shown here uses the parameters of Table 1 and the topography of Fig. 3 except that the upper layer inflow transport is 25 Sv, the lower layer 5 Sv. (from Hurlburt and Thompson, 1980).

In the two-layer model the value of g' in the table is multiplied by $(H_1 + H_2)/H_2$ to yield the same internal values for the gravity wave speed, Rossby wave speed and radius of deformation as in a reduced gravity model when $h_1 = H_1$. The inflow transport is spun up to a steady value with a time constant of 30 days to minimize the excitation of high frequency waves. Horizontal friction provides the only dissipation in the models. Because Laplacian friction is a crude parameterization, for convenience $Ah_i \nabla^2 \vec{v}_i$ was replaced by $A \nabla^2 \vec{v}_i$ (with minimal effect). Although this form is not compatible with the eddy-mean energetics calculations, it did not lead to significant imbalances in the energy box diagrams. Fig. 2 shows the large amplitude idealized Gulf of Mexico topography used in some of the numerical experiments.

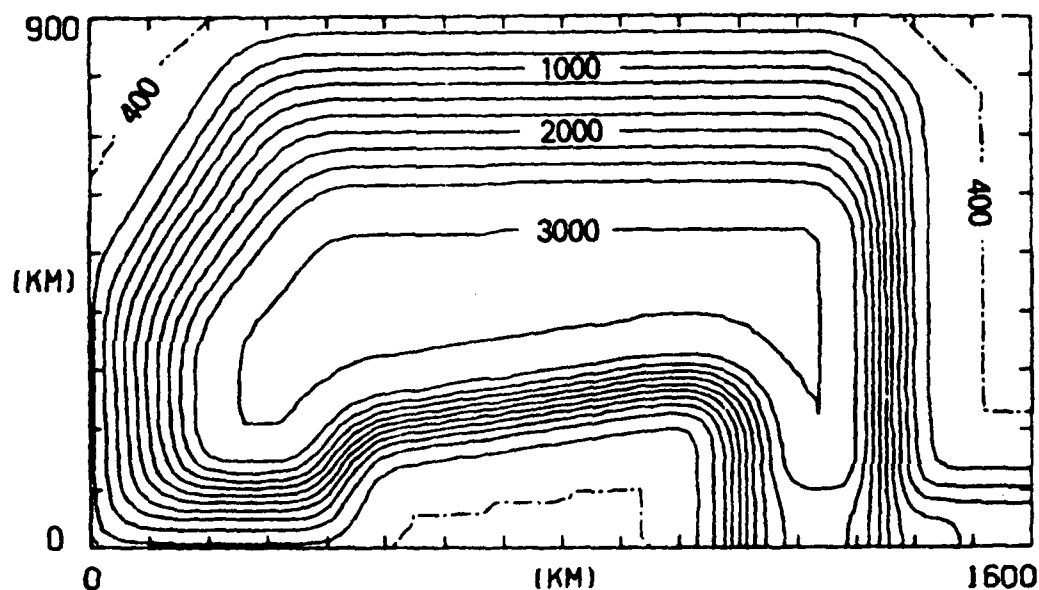


Fig. 2 Bathymetry of the idealized Gulf of Mexico model. The deepest water is at 3000 m and the shallowest topography is 400 m deep. The contour interval is 250 m. (from Hurlburt and Thompson, 1980)

3. AN EDDY-SHEDDING CYCLE AND SOME DYNAMICAL CHARACTERISTICS

Fig. 1 illustrates our first successful simulation of an eddy-shedding cycle (1978) in statistical equilibrium, using a sequence of four synoptic maps of the pycnocline anomaly (PA). The PA is the deviation of the interface between the layers from its initial flat elevation and is positive downward (upper layer thickness greater than initial). This experiment utilizes the parameters in Table 1 and the topography shown in Fig. 2 except that the upper layer inflow transport is 25 Sv and the lower is 5 Sv.

Fig. 1a shows the meander penetrating into the domain and beginning to form an anticyclonic eddy (warm core ring). In Fig. 1b the meander has bent westward and an eddy is about to break off. Fig. 1c shows the meander and an eddy just after an eddy-shedding event. In Fig. 1d the eddy has drifted westward and the meander has reamplified. In some regimes the eddy shedding cycle is quite different from that illustrated here, but in almost all cases it is repetitive in this geometry. The cycles may or may not be alike and the period may or may not exhibit substantial irregularity with steady inflow. In this case they are mildly different and mildly irregular with an average period of about 290 days.

As found by Hurlburt and Thompson (1980, 1982), useful information about dynamical characteristics of the eddy-shedding meanders can be obtained from reduced gravity models when a horizontal shear instability is the dominant instability mechanism. This is the case in Fig. 1. Based on CAV (constant absolute vorticity) trajectories, Rossby wave theory, scale analysis, and the parameters in Table 1, Hurlburt and Thompson (1982) present the following scales: eddy radius, $r = (v_c/\beta)^{1/2} = 191$ km, distance from the southern boundary to the latitude of westward bending, $L_{\beta I} = r$, the maximum northward penetration of the meander, $L_{np} = L_{\beta I} + 2r = 573$ km, the β Rossby number, $R_\beta = v_c/\beta r^2 = 1$, and the westward propagation speed of shed eddies is the internal Rossby wave speed with dispersion included, $c_r = \beta/(k^2 + \ell^2 + \lambda^{-2}) = 3.5$ cm/sec., where v_c is the speed at the core of the current and k and ℓ are wavenumbers calculated by assuming circular eddies with radius, r . The eddy-shedding period, p_e , was found to be proportional to r/c_r . The prescribed inflow angle also affects $L_{\beta I}$, L_{np} , and p_e . Most of the results from the reduced gravity numerical model agreed closely with the theoretical predictions.

The CAV trajectory analysis also showed how the current could increasingly tend to loop back on itself as the current just beyond the first inflection point after inflow increasingly bent westward under the influence of Rossby wave propagation (see Fig. 1). Thus, the westward bending of the meander and the tendency for it to loop back on itself can be understood without invoking an instability mechanism. In these experiments, where an instability is not required for the initial amplification of the meander, an instability mechanism appears essential only to explain the separation of the eddy from the meander. As a result the eddy shedding period is not determined primarily by the growth rate of an instability, but by the time required for the meander to penetrate into the domain and bend westward into an unstable configuration. Thus, $p_e \propto r/c_r$. See Hurlburt and Thompson (1982) for a much expanded discussion.

The extent to which the results in the two-active-layer model agree with the preceding results for reduced gravity models with a single vertical mode, depends strongly on the rate at which energy is transferred to the lower layer. As this rate is increased, the upper ocean eddies which are shed by the meander become increasingly weaker and smaller, and the shedding period is decreased. When baroclinic instability is important they are much weaker, the diameter is less than half, the westward propagation speed is 2-3 times faster, and the shedding period is 5-6 times shorter.

4. EDDY-MEAN ENERGETICS

In this section we survey the eddy-mean energetics for the seven numerical experiments listed in Table 2. In following sections we illustrate some characteristic features of the different regimes using synoptic maps of upper and lower layer pressure (p_1 and p_2) and curves of domain-averaged energy vs. time. Fig. 3 shows the eddy-mean energetics in terms of energy box diagrams. Fig. 3a labels the energy transfers. See the Appendix for symbol definitions and Hurlburt and Thompson (1982) for the derivation of the energetics. All of the model domain was used in calculating the energetics except the parts within 100 km of the eastern boundary and 37.5 km of the southern boundary. Thus, the eastern and southern boundaries of the energetics calculations are open. Kinetic energy and pressure work fluxes through these open boundaries are represented by arrows at the top (bottom) of the K_1 (K_2) boxes.

TABLE 2

Model experiments

Exp #	Differences from standard two-layer flat-bottom experiment in Table 1
1	None
2	$\theta_1 = 27^\circ$, $Sv_2 = 0$
3	Reduced gravity, Yucatan and Florida Straits added to model domain
4	$A = 3 \times 10^6 \text{ cm}^2/\text{s}$, $Sv_2 = 0$
5	$A = 3 \times 10^6 \text{ cm}^2/\text{s}$, $Sv_2 = 0$, Fig. 2 topography
6	$Sv_1 = 25$, $Sv_2 = 0$
7	$Sv_1 = 25$, $Sv_2 = 0$, Fig. 2 topography

Sv_i is the inflow in layer i in $10^6 \text{ m}^3/\text{s}$ or Sv .

In all cases most of the energy flows into \bar{K}_1 . In some cases there is significant efflux from K'_1 , but always must be less than the $\bar{K}_1 \rightarrow K'_1$ transfer. The arrows pointing outward from the sides represent dissipation of a particular type of energy due to Laplacian horizontal friction. Arrows between the boxes represent conversions of energy from one type to another as indicated by the direction of the arrow.

Fig. 3b shows the eddy-mean energetics for Exp. 1 in Table 2, a two-layer flat-bottom experiment using the standard parameters given in Table 1. The $\bar{K}_1 \rightarrow K'_1$ energy conversion is characteristic of a barotropic instability. The potential energy transfer is actually reversed with eddy potential energy (P') feeding the mean.

Angling the inflow 27° west of normal in the standard two-layer flat-bottom model (Exp. 2) produced a dramatic change in the eddy-mean energetics which is shown in Fig. 3c. (The lower layer inflow was also reduced to zero, but other experiments show this has a relatively minor role in altering the energetics in this case). Fig. 3c illustrates a classic signature of baroclinic instability in the eddy-mean energetics with $\bar{P} \rightarrow P'$ dominating the mean to eddy energy transfer and feeding the upper and lower layers almost equally. There is even a reverse cascade in the kinetic energy ($K'_1 \rightarrow \bar{K}_1$) with eddies feeding the mean flow.

The eddy-mean energetics for the reduced gravity model with a single vertical mode (Exp. 3 and Fig. 3d) illustrates a pure barotropic instability, since this model excludes baroclinic instability. In this case the dominant

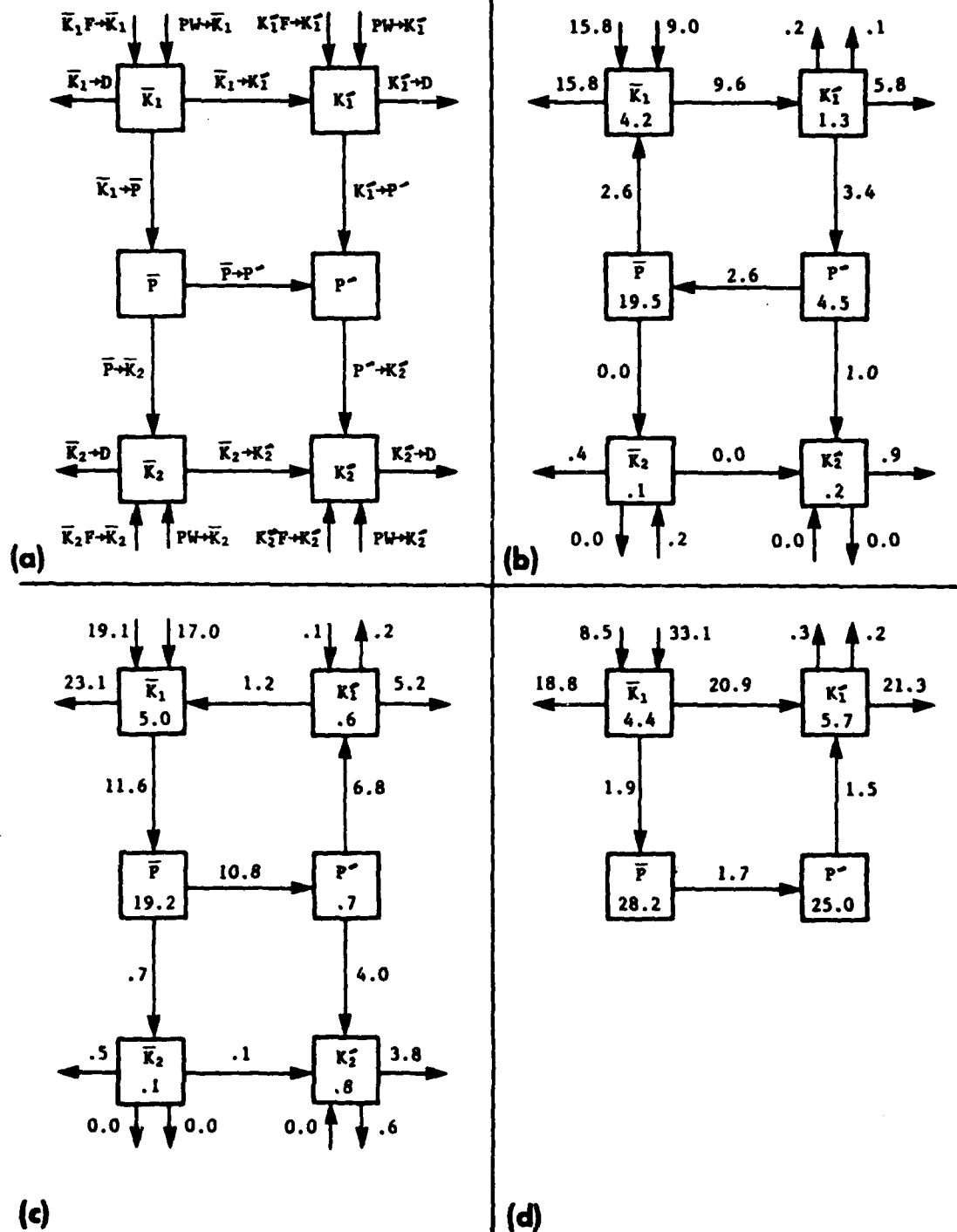


Fig. 3. Eddy-mean energetics for the experiments listed in Table 2: (a) labels for the energy pathways and energy reservoirs, (b) energetics for Experiment 1, standard flat-bottom case, (c) Experiment 2, flat bottom with non-normal inflow, (d) Experiment 3, reduced gravity, (e) Experiment 4, flat bottom with low

viscosity, (f) Experiment 5, same as the preceding but with topography, (g) Experiment 6, flat bottom, (h) Experiment 7, same as preceding but with topography. The energy reservoirs are in units of 10^{15} joules and the energy transfers are in units of 10^8 joules/s. (From Hurlburt and Thompson, 1982).

mean to eddy transfer is $\bar{K} \rightarrow K'$. Even though this is a pure barotropic instability, there is a net transfer from $\bar{P} \rightarrow P'$. Thus, the existence of such a transfer does not necessarily imply any contribution from baroclinic instability.

Fig. 3e is particularly interesting because it illustrates a mixed instability and because it demonstrates the value of separating the kinetic energy into upper and lower layer components. These results were obtained primarily by reducing the eddy viscosity in the two-layer flat-bottom model by a factor of three (Exp. 4). If K_1 and K_2 were combined to produce a 4-box diagram, the results would look much like those for the reduced gravity model and we might conclude that this is a case of barotropic instability. In contrast, the 6-box diagram (Fig. 3e) illustrates a striking result. Although a barotropic energy conversion ($\bar{K}_1 \rightarrow K'_1$) is dominant in the upper layer, the lower layer eddies are fed almost equally by transfers from $\bar{P} \rightarrow P'$ and $K'_1 \rightarrow P'$. In view of the reduced gravity results, this is insufficient evidence for an important contribution from baroclinic instability to the lower layer eddies. Additional evidence for this will be provided shortly.

Figs. 3e and 3f compare the results for Exps. 4 and 5. The experiments are identical except that Exp. 4 (Fig. 3e) has a flat bottom and Exp. 5 (Fig. 3f) includes the idealized Gulf of Mexico topography shown in Fig. 2. The topography strongly suppresses the baroclinic instability. With the topography added, the energy box diagram (Fig. 3f) indicates a strong barotropic instability ($\bar{K}_1 \rightarrow K'_1$) and a strong reverse potential energy flux ($P' \rightarrow \bar{P}$).

Figs. 3g and 3h again compare experiments with and without the topography of Fig. 2 (Exps. 6 and 7). They differ from the preceding by a three-fold increase in the eddy viscosity and a 25% increase in the upper layer inflow. The experiment with the topography (Fig. 3h) exhibits essentially the same energy pathways as the previous frame with the same topography (Fig. 3f). The reverse potential energy transfer ($P' \rightarrow \bar{P}$) is even stronger. Almost 1/3 of the eddy energy makes a complete circuit. Although this reverse transfer is clearly augmented by the topography, it is not restricted to experiments with topography (see Fig. 3b). In the corresponding flat-bottom case (Exp. 6, Fig. 3g), eddies in both layers are fed by energy conversions appropriate for a barotropic instability, the lower layer fed indirectly via energy transfer from the upper layer. In this case, increasing the eddy viscosity has suppressed the apparent contribution from baroclinic instability. Exp. 6 (Fig. 3g) differs from Exp. 1

(Fig. 3b) by having 25% greater inflow in the upper layer and none in the lower layer. The energy pathways in the two experiments are similar, but Fig. 3g shows more energy transfer to the lower layer and lacks the reverse ($P' \rightarrow \bar{P}$) transfer of the standard flat-bottom experiment (Fig. 3b).

The energy transfers in all these experiments are strongly inhomogeneous in space. Thus, as stressed by Harrison and Robinson (1978), energy transfers averaged over the model domain may not be characteristic of any important subregion.

5. KINETIC ENERGY VS. TIME

In the following discussion, we will illustrate features of the flow which are characteristic of the three regimes identified in the eddy-mean energetics with barotropic, baroclinic, and mixed instabilities. We will utilize the four experiments which do this most simply and clearly, (a) Exp. 1 for barotropic instability with a flat bottom, (b) Exp. 7 for barotropic instability with topography, (c) Exp. 2 for baroclinic instability, and (d) Exp. 4 for mixed instability. Fig. 4 shows the curves of K_1 and K_2 vs. time for these four experiments.

Fig. 4 a, b represents the barotropically unstable experiments and clearly shows a relatively long period for the eddy shedding cycle, 273 days for Exp. 1 (Fig. 4a) and 250 days for Exp. 7 (Fig. 4b). Fig. 4c shows a much faster 57 day oscillation for the baroclinically unstable experiment, Exp. 2. The corresponding reduced gravity experiment (not shown), in which baroclinic instability is not permitted, has a 284 day period. The period in Fig. 4 is very similar to that found by Holland and Lin (1975) for mid-latitude mesoscale eddies in a two-layer model with baroclinic instability. They also noted a similar maximum in K_1 near the onset of baroclinic instability which is followed by a rise in K_2 . We have not found this type of signature in any of our barotropically unstable experiments. Fig. 4d shows K_1 and K_2 vs. time for Exp. 4, the experiment for which the eddy-mean energetics (Fig. 3e) suggest a mixed instability. Two periods which are not harmonically related are clearly indicated, a long period of 300 days, which is typical of barotropically unstable experiments, and a much shorter 56 day period similar to that for the baroclinically unstable experiment. Also notable are the dramatic spikes in K_2 lagging the maximum in K_1 . This resembles the behavior of K_2 at the onset of baroclinic instability shown in Fig. 4c.

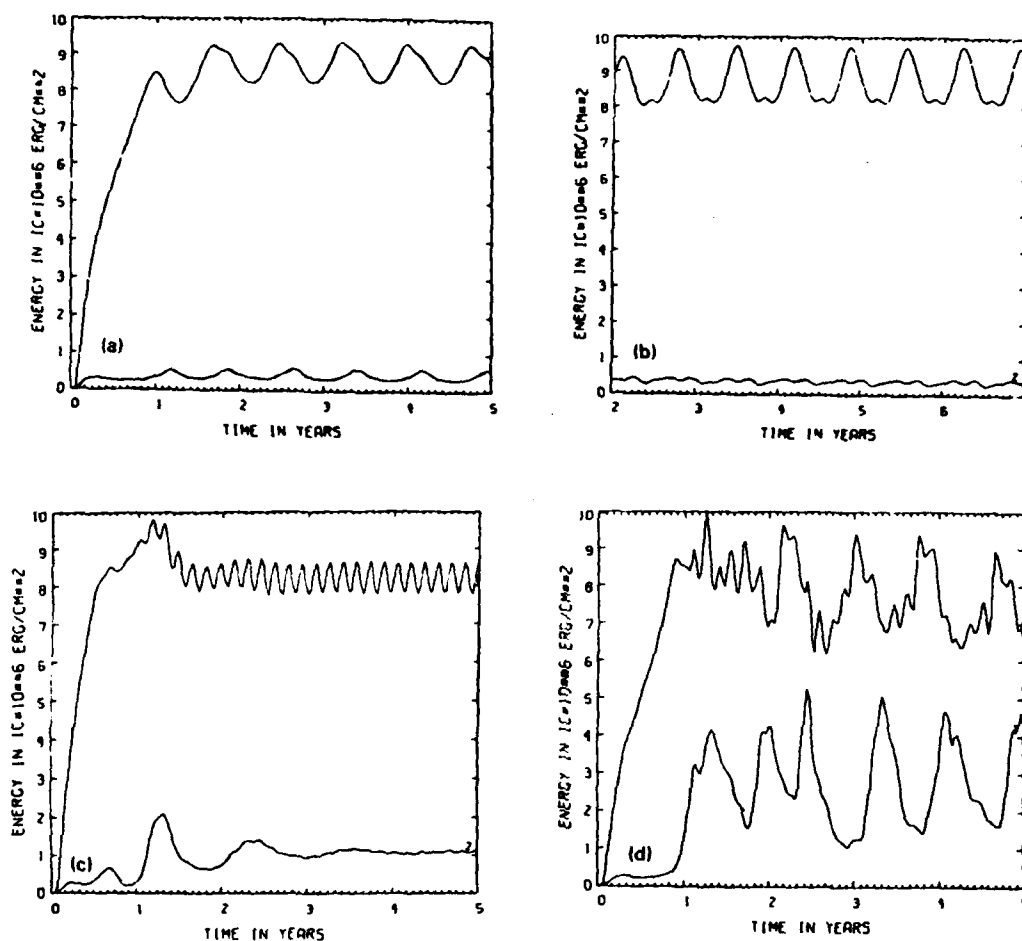


Fig. 4. Average kinetic energy over the rectangular domain (upper curve for upper layer) for (a) Experiment 1, the standard two-layer flat-bottom case, (b) Experiment 7, with the topography of Fig. 2 (c) Experiment 2, with non-normal inflow, and (d) Experiment 4, identical to Experiment 1 but with $A = 3 \times 10^6 \text{ cm}^2/\text{s}$ and $Sv_2 = 0$. The value of IC is (a) .5, (b) 1.0, (c) .55, (d) .7. (From Hurlburt and Thompson, 1982).

6. MODON GENERATION IN THE BAROTROPICALLY UNSTABLE EXPERIMENTS

We begin examining the characteristic features of the flow in different regimes by studying two experiments where the eddy-mean energetics indicate barotropic instability. One experiment has a flat bottom, and the other includes the idealized Gulf of Mexico topography shown in Fig. 2. The two experiments which illustrate the basic features of this flow in the simplest and clearest fashion are Exp. 1 with Fig. 3b energetics (the standard flat-bottom experiment) and Exp. 7 with Fig. 3h energetics.

Fig. 5 shows synoptic views of p_1 and p_2 for Exp. 1. At day 1710, p_1 (Fig. 5a) shows the meander penetrating into the basin and beginning to bend westward. An eddy shed earlier lies in the western part of the domain. A characteristic feature of the barotropically unstable experiments is the generation of a modon in the lower layer as the meander begins to form an eddy (Fig. 5b). This is due to vortex stretching:

$$\begin{aligned} \zeta_{2t} + \vec{v}_2 \cdot \nabla \zeta_2 - (f + \zeta_2) h_{2t} / h_2 + B v_2 &\approx A \nabla^2 \zeta_2 \\ h_{2t} &\approx -h_{1t} \end{aligned}$$

In Fig. 5a the embryonic eddy is moving WNW with h_1 increasing on the leading side and decreasing on the trailing side. The result in the lower layer is anticyclonic vorticity generation to the WNW of the upper ocean anticyclonic eddy and cyclonic vorticity generation to the ESE. The consequence of this is shown in Fig. 5b. The relationship between p_1 and p_2 can be seen clearly by superimposing the fields. The modon intensity tends to follow that of the generating eddy in the upper layer. In this experiment the modon intensity is insufficient for mutual advection to significantly influence the movement of the upper layer vortex, which still propagates westward at close to the internal Rossby wave speed.

The axis of the modon is oriented close to the direction of propagation by the upper layer vortex with the anticyclonic member leading and the cyclonic member trailing. The orientation of the modon generated here is quite different from that found by McWilliams and Flierl (1979) for isolated, nearly circular vortices, but the tendency of the eddy in the upper layer to propagate toward the member of the modon with like rotation is similar. However, in this case the westward propagation speed of the modon slightly exceeds that of the upper layer vortex. Thus the flow actually becomes more baroclinic and in Fig.

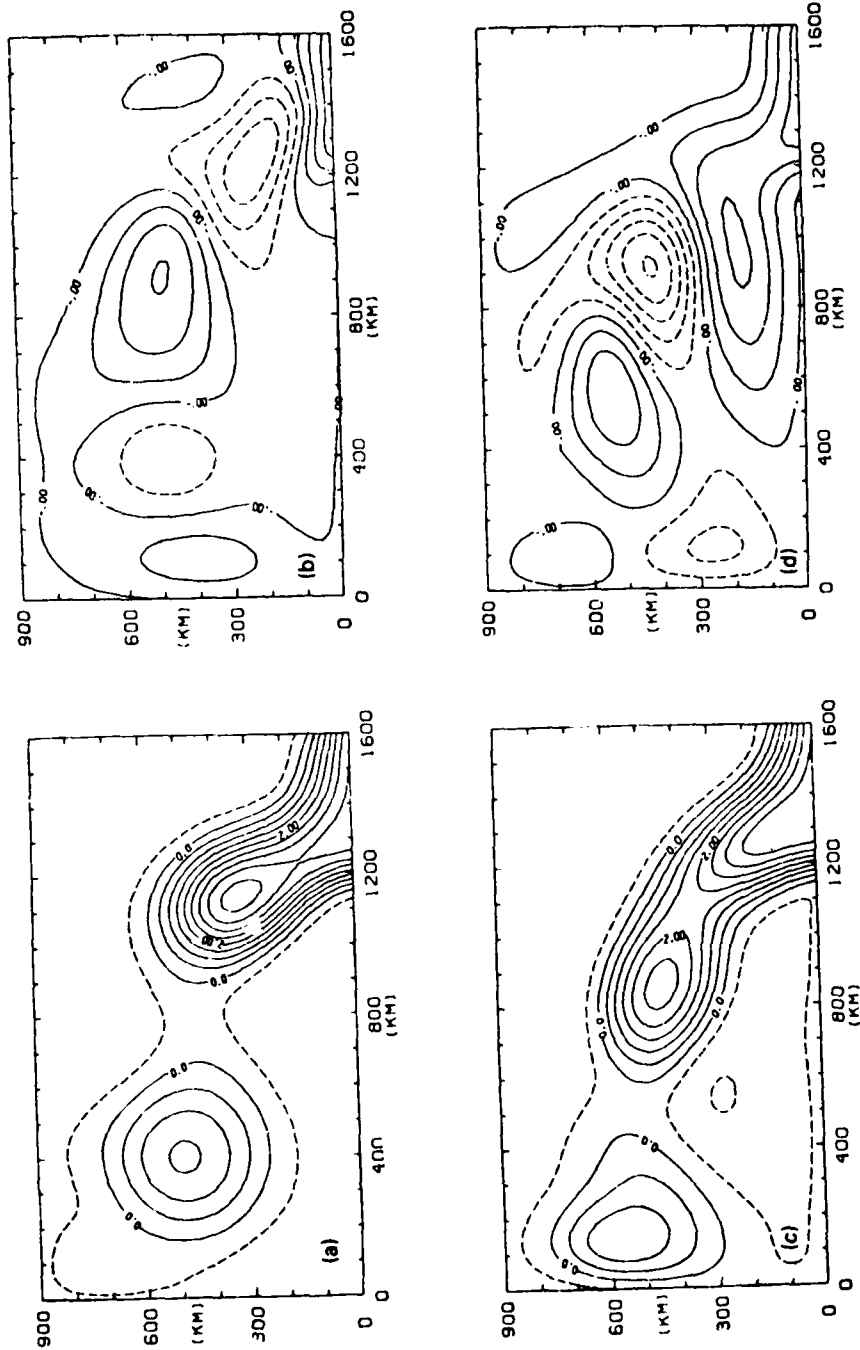


Fig. 5. (a) p_1 and (b) p_2 at day 1710 and (c) p_1 and (d) p_2 at day 1800 for Experiment 1. The contour interval is $.5 \text{ m}^2/\text{s}^2$ for p_1 and $.05 \text{ m}^2/\text{s}^2$ for p_2 . (From Hurlburt and Thompson, 1982).

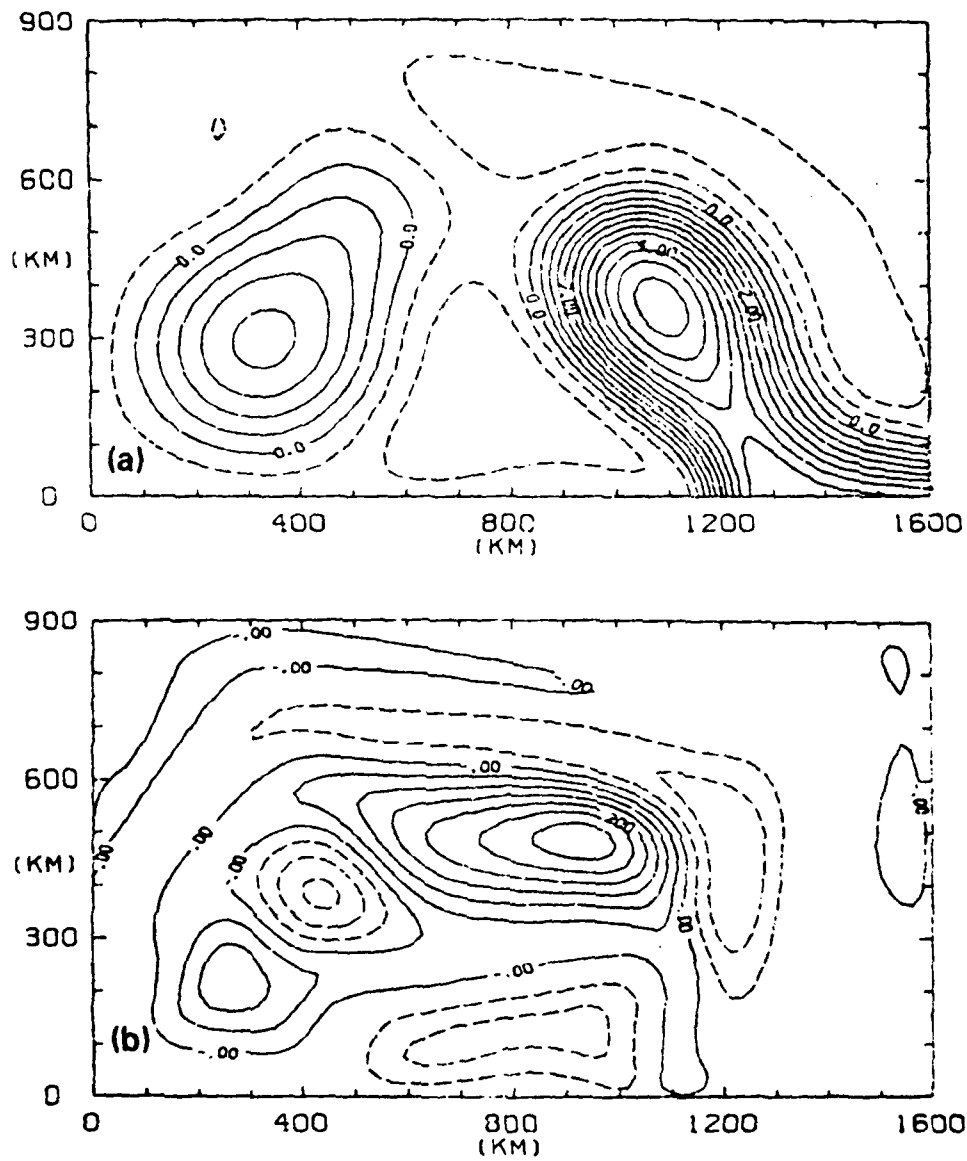


Fig. 6. (a) p_1 and (b) p_2 at day 1760 for Experiment 7. The contour interval is $0.5 \text{ m}^2/\text{s}^2$ for p_1 and $0.05 \text{ m}^2/\text{s}^2$ for p_2 . (From Hurlburt and Thompson, 1982)

5a, b we see the anticyclonic eddy in the upper layer situated over the cyclonic member of the modon. This behavior is common but not universal in our numerical experiments. It is quite unlike the coupled behavior of the isolated baroclinic vortex and barotropic modon studied by McWilliams and Flierl (1979). In their results the modon member with rotation unlike the baroclinic vortex eventually broke away and the barotropic and baroclinic vortices tended to become superimposed and to approach a state of deep compensation (no signature of the vortex in the lower layer). When the upper layer vortex reaches the western boundary and propagates northward (Fig. 5c), it is again associated with a modon in the lower layer (Fig. 5d) and again the modon is oriented in the direction of propagation with the like (anticyclonic) member leading and the opposite member trailing.

Fig. 6 shows a synoptic view of p_1 and p_2 at day 1760 for a barotropically unstable experiment with Fig. 2 topography (Exp. 7 with Fig. 3h energetics). This experiment exhibits coupled upper layer vortex, lower layer modon behavior similar to the flat bottom experiment, except that the modon is mostly confined to the abyssal plain. Another difference is that the upper layer vortex remains between the modon pair. The modon is partially steered by the topography. Apparently, the back interaction from the modon to the upper layer is sufficient that the trajectory of the upper layer vortex is also modified by the topography. Fig. 7 compares upper layer eddy trajectories for Exps. 6 and 7, two experiments with no flow through the ports in the lower layer. The experiments are identical except that Exp. 6 has a flat bottom and Exp. 7 includes Fig. 2 topography. Because Exp. 7 includes no flow through the ports in the lower layer, there is no current following the f/h contours. The addition of such a current had no major effect on the modon, provided the current was weak enough to permit the normal eddy shedding to occur (see Hurlburt and Thompson, 1980).

Although eddy activity in the lower layer modified the propagation of the upper layer vortex, the propagation of both the upper layer vortex and the associated modon was dominated by internal Rossby wave propagation in both the reduced gravity and two active layer experiments which exhibited discrete eddy shedding and a horizontal shear (barotropic) instability of the internal mode. As we will see shortly, this is not the case in the experiment with a baroclinic instability.

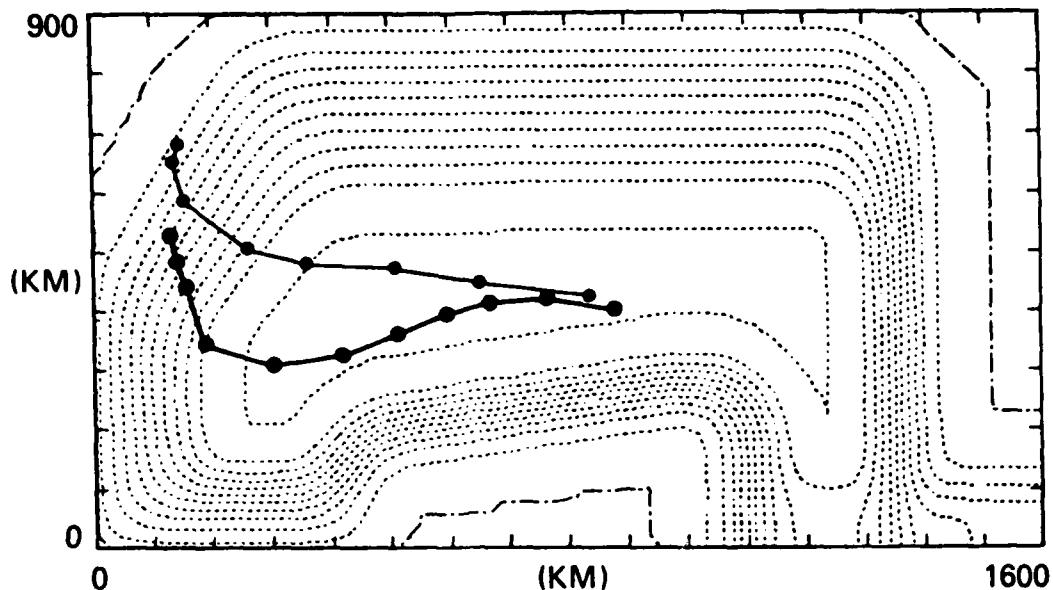


Fig. 7. Shows the effect of bottom topography on eddy trajectories for identical experiments except that Experiment 6 (upper trajectory) had a flat bottom and Experiment 7 (lower trajectory) included the topography of Fig. 2 which is used as background in this figure. The trajectories are dotted at 30 day intervals. (From Hurlburt and Thompson, 1982).

7. FLOW CHARACTERISTICS ASSOCIATED WITH BAROCLINIC INSTABILITY

Fig. 8 shows a synoptic view of p_1 and p_2 for Exp. 2 where the upper layer inflow is angled 27° west of normal and there is no flow through the ports in the lower layer. The eddy-mean energetics (Fig. 3c) indicate the occurrence of baroclinic instability. This experiment exhibits modon-like generation similar to that earlier associated with a barotropic instability. However, the eddies tend to be smaller and the greater population of eddies tends to mask the modon character of the eddy generation. The upper and lower layer eddies near the eastern part of the meander bear a phase relationship which is similar to the barotropically unstable experiments. The modon axis is oriented close to the direction of propagation of the anticyclonic eddy in the upper layer, with the anticyclonic modon member leading and the cyclonic one trailing. One difference is that the modon axis is south of the upper layer vortex. Thus, the lower layer eddies tend to be strongest under the westward-flowing arm of the meander as expected for a baroclinic instability (Gill, et al, 1974; Philander, 1976). Later, in the central basin the leading modon member shifts northward, away from the westward propagating vortex in the upper layer. The trailing vortex remains under the westward

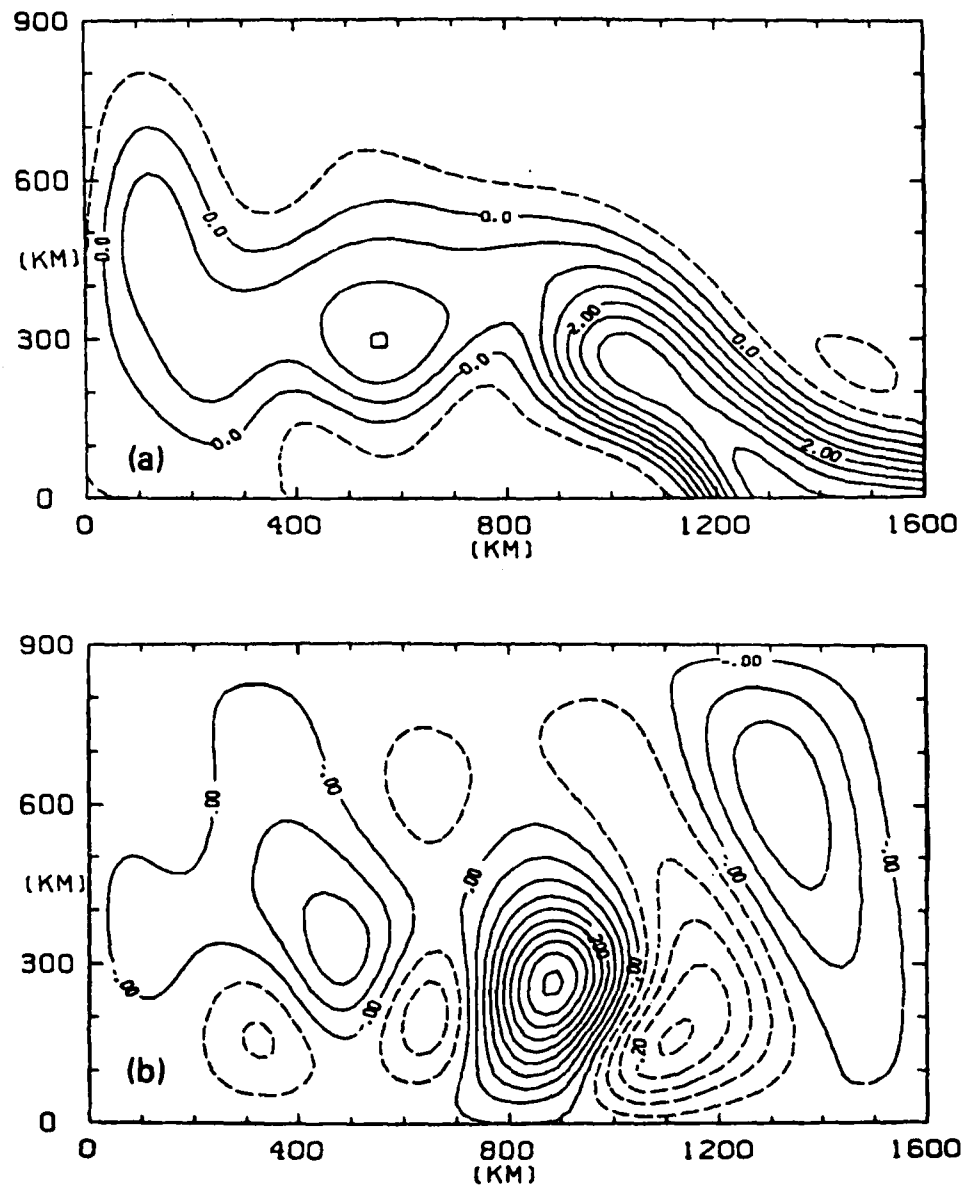


Fig. 8. (a) p_1 and (b) p_2 at day 2450 for Experiment 2. The contour interval is $0.5 \text{ m}^2/\text{s}^2$ for p_1 and $0.05 \text{ m}^2/\text{s}^2$ for p_2 . (From Hurlburt and Thompson, 1982).

branch of the meander. Thus the modon axis is no longer aligned with the direction of propagation. In general, the lower layer eddies tend to be elongated meridionally in the eastern part of the basin where they originate and zonally in the western part of the basin where they decay. In the western part of the basin the eddies also show some tendency toward barotropy. Except for the initial meridional elongation, these tendencies are consistent with results presented by Rhines (1977).

The most dramatic difference between the experiments with barotropic and baroclinic instability lies in the propagation speed of the eddies. In the barotropically unstable experiments with discrete eddies the internal Rossby wave speed associated with the upper layer vortex exerts primary control on the propagation in both layers. Even though the eddies in the baroclinically unstable case are smaller, they propagate westward at ~ 10 cm/sec, typically 2 to 3 times faster than in the barotropically unstable experiments. Although it is difficult to estimate an appropriate shear velocity, the propagation speeds in our numerical model are quite consistent with those for baroclinic instability in a linearized two-layer model with a horizontally uniform basic flow (Pedlosky, 1979).

Gill et al (1974) have suggested the upper to lower layer phase shift as a means of detecting baroclinic instability. In our results we find this is not very useful because the barotropic instability which occurs in the upper layer generates a modon in the lower layer with upper-lower layer phase relationships which are much like those of the baroclinic instability. In our results the westward propagation speed of the eddies is a much clearer distinguishing characteristic.

8. FLOW CHARACTERISTICS OF A MIXED INSTABILITY

Fig. 9 shows two synoptic views of p_1 and p_2 for Exp. 4 which has a flat bottom, no inflow in the lower layer, and one-third the eddy viscosity of the experiments discussed in Sections 6 and 7. The eddy-mean energetics (Fig. 3e) suggest that a mixed instability occurs in this experiment. Since there is no flow through the ports in the lower layer, all the energy in the lower layer is received from the upper layer. Apart from this the flows in the two layers are much more independent than those discussed in the two preceding subsections.

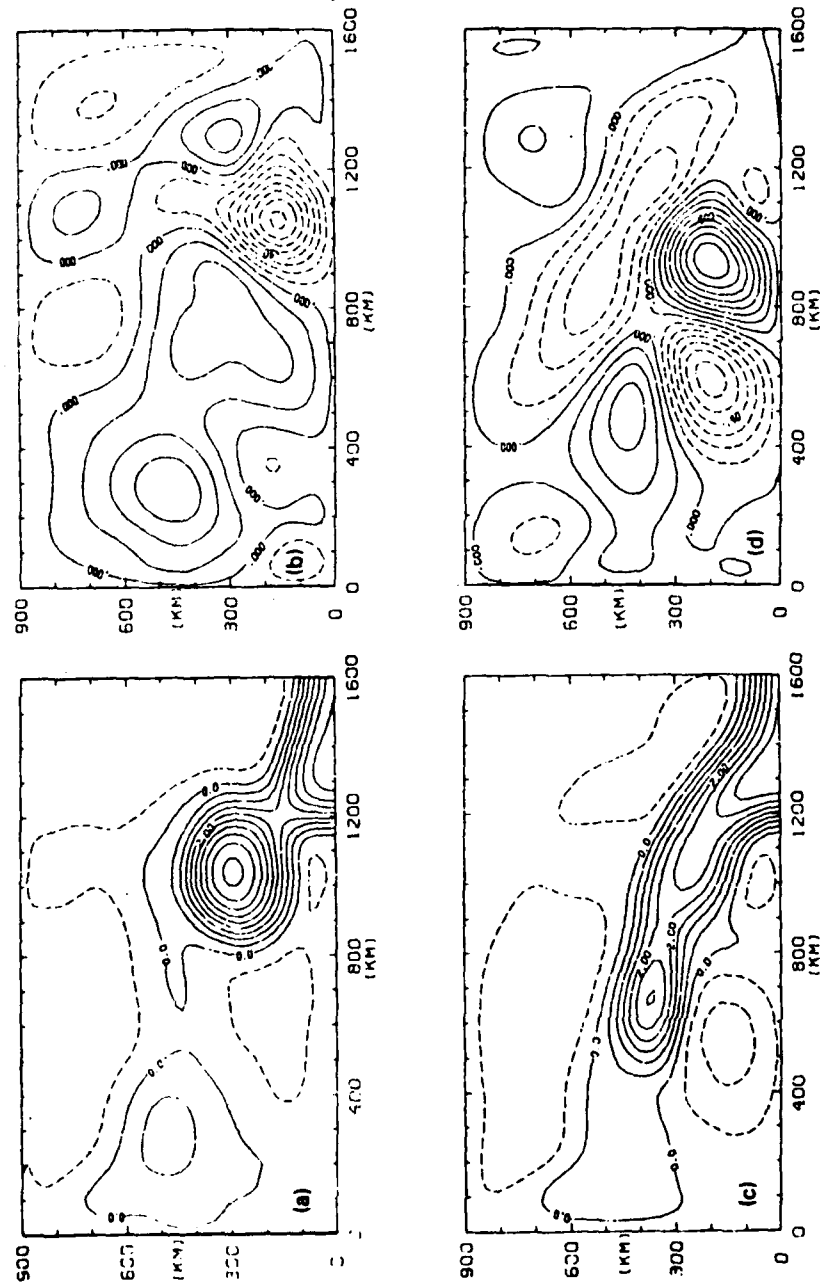


Fig. 9. (a) p_1 and (b) p_2 at day 1720 and (c) p_1 and (d) p_2 at day 1760 for Experiment 4. The contour interval is $.5 \text{ m}^2/\text{s}^2$ for p_1 and $.1 \text{ m}^2/\text{s}^2$ for p_2 . (From Hurlburt and Thompson, 1982).

Eddies in the lower layer propagate westward at approximately the external Rossby wave speed (~ 10 cm/sec), and those with like rotation pass a given point with a periodicity of about 60 days. Unlike the experiments discussed in Sections 6 and 7 there is no clear phase relationship between the eddies in the lower layer and the eddy which forms on the meander in the upper layer. This is true during most, but not all, of the eddy-shedding cycle of the meander. In this experiment the eddy-shedding period is about 300 days and is depicted as a slow oscillation in κ_1 (Fig. 4d). There is a back interaction from the lower layer eddies to the meander in the upper layer which causes a strong undulation of the meander with approximately a 60 day period. This is depicted in Fig. 4d as the high frequency oscillation in κ_1 . Except for this undulation, the meander penetrates into the domain, bends westward and begins to form an eddy structure just as in the barotropically unstable experiments, but near the time an eddy would break off (Fig. 9a) in a barotropically unstable experiment, something quite different occurs. The meander suddenly shoots far to the west at a speed appropriate for baroclinic instability and breaks into a series of smaller eddies. During this process lower layer eddies under the south side of the meander strengthen dramatically and the upper and lower layer eddies develop distinct phase relationships. An anticyclonic eddy in the lower layer leads the westward advance of the meander. At this stage phase relationships in the upper and lower layers are very similar to those for the baroclinically unstable case, and they exhibit the same differences from the barotropically unstable experiments. These phase relations disintegrate as soon as the rapid westward advance of the meander is halted. Thus we have a picture of episodic baroclinic instability associated with a small part of each 300 day eddy-shedding cycle of the meander. This instability is strong enough to show up in the domain-averaged eddy-mean energetics (Fig. 3e) and to provide a sharp spike in the curve of K_2 vs. time (Fig. 4d). Day 1720 (Fig. 9b) is near the foot of the last spike and day 1760 (Fig. 9d) is near the top of it.

The much weaker coupling for the two layers than found in either the barotropically or baroclinically unstable experiments is explained in part by the peculiar episodic nature of the baroclinic instability in Exp. 4 and in part by the 3 times lower eddy viscosity. Because the eddies in the lower layer are governed by external Rossby wave propagation, they are dispersive in nature. With the lower eddy viscosity they are not dissipated as soon after generation and have greater opportunity to disperse and fill the basin. The importance of dispersion in spreading the eddy population in the lower layer has

been noted by Rhines (1977) and in the study of isolated vortices by McWilliams and Flierl (1979).

A comparison of Fig. 6 (for the experiment with Fig. 2 topography) and Fig. 9 (for the flat-bottom experiment with a mixed instability) indicates how the topography can suppress the episodes of baroclinic instability found in the latter case. When the topography of Fig. 2 is present, the eddies in the lower layer are mostly confined to the abyssal plain. Lower layer eddy generation over the strongly sloping topography is prevented because the eddy flow would have to cross the closely packed f/h contours at large angles, behavior not anticipated in geostrophically balanced flow which conserves potential vorticity. The strong eddies in Fig. 9d which form under the westward-flowing branch of the meander would lie over the wide shelf and its slope just west of the inflow port. Thus, they are prevented from forming when the topography of Fig. 2 is included. We can now appreciate why the two-layer model with topography produces results more like the reduced gravity model than does the two-layer flat-bottom model. If the westward branch of the meander were to flow over the abyssal plain, we might expect the model to exhibit episodes of baroclinic instability even when the topography is included.

ACKNOWLEDGEMENTS

We extend our appreciation to Dr. L. B. Lin, who developed much of the analysis and display software, including the eddy-mean energetics. We thank Ruth Preller, John Harding, Monty Peffley, Marla Burson and Cynthia Seay for assisting us in various aspects of manuscript preparation. Dr. Daniel Moore of Imperial College, London provided the fast vectorized Helmholtz solver. Some of the graphics software was supplied by the National Center for Atmospheric Research, which is sponsored by the National Science Foundation. Computations were performed on the two-pipeline Texas Instruments Advanced Scientific Computer at the Naval Research Laboratory in Washington, D.C. Portions of this paper were excerpted from Section 8 of Hurlburt and Thompson (1982). We thank Charlene Parker and Leah Wheatley for typing the manuscript.

APPENDIX

List of Symbols

A	horizontal eddy viscosity
c_r	internal Rossby wave speed including dispersion
f, f_0	Coriolis parameter; f_0 taken at southern boundary (y_0)

g	acceleration due to gravity
g'	reduced gravity, $g(\rho_2 - \rho_1)/\rho$
$H_1, H_2(x,y)$	initial thickness of the layers
h_1, h_2	instantaneous local thickness of the layers
k_i, \bar{K}_i, K_i'	kinetic energy $\frac{1}{2}\rho h_i(u_i^2 + v_i^2)$; of the mean flow; mean of the eddy flow
k, ℓ	zonal and meridional wave numbers
$L_{\beta I}$	minimum inertial length scale over which β is important, $(v_c/\beta)^{\frac{1}{2}}$
L_{np}	maximum northward penetration of the meander
P, \bar{P}, P'	potential energy $\frac{1}{2}\rho(g\eta_1^2 + g'\eta_2^2)$; of the mean flow; mean of the eddy flow, respectively.
p_1	upper layer density-normalized pressure, $g\eta_1$.
p_2	lower layer density-normalized pressure, $g\eta_1 - g'(h_1 - H_1)$
p_e	eddy shedding period
R_β	beta Rossby number, $v_c/\beta r^2$
r	eddy radius
t	time
Δt	time increment in the numerical integration
u_1, u_2, v_1, v_2	x and y-directed components of current velocity
v_c	speed at the core of the current
\vec{v}_1, \vec{v}_2	$h_1 \vec{v}_1, h_2 \vec{v}_2$
x, y, z	tangent plane Cartesian coordinates: x positive eastward, y positive northward, z positive upward
x_L, y_L	east-west and north-south domain size
$\Delta x, \Delta y$	horizontal grid increments
β	differential rotation, df/dy
ζ	relative vorticity, $v_x - u_y$
η_1	free surface anomaly; height of the free surface above its initial uniform elevation; $\eta_1 = h_1 + h_2 - H_1 - H_2$
η_2	$\eta_2 = H_1 + \eta_1 - h_1 = h_2 - H_2 = -\eta_1$
θ_I	angle of inflow with respect to the positive x-axis
λ	internal radius of deformation
ρ, ρ_1, ρ_2	densities of sea water
τ_i^x, τ_i^y	x and y directed tangential stresses at the top (i) and bottom (i + 1) of layer i

REFERENCES

- Gill, A. E., J.S.A. Green, and A. J. Simmons, 1974: Energy partition in the large-scale ocean circulation and the production of mid-ocean eddies. *Deep-Sea Research*, 21, 499-528.
- Harrison, D. E., and A. R. Robinson, 1978: Energy analysis of open regions of turbulent flows-mean eddy energetics of a numerical ocean circulation experiment. *Dyn. Atmos. Oceans*, 2, 185-211.
- Holland, W. R., and L. B. Lin, 1975: On the generation of mesoscale eddies and their contribution to the oceanic general circulation. I. A preliminary numerical experiment. *J. Phys. Oceanogr.*, 5, 642-657.
- Hurlburt, H. E. and J. D. Thompson, 1980: A numerical study of Loop Current intrusions and eddy shedding. *J. Phys. Oceanogr.*, 10, 1611-1651.
- Hurlburt, H. E. and J. D. Thompson, 1982: The dynamics of the Loop Current and shed eddies in a numerical model of the Gulf of Mexico. *Hydrodynamics of Semi-enclosed Seas*, J. C. J. Nihoul, Ed., Elsevier Scientific Publishing Company, 243-297.
- Kwizak, M. and A. J. Robert, 1971: A semi-implicit scheme for grid point atmospheric models of the primitive equations. *Mon Wea. Rev.*, 99, 32-36.
- McWilliams, J. C. and G. R. Flierl, 1979: On the evolution of isolated, nonlinear vortices. *J. Phys. Oceanogr.*, 9, 1155-1182.
- Pedlosky, J., 1979: *Geophysical Fluid Dynamics*, Springer-Verlag, 624 pp.
- Philander, S. G. H., 1976: Instabilities of zonal equatorial currents. *J. Geophys. Res.*, 81, 3725-3735.
- Rhines, P., 1977: The dynamics of unsteady currents. *The Sea*, Vol. 6, E. D. Goldberg, I. N. McCave, J. J. O'Brien and J. H. Steele, Eds., Wiley Interscience, 189-318.
- Stern, M. E., 1975: Minimal properties of planetary eddies. *J. Mar. Res.*, 33, 1-13.



An Analysis of the Potential Vorticity Distribution across the Gulf Stream

Elizabeth Messenger Johns

D. Randolph Watts

University of Rhode Island

Potential vorticity, $\Pi = \omega_a \cdot \nabla \rho$, (where ω_a is the absolute vorticity and $\nabla \rho$ is the gradient of the density), is a conservative property of ocean circulation wherever dissipative and non-adiabatic effects are negligible (Ertel, 1942; Pedlosky, 1979). The significant terms of Π in the Gulf Stream are

$$(1) \quad \Pi = (f + \kappa v + \partial v / \partial n) \cdot \partial \rho / \partial z - \partial v / \partial z \cdot \partial \rho / \partial n$$

where f is the planetary vorticity, κv and $\partial v / \partial n$ are the curvature and horizontal shear vorticities, $\partial v / \partial z$ is the vertical shear, and $\partial \rho / \partial z$ and $\partial \rho / \partial n$ are the vertical and cross-stream density gradients.

The various terms in (1) can be estimated from hydrographic sections and appropriately chosen or measured reference velocities across the Gulf Stream. Results from such an analysis are presented below for a section taken in July 1967 off Cape Hatteras (Richardson, 1970) which utilized transport floats in addition to hydrographic measurements. This section was chosen for its similarity in geographic location and measurement techniques to CTD and transport float work which will be done in July 1982 on the R/V Endeavor.

The section (figure 1) was positioned across the continental slope off Cape Hatteras, between 34 and 35.5° North and 74 and 76° West. The temperature structure is shown in figure 2, and the geostrophic velocity

contours in figure 3. The arrows mark the hydrographic station locations, with only the Gulf Stream portion of the transect included in the following analysis. (Thus, the origin of the cross-stream axis in figures 2 through 6 corresponds to about 40 km along the line shown in figure 1). Transport floats were used to obtain a reference velocity for each hydrographic station pair.

Equation (1) simplifies to

$$(2) \quad \Pi = (f + \partial v / \partial n) \cdot \partial \rho / \partial z$$

for this particular section, as κv is significant only in regions of strong curvature such as Gulf Stream rings and sharp meanders, and in most cases the term $\partial v / \partial z \cdot \partial \rho / \partial n$ is negligible compared to $\partial v / \partial n \cdot \partial \rho / \partial z$. Further work will examine where, and to what extent, these neglected terms are significant. Finally, for simplicity, ρ has been replaced by T in the calculation. This is a valid approximation across most of the section, especially on the anticyclonic side where a tight TS relationship is established.

The results of the potential vorticity calculation are shown in figure 4. Main features of the Π distribution on the anticyclonic side (the seaward 2/3 of the figure), where potential vorticity is expected to be a conservative property, are:

- a.) The 18° water is a lens of minimum Π , with a tendency to increase gradually from $<.4$ to $\geq 1.5 \cdot 10^{-6} \text{ } ^\circ\text{C m}^{-1} \text{ s}^{-1}$ in the onshore direction;

b.) The upper thermocline waters (12 to 17° C) are a relative Π maximum, with values between 1.5 and $2 \cdot 10^{-6} \text{ } ^\circ\text{C m}^{-1} \text{ s}^{-1}$; and

c.) The deep waters ($\leq 5^\circ\text{C}$) again show low ($.5 \cdot 10^{-6}$) Π values, due mostly in this case to the $f\partial T/\partial z$ term, as the velocity shear in the deep water is small.

On the anticyclonic side of the Stream there is a definite tendency for Π contours to be aligned with T or ρ contours; i.e. to the first approximation layers of constant density do have "uniform" Π as is generally assumed in theoretical Gulf Stream models.

There is a sharp increase in Π in the surface layer ($T \geq 19^\circ\text{C}$). Because this layer is exposed to mixing and heating or cooling effects, Π is not expected to be conserved here. There is another sharp frontal increase in Π near the north wall for all waters warmer than 12°C , representing the change from an anticyclonic to a cyclonic current shear regime (where $\partial v/\partial n$ reverses sign), as well as the steep increase in $\partial T/\partial z$ found on the slope water side of the Stream. The potential vorticity is not expected to be conserved on the cyclonic side, either, as dissipative influences may be significant there. Thus, the emphasis in the following discussion is on the anticyclonic side of the Gulf Stream, in waters colder than 19°C , where Π will be considered a conservative property.

The potential vorticity profiles along two particular isotherms, 18°C and 5°C , are illustrated in figures 5 and 6. The distributions in these two layers are quite different: In the 18° water, Π increases

systematically in the onshore direction from $.4$ to $\geq 1 \cdot 10^{-6} \text{ } ^\circ\text{C m}^{-1} \text{ s}^{-1}$ on the anticyclonic side (seaward of 40 km). In the deep water, however, Π is nearly constant along 5°C all the way across the Stream, with a value $\approx .25 \cdot 10^{-6} \text{ } ^\circ\text{C m}^{-1} \text{ s}^{-1}$.

These potential vorticity trends in the Gulf Stream are of significance within the context of the general North Atlantic circulation. In the central ocean, where the relative vorticity $\partial v / \partial n$ is much smaller than f , Π is approximately equal to $f \partial T / \partial z$. Figures 7 and 9 show $f \partial T / \partial z$ contours estimated from the thickness of the $17\text{-}19^\circ\text{C}$ and $4\text{-}6^\circ\text{C}$ layers for the North Atlantic from Fuglister(1960)'s atlas¹. These two figures exhibit the following features:

In the 18° water, $f \partial T / \partial z$ shows a minimum ($< .4 \cdot 10^{-6} \text{ } ^\circ\text{C m}^{-1} \text{ s}^{-1}$) in the central part of the Gulf Stream recirculation gyre for warm North Atlantic waters (figure 7), and increases outward from the center of the gyre to values as high as 1 to $2 \cdot 10^{-6}$ in the Caribbean Sea. The variation of Π across the Gulf Stream (figure 5) is similar to the distribution along 70° West running southward in figure 7 through the subtropical gyre. If Π is interpreted as a "dynamical tracer", a laminar pattern of inflow to the Gulf Stream is suggested which closely resembles the circulation diagram for waters warmer than 17°C suggested by Worthington (1976) and shown in figure 8. Water joining the Stream from the Sargasso Sea, north of the Florida Straits, carries a very low ($.4 \cdot 10^{-6}$) Π signature. Nearer-shore waters in the high velocity Gulf Stream core originate from farther south in the gyre, and from the Caribbean via the

1 A more complete $f \partial \rho / \partial z$ analysis is presented in McDowell, Rhines and Keffer(1982). The general patterns are the same as those shown here for $f \partial T / \partial z$.

Florida Current; they carry a higher (1 to $2 \cdot 10^{-6}$) Π signature, consistent with the $f\partial T/\partial z$ contours in figure 7, and the streamlines in figure 8. Other water mass tracers such as the Subtropical Underwater salinity maximum and the oxygen minimum corroborate this scheme (c.f. Watts, 1982).

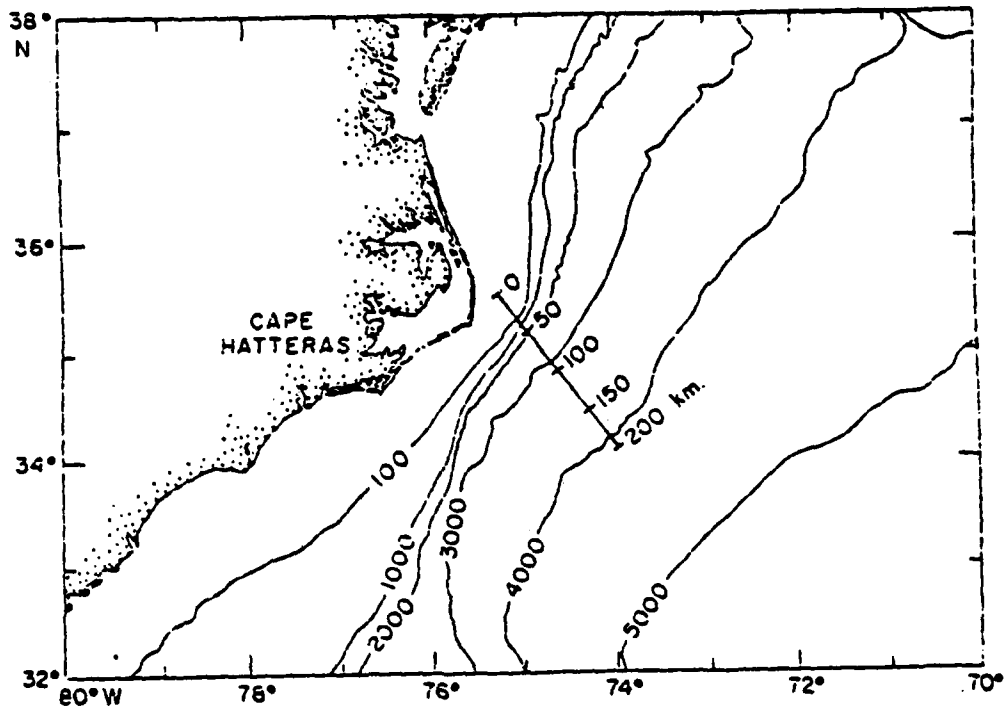
In the deep water, in contrast to the warmer water, the mid-ocean $f\partial T/\partial z$ distribution shown in figure 9 tends to be more zonally oriented. Worthington's recirculation gyre for this layer is also zonally restricted to between 30 and 40° North, as seen in figure 10. In this layer, Π is relatively uniform ($.25$ to $3 \cdot 10^{-6} \text{ }^\circ\text{C m}^{-1} \text{ s}^{-1}$) throughout the closed recirculation region and across the entire Gulf Stream, suggestive of a freer cross-stream exchange of water at depth.

Further work will be directed toward an examination of geostrophy and potential vorticity in the Gulf Stream downstream of Cape Hatteras, primarily using data gathered in July 1982². It is hoped that this study will supplement other research on Π in the North Atlantic to yield a more complete understanding of the Gulf Stream and its role in the general circulation.

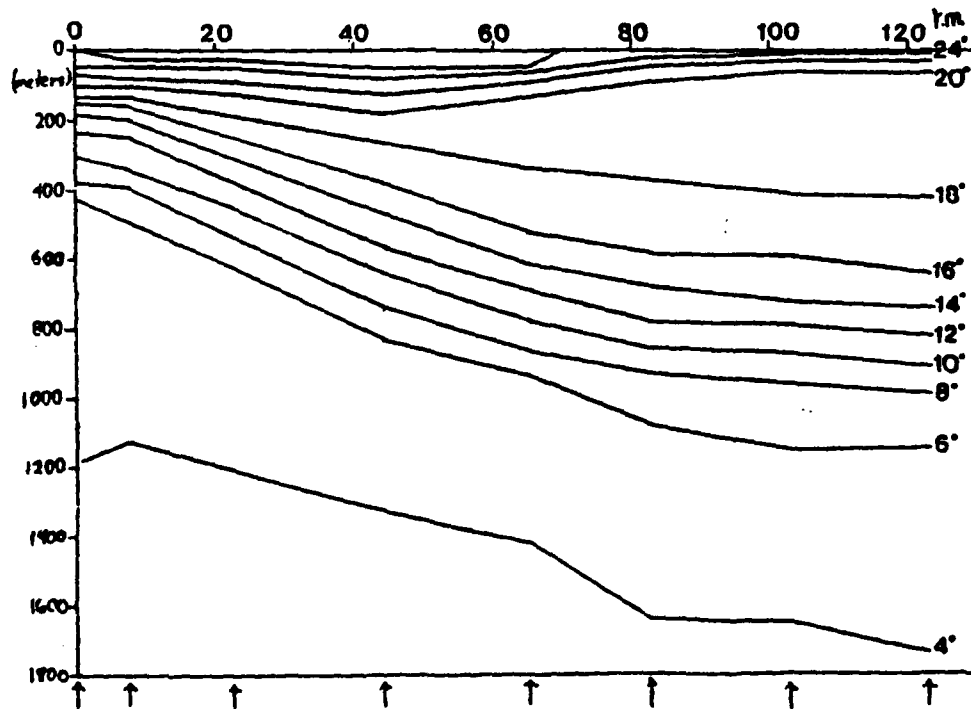
2 A two ship operation involving Tom Rossby's Pegasus-derived direct velocity measurements and our CTD/transport float work was successfully completed since the time of the Gulf Stream Workshop.

References

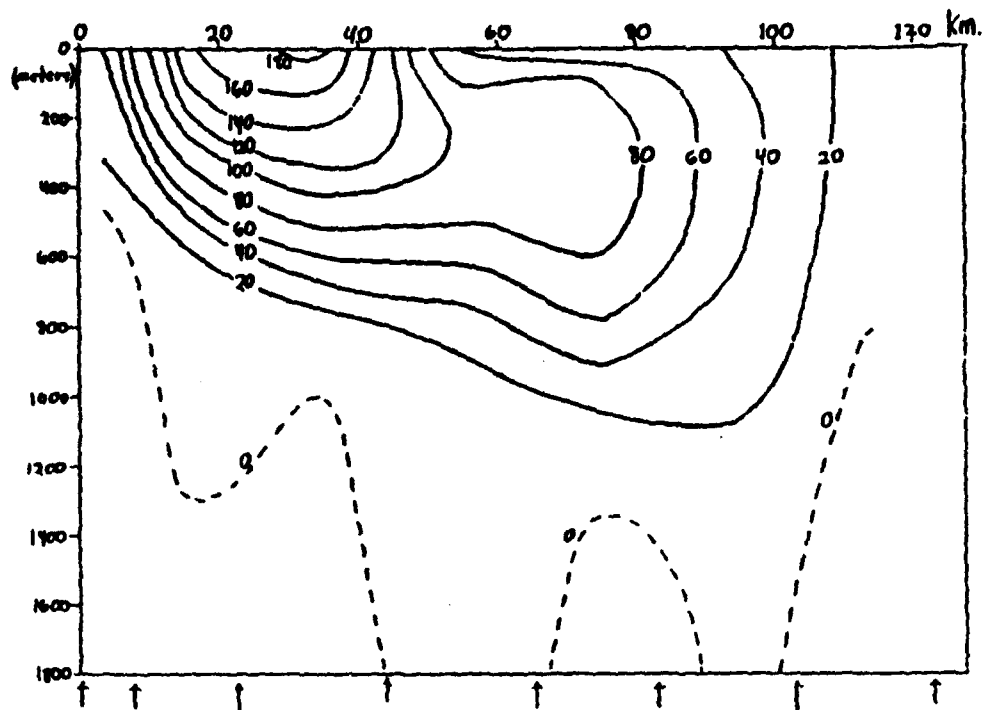
- Ertel, H., Ein neuer hydrodynamischer Wirbelsatz, Meteorologische Zeitschrift, 59, 277-282, 1942.
- Fuglister, F.C., Atlantic Ocean Atlas of Temperature and Salinity profiles and Data from the International Geophysical Year of 1957-58, Woods Hole Oceanographic Institution Atlas Series, 1, 209 pp., 1960.
- McDowell, S., P. Rhines, and T. Keffer, North Atlantic Potential Vorticity and its Relation to the General Circulation, preprint, 1982.
- Pedlosky, J., Geophysical Fluid Dynamics, 624 pp., Springer-Verlag New York, Inc. N.Y., 1979.
- Richardson, P.L., Transport and Velocity of the Gulf Stream at Cape Hatteras, MS Thesis, U. of Rhode Island, 1970.
- Watts, D.R., Gulf Stream Variability, in: Eddies in Marine Science, ed. A. Robinson, in press, 1982.
- Worthington, L.V., On the North Atlantic Circulation, 110 pp., The Johns Hopkins University Press, Baltimore, MD., 1976.



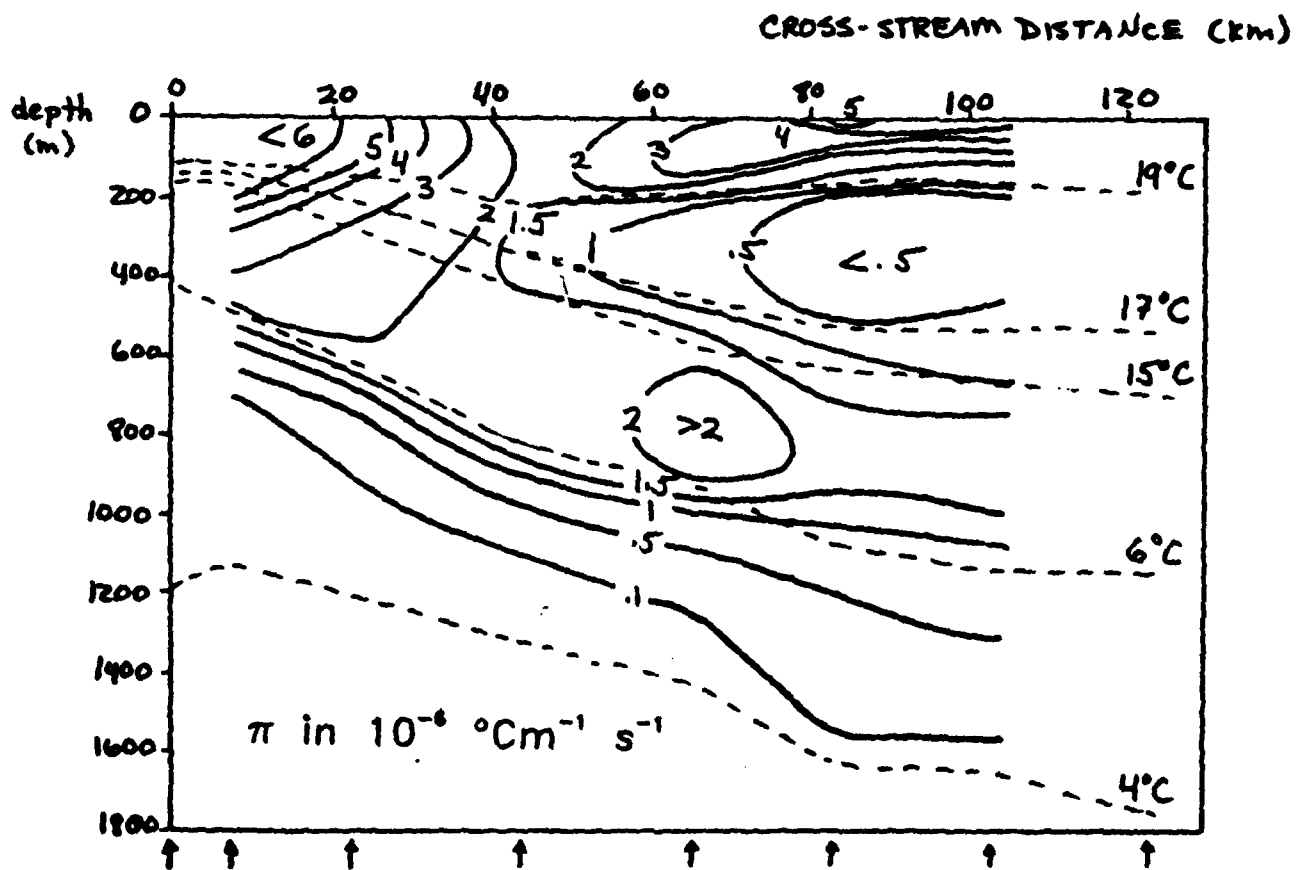
1. Location of the section analyzed, taken in July 1967 by J. Knauss and P. Richardson.



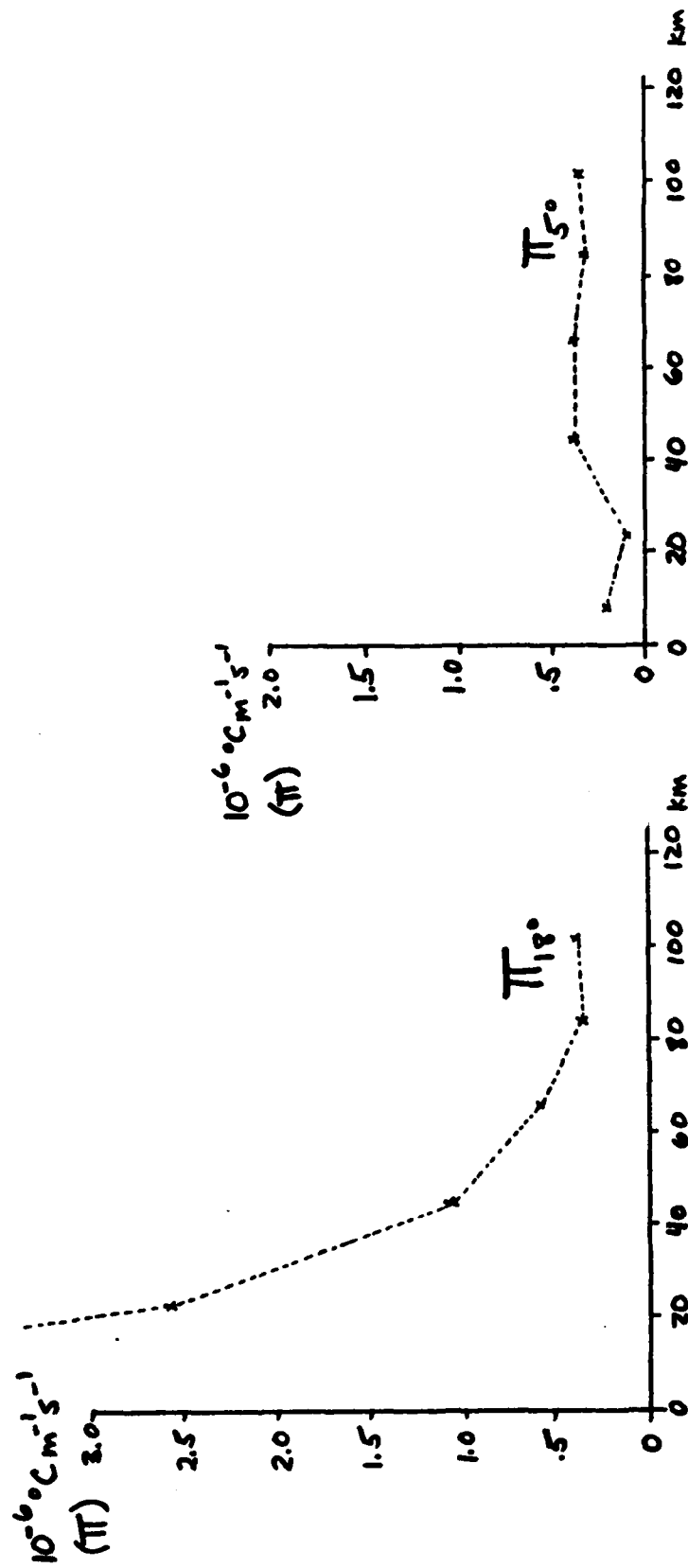
2. Isotherm depths vs. cross-stream distance.



3. Geostrophic velocity contours (from hydrographic stations, referenced to transport float data).

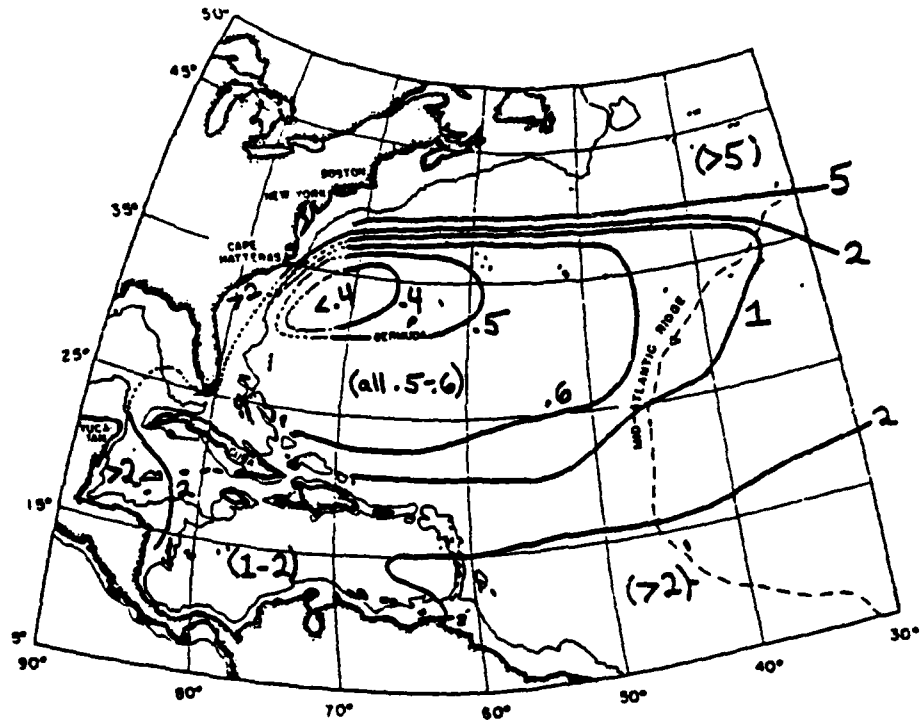


4. Results of the potential vorticity calculation.

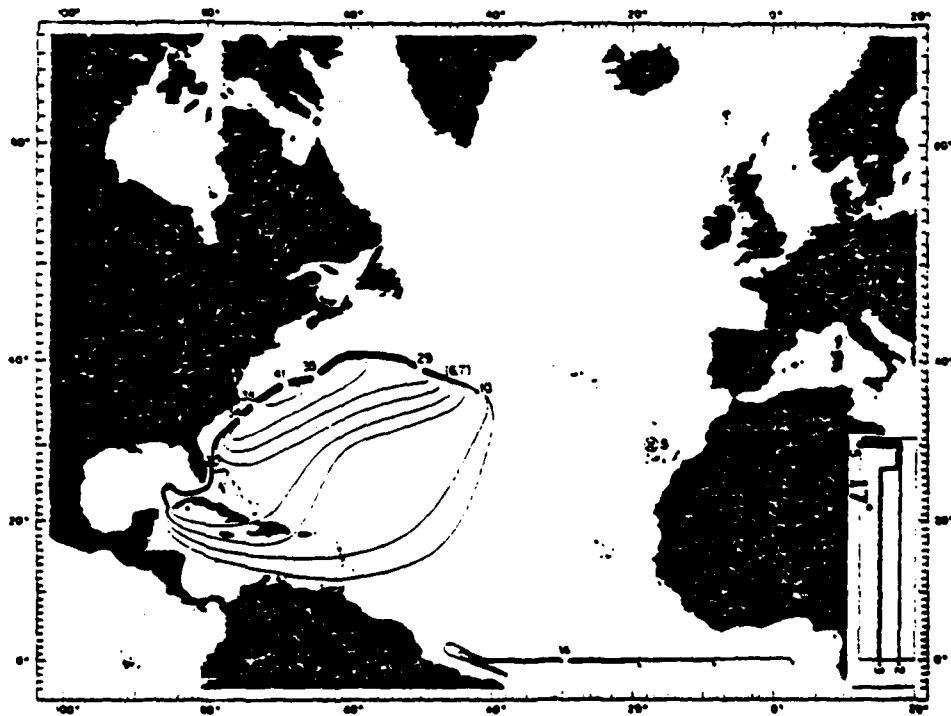


5. Potential vorticity along the 18°C isotherm, across the Gulf Stream.

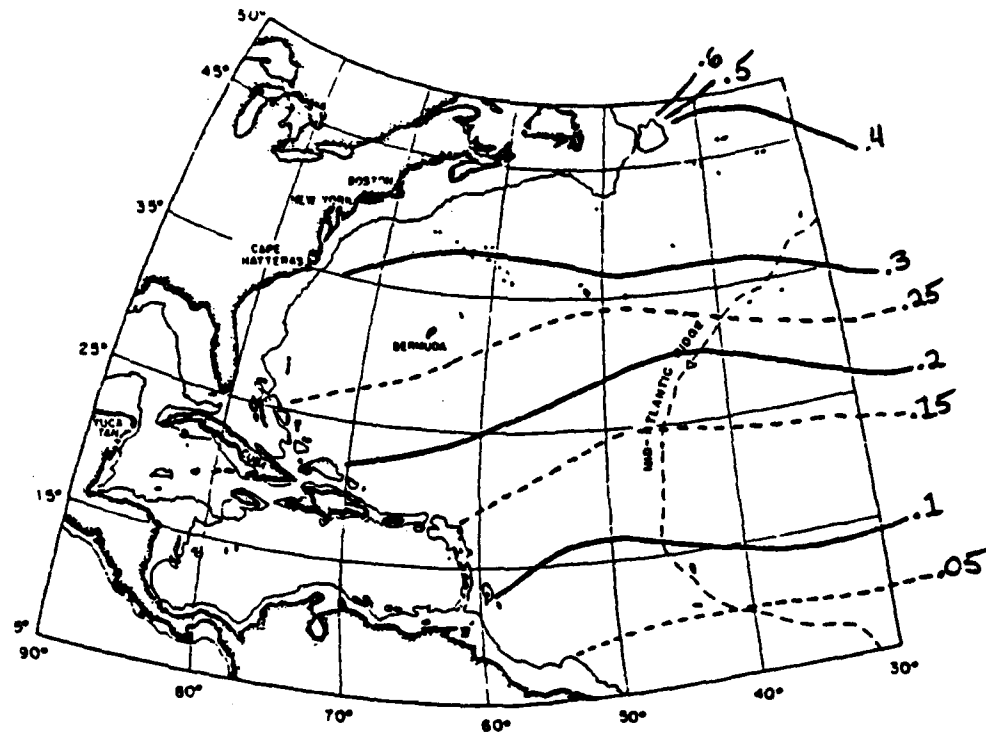
6. Potential vorticity along the 5°C isotherm, across the Gulf Stream.



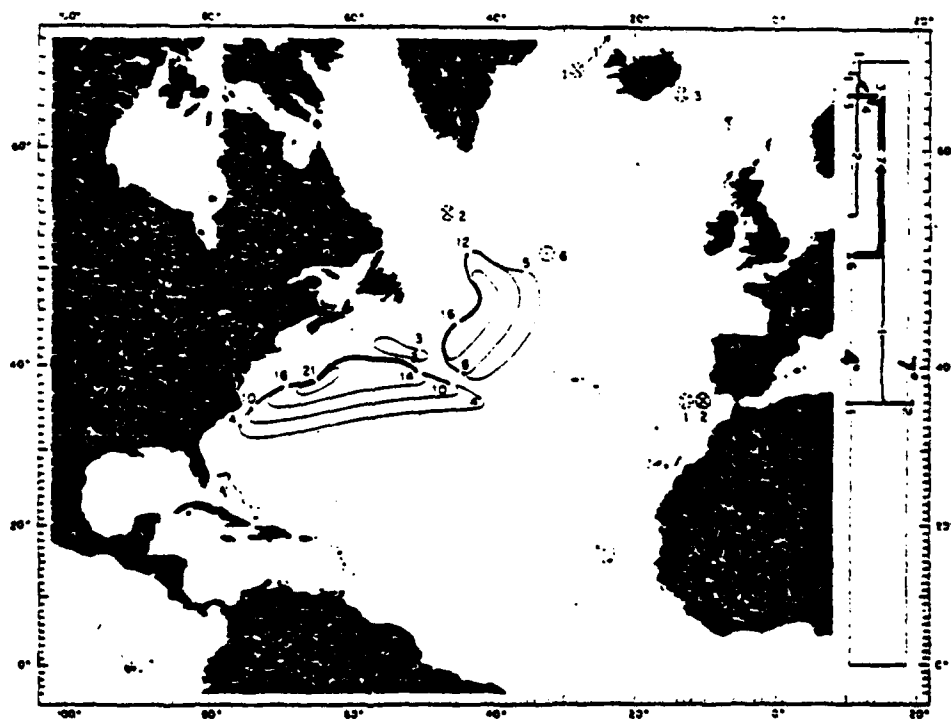
7. Contours of $f\partial T/\partial z$ in the North Atlantic for the 17-19°C layer.



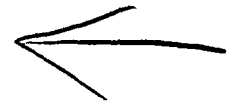
8. Western North Atlantic gyre for $T > 17^\circ\text{C}$ from Worthington (1976).



9. Contours of $f\theta T/\theta z$ in the North Atlantic for the 4-6°C layer.



10. Western North Atlantic gyres for the 4-7°C water, from Worthington (1976).



Observations on the Vertical Coherence of Gulf Stream Meanders

William E. Johns
University of Rhode Island
Kingston, RI

I. Introduction

Recent results (Watts and Johns, 1982) have shown that sub-inertial thermocline depth fluctuations east of Cape Hatteras, N.C. are closely tied with the variability in offshore-onshore location of the near-surface Gulf Stream front. Variations in thermocline depth have also been positively correlated with the location of the surface temperature front determined by satellite imagery (Cornillon, 1982). During several measurement periods spanning two years, these fluctuations consistently show downstream (\sim NE) phase propagation at speeds of 20-40 km/day.

By contrast, low-frequency currents and temperatures beneath the Gulf Stream east of Cape Hatteras show a dominant southward phase propagation of approximately 10-12 km/d (Luyten, 1977). Furthermore, these fluctuations have wave properties consistent with the bottom-intensified, baroclinic variety of topographic Rossby wave first proposed by Rhines (1970) (Thompson, 1977; Hogg, 1981). This suggests that meanders do not contribute significantly to the deep water energetics here, and raises the question of whether or not there exists a vertically-coherent, barotropic variability associated with Gulf Stream meanders east of Cape Hatteras or if perhaps instead the meanders are trapped to the upper layers of the water column. This question must be resolved in order to determine the extent to which topography influences meander dynamics. This paper examines the vertical coherence and structure of Gulf Stream meanders in the region just downstream of Cape Hatteras where the Stream flows down across the continental slope. Here the meanders are

--known to exhibit rapid spatial growth, yet the amplitudes are still small enough so that the convoluted paths associated with eddy formation may be avoided.

II. Observations

During 1979-80 an instrument array consisting of Inverted Echo Sounders (IES) and deep current meters (VACM's) was deployed 100-200 km northeast of Cape Hatteras, N.C. in 3000-4000 m depth. The instrument locations are shown in Figure 1. Currents and temperatures 1000 m off the bottom were obtained at site 1 during May-November 1979, at site 2 during May-August 1979 and November 1979-July 1980, and at site 3 during November 1979-July 1980. IES sites were maintained along sections A, B, and C during these time periods to monitor fluctuations in the location of the Stream's north-wall (15°C at 200 m), according to the method established by Watts and Johns (1982) (hereafter WJ 82). All of the data records have been low-pass filtered with a 24-hour half-width Gaussian window, and then subsampled at 12 hr. intervals.

This report will be essentially confined to a description and interpretation of (vertical) cross-spectra between Gulf Stream north-wall position along section B and temperatures measured at current meter site 3. Relevant current meter statistics and horizontal current meter cross-spectra are also briefly discussed. Other aspects of the data set are presented in WJ 82 and Johns and Watts (1983) (in preparation).

III. Results

The dispersion relation for Gulf Stream meanders within the survey area of Figure 1 is displayed as a solid line in Figure 2, plotting downstream phase speed vs. frequency (WJ 82). This curve is obtained from the along-stream phase lags between IES-determined lateral displacements of the north wall

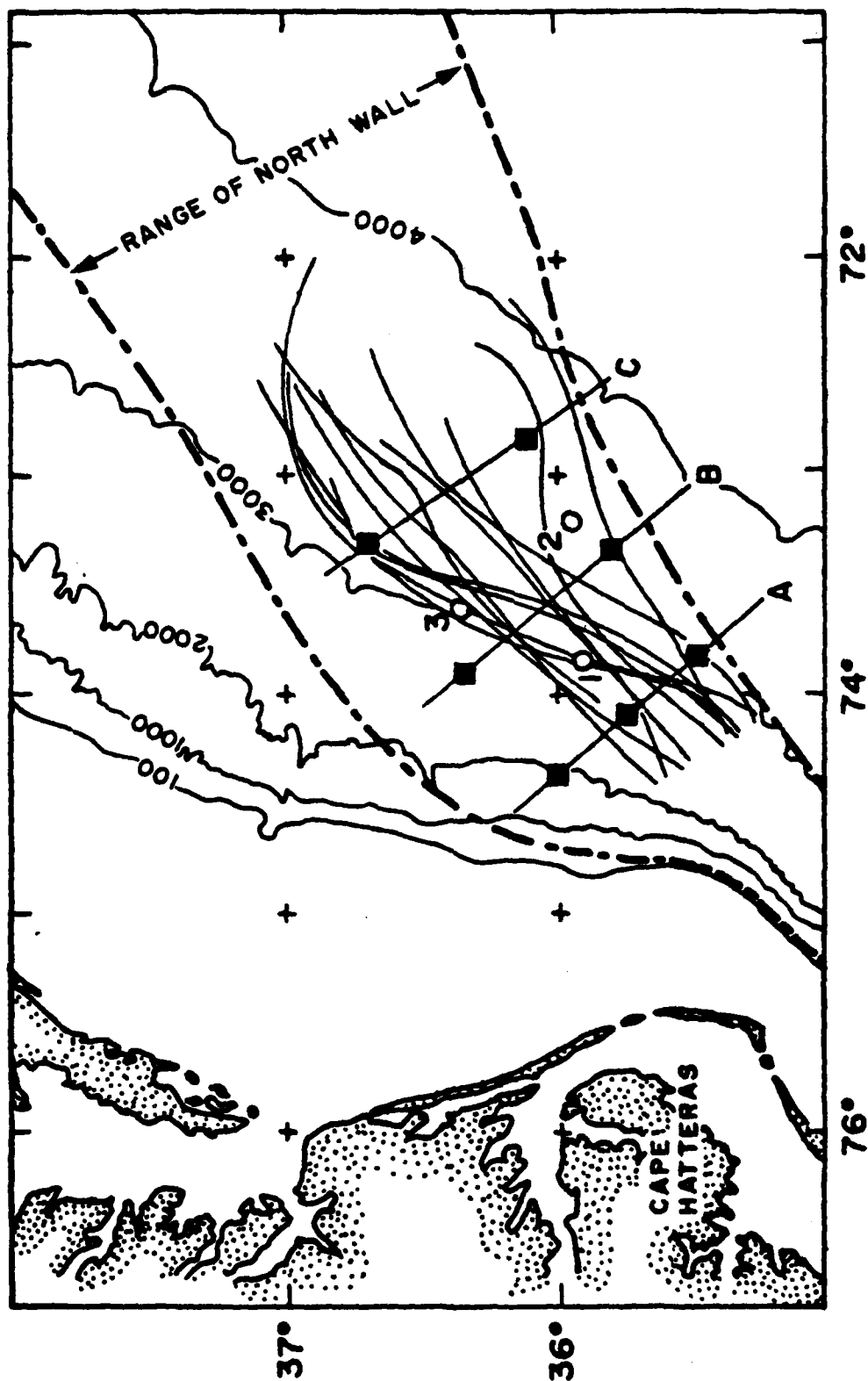


Figure 1. Survey area. IES's are shown in black squares, along sections A,B,C. Current meter sites are indicated by open circles. Light solid lines are composite paths taken from 1979-80 XBT surveys. The north-wall envelope has been constructed from historical paths using shipboard (XBT and towed thermistor) and AXBT surveys.

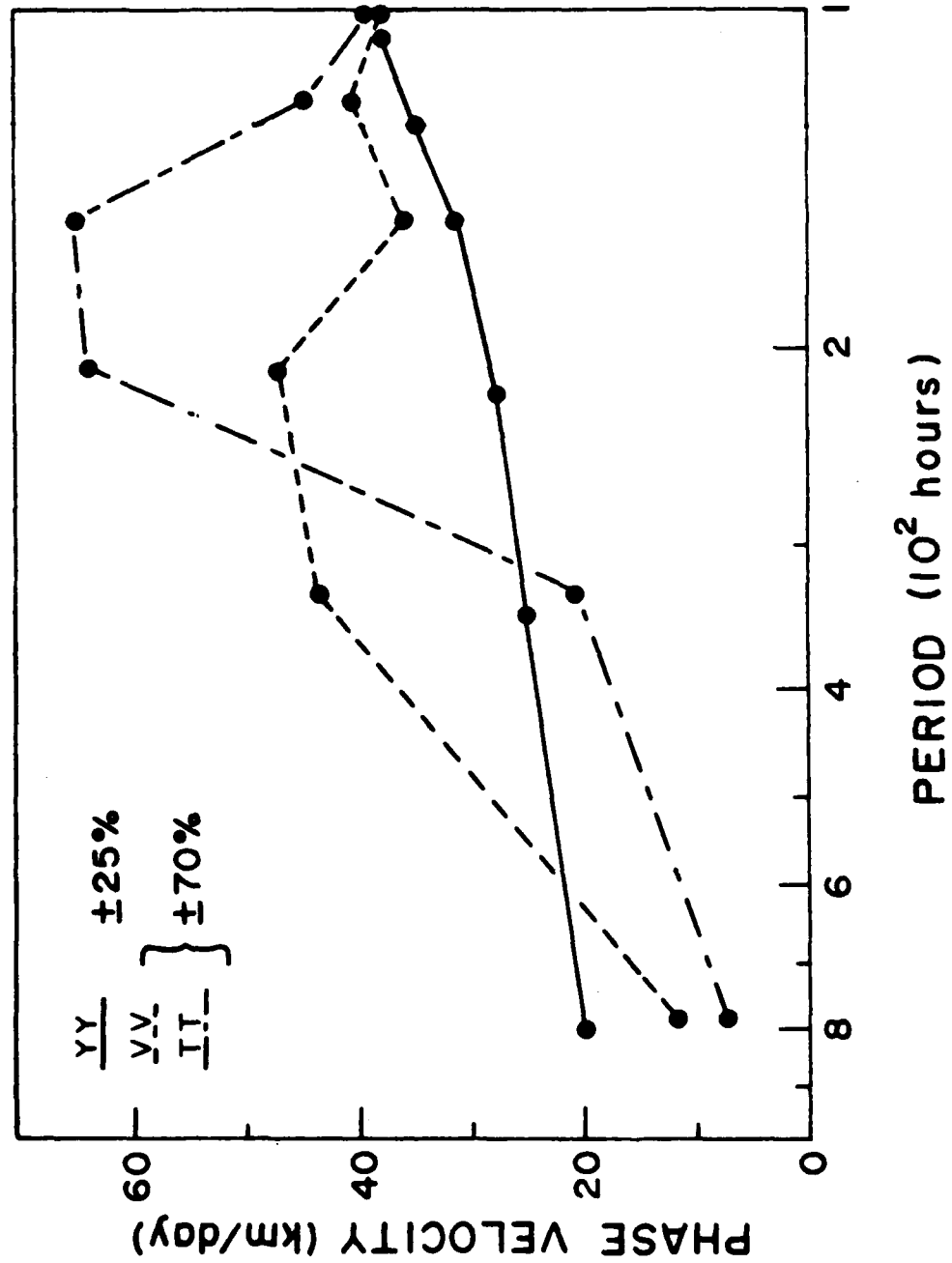


Figure 2. Downstream phase speed of north-wall displacements determined by IES (solid) compared with downstream phase speed of temperature (dash-dotted) and cross-stream velocity (dashed) fluctuations at current meter sites 1 and 2.

(15°C/200 m), and represents the ensemble of two measurement periods totalling one year. The phase speed increases smoothly from 20 km/d at a period of 800 hours (~ 1 mo.) to almost 40 km/d at a period of 100 hours (~ 4 d.)

Also plotted in Figure 2 are dispersion curves derived from the 3½-month cross-spectrum of temperature T (dotted) and of onshore-offshore (positive NW) velocity V (dashed) between CM 1 and CM 2. The current meters were 1000 m off bottom at depths of 1950 and 2680 m, respectively, and had a zonal separation of 50 km. The coherence (not shown) for both T and V was above the 90% confidence level over the entire frequency range shown.

With only two sites, it is not possible to compute the wavenumber vectors. This being the case, we have assumed a northeasterly direction of propagation in interpreting the phase delays. The phase speed magnitudes of Figure 2 are therefore the (possibly enlarged) values $|c| = \omega/\vec{k} \cdot \hat{i}$, based on the projection of the wavenumber vector \vec{k} onto a northeast unit vector \hat{i} .

The picture in Figure 2 is that of smaller downstream-component phase speeds in the deep water at low frequency, gradually rising above the IES curve to a maximum of 40-60 km/d near 10 d, and then a convergence of all three curves to essentially identical phase speed values at periods approaching 4 d. Due to the shortness of the current meter records, the (T,V) phase estimates have $\pm 70\%$ error limits and as a result these curves are not quantitatively distinct from the IES curve. Nevertheless, the agreement near 4-5 days suggests that the deep fluctuations in this band are coupled to those in the upper layer. The disagreement at long and especially at the intermediate periods may indicate a lack of vertical coupling at these frequencies.

Figure 3 shows time series of cross-stream velocity $(V)^+$ and temperature (T)

^+V is the velocity component perpendicular to 051° true, which was the mean orientation of the Gulf Stream during this period.

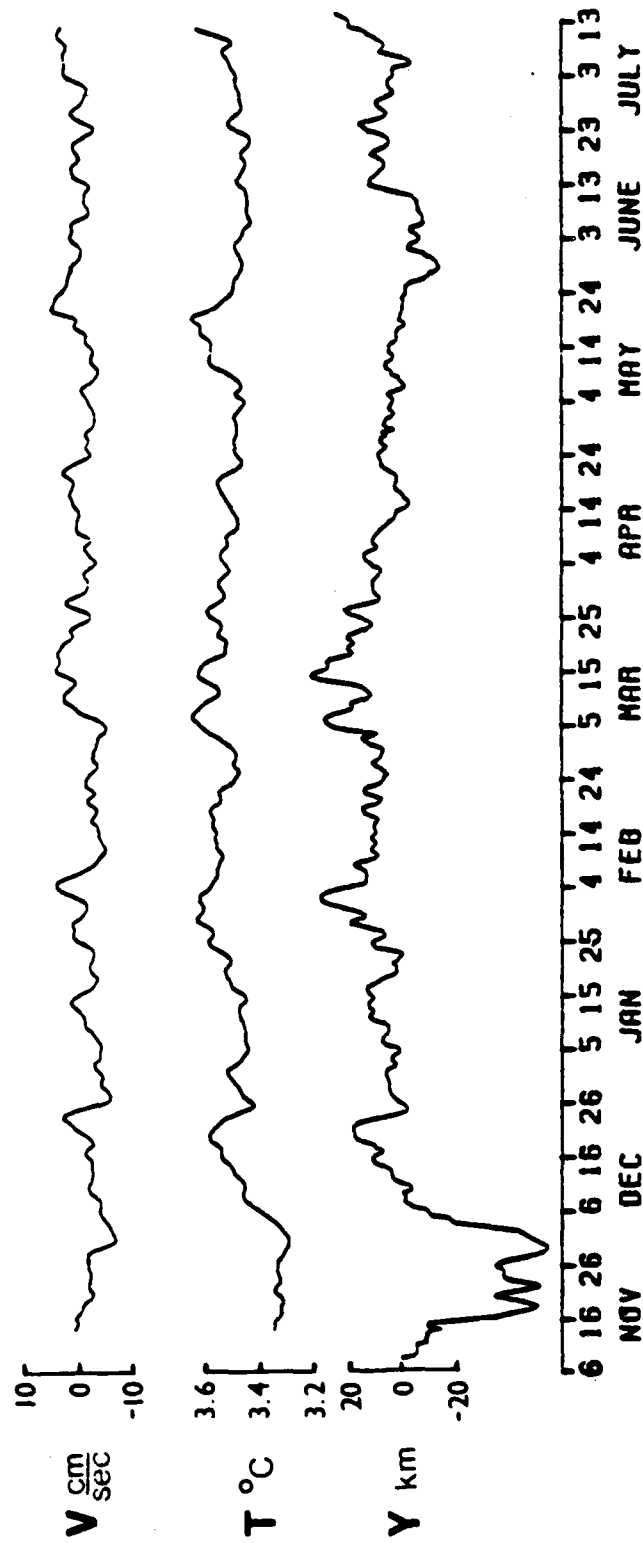


Figure 3. Time series of north-wall position (Y) along IES section B, compared with temperature (T) and cross-stream velocity (V) at current meter site 3. The north wall was nearly overlying site 3 from December 1979 through July 1980.

at CM site 3, along with the time series of north-wall displacement (Y) along IES section B, relative to its mean position $Y=0$. Several events of onshore movement (decreasing Y) with periods of approximately 10 d and less are clearly correlated with increases in T and V (e.g. near December 20, February 3, and March 5-15).

Let the location of the horizontal temperature front be given by the Fourier sum $y(x,z,t) = \sum_n Y_n(x,z,t) = \sum_n \hat{Y}_n(z) e^{i\phi_n(z) + ik_n(x-c_nt)}$. $\hat{Y}_n(z)$ is therefore the depth-varying amplitude of a given constituent wave n travelling in the mean downstream direction x at speed $c_n(k_n)$. The phase ϕ_n of the wave may also vary with depth. Changes in lateral displacement of the front at a current meter site, at some level z_2 , are

$$dy(z_2) = \sum_n dY_n(z_2) = \left[\frac{\partial T}{\partial y}(z_2) \right]^{-1} \cdot dT(z_2)$$

We may relate the deep front displacement $\hat{Y}_n(z_2)$ to the near-surface displacements $\hat{Y}_n(z_1)$ measured by IES:

$$R_n = \frac{\hat{Y}_n(z_2)}{\hat{Y}_n(z_1)} = \left[\frac{\partial T}{\partial y}(z_2) \right]^{-1} \cdot \left[\frac{G_{T_n}(z_2)}{G_{Y_n}(z_1)} \right]^{\frac{1}{2}} \quad (1)$$

where G_{T_n} and G_{Y_n} are the temperature and displacement auto-spectra, respectively. The phase between $T(x_2, z_2)$ and $Y(x_1, z_1)$ is:

$$\phi_n = \phi_n(Z_2) - \phi_n(Z_1) + \psi_n(\delta x) \quad (2)$$

where $\psi_n(\delta x) = k_n(x_2 - x_1)$ is the (small) phase difference due to along-stream separation δx .

Given that T and Y are coherent, (1) gives an estimate of the amplitude ratio $\hat{Y}_n(Z_2)/\hat{Y}_n(Z_1)$, and (2) an estimate of the vertical phase tilt $\phi_n(Z_2) - \phi_n(Z_1)$. In (2), $\psi_n(\delta x)$ will be computed based on WJ82's dispersion relation for Gulf Stream meanders, and $\frac{\partial T}{\partial y}(Z_2)$ in (1) will be estimated from historical data.

During the time between November 1979 and July 1980, the current meter at site 3 was in an ideal location for testing the model. The mean north wall position during this time period was nearly overlying the site, and with the exception of the first month, the deviations from this mean were 0(20 km) or less.

Before proceeding, $\frac{\partial T}{\partial y}(Z_2)$ must be chosen. We have used for reference three deep sections of the stream which were normal to the instantaneous path [Barrett and Schmitz(1971), Richardson and Knauss (1971), Warren and Volkman (1968)]. From each section the average $\frac{\partial T}{\partial y}$ was computed over approximately one Rossby deformation radius (35 km), centered on $T = 3.5^\circ\text{C}$ and $Z = 2000$ m (The mean temperature at site 3 was 3.5°C). The values are remarkably consistent; 0.0055°C/km , 0.0049°C/km , and 0.0045°C/km ; we therefore take $\frac{\partial T}{\partial y}(3.5^\circ\text{C}, 2000\text{ m}) = 0.0050^\circ\text{C/km} (\pm 10\%)$.

Figures (4a,b) show the cross-spectrum between north-wall position Y along IES section B and site 3 temperature T. To retain the desired resolution, only 4 adjacent bands have been averaged, and as a result, the indicated 90% confidence limits are rather large. Even so, the coherence is significant within a band from 100 - 220 hours (4 - 9 days), except for one estimate near 150 hours. Outside this band, the coherence

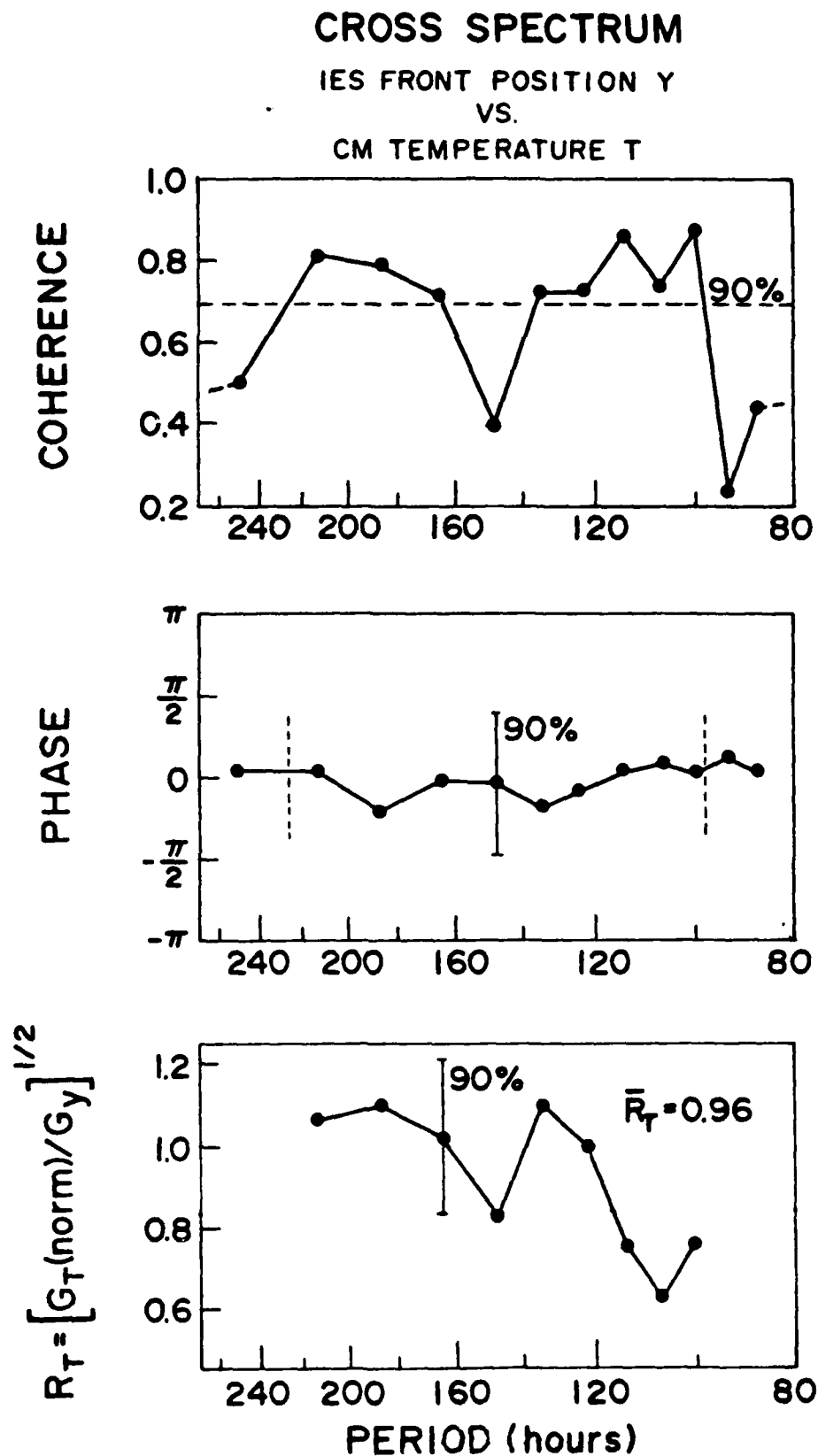


Figure 4. Cross-spectrum between north-wall position along section B and temperature at site 3: (a) coherence, (b) phase, and (c) vertical amplitude ratio.

drops off sharply, especially at the high frequencies. In Figure 4b, $\psi_n(\delta x)$ has been subtracted from the observed phase so that the plot indicates purely the vertical phase tilt $(\phi_n(z_2) - \phi_n(z_1))$. Over the frequency range of interest this phase difference is indistinguishable from zero. There is thus no indication of a phase tilt opposing the mean vertical shear (i.e. lower layer leading the upper layer), which according to baroclinic instability theory would signify that the perturbations are drawing energy from the mean flow.

The amplitude ratio R_n computed from (1) is shown in Figure 4c. Its average value for the 4-9 day band is $\bar{R} = \left(\frac{\partial T}{\partial Y}\right)^{-1} \frac{\sum_n G_T T_n}{\sum_n G_Y Y_n} = 0.96$, with a trend toward smaller R_n values (~ 0.7) at the 4-5 day periods. This trend is insignificant, based on the combined uncertainties in G_T and G_Y , but may indicate that the 4-5 day meanders are weakly surface-trapped. The vertical structure will be investigated in more detail using a vertical array of current meters to be deployed in the Gulf Stream later this year. In summary, the 4-9 day fluctuations appear to be coherent and in-phase vertically, and are nearly barotropic ($\bar{R} \sim 1.0$).

Deep Currents

Perhaps the most surprising result thus far is the lack of vertical coherence for periods of 10 days and longer, especially when considering that the near-surface path displacements are dominated by long periods (WJ82). To examine this in more detail a rotary spectrum analysis was performed on each of the individual current records. Initially four basic frequency bands were averaged, yielding a lowest frequency spectral

estimate at 80 days for sites 2 and 3, and at 60 days for site 1. The mean currents and current variance ellipses for all three sites are shown in Figure 5. We have divided the variance into two period bands: 10-80 days and 4-10 days, based on the marked change in orientation of the major axes which occurred in all cases near 10 days. Periods shorter than 4 days are not of particular interest here since meanders are known to have little energy at these frequencies (WJ82).

The 4-10 day variance ellipses are smaller by almost one order of magnitude than the 10-80 day ellipses, and tend to be more isotropic. Yet they are still somewhat elongated and point consistently NNW-SSE. This orientation is nearly perpendicular to the mean direction of flow (051°) taken by the surface Gulf Stream during this period. By contrast, the low-frequency ellipses are closely aligned with the mean isobaths and are quite elongated, having major axes of approximately $30 \text{ cm}^2/\text{sec}^2$. The current vectors show no preferred sense of rotation (i.e. the clockwise and anticlockwise spectra have nearly equal energies), and the velocity components are nearly 180° out of phase. This suggests that the oscillations are transverse. The deep currents are also highly coherent vertically at 500 m and 1000 m off the bottom for periods longer than 10 days (at site 2 a second meter was placed 500 m off the bottom). These characteristics are very similar to those of current records taken in water depths shallower than 4000 m during the 1974 WHOI 'Rise Array' experiment (Luyten, 1977), and also to those taken near WHOI site D ($39^{\circ}10'N$, $70^{\circ}W$) on the continental rise south of Cape Cod (Thompson and Luyten, 1976).

From the 'Rise Array' data, Thompson (1977) has obtained good agreement between observed phase propagation of motions with periods from 8-32 days and those predicted by a linear bottom-trapped topographic wave

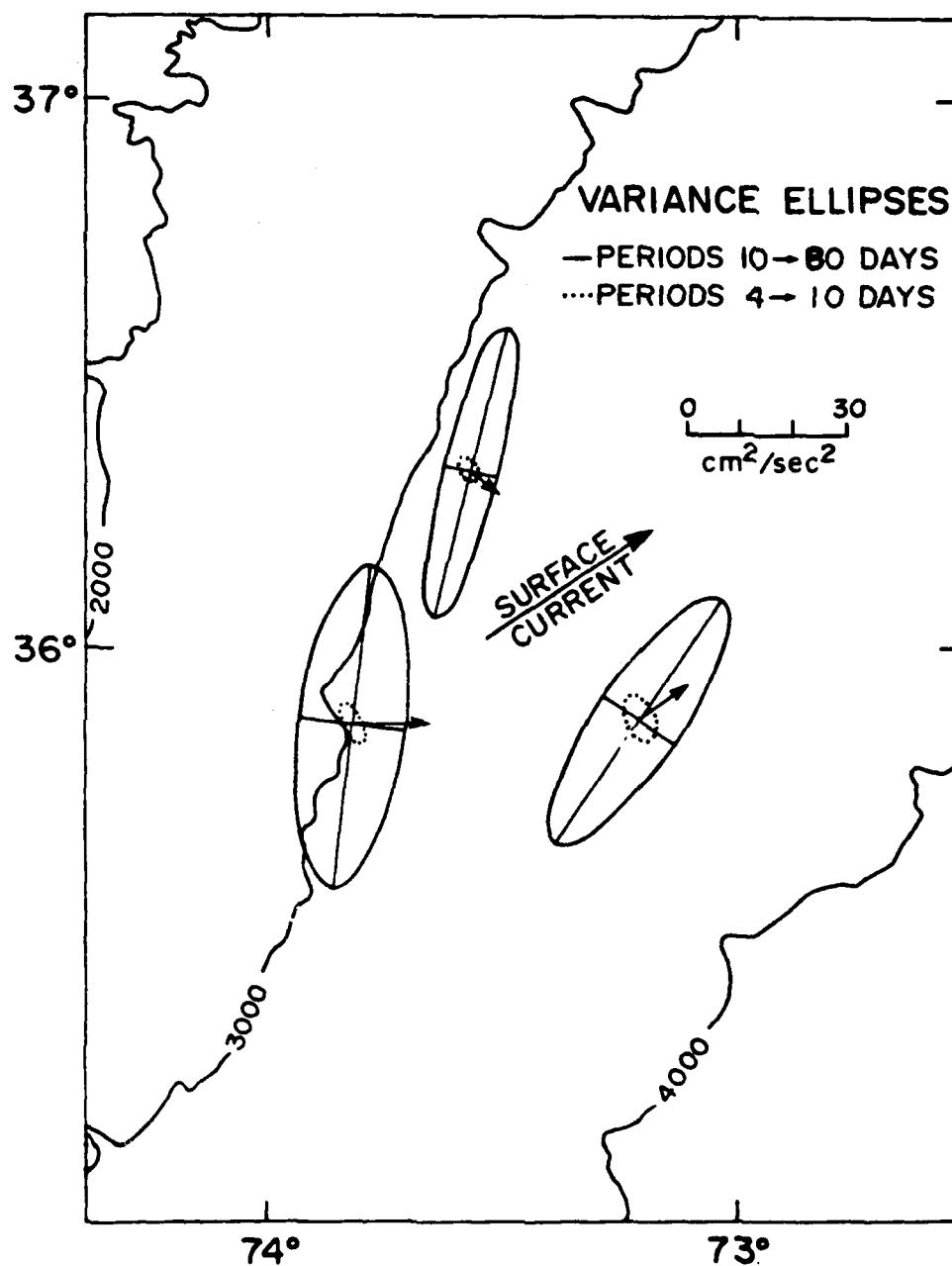


Figure 5. Mean currents and variance ellipses for sites 1, 2, and 3, all 1000 m off bottom. (Solid, dotted) ellipses represent the summed variance for periods (10-80 days, 4-10 days), respectively.

model. It can be shown (Thompson and Luyten, 1976) that for sufficiently short waves ($\lambda \gtrsim 150$ km), the frequency of the bottom-trapped mode is given approximately by $\omega = \alpha N \sin \theta$, where α is the bottom slope, N is the Brunt-Väisälä frequency, and θ is the angle measured clockwise between the wavenumber vector \vec{k} and downslope. As frequency increases, the phase propagates in a direction farther to the right of downslope. The fluid velocity is in the plane of the wavefronts, so that in the zero frequency limit the velocity fluctuations should be back and forth along the isobaths and in the high-frequency limit $\omega = \alpha N$ the fluctuations should be up and downslope. Taking $\alpha = 10^{-2}$ and $N = 10^{-3} \text{ sec}^{-1}$, the shortest period to be expected is $2\pi/\alpha N \approx 8$ days.

Observationally, the variance ellipses and wavenumber vectors are very nearly perpendicular (Thompson, 1977), but away from the bottom they do not rotate with increasing frequency as much as the short-wave theory predicts. Thompson and Luyten (1976) discuss why this might be so. Table 1 summarizes Thompson's (1977) and Thompson and Luyten's (1976) results, and compares them to our results for periods between 32 days and 8 days. The agreement is reasonable for periods longer than 12 days. Our principal axis angles are in the proper quadrant relative to the bathymetry, and with the exception of $T=30$ days whose axes lie directly along the isobaths, they have comparable magnitudes. In addition, the low-frequency phase relationship between the currents at sites 1 and 2, which we recall was not consistent with meander propagation, is in much better agreement with propagation at our observed θ 's and with the historically documented phase speeds of Table 1. Our observations, although limited, therefore tend to support the previous observations of energetic low-frequency topographic

TABLE 1

<u>T (d)</u>	<u>λ (km)</u>	<u>c (km/d)</u>	<u>θ (deg)</u>	<u>Reference</u>	<u>T (d)</u>	<u>θ (deg)</u>
32	230	7	15	Thompson(77) site'D'	30	-1 *
	270	8	11	Thompson(77) 'Rise'		
	-	-	13 *	Thom.& Luyten(76) site'S'		
16	290	18	16	"	20	9 *
	160	10	27		15	16 *
	160	10	10 *			
10.7	140	13	37	"	12	4 *
	240	22	34		10	-24 *
	130	12	32 *			
8	190	24	49	"	8.5	-45 *
	160	20	47			
	90	11	35 *			

Table 1: Comparison of previous results (left) for topographic waves with our results (right). A * indicates principal axis angle, when the wave-number direction was unknown.

wave activity along the Western North Atlantic continental rise. This is unfortunate from the viewpoint of this study, since the energy of these low-frequency motions is so large that it may effectively mask any meander-associated variability which does exist at these frequencies.

IV. Conclusions

These observations show that lateral displacements of the Gulf Stream temperature front with periods between 4 and 9 days penetrate to within 1000 m of the bottom without significant phase variation or

attenuation with depth. Within this band most of the temperature variance in deep water is produced by offshore-onshore excursions of the mean cross-stream temperature field in association with downstream-propagating meanders.

At lower frequencies ($T \geq 10$ days) the major fluctuations in deep water are not directly coupled to the near-surface variability, but are characteristic of baroclinic topographic wave motions which decay upward from the bottom. The dominance of the low-frequency spectrum by these waves makes it virtually impossible to isolate any barotropic motions which may actually be present at these frequencies. It is significant that the emergence of vertically coherent meander variability seen at periods shorter than 9 days corresponds closely with the expected disappearance of this bottom-trapped mode near its high-frequency cutoff at $T \approx 8$ days.

REFERENCES

- Barrett, J. and W. Shmitz (1971) Transport float measurements and hydrographic station data from three sections across the Gulf Stream near 67° W. WHOI Tech. Report no. 71-66.
- Cornillon, P. (1982) The edge of the Gulf Stream: Satellite versus Inverted Echo Sounder determinations. EOS Trans. AGU 63, 363, 1982.
- Hogg, N. (1981) Topographic waves along 70° W on the Continental Rise. Jour. Mar. Res., 39(4), 627-649.
- Johns, W.E. and D.R. Watts (1983) On the relationship of deep currents east of Cape Hatteras to Gulf Stream meanders. (in preparation).
- Luyten, J.R. (1977) Scales of motion in the deep Gulf Stream and across the Continental Rise. Jour. Mar. Res., 35, 49-74.
- Rhines, P.B. (1970) Edge-, bottom-, and Rossby waves in a rotating stratified fluid. Geophys. Fluid Dyn., 1, 273-302.
- Richardson, P.L. and J.A. Knauss (1971) Gulf Stream and Western Boundary Undercurrent observations at Cape Hatteras. Deep-Sea Res., 18, 1089-1109.
- Thompson, R.O.R.Y. (1977) Observations of Rossby waves near site D. Prog. in Ocean., 7, 1-28.
- Thompson, R.O.R.Y. and J.R. Luyten (1976) Evidence for bottom-trapped topographic Rossby waves from single moorings. Deep-Sea Res., 23, 629-635.
- Warren, B.A. and G.H. Volkmann (1968) Measurement of volume transport of the Gulf Stream south of New England. Jour. Mar. Res., 26(2), 110-126.
- Watts, D.R. and W.E. Johns (1982) Gulf Stream Meanders: Observations on propagation and growth. Jour. Geophys. Res., (in press).



Preliminary Results on Normalization of Hydrographic Sections
of the Gulf Stream

by

Timothy W. Kao

Department of Civil Engineering

The Catholic University of America; Washington, D.C. 20064

ABSTRACT

Gulf Stream sections north of Cape Hatteras are normalized by a length scale and a depth scale to test whether all sectional σ_t -profiles will collapse into a universal plot. Such a plot is of interest per se since it will display the inherent similarity of Gulf Stream sections. Furthermore it sets the stage for a quantitative comparison between field data and model results. To determine the appropriate length scale we first compute the sea-surface height changes relative to a reference level from the density structure of the hydrographic section. From these we obtain the length scale

$$\lambda = \Delta h_m / (dh/dx)_m$$

where Δh_m is the maximum rise height across the stream and $(dh/dx)_m$ is the maximum slope of the height profile. The depth scale is the depth of the 10% density anomaly between the Sargasso Sea warm pool and bottom North Atlantic water. The above length scale has been shown by Kao and Cheney (1982) to correlate the sea-surface height profiles of the Gulf Stream from SEASAT altimeter results.

In a recent paper, Kao and Cheney (1982) introduced a length scale which correlated well with the width of the sea-surface height anomaly across the Gulf Stream (GS) front north of Hatteras as derived from SEASAT altimeter data. The length scale is given by

$$\lambda = \frac{g}{f} \frac{\Delta h_m}{v_m} \quad (1)$$

where Δh_m is the maximum height change across the anomaly and v_m is the maximum along-front geostrophic velocity, and g and f denote the gravitational acceleration and Coriolis parameter respectively. We note that $v_m = \frac{g}{f} \left(\frac{dh}{dx} \right)_m$ where x is the cross-stream distance and $\left(\frac{dh}{dx} \right)_m$ is the maximum slope of the height profile.

The sea-surface height anomaly is of course the surface manifestation of the density anomaly between the pool of warmer, saltier water in the Sargasso Sea and the slope water. It should therefore be anticipated that the subsurface GS frontal structure should be similarly scaled by λ .

→ In this paper, we present the preliminary results of the normalization of the cross-stream density data compiled from three transects (Sections I, II, and III) of the Gulf Stream '60 data (Fuglister, 1963). All three sections are approximately perpendicular to the Stream direction.

The procedure for the analysis is as follows: from the computed density field, we calculate first the sea-surface height anomaly across the front using 1500 m as the reference level. From the sea-surface height profile, we then estimate the value of the maximum slope of the profile, $\left(\frac{dh}{dx} \right)_m$, and the maximum height change across the anomaly, Δh_m . From these, λ is readily obtained.

λ is used to normalize the cross-stream distance x . For the vertical scale, we choose arbitrarily the depth D of the isopycnic

$0.9 \Delta\sigma / \Delta\sigma_m$ representing 10% of the total density deficit $(\Delta\sigma)_m$ between the near surface Sargasso Sea water and the deep water below 1500 m, just at the Sargasso Sea side of the front. The values of $(\Delta h)_m$, λ and D are tabulated below for the three sections.

	Longitude	$(\Delta h)_m$	λ (km)	D (m)
Section I	68°30'W	1.18	70	1375
Section II	66°30'W	0.95	110	1330
Section III	64°30'W	1.00	91	1450

The composite sea-surface height profiles across the GS front for the three sections when normalized by λ and by $(\Delta h)_m$ is shown in Fig. (1), with a different symbol indicating each different section. It is seen that the front is spanned by approximately 2λ in each case. The solid curve is the sea-surface height rise profile given by Kao's (1980) model. The agreement is rather similar to the SEASAT data presented by Kao and Cheney (1982).

The subsurface plots of the isopycnics representing $\Delta\sigma / (\Delta\sigma)_m$ equal to 0.1, 0.6 and 0.9 for Sections I, II, and III are shown in Figs. (2), (3), and (4) respectively. It is seen that in each case the sub-surface front as represented by the sloping isopycnics is spanned very well by 2λ also. Furthermore the frontal structure is similar in all the plots. The choice of D is rather arbitrary, as mentioned before. Perhaps a better choice is to take the average depth \bar{D} of the same isopycnic beneath the Sargasso Sea.

Acknowledgments. The author wishes to thank Fuh-Shing Pan and Despina Michael for their help in the data analysis and reduction. This work is

supported by the NSF under Grant OCE 79-25061.

REFERENCES

- Fuglister, F. C., Gulf Stream '60, in Progress in Oceanography, Vol. 1, ed. by M. Sears, pp. 265-573, Macmillan, New York, 1963.
- Kao, T. W., The dynamics of oceanic fronts, 1, the Gulf Stream, J. Phys. Oceanogr., 10, 483-492, 1980.
- Kao, T. W., and R. E. Cheney. The Gulf Stream Front: A comparison between SEASAT altimeter observations and theory, J. Geophys. Res., 87, 539-545, 1982.

AD-A128-789

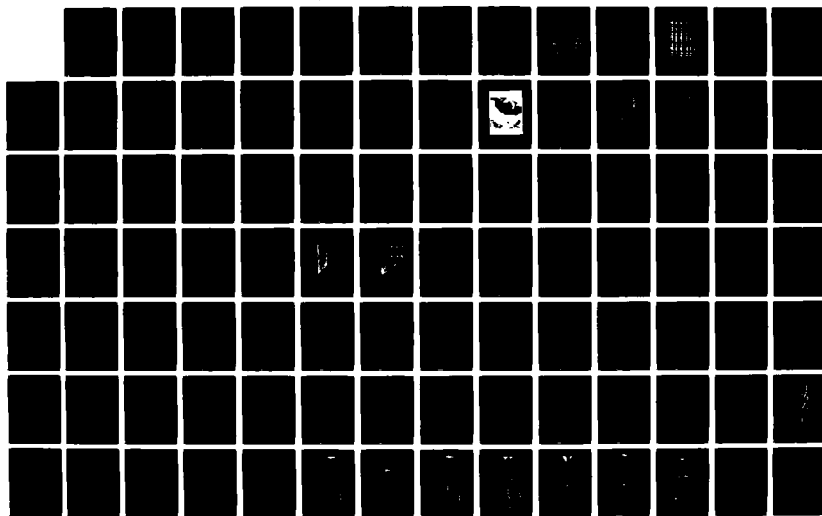
PROCEEDINGS OF THE WORKSHOP ON GULF STREAM STRUCTURE
AND VARIABILITY HELD... (U) NORTH CAROLINA UNIV AT CHAPEL
HILL APR 82 N00014-82-G-0059

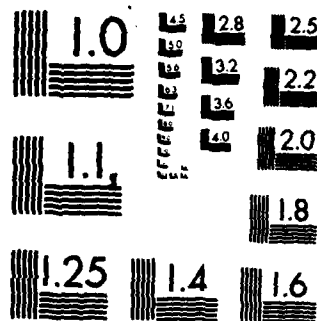
3/5

UNCLASSIFIED

F/G 8/3

NL





MICROCOPY RESOLUTION TEST CHART
NATIONAL BUREAU OF STANDARDS-1963-A

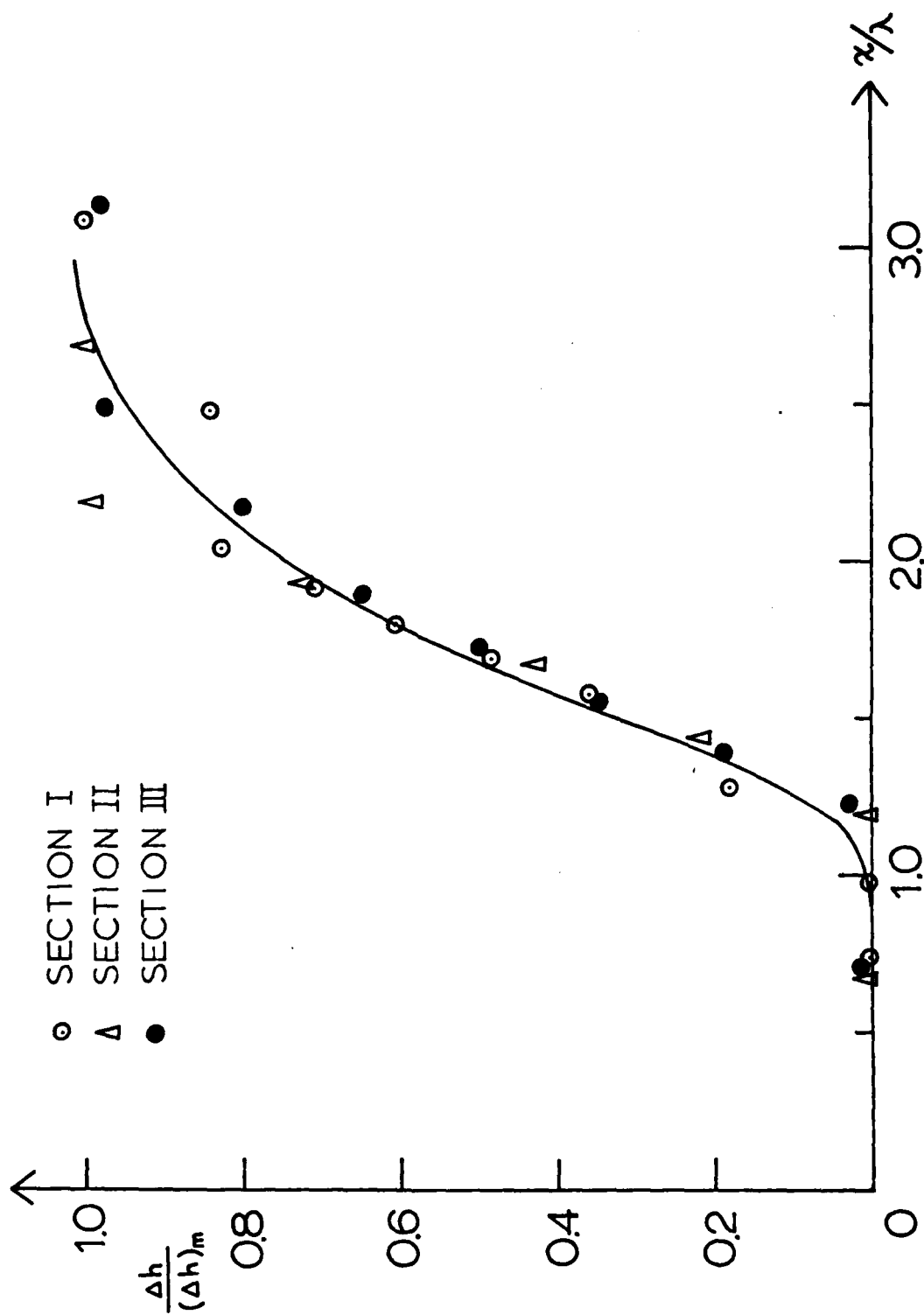
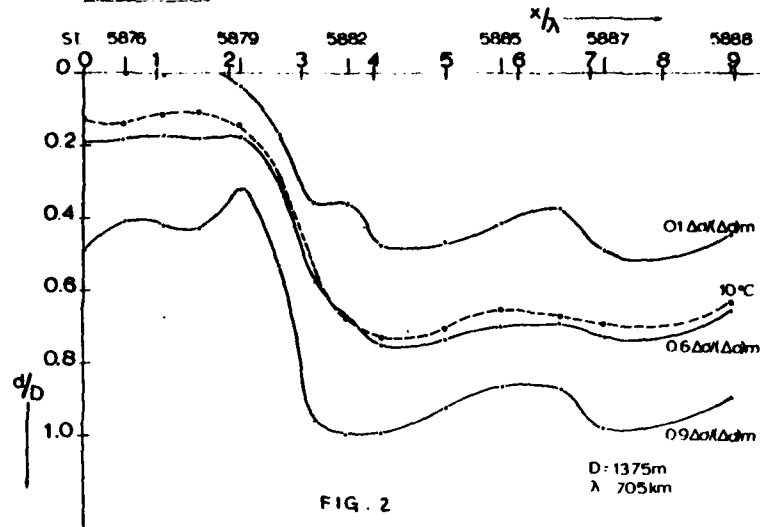
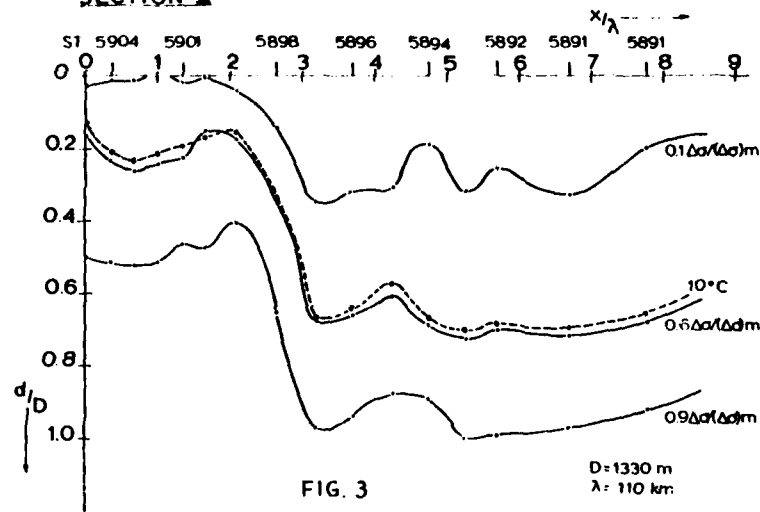


FIG. 1

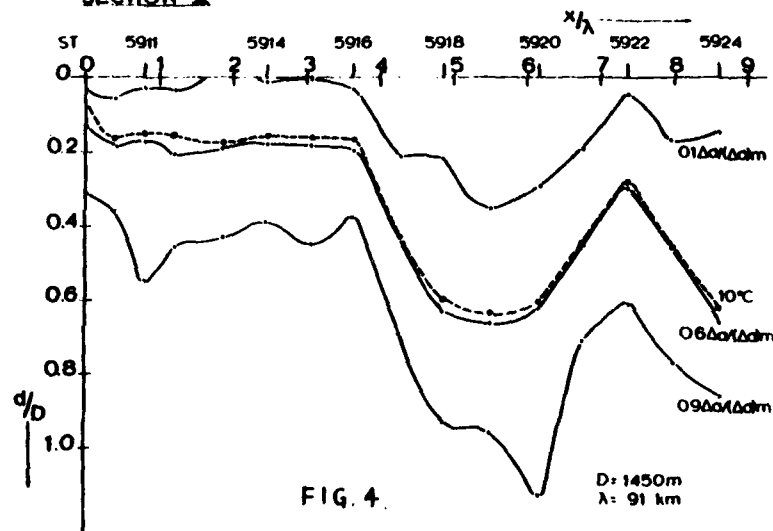
SECTION I



SECTION II



SECTION III



AD P001052

186

ON GULF STREAM FRONTAL EDDIES
ALONG THE SOUTHEAST U.S. OUTER CONTINENTAL SHELF

Thomas N. Lee
RSMAS/MPO, University of Miami
4600 Rickenbacker Causeway, Miami, FL 33149

Larry P. Atkinson
Skidaway Institute of Oceanography
P.O. Box 13687, Skidaway Island
Savannah, Georgia 31406

ABSTRACT

Low-frequency current and temperature time series from the outer shelf between Cape Canaveral, FL and Cape Romain, SC are compared to shipboard hydrographic data, satellite VHRR, coastal and buoy winds and coastal sea level during the period from February to June 1980. Low-frequency current and temperature variability along the shelf break was primarily produced by cyclonic, cold-core Gulf Stream frontal eddies. These disturbances traveled to the north at speeds of 50 to 70 cm/s^{-1} with periods of 5 to 9 days throughout the experiment and produced cold cyclonic perturbations of the northward mean flow and temperature fields over an along-shelf coherence scale of 100 km. Frontal eddies appear to be an important mechanism in the observed eastward transport of northward momentum and heat along the shelf edge. They also appear to play a key role in the transfer of eddy kinetic and potential energy back to the mean flow, which suggests an upstream formation region and shear induced dissipation. Upwelling velocities of about $(10^{-2} \text{ cm s}^{-1})$ in the cold core provide the major source of new nutrients to the outer shelf.

0.01 cm/s

INTRODUCTION

The effect of Gulf Stream forcing in the southeast U.S. outer continental shelf has been investigated using moored current meter, hydrographic, wind and satellite VHRR data collected as part of a Department of Energy and Bureau of Land Management supported interdisciplinary study of the region.

Shelf topography is particularly simple along the southeast U.S., consisting of a broad shallow shelf that slopes gently to a rather sharp shelf break at about the 75 m depth (Fig. 1). Shelf widths vary from a minimum of about 50 km off Cape Canaveral to a maximum of 120 km off Brunswick and Savannah, GA. Isobaths tend to follow the slight cusped shape of the coast with diverging isobaths north of Cape Canaveral and convergence at Cape Romain. A shallow shoal extending from Cape Fear forms the northern boundary of the region and has considerable influence over the flow in that region (Pietrafesa, unpublished report). East of Savannah a topographic anomaly of the slope known as the "Charleston Bump" (Brooks and Bane, 1978) protrudes into the Gulf Stream. Low-frequency flow variability and water exchange in the outer shelf (41-75 m) is primarily produced by Gulf Stream frontal disturbances such as northward propagating wave-like meanders and cold cyclonic frontal eddies, which occur on time scales of 2-days to 2-weeks (Lee and Brooks, 1979; Lee, Atkinson and Legeckis, 1981). South of 32°N the western edge of the Gulf Stream generally lies within ± 15 km of the shelf break (Bane and Brooks, 1979). Frontal eddies have been shown to propagate along the outer shelf in this region causing an exchange of water and momentum and a net flux of nutrients to the shelf (Lee, Atkinson and Legeckis, 1981). Yoder, et al. 1981, found a significant phytoplankton response to upwelling in the cold core of frontal eddies. Between 32 and 33°N the "Charleston Bump"

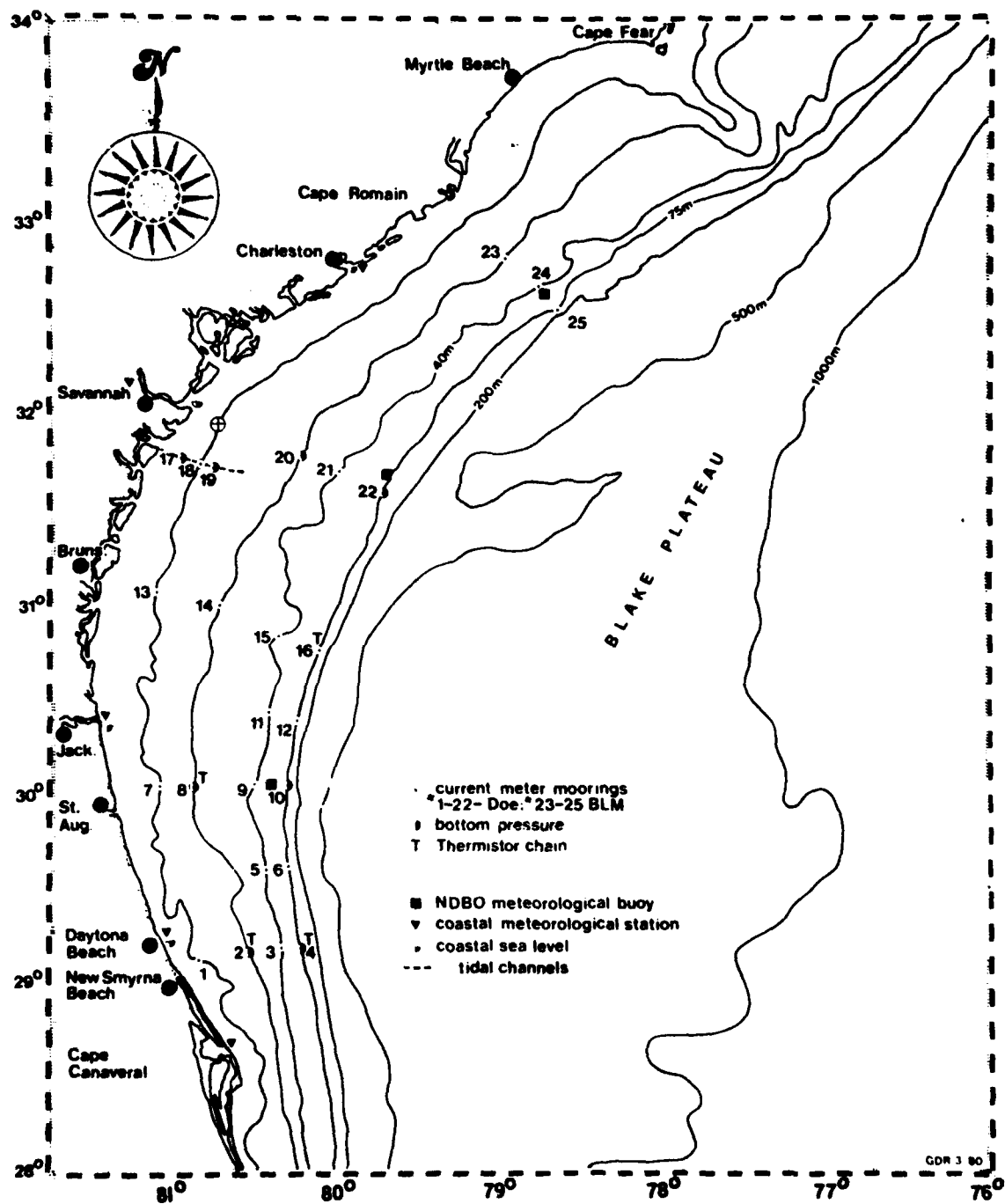


Fig. 1. GABEX-I subsurface current meter array, Feb. 17 to June 26, 1980.

appears to force an offshore meander of the Gulf Stream (Brooks and Bane, 1978; Pietrafesa, Atkinson and Blanton, 1978; Legeckis, 1979). Downstream of the "Bump" enlarged wavelike meanders can displace the Gulf Stream front up to 100 km from the shelf break (Legeckis, 1979; Bane and Brooks, 1979). These enlarged "meanders" have similar kinematic properties (Brooks and Bane, 1981; Bane, Brooks and Lorenson, 1981) as observed in the smaller frontal eddies off the Georgia shelf and suggest a dynamic connection.

During the winter/spring of 1980 a multi-institutional study of physical, chemical and biological processes on the southeast U.S. shelf was undertaken. The University of Miami effort involved moored current meter measurements along the 40 and 75 m isobaths (outer shelf) from Savannah, GA to New Smyrna Beach, FL. North Carolina State University was responsible for the mid- and inner-shelf moorings in this region and Science Applications, Inc., for the moorings off Cape Romain. In this paper we present findings from the outer shelf.

OBSERVATIONAL METHODS

Seven cross-shelf pairs of subsurface, taut-wire current meter moorings were deployed on the 40 and 75 m isobaths between Cape Canaveral, FL and Cape Romain, SC for a 4-month period from February 16 to July 2, 1980 (Fig. 1). The array was designed to investigate the effects of propagating Gulf Stream frontal disturbances on shelf processes over a wide range of spatial scales. Standard Aanderaa current meters were deployed at depths of 17, 45 and 72 m on most of the shelf break moorings, and 17 and 37 m on the moorings at the 40 m isobath, with upper flotation at 15 m. Vertical resolution was enhanced at the 30°N transect with 6 current meters at the 75 m isobath at depths of 7, 17, 27, 45, 60 and 72 m (mooring 10), and 4 current meters at the 40 m isobath at depths of 7, 17, 27 and 37 m (mooring 9). Local shelf wind data were obtained from an NDBO buoy stationed between moorings 9 and 10. Additional wind and sea level data were

obtained from coastal stations. Low-frequency (subtidal) time series of all data sets were obtained by filtering with a 40 h low-pass Lanczos filter kernel to remove variance associated with tidal and inertial motions. Semi-diurnal tides are attenuated by more than 10^5 by the filter, which results in a 4 day truncation at the start and end of the records. The filtered data were sub-sampled every 6 h and current and wind vectors were rotated to align with the local topography, such that the velocity components (u , v) are positive in the offshore and northward along-shelf directions, respectively.

LOW-FREQUENCY CURRENT AND TEMPERATURE FLUCTUATIONS

Time Domain

Low-frequency wind and upper layer currents along the outer shelf are shown in Fig. 2. The influence of the Gulf Stream is clearly indicated at the shelf break where current speeds were greater than 100 cm s^{-1} . South of 30°N strong northward flows persisted for most of the measurement period and current fluctuations were visibly coherent between stations (moorings 4, 6 and 10). Only 5 flow reversals were observed at the St. Augustine transect (mooring 10) during the 4 month study. The persistent northward flow was not observed at the shelf break off Savannah, GA (mooring 22) and the number of flow reversals increased. At the Cape Romain transect (moorings 24 and 25) prolonged southward flow events were observed at the shelf break that show little visual similarity to the currents off Savannah (mooring 22). Along the 40 m isobath low-frequency currents in the upper layer were generally poorly correlated to events at the shelf break. However, significant visual coherence did occur between events along the 40 m isobath sites and shelf winds. Current amplitudes were also similar in magnitude between the 40 m sites with little indication of any seasonal trend.

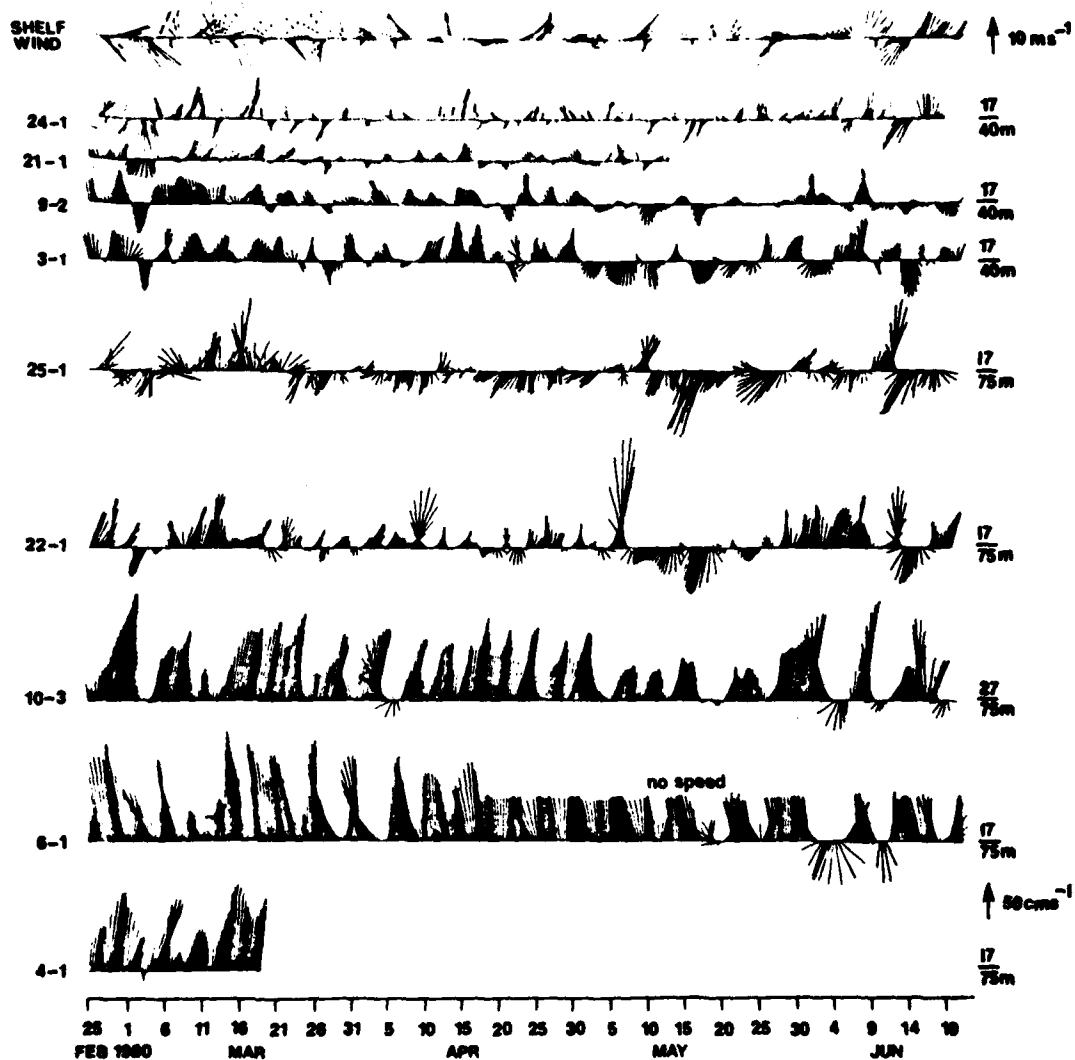


Fig. 2. Time series of 6-h rotated 40-HLP wind and current vectors from the upper layer for Feb. 25 to June 21, 1980. Current meter identification is given on the left, instrument and water depths on the right with scale arrows.

The vertical distribution of subtidal currents and temperature at the shelf break on the St. Augustine transect is shown in Figs. 3 and 4. Current and temperature fluctuations were strongly coupled at the shelf break throughout the water column. Onshore flow events that occurred nearly simultaneously over the vertical array were followed closely by decreasing along-shelf currents and decreasing temperatures. Thus, cold temperature anomalies occurred with cyclonic perturbations of the basic northward flow and the effect was observed over the total water column. Over the total 4-month experiment approximately 20 disturbances of this type were observed, giving an average period of about 6 days (Fig. 4, events 1-14). Vertical shears at the shelf break ranged from about $2 \times 10^{-3} \text{ s}^{-1}$ to $1 \times 10^{-2} \text{ s}^{-1}$ in the fluctuations and $1 \times 10^{-2} \text{ s}^{-1}$ in the mean, indicating a significant baroclinic component in both the fluctuating and mean parts of the flow. The baroclinicity was greatest at times of maximum northward currents, indicating periods when the Gulf Stream front was located near the shelf break.

Shelf break current and temperature records indicate that the largest amplitude fluctuations occurred in a 2-day to 2-week period band. Therefore, the data were band-pass filtered about this band by smoothing the low-frequency time series with a 2-week high frequency cut-off, which removes fluctuations with periods less than 40 hours and greater than 2 weeks. The band-pass cross-shelf (u), along-shelf (v) and temperature (T) time series from the lower layer were compared to the band-pass shelf wind components and coastal sea level measured at the mouth of the Savannah River for the period from May 15 to June 17, 1980 (Fig. 5).

Cold, cyclonic perturbations are observed to propagate northward along the shelf break at about 55 cm s^{-1} . Legeckis (1979) observed a 46 cm s^{-1} mean northward propagation speed of meanders downstream of the Charleston Bump. The propagation is clearest in the lower layer due to the greater number of available instruments but is also readily apparent in the upper layer. Events 10-14

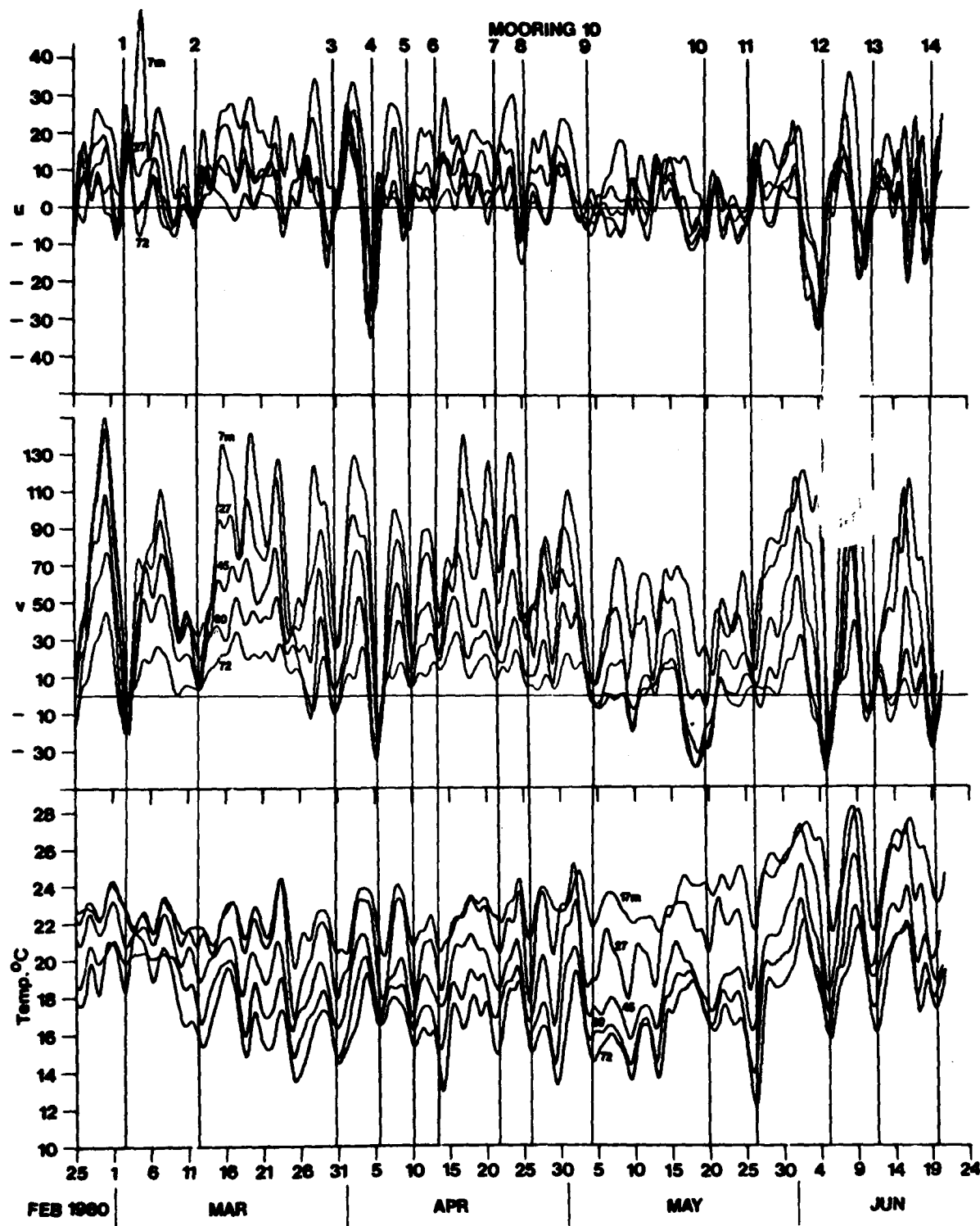


Fig. 4. Time series of 6-h rotated 40-HLP u, v, and T from mooring 10. Vertical lines are for event identification.

traveled to the north at nearly a constant speed. Event 12 was clearly recognizable over along-shelf distances of up to 425 km. The signature of these perturbations appears more pronounced at the Cape Romain transect, especially the cross-shelf component which was larger in magnitude than the along-shelf component in the upper layer at mooring 25. This location is downstream of the Charleston Bump in a region of observed meander amplification (Bane, 1983). Cold, cyclonic perturbations were observed to propagate northward along the shelf break at speeds of $50\text{--}70\text{ cm s}^{-1}$ throughout the 4-month study (Fig. 4; events 1-14) and were not visually correlated with either wind or coastal sea level events. Propagating disturbances were sometimes observed at 40 m and were visibly coherent with events at the shelf break (events 11, 12, 13 and 14, Fig. 5).

However for most of the records propagating disturbances were difficult to identify at the 40 m isobath. At the 37 m level u and v appear to be 180° out of phase (rectilinear) for a large part of the records and not significantly related to temperature fluctuations. Nonpropagating events were many times observed at the 40 m isobath when northward (southward) current fluctuations occurred simultaneously over the along-shelf extent of the array following northward (southward) winds and coastal sea level set-down (set-up) (Fig. 5, events a-d). Nonpropagating events of this type are occasionally observed at the shelf break (event a). Mixed responses also appear to occur when propagating and stationary events interact and large amplitude current fluctuations may occur when these events are in phase (events c and d at mooring 25).

Frequency Domain

Cross-spectra of cross-shelf and along-shelf low-frequency velocity components from mooring 10 at the shelf break and shelf winds are presented in Fig. 6. Spectra from records taken at the 27 m level at the shelf break are shown, for

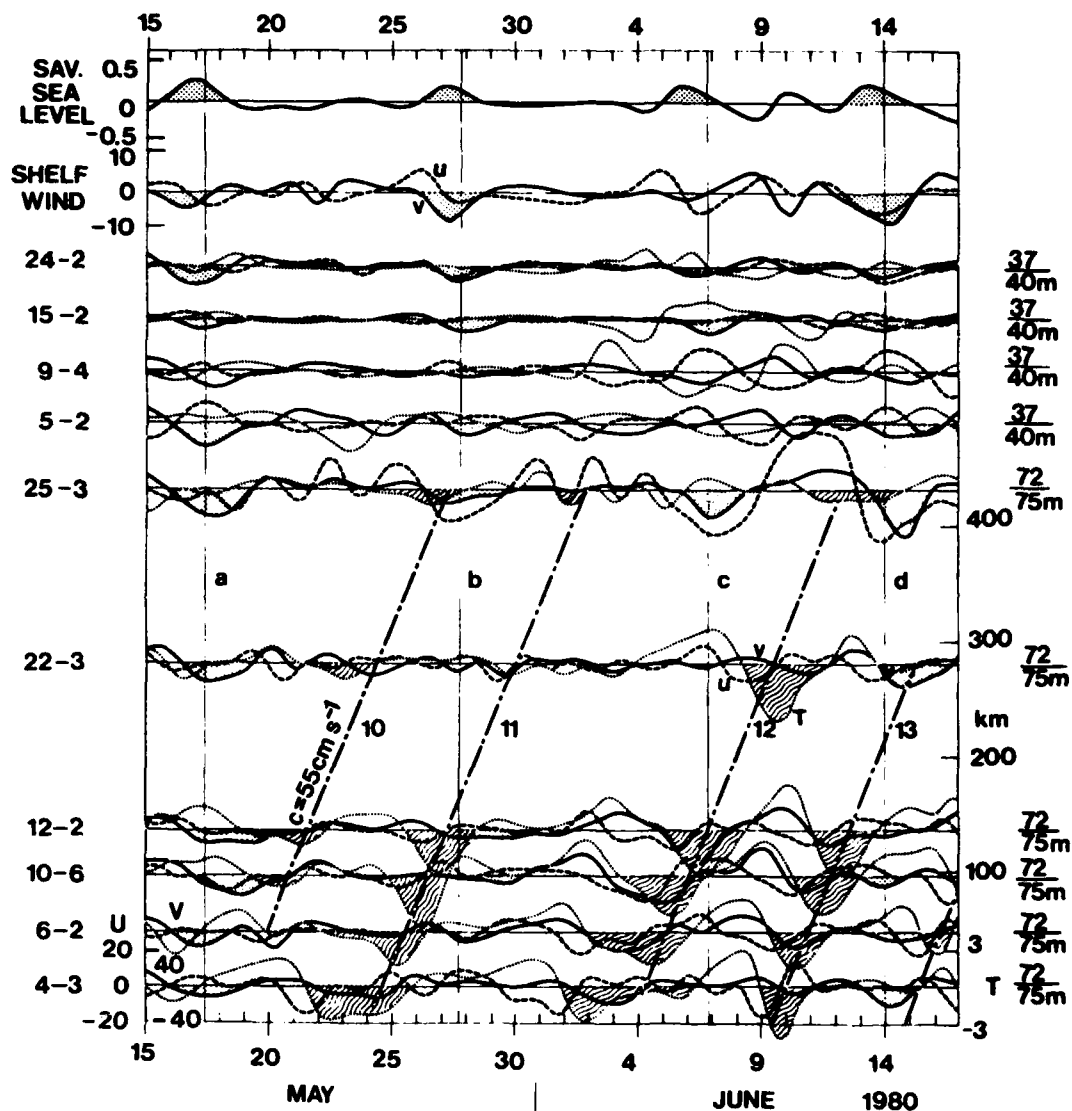


Fig. 5. Time series of 6-h rotated, band pass filtered lower layer current components (cm s^{-1}) u (dashed lines), v (solid lines) and T (dotted lines); shelf wind components (m s^{-1}) u (dashed lines), v (solid lines) for the period May 15 to June 17. Propagating events (#10-13) shown by slanted lines with phase speed $c = 55 \text{ cm s}^{-1}$ connecting cold anomalies at the shelf break (wavy shading). Non-propagating events (a-d) shown by vertical lines connecting southward wind and current events (dotted shading) and coastal sea level set-up (dotted shading).

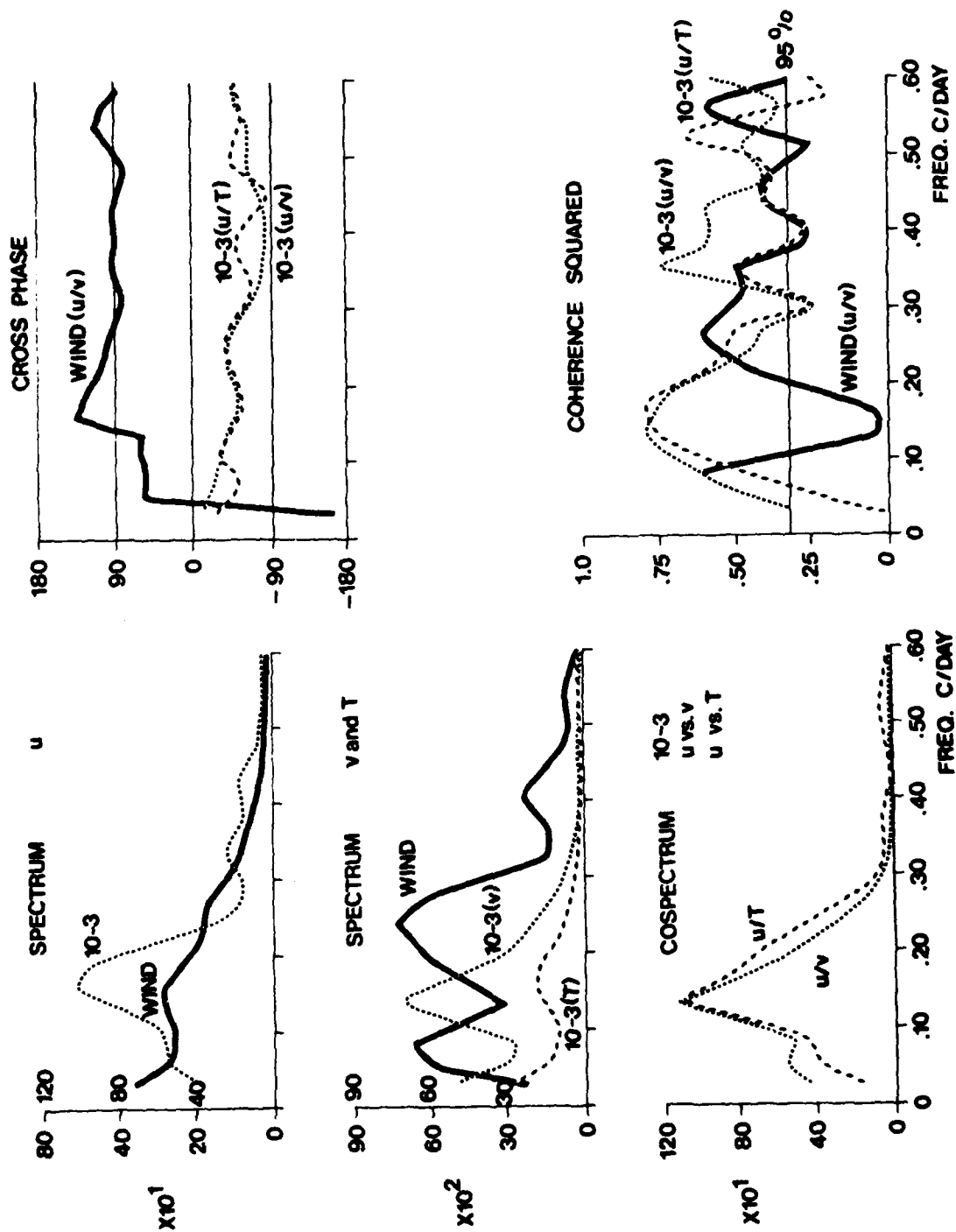


Fig. 6. Spectra ($\text{cm}^2\text{s}^{-2}\text{CPD}^{-1}$), cospectrum, cross-phase and coherence squared between u and v 40-HLP rotated velocity components of buoy winds, 10-3 currents and temperature (T) for GABEX-I. Degrees of freedom = 16.8, number of lags = 74, effective bandwidth = 0.036 CPD. Spectra scale on left is for currents and on right is for wind.

they are typical of the total water column at this location. Low-frequency currents at the shelf break show well-defined energy peaks at periods of 5 to 6 days for u and 7 to 9 days for v . The velocity components were coherent at these periods with u leading v by about 50 to 70° , which is indicative of propagating cyclonic fluctuations. Coherence was also significant at periods of 3, 2.5 and 2 days but the energy levels were considerably reduced. Shelf winds had energetic coherent fluctuations at periods of about 2 to 4 and 12 days. There was a spectral gap in energy and coherence of wind components in the 5 to 9 day period band where energy levels and coherence was highest in the shelf break currents.

Coherence and phase of the velocity and temperature fluctuations in the 7 to 9 day period band are plotted against along-shelf separation distance from combinations of current meter pairs along the shelf break in Figs. 7-9. The kinetic energy density in the upper and lower layer at each mooring site is also shown. Coherence falls off rapidly at the shelf break and defines an along-shelf coherent length scale of approximately 100 km for u , v and T in the energetic 7 to 9 day period band. Phase estimates show a near linear increase of negative phase with separation for distances less than the coherent length scale. Negative phase lags indicate northward propagation, and the scatter of points tend to fall around a line equivalent to a constant phase speed of 55 cm s^{-1} . The kinetic energy of along-shelf fluctuations in the 7 to 9 day period band was highest in the upper layer in the southern portion of the array and decreased northward. Minimum fluctuation energy occurred off Savannah (mooring 22). No significant differences in energy levels occurred between mooring sites for the along-shelf flow in the lower layer or the cross-shelf flow for upper and lower layers. The amplitudes of temperature fluctuations were larger over the southern portion of the array, without any significant differences between upper and lower layers.

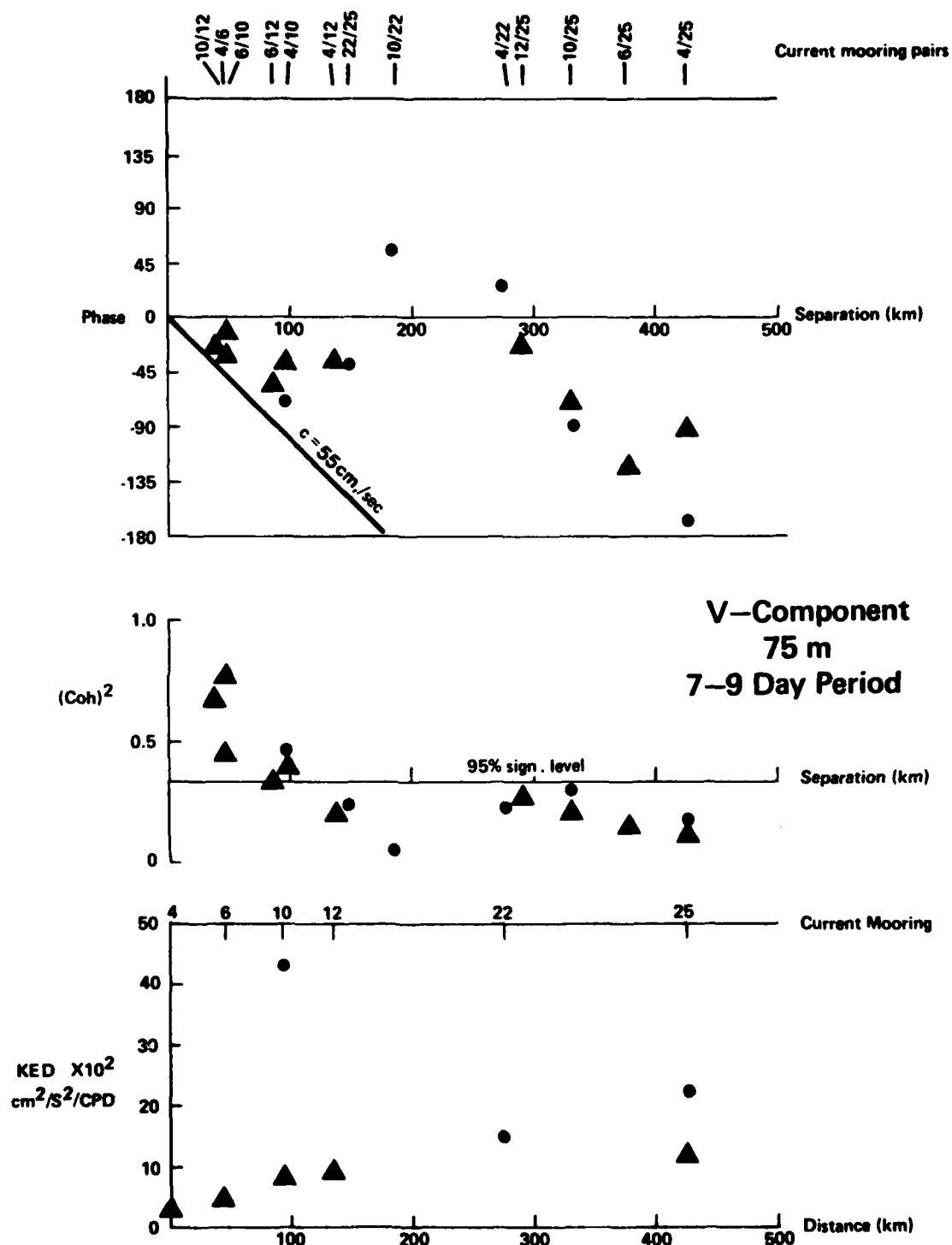


Fig. 7. Along-shelf coherence squared, phase and energy density for the 40-HLP rotated v component from current meter pairs at shelf break in 7-9 day period band; dots are for upper layer and triangles for lower layer.

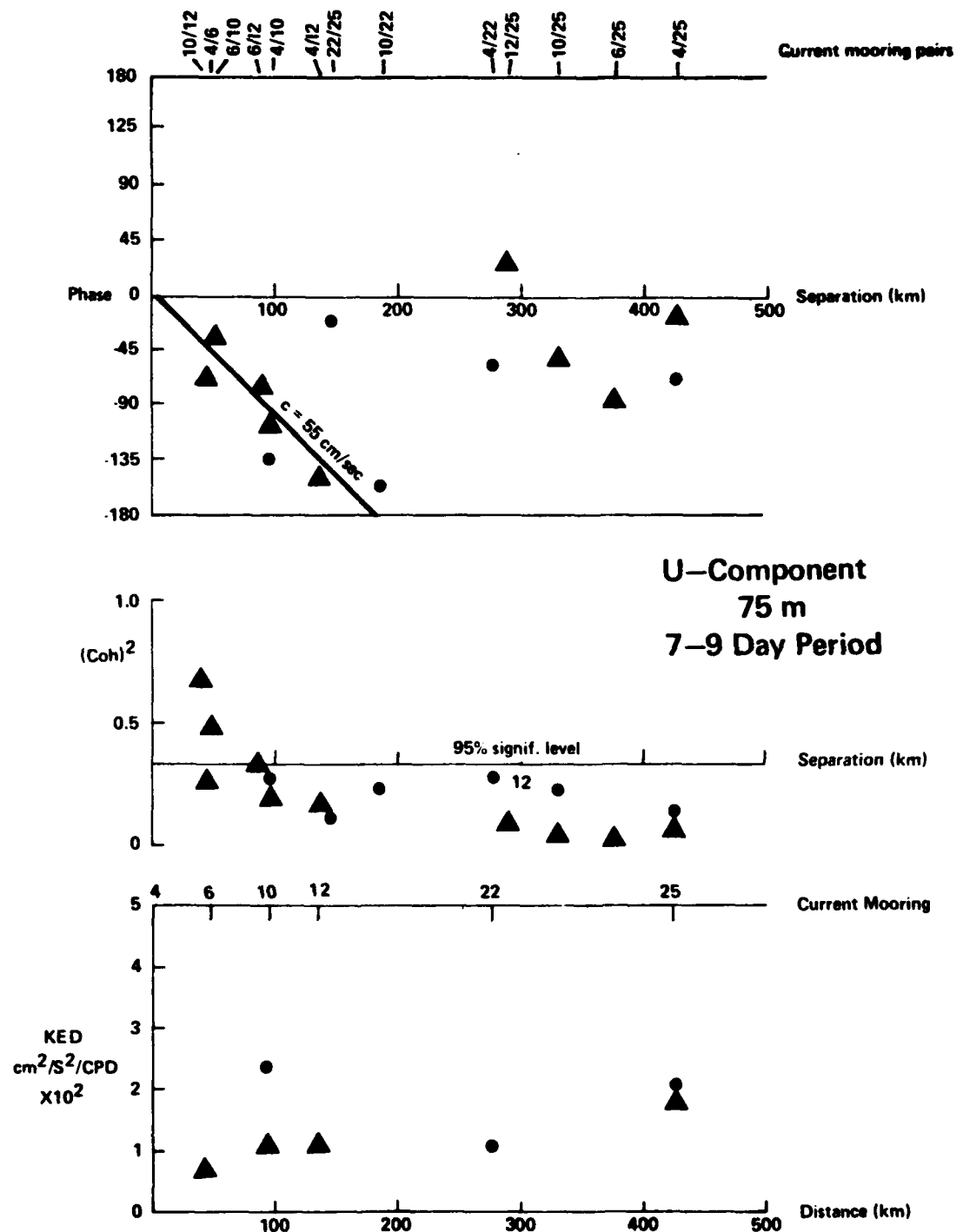


Fig. 8. Along-shelf coherence squared, phase and energy density for the 40-HLP rotated u component from current meter pairs at shelf break in 7-9 day period band; dots are for upper layer and triangles for lower layer.

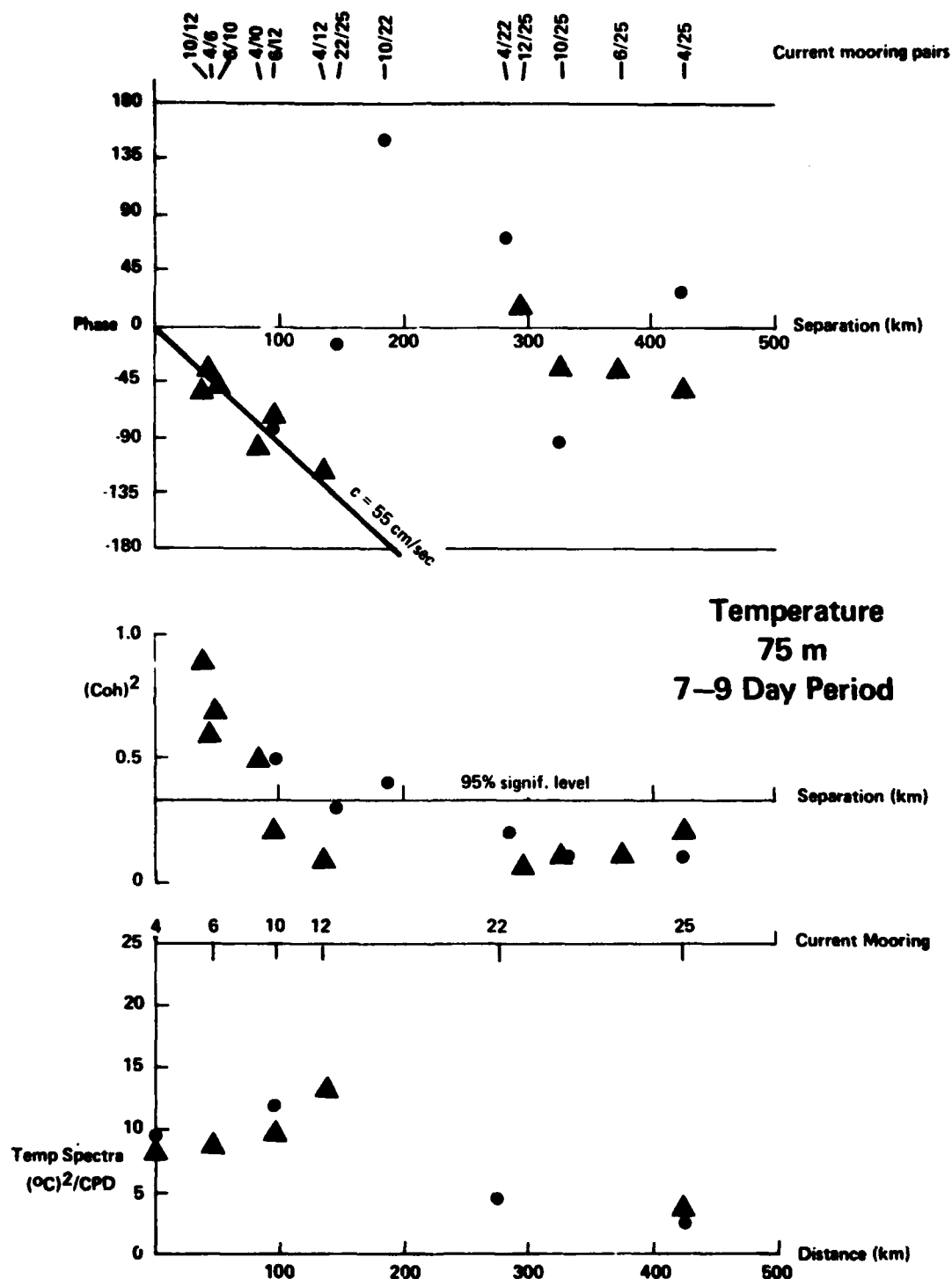


Fig. 9. Along-shelf coherence squared, phase and energy density for the 40-HLP temperature from current meter pairs at shelf break in 7-9 day period band; dots are for upper layer and triangles for lower layer.

Similar estimates for the 40 m isobath (not shown) show that coherence of along-shelf current fluctuations in the 7 to 9 day band was high over along-shelf distances of up to 425 km with small and nearly constant phase lags, which is indicative of nonpropagating fluctuations. The cross-shelf velocity components and temperature did not show any consistent along-shelf coherent features, so they are not presented. Also, along-shelf coherence and phase estimates computed for fluctuations in the 5 to 6 day period band were similar to those shown for the 7 to 9 day band at both the 75 and 40 m isobaths, and so they are not presented.

Gulf Stream Frontal Eddies

Hydrographic and biological observations of shelf waters in the region of the current meter array and the adjacent Gulf Stream front were made during April 10 to 26. Two ships were involved: EASTWARD and COLUMBUS ISELIN. The EASTWARD was used to investigate shelf processes while the COLUMBUS ISELIN was used to locate and track Gulf Stream frontal disturbances with the aid of a telefax system for receiving satellite sea surface temperature (SST) images from the NOAA-NESS field station in Miami. The ISELIN also received a detailed SST map every 3 days from a U.S. Coast Guard aircraft equipped with an airborne radiation thermometer. Current and temperature records from the outer shelf indicate that a succession of 4 cold cyclonic perturbations of the strong northward mean flow occurred during the shipboard sampling period (Figs. 3 and 4, events 5, 6, 7 and 8). These events were advected northward at a mean speed of about 60 cm s^{-1} which is close to the mean northward speed observed at the shelf break and also close to the northward propagation speed determined for u , v , T fluctuations in the 5 to 9 day period band (Figs. 7-9). The onset of each disturbance produced onshore flow followed by decreasing temperature and northward current speeds throughout the water column at the shelf break. The end of the

events produced offshore flow coupled with increasing temperature and northward speeds. A similar but less pronounced response occurred at the 40 m isobath. Shipboard observations indicate that the cold anomalous waters consisted of newly upwelled nutrient enriched North Atlantic Central Water (Dunstan and Atkinson, 1976; Yoder et al., 1981).

The formation, growth and northward movement of event 8 was observed with shipboard hydrography and remote thermal imagery from April 21 to 27. It was first observed with shipboard SST mapping as a small disturbance of the Gulf Stream surface thermal front off Cape Canaveral on April 21 (Lee, unpublished report). On April 22 and 23 it was clearly observable in satellite thermal imagery as a well-defined frontal "shingle" (Von Arx, Bumpus and Richardson, 1955) seaward of Cape Canaveral (Fig. 10). The shingle thermal pattern has been found to be the characteristic SST signature of cyclonic cold-core frontal eddies in this region (Lee, Atkinson and Legeckis, 1981). Detailed hydrographic sampling was obtained through the disturbance during a 20 hour period on April 24 and 25 and again over a 37 hour period on April 25 and 26 (Figs. 11 and 12). It took the combined effort of two ships to resolve the thermal field of this rapidly moving event.

The northward speed of the event was estimated using remote imagery, shipboard mapping and current meter records, all of which indicated a speed of about 55 cm s^{-1} . A warm filament of 23 to 24 C Gulf Stream water approximately 15 to 20 m in depth extended southward from the front around a cold-core with a minimum surface temperature of 22 C. The along-shelf dimension of the feature was approximately 130 km and the cross-shelf distance from western edge of the filament to the center of the cold core was about 25 km. A typical temperature, density and nitrate section through the center of the feature is shown in Fig. 13. Up-lifted temperatures in the cold dome extended across the outer shelf beneath the warm filament in a cold subsurface intrusion of nutrient enriched waters. Euphotic

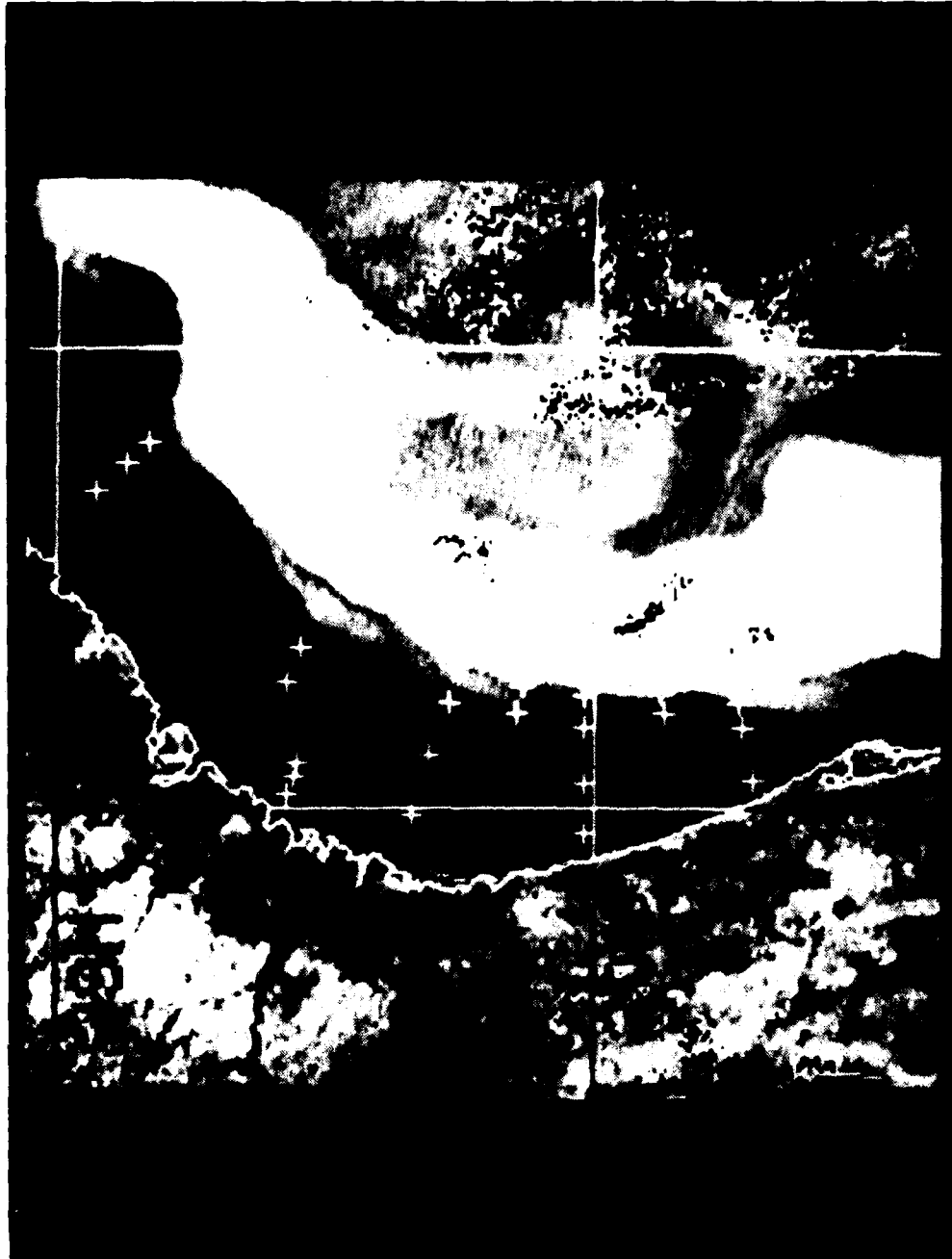


Fig. 10. Satellite VIRR thermal image of the Gulf Stream at 1258 Z on April 22, 1980; crosses are for current mooring locations (prepared by Otis Brown and Bob Evans of University of Miami).

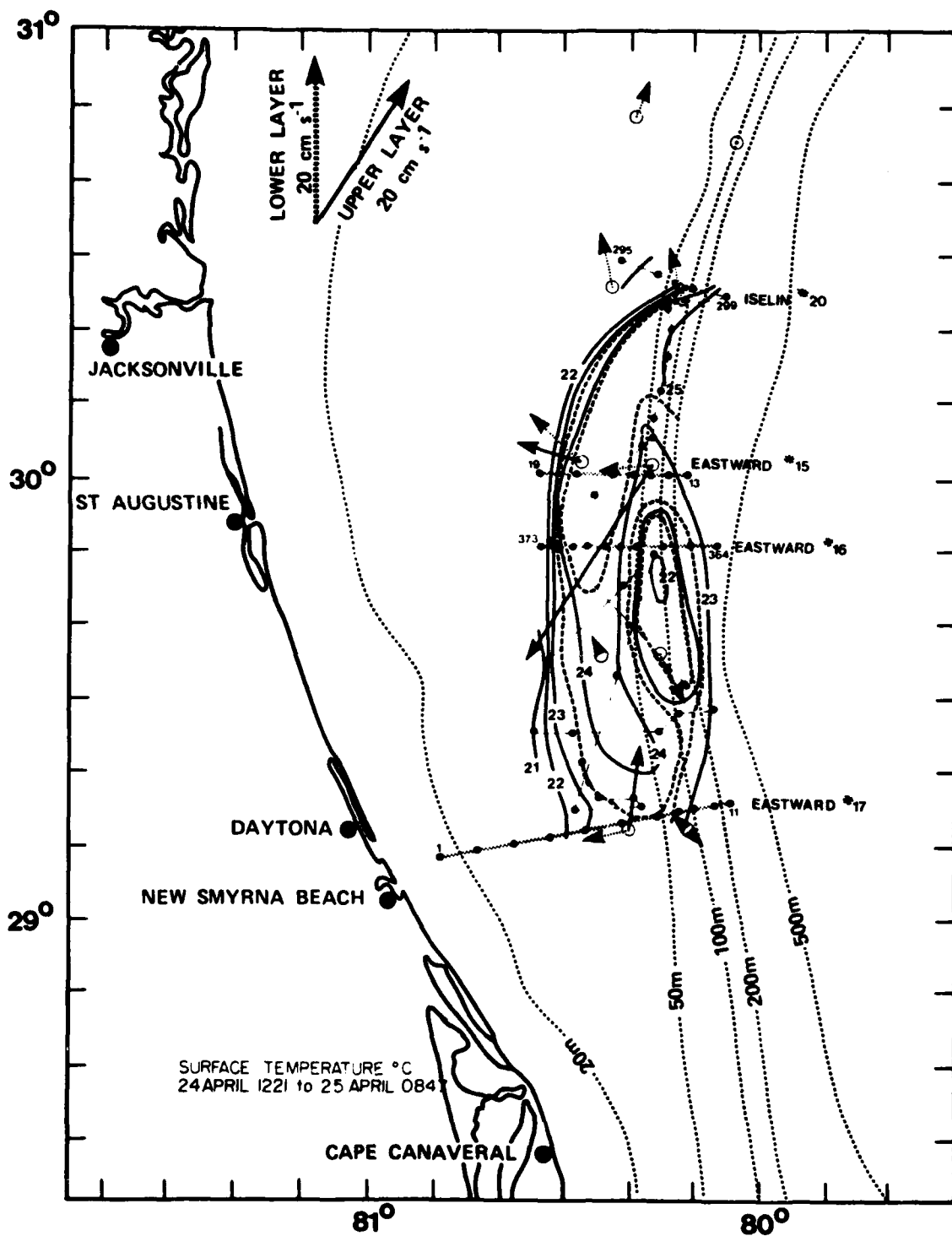


Fig. 11. Ship measured surface temperature ($^{\circ}\text{C}$) on April 24 (1221 hr) to April 25 (0847 hr). Straight lines with dots show ISELIN ship track and stations. Wavy line and dots show EASTWARD track and stations. Hydrographic sections are labeled with ship name and end point station numbers. Daily averaged currents on April 25 are shown with arrows.

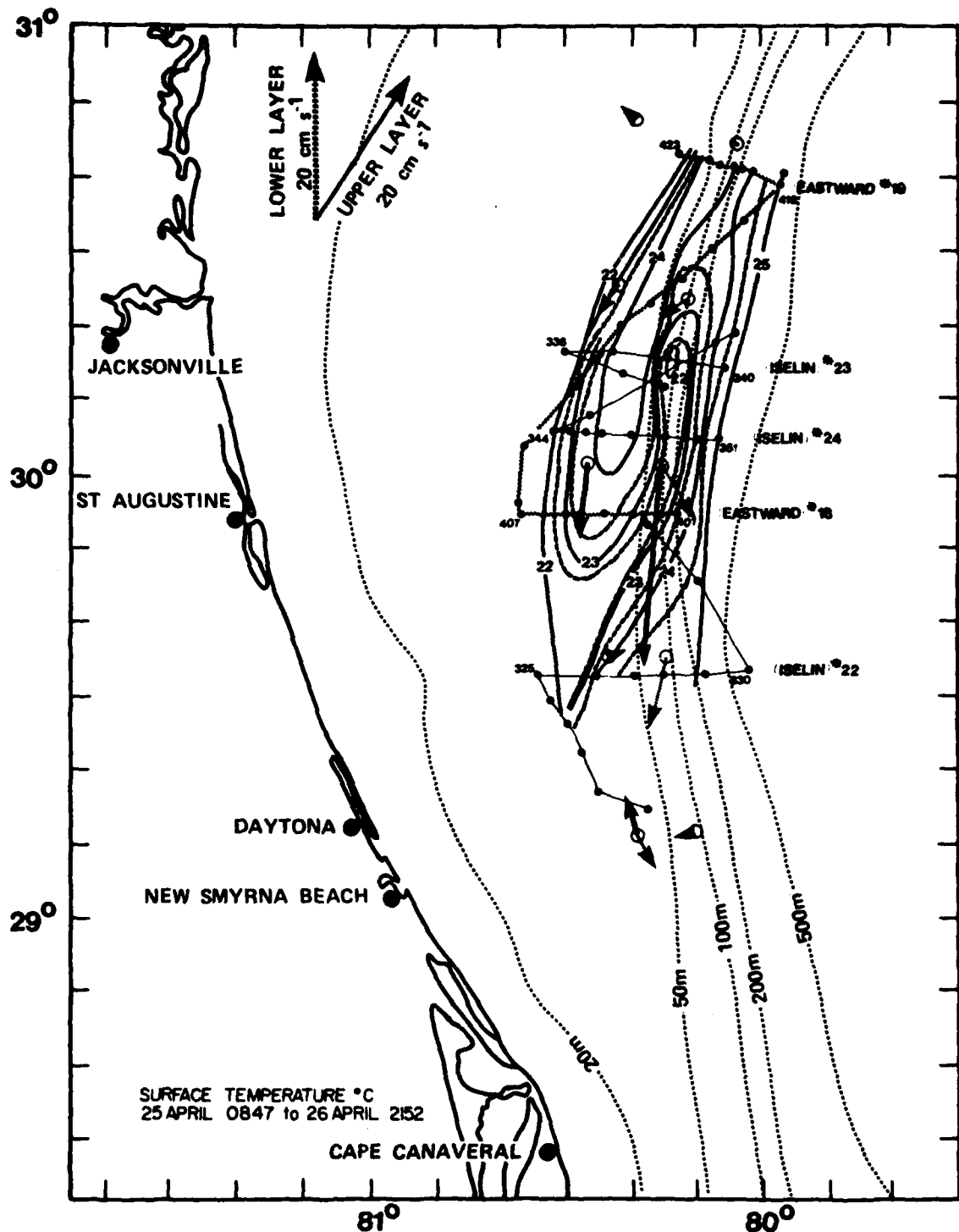


Fig. 12. Ship measured surface temperature ($^{\circ}\text{C}$) on April 25 (0847 hr) to April 26 (2152 hr). Straight lines with dots show ISELIN ship track and stations. Wavy line and dots show EASTWARD track and stations. Hydrographic sections are labeled with ship name and end point station numbers. Daily averaged currents on April 26 are shown with arrows.

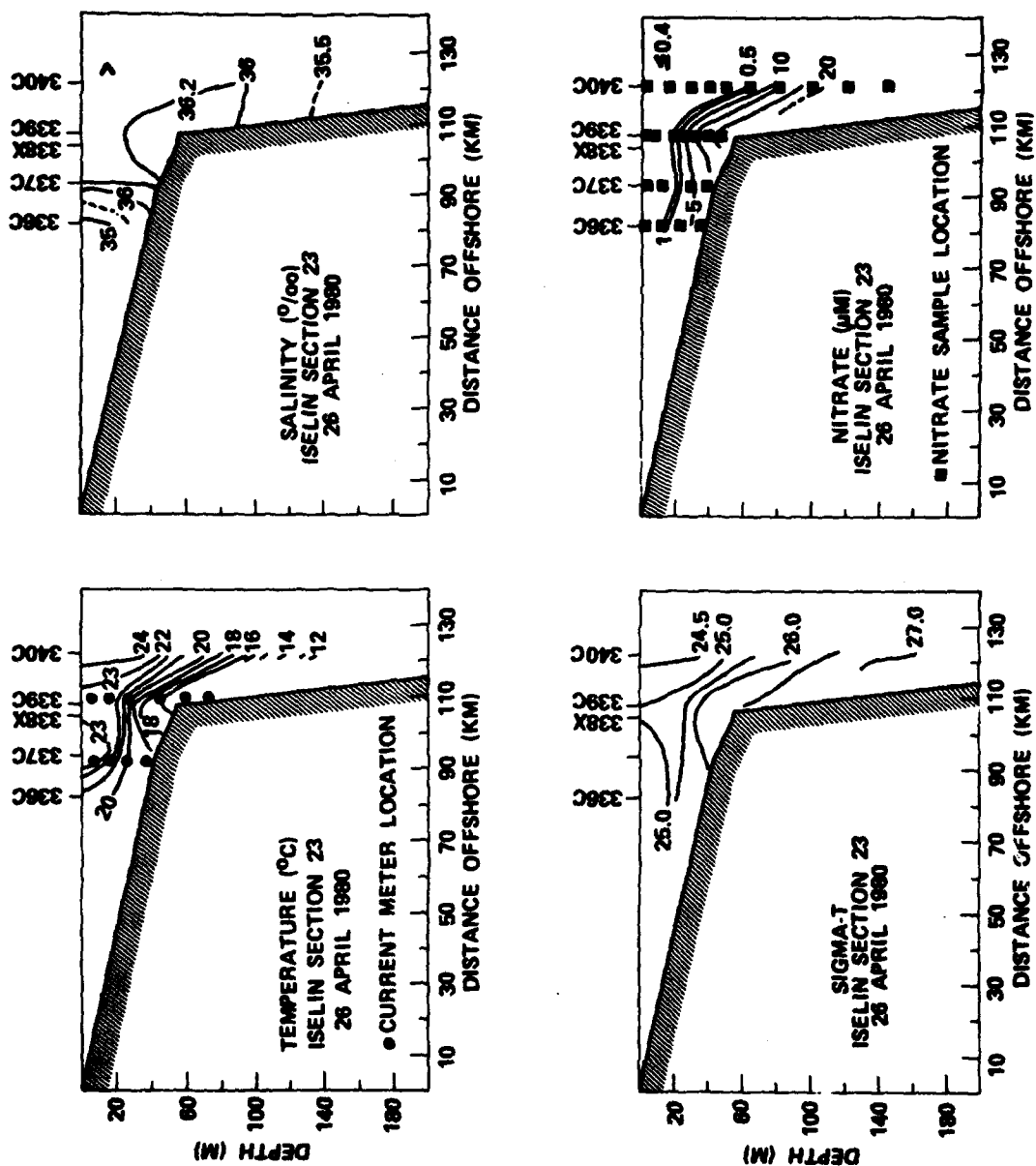


Fig. 13. Temperature ($^{\circ}\text{C}$), salinity ($^{\circ}/_{\infty}$), density (σ_t) and nitrate (μM) sections across a Gulf Stream frontal eddy on April 26 (0028 to 0757 hr). Stations are numbered along the top from ISELIN section #23 (Figure 21).

zone nitrate concentrations of $5 \mu \text{ moles } \ell^{-1}$ were observed beneath the warm filament and $10 \mu \text{ moles } \ell^{-1}$ near the shelf break.

SST and hydrographic section data (Figs. 11-13) indicate that the cold core of event 8 passed directly through mooring 10 and the western edge of the warm filament passed through mooring 9. The low-frequency temperature records from mooring sites 9 and 10 further substantiates this movement (Fig. 4). At mooring 10 temperature decreased then increased at all vertical positions between April 24 and 27, which was the time the cold core passed the mooring. Temperature from mooring site 9 (not shown) first increased from April 24 to 25 at all levels then decreased in the lower 13 m and remained high in the upper 17 m. The initial temperature increase appears related to the passage of the warm filament, which caused the temperature to remain high in the upper 17 m for the duration of the event. Below the level of the warm filament temperatures decreased as the cold subsurface intrusion passed through the mooring.

The uplifted density structure in the cold core of the disturbance indicates a cyclonic circulation with southward flow west of the core and northward flow on the east. Previous investigations of Gulf Stream frontal eddies on the Georgia shelf (Lee, Atkinson and Legeckis, 1981) and in the Florida Straits (Lee, 1975; Lee and Mayer, 1977) have observed cyclonic current reversals in current meter records as shingles with similar properties as found in event 8 were encountered. However low-frequency current records from moorings 9 and 10 during April show a persistent northward flow that is perturbed by a succession of cyclonic cold anomalies, but no flow reversals (Figs. 2, 3 and 4). A fixed current meter records the mean flow (\bar{v}) plus eddy motions (v'), written as: $v = \bar{v} + v'$ for the along-shelf component. If the mean flow is larger than the eddy motion a current reversal will not be observed at a fixed station. Band pass filtering the data from 40 hours to 2 weeks removes the effect of the mean and shows cold cyclonic perturbations propagating northward along the shelf break at about 55 cm s^{-1} , which was

nearly the same speed as the mean (Fig. 5). When the effect of the mean flow is removed cyclonic flow reversals are observed at all levels at sites 9 and 10 during the passage of event 8 (Fig. 14).

Southward flows within event 8 appear to be in approximate geostrophic balance with the uplifted density structure in the cold core as determined from the thermal wind equation:

$$\frac{\partial v}{\partial z} = \frac{g}{\rho f} \frac{\partial \rho}{\partial x} \quad (1)$$

The daily averaged vertical shear measured at mooring 9 during the passage of event 8 (April 26) was about $5 \times 10^{-3} \text{ s}^{-1}$ beneath the warm filament. The horizontal density gradient, right hand side of (1), was about $4 \times 10^{-3} \text{ s}^{-1}$ at the 17 m level and $3 \times 10^{-3} \text{ s}^{-1}$ at 37 m (from stations 337 and 339 of ISELIN section 24). Anti-cyclonic circulation was not observed in currents within the filament (7 m level), presumably due to the stronger cyclonic circulation within the larger cold anomaly. However, station spacing was not sufficient to resolve the relative density field of the warm filament. Thus the propagating cold cyclonic perturbations described here appear to be the same type of frontal eddies as found previously (Lee, Atkinson and Legeckis, 1981). The only observable difference is that the northward propagation velocities were larger than eddy velocities for most of the events.

Upwelling Velocity in Frontal Eddies

Upwelling velocities (w) in event 8 can be estimated by comparing vertical positions of isotherms in the cold core while tracking the feature. The 17 C isotherm was uplifted 13 m in the core in a 37.8 hour period between EASTWARD station 366 (EASTWARD section 16, Fig. 11) and ISELIN station 339 (ISELIN section 23, Fig. 12), which gives a vertical velocity of $10^{-2} \text{ cm s}^{-1}$. Since subsurface temperature measurements can be aliased by internal tides it becomes useful to also estimate w from the conservation of relative vorticity (ζ) along a streamline.

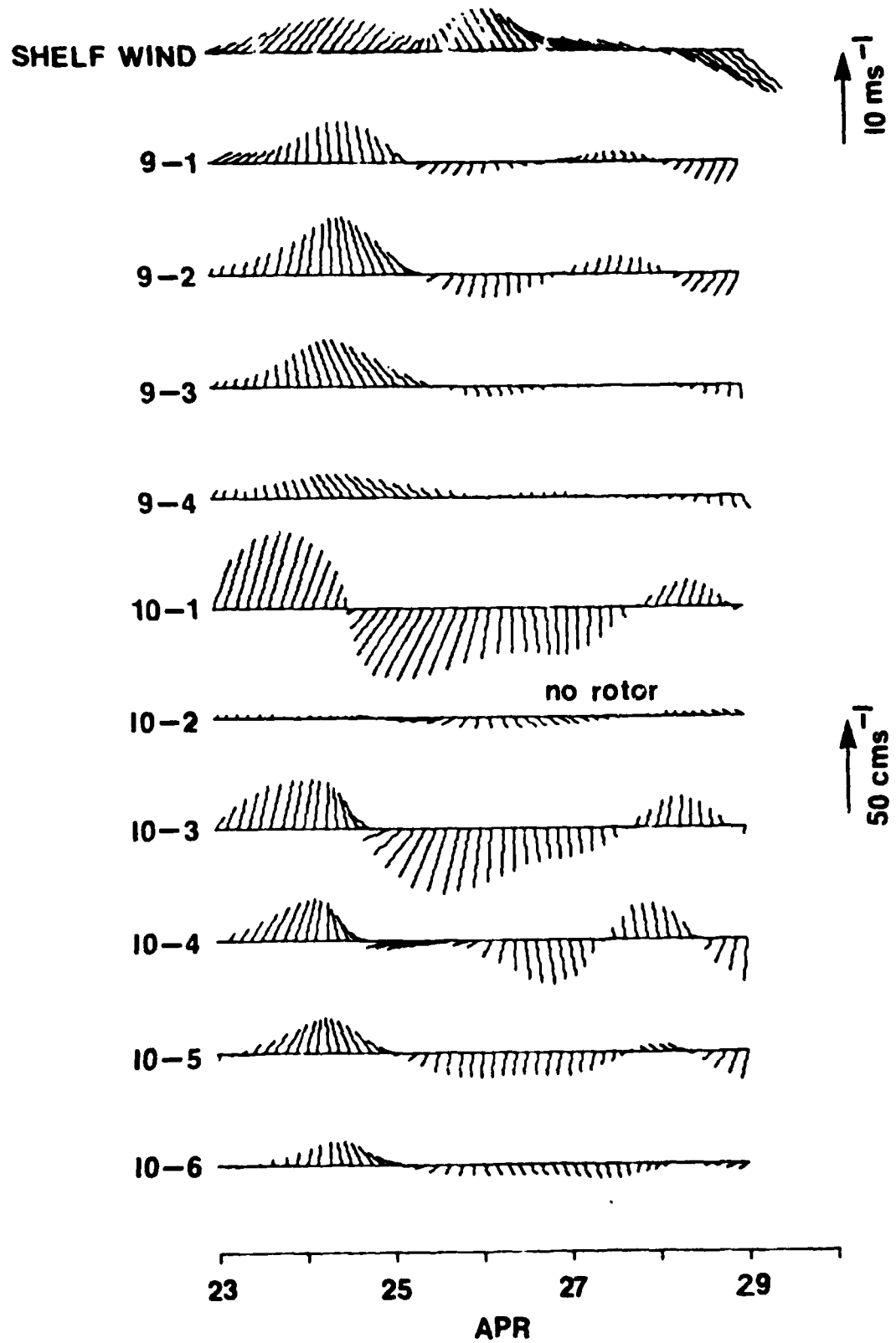


Fig. 14. Time series of 3 HLP band pass filtered wind and current vectors from moorings 9 and 10 during event #8.

Following Arthur (1965) the conservation of relative vorticity in natural coordinates is:

$$f \frac{dw}{dz} = \frac{d\zeta}{dt} + \beta V \quad (2)$$

where $\zeta = \frac{V}{R} - \frac{dV}{dn}$, and β is the change in planetary vorticity (f) with latitude; $\beta = 1.35 \times 10^{-13} \text{ cm}^{-1} \text{ s}^{-1}$. Assuming a uniform flow V which tends to follow the temperature pattern shown in Fig. 11 with cyclonic curvature of radius R around the cold core (the shear vorticity $\frac{dV}{dn}$ in the filament is assumed zero), then the vertical velocity at depth h is given by:

$$w_h = - \frac{h}{f} \frac{d\zeta}{dt} - \frac{h\beta V}{f} \quad (3)$$

The tangential velocity V is assumed equal to the eddy velocity of event 8 or approximately 40 cm s^{-1} (Fig. 14) and has a radius of curvature R of 22 km north of the cold core and $R = \infty$ west of the core where the flow is southward in the warm filament, therefore $\frac{d\zeta}{dt} = -2 \times 10^{-10} \text{ s}^{-2}$; $\beta V = 5.4 \times 10^{-12} \text{ s}^{-2}$; and the vertical velocity at 50 m is: $w = 1.4 \times 10^{-2} \text{ cm s}^{-1}$, which is quite close to the estimate made following rising isotherms. The strength of the vertical velocity depends primarily on the change in curvature vorticity along a streamline. The curvature is cyclonic around the cold core of a frontal eddy which gives a positive (upwelling) vertical velocity. The strength of the upwelling velocity is about $.01 \text{ cm s}^{-1}$ or 8.6 m day^{-1} .

Vorticity Conservation in Frontal Eddies

The conservation of potential vorticity can be written:

$$\left(\frac{V}{R} - \frac{\partial V}{\partial n} + f \right) N^2 = \text{constant} \quad (4)$$

where $\zeta = \frac{V}{R} - \frac{\partial V}{\partial n}$ is the same as in (2) and the static stability $N^2 = \frac{g}{\rho_0} \frac{\Delta \rho}{\Delta z}$ depends on the strength of the pycnocline, with density difference $\Delta \rho$ between

two isopycnals separated in the vertical by Δz . Considering a cyclonic cold core eddy both the curvature vorticity and shear vorticity will lead to an increase in potential vorticity, which must be compensated for by a decrease in static stability. The shear vorticity produces a positive effect since in a natural coordinate system n increases to the left of the flow making the shear term negative on the inside (east) of the warm tongue and when combined with the minus sign gives a positive effect. On the outside (west) of the warm tongue the shear is positive and so can compensate for the cyclonic curvature by closing up streamlines. Thus in the cold core region static stability must decrease to compensate the increase in curvature and shear vorticity (changes in planetary vorticity are small). In the cold core of event 8 N^2 was observed to decrease by about a factor of 2 compared to estimates in the frontal region north and south of the event. Similar results were found for the 1977 frontal eddy reported on by Lee, Atkinson and Legeckis (1981).

Kinematics of Frontal Eddies

Reynolds stress ($\overline{u'v'}$) averages over the 4 month experiment were generally offshore (positive) along the shelf break, indicating an average offshore transport of northward momentum. The only net onshore transport of momentum observed over the total period was near-bottom at the southern mooring (current meter 4-5). Cumulative weekly averages indicate that Reynolds stress estimates became reasonably stable (within $\pm 10\%$ of the total record average) for averaging periods of 12 to 15 weeks. Maximum offshore momentum transport of about $260 \text{ cm}^2 \text{ s}^{-2}$ occurred in the upper layer at 30°N (10-1) and decreased rapidly with depth. The mean horizontal shear $\frac{\partial \bar{v}}{\partial x}$ in the upper layer at this latitude was approximately $2.6 \times 10^{-5} \text{ s}^{-1}$ which gives a horizontal eddy viscosity $A_H = -\rho \overline{u'v'} / \frac{\partial \bar{v}}{\partial x}$ of $-8 \times 10^6 \text{ cm}^2 \text{ s}^{-1}$. The overbar represents a time average over the record length and the primes denote deviations from the average. Density ρ is taken as 1 g cm^{-3} .

and x increases in the offshore direction. A negative viscosity was also found in the region of the cyclonic Gulf Stream front off Onslow Bay, NC (Webster, 1961a; Brooks and Bane, 1981), and in the Florida Straits (Schmitz and Niiler, 1968; Brooks and Niiler, 1977) and is believed to indicate a baroclinic instability process where kinetic energy is transferred from the fluctuations to the mean flow (Orlanski, 1969; Orlanski and Cox, 1973). The rate of net energy transfer can be estimated with current meters at 30°N from $\rho \overline{u'v'} \frac{\partial \bar{v}}{\partial x}$ (Webster, 1961b; Schmitz and Niiler, 1968; Brooks and Niiler, 1977). Brooks and Niiler (1977) found that the net conversion rate of perturbation kinetic energy can be estimated from:

$$\frac{d}{dt} \left\{ \frac{1}{2} (\overline{u'^2} + \overline{v'^2}) \right\} = - \left\{ \overline{u'^2} \frac{\partial \bar{u}}{\partial x} + \overline{v'^2} \frac{\partial \bar{v}}{\partial y} + \overline{u'v'} \frac{\partial \bar{v}}{\partial x} \right\} \quad (8)$$

Their estimates for the Florida Current between Miami, FL and Bimini, Bahamas, indicated that the total local kinetic energy conversion was dominated by the 2nd term on the right hand side but for the sectional area average this term was small and the 1st and 3rd terms were larger and of similar magnitude.

The net local perturbation kinetic energy at the shelf break at 30°N can be estimated using current meter data from moorings 4, 9 and 10. The results for the middle to upper water column and near-bottom layer are given in Table 1. In the upper layer the net local conversion of perturbation kinetic energy was dominated by $\overline{u'v'} \frac{\partial \bar{v}}{\partial x}$ which was about an order of magnitude larger than the 1st and 2nd terms of (8). Near-bottom estimates are two orders of magnitude smaller and not significant. The positive net value indicates that there was a net transfer of kinetic energy from the fluctuations to the mean flow at this location, consistent with similar findings in the Gulf Stream cyclonic frontal region off Onslow Bay in the surface layer (Webster, 1961a) and middle to lower water column (Brooks and Bane, 1981). Brooks and Niiler (1977) also found a region of kinetic

TABLE 1. Net Kinetic Energy Exchange Rate at the Shelf Break from February 25 to June 21, 1980.

Quantity	Units	Net Value Upper Layer (27-45m depths)	Net Value Lower Layer (3m above bottom)
$\overline{u'^2}$	$\text{cm}^2 \text{s}^{-2}$	106	34
$\overline{v'^2}$	$\text{cm}^2 \text{s}^{-2}$	1198	184
$\overline{u'v'}$	$\text{cm}^2 \text{s}^{-2}$	194	13
$\overline{\frac{\partial u}{\partial x}}$	s^{-1}	4.2×10^{-6}	2.0×10^{-6}
$\overline{\frac{\partial v}{\partial y}}$	s^{-1}	2.5×10^{-7}	-3.1×10^{-7}
$\overline{\frac{\partial v}{\partial x}}$	s^{-1}	2.6×10^{-5}	2.0×10^{-6}
$\overline{\rho u'^2} \frac{\partial \overline{u}}{\partial x}$	ergs $\text{cm}^{-3} \text{s}^{-1}$	4.4×10^{-4}	0.7×10^{-4}
$\overline{\rho v'^2} \frac{\partial \overline{v}}{\partial y}$	ergs $\text{cm}^{-3} \text{s}^{-1}$	3.0×10^{-4}	-0.6×10^{-4}
$\overline{\rho u'v'} \frac{\partial \overline{v}}{\partial x}$	ergs $\text{cm}^{-3} \text{s}^{-1}$	50.4×10^{-4}	0.3×10^{-4}
$\overline{\rho u'^2} \frac{\partial \overline{u}}{\partial x} + \overline{\rho v'^2} \frac{\partial \overline{v}}{\partial y} + \overline{\rho u'v'} \frac{\partial \overline{v}}{\partial x}$	ergs $\text{cm}^{-3} \text{s}^{-1}$	57.8×10^{-4}	0.4×10^{-4}

energy flux to the mean flow over the total water column in the cyclonic front of the Florida Current off Miami. However, the region was displaced about 8 km east of the shelf break and energy was transferred to the fluctuations at shelf break. A similar result was found from current meters positioned at the shelf break in the Florida Straits (Lee, 1975; Lee and Mayer, 1977), indicating that the shelf break strip was a region of mean energy removal. However, between Cape Canaveral and Savannah the Gulf Stream front follows the shelf break closely and the fluctuations release kinetic energy to the mean flow at about the same rate ($58 \times 10^{-4} \text{ ergs cm}^{-3} \text{ s}^{-1}$) as was found off Onslow Bay and in the Florida Straits (Brooks and Bane, 1981; Brooks and Niiler, 1977). The co-spectrum of the u vs. v velocity components at the shelf break (Fig. 6) shows that the positive (off-shore) momentum flux was selectively grouped in the 5 to 9 day period band where propagating cold cyclonic perturbations were found to produce coherent u and v fluctuations. Thus the net conversion of perturbation to mean kinetic energy appears to occur throughout the water column at the shelf break and is being driven by fluctuations occurring in the 5 to 9 day period band.

The heat flux $\overline{u'T'}$ at the shelf break averaged over the 4 month study period was positive within the water column and decreased to small negative values near the bottom. A positive heat flux indicates a net offshore heat transport similar to that found in the Gulf Stream frontal region off Onslow Bay (Oort, 1964; Brooks and Bane, 1981) and in the Florida Straits (Brooks and Niiler, 1977). Following Brooks and Niiler (1977) the net conversion rate of potential energy can be estimated from:

$$\frac{d}{dt} \left\{ \frac{g}{2} \overline{\rho'^2} / \left| \frac{\partial \bar{\rho}}{\partial z} \right| \rho_o \right\} = - \left\{ g \overline{u' \rho'} \frac{\partial \bar{\rho}}{\partial x} / \rho_o \left| \frac{\partial \bar{\rho}}{\partial z} \right| + g \overline{v' \rho'} \frac{\partial \bar{\rho}}{\partial y} / \rho_o \left| \frac{\partial \bar{\rho}}{\partial z} \right| \right\} \quad (9)$$

Gulf Stream water present in the outer shelf produces a reasonably constant T-S relationship (Lee, Atkinson and Legeckis, 1981) that is used with temperature

from current meters on moorings 4, 9 and 10 to evaluate rates of potential energy conversion in the same manner as kinetic energy conversion. The results are presented in Table 2. There was a net transfer of perturbation potential energy from the fluctuations to the mean at the shelf break that can be largely accounted for by $g \overline{u' \rho'} \frac{\partial \bar{\rho}}{\partial x} / \left| \frac{\partial \bar{\rho}}{\partial z} \right|$. The co-spectrum of u vs. T (Fig. 6) is quite similar to the co-spectrum of u vs. v and indicates that coherent current and temperature fluctuations occurring in the 5 to 9 day period band were the cause of the local generation of mean potential energy at the shelf break.

CONCLUSIONS

Low-frequency current and temperature variability along the outer shelf of the southeastern U.S. continental shelf appears to result from a combination of wind forcing and interaction with the Gulf Stream. Subtidal current and temperature fluctuations along the shelf break result primarily from propagating disturbances in the Gulf Stream front. Along the 40 m isobath low-frequency variability appears to be a mixed response to wind and Gulf Stream forcing with non-propagating wind effects more clearly observable.

Low-frequency current and temperature variability, and fluxes of momentum, and heat at the shelf break result largely from northward propagating Gulf Stream frontal disturbances. Current meter, hydrographic and satellite observations indicate that these disturbances are cold cyclonic eddies embedded in the Gulf Stream front. These features were observed to propagate to the north at speeds of 50 to 70 cm s⁻¹ and produce coherent fluctuations of cross-shelf and along-shelf velocity components and temperature throughout the water column in the 5 to 9 day period band over along-shelf coherence scales of 100 km. The frontal eddy signature in along-shelf pairs of current meters at the shelf break consists of a propagating cyclonic perturbation of the northward mean flow coupled to a sharp drop in temperature. The response is observed throughout the water column

TABLE 2. Net Potential Energy Exchange Rate at the Shelf Break from February 25 to June 21, 1980.

Quantity	Units	Net Value Upper Layer (27-45 m depths)
$\overline{u'\rho'}$	$\text{gm cm}^{-2}\text{s}^{-1}$	-1.7×10^{-3}
$\overline{v'\rho'}$	$\text{gm cm}^{-2}\text{s}^{-1}$	-1.2×10^{-2}
$\frac{\partial \bar{\rho}}{\partial x}$	gm cm^{-4}	-3.1×10^{-10}
$\frac{\partial \bar{\rho}}{\partial y}$	gm cm^{-4}	-0.1×10^{-10}
$ \frac{\partial \bar{\rho}}{\partial z} $	gm cm^{-4}	2.7×10^{-7}
$g \overline{u'\rho'} \frac{\partial \bar{\rho}}{\partial x} / \frac{\partial \bar{\rho}}{\partial z} $	$\text{ergs cm}^{-3}\text{s}^{-1}$	19.1×10^{-4}
$g \overline{v'\rho'} \frac{\partial \bar{\rho}}{\partial y} / \frac{\partial \bar{\rho}}{\partial z} $	$\text{ergs cm}^{-3}\text{s}^{-1}$	4.4×10^{-4}
$g \overline{u'\rho'} \frac{\partial \bar{\rho}}{\partial x} / \frac{\partial \bar{\rho}}{\partial z} + g \overline{v'\rho'} \frac{\partial \bar{\rho}}{\partial y} / \frac{\partial \bar{\rho}}{\partial z} $	$\text{ergs cm}^{-3}\text{s}^{-1}$	23.5×10^{-4}

with larger temperature fluctuations usually occurring in the lower layer. A cyclonic current reversal may occur on the western side of an eddy if the eddy velocity is larger than the northward mean flow.

Eddy SST signature consists of the "shingle" pattern (Von Arx, Bumpus and Richardson, 1955) which develops as a warm filament of near surface Gulf Stream water 10 to 15 m deep, is pulled out of the front and wraps around a cold core, presumably by the cyclonic eddy circulation in much the same manner as "streamers" associated with warm and cold core rings (Vulkovich and Grissman, 1978). The eddy circulation appears to be in quasi-geostrophic equilibrium with uplifted density surfaces in the cold core. There was no indication in current and temperature records of anticyclonic circulation in the warm filaments as was suggested by Chew (1981). The movement of a warm filament with anticyclonic circulation should produce a propagating anticyclonic perturbation of the northward mean flow coupled to an increase in temperature, which was not observed at the outer shelf current meter sites.

The formation process of frontal eddies is not well understood. The shingle signature observed in satellite imagery appears to be connected to growing wave-like meanders of the Gulf Stream front (Legeckis, 1975; Stumpf and Rao, 1975; Legeckis, 1979). Theoretical investigations predict that both barotropic (Niiler and Mysak, 1971) and baroclinic (Orlanski, 1969; Orlanski and Cox, 1973) instabilities can exist in the frontal region with wave properties for the fastest growing waves that match reasonably well with the satellite observations, i.e. wave lengths of 100 to 200 km and periods ≈ 10 days. Our observations show that cyclonic eddies travel in conjunction with the offshore meander portion of the waves. Similar findings were reported from the Florida Straits (Lee and Mayer, 1977) and off Onslow Bay, NC (Bane, Brooks and Lorenson, 1981). Frontal eddies do not appear to be directly or simply connected to wind forcing. However wind events may act to trigger a frontal instability which could grow into an eddy.

Frontal eddies are short-lived phenomena. They can form in only a few days and possibly dissipate just as fast. Satellite imagery suggests that the total cycle takes place in 1 to 3 weeks. The eddy process appears to be an important component in the Gulf Stream energy balance. Between New Smyrna Beach, FL, and Savannah, GA, frontal eddies transport momentum and heat to the Gulf Stream as part of the process of transferring both perturbation kinetic and potential energy to the mean flow. Eddy production of mean energy in the area of the current meter array suggests an upstream formation region, possibly where the shelf widens north of Jupiter, FL, as the Gulf Stream leaves the Florida Straits. Dissipation appears to occur through a rapid elongation process brought about by the large horizontal shear across the Gulf Stream front. Dissipation of this type is consistent with the estimated energy transfer and should cause a strengthening of the front. A similar process may occur off Onslow Bay, NC. The kinematic and dynamic properties of the enlarged frontal disturbances that form downstream of the Charleston bump appear to be consistent with the eddies we observed upstream of the bump (Bane, Brooks and Lorenson, 1981; Brooks and Bane, 1981). Occasionally shingles are observed in satellite imagery that maintain recognizable integrity as they propagate from the upstream to downstream region with considerable enlargement occurring downstream of the bump (Lee, Atkinson and Legeckis, 1981). However, positive identification of events in satellite imagery requires about one week of consecutive cloud-free days, which rarely occurs. Our shelf break current meter records also indicate that frontal disturbances can maintain continuity between regions and produce larger fluctuations downstream of the bump.

Frontal eddies are observed to have considerable influence on primary production in the outer shelf (Lee, Atkinson and Legeckis, 1981). Upwelling in the cold core, together with onshore flow in the cyclonic circulation, transports deeper nutrient enriched Gulf Stream waters into the euphotic zone for


phytoplankton uptake. Upwelling velocities are estimated at 8.5 m day^{-1} . Rapid utilization of newly upwelled nutrients results in elongated patches of high chlorophyll that propagate with the cold core and have similar dimensions (Yoder et al., 1981). Since the demise of frontal eddies appears to occur as a shear induced dissipation process rather than a collapse of isopycnal surfaces the upwelled nutrients should remain in the outer shelf, possibly causing chlorophyll bands in the Gulf Stream front.

Acknowledgements. We thank the crew of the R/V COLUMBUS ISELIN for their aid in field operations. Special thanks are extended to Phil Bedard, Ted Tankard, Paula Anderson, Nedra Chalker, Jere Green, Robert Guest, Paul Galbreath and Gary Rosiello for technical assistance. We appreciate discussions with Don Olson, Chris Mooers, Claes Rooth, John Woods and Jim Yoder. We particularly wish to acknowledge the help of Steve Baig of NOAA-NESS, Miami, who transmitted satellite images to the ship, and the United States Coast Guard, especially Joe Deaver, who participated in the study in providing SST maps with Coast Guard aircraft. We thank Otis Brown and Bob Evans for supplying the satellite thermal images shown in Fig. 10.

This research was supported by the Department of Energy under contracts EY-76-S-05-5163 and EY-76-S-09-0889, and Bureau of Land Management prime contract number AAT851-CT1-25 to Science Applications, Inc., of Raleigh, NC, subcontract number 11-820294-11.

REFERENCES

- Arthur, R.S., On the calculation of vertical motion in eastern boundary currents from determinations of horizontal motion, *J. Geophys. Res.*, 70, 2799-2803, 1965.
- Bane, J.M., Jr., and D.A. Brooks, Gulf Stream meanders along the continental margin from the Florida Straits to Cape Hatteras, *Geophys. Res. Lett.*, 6, 280-282, 1979.
- Bane, J.M., Jr., D. A. Brooks, and K.R. Lorenson, Synoptic observations of the three-dimensional structure, propagation and evolution of Gulf Stream meanders along the Carolina continental margin, *J. Geophys. Res.*, (in press).
- Bane, J.M., Initial observations of the subsurface structure and short-term variability of the seaward deflection of the Gulf Stream off Charleston, SC, (submitted to *J. Geophys. Res.*, special issue on SAB), 1983.
- Brooks, I.H., and P.P. Niiler, Energetics of the Florida Current, *J. Mar. Res.*, 35, 162-191, 1977.
- Brooks, D.A., and J.M. Bane, Jr., Gulf Stream deflection by a bottom feature off Charleston, SC, *Science*, 201, 1225-1226, 1978.
- Brooks, D.A., and J.M. Bane, Jr., Gulf Stream fluctuations and meanders over the Onslow Bay upper continental slope, *J. Phys. Oceanogr.*, 11(2), 247-256, 1981.
- Chew, F., Spin-off eddies and an hypothesis, *Deep Sea Res.*, 28, 329-391, 1981.
- Dunstan, W.M., and L.P. Atkinson, Sources of new nitrogen for the South Atlantic Bight, in Wiley (ed), *Estuarine Processes*, vol. 1, p. 69-78, Academic Press, 1976.
- Lee, T.N., Florida current spin -off eddies, *Deep Sea Res.*, 22, 753-765, 1975.
- Lee, T.N., and D. Mayer, Low frequency current variability and spin-off eddies on the shelf off southeast Florida, *J. Mar. Res.*, 35, 193-220, 1977.
- Lee, T.N., and D.A. Brooks, Initial observations of current, temperature and coastal sea level response to atmospheric and Gulf Stream forcing on the Georgia shelf, *Geophys. Res. Lett.*, 6, 321-324, 1979.
- Lee, T.N., L.P. Atkinson and R. Legeckis, Observations of a Gulf Stream frontal eddy on the Georgia continental shelf, April 1977, *Deep Sea Res.*, 28(4), 347-378, 1981.
- Legeckis, R., Applications of synchronous meteorological satellite data to the study of time dependent sea surface temperature changes along the boundary of the Gulf Stream, *Geophys. Res. Lett.*, 2, 435-438, 1975.
- Legeckis, R., Satellite observations of the influence of bottom topography on the seaward deflection of the Gulf Stream off Charleston, South Carolina, *J. Phys. Oceanogr.*, 9, 483-497, 1979.

- Niiler, P.P., and L.A. Mysak, Barotropic waves along an eastern continental shelf, *Geophys. Fluid Dynamics*, 2, 273-278, 1971.
- Orlanski, I., The influence of bottom topography on the stability of jets in a baroclinic fluid, *J. Atmospheric Science*, 26, 1216-1232, 1969.
- Orlanski, I., and M.D. Cox, Baroclinic instability in ocean currents, *Geophys. Fluid Dynamics*, 4, 297-332, 1973.
- Pietrafesa, L.J., L.P. Atkinson and J.O. Blanton, Evidence for deflection of the Gulf Stream by the Charleston Rise, *Gulf Stream*, IV(9), 3-7, 1978.
- Schmitz, W.J., Jr., and P.P. Niiler, A note on the kinetic energy exchange between fluctuations and mean flow in the surface layer of the Florida current, *Tellus*, 21, 814-819, 1969.
- Von Arx, W.S., D.F. Bumpus, and W.S. Richardson, On the fine structure of the Gulf Stream front, *Deep Sea Res.*, 3, 46-65, 1955.
- Vukovich, F.M., and B.W. Grissman, Further studies of a cold eddy on the eastern side of the Gulf Stream using satellite data and ship data, *J. Phys. Oceanogr.*, 8, 838-843, 1978.
- Webster, F.A., A description of Gulf Stream meanders off Onslow Bay, *Deep Sea Res.*, 8, 130-143, 1961a.
- Webster, F.A., The effect of meanders on the kinetic energy balance of the Gulf Stream, *Tellus*, 13, 391-401, 1961b.
- Yoder, J.A., L.P. Atkinson, T.N. Lee, H.H. Kim and C.K. McClain, Role of Gulf Stream frontal eddies in forming phytoplankton patches on the outer southeastern shelf, *Limnol. and Oceanogr.*, 26, 1103-1110, 1981.
- 

AD P001053

ON GULF STREAM VARIABILITY AT 30°N

Thomas N. Lee
RSMAS/MPO, University of Miami
4600 Rickenbacker Causeway, Miami, FL 33149

Evans Waddell
Science Applications, Inc.
4900 Waters Edge Drive, Suite 255
Raleigh, North Carolina 27606

ABSTRACT

Current and temperature variability of the Gulf Stream at 30°N was observed with a subsurface array of current meter moorings from August 1980 to October 1981. Energetic current fluctuations in the 2 to 14 day period band accounted for 45 to 70% of the total observed variability. Flow perturbations in the cyclonic shear zone tended to have a cyclonic sense of rotation and were 180° out of phase from anticyclonic flow perturbations within the anticyclonic shear region. These fluctuations appear to result from northward propagating wave-like meanders of the Gulf Stream axis. The fluctuations do not appear to be directly related to local wind forcing.

Observations of near-bottom flow on the Blake Plateau east of the Gulf Stream showed periods of prolonged southward currents lasting up to 40 days with speeds in excess of 30 cm s⁻¹. The mean flow was also southward due to these strong events. The source of the southward flow is unknown. It may be connected to cold-core eddies that are not detectable in the surface with remote sensing or possibly a remnant of the southward undercurrent that has been observed beneath the Gulf Stream off Cape Hatteras and on the deep slope of the Blake Escarpment.

INTRODUCTION

The low-frequency variability of the Gulf Stream flow over the Blake Plateau is investigated using a cross-stream array of subsurface current meter moorings

at 30°N (Fig. 1). The array was deployed for a 13 month period from August 1980 to October 1981 as part of a Bureau of Land Management study of the region.

Meanders and Eddies

A significant part of the Gulf Stream variability observed in the South Atlantic Bight (SAB: Continental shelf and slope region between Cape Canaveral, FL, and Cape Hatteras, NC) occurs within a period band 2 to 14 days. These fluctuations were first systematically observed by Pillsbury (1890) and later by Parr (1937). Webster (1961a) found the Gulf Stream surface front and current axis to be meandering ~ 10 km in the onshore-offshore direction off Onslow Bay on a time scale of 4 to 7 days with estimated wave lengths of about 100 km.

Schmitz and Richardson (1968) reported east-west meanders of the Florida Current occurring on a 1-week time scale with amplitudes of about 5 km. Düing (1975) analyzed 2 weeks of current profiles sampled from 4 ships anchored off Miami and noted a barotropic current meander with a 4 to 6 day time scale. Comparison of the ship measured transport data with transport estimated from the electrical potential on a submarine cable off Jupiter, FL, indicated that the several day "meander" was produced by a wave traveling to the north at 47 cm s^{-1} and wave length of 200 km. Düing described 2 cases for meanders: deep southward flow appeared to occur over the Miami Terrace during an offshore meander (current axis displaced to the east) and deep northward flow occurred over the Terrace during an onshore meander stage (axis displaced to the west). In general it appeared that flow variations on the cyclonic shear side of the axis were about 180° out of phase with the anticyclonic side.

More recently Brooks (1979) found similar results from dropsonde transects of the Florida Current off Miami over an 83 day period in the summer of 1974. Transport fluctuations within the 2 to 14 day period band were highly coherent and in phase at stations in the cyclonic shear region as were stations in the anticyclonic region but the two regions were 180° out of phase. Brooks also

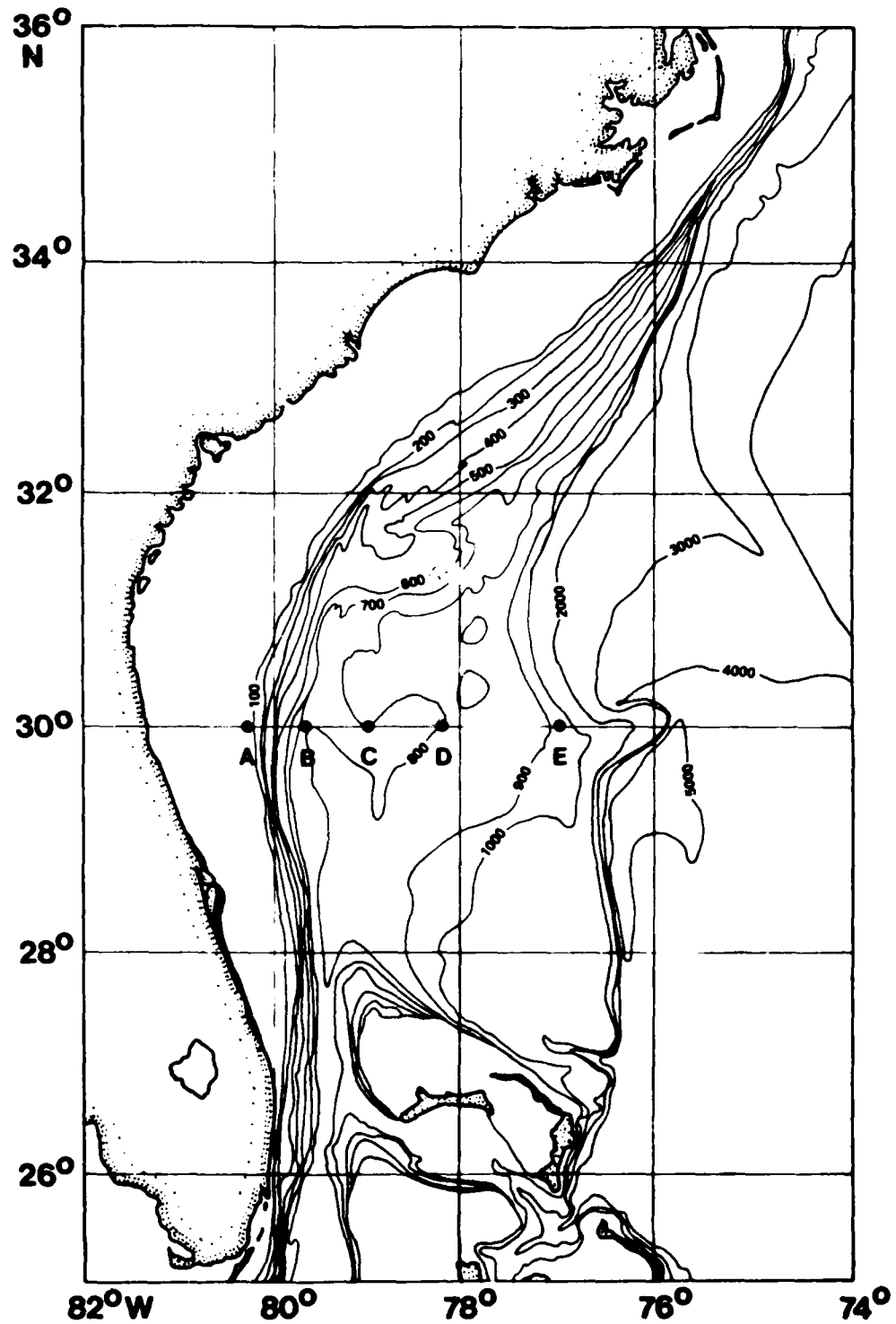


Figure 1 Location of Blake Plateau current meter mooring sites; August 26, 1980 to October 6, 1981.

found fluctuations in the total transport that were visually coherent and in phase with the variations on the anticyclonic side. During the experiment the current axis meandered a total distance of approximately 24 km. An offshore (onshore) meander was associated with a transport increase (decrease) on the eastern side of the current, a transport decrease (increase) on the western side and an increase (decrease) of total transport. Current records from an array of near bottom current meters, spanning the Florida Straits at the same location and time as the Brooks dropsonde measurements, showed energetic fluctuations of the downstream component with well defined spectral peaks at periods of 9 to 12 days that were coherent across the entire Florida Straits (Düing, Mooers and Lee, 1977). The downstream coherence scale of these fluctuations was estimated at 55 km from a current meter array along the continental slope (Lee, Brooks and Düing, 1977).

Brooks and Bane (1981) and Bane, Brooks and Lorenson (1981) used current meter data from the continental slope, satellite infrared images and AXBT temperature profiles to describe Gulf Stream meanders off Onslow Bay. Their results are consistent with Webster's (1961a) findings and indicate that the meanders were produced by northward propagating skewed waves with a weekly period. Approaching wave crests (shoreward excursions of the SST front) produced in-phase increases in northward speeds and temperature at the mooring locations. Decreasing speeds and temperatures occurred following the crest's passage.

Cyclonic, cold-core eddies have been observed embedded in the Gulf Stream front in the Florida Straits region (Lee, 1975; Lee and Mayer, 1977) and along the Florida/Georgia outer shelf (Lee, Atkinson and Legeckis, 1981; Lee and Atkinson, 1983). These eddies occur on the shoreward side of offshore meanders and appear to be phase-locked to the meander; traveling to the north at the same speed as the meander (30 to 70 cm s^{-1}) and growing in size as the meander develops. Upwelling in the cold-core has been observed to uplift the density structure of

the front in the upper 200 m. They occur on the average of about 1 per week and have a life span of about 1 to 3 weeks. Satellite images (Legeckis, 1975; Stumpf and Rao, 1975) suggest that the eddies evolve from growing frontal meanders. Their surface manifestation consists of warm, southward-oriented streamers of Gulf Stream water than wrap around the cold-core. These features were first described as "shingles" by Von Arx, Bumpus and Richardson (1955).

Satellite imagery shows that wave-like meanders and eddies are a consistent feature of the Gulf Stream front all along the southeast U.S. In the Florida Straits eddy dimensions are usually less than 50 km and east-west displacements of the surface front are on the order of 10 km. North of Jupiter, FL, where the shelf begins to widen and the Bahama Bank falls off into the Blake Plateau, eddy dimensions increase in the downstream direction to 100-200 km, and east-west meanders of 30 km are observed (Lee, Atkinson and Legeckis, 1981; Bane and Brooks, 1979). A second elongation is observed north of the "Charleston bump" (a topographic anomaly of the slope extending seaward into the Gulf Stream) where downstream dimensions can reach 300 km (Legeckis, 1979) and meanders with 100 km displacements occur (Legeckis, 1979; Bane and Brooks, 1979; Brooks and Bane, 1981; Bane, Brooks and Lorenson, 1981).

The Gulf Stream is observed to have a quasi-persistent eastward displacement downstream of the "bump", which is believed to be the cause of the larger meanders and eddies between the "bump" and Cape Hatteras (Pietrafesa, Atkinson and Blanton, 1978; Brooks and Bane, 1978; Bane and Brooks, 1979; Legeckis, 1979). East of Cape Hatteras, Gulf Stream meanders are no longer restricted by the continental shelf as along the southeast U.S. coast and the well-known warm and cold core "rings" develop north and south of the Stream, respectively.

METHODS

Current and temperature variability over the Blake Plateau at 30°N was measured with a cross-stream array of 5 subsurface taut-wire current meter

moorings (Fig. 1). The array was in place for a total of 13 months from August 27, 1980 to October 6, 1981 with a mooring exchange in March, 1981. The array was equipped with 9 Niskin Wing Current Meters (NWCN's). The vertical distribution of instruments is shown superimposed on the temperature section made across the array by Skidaway Institute of Oceanography on September 8 and 9, 1980 (Fig. 2a); and on a velocity section made by Richardson, Schmitz and Niller (1969) 37 km north of the array (Fig. 2b). The array extended from the shelf edge ($80^{\circ}15'W$) to the Blake Escarpment ($77^{\circ}W$). The shelf edge mooring (#A) was deployed at the 75 m isobath with a single current meter 3 m above the bottom. Moorings B and C were installed in water depths of about 800 m with instruments located near depths of 400, 600 and 797 m. Mooring B was located near the subsurface extension of the Gulf Stream axis as shown in Fig. 2b and Mooring C was near the seaward edge of the Stream. Moorings D and E were near bottom moorings with current meters located 3 m above the bottom in water depths of about 800 and 970 m respectively. Mooring E was located at the seaward edge of the Blake Plateau near the Blake spur. The 600 m level current meter on mooring C did not operate properly during the first deployment so is not listed. The lower layer instrument on mooring B lost a fin at the start of the second deployment giving low speeds. Also temperature from the top meter on mooring B of the second deployment was in error.

Current and temperature were recorded on cassette tapes every 15 minutes. All data were smoothed with a 3-hour low pass (HLP) Lanczos filter kernel and resampled every hour to form the basic time series. The hourly values were then refiltered with a 40-HLP Lanczos filter to remove fluctuations with tidal or inertial periods and resampled every 6 hours to form the low-frequency time series. Current vectors were converted into component time series with u (cross-stream) + toward the east and v (along-stream) + toward the north.

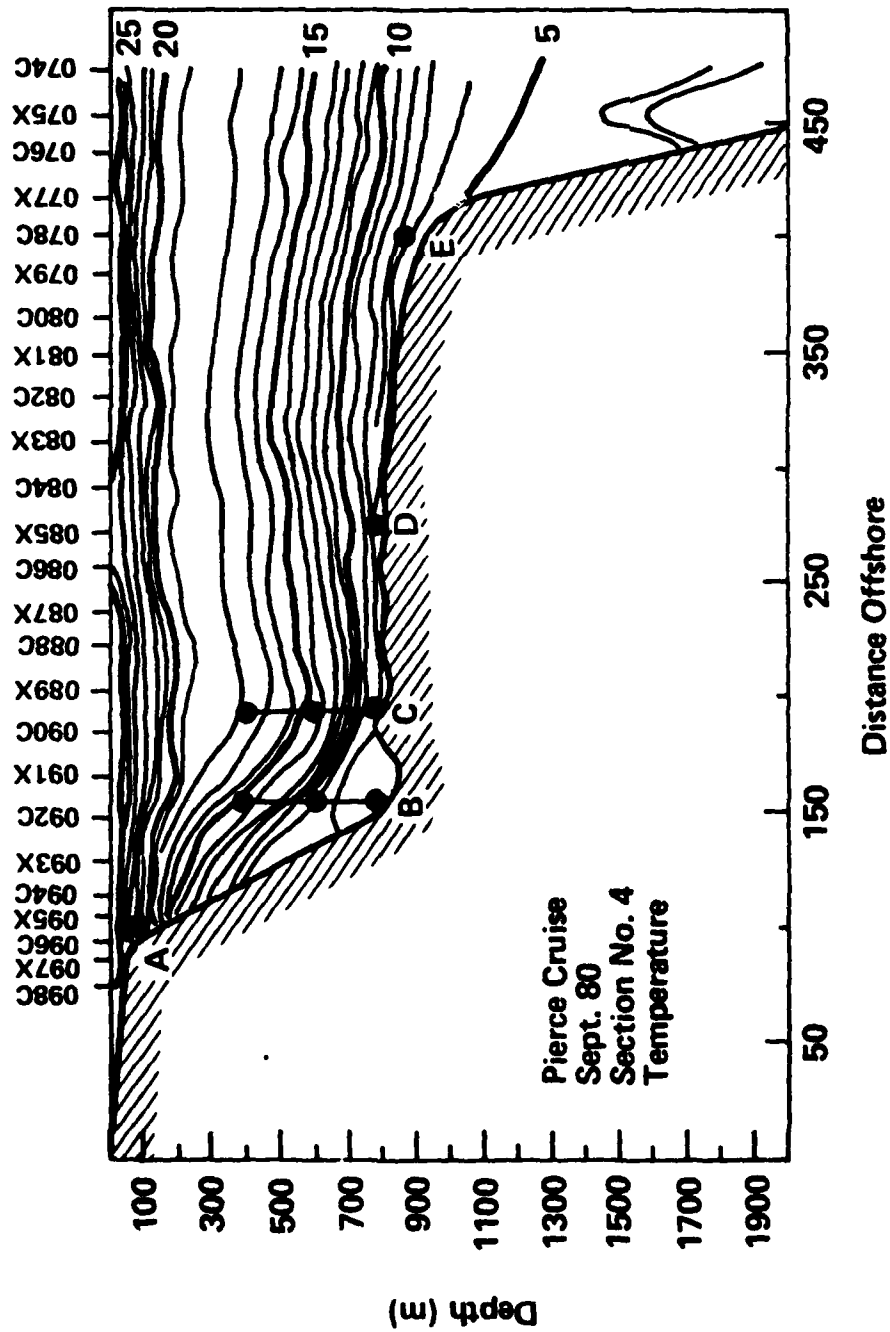


Figure 2a Vertical configuration of current meters superimposed on a temperature section of September 8 and 9, 1980 made by Skidaway Institute of Oceanography.

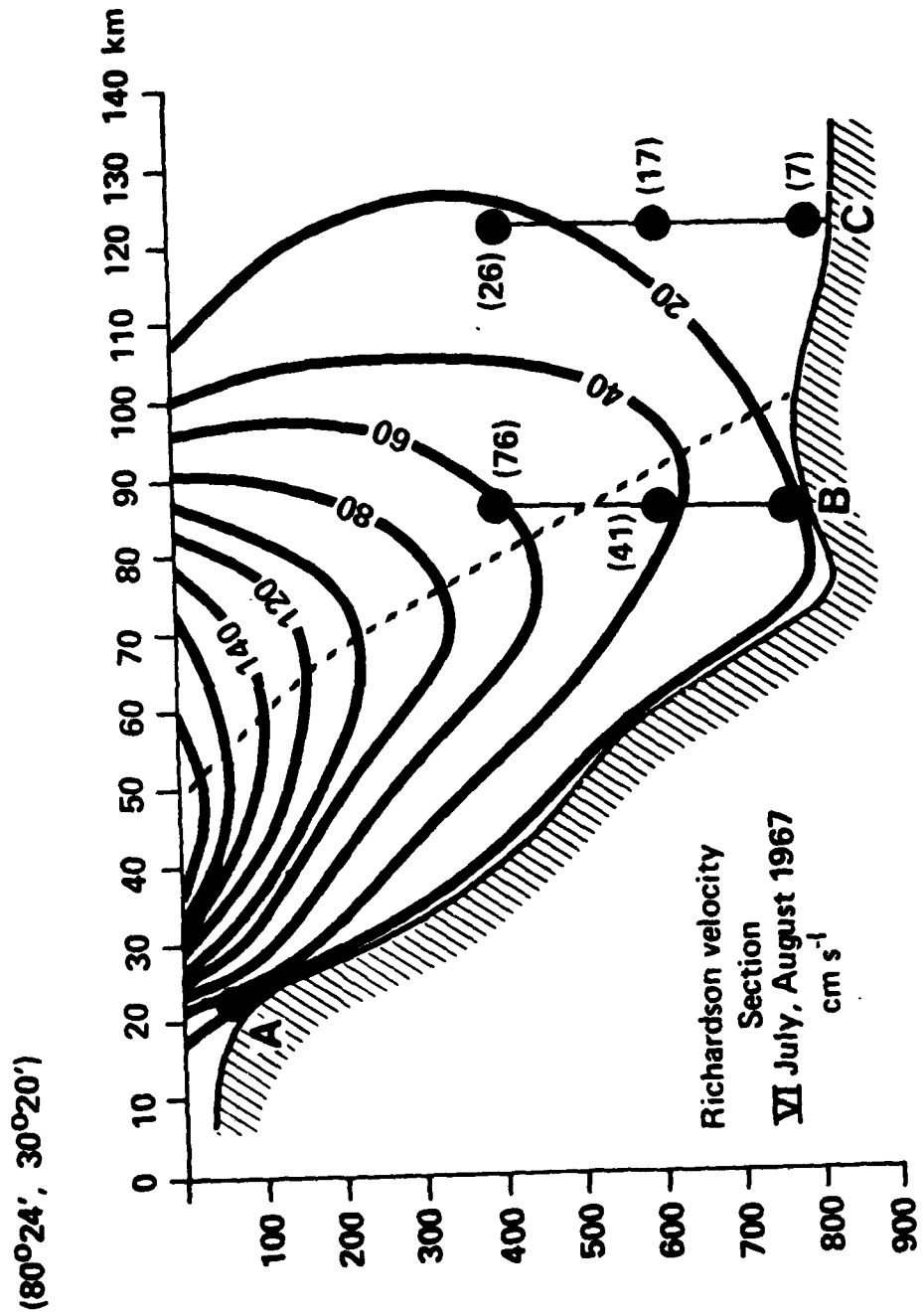


Figure 2b Vertical configuration of moorings A, B and C superimposed on a velocity section made by Richardson et al. (1969) during July and August 1967. Mean downstream velocities at each current meter during the 2nd deployment are shown

OBSERVATIONS

An example of the 40-HLP current vector time series across the Blake Plateau is shown in Fig. 3. Moorings B and C were apparently located within the Gulf Stream judging from the strong persistent northward flow at both locations. Downstream mean velocities agree remarkably well with the Richardson et al. (1969) velocity section shown in Fig. 2b indicating that mooring B was located near the subsurface extension of the current axis and mooring C was located near the eastern edge of the current. Mean downstream velocities were about 62 cm s^{-1} at B (top) during the first deployment and 76 cm s^{-1} during the second deployment, which suggests a seasonal trend consistent with the summer transport maximums observed by Niiler and Richardson (1973). Mean flows at C were about half as strong as at B and showed little change between the deployment periods. Mean vertical shears were about $-1.7 \times 10^{-3} \text{ s}^{-1}$ at B and $-0.5 \times 10^{-3} \text{ s}^{-1}$ at C over both deployment periods, indicating little seasonal change in baroclinic transport between B and C. Maximum downstream flow at B reached 109 cm s^{-1} at the 400 m level during the second deployment and maximum flow at C was 87 cm s^{-1} during the first deployment. Standard deviations of the cross-stream and downstream components were approximately equal at each instrument of moorings B and C during both deployments and ranged from a minimum of $\pm 7 \text{ cm s}^{-1}$ near the bottom to a maximum of $\pm 18 \text{ cm s}^{-1}$ at 400 m.

Low-frequency velocity fluctuations appear to be visibly well correlated over the 400 m vertical separation at both moorings B and C (Fig. 3). Both cyclonic and anticyclonic perturbations appear to occur with cyclonic perturbations more common at mooring B and anticyclonic more prevalent at C. At times cyclonic perturbations at B appear to occur simultaneously with anticyclonic events at C and cyclonic events at A. Cold, cyclonic fluctuations at the shelf edge have been shown to be produced by northward propagating cyclonic, cold-core eddies embedded in the Gulf Stream front (Lee and Atkinson, 1983). These

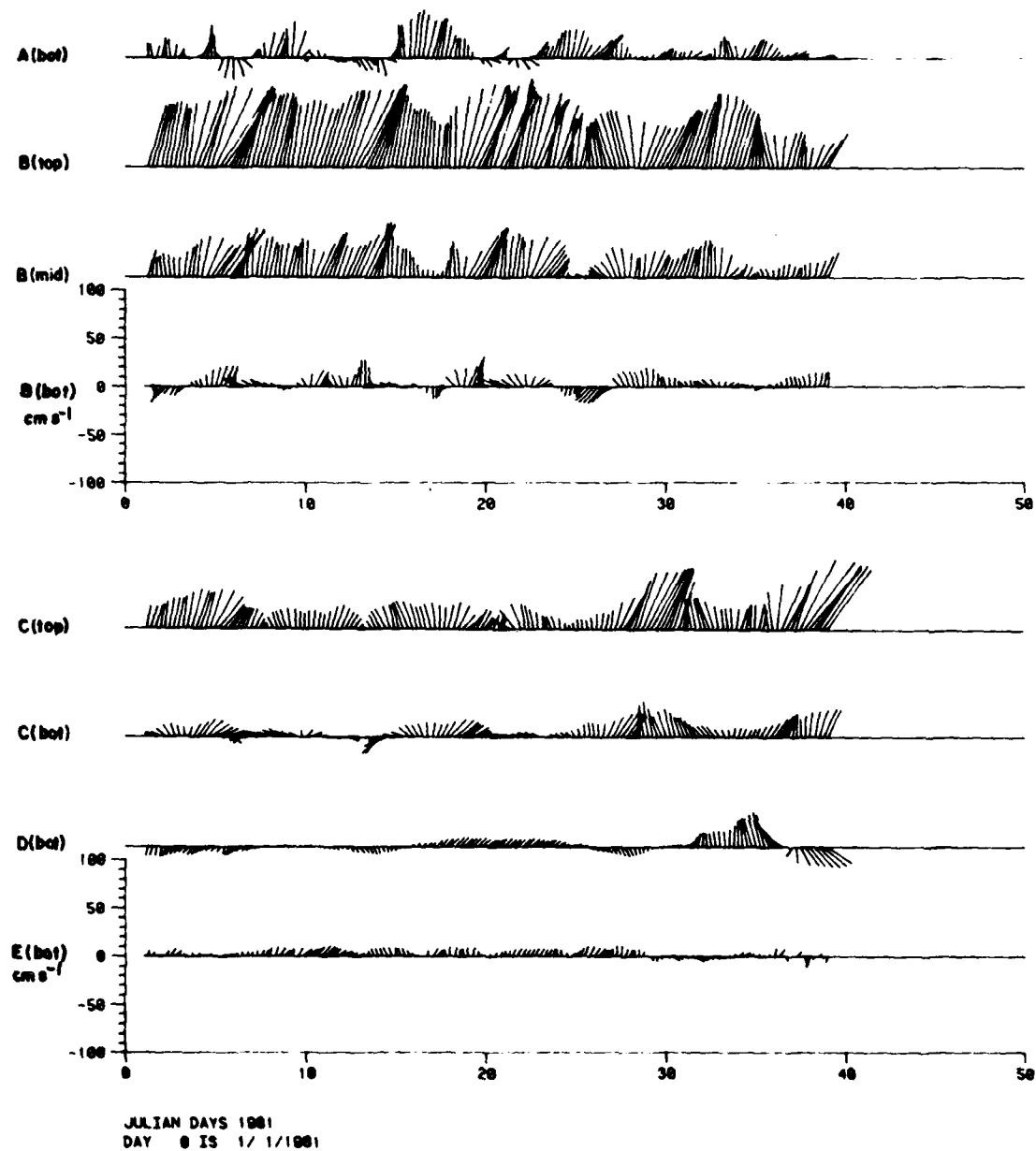


Figure 3 6-hourly current vectors from 40-HLP filtered time series during winter.

types of events appear to be a common feature at A throughout the year.

Near bottom flow at site D shows little visual similarity to the currents at sites C or E. Prolonged southward flows occurred that persisted for periods up to 42 days and reached speeds in excess of 30 cm s^{-1} (Fig. 3). Mean flows at D were southward at -7 and -2 cm s^{-1} during the first and second deployments respectively. The near bottom mean flow at the seaward edge of the Plateau (site E) was primarily in the offshore direction at about 5 cm s^{-1} during the first deployment and 7 cm s^{-1} during the second deployment. Maximum currents at E reached speeds of about 35 cm s^{-1} in the offshore and southerly directions. Standard deviations ranged from ± 7 to $\pm 15 \text{ cm s}^{-1}$. Cold-core, cyclonic rings have been observed to cross the Plateau in this region and coalesce with the Gulf Stream (Cheney and Richardson, 1976; Perkins and Wimbush, 1976; Vukovich and Grissman, 1978).

Energy Partitioning

If the velocity field is decomposed into mean and fluctuating components, i.e., $u = \bar{u} + u'$, then total kinetic energy can be estimated from

$$\frac{1}{T} \int_0^T |V|^2 dt = (\sigma_u^2 + \sigma_v^2) + (\bar{u}^2 + \bar{v}^2) \quad (1)$$

where V is the current vector and σ^2 = variance. In this decomposition the second term on the right is approximately proportional to the kinetic energy of the mean flow and the first term is proportional to kinetic energy due to velocity fluctuations, i.e. eddy or perturbation kinetic energy (PKE). The various major components in (1) are shown in Table 1 for the first measurement period.

The locally dominant Gulf Stream influence is apparent at moorings B and C from the large total kinetic energy levels observed away from the bottom. Division into time varying and steady components shows this Gulf Stream contribution

TABLE I. Energy partition for first deployment period,
units are cm^2s^{-2} .

Current Meter I.D.	Perturbation Kinetic Energy ($\sigma_u^2 + \sigma_v^2$)	+	Kinetic Energy of Mean Flow = ($\bar{u}^2 + \bar{v}^2$)	=	Total Kinetic Energy
A (bot)	435 (84%)		80 (16%)		515 (100%)
B (top)	519 (11%)		4104 (89%)		4623 (100%)
B (mid)	295 (25%)		884 (75%)		1179 (100%)
B (bot)	178 (80%)		44 (20%)		222 (100%)
C (top)	560 (37%)		945 (63%)		1505
C (mid)	---		NO DATA		---
C (bot)	255 (69%)		116 (31%)		371 (100%)
D (bot)	520 (92%)		48 (8%)		568 (100%)
E (bot)	184 (88%)		26 (12%)		210 (100%)

results substantially from mean flow having strong vertical shear, i.e. baroclinicity in the mean. In contrast, perturbation kinetic energy is of lower relative magnitude near the Gulf Stream core and has weaker vertical gradients. Away from the Gulf Stream only near-bottom measurements were made so it is not possible to determine the importance of mean interior flows to energetics at non-Gulf Stream sites. However, even near the Gulf Stream the time varying velocity dominated energetics at the bottom.

Because of the overall importance of the time varying velocity component, the kinetic energy was partitioned as a function of period (Table 2). The high frequency component containing tidal and inertial fluctuations was a major contributor to PKE only at those sites close to a topographic break (moorings A and E) at the shelf break and the Blake Escarpment respectively. At those sites having a substantial Gulf Stream influence (moorings B and C) the 40 hr to 14 day band tended to be the major contributor to PKE. Available data suggest this relative contribution increased with depth as might be expected for barotropic fluctuations of a baroclinic mean flow.

The lowest frequency component (period >14 days) was significant only for the 400 m flow in the vicinity of the Gulf Stream and near bottom flow on the middle and outer Blake Plateau. During the first deployment the contribution to the total velocity variance observed at 400 m locations on moorings B and C from motions with periods >14 days was equal to or slightly higher than the variance in the 40 hr to 14 day band. In contrast, during the second deployment fluctuations with periods >14 days accounted for significantly less variance than 40 hr to 14 day motions at B and were about equal with values from C.

At the mid and outer Blake Plateau stations (moorings D and E) and for interior positions near or in the Gulf Stream, approximately 6 month records do not produce stationary means or variance although the patterns do generally seem to be consistent. This is clearly evident in the magnitude of the mean and fluctuating components of kinetic energy.

TABLE 2. Decomposition of Perturbation Kinetic Energy (PKE) into periodicities for first deployment period, units are $\text{cm}^2 \text{s}^{-2}$.

Current Meter I.D.	(3-40 Hr)	+	(40 Hr - 14 Day)	+	(>14 Day)	=	PKE
A (bot)	210 (48%)		180 (41%)		45 (10%)		435 (100%)
B (top)	17 (3%)		236 (45%)		266 (52%)		519 (100%)
B (mid)	42 (14%)		274 (59%)		79 (27%)		295 (100%)
B (bot)	28 (16%)		111 (62%)		39 (22%)		178 (100%)
C (top)	18 (3%)		221 (39%)		321 (57%)		560 (100%)
C (mid)	---		NO DATA		---		---
C (bot)	50 (20%)		158 (70%)		47 (18%)		255 (100%)
D (bot)	91 (18%)		89 (17%)		340 (65%)		520 (100%)
E (bot)	72 (39%)		18 (10%)		94 (51%)		184 (100%)

Spectra

Spectra, coherence squared and phase computed for the 40-HLP time series of cross-stream and along-stream velocity components from the first deployment of moorings B and C are shown in Figs. 4 and 5. Similar results were obtained from the second deployment. Energetic fluctuations of the cross-stream and along-stream velocity components at 400 m were coherent over the 37 km separation in the 3 to 5 and 8 to 12 day period bands. Cross-stream current variations at C appear to lead those at B by about 45° phase in the 3 to 4 day band and about 90° phase in the 8 to 12 day band. Along-stream current fluctuations were almost 180° out of phase for periods less than 1 week. For periods longer than 1 week C lead by about 90 to 100° phase. Temperature (not shown) was nearly in phase over these periods. Similar results were found for the lower layer between sites B and C except that fluctuations in the cross-stream components were nearly in phase and along-stream variations at C lead those at B by about 90° in phase.

Co-spectra, coherence squared and phase of u vs. v from the 400 m level at sites B and C are shown in Fig. 6. The velocity components were coherent at each site in the 3 to 4 and 8 to 12 day period bands. At site B the phase was positive at these periods, indicating that u was leading v by about 45 to 60° which would occur for cyclonic motion. At site C the phase was negative over the 2 to 4 day period band indicative of anticyclonic fluctuations. Anticyclonic motion also appeared to occur in the near bottom flow at site D (not shown), whereas the coherent part of the bottom flow near the Blake Escarpment (site E) appeared to occur as cyclonic fluctuations. Cross-spectra between coastal winds at Jacksonville FL, and currents from B and C revealed no significant coherence.

At the shelf edge location (site A) the low-frequency velocity variations occurred as cyclonic motions that were coherent at periods of about 5, 3.5, 2.5 and 2 days (not shown). Along-stream fluctuations at the shelf edge had well-defined energy peaks with about an order of magnitude higher energy levels than

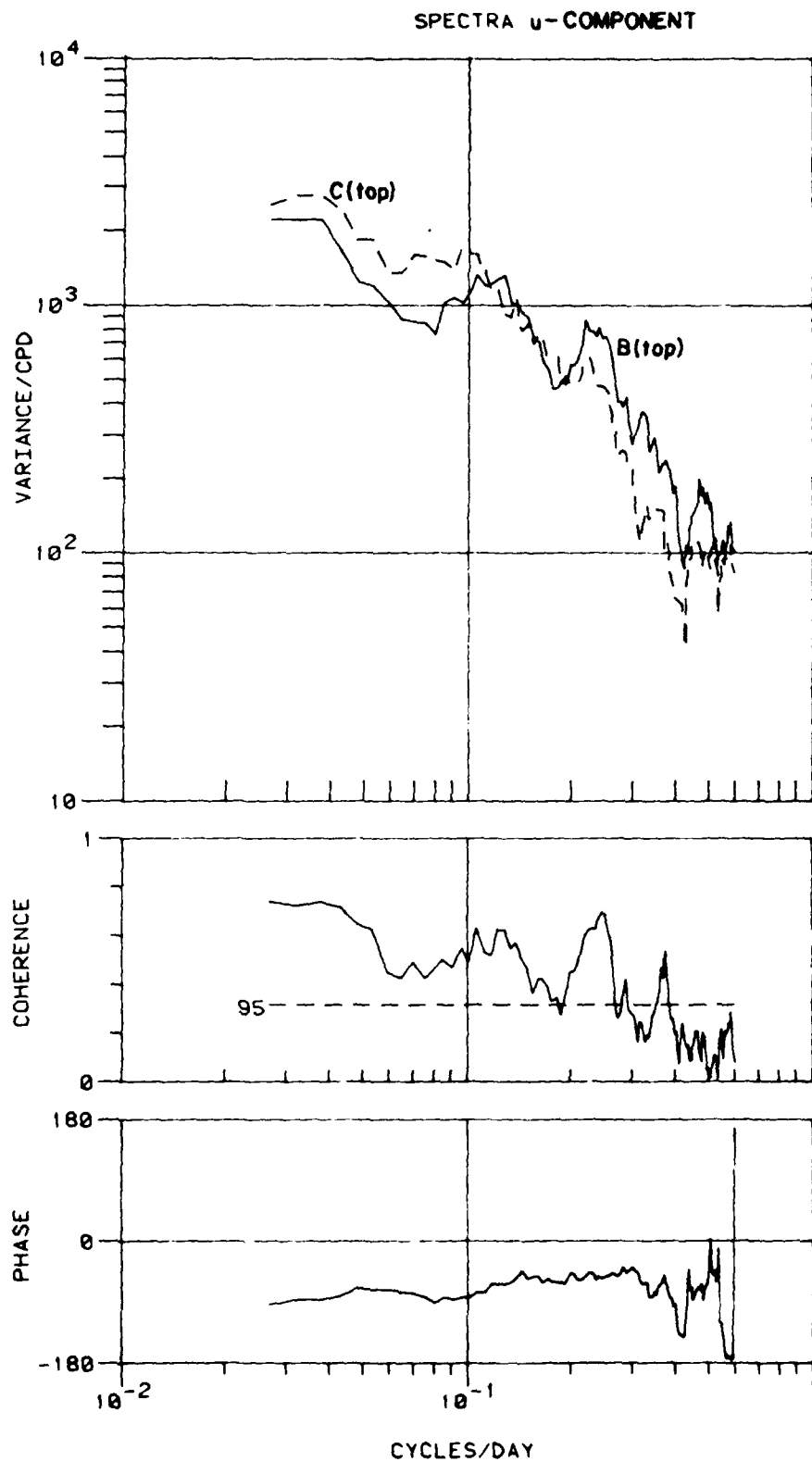


Figure 4 Spectra, coherence squared and phase between u-component 40-HLP time series from current meters B (top) and C (top). Degrees of freedom = 18; bandwidth = 0.048; data length = 188 days.

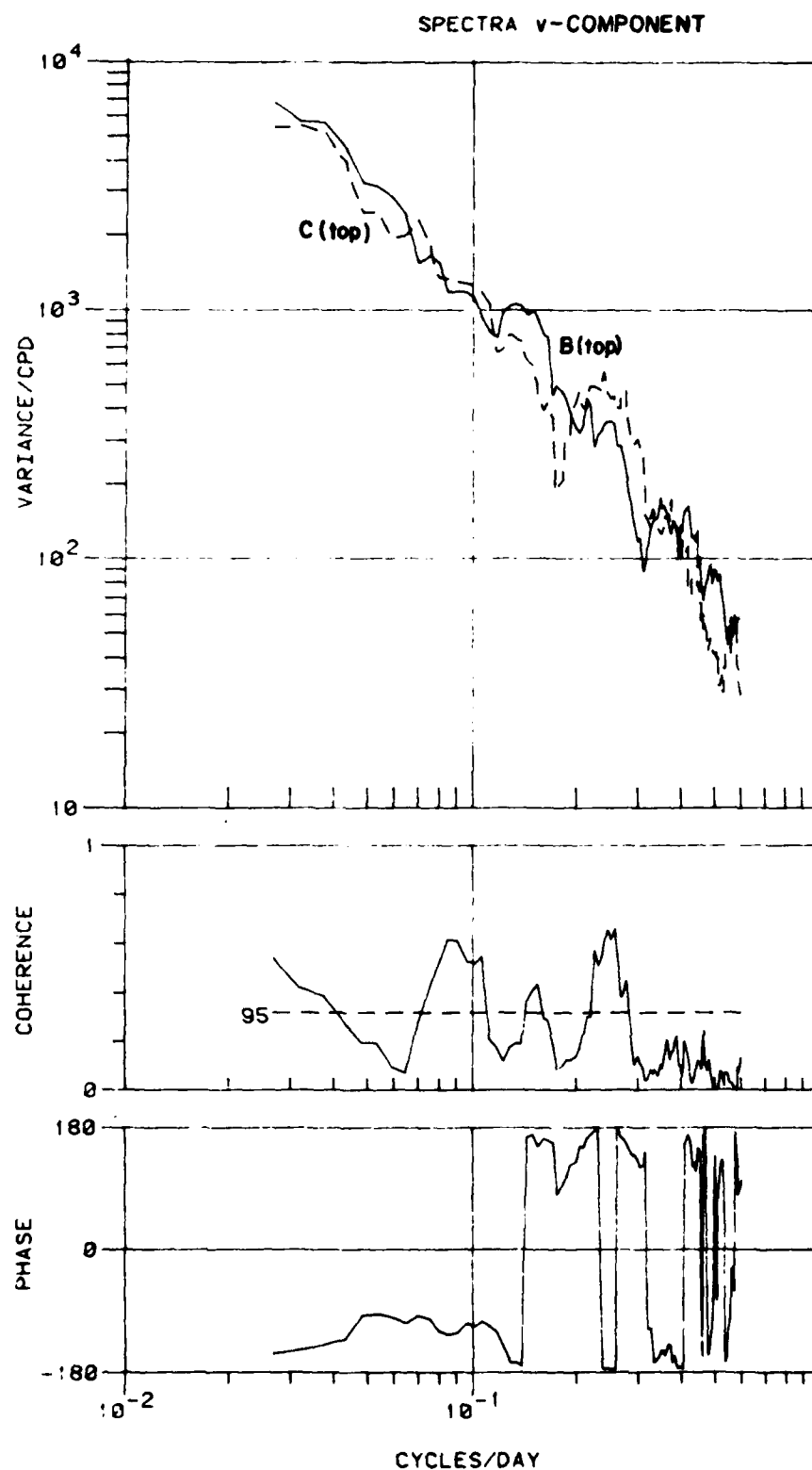


Figure 5 Spectra, coherence squared and phase between v-component 40-HLP time series from current meters B (top) and C (top). Degrees of freedom = 18; bandwidth = 0.048; data length = 188 days.

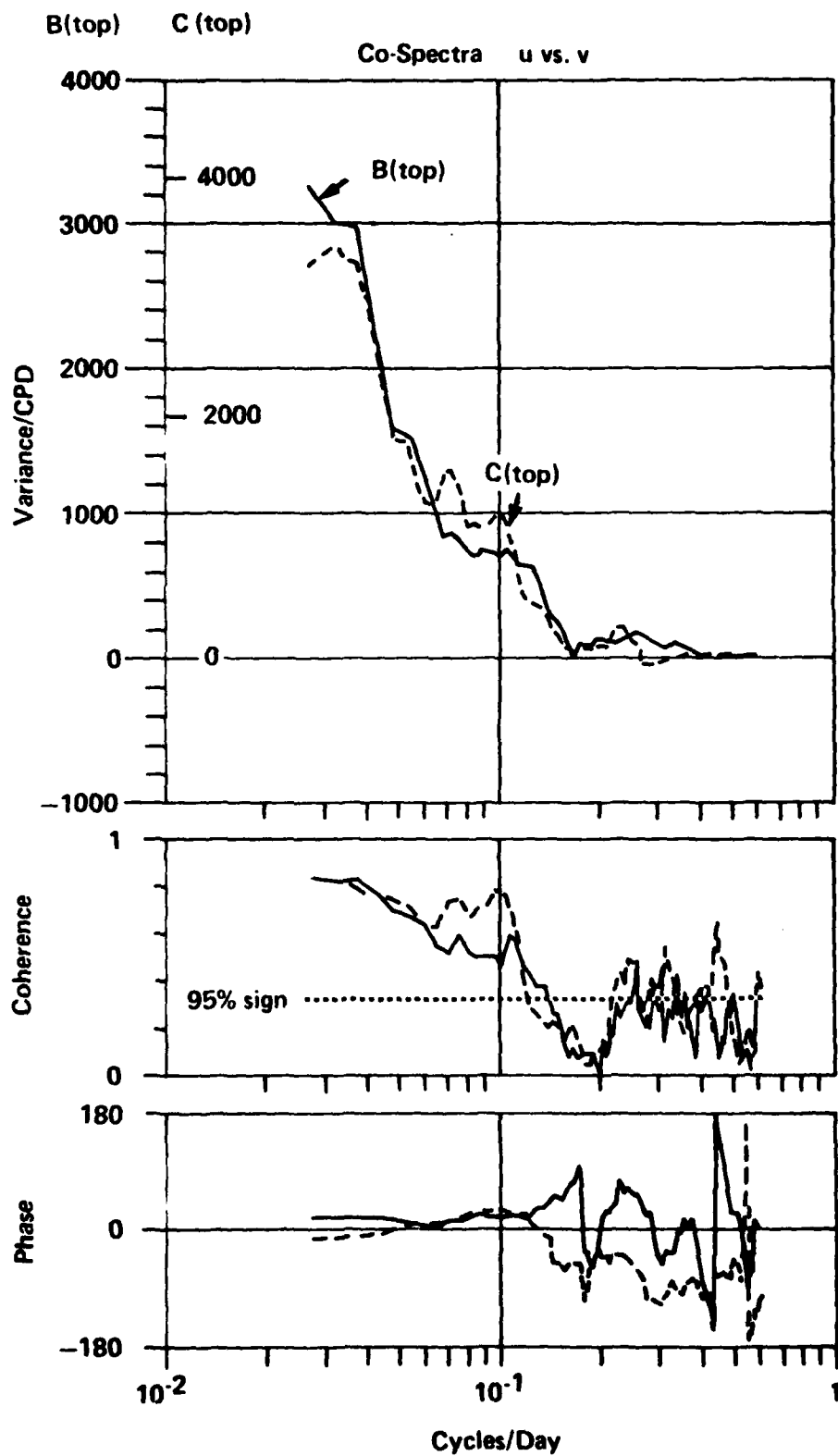


Figure 6 Co-spectra, coherence squared and phase of u and v components from current meters B (top) (solid lines) and C (top) (dashed lines). Degrees of freedom = 18; bandwidth = 0.048; data length = 188 days.

the cross-stream for periods longer than 3 days. In contrast, energy spectra from the Blake Plateau sites continued to increase with decreasing frequencies without well-resolved energy peaks. Also the level of energy was nearly the same for the cross- and along-stream components.

Significant coherence was observed over the 400 m vertical separation (not shown) at site B for the cross-stream component at periods of 3 to 5 days; for the along-stream component at periods longer than 1 week; and for temperature at periods of 2.5 and 5 to 10 days with small phase lags for all variables. At site C significant vertical coherence was observed at periods of 2 to 7 days for u , 4 to 5 and 7 to 12 days for v and 4 to 12 days for T , again with small phase lags.

DISCUSSION

Low-frequency time series and spectra of current and temperature from the Gulf Stream region indicate that cold, cyclonic perturbations of the basic northward flow at site B tend to be coherent and 180° out of phase with anticyclonic flow events at site C. Fluctuations of this type appear to occur at periods of 2 to 7 days and are more clearly recognizable after removing the effect of the strong northward Gulf Stream mean flow by band-pass filtering the data over a 40 hr to 2 week period band. This removes fluctuations with periods less than 40 hr and greater than 2 weeks. Figs. 7 and 8 show examples of band-pass filtering. Current perturbations at sites A and B generally show a cyclonic sense of rotation and were at times 180° out of phase. At site C anticyclonic rotation that was 180° out of phase with the flow at site B tends to be more common. Current amplitudes were approximately equal at all instrument levels at sites A, B and C. Vertical shears in the fluctuations were weak, on the order of 10^{-4} s^{-1} which is about an order of magnitude less than the mean shears and indicates a significant barotropic component to the fluctuations. Temperature fluctuations were

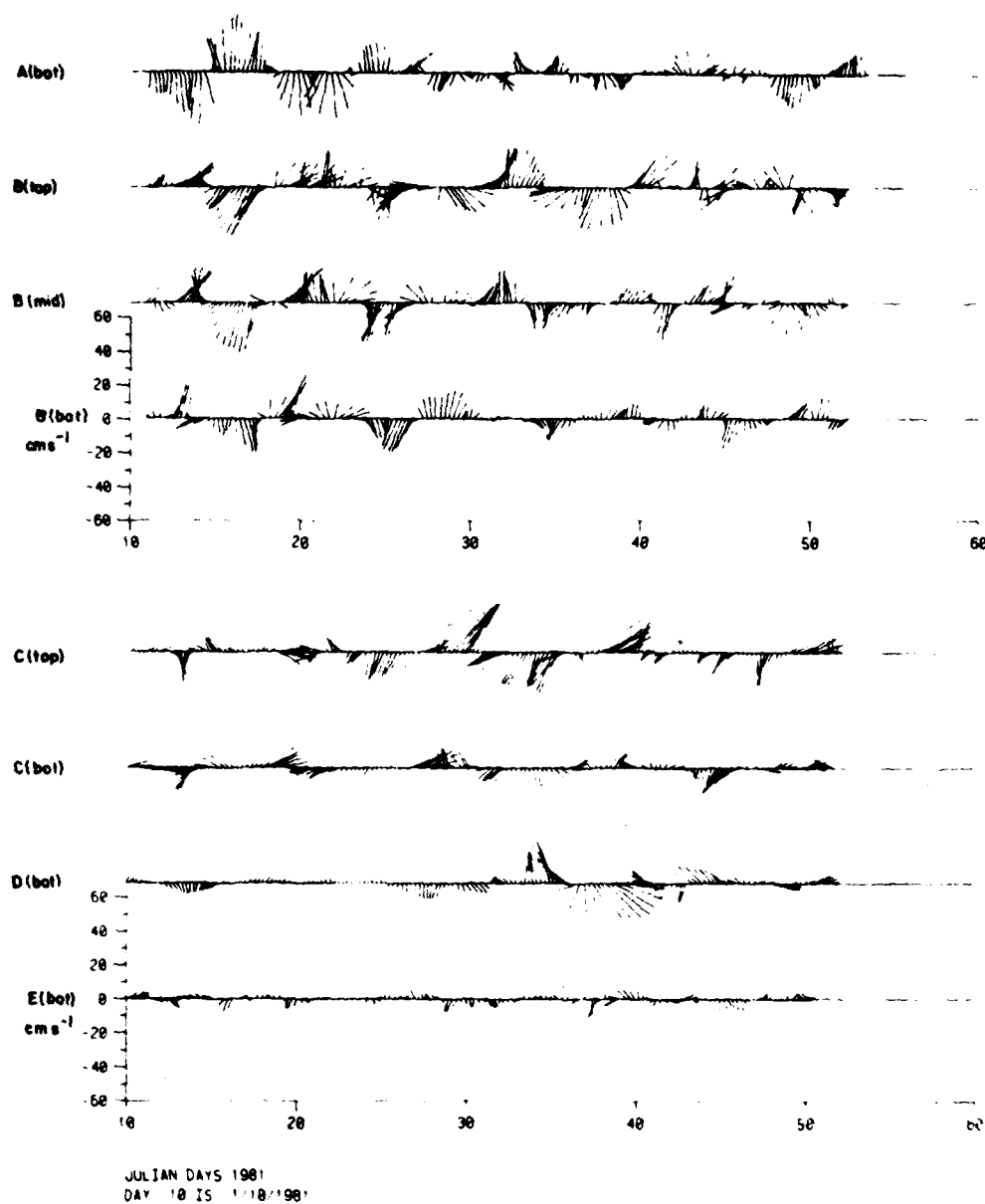


Figure 7 6-hourly current vectors from 40 hr-to-14 day band pass filtered time series during Julian days 1-50, 1981.

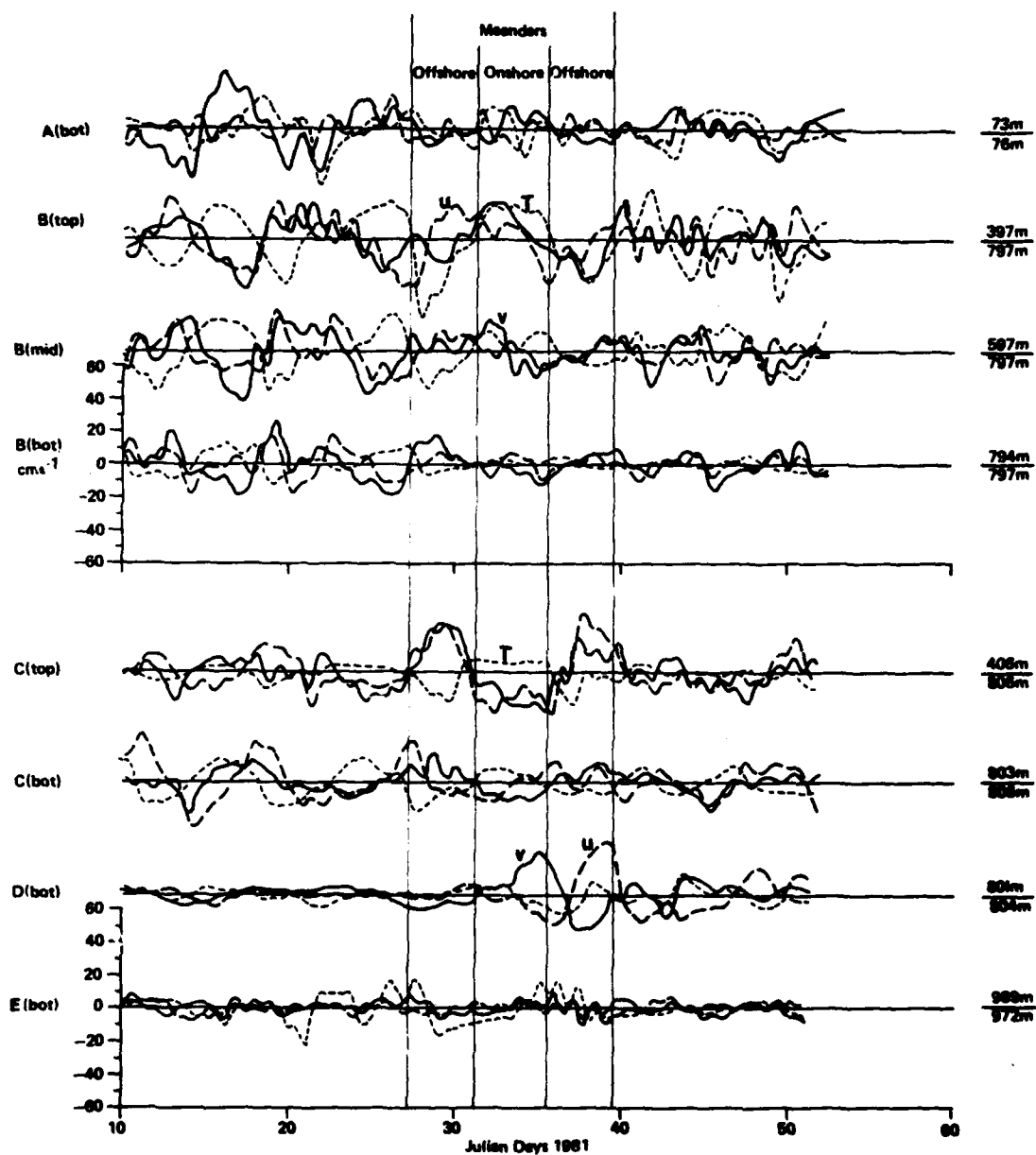


Figure 8 Band-pass filtered cross-stream (u) and along-stream (v) velocity components and temperature (T) during Julian days 1-50, 1981. Vertical lines are for meander event identification, instrument depth and water depth is shown at the right.

approximately 180° out of phase with the cross-stream velocity component at sites B and C.

During days 27 to 40 temperature was in phase with the along-stream velocity at site B and out of phase at site C and appears to be a reasonably clear example of an offshore/onshore/offshore Gulf Stream meander with a period of about 8 to 9 days. Assuming the current axis was located near mooring B as indicated in Fig. 2 then a meander of the Stream (east/west shift of the velocity and temperature fields) could account for the observed changes in velocity and temperature. An offshore meander could cause an offshore component in the flow and decreasing temperatures at B and C coupled with an increase in along-stream flow at C and decrease at B (as the axis approaches C). The observations on days 27 to 31 and 35 to 40 are typical examples of this type of offshore meander behavior. An onshore meander would result in an onshore current component and increasing temperatures at B and C while the along-stream flow increased at B, with the approaching axis, and decreased at C. The observations on days 31 to 35 are representative of changes occurring during an onshore meander.

Assuming that the dominant time varying component of cross-stream velocity occurring at 2.5 - 5 day periods in the vicinity of the Gulf Stream is a result of the lateral motion of the main stream, then a first order estimate of this displacement can be made by examining the time integral of u over a half cycle, i.e. between zero crossings. Results show this approximation to be ~ 25 km with a mean offshore or onshore velocity of $\sim 14 \text{ cm s}^{-1}$, which is in reasonable agreement with 30 km estimate for the Gulf Stream surface front in this region (Bane and Brooks, 1979).

A significant fraction of the low-frequency current and temperature variability at sites A, B and C appears to have been produced by Gulf Stream meanders similar to that found north of the Charleston bump by Brooks and Bane (1981) and Bane, Brooks and Lorenson (1981). Theoretical investigations indicate that both

barotropic and baroclinic instabilities can occur for the Gulf Stream flow in this region (Niiler and Mysak, 1971; Orlanski, 1969; Orlanski and Cox, 1973). Theory predicts wave lengths of 100 to 200 km and wave periods of about 10 days for the fastest growing northward propagating waves, which appears to match reasonably well with satellite observations of the surface thermal front (Legeckis, 1979); current meter data from the shelf edge upstream of the Charleston bump (Lee and Atkinson, 1983); on the continental slope downstream of the bump (Brooks and Bane, 1981); and those data presented here. Luther (personal communications) modeled spatially unstable waves in the Gulf Stream off the southeast U.S. and found cyclonic perturbations west of the axis and anticyclonic perturbations east of the axis, similar to our findings.

Energy Transfer

Meanders have been shown to play an important role in the flux of momentum and heat and redistribution of kinetic and potential energy within the Gulf Stream. The transfer of eddy kinetic energy was found to be distributed horizontally across the Stream off Miami, whereas the transfer of perturbation potential energy was vertically distributed (Brooks and Niiler, 1977). Perturbation kinetic energy was transferred from the fluctuations to the mean flow in the cyclonic shear region of the current, and from the mean to the fluctuations in the anticyclonic shear region (Webster, 1961b; Schmitz and Niiler, 1968; Brooks and Niiler, 1977). Perturbation potential energy was transferred from the mean to the fluctuations in the lower half of the current and in the vicinity of the current axis (Brooks and Niiler, 1977). Orlanski (1969) and Orlanski and Cox (1973) concluded that energy transfers of this type can best be explained by a baroclinic instability process, where disturbances can grow by feeding on the potential energy of the mean current and then transfer their kinetic energy back to the mean flow. Brooks and Niiler (1977) determined that Gulf Stream fluctuations caused an internal redistribution of energy with no appreciable net energy

transfer over the current cross-sectional average. They showed that the net conversion rate of perturbation kinetic energy can be estimated from:

$$\frac{d}{dt} \left\{ \frac{1}{2} (\overline{u'^2} + \overline{v'^2}) \right\} = - \left\{ \overline{u'^2} \frac{\partial \bar{u}}{\partial x} + \overline{v'^2} \frac{\partial \bar{v}}{\partial y} + \overline{u'v'} \frac{\partial \bar{v}}{\partial x} \right\} \quad (2)$$

where the overbar represents a time average and the primes are deviations from the mean. The first and third terms on the right hand side of (2) were evaluated from the 400 m and near bottom depths at sites B and C. The second term involves downstream derivative of \bar{v} which could not be calculated from the cross-stream array. However, since the cross-stream and along-stream current fluctuations (u' , v') were about the same magnitude and $\frac{\partial \bar{v}}{\partial x} \gg \frac{\partial \bar{v}}{\partial y}$ then the second term should be small compared to the third. The results of these calculations are given in Table 3. The dominant term in the energy transfer is $\overline{u'v'} \frac{\partial \bar{v}}{\partial x}$. The negative sign indicates that there was a net transfer of perturbation kinetic energy from the mean flow to the fluctuations over the 7 month averaging period. This is consistent with the finding of Schmitz and Niller (1968) and Brooks and Niller (1977) for the anticyclonic shear zone. The rate of transfer was about -140×10^{-4} ergs $\text{cm}^{-3} \text{s}^{-1}$ at mid-depth and was insignificant near the bottom. The net transfer of perturbation energy to the fluctuations in this region was produced by the combined effects of a net offshore flux of northward momentum of $1.4 \times 10^3 \text{ cm}^2 \text{s}^{-2}$ occurring in a zone of mean anticyclonic shear of about $-9 \times 10^{-6} \text{ s}^{-1}$. using these values the horizontal eddy exchange coefficient, $A_h = -\overline{u'v'} / \frac{\partial \bar{v}}{\partial x}$, is estimated at $2 \times 10^8 \text{ cm}^2 \text{s}^{-1}$. Co-spectra of the velocity components from 400 m at sites B and C indicates that the offshore flux of northward momentum increased rather evenly for increasing periods at both sites, without any well-defined peaks (Fig. 6). This suggests that either the energy transfer was distributed over a broad range of periodicities or that the record lengths were too long, causing the energy density of near-period motions to merge, thus producing a red spectrum.

Table 3. Net kinetic energy exchange rate at sites B and C for the period September 2, 1980 to March 13, 1981

Quantity	Units	Net value mid-depth (400 m)		Net value near-bottom (800 m)	
		Mooring B	Mooring C	Mooring B	Mooring C
$\overline{u'^2}$	$\text{cm}^2 \text{s}^{-2}$	624	324	84	118
$\overline{v'^2}$	$\text{cm}^2 \text{s}^{-2}$	4114	1237	104	216
$\overline{u'v'}$	$\text{cm}^2 \text{s}^{-2}$	1394	468	-10	6
$\frac{\partial \overline{u}}{\partial x}$	s^{-1}	-2.7×10^{-6}		0.9×10^{-6}	
$\frac{\partial \overline{v}}{\partial x}$	s^{-1}	-8.6×10^{-6}		1.5×10^{-6}	
$\overline{\rho} \overline{u'^2} \frac{\partial \overline{u}}{\partial x}$	$\text{ergs cm}^{-3} \text{s}^{-1}$	-16.8×10^{-4}		0.8×10^{-4}	
$\overline{\rho} \overline{u'v'} \frac{\partial \overline{v}}{\partial x}$	$\text{ergs cm}^{-3} \text{s}^{-1}$	-119.9×10^{-4}		-0.2×10^{-4}	

Seasonality

Niiler and Richardson (1973) determined from transport sections between Miami and Bimini that there was a seasonal variation in volume transport of the Florida Current that could account for about 45% of the total transport variability. A seasonal maximum transport of $33.6 \times 10^6 \text{ m}^3 \text{ s}^{-1}$ was observed during early summer and a minimum of $25.4 \times 10^6 \text{ m}^3 \text{ s}^{-1}$ was found during December. Overall the seasonal cycle results in a fluctuation bound of about $8 \times 10^6 \text{ m}^3 \text{ s}^{-1}$.

Seasonal variations in the Gulf Stream at mooring sites B and C were investigated by computing 2-weekly averages of the along-stream velocity components which were then used to construct a time series of the 2-weekly along-stream transport (M_y) flowing through the 15 km^2 area between the moorings. These data are shown in Fig. 9 along with estimates of the 2-weekly averaged vertical and horizontal shear for the 400 to 600 m level between sites B and C, and the vertically averaged current at site B over the 400 to 600 m levels.

The mean transport between moorings B and C for the year-long measurements was about $4 \times 10^6 \text{ m}^3 \text{ s}^{-1}$, which is approximately 10% of the Gulf Stream transport estimated by Richardson et al. (1963) for this region. Even though the moorings encompassed only a small fraction of the total transport there still appears to be a seasonal trend consistent with that found by Niiler and Richardson (1973). Amplitude of the seasonal cycle was approximately $\pm 1 \times 10^6 \text{ m}^3 \text{ s}^{-1}$ with minimum values occurring during the fall and winter months and maximum values during spring and summer. This variation appears to have been produced by a summertime increase in the barotropic component of the flow at site B (increase in $\langle \bar{v} \rangle$). The baroclinic component ($\partial \bar{v} / \partial z$) of the flow at site B appears to have remained relatively constant for the year except for a large event during the first 2 weeks. The mean horizontal shear ($\partial \bar{v} / \partial x$) at the 400 m depth showed a general decreasing trend.

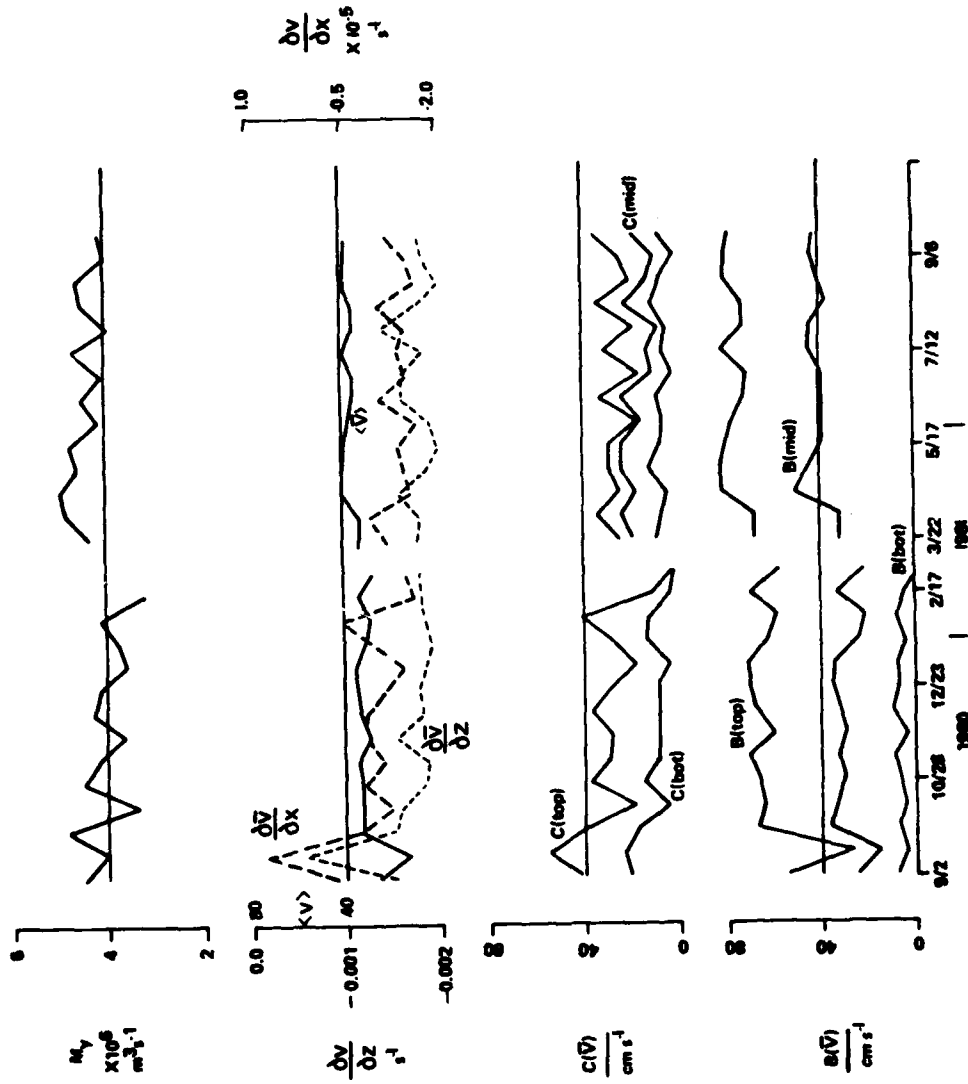


Figure 9 Two-weekly averages of volume transport (M_y) between moorings B and C; vertical shear ($\partial \bar{v} / \partial z$) at B over the 400 to 600 m depths; horizontal shear ($\partial \bar{v} / \partial x$) between B (top) and C (top); vertically averaged currents ($\langle \bar{v} \rangle$) at B over the 400 to 600 depths, and along-stream currents from moorings B and C.

SUMMARY AND CONCLUSIONS

Observations of Gulf Stream variability at 30°N showed energetic current and temperature fluctuations within a period band of 2 to 14 days. Flow perturbations on the cyclonic side of the Gulf Stream generally had a cyclonic sense of rotation, whereas on the anticyclonic side the fluctuations were anticyclonic and 180° out of phase with flow variations on the cyclonic side. These events appear to account for 45 to 70% of the total observed variability throughout the year. Fluctuations of this type can be explained by east-west meanders of the Gulf Stream. An offshore meander results in an offshore flow and decreasing temperature at locations on both sides of the current axis, coupled with increasing downstream flow in the anticyclonic shear region and decreasing downstream flow in cyclonic shear zone. The opposite occurs for an onshore meander: onshore flow and increasing temperature in both regions correlated to increasing downstream flow in the cyclonic zone and decreasing downstream flow in the anticyclonic shear region.

Gulf Stream meanders appear to be produced by waves propagating to the north at speeds of 30 to 70 cm s⁻¹, wave lengths of 100 to 200 km and periods of several days to one week. Indications are that these waves may be unstable through either a barotropic or baroclinic instability process which tends to redistribute the kinetic and potential energy between the fluctuations and the mean flow. Fluctuations on the anticyclonic side of the Stream appear to derive perturbation kinetic and potential energy from the mean flow, whereas on the cyclonic side fluctuations tend to supply energy to the mean flow. No significant coherence was observed between the low-frequency current fluctuations and local winds.

Low-frequency flow variability near the bottom at the shelf edge appears to be related to Gulf Stream meanders. Indications are that cold, cyclonic perturbations occur at times of offshore meanders due to the formation of cyclonic eddies in the frontal region. During the onshore meander stage the western edge

of the Stream is closer to the shelf and northward near-bottom flows occur with increased temperatures.

Near-bottom flows on the Blake Plateau east of the Gulf Stream show prolonged southward flow events that lasted up to 42 days and reached speeds in excess of 30 cm s^{-1} . These events were not correlated with flows at any other site and it is not clear as to the nature of the generating mechanism. A possible explanation may be the southward undercurrent that has been observed beneath the Gulf Stream off Cape Hatteras. Near-bottom flows at this location and at the seaward edge of the Plateau may at times be affected by cyclonic, cold-core eddies that are observed to move across the Plateau and merge with the Stream in this region. However without additional current measurements or supporting hydrographic and satellite data it is difficult to be more specific.

Mean flows in the vicinity of the Gulf Stream axis were toward the north at about 60 to 75 cm s^{-1} at the 400 m level. A maximum downstream current of 109 cm s^{-1} also occurred at this location. The mean vertical shear near the axis was approximately $-2 \times 10^{-3} \text{ s}^{-1}$ and showed little variation with season. The mean transport through the mooring array was $4 \times 10^6 \text{ m}^3 \text{ s}^{-1}$ which is about 10% of the total transport observed at 30°N . A seasonal change in transport of about $2 \times 10^6 \text{ m}^3 \text{ s}^{-1}$ was observed with minimum transport occurring in late fall-early winter and maximum values in late spring-early summer, consistent with the seasonal change in total transport observed by Niiler and Richardson (1973). The seasonal change in transport appeared to be produced by an increase in the barotropic component of the flow.

Acknowledgements. We appreciate the assistance given by the able crews of the R/V COLUMBUS ISELIN and G.W. PIERCE during field operations. We thank Phil Bedard, Ted Tandard, B. Haldane, Ed Koschen, Mark Graham, Paul Galbreath, Robert Guest, Jere Green, Joe Karpen and Bill Quinn for their valuable technical assistance.

This research was supported by the Bureau of Land Management prime contract number AA851-OT0-35 to General Oceanics, Inc., Miami, FL, subcontract number 851-01.

REFERENCES

- Bane, J.M., Jr., and D.A. Brooks, Gulf Stream meanders along the continental margin from the Florida Straits to Cape Hatteras, *Geophys. Res. Lett.*, 6, 280-282, 1979.
- Bane, J.M., Jr., D. A. Brooks, and K.R. Lorenson, Synoptic observations of the three-dimensional structure, propagation and evolution of Gulf Stream meanders along the Carolina continental margin, *J. Geophys. Res.* (in press).
- Brooks, D.A., and J.M. Bane, Jr., Gulf Stream deflection by a bottom feature off Charleston, SC, *Science*, 201, 1225-1226, 1978.
- Brooks, D.A., and J.M. Bane, Jr., Gulf Stream fluctuations and meanders over the Onslow Bay upper continental slope, *J. Phys. Oceanogr.*, 11, 247-256, 1981.
- Brooks, I. and P.P. Niiler, Energetics of the Florida Current, *J. Mar. Res.*, 35, 163-191, 1977.
- Brooks, I., Fluctuations in the transport of the Florida Current at periods between tidal and two weeks, *J. Phys. Oceanogr.*, 9, 1048-1053, 1979.
- Cheney, R.E., and P.L. Richardson, Observed decay of a cyclonic Gulf Stream ring, *Deep Sea Res.*, 23, 143-155, 1976.
- Duing, W., Synoptic studies of transients in the Florida Current, *J. Mar. Res.*, 33, 53-73, 1975.
- Duing, W., C.N.K. Mooers and T.N. Lee, Low-frequency variability in the Florida Current and relations to atmospheric forcing from 1972 to 1974, *J. Mar. Res.*, 35, 129-161, 1977.
- Lee, T.N., Florida current spin-off eddies, *Deep Sea Res.*, 22, 753-765, 1975.
- Lee, T.N., and D. Mayer, Low-frequency current variability and spin-off eddies on the shelf off southeast Florida, *J. Mar. Res.*, 35, 193-220, 1977.
- Lee, T.N., I. Brooks and W. Duing, The Florida Current - its structure and variability, U. of Miami Technical Report/RSMAS 77003, 275 pp.
- Lee, T.N., L.P. Atkinson and R. Legeckis, Observations of a Gulf Stream frontal eddy on the Georgia continental shelf, April 1977, *Deep Sea Res.*, 28A, 347-348, 1981.
- Lee, T.N. and L.P. Atkinson, Low-frequency current variability from Gulf Stream frontal eddies and atmospheric forcing along the southeast U.S. outer continental shelf, submitted to special issue of *J. Geophys. Res.* on the South Atlantic Bight, 1983.

- Legeckis, R., Applications of synchronous meteorological satellite data to the study of time dependent sea surface temperature changes along the boundary of the Gulf Stream, *Geophys. Res. Lett.*, 2, 435-438, 1975.
- Legeckis, R., Satellite observations of the influence of bottom topography on the seaward deflection of the Gulf Stream off Charleston, SC, *J. Phys. Oceanogr.*, 9, 483-497, 1979.
- Niiler, P.P., and L.A. Mysak, Barotropic waves along an eastern continental shelf, *Geophys. Fluid Dynamics*, 2, 273-278, 1971.
- Niiler, P.P., and W.S. Richardson, Seasonal variability of the Florida Current, *J. Mar. Res.*, 31, 144-167, 1973.
- Orlanski, I., The influence of bottom topography on the stability of jets in a baroclinic fluid, *J. Atmos. Sci.*, 26, 1216-1232, 1969.
- Orlanski, I., and M.D. Cox, Baroclinic instability in ocean currents, *Geophys. Fluid Dynamics*, 4, 197-221, 1973.
- Parr, A.E., Report of hydrographic observations at a series of anchor stations across the Straits of Florida, *Bull. of the Bingham Oceanographic Laboratory, Yale University*, 6, 1-63, 1937.
- Perkins, H., and M. Wimbush, A cyclonic mini-eddy near the Blake Escarpment, *Geophys. Res. Lett.*, 3, 625-628, 1976.
- Pietrafesa, L.J., L.P. Atkinson and J.O. Blanton, Evidence for deflection of the Gulf Stream by the Charleston Rise, *Gulf Stream, IV*, 3-7, 1978.
- Pillsbury, The Gulf Stream, Report of the U.S. Coast and Geodetic Survey for 1980, Appendix 10, 461-620, 1890.
- Richardson, W.S., W.J. Schmitz, Jr., and P.P. Niiler, The velocity structure of the Florida Current from the Straits of Florida to Cape Fear, *Deep Sea Res.*, 16, 225-231, 1969.
- Schmitz, W.J., Jr., and W.S. Richardson, On the transport of the Florida Current, *Deep Sea Res.*, 15, 679-693, 1968.
- Schmitz, W.J., Jr., and P.P. Niiler, A note on the kinetic energy exchange between fluctuations and mean flow in the surface layer of the Florida Current, *Tellus XXI*, 6, 814-819, 1969.
- Stumpf, H.G., and P.K. Rao, Evolution of Gulf Stream eddies as seen in satellite infrared imagery, *J. Phys. Oceanogr.*, 5, 388-393, 1975.
- Von Arx, W.S., D.F. Bumpus and W.S. Richardson, On the fine-structure of the Gulf Stream front, *Deep Sea Res.*, 3, 46-65, 1955.
- Vukovich, F.M., and B.W. Grissman, Further studies of a cold eddy on the eastern side of the Gulf Stream using satellite data and ship data, *J. Phys. Oceanogr.*, 8, 838-843, 1978.
- Webster, F.A., A description of Gulf Stream meanders off Onslow Bay, *Deep Sea Res.*, 8, 130-143, 1961a.
- Webster, F.A., The effect of meanders on the kinetic energy balance of the Gulf Stream, *Tellus*, 13, 391-401, 1961b.



Spatially Unstable Waves in the Gulf Stream
Over the Carolina Continental Slope

Mark E. Luther

Mesoscale Air-Sea Interaction Group
Meteorology Annex
The Florida State University
Tallahassee, FL 32306

Abstract

A numerical model is presented investigating the unstable normal modes of oscillation of a realistic boundary current. The model background current approximates the Gulf Stream south of Cape Hatteras, N.C., possessing both vertical and horizontal shear, and flowing along a sloping bottom topography. Small amplitude, alongshore propagating perturbations to the background flow are sought with real frequency and complex alongshore wave number as eigenvalues. A non-zero imaginary component of the wave number implies that the wave amplitude grows in the alongshore direction.

Observations in the Gulf Stream south of Cape Hatteras, N.C., have revealed a persistent wave-like meander pattern with a dominant period of 8 days, henceforth called the 8-day wave. This wave form propagates in the downstream direction with a phase speed of about 40 km/day and is uncorrelated with any known forcing. The observed 8-day wave appears as a eigenmode of the model. The perturbation velocity fields from the model 8-day wave are consistent with observations. The instability mechanism of the model wave is of the mixed barotropic-baroclinic type, with the majority of the perturbation energy coming from the potential energy of the background flow (about 80%). Warm filaments are formed on the inshore side of the background current, separated from the core of the current by a cool dome of upwelled water.

Observations in the Gulf Stream south of Cape Hatteras, North Carolina, have revealed the existence of wave-like meander patterns in the path of the Stream (Webster, 1961; Legeckis, 1979; Bane et al., 1981; Brooks and Bane, 1981). Figure 1 shows a typical meander pattern mapped from an AXBT survey by Bane et al. (1981). Contours inside the box are of temperature at 1 m below the surface, while contours outside the box are of bathymetry. Two large amplitude meanders are evident downstream of Charleston, South Carolina. These wave forms propagate along the Stream to the northeast (i.e., the downstream direction) with a phase speed of about 40 km/day. Their wavelength is approximately 200 km, and their period is near 8 days. We will henceforth call this meander pattern the 8-day wave. This wave does not appear to be correlated with any known forcing which suggests that it may be a natural mode of oscillation of the Gulf Stream. The sudden emergence of this wave downstream of a bottom topographic feature off Charleston known as the Charleston Bump indicates that this wave may be the result of an instability of the Stream triggered by the Bump.

A numerical model is developed to investigate these possibilities. The model geometry is shown in Fig. 2. A background current in geostrophic balance with the background density field flows along a straight coastline over a sloping bottom topography. The background fields are continuous functions of x and z only, and the depth is a monotonically increasing function of x only. The background current possesses both horizontal and vertical shear, admitting the possibility of both barotropic and baroclinic instability. The fluid motion is assumed to be inviscid, hydrostatic and Boussinesq, but not quasigeostrophic. Variations in the Coriolis parameter f are neglected. The equations of

motion for small amplitude perturbations are linearized about the background state, so that the perturbation quantities are affected by the background, but the background remains unaffected by the perturbations. Since all coefficients in the equations of motion are independent of alongshore (along-stream) distance y and time t , the perturbation variables can be assumed to have the form

$$(u', v', w', \pi', b') = \text{Re}\{(u, v, w, \pi, b) \exp[i(\sigma_0 t + \lambda y)]\} \quad (1)$$

where $\text{Re}\{ \}$ denotes the real part of the bracketed expression, (u', v', w') are the (x, y, z) components of the perturbation velocity, π' is the non-hydrostatic perturbation pressure per unit density, b' is the perturbation buoyancy, σ_0 is the wave frequency, and λ is the along-stream wave number. The perturbation amplitudes (u, v, w, π, b) are thus complex functions of (x, z) only. The dimensionless equations of motion are then

$$i\sigma u - v = -\pi_x \quad (2a)$$

$$i\sigma v + (1 + R_0 V_x)u + R_0 V_z w = -i\lambda \pi \quad (2b)$$

$$0 = -\pi_z + b \quad (2c)$$

$$u_x + i\lambda v + w_z = 0 \quad (2d)$$

$$i\sigma b + \alpha S^2 M^2 u + S^2 N^2 w = 0 \quad (2e)$$

where $\sigma = \sigma_0 + R_0 V \lambda$ is the intrinsic or Doppler-shifted frequency, V is the background velocity, N^2 and M^2 are measures of the vertical and horizontal density gradients, respectively, i.e., the Brunt-Vaisala frequency and its horizontal analog (Mooers, 1975) and subscripts denote differentiation. The dimensionless parameters are the background Rossby number $R_0 = \frac{V_0}{fL}$, a stratification parameter or Burger number $S^2 = \frac{N_0^2 H^2}{f^2 L^2}$, and an aspect ratio for the background density field $\alpha = \frac{M_0^2 L}{N_0^2 H}$, where L and H are length scales for the horizontal and vertical coordinates, respectively, and V_0 , N_0^2 and M_0^2 are reference values for V , N^2 and M^2 ,

respectively. For the Gulf Stream, S^2 and α are $O(1)$ quantities. Eqs. (2a-e) are combined to give a governing equation in π with σ_0 and λ as parameters. The boundary conditions are that there is no flow normal to the top, the bottom, or the coast, and that the solutions decay far offshore. For a fixed value of along-stream wave number λ , this forms an eigenvalue problem for σ_0 with π as the eigenfunction. The frequency σ_0 is assumed to be real while the wave number is complex, i.e. $\lambda = \lambda_r + i\lambda_i$. If an eigenmode can be found with the imaginary part of λ non-zero, then that wave will grow or decay as it propagates in the y direction, depending on the sign of λ_i , since

$$\text{Re}\{\pi \exp[i(\sigma_0 t + \lambda y)]\} = |\pi| \cos(\sigma_0 t + \lambda_r y + \theta_\pi) \exp[-\lambda_i y] \quad (3)$$

where $|\pi| = (\pi_r^2 + \pi_i^2)^{1/2}$

and $\theta_\pi = \tan^{-1}(\pi_i/\pi_r)$

are the amplitude and phase of the complex function π . This is consistent with the concept of an instability generated or triggered by a stationary mechanism such as a topographic feature (Hogg, 1976).

Fig. 3 shows a velocity section across the Gulf Stream off Cape Fear, North Carolina, after Richardson, Schmitz and Niller (1969). The background velocity used in this model is chosen to approximate this section as closely as possible. It is shown in Fig. 4. Both the vertical and horizontal shears and the total transport compare well with those of the Cape Fear section. The corresponding background temperature field is shown in Fig. 5. This is the apparent temperature, in that salinity effects are taken into account so that the density can be computed from the temperature alone. The bottom topography has a hyperbolic tangent form, and approximates the bottom slopes found in Long and Onslow Bays off North Carolina. The coastline in this area is oriented approximately

northeast. The background variables and the bottom topography for the model can be easily adjusted by varying several input parameters, but only the case approximating the Gulf Stream off the Carolina coast will be presented here.

Given the background configuration, for a particular value of wave number k the eigenvalues of σ_0 and the corresponding eigenfunctions for π are found by varying the frequency of an arbitrary wind stress curl forcing and searching for the resonance response. The response is defined as the \log_{10} of the integrated total energy of the perturbation. For a particular (σ_0, k) pair, the governing equation with the appropriate boundary conditions is solved numerically on a 100×40 (x, z) mesh. The vertical coordinate is stretched so that the solution can be obtained on a rectangle. One such resonance search is illustrated in Fig. 6. Several peaks in the response are clearly evident, and these peaks are taken to be an indication of a near-resonance response. Four distinct modal structures can be identified with the resonance peaks. All are surface trapped, and are numbered according to the number of nodes in perturbation pressure along the surface. By performing this resonance search for many different values of wave number, one can investigate the eigenvalue relationships for the different modes and construct a dispersion "space". Some slices through this space are shown in Fig. 7.

The most interesting thing to note about the dispersion surfaces is that if one plots the frequency and real wave number for the observed 8-day wave, it falls on the mode 2 dispersion surface for a wide range of growth rates. For that reason, this discussion will focus on the mode 2 wave. The perturbation pressure amplitude and phase are shown in Fig. 8 along with the real part of the intrinsic frequency for mode 2. The

pressure has two nodes across which the phase undergoes 180° phase jumps. Otherwise the phase is essentially constant where the amplitude is non-zero. There is some tilt of the phase lines with height, implying an energy conversion from the background to the perturbations. The cross-stream component of the perturbation velocity, u , is shown in Fig. 9. As with the pressure, u has two nodes with 180° phase jumps at the nodes, and the phase lines tilt in the vertical. The along-stream velocity, v , is shown in Fig. 10. It has one more node than π or u , and again has 180° phase jumps across the nodes. Note the strong jet in the inshore frontal zone of the background current. Fig. 11 shows the vertical velocity w . It has a maximum in the inshore frontal zone of the background current, indicating that this is an area of intense upwelling or downwelling. The phase for w is not constant over large areas where the amplitude is significant. It can be seen from (2e) that this implies a buoyancy flux and hence conversion of mean potential energy to perturbation energy through the $-\overline{u'v'} M^2/N^2$ term in the energy equation. Contours of this potential energy conversion term (PEC) are shown in Fig. 12. The energy conversion is a maximum in center of the background current, where the vertical shear is greatest and where the phase of w is changing most rapidly in the vertical, i.e., where the phase lines have the greatest tilt. The conversion of background kinetic energy to perturbation energy is also significant and accounts for about 20% of the total energy conversion. Contours of the kinetic energy conversion term, $KEC = -\overline{u'v'} V_x$, are shown in Fig. 13. This is the kinetic energy conversion due to the horizontal shear only, as that due to the vertical shear is two orders of magnitude less. It is maximum in the inshore frontal zone of the background current, since that is where the horizontal

shear is greatest. These energy conversion terms must be viewed as relative energy conversion tendencies only, since to compute the magnitude of the energy conversions would require the solution of the full set of nonlinear equations.

Of course, linear theory cannot predict the amplitude of the unstable disturbance and is merely suggestive of what disturbances are preferred by the background state. But to illustrate the form the mode 2 wave would take if realized in finite amplitude, the perturbation velocities are superimposed on the background velocity with an amplitude of 20% of the maximum background velocity. The horizontal currents near the surface are shown in Fig. 14a. This current pattern is strikingly similar to that inferred from observations of the 8-day wave (Bane et al., 1981; Brooks and Bane, 1981; Lee et al., 1982). The vertical velocity and buoyancy are shown in Fig. 14b, c respectively. The core of the current meanders from side to side, with a warm filament-like structure trailing a meander crest (the shoreward-most excursion of the current). The filament has an anticyclonic circulation around it, and is separated from the core of the current by a cold dome of upwelled water, about which there is a cyclonic circulation. The structure of the cold dome is quite similar to that proposed by Chew et al. (1982) for the observed 8-day wave, with upwelling in the leading portion of the dome, and downwelling in the trailing portion. The water in the center of the dome is neither being upwelled nor downwelled. The residence time of the water in the dome would be about one wave period. There are smaller eddies and filaments on the offshore side of the current, with circulations in the opposite sense to those on the inshore side.

The favorable comparison between the results of this linear model and the observed 8-day wave is remarkable, and is due mainly to the inclusion of a very realistic background state. The model does not, however, address the triggering mechanism for these waves. Brooks and Bane (1982) have found a seasonal variation in the meander process, with dominant periods of 8-10 days in winter and 5-7 days in summer. This is possibly due to the variations in the background state between summer and winter seasons. It has been shown in similar models that small variations of the background state can influence the perturbations considerably (Salby, 1981). This possibility has yet to be investigated.

Acknowledgements

The author would like to thank Dr. John M. Bane of the University of North Carolina for suggesting this research, and for many helpful discussions and suggestions along the way. Thanks are also due to Prof. James J. O'Brien of the Florida State University for providing working space and computer resources during the completion of this work. This project was supported by the National Science Foundation under grant number OCE-79-23413 and by the Office of Naval Research under contract number N00014-77-C-0354. Computing services were provided by the National Center for Atmospheric Research, which is supported by the National Science Foundation.

References

- Bane, J. M., Jr., D. A. Brooks and K. R. Lorenson, 1981: Synoptic observations of the three-dimensional structure and propagation of Gulf Stream meanders along the continental margin. J. Geophys. Res., 86, 6411-6425.
- Brooks, D. A., and J. M. Bane, Jr., 1981: Gulf Stream fluctuations and meanders over the Onslow Bay upper continental slope. J. Phys. Oceanogr., 11, 247-256.
- Brooks, D. A., and J. M. Bane, Jr., 1982: Gulf Stream meanders off North Carolina: A seasonal comparison of their observed characteristics. EOS, 63, 362 (Abstract).
- Chew, F., J. M. Bane, Jr., and D. A. Brooks, 1982: The propagation of a cold-dome meander, a conceptual model. Unpublished Manuscript.
- Hogg, N. G., 1976: On spatially growing baroclinic waves in the ocean. J. Fluid Mech., 78, 217-235.
- Lee, T. N., L. P. Atkinson, and R. V. Legeckis, 1982: Detailed observations of a Gulf Stream frontal eddy on the Georgia continental shelf, April, 1977. Deep Sea Res., in press.
- Legeckis, R. V., 1979: Satellite observations of the influence of bottom topography on the seaward deflection of the Gulf Stream off Charleston, South Carolina. J. Phys. Oceanogr., 9, 483-497.
- Mooers, C. N. K., 1975: Several effects of a baroclinic current on the cross-stream propagation of inertial-internal waves. Geophys. Fluid Dyn., 6, 245-275.
- Richardson, W. S., W. J. Schmitz, and P. P. Niiler, 1969: The velocity structure of the Florida Current from the Straits of Florida to Cape Fear. Deep Sea Res., 16, 225-231.
- Salby, M. L., 1981: Rossby normal modes in nonuniform background configurations. Part I: Simple fields. Part II: Equinox and Solstice conditions. J. Atmos. Sci., 38, 1803-1840.
- Webster, F., 1961: A description of Gulf Stream meanders off Onslow Bay. Deep Sea Res., 9, 130-143.

Figure Legends

- Fig. 1: Temperature at 1 m below the surface from an AXBT (airborne expendable bathythermograph) survey on 10-11 Feb. 1979 (from Bane et al., 1981).
- Fig. 2: Schematic diagram of model geometry.
- Fig. 3: Velocity section across the Gulf Stream off Cape Fear, N.C. Contours are isotachs of velocity into the page in cm/sec (from Richardson et al., 1969).
- Fig. 4: Model background velocity field. Contours are isotachs of velocity into the page in m/sec. Contour interval is 0.1 m/sec.
- Fig. 5: Model background temperature field. Contour interval is 4°C.
- Fig. 6: Energy response vs. frequency for $\lambda = (5.0, -0.5)$ in dimensionless units.
- Fig. 7: Dispersion diagrams for two values of growth rate. Dashed lines indicate uncertainties in location of a dispersion surface, while cross-hatched areas indicate a general enhanced response, with no discrete surfaces discernable.
- Fig. 8: (a) Pressure structure for the mode 2 wave at frequency and wavelength corresponding to the 8-day wave. Amplitude (top) is in dimensionless units, while phase (bottom) is in degrees. (b) Real part of intrinsic (Doppler-shifted) frequency in dimensionless units.
- Fig. 9: Cross-shelf or cross-stream velocity for the mode 2 wave. Amplitude (top) is in dimensionless units, phase (bottom) is in degrees.
- Fig. 10: Along-shore or along-stream velocity for the mode 2 wave. Amplitude (top) is in dimensionless units, phase (bottom) is in degrees.

- Fig. 11: Vertical velocity for the mode 2 wave. Amplitude (top) is in dimensionless units, phase (bottom) is in degrees.
- Fig. 12: Potential energy conversion term (PEC) for the mode 2 wave in dimensionless units. Contour interval is 10.0.
- Fig. 13: Kinetic energy conversion term (KEC) due to the horizontal shear of the background current in dimensionless units. Contour interval is 8.0.
- Fig. 14: Horizontal structure of the mode 2 wave at the uppermost interior mesh points.
- (a) Horizontal perturbation velocity superimposed on background current. One unit in x or y equals 200 km.
 - (b) Vertical velocity in dimensionless units. Note the skewness in the pattern around the filament-like structures.
 - (c) Perturbation buoyancy in dimensionless units. Dashed contours correspond to negative values, or cooler water.

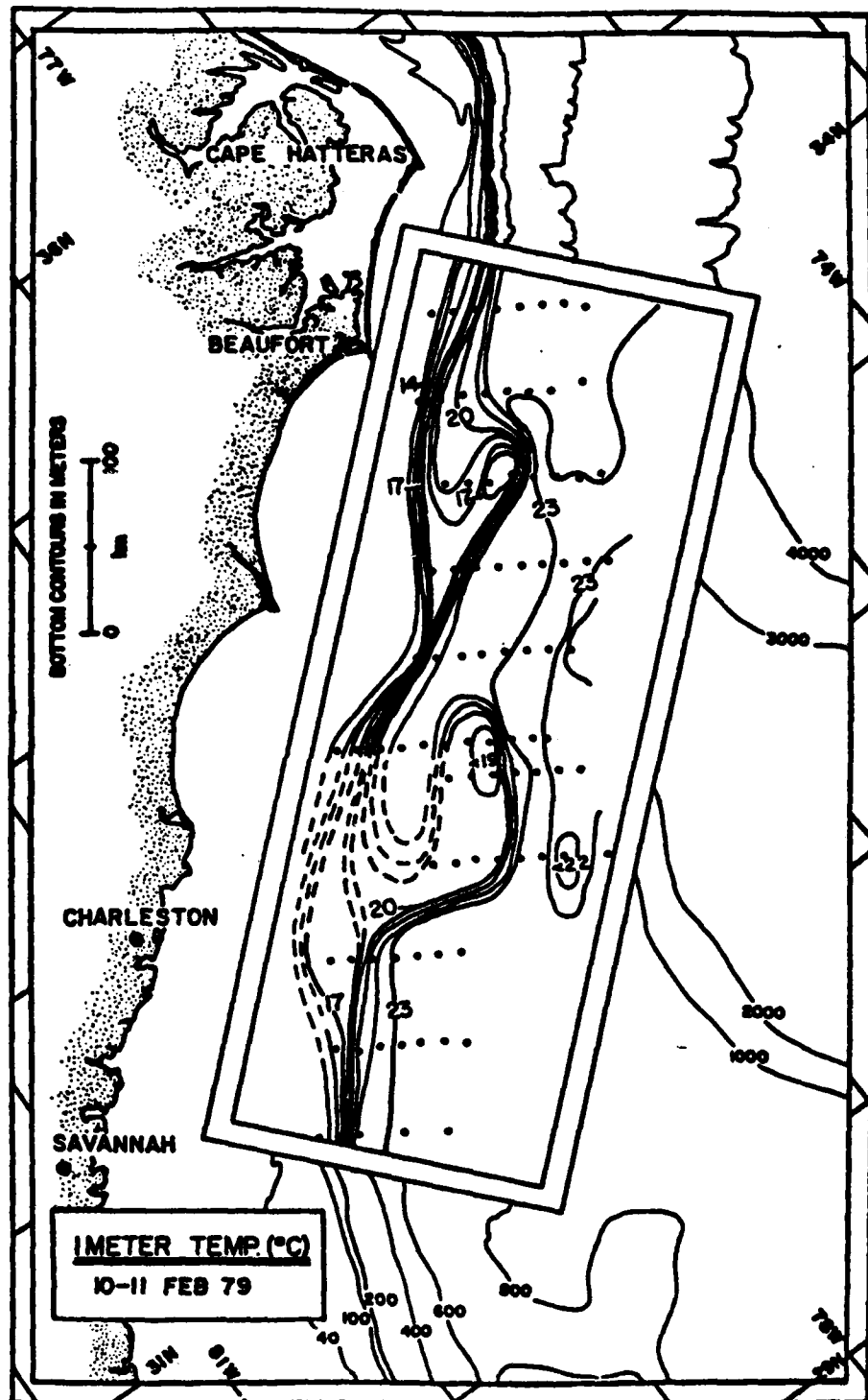


Fig. 1

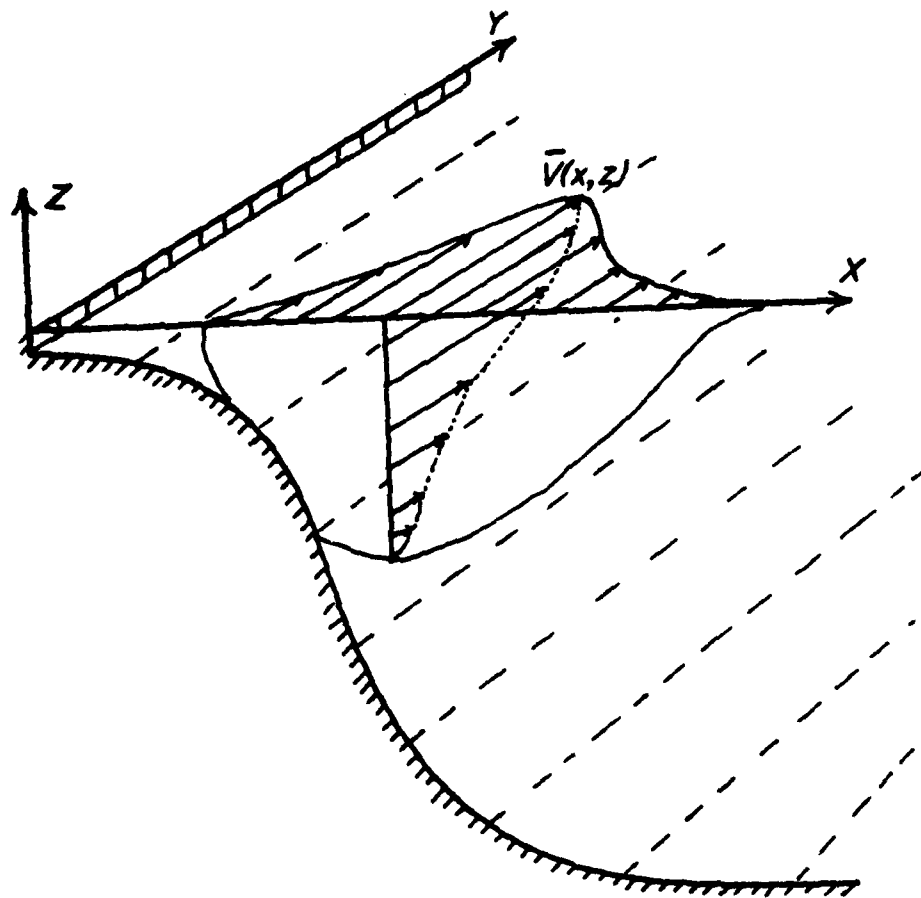
MODEL GEOMETRY

Fig. 2

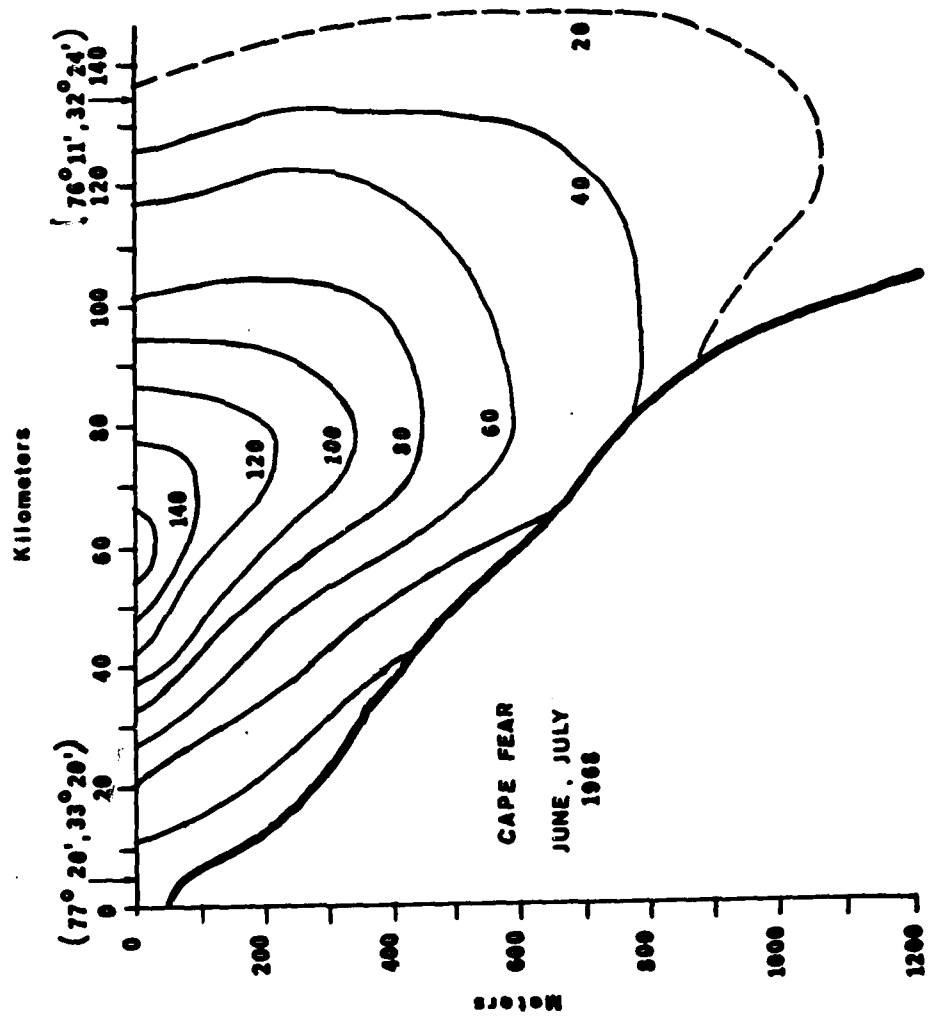


Fig. 3

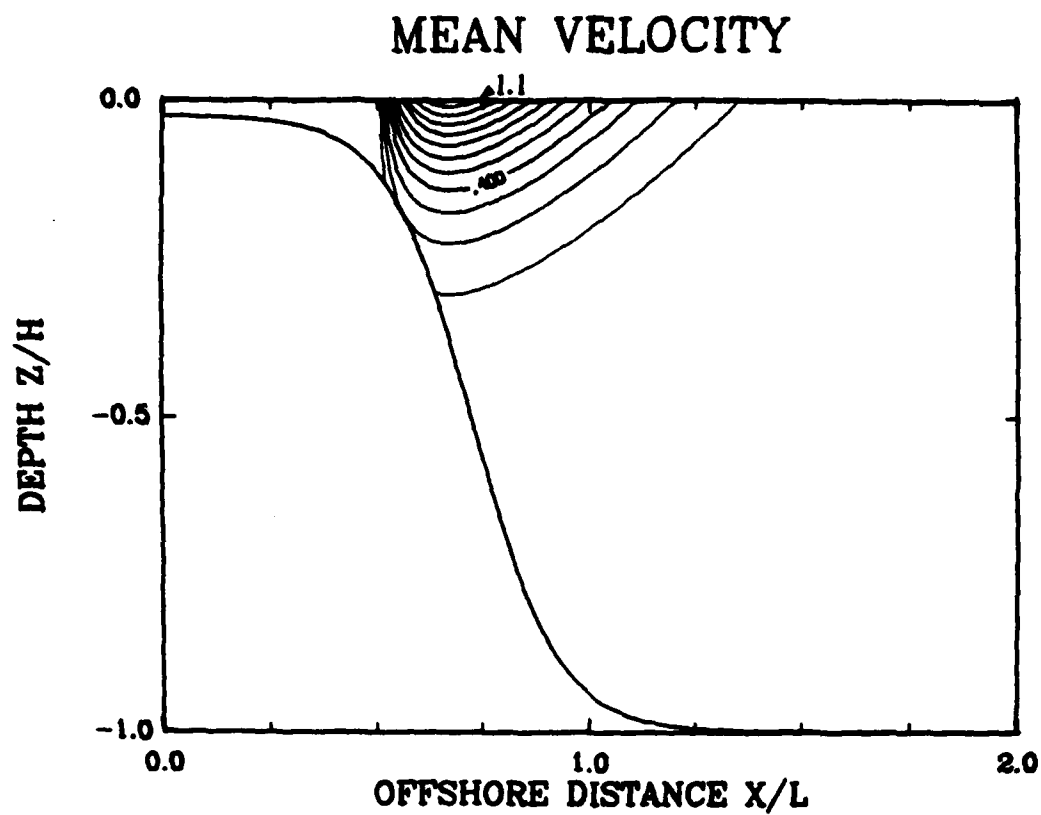


Fig. 4

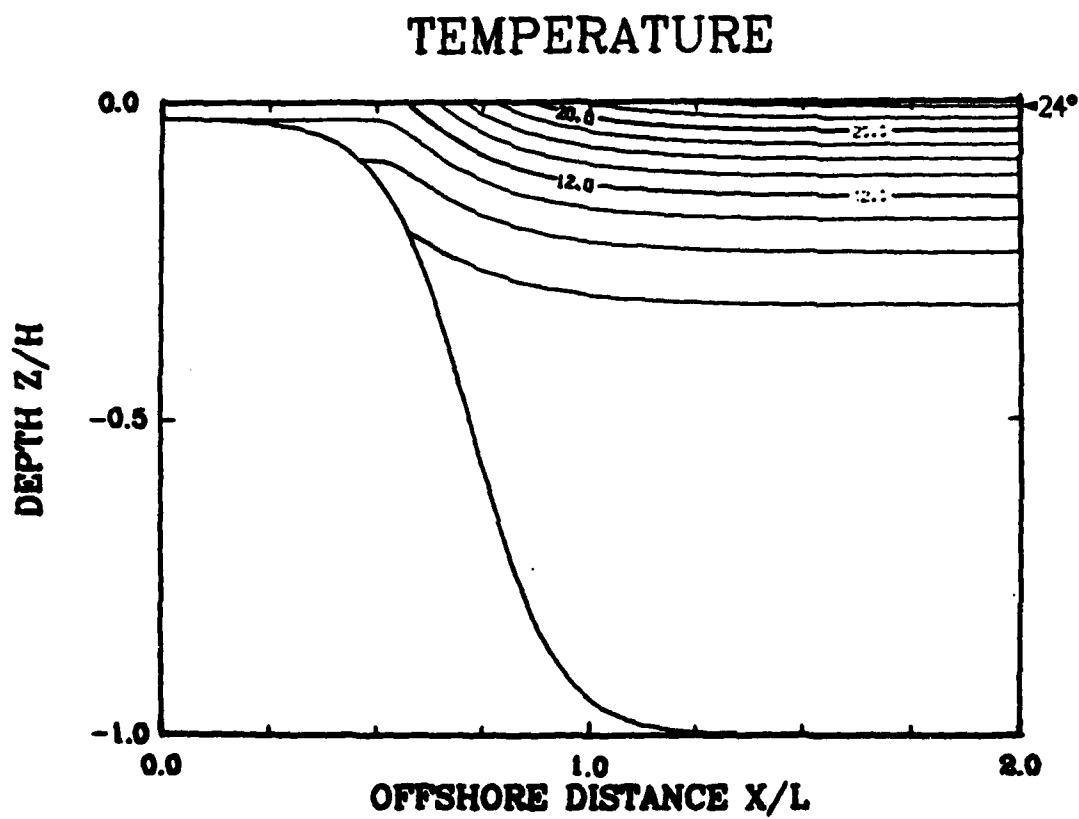


Fig. 5

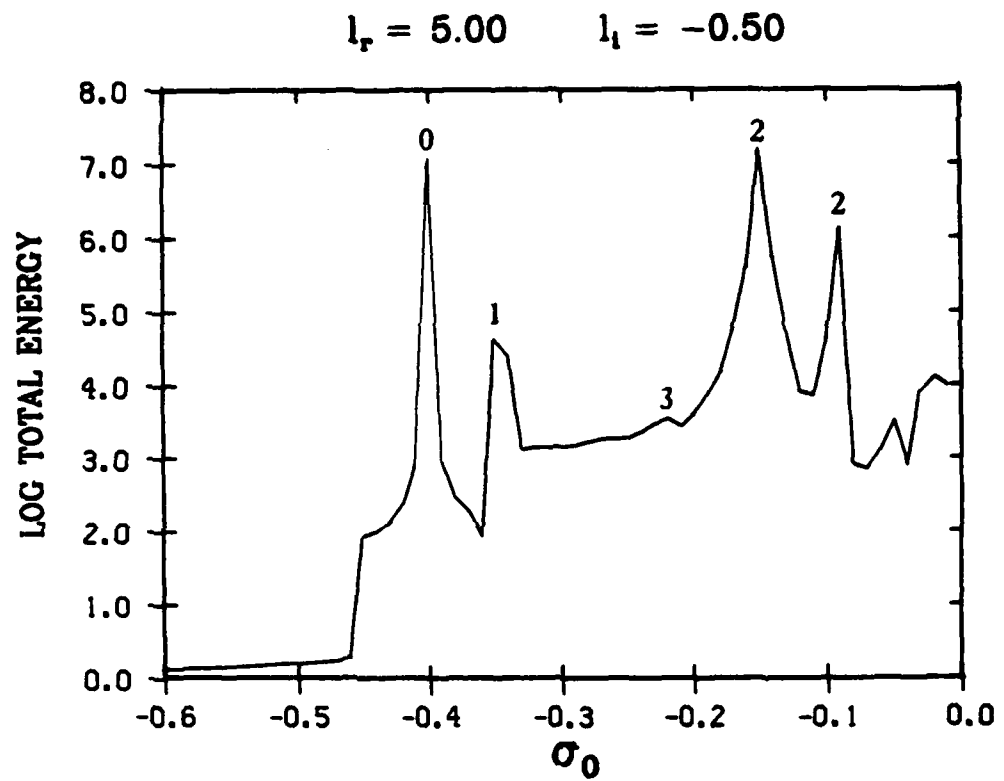


Fig. 6

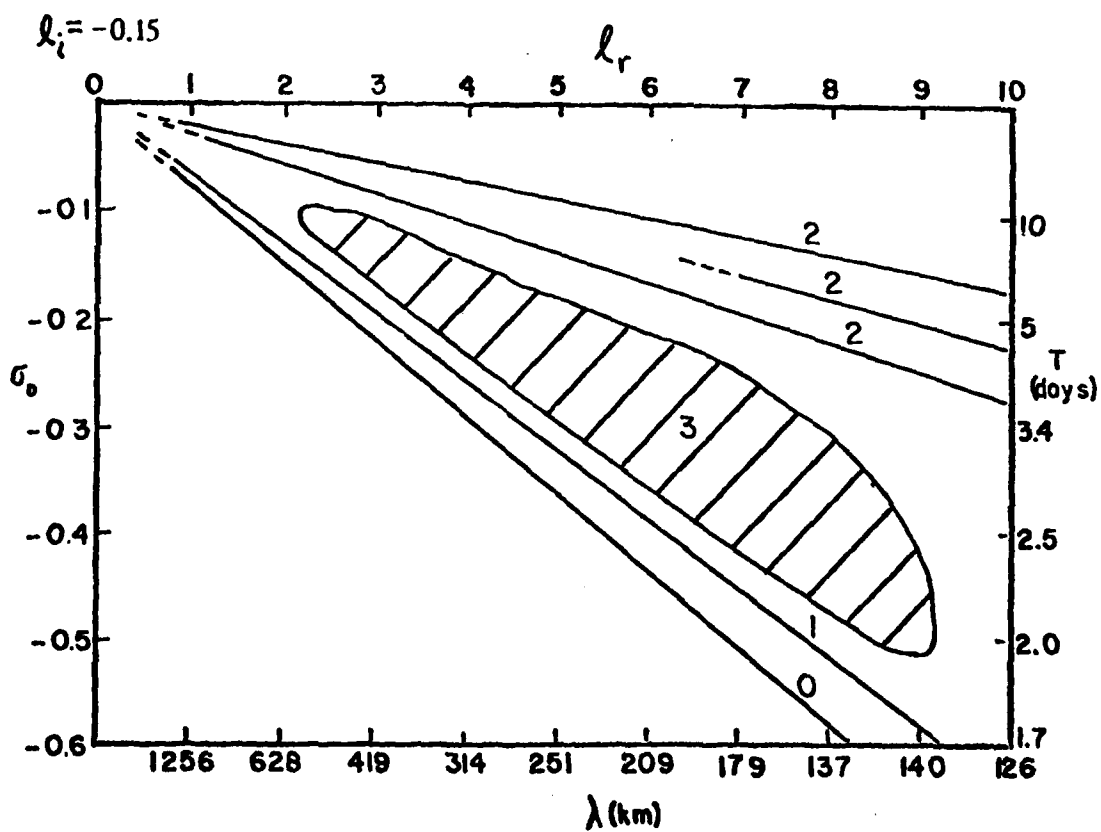
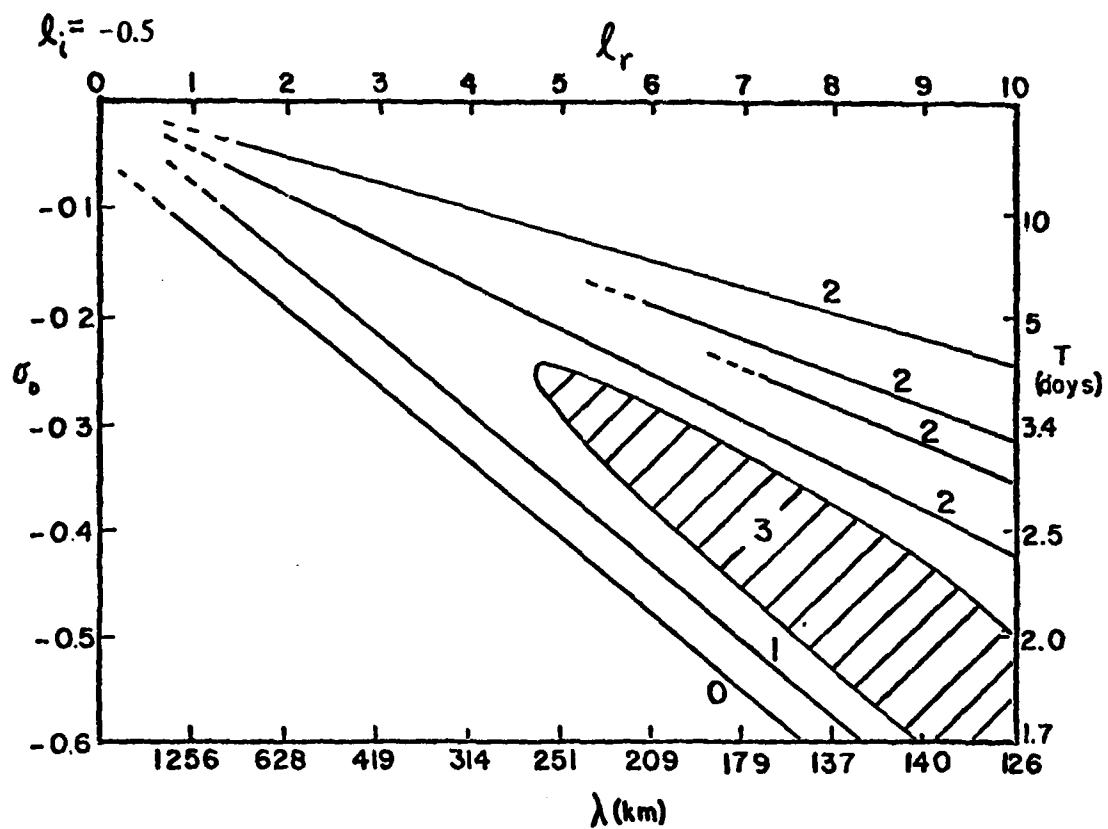


Fig. 7

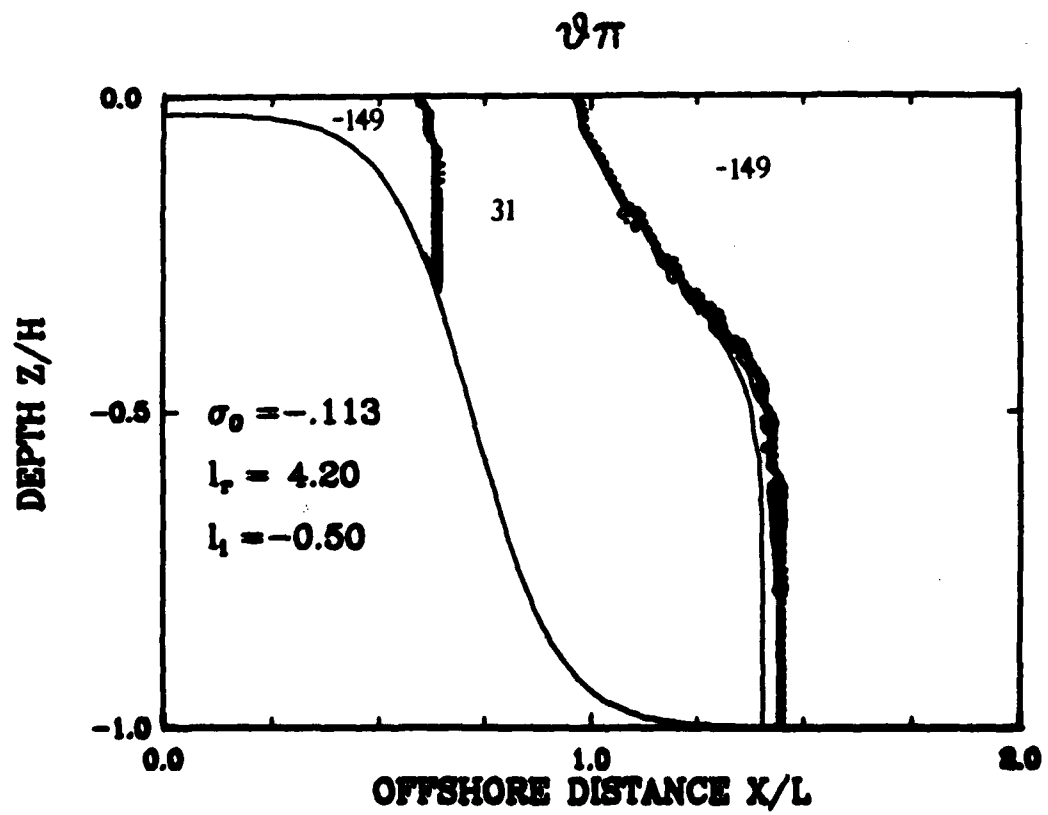
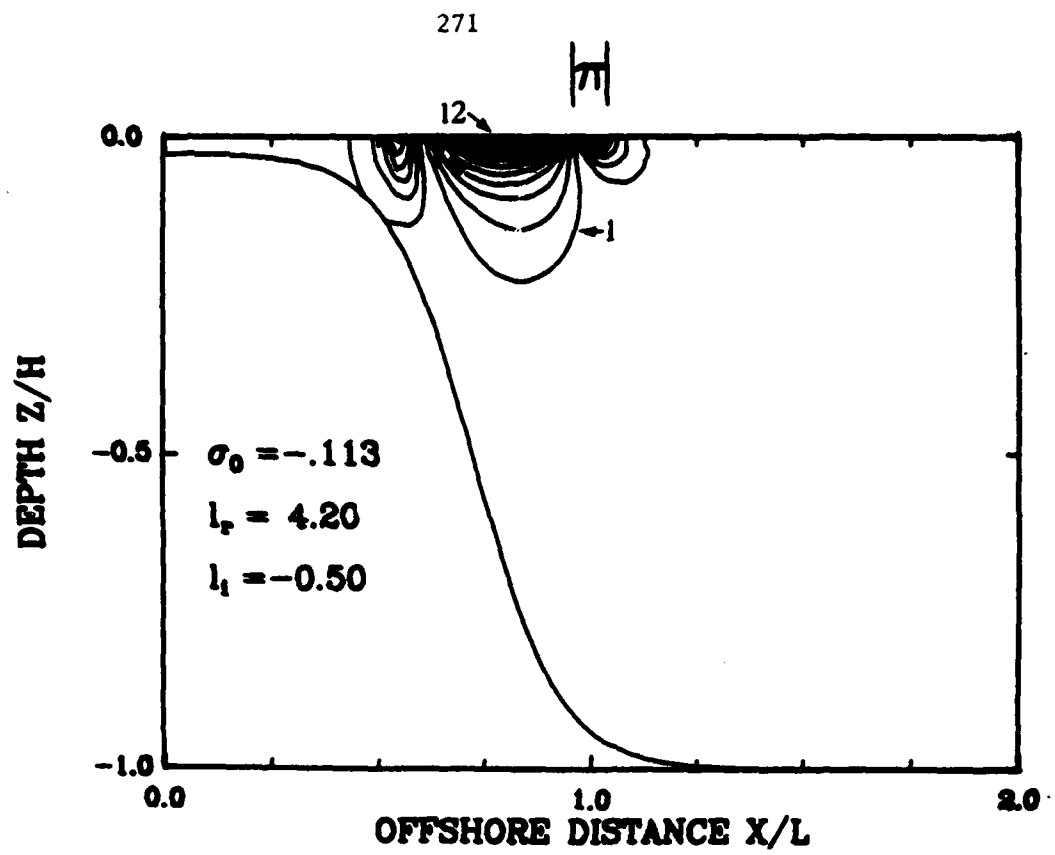


Fig. 8(a)

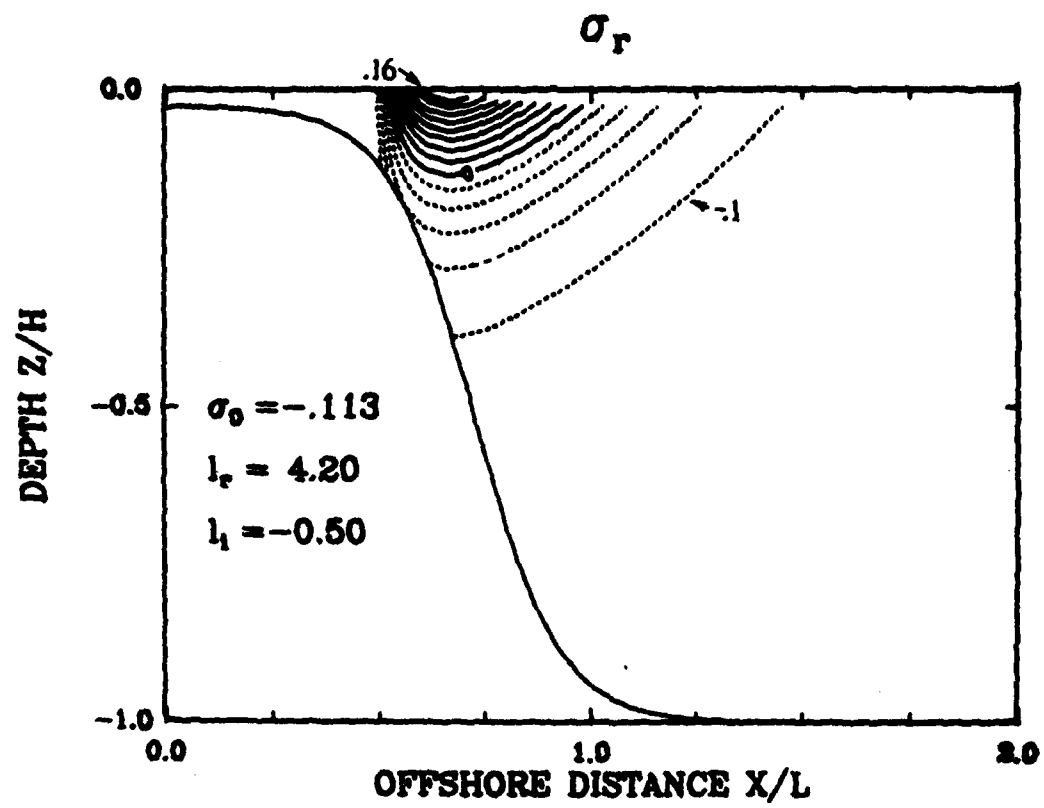


Fig. 8(b)

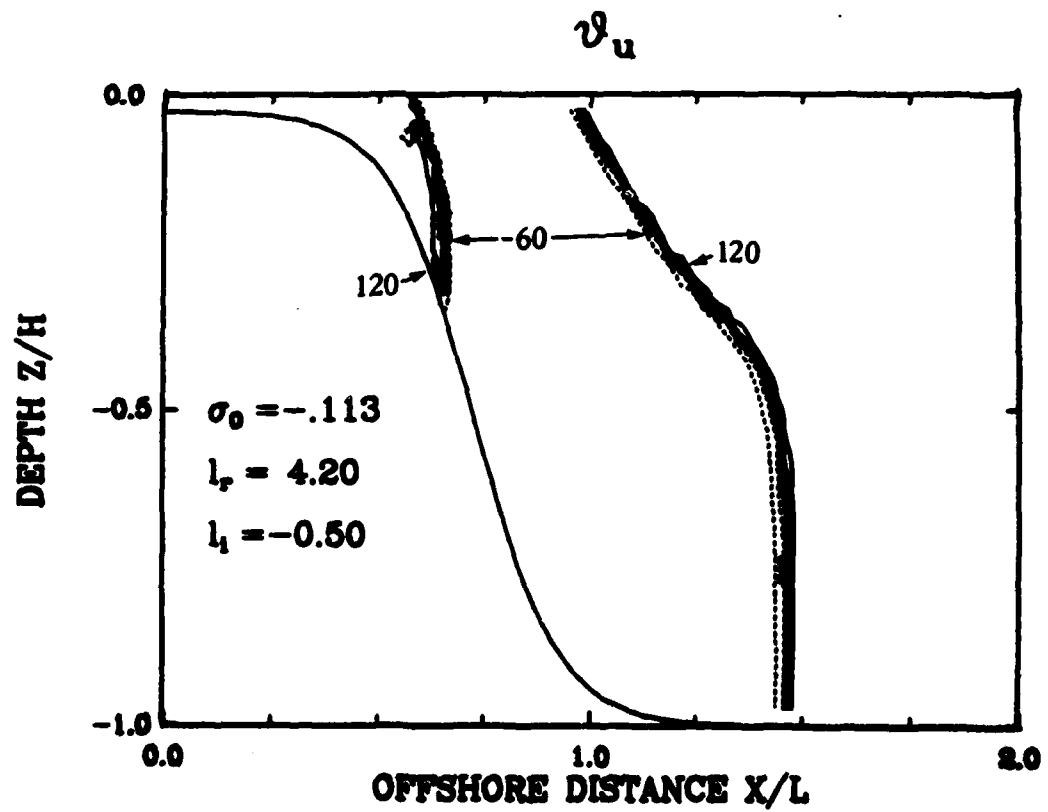
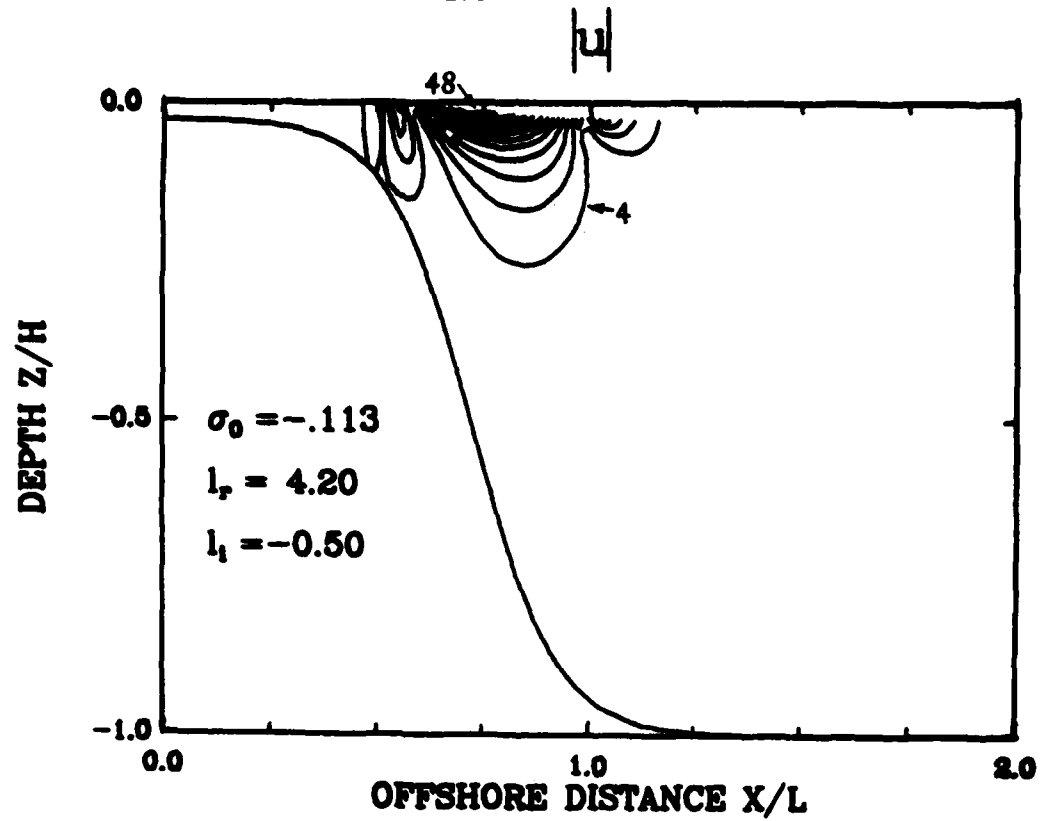


Fig. 9

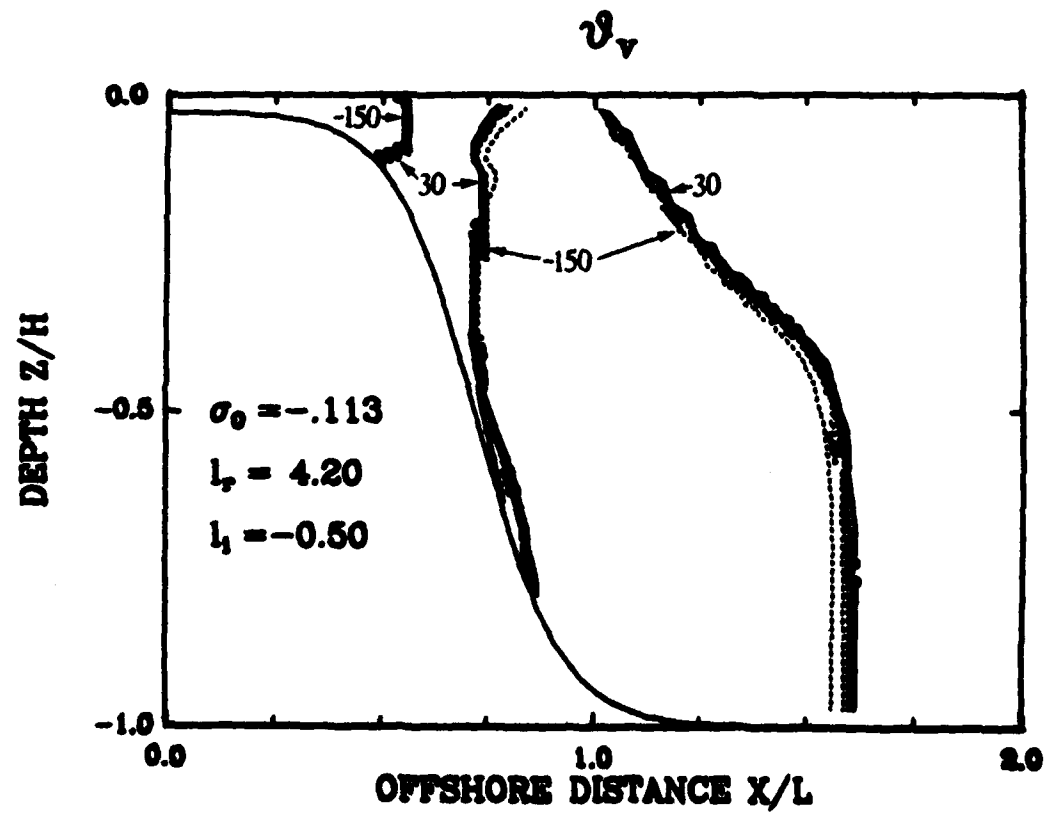
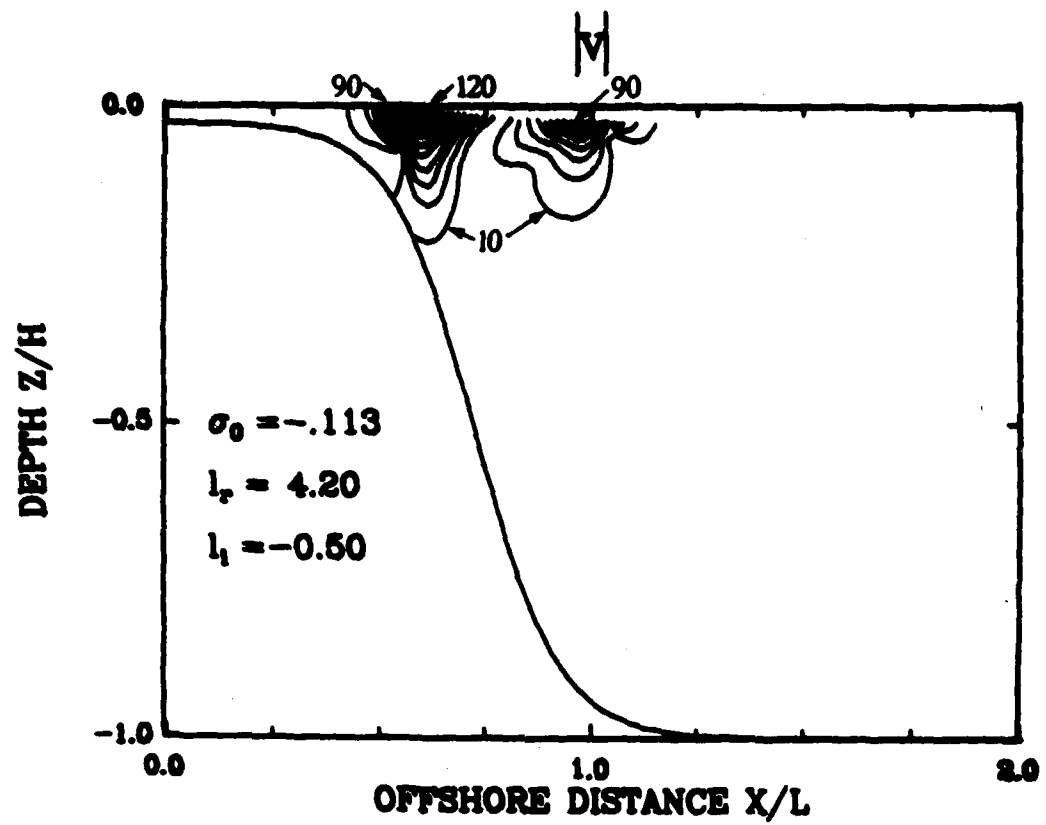


Fig. 10

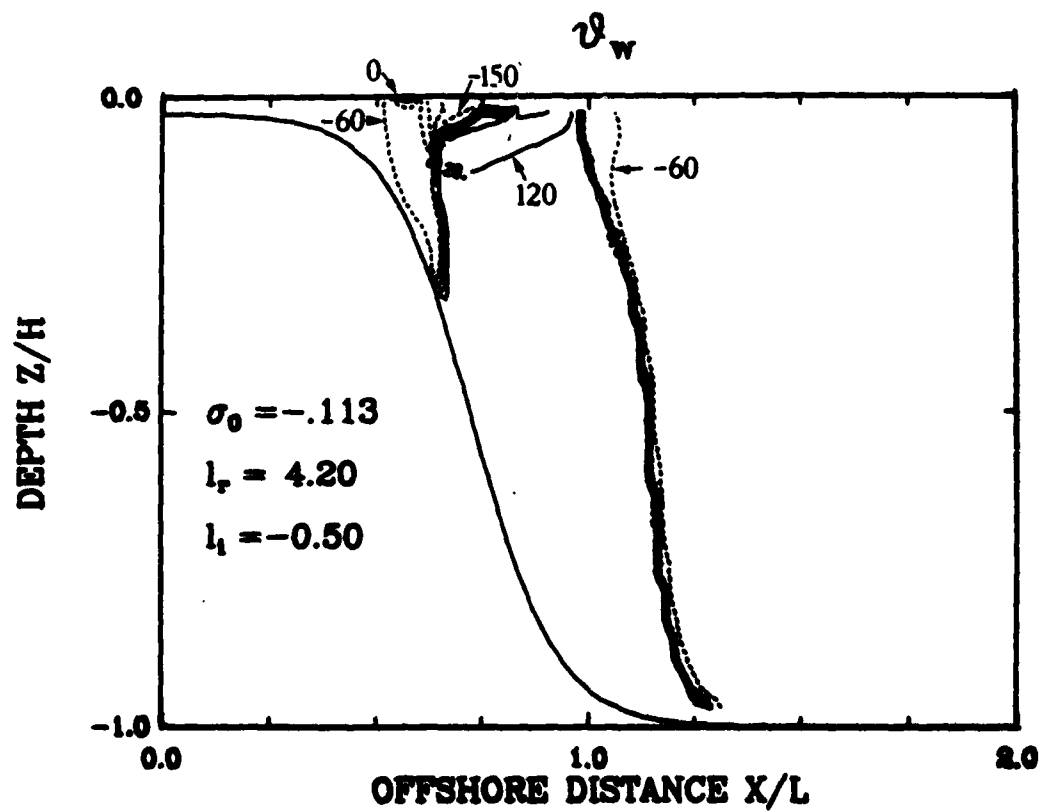
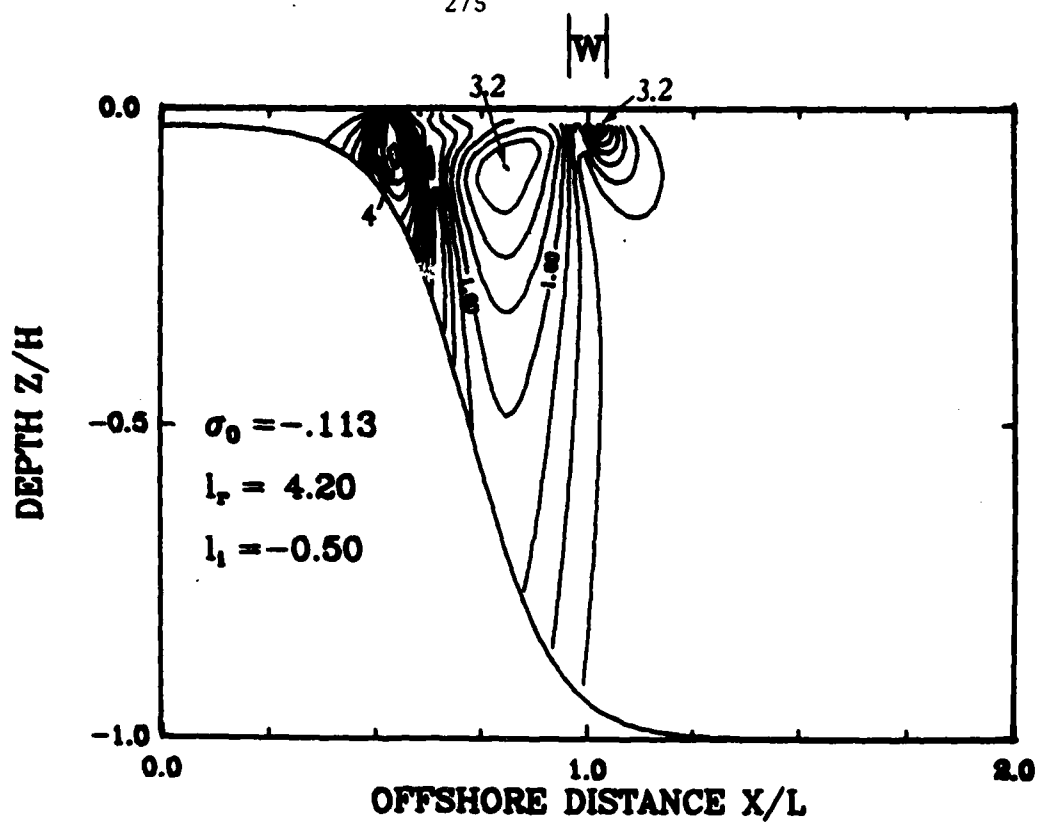


Fig. 11

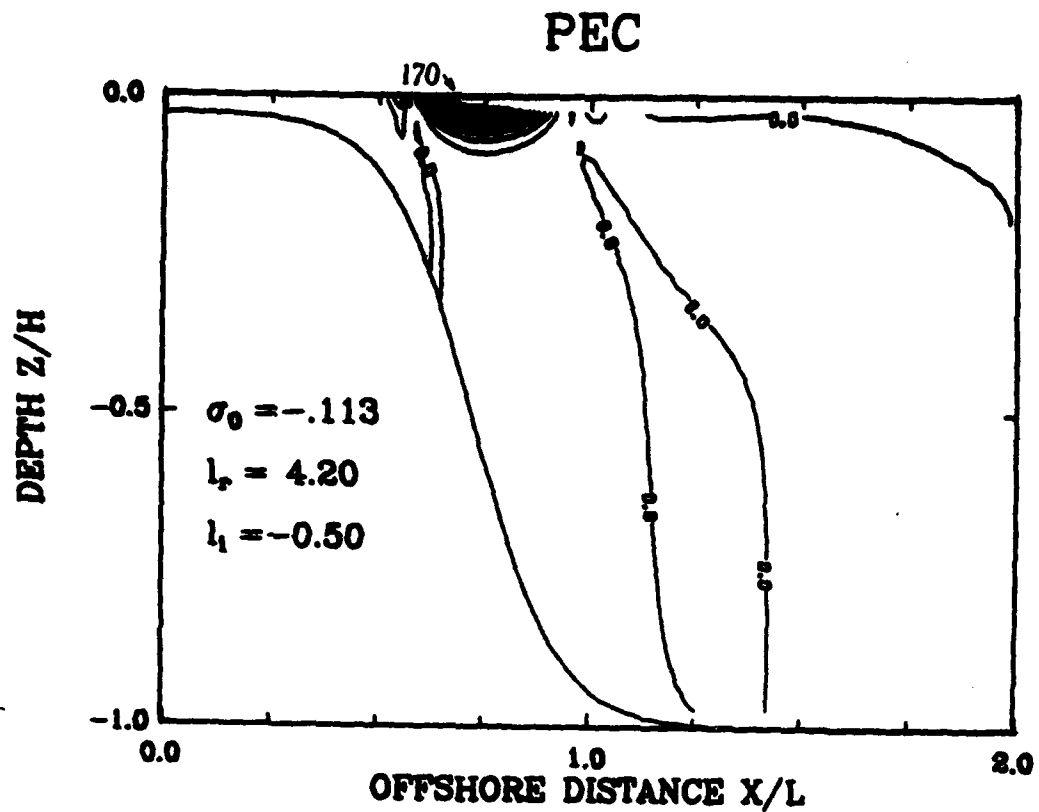


Fig. 12

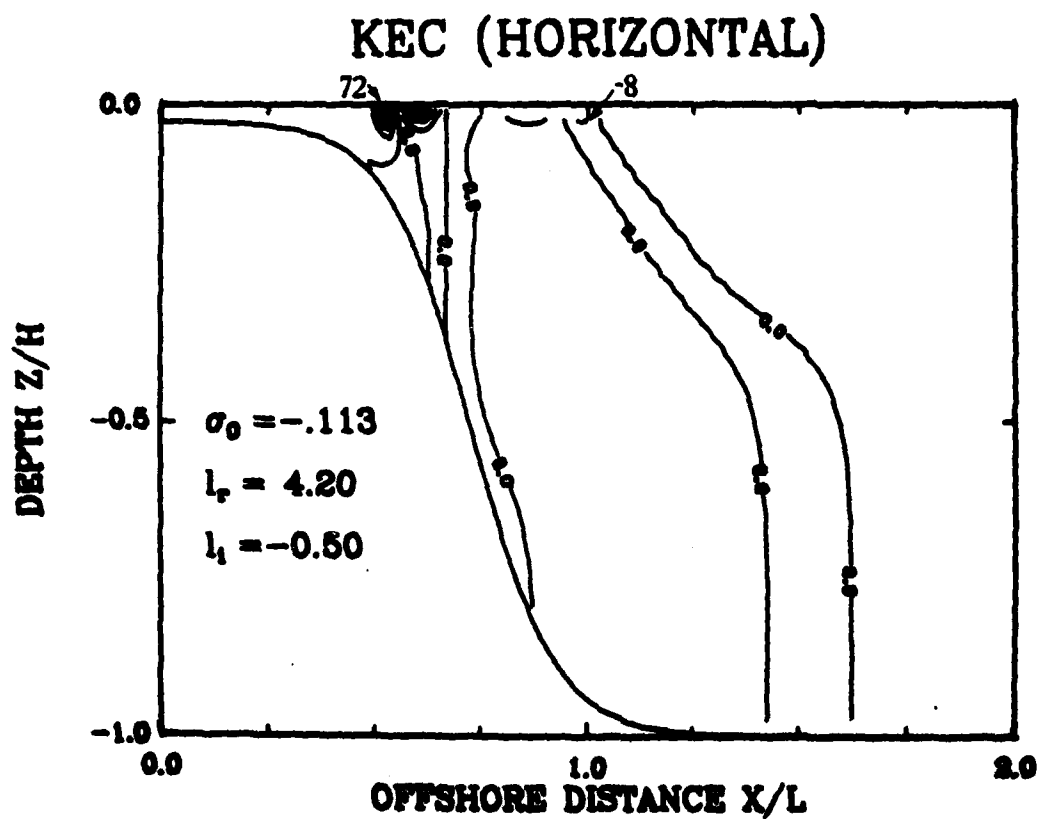


Fig. 13

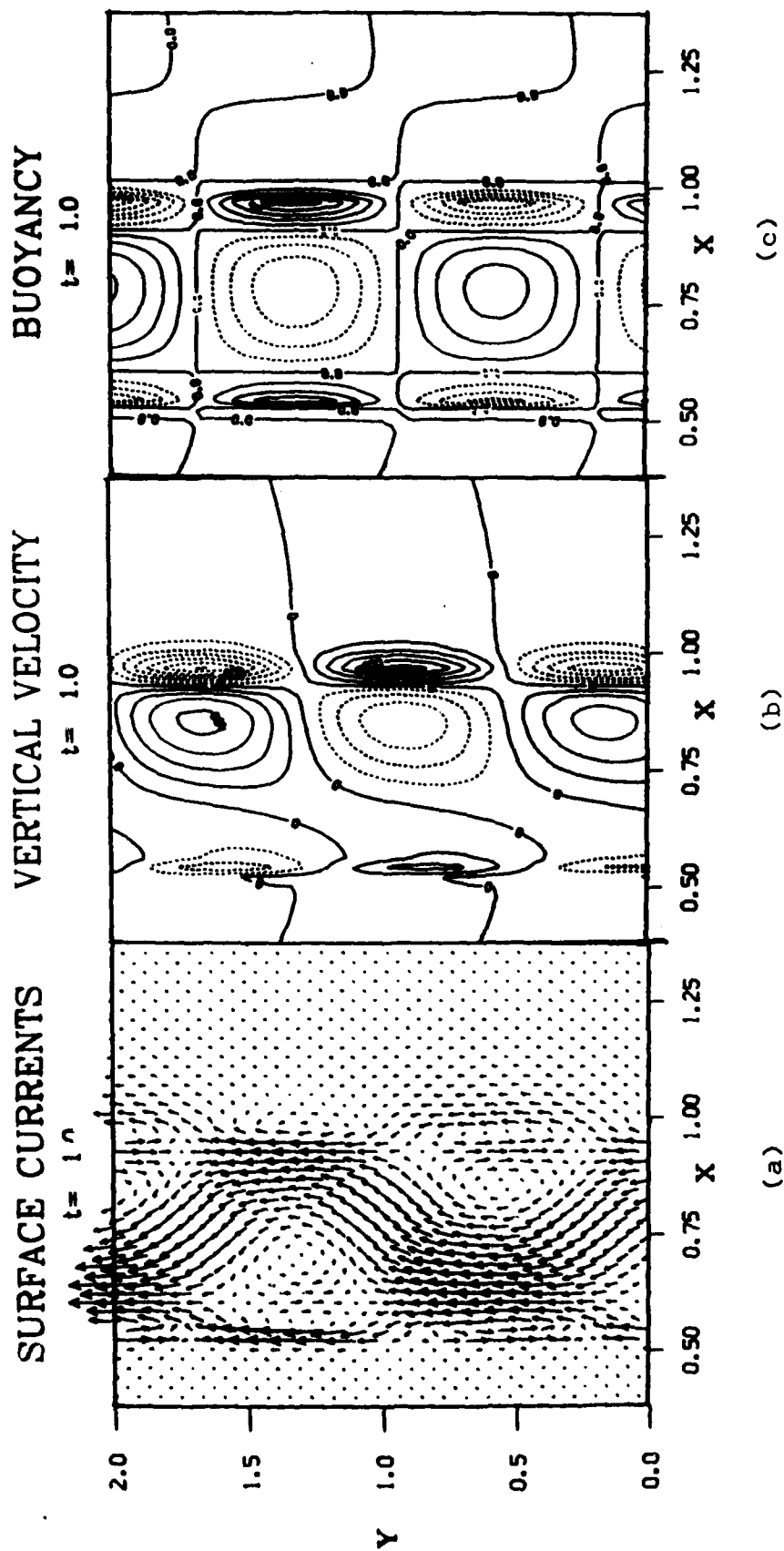


Fig. 14

Gulf Stream Frontal Statistics from Florida Straits to Cape Hatteras

Derived from Satellite and Historical Data

Donald B. Olson, Otis B. Brown

and

Steven R. Emmerson

Rosenstiel School of Marine and Atmospheric Science

1. Abstract:

Gulf Stream Frontal Statistics from the Florida Straits to Cape Hatteras Derived from Satellite and Historical Data

A five year record (1976-1980) of weekly Gulf Stream paths digitized from the U.S. Navy Ocean Frontal Analysis is analyzed to define a mean Gulf Stream path and weekly space-time series of fluctuations about the mean between the Florida Straits and Cape Hatteras. This satellite derived Gulf Stream frontal mean locus is used as a natural coordinate system in which NODC expendable bathythermograph (XBT) data is averaged to determine the mean cross stream thermal structure. The results show that the 15°C isotherm crosses the 200 m level at the mean location of the satellite derived front, that is, the cold wall of the stream as derived from IR imagery is in good agreement with a classical definition of the stream path. The Gulf Stream path is discussed in relationship to the bottom topography. Frontal location time series at various locations along the Gulf Stream are analyzed to generate occupation statistics and spectra for stream position. A steady increase in the variance of stream position occurs from Cape Canaveral to the Charleston Bump. This trend is followed by a sharp increase in variance just downstream of the bump and then a gradual decay from approximately 33°N to Cape Hatteras. A similar distribution of variance is found in the depth of the 15°C isotherm. An annual signal is seen in the path data all along the U. S. east coast. The stream front north of Charleston (32°N) exhibits the strongest annual variation with the surface front being further off-shore in the late winter and early spring. This annual signal is not obvious at the thermocline level (15°C). It is consistent, however, with observed shifts in the isotherm patterns in the upper 100 m.

2. Introduction:

The Gulf Stream between the Florida Straits and its separation from the coast at Cape Hatteras is the prototype of the 'classical' western boundary current. The mean path of the stream along the east coast is controlled by a combination of boundary shape, bottom topography, entrainment of fluid from the gyre interior, and the adjustment of the flow to the increase in planetary vorticity as fluid is advected northwards. Temporal variability in the stream can arise from changes in inflow conditions, instability of the mean flow, or forcing either by the wind, topography, diabatic cooling, or the interior mesoscale eddy field. In the present paper the mean path and cross stream structure of the stream are calculated from a combination of remotely sensed weekly frontal positions and historical expendable bathythermograph (XBT) data. Low frequency fluctuations in the stream are also considered with the same data. The work concentrates on the observed variability in the stream rather than on the forcing except to the extent that they have been discussed by other authors.

A large literature exists on the Gulf Stream and its variability between the Florida Straits and Cape Hatteras. Much of the work concentrates on short time scale fluctuations (Webster, 1961 μ Lee, 1975 μ Lee and Mayer, 1977 μ Legeckis, 1979 μ Brooks and Bane, 1981). A number of authors discuss the stream deflection south of Charleston and the increased stream variability downstream of the topographic feature located there (Knauss, 1969 μ Pashinski and Maul, 1973 μ Brooks and Bane, 1978 μ Legeckis, 1979). Variations in the Gulf Stream on the annual scale are considered by Iselin, 1940 μ Fuglister, 1952, 1972 μ and Niiler and Richardson, 1973. Studies of the longer time scale changes and the mean stream are limited by the data records available. One the most promising means of acquiring long time series is by satellite remote sensing. Studies by Maul et al., 1978 μ Legeckis, 1979 μ and Baig et al., 1981 provide an example of the time scales which can be examined from this data base. One difficulty which arises is the question of the connection between the surface and the deeper structure in the stream. Hansen and Maul (1970) in a short study suggest that the features at these levels are coherent. This conclusion is not obvious, however, in the synoptic data presented by Bane et al. (1981). Examining the connection between the surface front which can be observed from space and the deeper thermocline Gulf Stream front in the mean and at long time scales is the purpose of this study.

In the present study a five year time series of Gulf Stream path position from the U.S. Navy Ocean Frontal Analysis is examined in conjunction with available expendable bathythermograph (XBT) profiles from the NODC archives. The Ocean Frontal Analysis (Perchal, 1976 μ Bane and Brooks, 1979 μ Halliwell and Moores, 1979, 1982) is a weekly facsimile product derived from polar orbiter IR imagery along with some ship

AD-A128-789

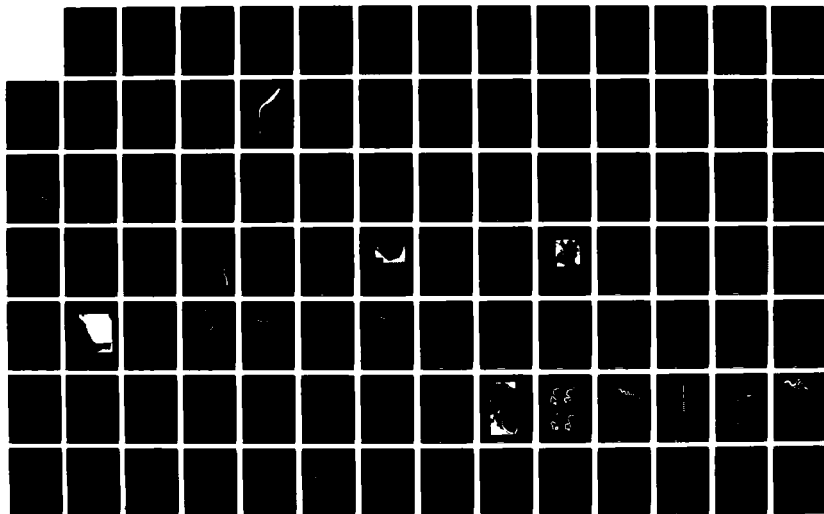
PROCEEDINGS OF THE WORKSHOP ON GULF STREAM STRUCTURE
AND VARIABILITY HELD... (U) NORTH CAROLINA UNIV AT CHAPEL
HILL APR 82 N00014-82-G-0059

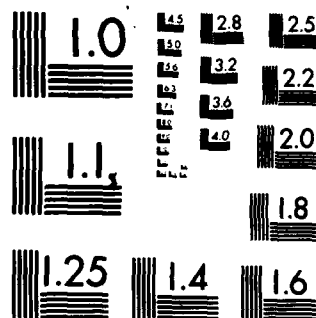
4/5

UNCLASSIFIED

F/G 8/3

NL





MICROCOPY RESOLUTION TEST CHART
NATIONAL BUREAU OF STANDARDS-1963-A

observations. The analysis was produced as an experimental product by NAVOCEANO from 1976 to 1979 and as an operational product from 1980 on by NAVEASTOCEANCEN, Norfolk, Virginia. The stream path on the facsimile is drawn at the location of the high sea surface thermal gradient along the western side of the stream. This corresponds to what is typically referred to as the cold wall of the stream in the literature (Stommel, 1960). Here this feature will be called either the stream path, cold wall, or the Gulf Stream surface front. The product varies considerably in detail and quality. In particular there is one facsimile in 1980 which has the stream flowing over the tip of Florida as outlined in the range of paths in Fig. 6 below. A test of Gulf Stream frontal statistics on a yearly basis fails to show any gross changes in the data over the 5 year period. Therefore, in the analysis all weekly data for the 5 years was kept. The weekly sampling period renders the product of limited use for following the rapidly propagating shingles or spin-off eddies (Lee, 1975; Lee and Mayer, 1977) on the western side of the stream. With appropriate analysis, however, the 5 years of data makes the facsimile product a unique source of data for a study of the mean and low frequency behavior of the stream.

The XBT data set spans an 11 year period from 1969-1980 and includes the period covered by the Navy surface front analysis. The 12446 XBT's in the region of interest contain information on the thermal structure of the stream above 750 m. The irregular distribution of XBT profiles in time and space introduces a difficult problem in terms of utilizing the data to describe the properties of the Gulf Stream and its surroundings. The difficulty in choosing an appropriate spatial region over which to average the XBT data is resolved here by computing statistics relative to the mean satellite derived Gulf Stream path.

The XBT information on the distribution of the thermal field can be interpreted using a simple layered model to infer the distribution of the velocity field and the available potential energy in the mean and the eddy fields. In general the density field is a strong enough function of temperature that the thermal wind relationship can be used to identify regions of maximum vertical shear in velocity. A simple approximation to the vertical structure of the velocity is to treat the subtropical ocean as two layers with different densities. The interface between the two layers is then taken to be the upper thermocline as discriminated by the depth of the 15°C isotherm (h_{15}). This approximation is valid in the interior of the North Atlantic gyre and in Gulf Stream rings (Olson, 1980) with an empirical reduced gravity (equation) as determined from station data between 0.010 - .020 m s^{-2} . The baroclinic velocity component of the Gulf Stream under this approximation is given by

$$\bar{v} = \frac{g'}{f} k \times G h_{15} \quad (1)$$

The other quantity of interest in what follows is the available

potential energy (APE, Reid et al., 1981). Here the discussion focuses on the eddy component of the APE (A') which is given by

$$A' = \frac{g'}{2} (h_{15} - \bar{h}_{15})^2 = \frac{g'}{2} \sigma_{h_{15}}^2 \quad (2)$$

where the overbar denotes an ensemble average and ($\sigma_{h_{15}}^2$) is variance in the 15°C relative to the mean. It is important to note that it is necessary to include a correction for sloping bottom topography (Reid, personal communication). This factor tends to decrease the APE in regions when the lower layer is thin (eg. shallow topography).

Since the current data set does not include information on g' or the validity of the two-layer approximation the discussion below is limited to assertions as to the location of the baroclinic velocity maximum and to the distribution of eddy APE. In a similar sense the topography correction to APE only strengthens the conclusions made below concerning the eddy energy distribution, therefore it is not considered. Actual APE estimates are not given although the interested reader may complete the computation using Eq. 2 as long as the caveat involved with the topography and layered model is kept in mind.

The basic analysis carried out in this study is a calculation of mean Gulf Stream path between 25-35°N latitude using the frontal analysis, followed by a treatment of the XBT data. The data analysis proceeds with a comparison of statistical properties of the thermal field in relation to the Gulf Stream surface front which is treated as a natural coordinate system. This procedure allows direct consideration of the relationship between the Gulf Stream path as given by thermocline level thermal gradients and that obtained from tracing the maximum gradient in satellite imagery. Other variables which are derived include path and isotherm depth variability as a function of the along stream coordinate. The variance in isotherm depth is also presented as a function of cross stream position. By completing averages over different seasons it is possible to demonstrate the distribution of a significant annual period oscillation in stream position as a function of latitude and depth.

The paper will proceed by first discussing the calculation of the Gulf Stream mean path and the variability about this mean. This is followed by a description of the deeper thermal structure in relationship to the surface mean path. Finally the implications of the results to our knowledge of the Gulf Stream will be outlined.

3. Methods

The Navy frontal Analysis charts from May 1976 to December 1980 (231 charts) were first digitized on a tablet digitizer. The accuracy of the digitizing process is comparable to the width of the frontal line drawn on the facsimile product. The result is a set of stream realizations each consisting of a sequence of latitude, longitude points. Since the stream is curved and occasionally exhibits large amplitude meanders care must be taken in estimating the mean. For example a straightforward calculation which averages frontal longitude by latitude bins will always lead to mean stream estimates which fall inside of the mean curvature of the stream. In order to conserve the mean stream curvature and still provide an objective estimate of stream path an iterative procedure in pseudo-natural coordinates has been chosen.

A set of arbitrary two-dimensional curves does not possess a unique mean in that algebraic means in different coordinate systems will give different answers. Establishment of a well-defined mean curve demands a prior knowledge of the properties of the ensemble of answers, ie. to specify the mean position of a set of curves it is necessary to compute both their mean orientation and the mean position along a normal to this orientation. Here the mean will be calculated from an initial first guess path in an iterative procedure. The steps involved are shown schematically in Fig. 1a.

A first guess at the orientation is specified as the curve which follows the 200 m isobath along the U.S. east coast. This choice follows from the constraint that the Gulf Stream at first approximation follows the coast. This initial curve is treated as a natural coordinate system with $N = 10$ km increments (dy') along its length. Fig. 1a. Each individual realization of the stream front is also divided into N equal segments which of course have some other length dy'' . A new stream coordinate estimate is then obtained by calculating the mean of the displacement vectors between the n th dy' , dy'' elements. These mean displacement vectors are used to iteratively correct the curve to a new reference curve. The final step involves taking the mean over all normal displacements between a point in the new reference curve and each realization of the stream. The final statistics are then calculated relative to a set of means which fall on the normals of the new reference curve.

The method outlined above works well as long as the individual realizations are well-behaved in the sense that there are no events that reverse the path of the front or that produce large sections of front normal to the initial guess curve. It is possible to derive other schemes for calculating the mean frontal position. The present scheme, while not unique, is not prone to bias due to stream curvature and is relatively straightforward to code into a computer.

The XBT data is averaged over bins which are laid out in a natural coordinate system based on the mean stream path described above. The along stream boundaries of the bins are normals to the mean stream path. The other boundaries are everywhere parallel to the stream path and displaced some x' along the normals. A schematic of the areas for the averaging is shown in Fig. 1b. The data averaged consists of the interpolated depths of a set of isotherms. Statistics including the mean to fourth moment and information on the depth bias arising from shallow XBT casts are compiled for each square. By choosing bin sizes in x' , y' that encompass a reasonable number of XBT's, significant statistics on stream structure as a function of along and across path position are obtained. With the data base available as of 1980 it is possible to consider scales of 20 km cross stream and 100-200 km in the downstream direction with the choice of long bins of 20 km width was made in order to give the best resolution of the rapidly varying across stream thermal field. The confidence limits shown in the plots of the XBT data are at the 90% level.

The NODC data used includes both 450m T-4 and 760 m T-7 probes. The shallower T-4's lead to substantial isotherm depth bias (Ebbesmeyer and Taft, 1979) for the deeper isotherms. A major proportion of the data, however, is made up of T-4 XBT's. Therefore the comparisons with the surface front (Figs. 8 and 9) below make use of a merged data set (T-4's and T-7's) while the eddy statistics and large scale 15°C isotherm topography calculations are restricted to T-7's. Bias calculations for the T-7 data set by Williams (1982) suggest a bias of less than 25 m for the area considered here.

4. The mean path

The mean Gulf Stream path from the merged XBT data set is shown in relationship to the bottom topography in Fig. 2. The stream hugs the continental shelf from the Florida Straits up to 29°N . In this region the surface front is in general in less than 100 m of water. The bottom topography is comparatively uniform through this area with a slope of 2×10^{-2} . The gradient in the bottom topography increases by approximately a factor of two around 29°N . The stream axis leaves the shelf at 29°N and falls between the 300 and 400 m isobaths downstream to Cape Hatteras. The path does extend locally into deeper water over the Charleston bump (Brooks and Bane, 1978; Legeckis, 1979) between 31° and 32°N . The Gulf Stream surface front also moves back into slightly shallower water (300 m) north of 32°N . This shift coincides with a steady increase in the gradient of the bottom topography downstream of Charleston.

The path of the surface front corresponds approximately with the location of the 200 m isoline in the 15°C isotherm topography

as shown in Fig. 3. The solid lines in Fig. 3 include all XBT's while the dashed curves are for T-7's only. In the curves up to 32°N the depth bias is negligible out to 60 km. In the northernmost curves the bias with T-4's is larger perhaps because of the large cold wedges near the coast and larger meanders. The wedge of cold water trapped against the continental shelf increases downstream from 29°N . From Figs. 2 and 3 it can be seen that the largest volume of cold slope/shelf water resides between the Charleston bump ($31^{\circ}30'\text{N}$) and Cape Fear (33°N). If a two-layer approximation with the 15°C isotherm as the interface is taken as a model for the baroclinic velocity distribution the maximum current falls around $x' = 30$ km from the Florida Straits up to 32°N . In the northernmost section (32° - 34°N , Fig. 3) the region of maximum shear across the thermocline is shifted farther offshore to $x' = 60$ km. The near surface front as depicted by the 25°C isotherm exhibits large variations which make the mean calculation somewhat uncertain. In general, however, the surface front as determined from the XBT's agrees with the path analysis from satellite data.

5. Spatial distribution of Gulf Stream variability

The standard deviation and total range of cross-stream path deflections are shown in relationship to the Gulf Stream mean path in Fig. 4. Along the right margin of the figure are selected histograms of cross-stream displacement in the surface front. The standard deviation as shown in Fig. 5 is nearly constant in the Florida Straits followed by an approximately linear increase between 27° and 32°N . There is a sharp peak in the latitudinal variance distribution just downstream of the Charleston bump. Finally the deviation in frontal position decreases from around 33°N to Cape Hatteras. The envelope of path excursions is skewed towards the middle of the strait between 25° - 27°N . As the shelf broadens around 27°N the path histograms become skewed shoreward. This tendency is reversed in the region just upstream and over the Charleston bump where there is a trend to larger offshore excursions of the front as pointed out by several other authors.

The variations in height of the thermocline mirror the general trends in surface front deviations. The 15°C variance averaged over the 20 km bin just seaward of the mean frontal path and by 2° of latitude is displayed in Fig. 6a. The distribution of variance implies a 3 to 5 fold increase in eddy available potential energy between 27° - 28°N and the region just north of the topographic bump at $31^{\circ}30'\text{N}$. The statistics fail to show the same dramatic rise in variance found in the path at 32°N . This is likely due to the effects of the 2° average. The 15°C isotherm variance does reach a maximum between 32° - 33°N and then decreases downstream. This northward increase in thermocline

height variance occurs for a range of normal coordinate (x') between -25 and 150 km.

The cross stream distribution of h_{15} squared variance for two latitudinal bands as a function of x' is shown in Fig. 6b. These statistics are based on the deeper T-7 XBT data to avoid bias. The Gulf Stream core exhibits a distinct minimum in both latitude bands. The eddy signal doubles seaward on a scale of 20-40 km. This may reflect the influence of lateral dissipation, bottom drag, or a strong constraint against meandering of the stream due to the sloping bottom topography. The variations in h_{15} are fairly constant from the approximate location of the velocity maximum ($x' = 30-40$ km) out to 100 to 140 km. Beyond this there is a more complicated distribution of thermocline variance. A more detailed presentation of the far field variability can be found in Williams (1982).

Together the spatial distributions of frontal excursions and thermocline displacements support the general view of a region of eddy growth between the Florida Straits and 33°N followed by a zone of eddy decay. A conversion of eddy kinetic energy back into the mean stream has been documented off Onslow Bay ($34^\circ 30' \text{N}$) by Webster (1961) and Brooks and Bane (1981). The present results suggest a concurrent net conversion of eddy available potential energy. The distribution of h_{15} variance normal to the stream is consistent with either a dissipative or topographically constrained area on the inside of the stream. The low thermocline variances are inconsistent with a net source of mesoscale radiation in an otherwise uniform medium. The sources of eddy energy found in proximity to the western boundary are not obvious at this time and deserve more attention. The overall distribution might be construed as indicative of a source which is a combination of instability in the Gulf Stream and a vigorous eddy field in the interior produced elsewhere and brought into the region by propagation and advection in the Gulf Stream recirculation. A portion of the frontal fluctuations may be forced by changes in the surface transport upstream and direct atmospheric forcing.

6. Frequency distribution of Gulf Stream variations

The space-time series of Gulf stream position from the Navy facsimile product contains information on the frequency distribution of stream fluctuations with periods greater than a few weeks. The XBT data set can only resolve persistent longer period signals which display significant along stream coherence. Here the disturbances in the path of the surface front are analyzed first. The XBT data is then used to verify the dominant annual peak in the frontal data. The distribution of standard deviation in each of three spectral bands is plotted as a

function of latitude in Fig. 5. The dominate contribution to the standard deviation is split evenly between the 3 week to 3 month and the greater than 3 month bands. Both of these follow the general rise in variance northwards to a peak around 33°N . The residual variance exhibits a similar northward increase with a slightly enhanced contribution downstream of the Charleston bump. Spectra of the cross stream fluctuations are shown in Fig. 6 for two locations along the stream.

The spectra in Fig. 7 are average spectra over nominal 100 km increment in y' centered at 29°N (Fig. 7a) and $32^{\circ}45'\text{N}$ (Fig. 7b). The raw data have been detrended and then low passed with a filter having a half power point at 21 days. The dominant peak in both occurs between 200 and 500 days with a center indistinguishable from 365 days or a year. This annual peak appears in all of the spectra from the straits downstream to Hatteras. There is a tendency for broader peaks south of 32°N although it is not clear if this trend is significant. The spectra fall off rapidly out to a period around 40 days. All of the spectra consist of essentially white noise for resolvable frequencies below $.025 \text{ days}^{-1}$ (40 days). The white noise spectrum may reflect the influence of the unresolved higher frequency eddies known to occur along the edge of the stream. An example of a time series in cross-stream frontal displacement is shown in Fig. 8. The series is from $33^{\circ}33'\text{N}$, and has been low-passed with a 60 day filter. The annual signal is pronounced. The annual frontal oscillation begins with a rapid offshore shift which reaches a maximum between January and March. The corresponding onshore shift which completes the cycle takes place in fall quarter of the year.

The annual signal is also found in the XBT data. Due to the limitations in the quantity of XBT data a 3 month, 'seasonal' average is the shortest time interval for which averages over 2° of latitude and 20 km x' are significant. An average stratification for $32-34^{\circ}\text{N}$ in the thermal winter (January-March) and fall (October-December) is shown in Fig. 9. The average cross-sections are calculated over all cases in which a particular isotherm is found. The plots above the cross-sections give the percentage of cases for which the near surface isotherms were found. From the cross sections the 'surface' front as denoted by the surfacing of the 25° and 27°C isotherms occurs farther inshore in the fall period. The shift is more pronounced in the percentage occurrence curves where the peak in the warmest isotherms are shifted 50 km offshore in the winter case. Similar figures for the spring and summer are in agreement with these shifts although the stronger near surface stratification makes them more difficult to interpret. The mean distributions of the 15° and 10°C isotherms are the same for all three averaging periods. The implication is that the annual signal is either limited to the surface layers or at least surface intensified in the sense that it is not found deeper than 100 m.

The seasonal deflection of the surface front is in agreement with the two year time series presented by Fuglister (1974) farther downstream in the Gulf Stream extension. It is intriguing to compare the annual period oscillations observed here with the annual period variations in the Florida Straits transport measurements taken by Niiler and Richardson (1973) although such a connection is not supported in the present data. The transport fluctuations may be tied to the deflection of the surface front but there is no indication of a deeper signal which could account for a change in the baroclinic transport in the XBT data treated here. The variations in near surface conditions here may be of importance to the question of the northward heat flux in the western boundary current.

7. Conclusions

The present work encompasses the most basic questions which can be asked about the Gulf Stream with the two data sets used. The primary concern is the mean conditions and the distribution of stream variability in space and time. The relationship between the mean surface frontal position, the bottom topography, and the thermal field is possibly the most noteworthy result. The fact that the mean surface front is correlated with a constant water depth over long distances verifies the presence of a strong topographic influence on the stream. The regions where the front shifts relative to the topography are also places where there are substantial changes in the bottom topography. The mean cross stream isotherm field varies gradually as the stream proceeds from the Straits of Florida to Cape Hatteras. The major modification to the cross stream profiles as the stream flows north is the appearance of an increased amount of cold fluid trapped up against the bottom slope. The largest increase in the inner cold wedge occurs in the area of Charleston bump.

The distributions of both surface frontal position and thermocline variance exhibit a similar downstream dependence. The cross stream distribution of thermocline variance implies the presence of either strong topographic constraints against meandering or a dissipative regime along the inner edge of the stream. The temporal variations which can be resolved in the composite data set show a annual cycle in the near surface features of the Gulf Stream front. This result might be construed to indicate a possible problem in following the evolution of the Gulf Stream from satellite IR data. The comparison of the XBT data with the satellite product suggests that the surface front follows the thermocline signature of the Stream well in the mean. The seasonal computations, however, imply that there is a seasonal change in the relation between the core of the stream as measured by the depth of the 15°C isotherm and the high gradient in sea surface temperature. It also implies that part of the deflection observed at the Charleston Bump is not due to direct topographic effects since only the surface layers are affected. The present results based on combining satellite and more

conventional data in determining the structure of ocean currents indicate that such combinations utilizing the intense spatial/temporal satellite coverage with sparser in-situ observation can yield major insights into the mean and fluctuation characteristics of the ocean. It is possible to think of many ways of expanding the current work such as considering the co-variation of the surface front and the deeper structures with the data set. A number of extensions of this analysis are currently being planned.

Acknowledgements

The authors would like to thank Mr. Stan Hooker for the long hours he spent digitizing the Navy frontal analysis product. We also owe our gratitude to Ms. Elizabeth Williams who is responsible for bringing the historical XBT data on line. Mr. Terry Parks helped code some of the sorting routines used in this work. There were a number of helpful comments and suggestions made to the authors during the course of the effort. In particular we would like to thank Drs. Kevin Leaman and Tom Lee. The manuscript was typed by Mss. Jere Greene and Gay Ingram. This work was supported by ONR (OBB,DBO) and BLM (OBB) under contracts N00014-80-C-0042 and 11-920293, respectively.

REFERENCES

- Baig, S., D. Gaby and J. Wilder., A provisional Gulf Stream system climatology. *Mariners Weather Log.* 25(5):323-345., 1981.
- Bane, J.M. Jr., D.A. Brooks and K.R. Lorenson., Synoptic observations of the three-dimensional structure, propagation and evolution of Gulf Stream meanders along the Carolina continental margin. *J. Geophys. Res.*, 86,6411-6425., 1981.
- Bane, J.M. Jr. and D.A. Brooks., Gulf Stream meanders along the continental margin from the Florida Straits to Cape Hatteras. *Geophysical Res. Lett.* 6:280-282., 1979.
- Brooks, D.A. and J.M. Bane, Jr., Gulf Stream deflection by a bottom feature off Charleston, S.C. *Science.* 201:1225-1226., 1978.
- Brooks, D.A. and J.M. Bane, Jr., Gulf Stream fluctuations and meanders over the Onslow Bay upper continental slope. *J. Phys. Oceanogr.* 11:247-256., 1981.
- Ebbesmeyer, C.C. and B.A. Taft., Variability of potential energy, dynamic height and salinity in the main pycnocline of the western North Atlantic. *J. Phys. Oceanogr.* 9:1073-1089., 1979.
- Fuglister, F.C., Annual variations in current speeds in the Gulf Stream system. *J. Mar. Res.* 10:119-127., 1951.
- Fuglister, F.C., Cyclonic rings formed by the Gulf Stream 1965-66. In *Studies in physical oceanography - A Tribute to Georg Wust on his 80th birthday*, Vol. 1, A.L. Gordon, editor, Gordon and Breach, New York:137-168., 1972.
- Halliwel, G.R. Jr., The space-time structure and variability of the shelf water-slope water and Gulf Stream surface temperature fronts and associated warm-core eddies. *J. Geophys. Res.* 84:7707-7725., 1979.
- Halliwel, G.R. Jr. and C.N.K. Mooers., Meanders of the Gulf Stream downstream from Cape Hatteras, 1975 through 1978. (In prep.)
- Hansen, D.V. and G.A. Maul., A note on the use of sea-surface temperature for observing ocean currents. *Remote Sensing Environ.* 3:161-164., 1970.
- Iselin, C.O'D., Preliminary report on long-period variations in the transport of the Gulf Stream system. *Pap. Phys.*

- Oceanogr. Meteor. 8:1-41., 1940.
- Knauss, J.A., A note on the transport of the Gulf Stream. Deep-Sea Res. Supplement to Vol. 16:117-123., 1969.
- Lee, T.N., Florida Current spin-off eddies. Deep-Sea. Res. 22:753-765., 1975.
- Lee, T.N. and D.A. Mayer., Low-frequency current variability and spin-off eddies on the shelf off Southeast Florida. J. Mar. Res. 35:193-220., 1977.
- Legeckis, R., Satellite observations of the influence of bottom topography on the seaward deflection of the Gulf Stream off Charleston, S.C. J. Phys. Oceanogr. 9:483-497., 1979.
- Maul, G.A., The annual cycle of the Gulf Loop current, Part I: Observations during a one year time series. J. Mar. Res., 35:29-47., 1977.
- Maul, G.A., P. W. deWitt, A. Yanaway, and S. Baig., Geostationary satellite observations of Gulf Stream meanders: infrared measurements and time series analysis. J. Geophys. Res. 83:6123-6135., 1978.
- Niiler, P.P. and W.S. Richardson., Seasonal variability of the Florida Current. J. Mar. Res. 31:144-167., 1973.
- Olson, D.B., The physical oceanography of the two rings observed by the cyclonic ring experiment, Part II, Dynamics. J. Phys. Oceanogr. 10:514-528., 1980.
- Pashinsky, D. and G. A. Maul, Use of ocean temperature while coasting between the Straits of Florida and Cape Hatteras, Mar. Weather Log., 17, 1-3, 1973.
- Perchal, R.J. Comparison of Gulf Stream edges detected by airborne radiation thermometer and VHRR-IR satellite imagery during Subswex 1-76. Tech. Note 3700-52-76, 21 pp., U.S. Nav. Oceanogr. Office, Washington, DC., 1976.
- Reid, R.O., B.E. Elliott, and D.B. Olson, Available potential energy: A clarification. J. Phys. Oceanogr. 11:15-29., 1981.
- Stommel, H., The Gulf Stream, A physical and dynamical description. University of California Press, Berkeley and Los Angeles. 248 pp., 1960.
- Webster, F., The effect of meanders on the kinetic energy balance of the Gulf Stream. Tellus XIII(3):392-401., 1961.
- Williams, E.J., A reevaluation of the North Atlantic circulation from XBT data, Master's thesis, University of Miami, (in prep.)

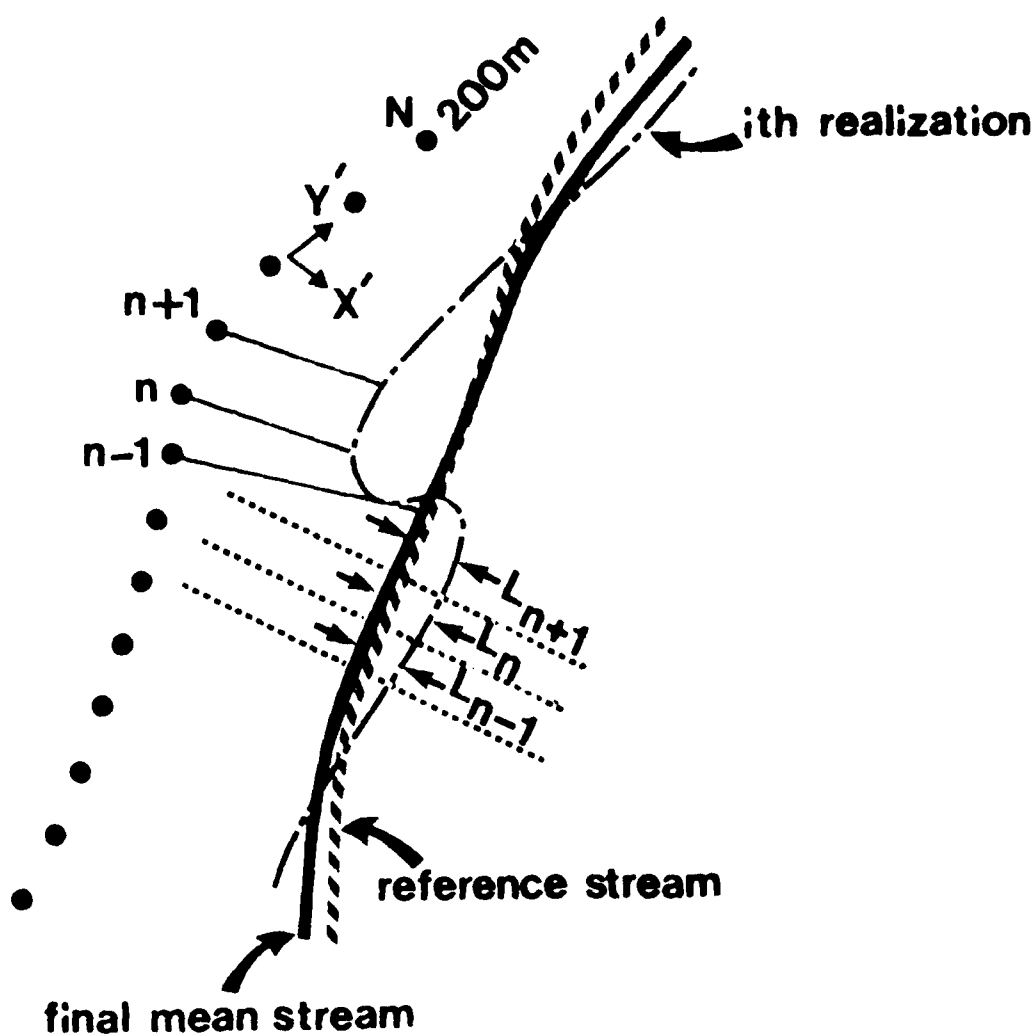


Fig. 1a. The method used in calculating the mean stream position is shown schematically. The iterative procedure starts with an initial estimate of the stream path as indicated by the dotted curve which in this case is the 200 m isobath. The calculation involves computing the mean vectors between the points marked $n-1$, n , $n+1$ and the corresponding locations along all realizations. This produces a reference stream curve. The final estimate of the mean stream is computed along normals (L_{n-1} , L_n , L_{n+1}) to this reference curve. For more details see the text.

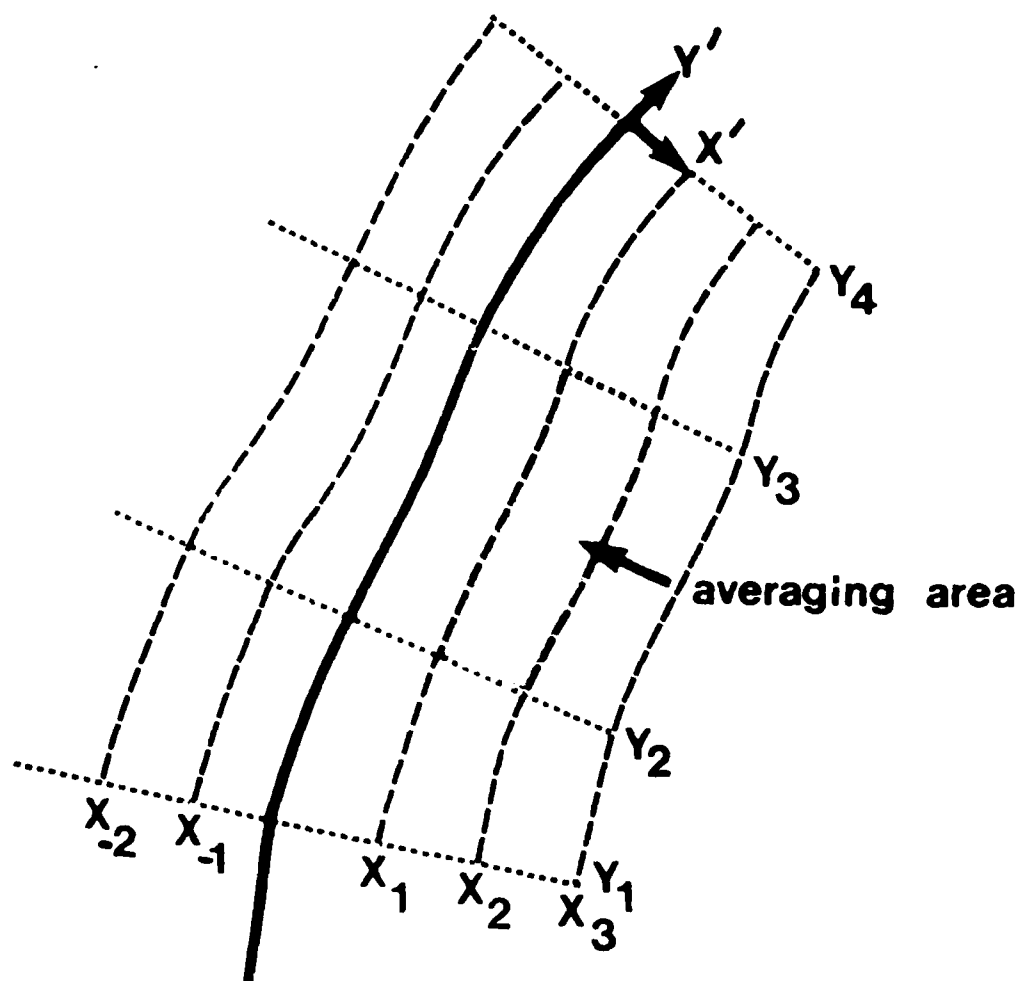


Fig. 1b. The XBT data is averaged over regions outlined by normals and parallels to the mean stream. This natural coordinate system and an example of an averaging area are shown in the figure.

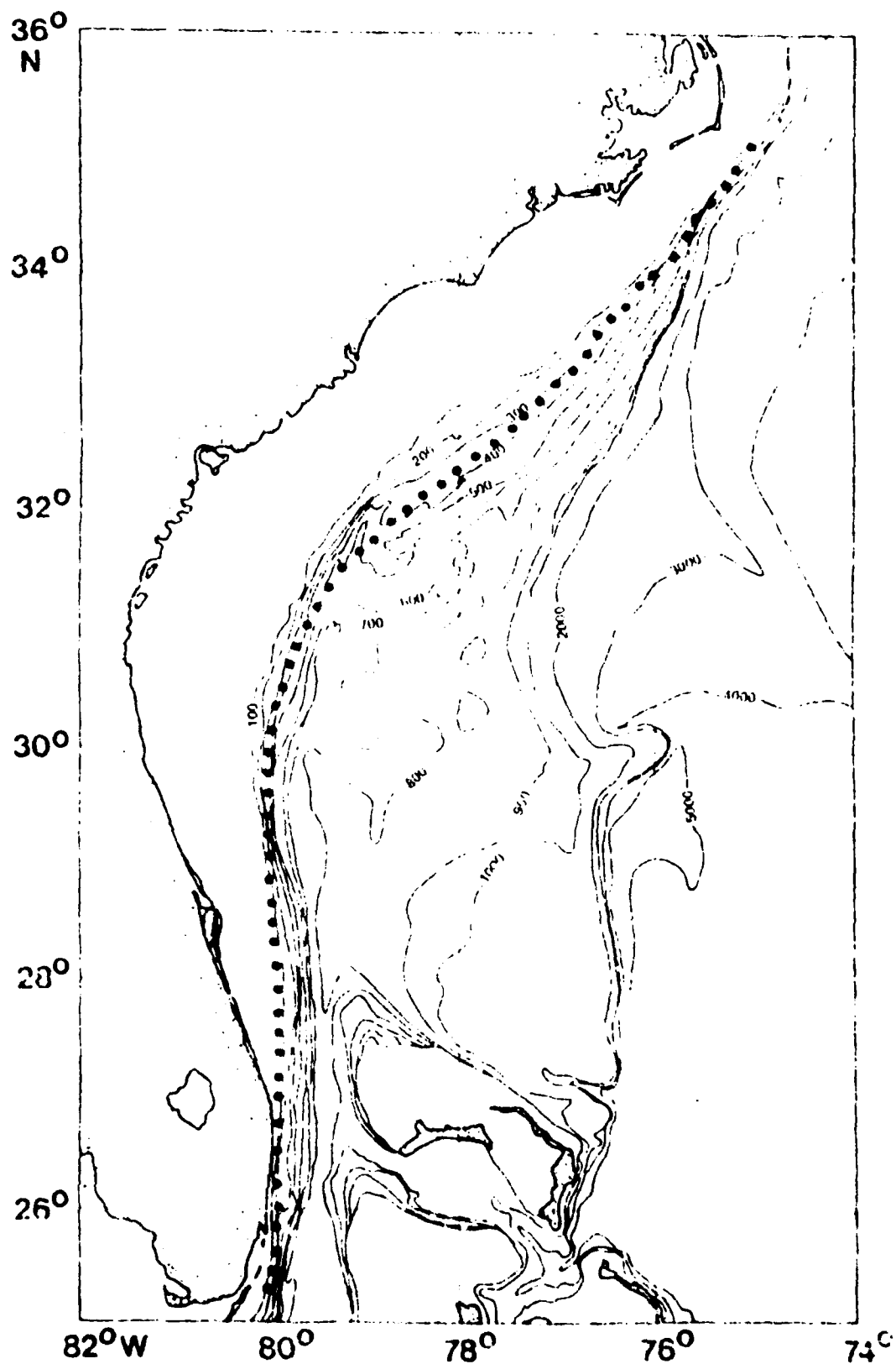


Fig. 2. The mean Gulf Stream plotted over the topography off the eastern coast of the United States.

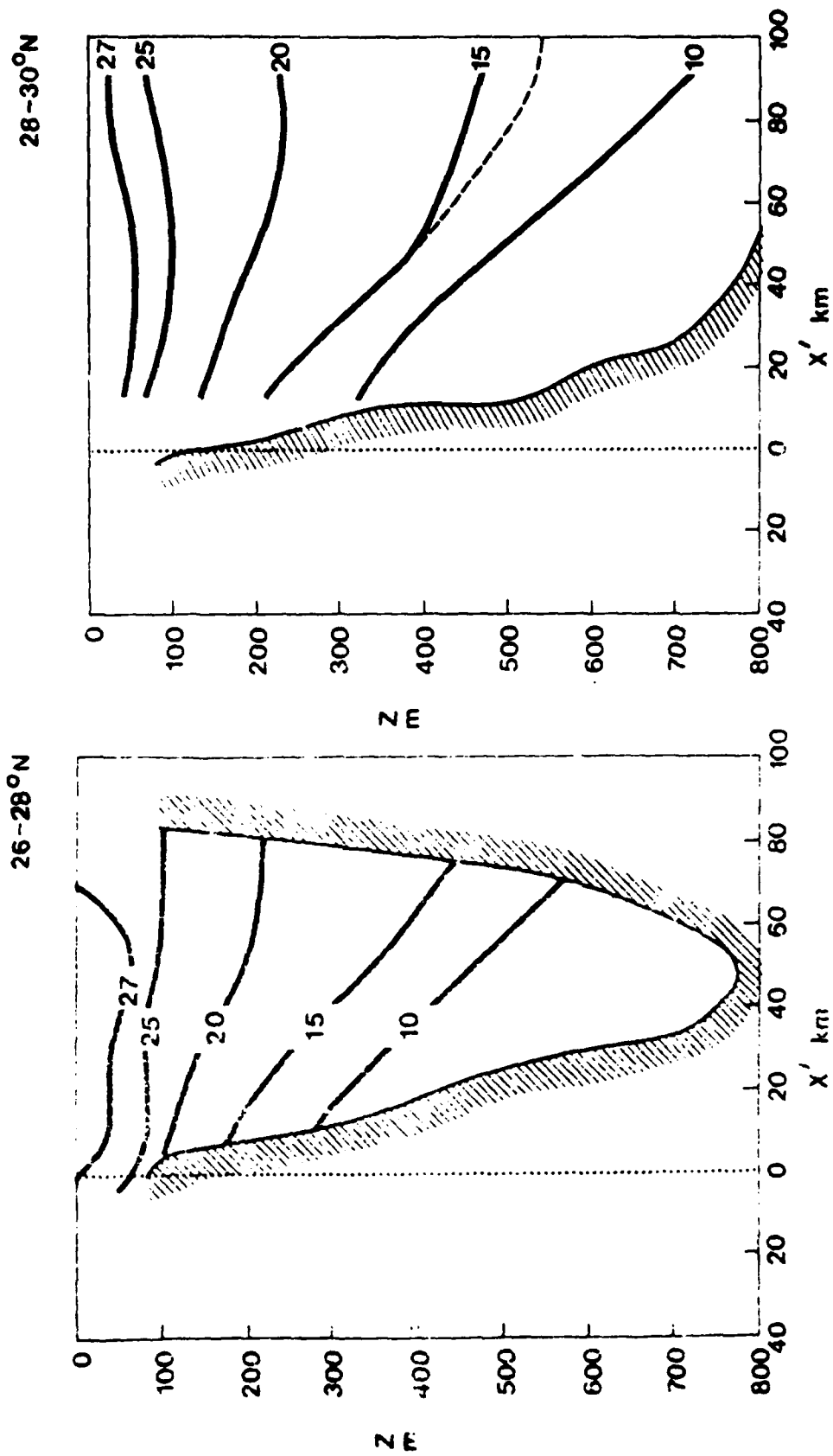


Fig. 3a. The mean cross-stream thermal structure for the region of the mean stream (Fig. 2) between 26° and 28° N.

Fig. 3b. Same as Fig. 3a but for 28° to 30° N.

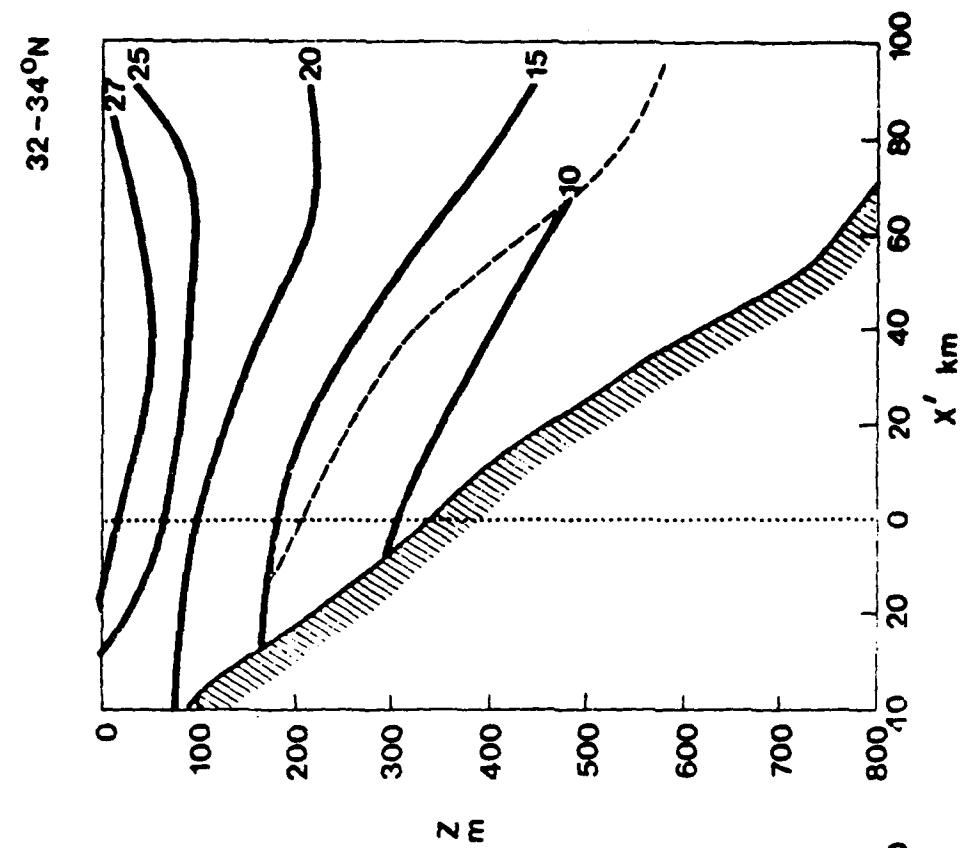


Fig. 3d. Same as Fig. 3a but for 32° to 34°N.

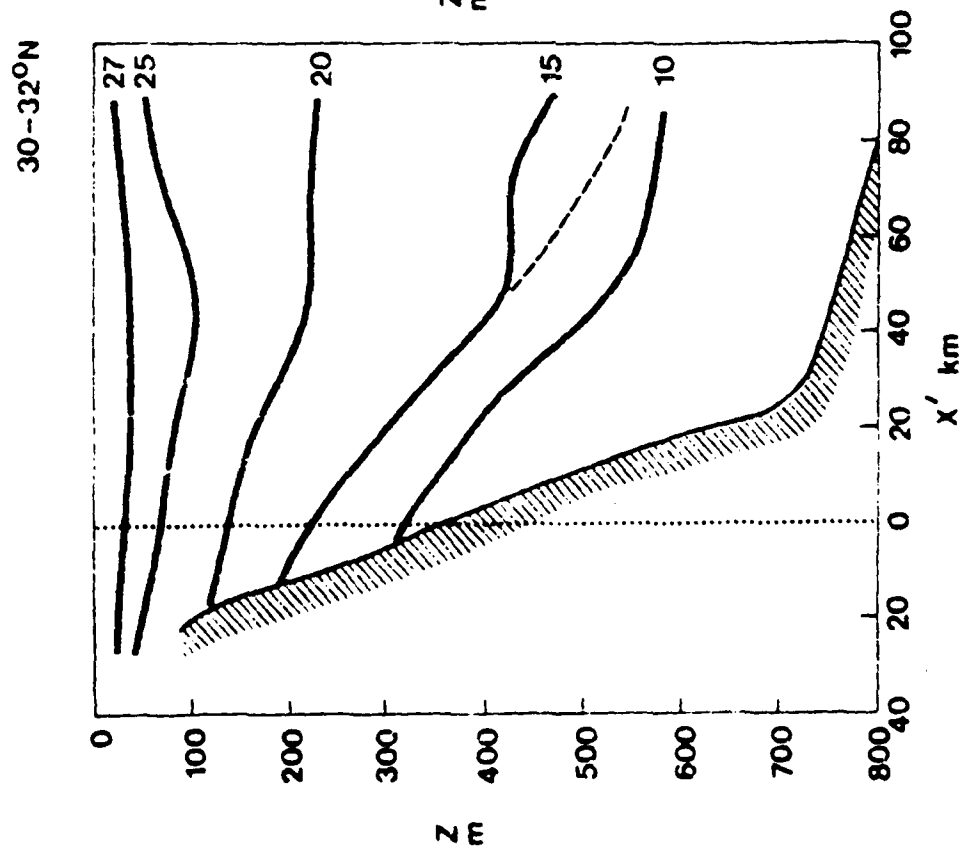
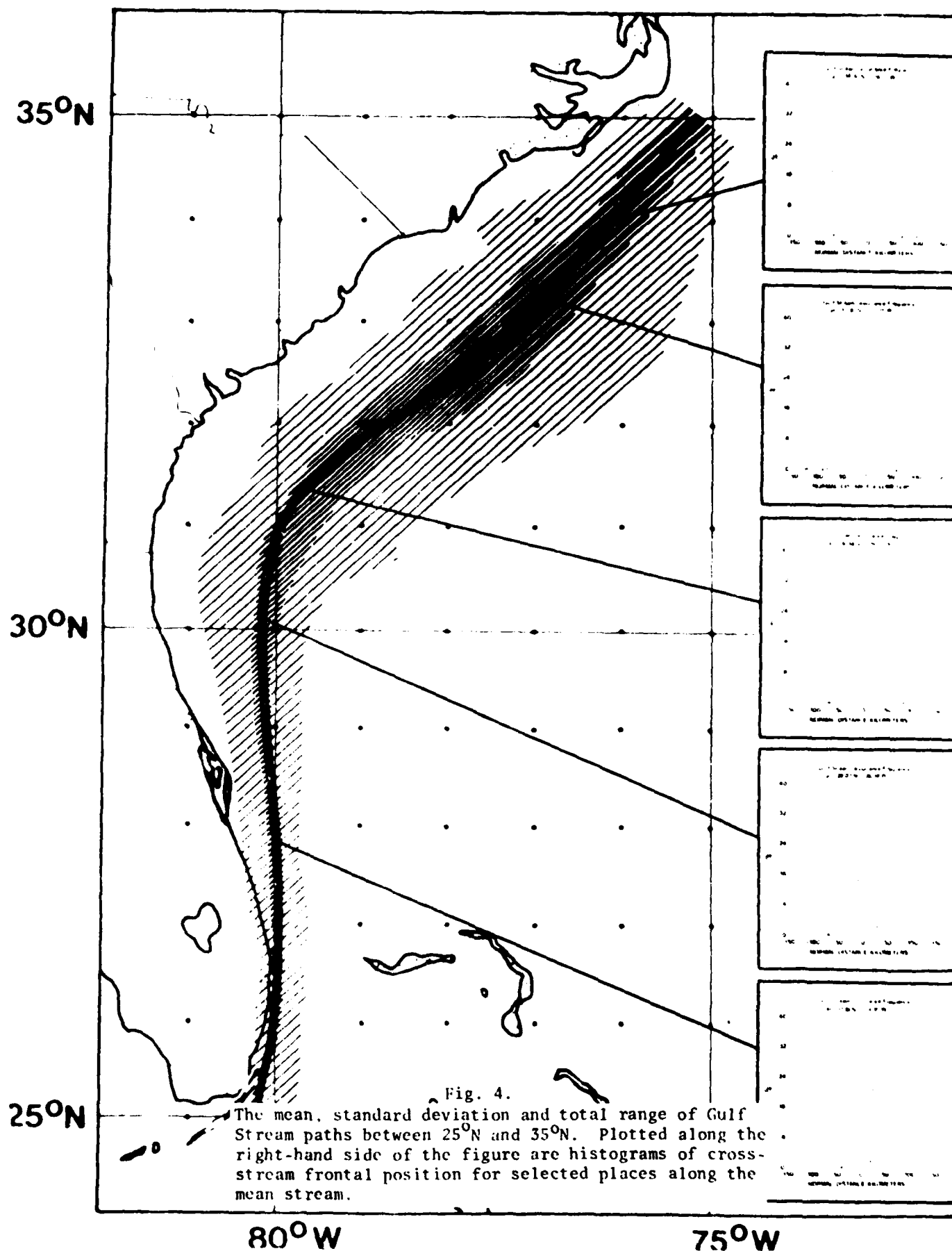


Fig. 3c. Same as Fig. 3b but for 30° to 32°N.

1976 - 1980 COLD - WALL POSITION



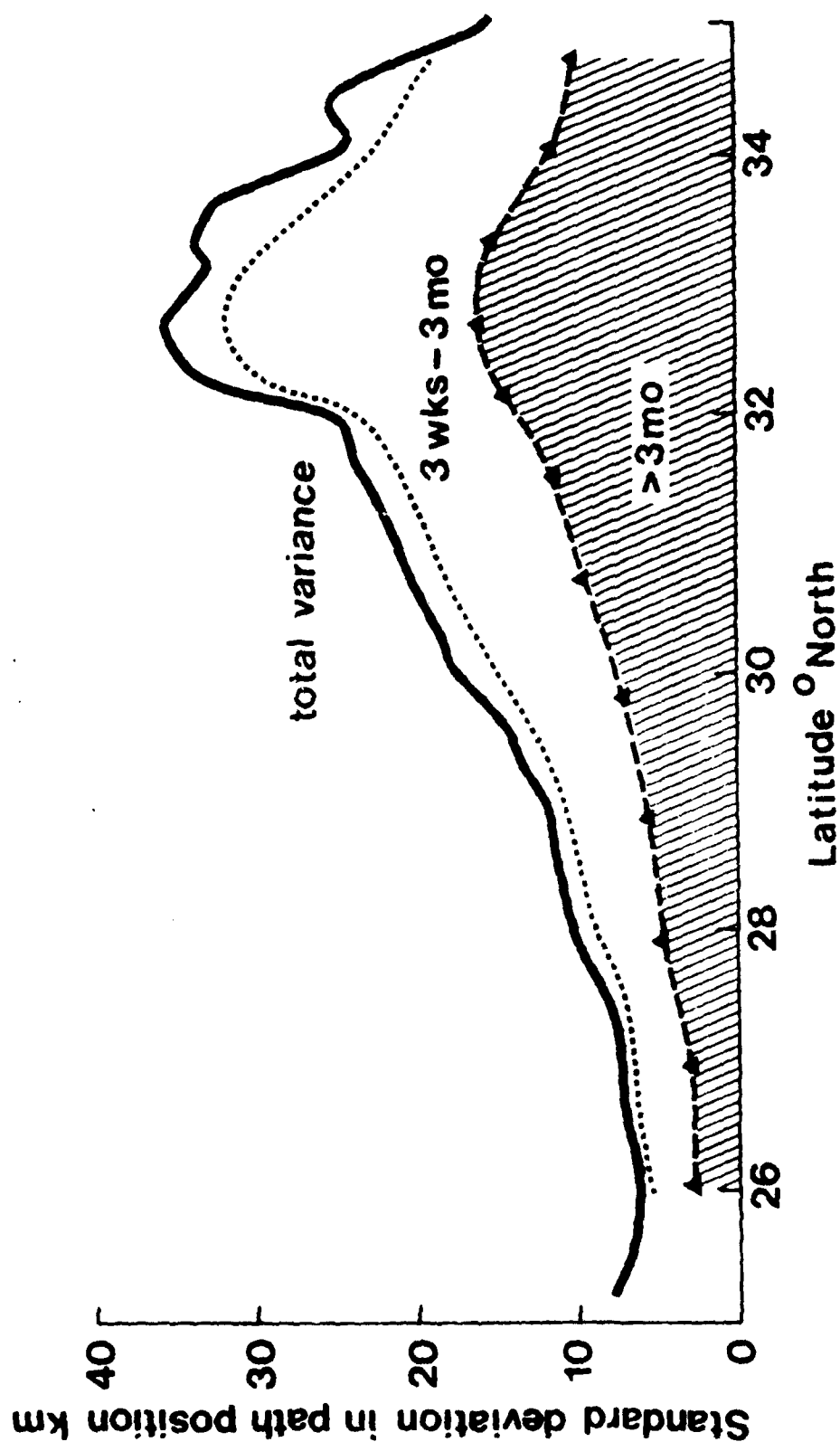


Fig. 5. The distribution of the standard deviation in cross-stream frontal displacement as a function of the latitude of the mean position. Included is a breakdown of the variations as a function of frequency.

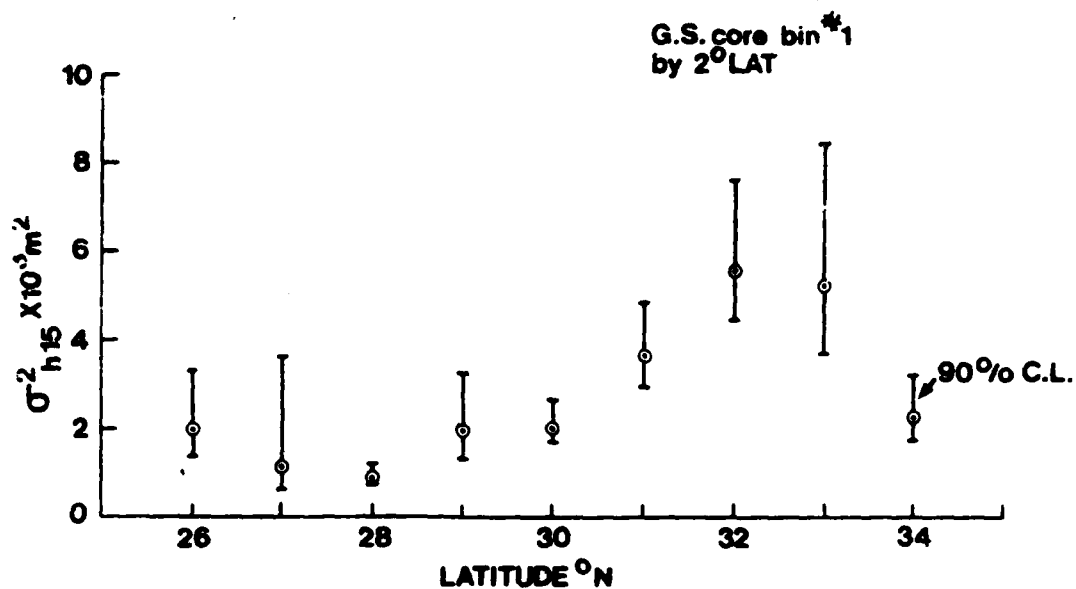


Fig. 6a. The variance in the 15°C isotherm depth for a strip between the mean stream path and a parallel curve 20 km to the seaward. The variance is plotted against the latitude of the mean path as in Fig. 5.

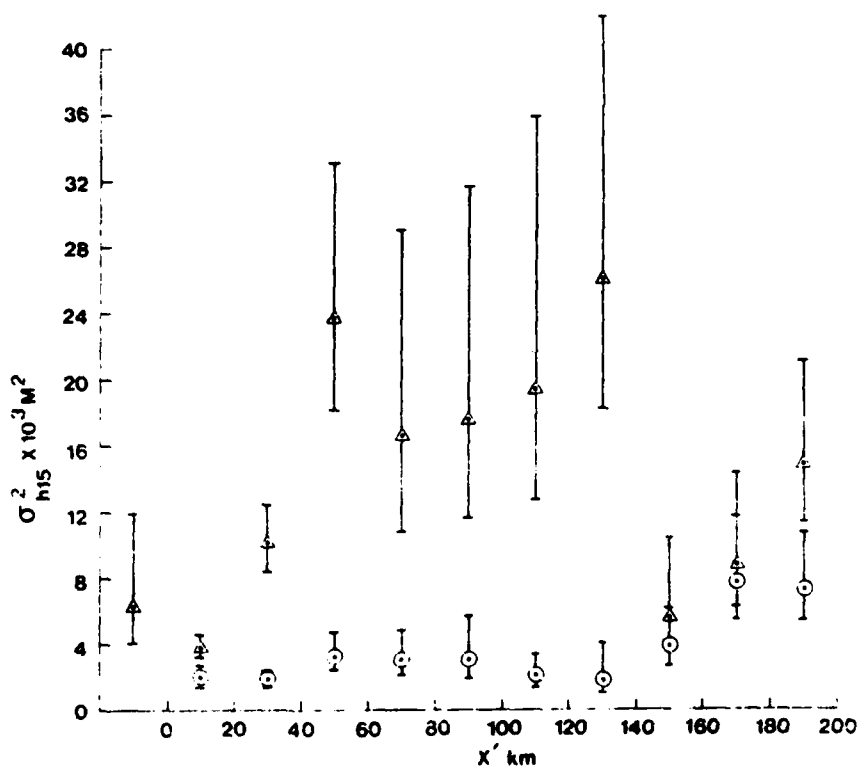


Fig. 6b. The cross-stream distribution of 15°C isotherm depth variance. The averaging is completed over T-7 SBT's only in order to minimize the depth bias. The circles (O) are for data between 25° and 30°N while the triangles (Δ) are for data in the range 30° to 35°N . The error bars are 90% confidence limits.

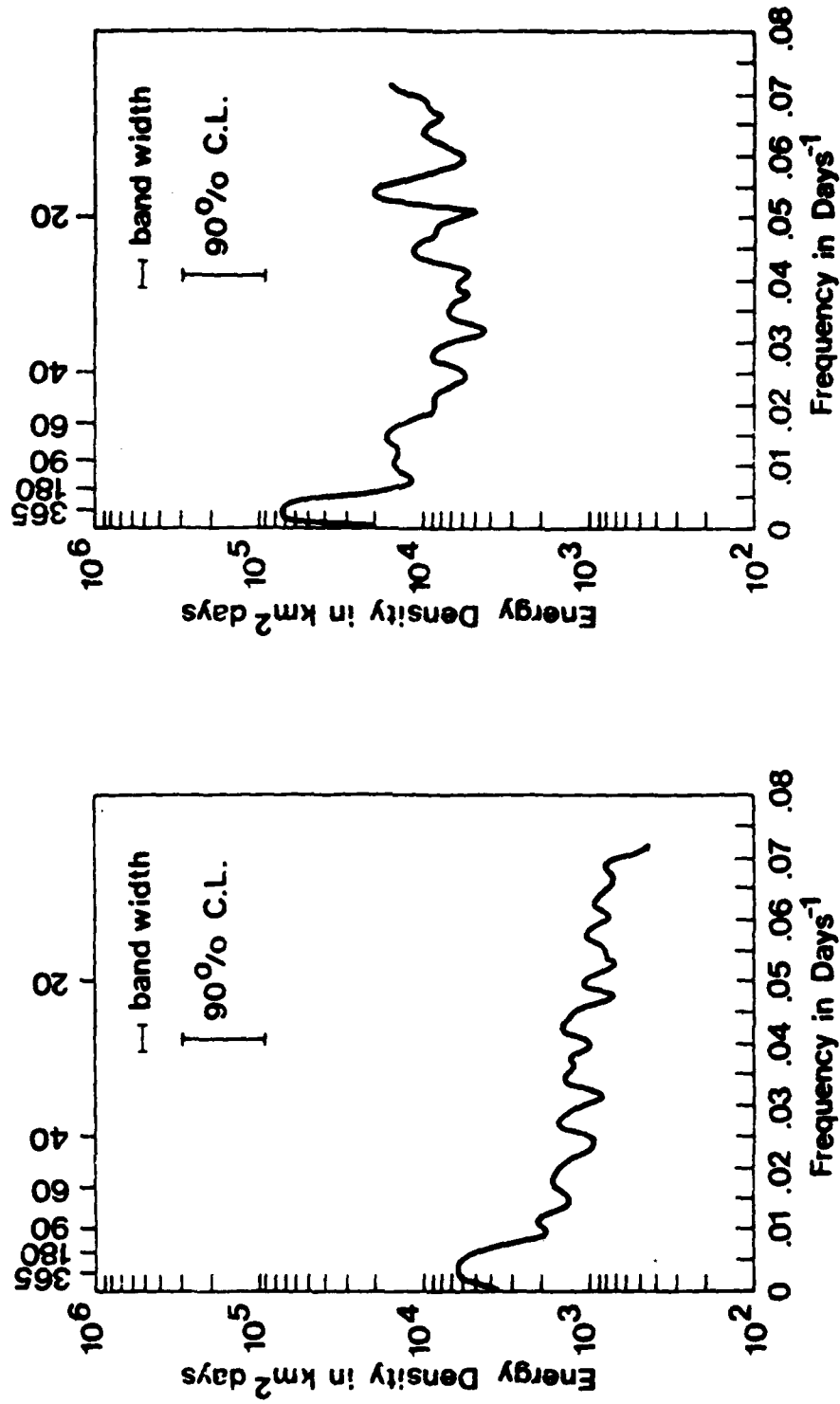


Fig. 7a. An average spectra of cross-stream deflections for the path between ± 50 km of 29°N . The raw signals have been detrended and low passed with a 21-day half power filter. The numbers along the top of the plots are the period in days.

Fig. 7b. Same as Fig. 7a but for 32°N .

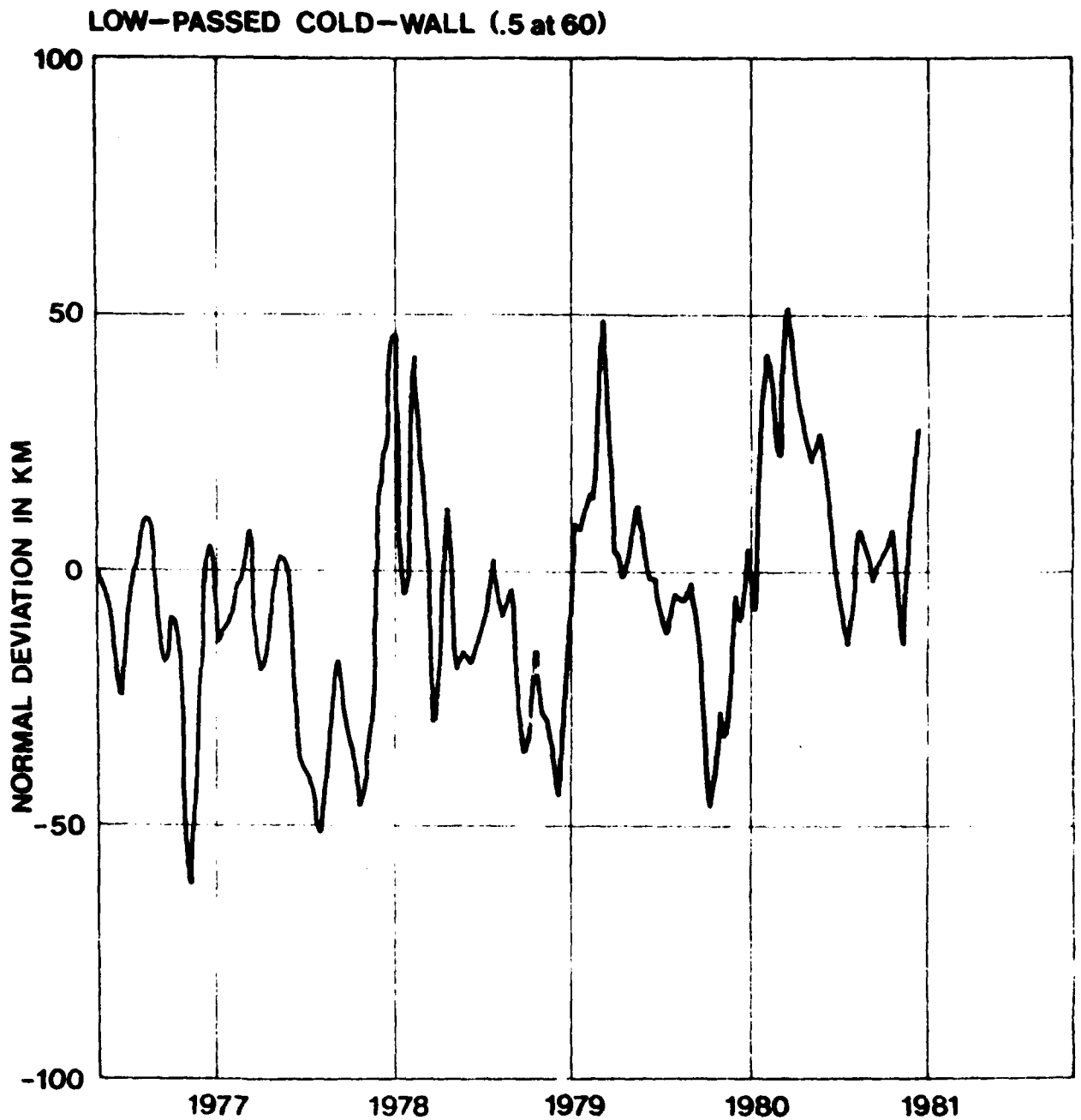


Fig. 8. The cross-stream deviations for the mean stream position of $33^{\circ}33'N$. The signal has been low passed with a filter with a half power point at 60 days.

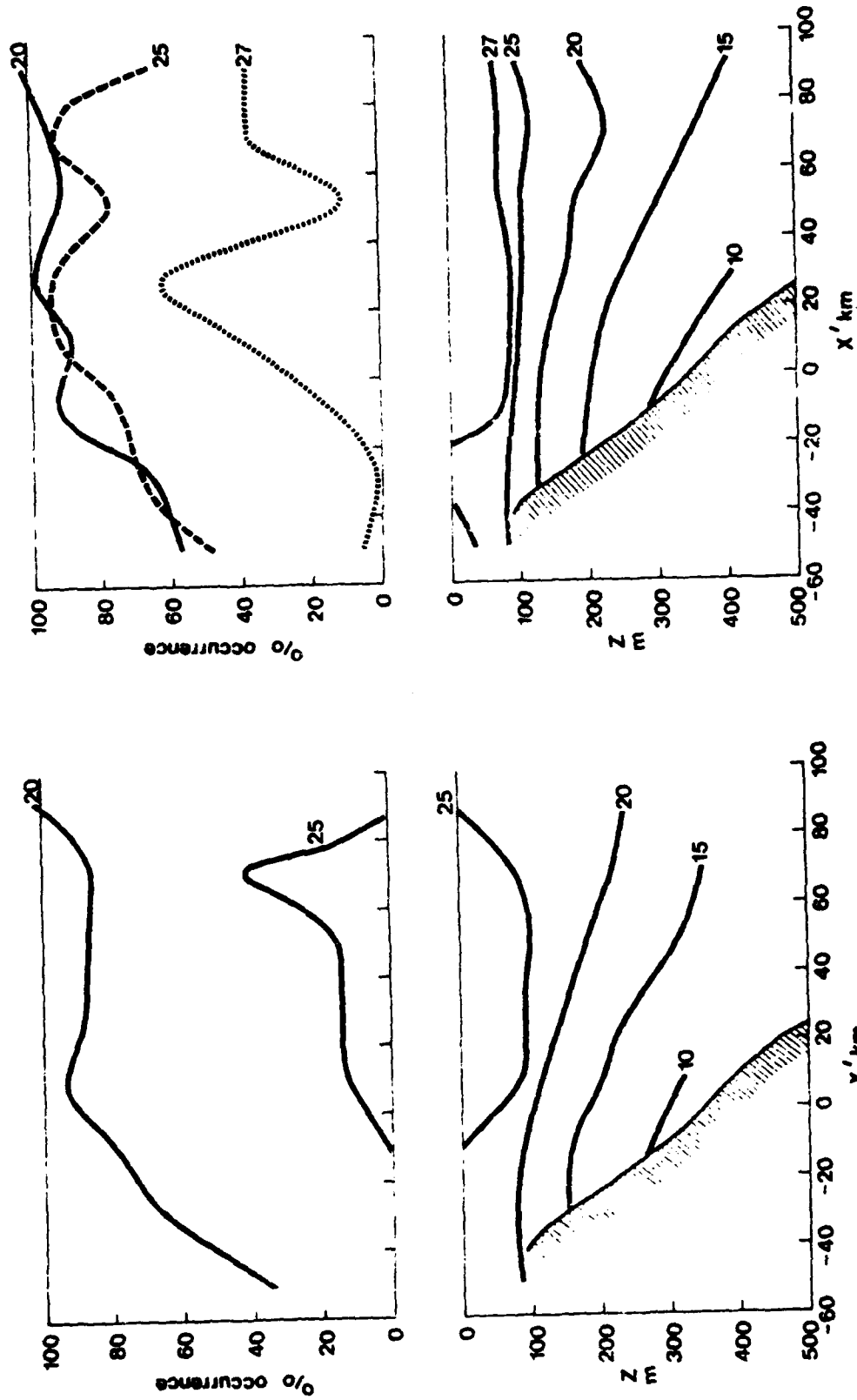


Fig. 9a. The average cross-stream thermal structure and percentage occurrence (upper plate) of near surface isotherms for all XBT's taken in January, February and March between the normals extending from the mean stream at 32° and 34° N.

Fig. 9b. Same as Fig. 9a but for the months October, November, and December.

AD P001056

THE PEGASUS PROGRAM EAST OF CAPE HATTERAS

T. Rossby and D. Halkin
Graduate School of Oceanography
University of Rhode Island
Kingston, R.I.

Since September 1980 we have maintained a program of bimonthly sampling of the velocity structure of the Gulf Stream. Each section consists of a set of velocity and temperature profiles taken along a 150 - 200 km long line centered at 36 N, 73 W from the Slope Waters to the Sargasso Sea. As of October 1982 the following sections have been taken:

1980	1981	1982	1983
	Jan(1)	Jan	Jan(4)
	Mar(1)	Mar	Mar(4)
	May(2)	May	May(4)
	Jul	Jul	
Sept	Aug	Sept	
Nov(3)	Nov(3)	Nov(4)	

(1) limited data due to weather, ship or equipment

- (2) no data due to ship
- (3) some weather problems
- (4) planned

During the first winter (and spring) we had rather serious weather and ship problems. For this reason we hope to add three additional sections in 1983. Since July 1981 the Pegasus instruments have been enclosed in glass spheres instead of aluminum tubes. This makes them lighter and easier to handle and permits us to profile to greater depths than before. The data are collected and stored in RAM using a microprocessor, and then secured on magnetic tape after each drop using the 20 ma SAIL loop. No data has been lost due to this use of "volatile" memory. The details of the instrument and the principles of operation are discussed by Spain, Dorson and Rossby (1981).

10-1-82 > The field program is designed to span two complete years. There are many scientific questions that motivate this effort. These include the determination of total mass transport, and the variations in mass and heat transport particularly with regard to the annual cycle. This will include a reexamination and redefinition of the corresponding integrals. We also expect to obtain rather accurate statistics on the mean and eddy kinetic energies in natural coordinates rather than geographical coordinates. Comparing the two should be instructive. Other objectives include a study of the local

dynamics(lateral/vertical structure of the vorticity field Reynolds stresses and their role). We also hope to determine what coupling, if any, there exists between the baroclinic and barotropic (deep) components of motion. This is of interest for its own sake and for any reexamination of the many hydrographic sections that have been taken in the past.

While we have only conducted very preliminary analyses of the uncorrected data thus far, there are several observations we would like to call attention to.

1) The total transport by the Stream between the surface and 2000 meters is 78 ± 11 Sv (based on six complete sections, to which the standard deviation refers). The typical width of the Stream (i.e. where the vertically averaged downstream velocity is 0 or < 10 cm/sec) is about 130 km. Numerically this is identical to Worthington's (1976) reanalysis of 30 hydrographic sections in this general area for which he assumed a level of no motion at 2000 meters. Our data, on the other hand, indicate a mean downstream velocity of 4-5 cm/sec at 2000 m. This would add 10-14 Sverdrups to his estimate. The reasons for this discrepancy are now being examined more closely.

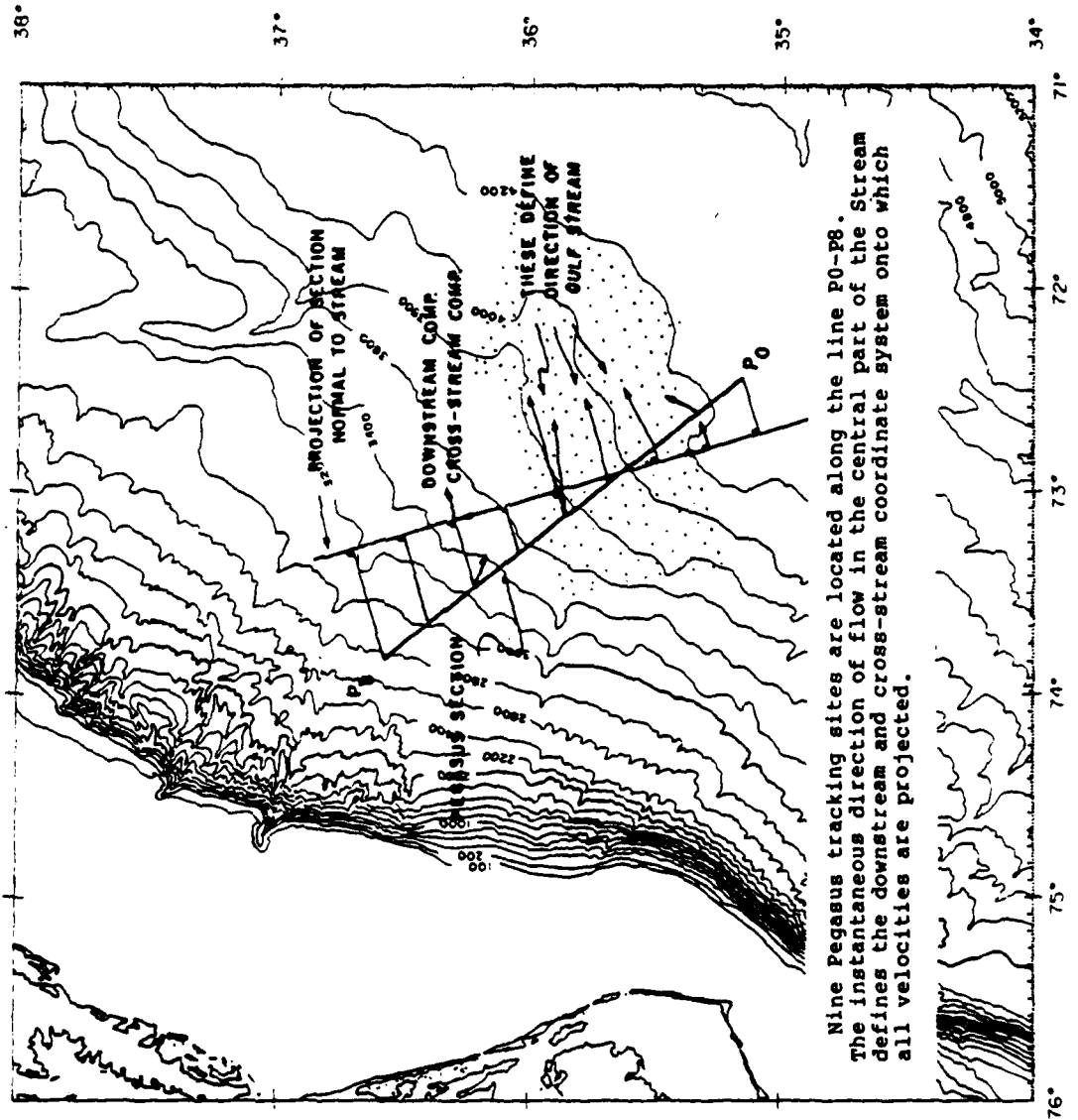
2) The Pegasus section is located in an area of evident entrainment from both the Sargasso Sea and the Slope Waters, with about twice as much being supplied by the latter. The

total inflow is equivalent to 20 Sv/100km. One should probably not attach too much numerical significance to this result until the entire data set has been collected and analyzed.

3) The velocity structure varies substantially from one section to another. This is, of course, expected since it is a derivative of the smoother density field. We have also, on several occasions, observed what appears to be discrete eddies embedded within and advected by the Stream.

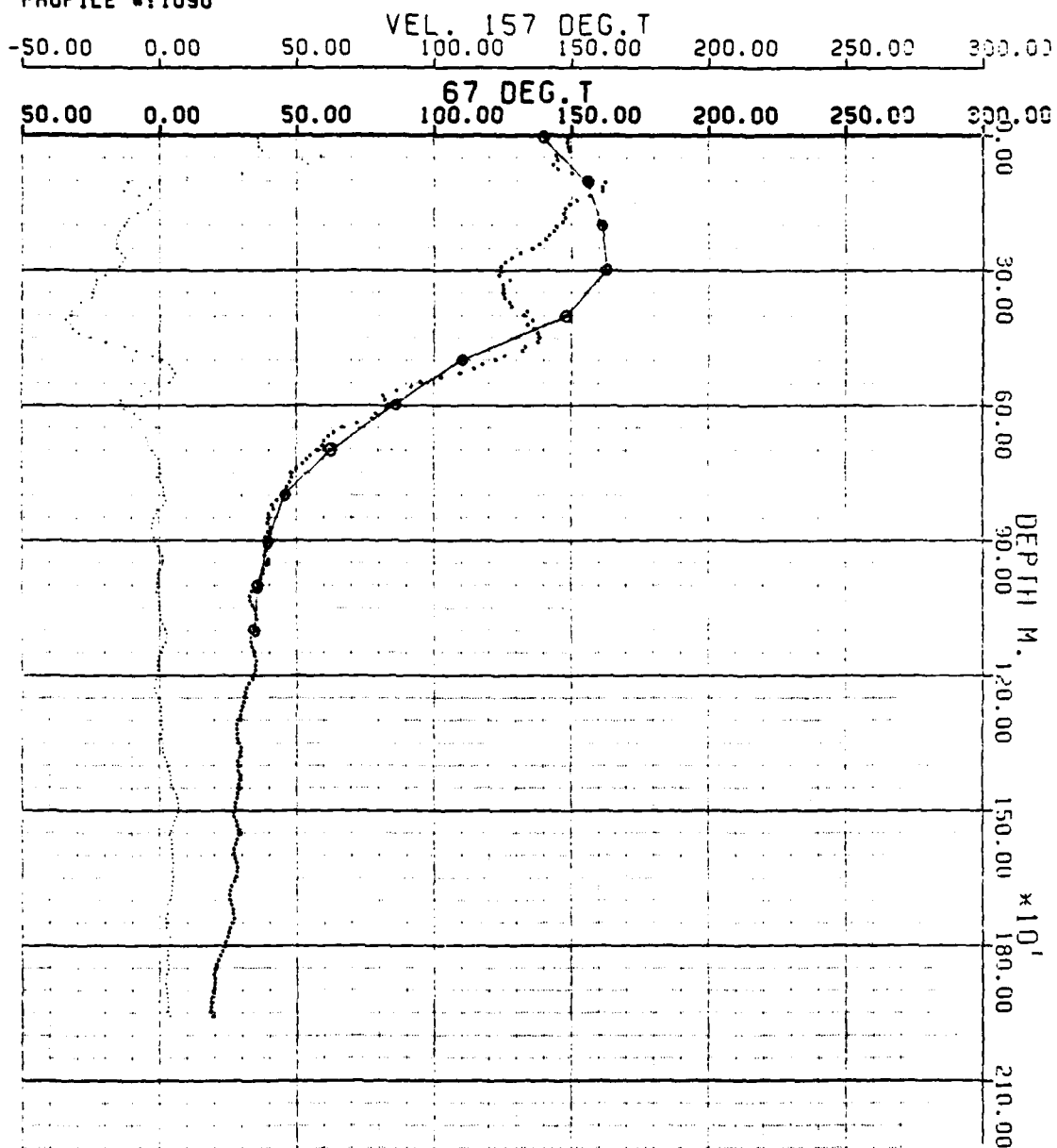
4) At 2000 meters, besides a weak path coherent velocity component of about 6 cm/sec, there is an isotropic(?) eddy field of the order of 5 cm/sec. This is remarkable, for it is about the same as that observed in the Polymode Local Dynamics Experiment (LDE) some 600 km to the southeast. We tentatively attribute these low kinetic energy levels to the small meandering envelope just east of Cape Hatteras.

The following figures and their commentary illustrate the nature of the information being collected.

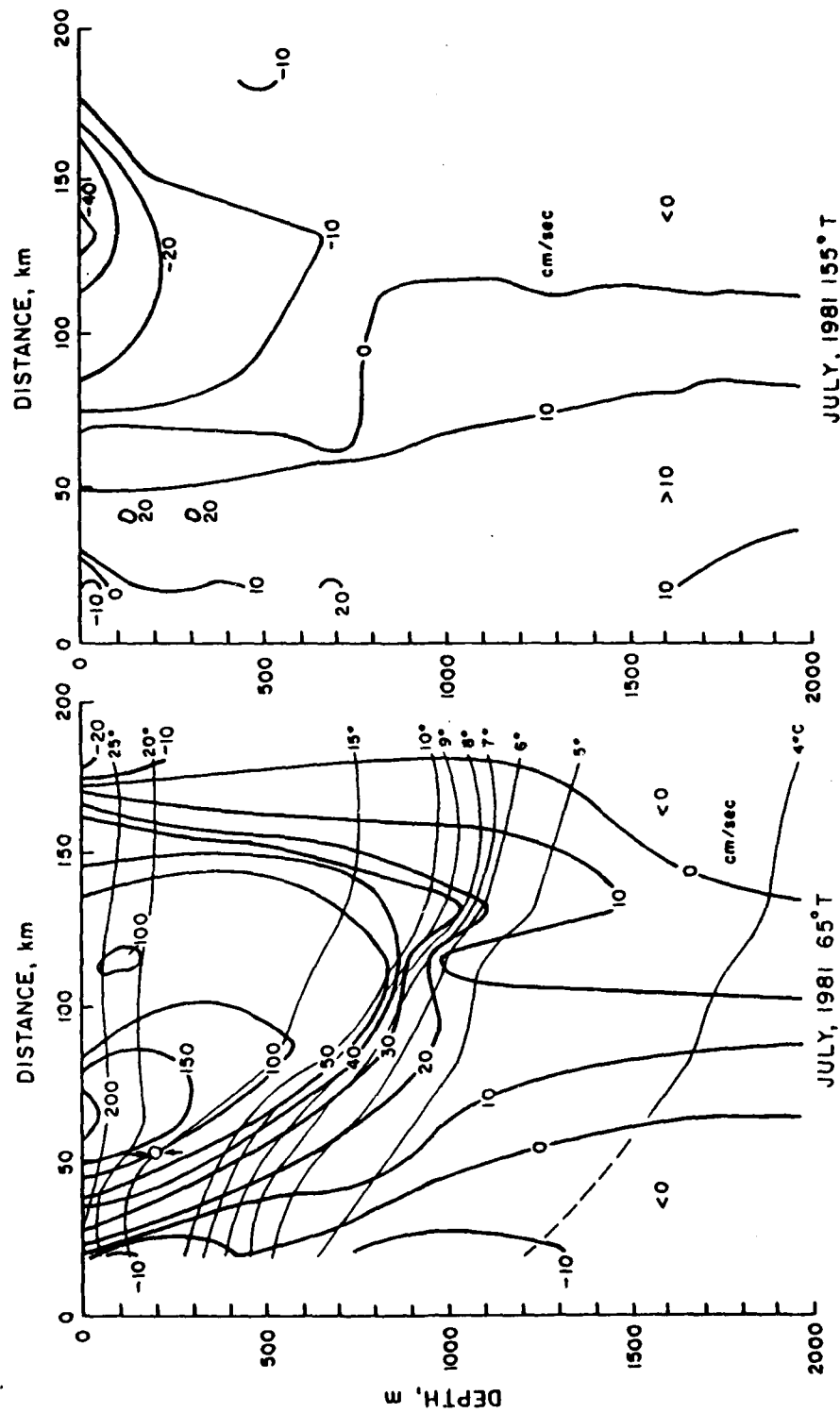


PEGASUS-G.S.MR.82#

PROFILE #:109U



A typical velocity profile from the center of the Stream with the downstream component shown in heavy dots. The circled solid line is a geostrophic velocity profile computed from two hydrocasts taken about 5 NM to either side of the Pegasus station.



This shows a typical section across the Stream with the downstream and cross-stream components contoured on the left and right panels respectively. Note that by the coordinate system used here the cross-stream component must show a region of zero motion near the center of the Stream.

VARIABILITY OF THE FLORIDA AND ANTILLES CURRENT

Friedrich Schott, Division of Meteorology and Physical Oceanography
Rosenstiel School of Marine and Atmospheric Science
University of Miami
Miami, Florida 33149

ABSTRACT

An experiment to measure low-frequency fluctuations of the Florida Current transport with several methods is described and the design of an array of moored current meters is discussed. Some preliminary results on a year long experiment with four moored current meter stations and several hydrographic surveys in the Antilles Current regime are presented.

1. Introduction

On the average, the Florida Current transports $32 \times 10^6 \text{ m}^3/\text{s}$ northward off Miami (Richardson *et al.*, 1969). As Leetmaa *et al.* (1977) have shown, about the same amount is carried southward by the Sverdrup transport in the interior of the subtropical Atlantic. On the seasonal time scale, however, there is no such nice balance between Florida Current and Sverdrup recirculation. The seasonal cycle of the Florida Current supposedly has a maximum of about $34 \times 10^6 \text{ m}^3/\text{s}$ in June and a minimum of about $25 \times 10^6 \text{ m}^3/\text{s}$ in December (Niiler and Richardson, 1973), but the anticyclonic wind stress curl, zonally averaged between the Bahamas and Africa, has a maximum in winter and a minimum in summer/fall (Leetmaa and Bunker, 1977). This means that if the relation between wind stress curl and Sverdrup transport is applicable also on the seasonal time scale, the seasonal cycle of the Florida Current and interior transport would be out of phase. In that case there must be compensatory flow east of the Bahamas to make up for this imbalance, because just a net northward transport of only a few $10^6 \text{ m}^3/\text{s}$ across the latitude of Miami into the closed North Atlantic for one month would result in a sea level rise of several tens of centimeters which is not observed. Where does this compensatory flow occur?

A good candidate is the Antilles Current where high variability has been observed but which analyses of historical data do not show to carry a significant mean

transport. We carried out an experiment with moored stations and hydrographic surveys during November 1980 - November 1981 to study the Antilles Current regime over the course of a year and also its relation to wind forcing and some preliminary results are reported below.

On the seasonal curve of the Florida Current in Niller and Richardson (1973) there is a large amount of scatter superimposed. Much of it is due to fluctuations in the tidal/inertial period range, and in the period range of days to weeks which have been extensively studied; but there must also be a significant amount of interannual variability which is evident in other indicators (winds, sea level) and which could not be successfully investigated with the earlier data. In the frame of the Subtropical Atlantic Climate Studies (STACS) program an extensive effort is being made to measure and understand the current and transport variability in the Florida Straits and devise a cost-effective measurement scheme to monitor transport of mass and temperature on a long-term basis.

2. The Florida Current Experiment

2.1. Variability of the Florida Current

Measurements of the seasonal cycle of the Florida Current of order $\pm 3 \times 10^6 \text{ m}^3/\text{s}$ and the yet unknown superimposed interannual variability, are difficult due to the very energetic higher frequency fluctuations. Variability studies by many investigators in the '60's to mid-70's in the Florida Current with moored stations and the dropsonde technique have revealed much on the fluctuations of currents and transports on the short-time scales. These studies attribute approximately 10-20% of the total variance to the tidal/inertial fluctuations (e.g. Schmitz and Richardson, 1968; Kielman and Düing, 1974; Brooks, 1979). Both diurnal components (K_1, O_1) and M_2 produce transport fluctuations of $\pm 3-4 \times 10^6 \text{ m}^3/\text{s}$ each. By adding up in phase at a particular time they can cause a big distortion of a transport measurement at that time.

Another energetic band, found by these and other investigators (e.g. Wunsch and

Wimbush, 1977; Düing et al., 1977), are fluctuations in the period range of a few days to two weeks, with maximum energy density in the 8-12 day period range. They seem to contribute about 20-30% of the total variance.

The problems with the earlier work on the low-frequency variability is that dropsonde transport values which took many hours to do, were aliased by the tides and that moored current meters were only deployed near the bottom at the boundary (Düing et al., 1977) because of the then less advanced mooring technology. Since the mean current is baroclinic and the fluctuations appear to be dominantly barotropic (Schott and Düing, 1976) near-bottom measurements would over-emphasize the contribution of the low-frequency fluctuations to the variance.

The first aim of the Florida Current Experiment is an "overkill" approach to the tidal and several day period fluctuations with a multitude of overlapping measurement methods in order to find out what the crucial measurements really are and to better understand the physics of the several-day period variability.

2.2. Experimental Setup

The site of the experiment selected was the location of the submarine cable, running across the Straits from Jupiter inlet to Settlement Point (Fig. 1). The program consists of the following components (with p.i.'s and their affiliations in parenthesis):

- five current meter moorings (146-150, Fig. 1) discussed in more detail in the following (F. Schott, T. Lee (U. of Miami))
- PEGASUS profiling at eight stations (1-8, Fig. 1) and shipboard profiling with an Aanderaa Profiler at the westernmost shallow station (PCM, Fig. 1). Intentions are for two-week long surveys, preferably with two ships simultaneously, at about three-monthly intervals (R. Molinari (NOAA), K. Leaman (U. of Miami))
- pressure difference measurements with bottom recorders across the Straits

- cable induction measurements (J. Larssen (U. of Washington))
- CODAR measurements over the western side of the Straits (R. Lyons/NOAA)
- shipboard velocity profiling with Ametek-Straza acoustic shiplog (F. Schott (U. of Miami), R. Molinari/ D. Bittermann (NOAA))
- at a later stage (1983), reciprocal acoustic transmission is expected to also be applied for velocity measurements (H. deFerrari (U. of Miami))

The overlap of these different methods will allow better than previously, regressions between the physically interesting quantities and the various parameters measured.

2.3. Moored Current Measurements

a) Results of a test mooring, November 1981

As preparation for the array, a test mooring was deployed for 2 weeks in November 1980, at site 145 (Fig. 1) off Miami at a water depth of 730 m. The configuration is shown in Fig. 2. The top instrument, a Niskin Wing Current Meter (NWCM) was located at 210 m (nominal) depth, at 310 m there was an Aanderaa instrument and right under it a second NWCM for intercomparison. At that depth there was also a tilt-meter, simply made from an older film recording NWCM firmly attached to the wire. Another Aanderaa current meter was located at 560 m depth. Fairing was used on the upper 200 m of wire to reduce drag and mooring tilt.

Profiles for time periods of high currents and low currents are shown in Fig. 3a, together with a profile for that position taken from the mean section of Niiler and Richardspn's (1973) dropsonde data for the winter situation, which fits right into our measurements.

An important part part of the test mooring study was to evaluate our mooring design program (based on the WHOI version) which describes mooring response to

given vertical profiles of horizontal currents and to determine the effect of fairings used on the top 200 m of wire.

Mooring behavior was calculated for the current profiles displayed in Fig. 3a. The depth increase at the 310 m level due to mooring tilt as predicted by the mooring program is shown versus the measured depth increase in Fig. 3b. The results are shown for two assumptions: first, that the drag on the top 200 m wire is not reduced by the use of fairings, i.e. choosing a drag coefficient for wire ($c_D=1.3$); and second, for a drag coefficient for fairings on the top 200 m ($c_D=0.4$).

Inspection of Fig. 3b shows that the observed depth increase is best represented by the case with no fairings and that with a reduced drag as given by the use of fairings the program shows too small a depth increase. This indicates that either the estimate of drag on the upper flotation used in the mooring program was too small or that the effective drag on the wire was higher than the static value due to stropping effects; the first option is rather unlikely.

A possible error source is the coarse vertical resolution of the current profile with no data below 560 m. We found, however, that it does not make much difference in the mooring program results how we extrapolate the current profile to the bottom below 560 m because the important drag is on the top.

The drag coefficient problem will be looked at more closely when we get more data back from the first array. At least, what we can tell from the test mooring behavior for the planned array, is that similar moorings equipped with fairings at the top should not lean over more than predicted by the program when applying the higher drag coefficient (for wire) to the top section covered by fairings.

b) Array Design

The location of the current meter array is shown in Fig. 1. It will be

positioned close to the existing submarine cable for transport intercomparisons. We use 25 current meters in five moorings. The velocity section by Richardson et al. (1969) at $27^{\circ}26'N$, i.e. about 50 km north of the proposed array site is shown in Fig. 4. A distribution of the five moorings across the current is also shown in Fig. 4. If transport calculations were the sole purpose of the study then we would use an array of moorings along a line across the Straits. However, we also want to obtain information on the propagation of eddy wave patterns. Therefore, we chose a saw-toothed shaped array. This configuration forms 3 triangles located on the eastern and western halves of the Straits and in the middle. The upstream distance of moorings 147 and 149 from a line of the northern three moorings is 20 km, which will allow phase propagation calculations on the energetic time scales. If averaged over a several day period fluctuations the currents at 147 and 149 can be projected into the line of the three northern moorings for calculation of mean transport sections.

Using the test mooring results to predict the mooring inclinations from the current distribution of Fig. 4 suggests that current meters can be positioned 50 m below the surface at mooring 146 with reasonable mooring tilt and that no problems should arise at the two eastern moorings, 149 and 150. However, if the moorings were extended to 100 m at the central positions near the current core the inclinations at mid depth would be too large for the Aanderaa meters ($\sim 30^{\circ}$). Also the vertical excursions of instruments with changing currents would be large because at times of low currents and small inclinations the top of the mooring would come very close to the surface in that case. If the top instruments are kept at 150 m at 147 and 200 m at 148 the inclinations do not exceed 20° which is acceptable for Aanderaa current meters.

It may be possible to further reduce mooring drag and measure closer to the surface under the current core by using torpedo shaped flotation instead of the

27" and 37" steel spheres shown in Fig. 2. However the floats are usually made from foam and experience has shown that besides being very expensive, they tend to soak up water in long term deployments and lose buoyancy. Therefore, we decided to continue with the more reliable spherical floats for the time being.

The vertical distribution of instruments on the current meter moorings is drawn in Fig. 4. We estimate that this distribution of moorings and instruments will cover approximately 55% of the total mean transport. The crowding of isotachs in Fig. 4 on the western side of the Straits suggests that higher instrument density should be used, whereas the low vertical shear on the eastern side could allow less vertical resolution. This would result in moorings with instruments located at different depth levels. But the calculation of energy flux terms requires the determination of horizontal gradients, i.e. would call for instruments to be positioned at constant levels across the stream. Horizontal directional spectral calculations have the same requirement. Furthermore, on shorter time periods, the velocity distribution is not as smooth as in Fig. 4 and even on the eastern side better resolution may be required for the study of fluctuations.

Therefore, we decided on a constant level instrumentation distribution with the Niskin Wing Current Meters (NWCN's) in the high speed areas (because of the danger of rotor losses there for Aanderaa instruments) and Aanderaas in the lower part. Pressure recordings at the top positions are obtained by a temperature pressure recorder (TP) because NWCN's are not equipped with pressure recorders.

c) Planned Deployments

The deployment of the first array is April-June 1982¹. The next three deployments are planned for six months duration each. Based on the results of the first array(s), the spacing of moorings might be changed in the subsequent arrays when

1. Note added later:

This array was successfully retrieved on 10 June and found to have performed very well.

the need arises to focus on a particular process besides continuing to measure the low-frequency transport changes.

2.4. Data Evaluation

At first, much of the data analysis will focus on the more technical issue of understanding what exactly the different methods measure and how that is related to the transport of mass and heat.

a) Tidal Predictability

First priority of the analysis from the moored station data is the predictability of the tidal components. Historical data suggest that about 50% of the variance is deterministic. This would permit partial detiding of spot measurements like Ametek-Straza and PEGASUS velocity sections.

b) Transport Prediction by Moored Array

The fraction of the transport covered by the moored array is about 55%. Regressions with complete sections obtained from PEGASUS profiles (and, if it would turn out to be an operational tool, from Ametek sections combined with moored current measurements at depth) will be carried out to determine how well the array can be used to predict the total transport and what the contribution of array components is to the prediction. These results will then be used to improve the design of later moored arrays.

c) Pressure Differences

If geostrophy applies across the Straits, sea level or near surface pressure differences would yield mean surface currents, and the question is how well these are correlated with transports. Evaluation of the data of Schmitz and Richardson (1968) shows a rather low correlation between mean surface speeds and transports on their sections.

d) Cable Data

Variability of cable inductions can be caused by meandering of a stream of

constant transport over varying topography. On a longer-term basis the moored station data should be usable to determine the meandering and after tackling question b) might be used to calibrate the low frequency fluctuations in the cable data. Hopefully, CODAR might be developed into an observational tool to monitor the position of the axis of the Stream later. Repeated sections with the PEGASUS profiler obviously are needed initially to find out what cable data really mean in terms of transport.

e) Processing of Low-frequency fluctuations

This work will first concentrate on the kinematics and dynamics of the fluctuations in the period range of days to weeks. An earlier study of barotropic and baroclinic energy fluxes of Brooks and Niiler (1977) was based on about 45 drop-sounde sections off Miami and there most likely is significant aliasing of these data by non-predictable components of the tides and other high-frequency noise. With the moored station data, we can establish better significance of such calculations. Also, the array pattern will allow better determination of wave parameters across the width of the Straits than possible with the earlier data (e.g. Schott and Düing, 1976).

The real issue, however, is the analysis of the very low-frequency variability of seasonal and interannual time scale. In addition to starting to collect the relevant observations ourselves we hope that the intercomparison of methods may allow reinterpretation of historical data, e.g. sea level, cable measurements.

3. The Antilles Current Experiment 1990/81

3.1 Moored Current Measurements

In early November 1980 four current meter moorings were deployed east of the Bahamas (Fig. 5) and retrieved after one year. Current meters were located at six depth levels ranging from 200-3000 m, and at three additional levels in the top part we had temperature recorders.

Time series of current vectors (stick plots) at the 400 m level are shown in Fig. 6. The time series are low-passed with a 30 h Lanczos filter to remove tidal, inertial and other high-frequency fluctuations. Obviously, the currents are dominated by eddies and a significant mean current does not exist over the year or over a season.

Despite the large variability, the mean current vectors for the one year long records, which are shown (Fig. 5) for the four positions and different depth levels show an organized large scale pattern:

- The mean flow along the boundary (stations 126, 127) is to the northwest in the top 1000 m with a southeastward countercurrent underneath. Taking the width of the boundary current as 150 km and the mean current over the top 1000 m from the data as 2.5 cm/s would yield a mean transport of $4 \times 10^6 \text{ m}^3/\text{s}$.
- Further offshore, at 125, the flow is northward and towards the boundary suggesting the feeding of the boundary current from the interior.
- At the northern station, 128, the strongest mean currents occur and they are oriented toward the boundary.
- There is no drastic change in this picture if one compares means over 6 months of summer or winter; especially, there is a net northward component at stations 126, 127 in both seasons and no reversal of boundary flow.

The westward current at 128 might be explained by dynamic topographies from historical data, e.g. Stommel *et al.* (1978), shown in Fig. 7, and from our own hydrographic measurements. There is a narrow high in the topography (Fig. 7) along the northern Antilles around which the Gulf Stream recirculation returns northward. The moored station, 128, could have been located in the southern margin of that return flow.

Our own hydrographic data from October/November 1980 also show an eddy off Abaco just north of Station 128. A similar observation was made by Gunn and Watts (1982). Also the inverse calculations of Wunsch and Grant (1982) for the case with the initial reference level at 2,000 m show an intensive recirculation cell, again with onshore flow at about the position of that northern moored station.

Is the northward mean after the year at stations 126, 127 representative for the overall mean? One would then expect a wedge of high-saline subtropical under-water just beneath the surface-mixed layer, extending along the boundary, which is not observed. Also a net mean northward transport east of the island arc would contradict the balance found by Leetmaa *et al.* (1977) between the mean Florida Current transport and the Sverdrup transport. That suggests the conclusion that for the boundary flow we have again only captured a transient stage of interannual variability over that year.

3.2. Low-frequency Fluctuations and Wind Forcing

The vertical distributions of the eddy kinetic energies (EKE) at the four stations over the one year time period is shown in Fig. 8. As already obvious from Fig. 6 the highest variance occurs at Station 128. It is interesting to note that the minimum EKE is recorded at the 1000 m level which also seemed to be a level of minimum mean currents. For comparison the EKE data from MODE at 500 m, and 1000 m (Richman *et al.*, 1978) have been added and also those from a 445 day long record at 69°30'N, 31°W (Owen *et al.*, 1982).

EKE's at 500 m and 1000 m at all stations are significantly higher than in the MODE region, and on the average, they are also higher than in the LDE area. A large amount of the current variance is situated in the period range of 2-3 months. It is interesting to note that there is also energy in that frequency band in the wind field.

We used twice-daily wind fields from the NOAA/Atoll Service with a 150 km

grid point distance and calculated stresses using a constant drag coefficient. There is a strong energy maximum in the zonal stress component at about 2 months period (fig. 9a). Coherence between currents and the stress time series are significant in that period range for instruments in moorings near the boundary, suggesting barotropic local response at the topography; but remote effects have also to be investigated because of the large zonal coherence scale of the zonal wind stress (Fig. 9b).

4. Concluding Remarks

The interest in North Atlantic circulation studies is shifting towards gyre scale variability. One of the most prominent indices of such variability are Florida Straits transports. We are working towards establishing those. However, other measurements must be carried out to understand the physics of Florida Straits transport variations, i.e. their significance for what goes on in the interior. Some national and international programs over the next few years focus on the Gulf Stream and the North Atlantic Current but except for the meridional ship sections planned along 20, 35 and 50°W, there is no organized effort planned to monitor the variability across the subtropical North Atlantic gyre.

The first steps should be institution of a ship-of-opportunity XBT program and installation of additional tide gauges. An efficient future monitoring tool for integral changes of the baroclinic structure and, through reciprocal transmission, also of the vorticity balance could be a large-scale tomography array (Munk and Wunsch, 1982) in the subtropical Atlantic.

Sensitivity studies with numerical models, especially using realistic topography in the west have to be carried out, applying various wind field cases.

Acknowledgements

The Antilles Current field work was carried out jointly with K. Leaman and D. Olson, the Florida Straits moored array work is a cooperative effort with

T. Lee (all of RSMAS/MPO). We appreciate the contribution of P. Bedard and the MPO technical group to the moored station work. Financial support by the Office of Naval Research under contract N-00014-80-C-0042 and by the National Oceanic and Atmospheric Administration under contract NA81RC00138 is gratefully acknowledged.

References

- Brooks, I.H., 1979: Fluctuations in the transport of the Florida Current at periods between tidal and two weeks. J. Phys. Oceanogr., 9, 1048-1053.
- Brooks, I.H. and P. P. Niiler, 1977: Energetics of the Florida Current. J. Mar. Res., 35, 162-191.
- Düing, W., C. N. K. Mooers and T. Lee, 1977: Low frequency variability in the Florida Current and relations to atmospheric forcing from 1972 to 1974. J. Mar. Res., 35, 129-161.
- Gunn, J. T. and D. R. Watts, 1982: On the currents and water masses north of the Antilles/Bahamas arc. J. Mar. Res., 40, 1-18.
- Kielman, J. and W. Düing, 1974: Tidal and sub-inertial fluctuations in the Florida Current. J. Phys. Oceanogr., 4, 227-236.
- Leetmaa, A., P. P. Niiler and H. Stommel, 1977: Does the Sverdrup relation account for the mid-Atlantic Circulation. J. Mar. Res., 35, 1-10.
- Leetmaa, A. and A. F. Bunker, 1978: Updated charts of the mean annual wind stress, convergences in the Ekman layer and Sverdrup transports in the North Atlantic. J. Mar. Res., 36, 311-322.
- Mooers, C. N. K., and D. A. Brooks, 1977: Fluctuations in the Florida Current, summer 1970. Deep-Sea Res., 24, 399-425.
- Munk, W. and C. Wunsch, 1982: Ocean acoustic tomography: large scale climatic measurements and modelling. Ocean Modelling, 42 (unpublished manuscript).

- Niiler, P. P. and W. S. Richardson, 1973: Seasonal variability of the Florida Current. J. Mar. Res., 31, 144-167.
- Owen, W. B., J. R. Luyten and H. L. Bryden, 1982: Moored velocity measurements at the edge of the Gulf Stream. J. Mar. Res., 40 (suppl.), 509-524.
- Richardson, W. S., W. J. Schmitz, Jr., and P. P. Niiler, 1969: The velocity structure of the Florida current from the Straits of Florida to Cape Fear. Deep-Sea Res., 16 (suppl.), 225-231.
- Rickman, J. G., C. Wunsch and N. G. Hogg, 1977: Space and time scales of meso-scale motion in the western North Atlantic. Rev. Geophys. and Space Phys., 15, 385-420.
- Sanford, T. B., 1982: Temperature transport and motional induction in the Florida Current. J. Mar. Res., 40 (suppl.), 621-639.
- Schmitz, W. J. Jr. and W. S. Richardson, 1968: On the transport of the Florida Current. Deep-Sea Res., 15, 679-693.
- Schott, F. and W. Düing, 1976: Continental shelf waves in the Florida Straits. J. Phys. Oceanogr., 6, 451-460.
- Wunsch, C. and M. Wimbush, 1977: Simultaneous pressure, velocity and temperature measurements in the Florida Straits. J. Mar. Res., 35, 75-104.
- Wunsch, C. and B. Grant, 1982: Towards the general circulation of the North Atlantic Ocean. Progress in Oceanography, 11, 1-59.

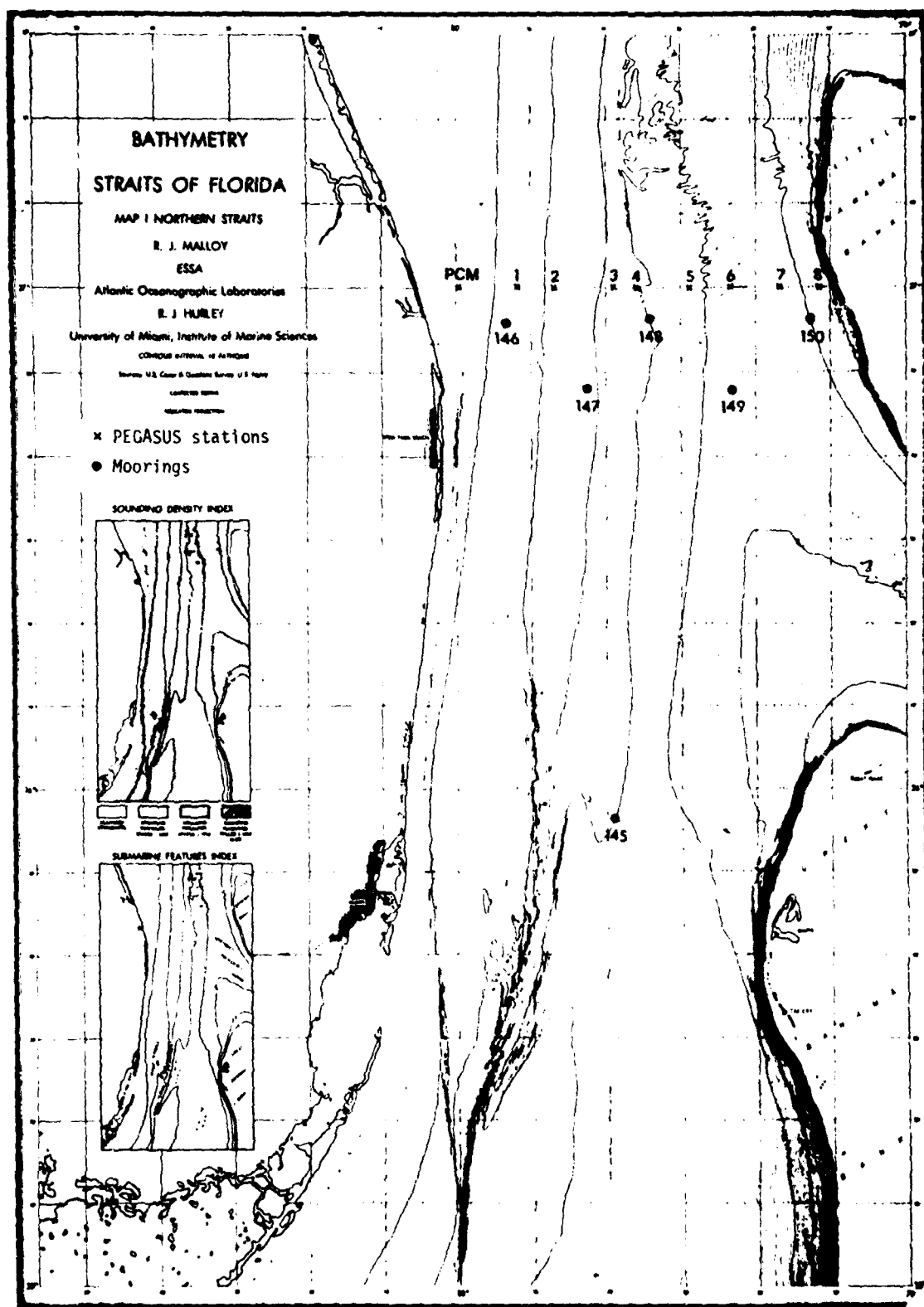


Fig. 1. Positions of the test mooring (145, deployed 23 Oct.-7 Nov., 1980) of moored array (146-150) and PEGASUS dropsites (1-8).

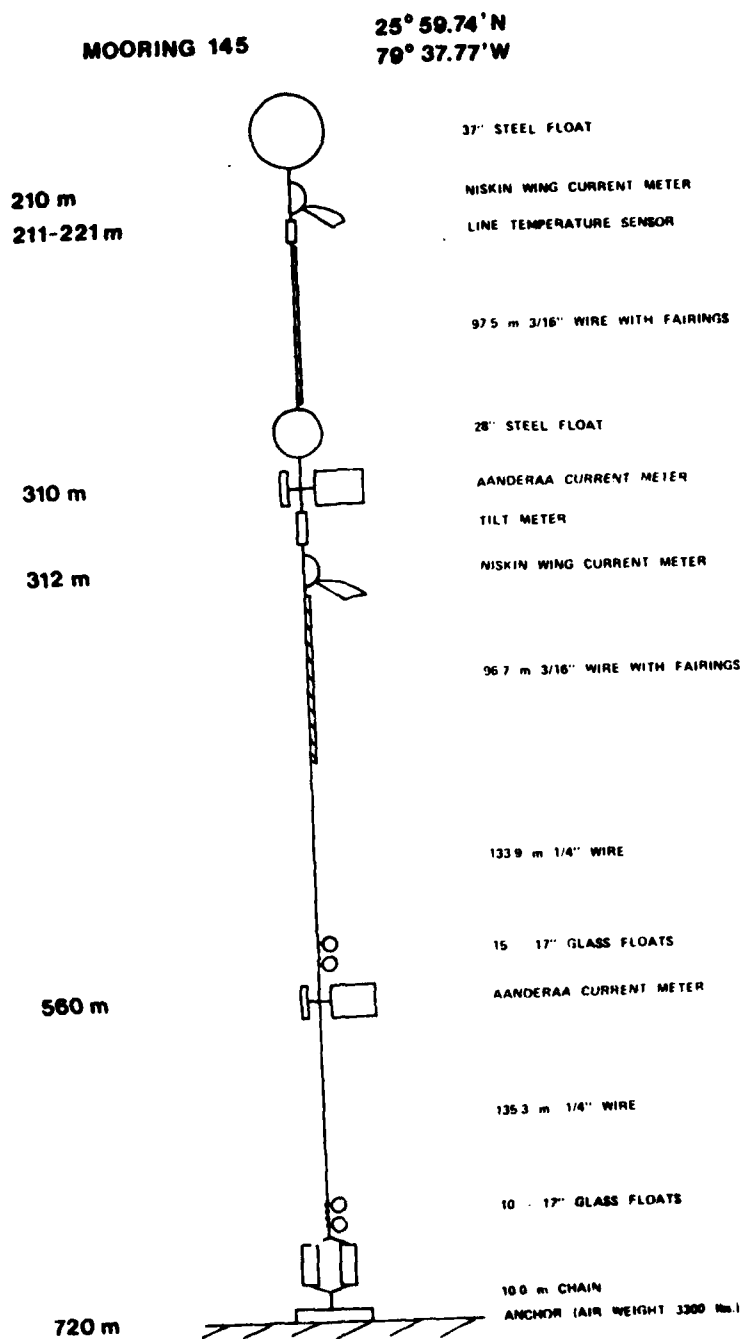


Fig. 2. Florida Current test mooring

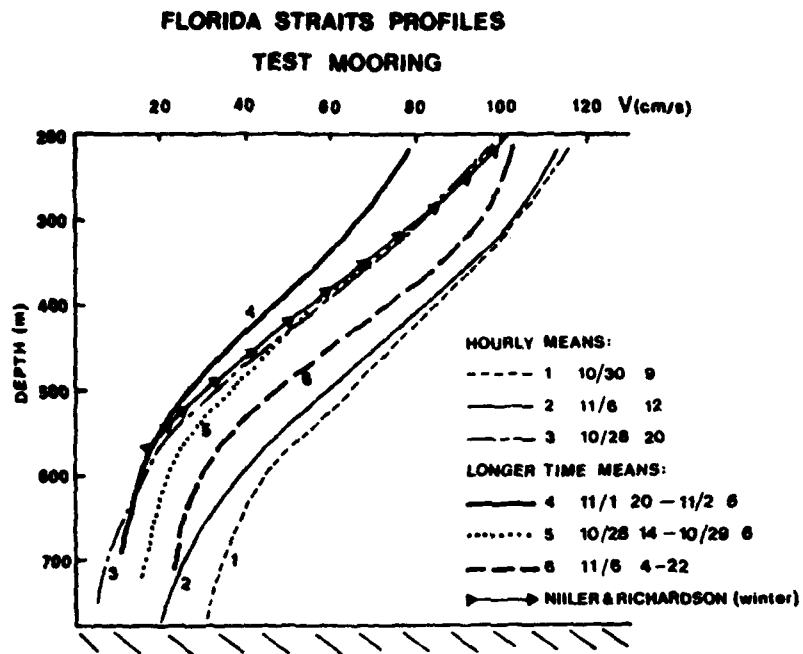


Fig. 3a. Vertical profiles of the downstream velocity components from the Florida Current test mooring averaged over hourly and longer periods.

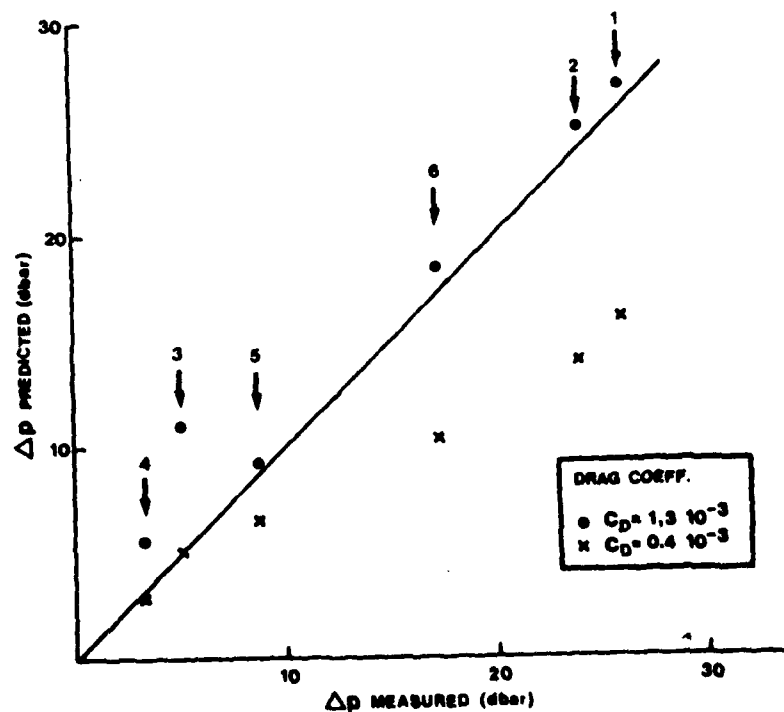


Fig. 3b. Pressure at the 310 m level in test mooring; measured vs predicted by mooring program, for profiles of Fig. 3a and two drag coefficients

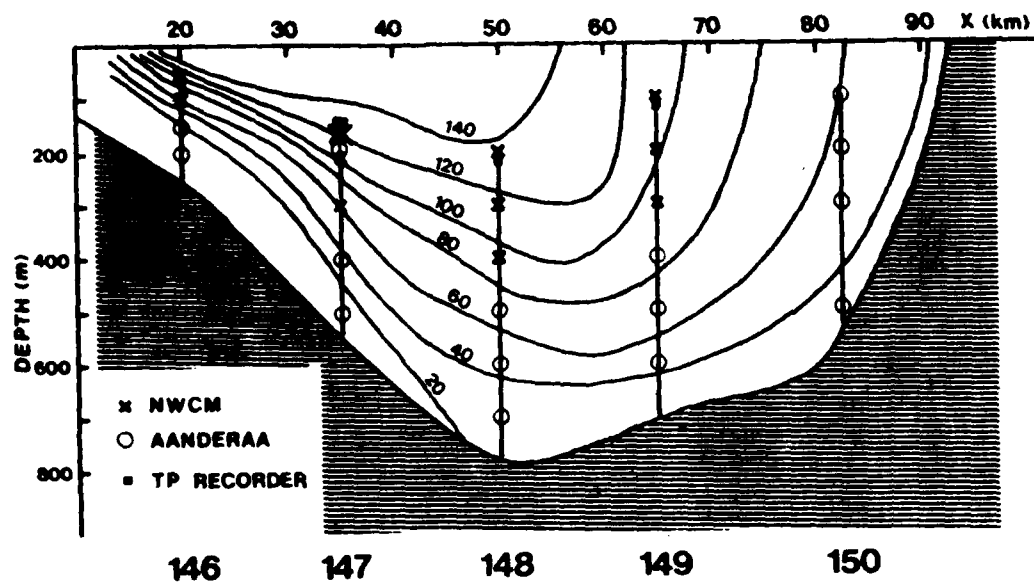


Fig. 4. Instrument position in moorings 146-150 (see Fig. 1) on mean velocity scheme at $27^{\circ}26'N$ (from Richardson *et al.*, 1969).

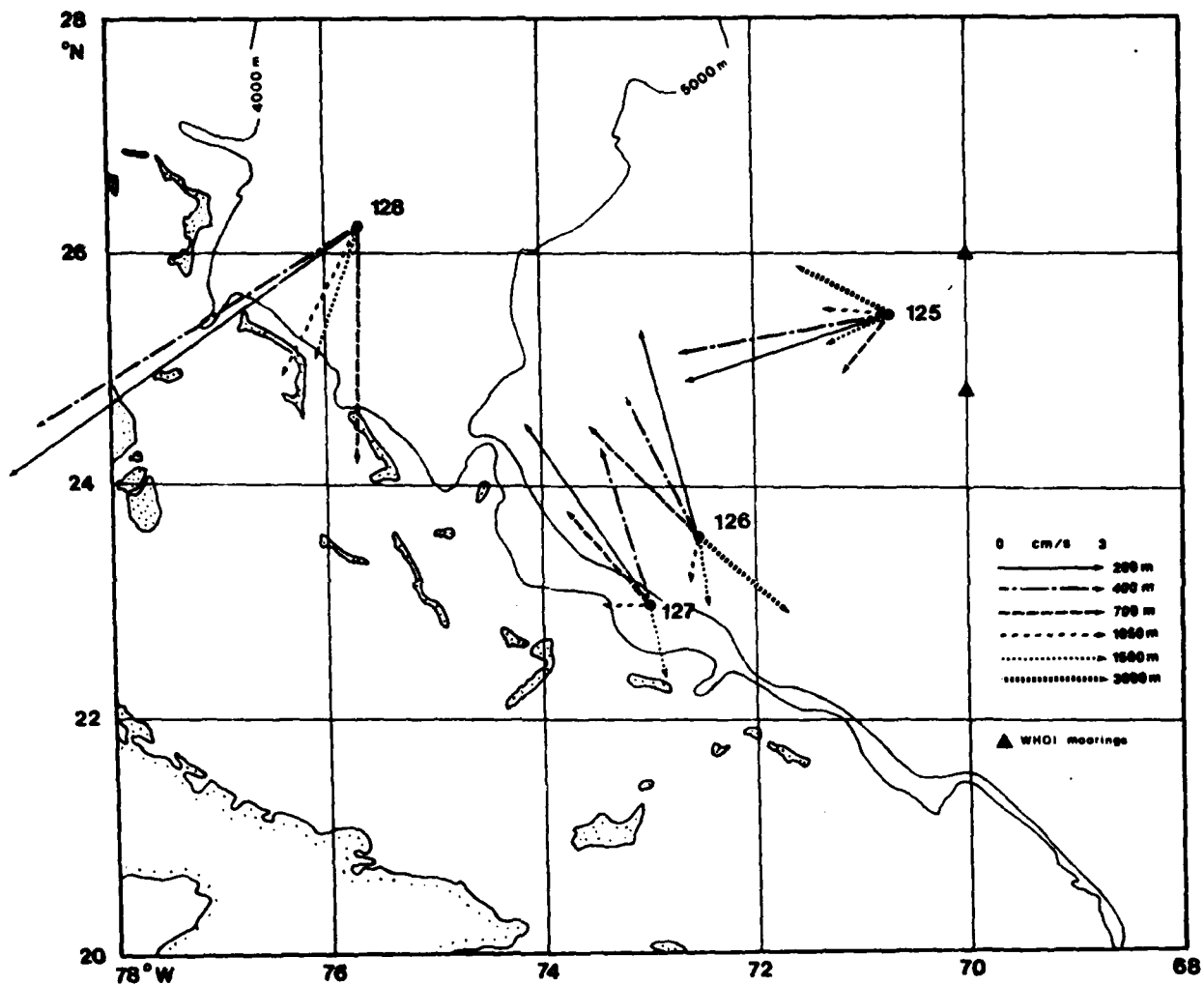


Fig. 5 Positions of moorings 125-128 and mean currents of one-year long record at various depths. Also included are positions of two WHOI moorings which were out from February-August 1981 for the Local Tomography Experiment (LTE).

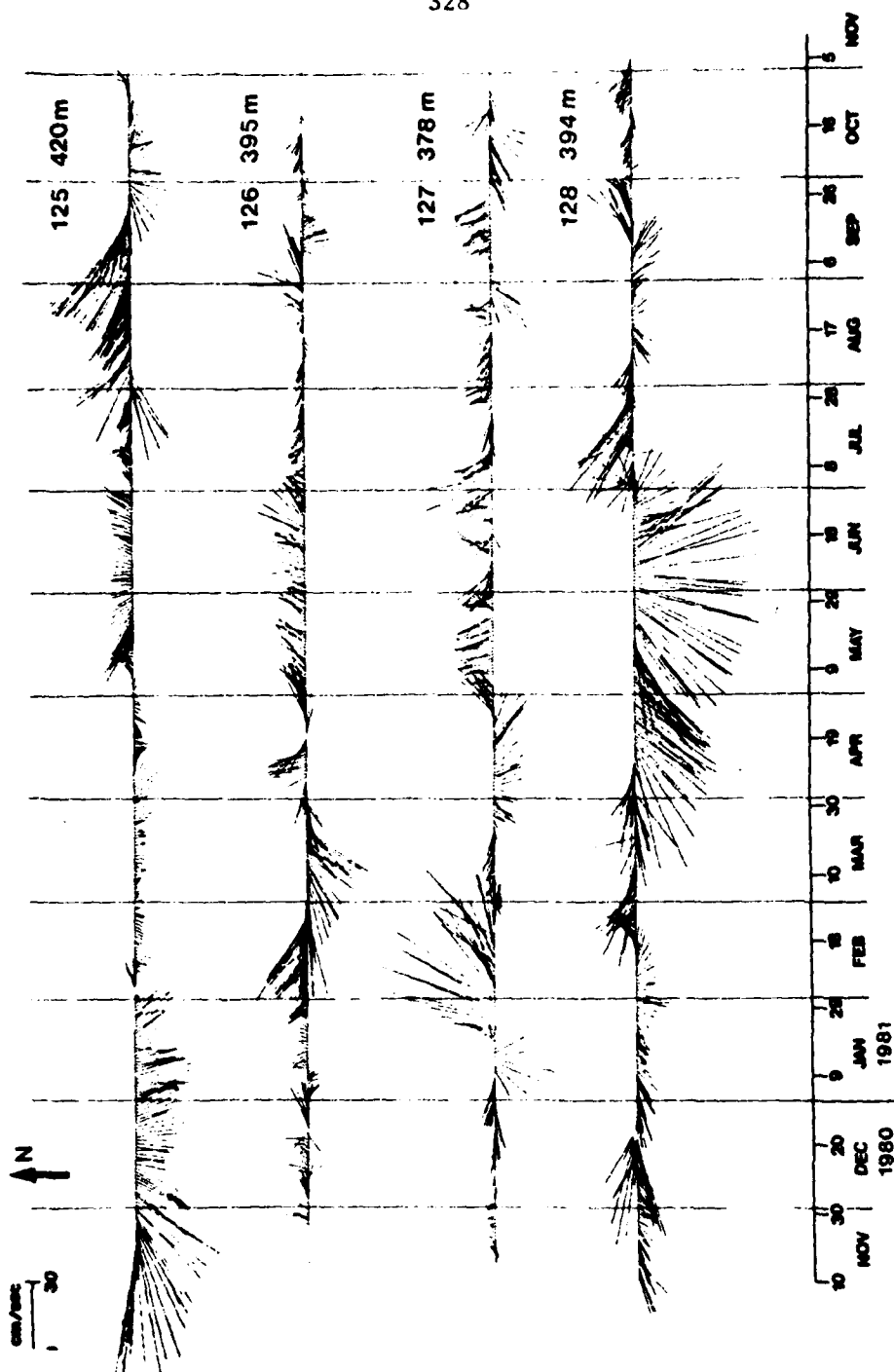


Fig. 6 Low-passed (periods <30 hours removed) current vector time series ("stick plots") at 400 m level at stations 125-128.



Fig. 7. Dynamic topography of 100 dbar rel to 1500 dbar (dyn. mm.), from Stommel et al. (1978).

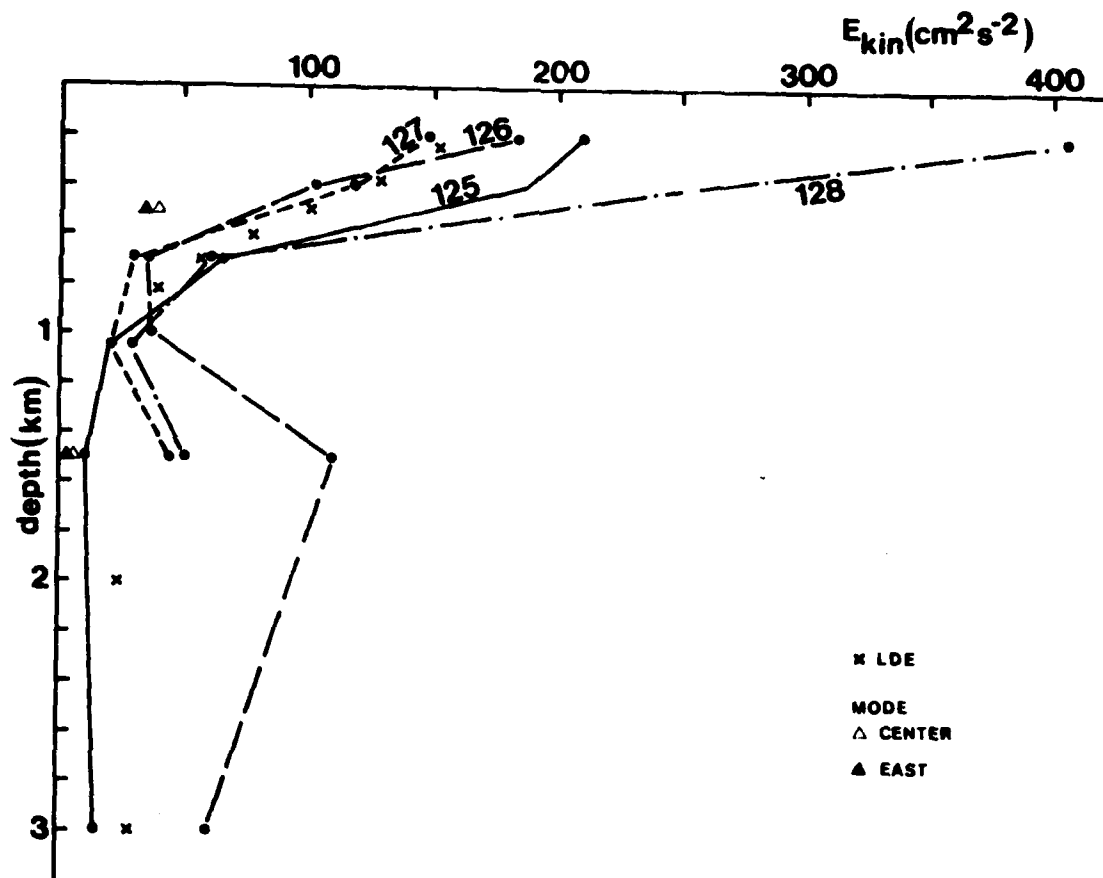


Fig. 8. Eddy kinetic energies, $\frac{1}{2}(\overline{u'^2} + \overline{v'^2})$ for year long records at stations 125-128. Also shown are EKE's from MODE-CENTER, MODE-EAST and a mooring in the Local Dynamics Experiment (LDE).

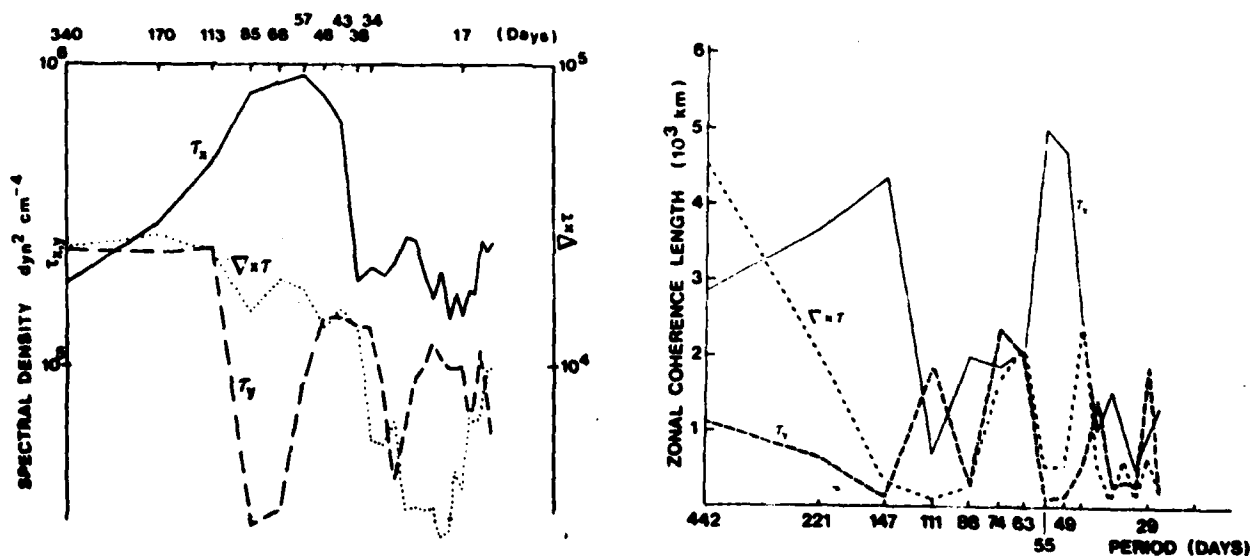


Fig. 9. Wind stress components and curl
a) energy spectra over Antilles Current area
b) zonal coherence scales

Synoptic Measurements of Sea Surface Temperatures in the Gulf Stream Frontal Zone Between Savannah, GA and Cape Hatteras, NC

Cynthia M. Seay
JAYCOR

205 South Whiting Street, Alexandria, VA 22304

In 1979, an observational study of meanders along the western edge of the Gulf Stream was conducted between Savannah, GA and Cape Hatteras, NC. This research, a portion of the Gulf Stream Meanders Experiment, was designed to investigate the structure, movement and evolution of mesoscale fluctuations in this region of the Stream. Figure 1 is an infrared satellite image of the Gulf Stream as it flowed along the eastern United States coast on 8 April 1977. Darker shadings indicate areas of higher sea surface temperatures (SST's) such as the Gulf Stream while lighter shadings indicate regions of colder coastal waters. Although cloud-free satellite data was unavailable during our study, many of the patterns seen here are quite similar to those we observed. These include (a) the seaward deflection of the Gulf Stream at 32°N and (b) large-amplitude meanders downstream of the deflection. Characteristic of these meanders are wavelengths of ≈ 200 km, downstream phase speeds of ≈ 35 km day $^{-1}$, and amplitudes of 40 to 80 km.

A series of eight aerial surveys was made in February 1979 which covered the Gulf Stream frontal zone between Savannah, GA and Cape Hatteras, NC as shown in Figure 2. The positions of four moored arrays of thermistors and current meters which recorded measurements at this time are also shown. During each flight measurements of subsurface temperatures were made with air-deployed, expendable bathythermographs (AXBT's) at 12.5 km intervals along a transect. Continuous measurements of SST were recorded with a Barnes PRT-5 Precision Radiation Thermometer. At an operational altitude of 1000 feet, the PRT-5 had an accuracy of $\pm 0.5^{\circ}\text{C}$. In general, either the northern or southern half of the flight grid was covered during a single flight resulting in survey times

of 3 to 4 hours. Such rapidly obtained measurements resulted in essentially synoptic views of the surface and sub-surface temperature fields during a single survey.

In the course of our flight series, two large-amplitude meanders were recorded by the PRT in the SST field as they progressed northeastward through the study area. During our third flight on 11 February 1979, both meanders were observed in the SST in the course of a single survey (Figure 3). The meanders possessed characteristic amplitudes (≈ 80 km), wavelength (150-100 km) and phase speeds (≈ 35 km day⁻¹). (In examining these features, a meander crest is taken to be the shoreward-most position of the front while a meander trough is the seaward-most position of the Gulf Stream front.) A large meander crest (along transect C) and trough (along transect C) are surface manifestations of the northeastern-most meander while the second crest (along transect I) and trough (offshore-most surface thermal front, transect K) are associated with the southwestern-most meander seen in this survey. Evidence of a trailing filament of warm water may be seen following the NE meander crest and indications of a filament are seen behind the SE meander crest. Comparison of SST patterns and one meter AXBT temperature patterns for 11 February 1979 (Figure 4) reveal nearly identical records of the two meanders. (Dotted lines on the one meter field indicate position of AXBT drops).

Due to the strong similarity in the surface and subsurface temperature fields, it is of interest to determine what differences may exist between these two fields. The temperature at one meter as measured by AXBT minus the PRT surface temperature was determined and plotted as a function of consecutive AXBT number during a flight (Figure 5). This ΔT value was found to be approximately 1°C for the 11 February flight and indicates that in general, one meter temperature values were 1°C warmer than SST values. This result may be due to surface cooling and/or insufficient instrument calibration.

Comparison of surface temperature patterns on 11 February (Figure 3) with the 50 meter AXBT field (Figure 6) indicate a strong similarity in meander structure. This vertical coherence includes the presence of trailing filaments as well as large-amplitude meanders.

Large-amplitude meanders observed in the SST field (Figure 3) are clearly visible to a depth of 250 meters (Figure 7); indicating a strong vertical coherence in these structures. However, trailing filament patterns are no longer visible and appear to be somewhat shallow features, extending to depths of less than 50 meters. In this figure, the positions of two of the current meter arrays are denoted.

Figure 8 is a cross-stream profile of transect K from 11 February in which the inshore-most thermal front is associated with the southern-most trailing filament in the SST field (Figure 3). As can be seen, this thermal feature extends to a depth of less than 50 meters. Also, notice that the offshore-most thermal front mapped along this transect in the SST field corresponds to the main thermocline of the Gulf Stream as seen in the AXBT profile. This confirms the position of the southwestern meander trough.

Current meters moored along the 200 and 400 meter isobaths off Onslow Bay provided current velocity and temperature data simultaneous with our aerial surveys (Figure 2). Velocity and temperature records from the top current meter (at a depth of 250m) at mooring B indicate the passage of both large-amplitude meanders through the study area in early February 1979. Meander passages appear in the current meter records as simultaneous increases in downstream (V) velocity and in temperature. Figure 9 is the record of the B-TOP current meter during the January - May mooring period. The vertical lines in each record indicate days on which flight surveys were conducted. The third vertical line indicates the 11 February survey. As seen here, there was a very strong increase in downstream velocity (V) and in temperature indicative of the passage of a Gulf Stream meander through the mooring site. By looking again at the 250 m AXBT

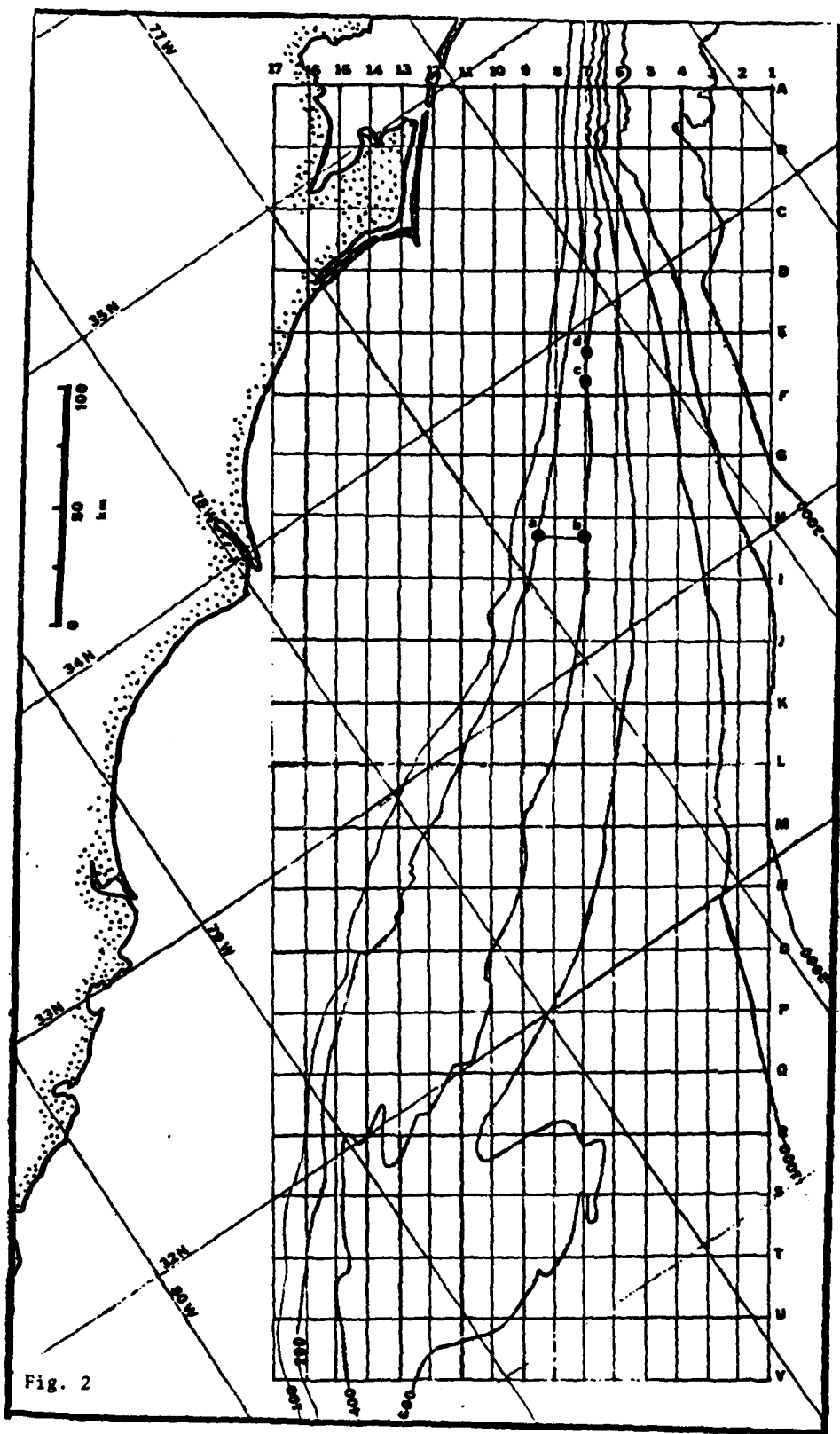
temperature field (Figure 7 where the position of B-TOP is indicated) it can be seen that on 11 February, current meter B-TOP was located in the crest of the southwestern meander. Therefore, it appears that Gulf Stream meanders seen in the SST field may also be accurately reflected in current meter records.

Conclusion

The results of this study indicate that large-amplitude, wave-like meander patterns observed in the SST field between Savannah, GA and Cape Hatteras, NC are reliable indicators of subsurface meandering of the Gulf Stream during typical wintertime conditions.



Fig. 1



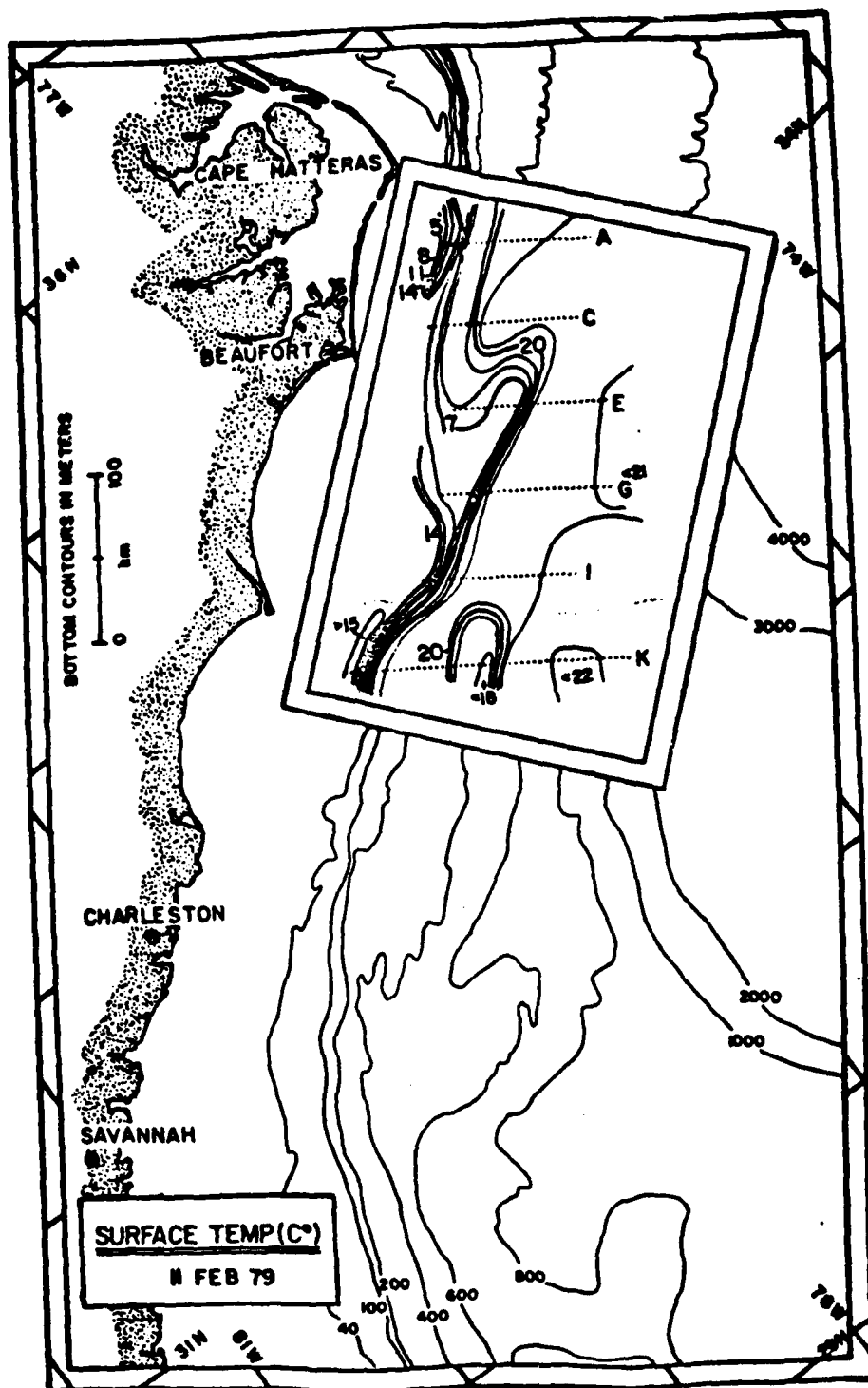


Fig. 3

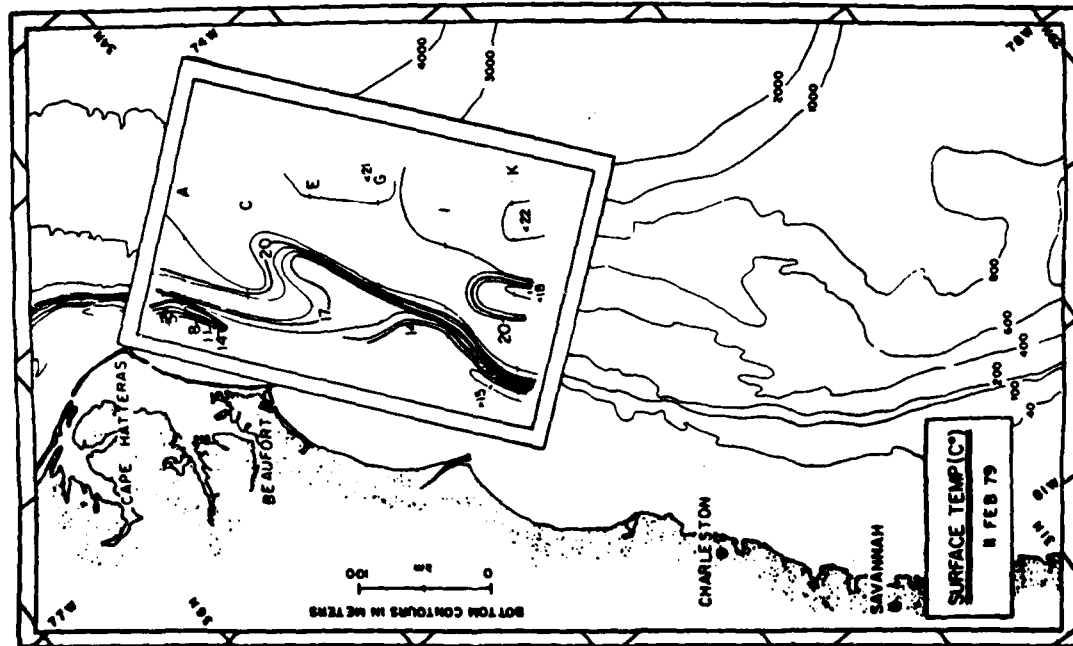
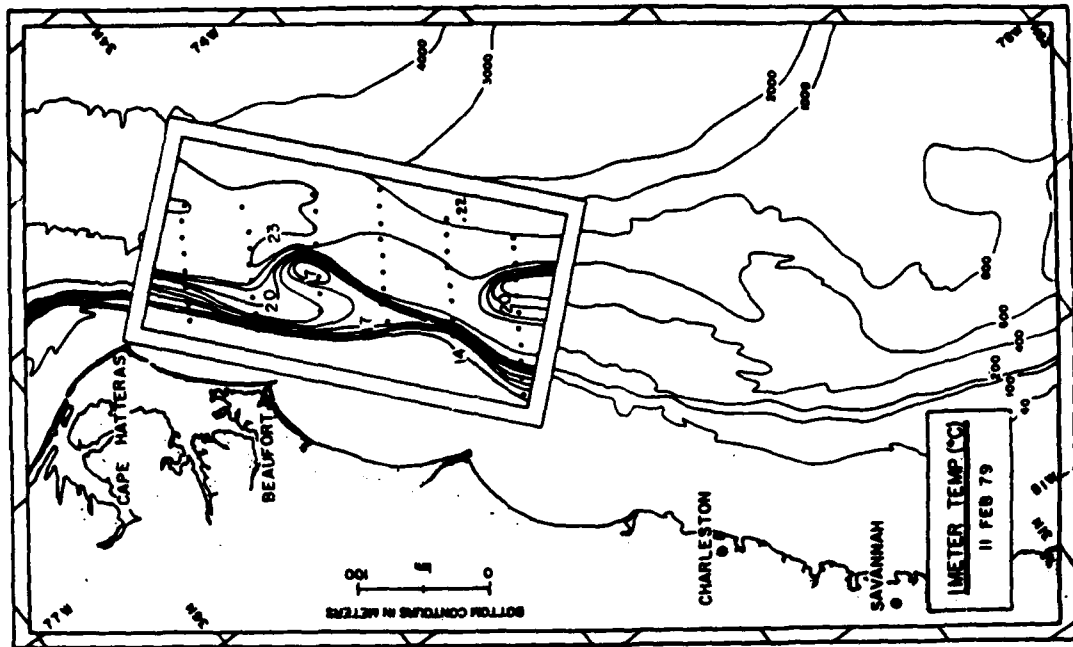


Fig. 4

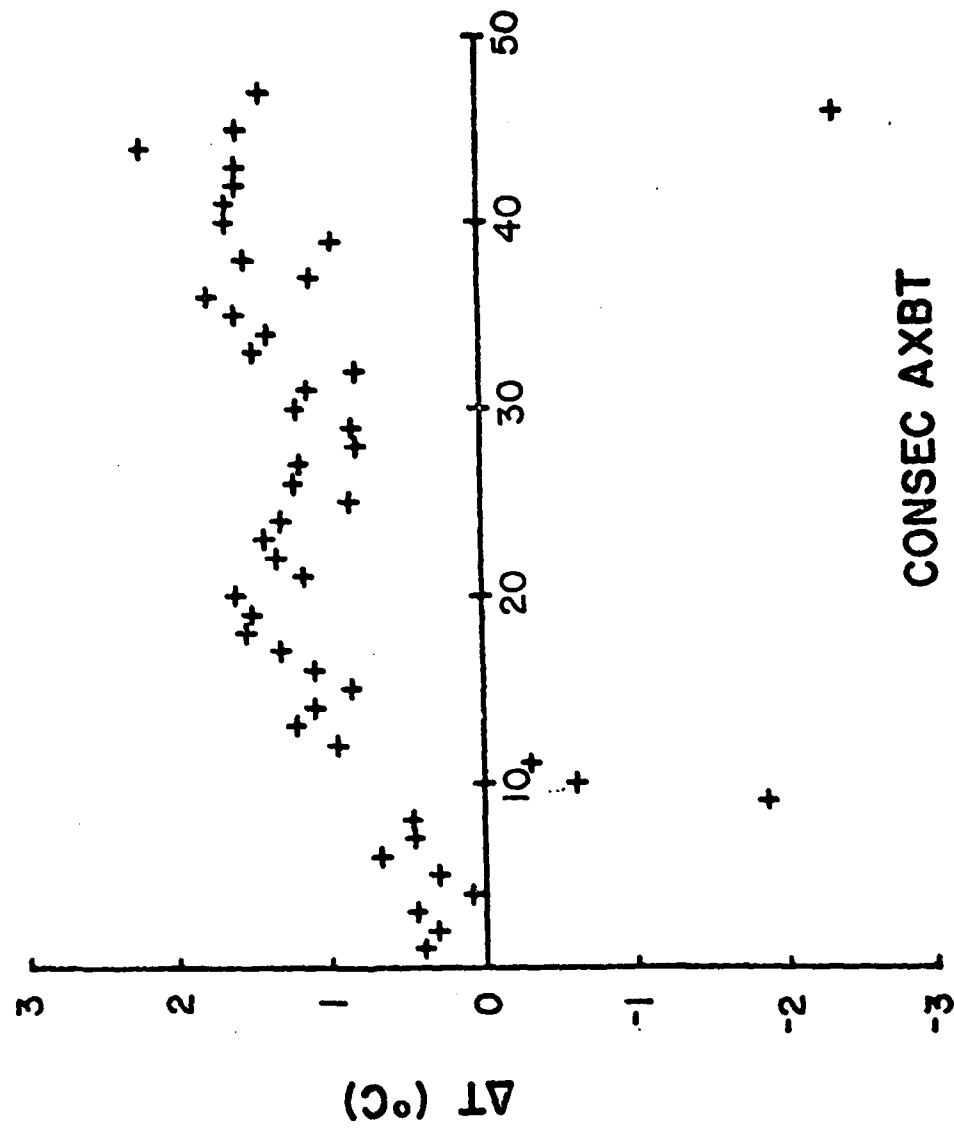


Fig. 5

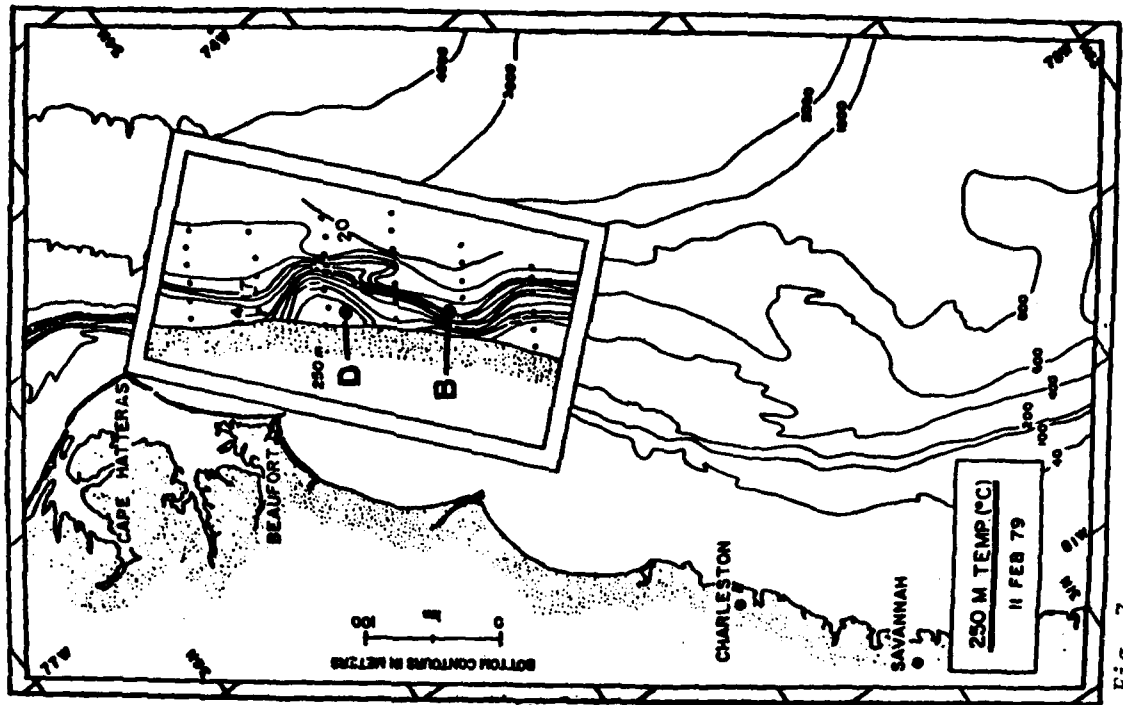


Fig. 7

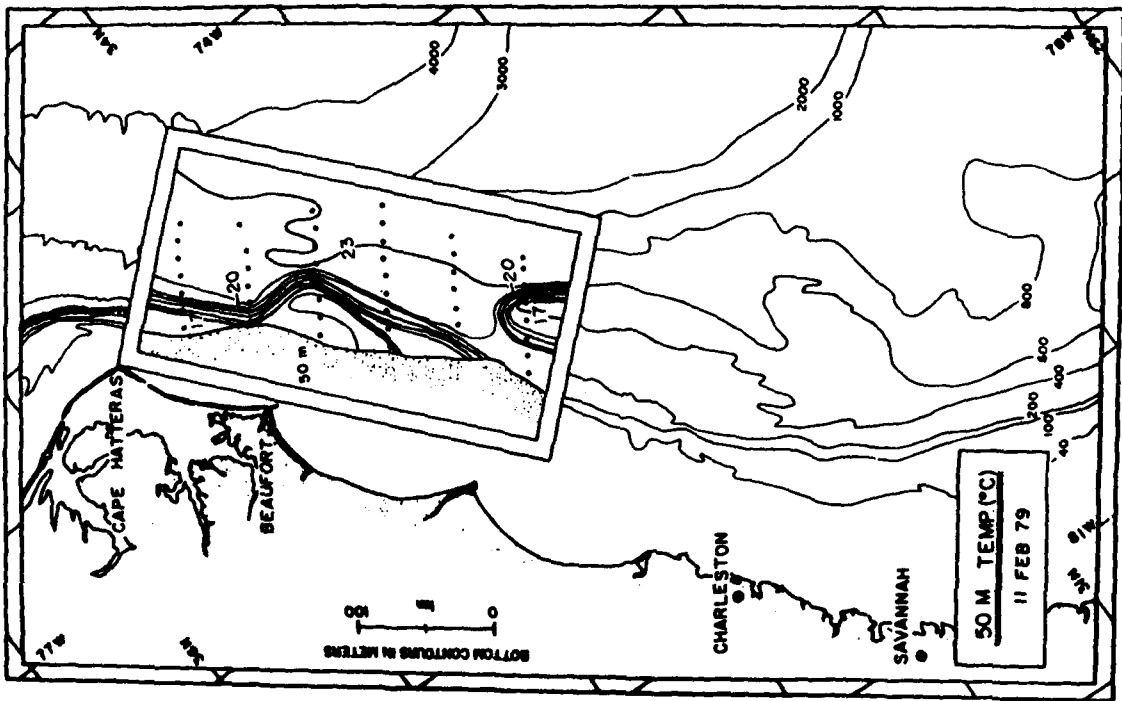


Fig. 6

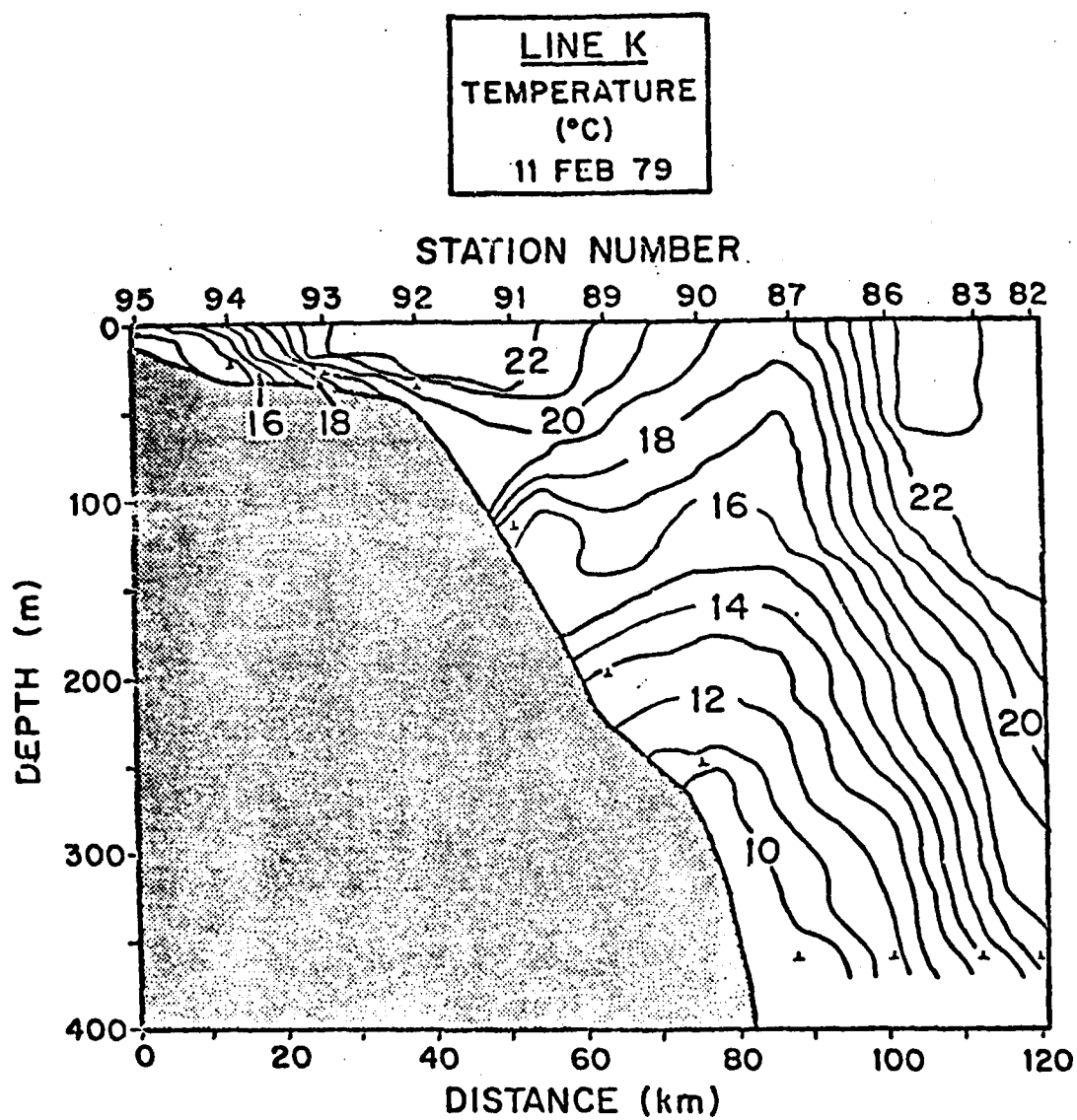


Fig. 8

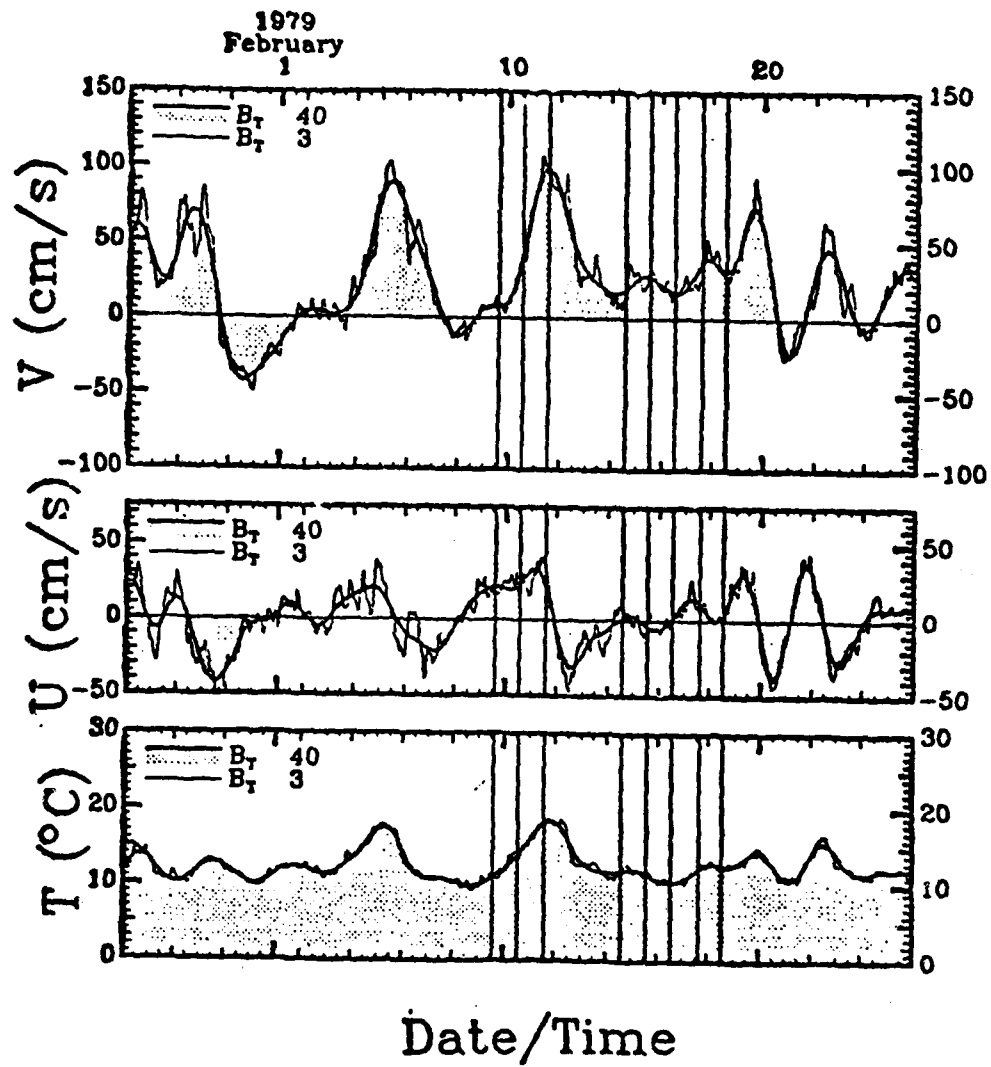


Fig. 9

TRAPPED AND RADIATING INSTABILITIES OF A TWO-LAYER JET,
APPLIED TO THE GULF STREAM

Lynn Talley
Woods Hole Oceanographic Institution
Woods Hole, MA 02543

Oceanic fluctuations are dependent on geographical location. Near intense currents; the eddy field is highly energetic and has broad meridional extent. It is likely that the energy arises from instabilities of the intense current. However, the meridional extent of the linearly most unstable modes of such intense jets is much narrower than the observed region of energetic fluctuations. It is proposed here that weaker instabilities, in the linear sense, which are very weakly trapped to the current, may be the dominant waves in the far field.

As a preliminary problem, the instability of parallel shear flow on the beta plane is discussed. An infinite zonal flow with a continuous cross-stream velocity gradient is approximated with segments of uniform flow, joined together by segments of uniform potential vorticity. This simplification allows an exact dispersion relation to be found. There are two classes of linearly unstable solutions. One type is trapped to the source of energy and has large growth rates. The second type are weaker instabilities of the shear flow which excite Rossby waves in the far field; the influence of these weaker instabilities extends far beyond that of the most unstable waves.

The central focus of the thesis is the linear stability of thin, two-layer, zonal jets on the beta plane, with both horizontal and vertical shear. The method used for the parallel shear flow is extended to the two-layer flow. Each layer of the jet has uniform velocity in the center, bordered by shear zones with zero potential vorticity gradient. The velocity in each layer outside the jet is constant in latitude. Separate linearly unstable modes arise from

the horizontal and vertical shear. The energy source for the horizontal shear modes is both kinetic and potential while the source for the vertical shear modes is nearly all potential. The most unstable waves are tightly trapped to the jet, within two or three deformation radii for small but non-zero beta. Rossby waves and baroclinically unstable waves (in the presence of vertical shear) exist outside the jet because of a nonzero potential vorticity gradient there. Weakly growing jet instabilities can force these waves when their phase speeds and wavelengths match. In particular, westward jets and any jets with vertical shear exterior to the jets can radiate in this sense. The radiating modes influence a large region, their decay scales inversely proportional to the growth rate. Two types of radiating instability are found: (1) a subset of the main unstable modes near marginal stability and (2) modes which appear to be destabilized neutral modes. Westward jets have more vigorously unstable radiating modes.

Applications of the model are made to the eddy field south of the Gulf Stream, using data from the POLYMODE setting along 55°W and farther into the gyre at MODE. The energy decay scale and the variation of vertical structure with latitude in different frequency bands can be roughly explained by the model. The lower frequency disturbances decay more slowly and become more surface-intensified in the far field. These disturbances are identified with the weak, radiating instabilities of the model. The higher frequency disturbances are more trapped and retain their vertical structure as they decay, and are identified with the trapped, strongly unstable modes of the jet.

EIGHTEEN DEGREE WATER VARIABILITY

The Eighteen Degree Water of the western North Atlantic is formed by deep convection in winter. Worthington (1959) defines the Eighteen Degree

Water as $\theta = 17.9^{\circ}\text{C} \pm 0.3^{\circ}\text{C}$, $S = 36.50\text{‰} \pm 0.10\text{‰}$, and $\sigma_t = 26.4 \text{ mg cm}^{-3}$.

The seemingly stable characteristics of the Eighteen Degree Water over the history of hydrographic measurements in the western North Atlantic point to a relatively stable circulation and forcing, as discussed by Warren (1972). The circulation and changing properties of Eighteen Degree Water are studied here using hydrographic data from a long time series at the Panulirus station ($32^{\circ} 10'\text{N}$, $64^{\circ}30'\text{W}$) and from the Gulf Stream '60 experiment. Due to its relative vertical homogeneity, which persists year-round, the Eighteen Degree Water can be identified by its low potential vorticity ($f/\rho \partial \rho / \partial z$). The Eighteen Degree Water is formed in an east-west band of varying characteristics offshore of the Gulf Stream. From a comparison of the Gulf Stream '60 results and the Panulirus station record, it appears that the Eighteen Degree Water formed at the eastern end of the subtropical gyre recirculates westward past the Panulirus station. Renewal of Eighteen Degree Water occurred regularly from 1954 to 1971, ceased from 1972 to 1975, and began again after 1975. The properties of Eighteen Degree Water seen at Panulirus were nearly uniform from 1954 to 1964. There was a shift in properties in 1964 and by 1972 the Eighteen Degree Water properties were 17.1°C , 36.4‰ . The new Eighteen Degree Water formed after 1975 had nearly the same characteristics as that of 1954.

The density, potential temperature, salinity and the temperature-salinity relation of the entire upper water column at the Panulirus station changed at the same time as the Eighteen Degree Water properties. The upper water was denser and colder from 1964 to 1975 than from 1954 to 1964 and after 1975.

Warren, B. A., 1972. Insensitivity of subtropical mode water characteristics to meteorological fluctuations. Deep-Sea Res. 19, 1-19.

Worthington, L.V., 1959. The 18° Water in the Sargasso Sea. Deep-Sea Res. 5, 297-305.

A Numerical Study of
the Influence of the New England
Seamount Chain on the Gulf Stream:
Preliminary Results

by

J. Dana Thompson¹
and
H.E. Hurlburt

Naval Ocean Research and Development Activity
Code 322
NSTL Station, MS 39529

¹Presently at the
Department of Marine, Earth and Atmospheric Sciences
North Carolina State University
Raleigh, N.C. 27650

Abstract

There is growing evidence that the New England Seamount Chain significantly influences the path of the Gulf Stream, deflecting it southeastward and generating large meanders downstream. A "ring meander" extending southward or southeastward near the seamounts also appears to be a semi-permanent feature (Richardson, 1981). Whether the ring remains attached to the stream for long periods of time or whether it repeatedly separates and reattaches is not known.

The dynamics of the interaction of the NESCS with the Gulf Stream is the focus of this research. Important similarities exist between this problem and the influence of large amplitude topography on the Loop Current in the Gulf of Mexico. There instabilities of the Loop Current in the upper layer produce large anticyclonic rings which in turn tend to drive modons in the lower layer. Back interaction of these modons with the Loop Current provides a mechanism by which topographic control is exerted on the path of the upper layer eddies and the Loop Current. Preliminary results from an ensemble of reduced-gravity and two-layer primitive equation experiments are presented which demonstrate how these dynamics may be appropriate for understanding the influence of the NESCS on the Gulf Stream.

1. Introduction

The New England Seamount Chain (NESC) extends from near Georges Bank southeastward to the Sohm Abyssal Plain in the western Atlantic. Some of these mountains rise 3 km above the surrounding sea floor. The Gulf Stream passes over the NESC and appears to be strongly influenced by them. For example, Richardson (1981) analyzed trajectories from 35 free-drifting buoys and found that the influence of the NESC on the Gulf Stream was manifest as (1) a quasi-permanent 100 km southeastward deflection of the Stream, (2) frequent occurrence of a ring meander over the seamounts, (3) large-amplitude meanders beginning at the seamounts and extending eastward and (4) small, 20 km diameter eddies which appear to be generated locally by individual seamounts. In addition, composites of the path of the Gulf Stream from satellite infrared imagery (Maul et al., 1978, and Legeckis, personal communication) clearly show a marked spreading of the envelope of Gulf Stream paths over the NESC.

Dynamics associated with the interaction of the NESC and the Gulf Stream are not well understood. Although models of broad, steady inertial flows impinging on a meridional ridge or a small bump (McCartney, 1976) are important, they are not particularly relevant to this highly time-dependent phenomena in which an intense barotropically/baroclinically unstable surface jet transfers momentum to the deep ocean. The resulting deep circulation interacts with the bottom topography and may in turn modify the stability properties of the upper flow. Furthermore, quasi-geostrophic numerical models may not be appropriate for this problem since they are restricted to seamounts and ridges of small amplitude.

We have chosen to study the dynamics of the interaction of the NESC and the Gulf Stream using an ensemble of experiments with reduced-gravity and

two-layer primitive equation numerical models. These models are time-dependent, nonlinear and can include large amplitude topography in the two-layer case. This report describes our initial model design, basic experiments and preliminary results.

2. Model Design

The numerical models are similar to those described by Hurlburt and Thompson (1980, 1982; henceforth referred to as HTa and HTb, respectively). The models retain a free surface and gravity waves are treated implicitly. A fixed-density contrast is specified between the two immiscible layers and in the reduced-gravity model the lowest layer is assumed infinitely deep and at rest. For details of the formulation see HTa and our companion paper in this volume.

Fig. 1 shows the model domain superimposed on a map of the western Atlantic from Richardson (1981). The domain is a 2500 x 1280 km rectangle rotated counterclockwise 28° from zonal. The boundary conditions are no-slip and kinematic except on outflow where a free-slip condition is specified. The location of the northwestern boundary approximates the position of the 200 m contour of the continental shelf. The Coriolis parameter is a function of latitude only and the β -plane approximation is used. The model is driven from rest by inflow through a port 100 km wide located 180 km from the sidewall boundary and is designed to simulate the Gulf Stream as it flows past Cape Hatteras. Mass balance is maintained precisely by outflow through a 200 km wide opening located in the vicinity of the mean position of the Gulf Stream as it flows past the Newfoundland Ridge.

The models are spun-up from rest by specifying an inflow transport increasing to $50 \times 10^6 \text{ m}^3/\text{sec}$ over 90 days. The transport distribution is parabolic across the port and normal to it. In no case is inflow transport specified in the lower layer. Model parameters for all experiments are

shown in Table I.

Table II lists the five basic model experiments. The first experiment uses the reduced-gravity model while four additional experiments use the two-layer model. The two-layer cases were: flat-bottom, large-amplitude ridge, large-amplitude seamounts and small-amplitude seamounts. The experiments were otherwise identical in every specified parameter, dimension and boundary condition. Each model was integrated to statistical equilibrium, as indicated by basin-wide average potential and kinetic energy curves. Typically, models reached statistical equilibrium in four years and were then integrated an additional three years.

3. Results

Fig. 2 shows a sequence of snapshots of the pycnocline height anomaly for the reduced-gravity experiment. The PHA is the deviation of the interface between layers from an initial horizontal rest position. Negative contours indicate a shallower fluid interface. Note the thermocline deepens about 500 m across the Gulf Stream. The large wavelength, large amplitude meanders dominate the flow pattern. In Fig. 2a a 500 km diameter cold-core cyclonic ring has broken off from the Stream by day 1620 and drifted to the southwest. Within 150 days the ring has been reabsorbed into the Gulf Stream and a new ring is in the process of breaking off. By day 1800 the first ring has moved farther downstream and a new cold core ring has broken off. This quasi-periodic break-off process occurs approximately every 200 days. The diameter of the rings immediately after separation is comparable to $2(V/\beta)^{1/2}$, where V is the speed at the core of the current (approximately 125 cm/sec) and β is the variation of the Coriolis parameter with latitude.

Both the amplitude of the meanders and the rings are unrealistically large in the reduced-gravity experiment. However, in this experiment no

momentum can be transmitted downward to the deep water through the pressure field. It is therefore logical to look to the two-layer experiments for more realistic simulations.

Fig. 3 is a snapshot of the density-normalized pressure anomaly field for the upper (p_1) and lower (p_2) layers in the two-layer flat-bottom experiment. We have used this measure to be consistent with our companion paper and HTb. All parameters and boundary conditions were maintained as in the reduced-gravity experiment and no flow was forced through the deep water inflow port.

In the flat bottom two-layer experiment the wavelengths of the meanders and the detached cold-core rings are considerably smaller than in the reduced-gravity experiment. The upper layer circulation is weaker than in the reduced-gravity case, consistent with the transmission of momentum to the deep water as indicated by p_1 and p_2 in Fig. 3b. The maximum currents in the deep water are about 15 cm/sec.

Inclusion of topography was accomplished in three experiments. In Fig. 4a a ridge with a Gaussian distribution varying only in x (not longitude) was added to the flat-bottom experiment. Maximum amplitude of the ridge was 2500 m. Recall the initial thickness of the lower layer was 4400 m. In Fig 4b the ridge was replaced by five Gaussian seamounts again with maximum amplitude of 2500 m. The third topography experiment retained the identical topography as Fig. 4b but with amplitude multiplied by .2.

Fig. 5 shows the mean p_1 and p_2 fields in the upper and lower layers for the flat-bottom, ridge, and large-seamount cases. The two-year averaging period was sufficiently long to insure stable statistics.

In the flat bottom experiment (Fig. 5a, b) an intense deep mean

circulation is generated below the mean axis of the Gulf Stream near inflow. The intense deep gyres are reminiscent of those reported by Holland and Rhines (1980) for a two-layer quasi-geostrophic model driven by wind stress. Note the presence of two intense gyres, one cyclonic and one anticyclonic, and two weaker gyres on either side. There is also an additional intense anticyclonic gyre not found by Holland and Rhines (1980) immediately downstream and below a mean upper-layer ridge. Weak standing waves still farther downstream are clearly evident in the flow patterns. For the ridge experiment (Fig. 5c, d) the p_1 pattern upstream of the ridge is significantly different from the flat-bottom case. An intense meander has formed about 300 km upstream from it. Essentially no deep mean flow crosses the ridge, and the deep anticyclonic gyre which was centered near $x = 800$ km, $y = 700$ km in the flat bottom experiment has vanished. Downstream of the ridge the deep mean gyres are more intense than in the flat bottom experiment.

The seamount experiment results shown in Fig. 5e, f are dramatically different from either the ridge case or the flat-bottom experiment. An extremely large anticyclonic meander of the stream occurs directly over the seamounts. A trough-ridge pair just downstream from the ridge is also of much larger amplitude than in the previous two-layer experiments. This feature is reminiscent of the "ring meander" Richardson (1980) suggests is a semipermanent feature of the Gulf Stream system. In the deep water a mean anticyclonic circulation is generated around each seamount with the flow tending to follow f/h contours. This deep-mean anticyclonic flow is reflected in p_1 via the large-amplitude meander over the seamounts. This is the back-interaction mechanism discussed in our companion paper and observed by HTb in the Gulf of Mexico model.

We have not yet examined in detail the influence of the seamounts on the eddy-field. However, an important result for the seamount experiment vis-a-vis the flat-bottom or ridge case is indicated in Fig. 6. Here a snapshot at day 2500 of p_1 and p_2 for the seamount experiment are shown. Warm-core rings are found to be generated in the vicinity of the seamounts. Such warm-core ring generation is consistently observed in this experiment and differs sharply from the flat-bottom and ridge experiments in which warm-core rings were very rarely generated. In the seamount case there are nearly as many warm-core rings generated as cold-core rings. Our results indicate that the deep anticyclonic circulation around the NESC may affect both the mean Gulf Stream path and ring formation. This very intriguing result requires considerable additional study.

Finally we have conducted an experiment to investigate the importance of seamount amplitude on the circulation. In this experiment we reduced the seamount amplitude by 80% so that the maximum amplitude was only 500 m instead of 2500 m. Fig. 7 shows the mean p_1 and p_2 fields in this experiment. Clear differences between the small seamount and large seamount cases are evident. The meander over the seamounts in the large-amplitude seamount case has practically disappeared in the small-amplitude case. The downstream trough-ridge pair is also considerably weaker in the small-amplitude case. The deep flow around the small-seamounts is weaker but the pattern of flow is not significantly different in the two cases. Further downstream the two anticyclonic gyres near outflow are stronger in the small-amplitude case, reflecting larger-amplitude meanders at the surface.

4. Conclusions

Preliminary results from a numerical study of the influence of the NESC on the Gulf Stream suggest that deep mean flows driven by a barotropically/

baroclinically unstable Gulf Stream can interact with the NESC and influence the path of the Gulf Stream. Results from a reduced-gravity model show unrealistically large meanders and cold-core rings while results from a two-layer flat-bottom model which allows vertical momentum flux to the deep water shows much more realistic meander patterns and cold-core rings. The influence of a ridge and a series of Gaussian seamounts on the deep mean circulation, the path of the Gulf Stream, and ring generation is dramatic. A deep mean anticyclonic circulation around the seamounts is reflected in the upper layer as a large anticyclonic meander of the Gulf Stream. The seamounts appear to enhance warm-core ring generation by the Gulf Stream.

Results from a small-amplitude seamount case are significantly different from the large-amplitude case. This suggests that quasi-geostrophic models of the interaction of the Gulf Stream-NESC may be inappropriate, since they are constrained to include only small amplitude topographic variations.

Although our preliminary results are suggestive, further analysis and additional experiments with significantly larger domains must be conducted. The larger domain experiments are required to remove constraints on the size and number of meanders and standing waves in the domain. Higher resolution experiments must also be conducted to better resolve the "spiky", small width-scale nature of the seamounts. A larger volume of parameter space and a variety of additional forcing functions must also be included in the study.

Acknowledgements: We thank Dr. Daniel Moore of Imperial College, London, for providing the fast vectorized Helmholtz solvers for the models. Graphics software was supplied by the National Center for Atmospheric Research, which is sponsored by the National Science Foundation. Computations were performed on the two-pipeline Texas Instruments Advanced Scientific Computer at the Naval Research Laboratory in Washington, D.C.

References

- Hurlburt, H.E. and J.D. Thompson, 1980: A numerical study of Loop Current intrusions and eddy shedding. J. Phys. Oceanogr., 10, 1611-1651.
- Hurlburt, H.E. and J.D. Thompson, 1982: The dynamics of the Loop Current and shed eddies in a numerical model of the Gulf of Mexico. Hydrodynamics of Semi-Enclosed Seas. J.C.J. Nihoul (editor), Elsevier Scientific Publishing Co., Amsterdam, 243-297.
- Maul, G.A., P.W. Dewitt, A. Yanaway, and S.R. Baig, 1978: Geostationary satellite observations of Gulf Stream meanders: infrared measurements and time-series analysis. J. Geophys. Res., 83, 6123-6135.
- McCartney, M.S., 1976: The interactions of zonal currents with topography with application to the Southern Ocean. Deep-Sea Res., 23, 413-427.
- Rhines, R.B. and W.R. Holland, 1979: A theoretical discussion of eddy-driven mean flows. Dynamics of Atmospheres and Oceans, 3, 289-325.
- Richardson, P.L., 1981: Gulf Stream trajectories measured with free-drifting buoys. J. Phys. Oceanogr., 11, 887-1042.

TABLE 1. Model Parameters

A	$3 \times 10^6 \text{ cm}^2 \text{ s}^{-1}$	horizontal eddy viscosity
f_0	$6.73 \times 10^{-5} \text{ s}^{-1}$	Coriolis parameter at southwest corner
g'	2.27 cm sec^{-2}	reduced gravity $g(\rho_2 - \rho_1)/\rho_0$
H_1	600 m	upper layer mean depth
H_2	4400 m	lower layer mean depth
β	$2 \times 10^{-13} \text{ cm}^{-1} \text{ sec}^{-1}$	differential rotation (df/dy)
$\Delta x, \Delta y$	20 km	grid spacing in x, y
Δt	4800 sec	time step
Domain size, x_L by y_L		2500 km x 1280 km
inflow port width		120 km
outflow port width		200 km
Upper layer inflow transport		$50 \times 10^6 \text{ m}^3 \text{ s}^{-1}$ (50 Sv)
Lower layer inflow transport		0

TABLE 2. List of Experiments

<u>Experiment No.</u>	<u>Description</u>
1	Reduced-Gravity 1-layer
2	2-layer flat-bottom
3	2-layer Ridge
4	2-layer Seamounts (Large Amplitude)
5	2-layer Seamounts (Small Amplitude)



Fig. 1

The model domain superimposed on a map of the mean temperature distribution at a depth of 450 m based on 1° square averages of the NODC data (from Richardson, 1981). Inflow is through a port just off Cape Hatteras and compensated by outflow through a port near the Newfoundland Ridge. Lateral boundaries are otherwise closed.

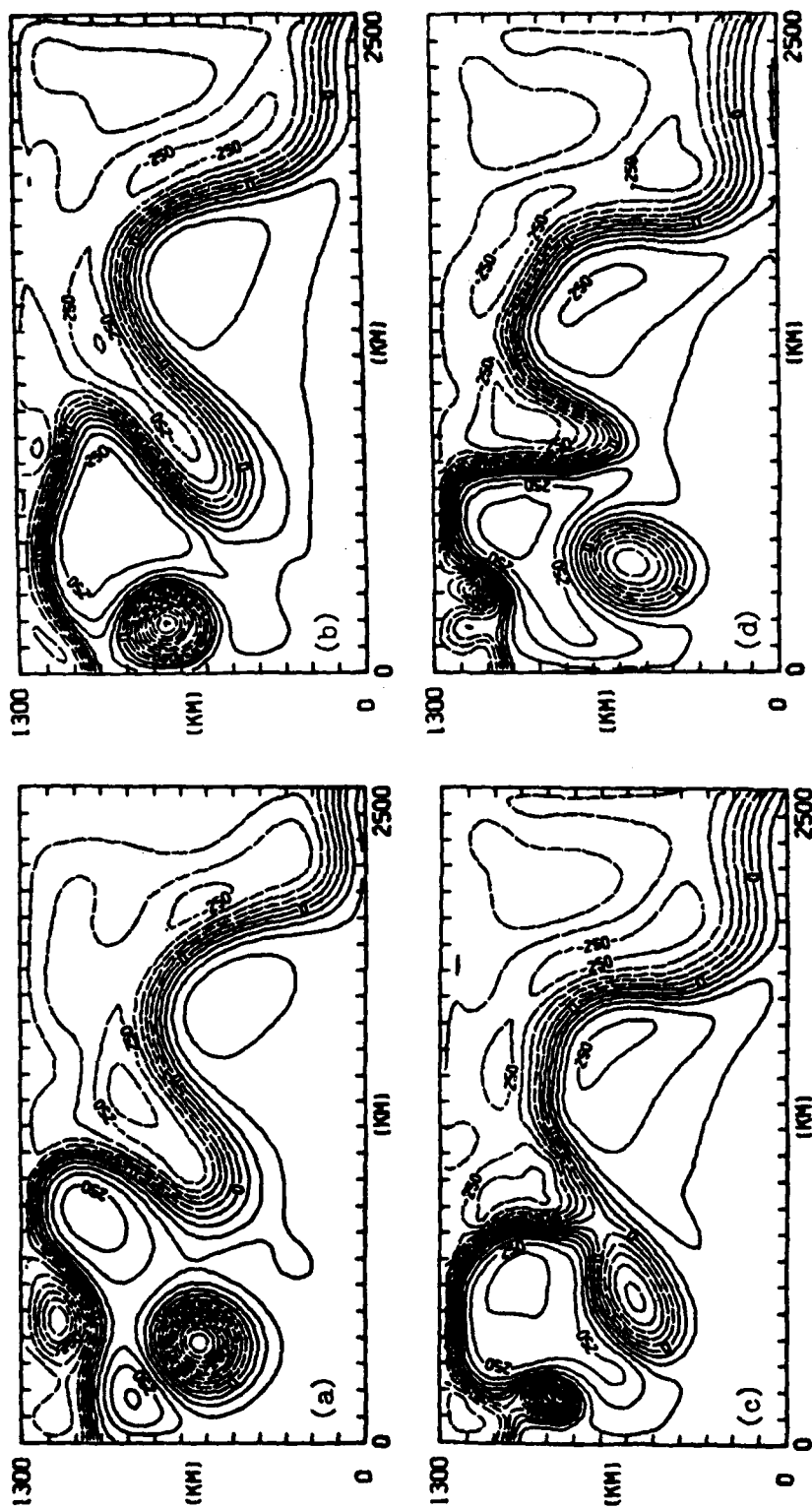


Fig. 2

Snapshots of pynocline height anomaly in meters at (a) day 1620, (b) day 1710, (c) day 1770, and (d) 1800 for the reduced gravity model. Negative values indicate an interface shallower than the rest state value. The contour interval is 50m.

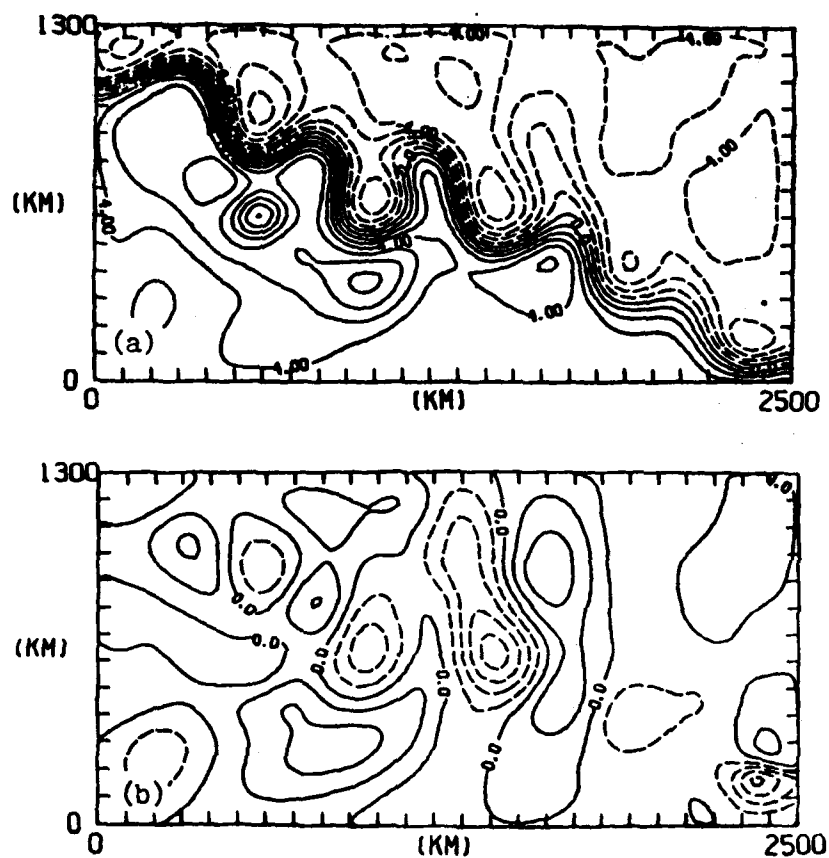


Fig. 3

Snapshots of p_1 and p_2 for the two-layer flat bottom case in the (a) upper-layer and (b) lower-layer. The contour interval is $1 \text{ m}^2/\text{sec}^2$ for (a) and $.5 \text{ m}^2/\text{sec}^2$ for (b).

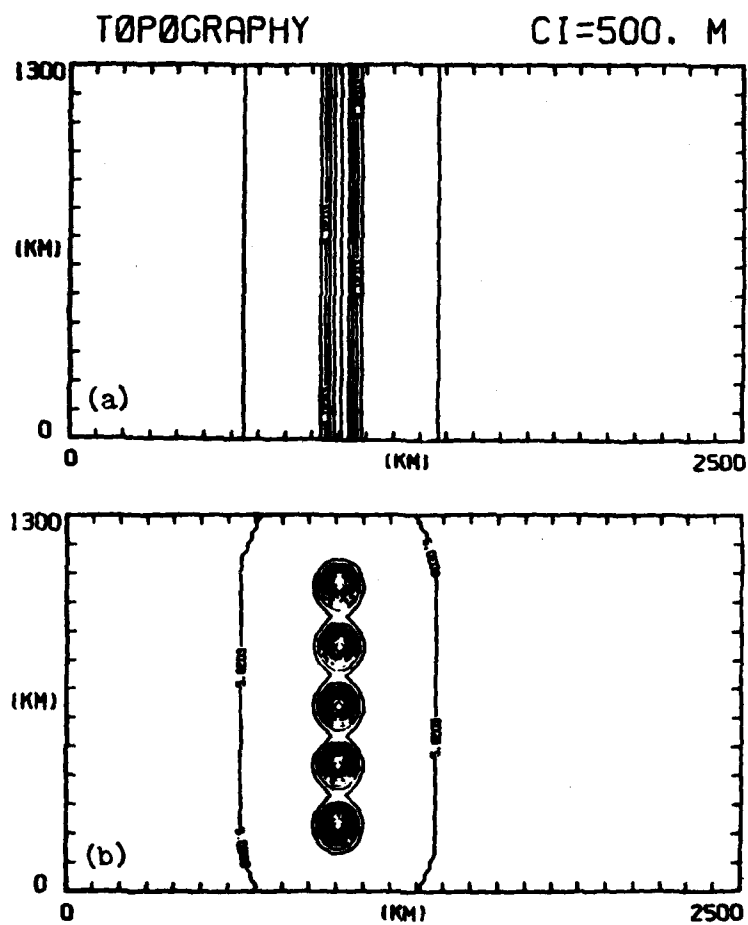


Fig. 4

Bottom topography for the ridge (a) and seamount (b) cases. Maximum amplitude of the bottom height is 2500m. The contour interval is 250m.

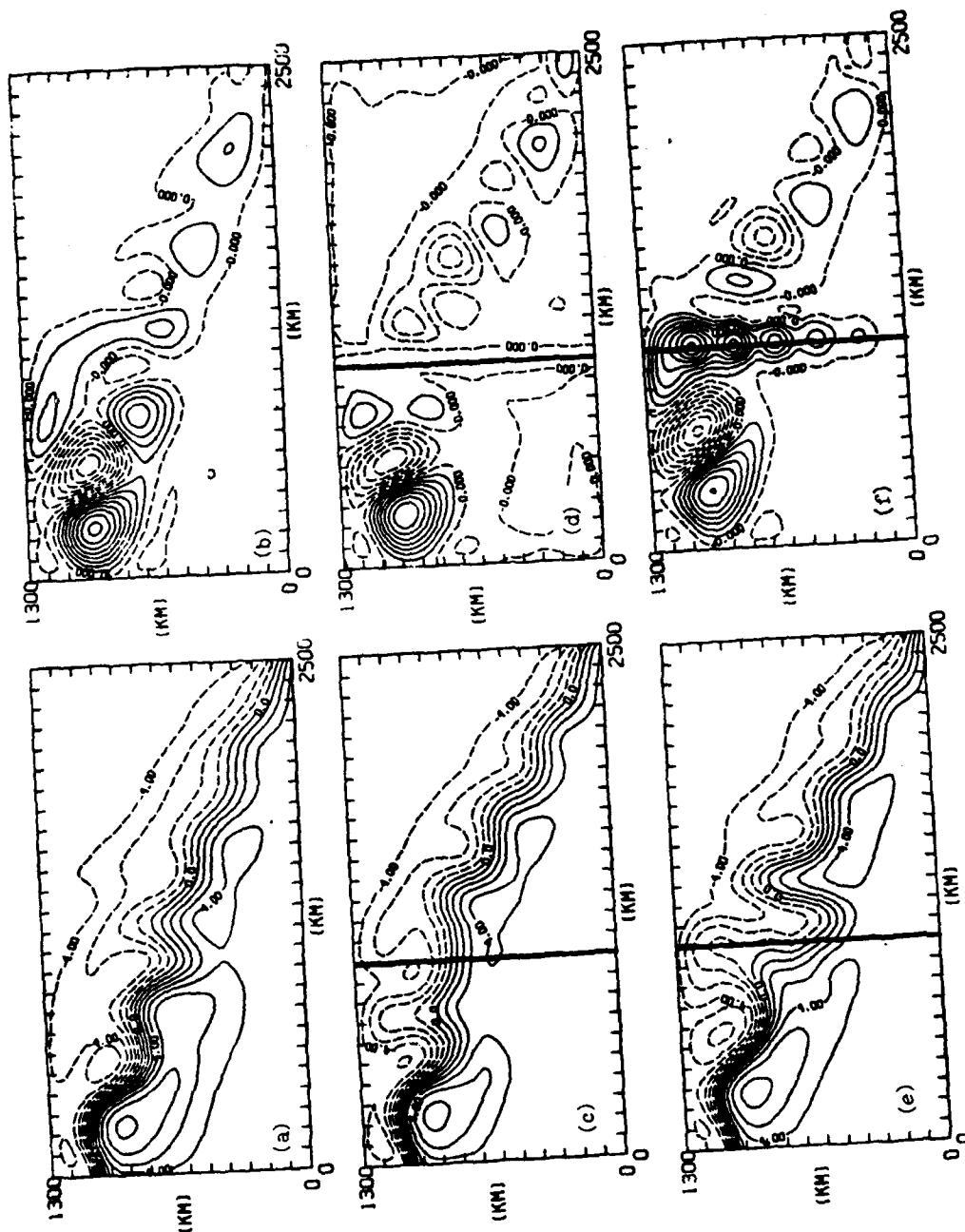


Fig. 5

Mean P_1 fields for the (a) flat-bottom, (c) ridge, and (e) large-amplitude seamount experiments. Panels (b), (d), and (f) are P_2 for the for each experiment, respectively. The contours are 1 m/sec^2 for the upper layer and $.2 \text{ m/sec}^2$ for the lower layers.

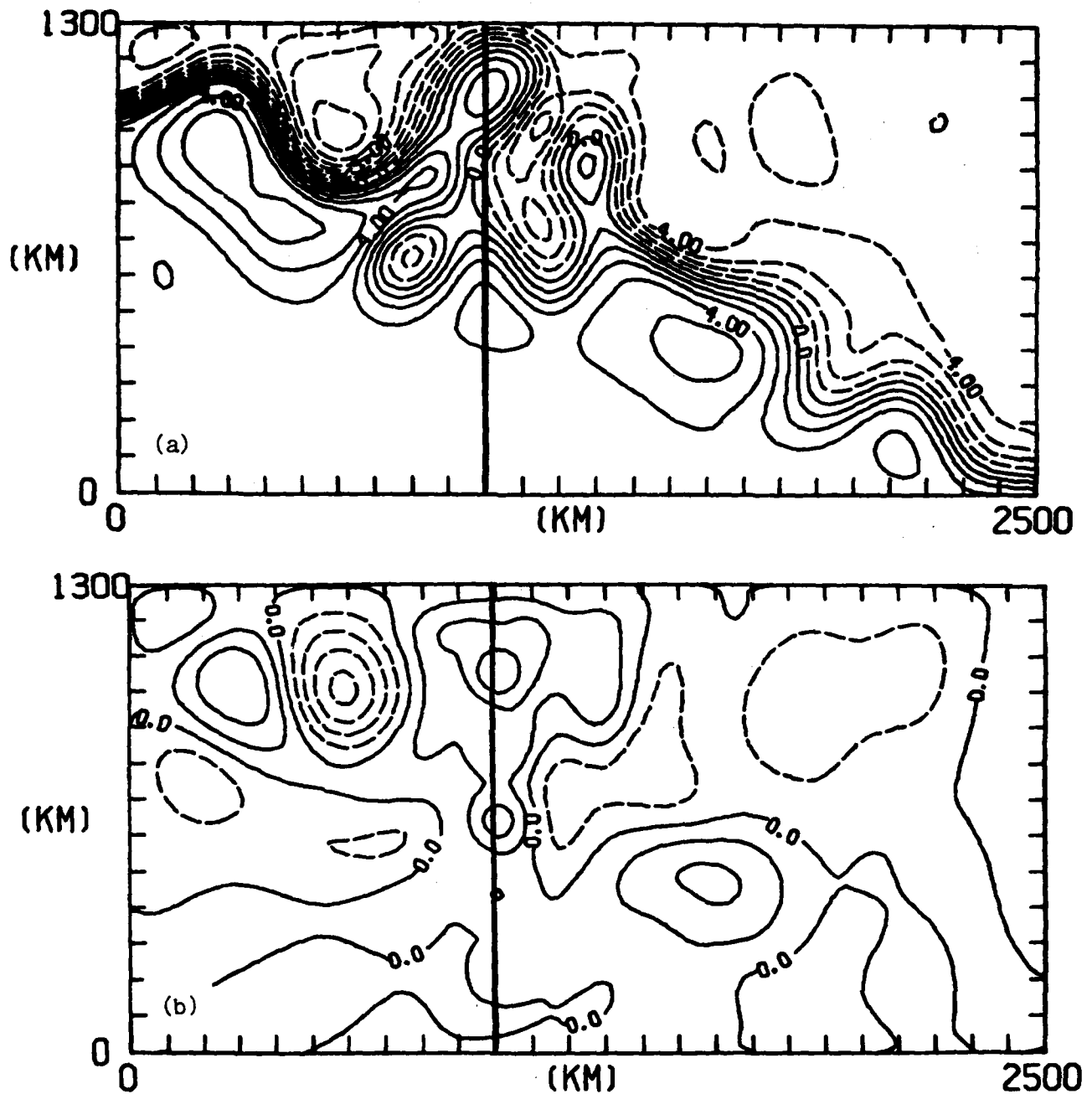


Fig. 6

Snapshots of the pressure anomaly field for the two-layer large-amplitude seamount case in the (a) upper-layer and (b) lower-layer. Contour intervals are $1 \text{ m}^2/\text{sec}^2$ for (a) and $0.5 \text{ m}^2/\text{sec}^2$ for (b).

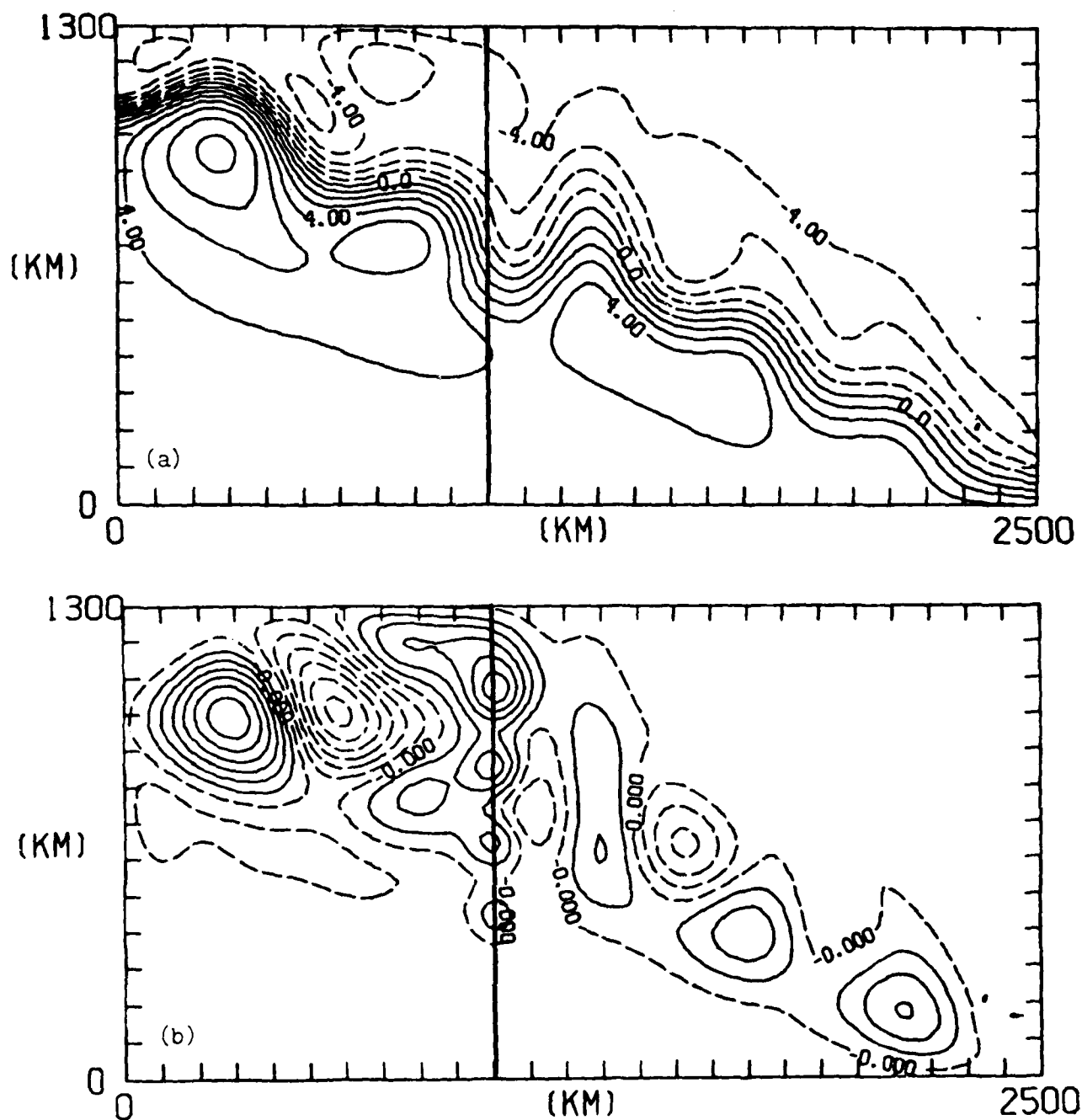


Fig. 7

Mean (a) p_1 and (b) p_2 fields for the small-amplitude seamount case. Contour intervals are as in Fig. 5.

PRELIMINARY ESTIMATES OF SURFACE VORTICITY AND DIVERGENCE IN
GULF STREAM WESTERN BOUNDARY PERTURBATIONS USING SATELLITE AND BUOY DATA

Fred M. Vukovich
Research Triangle Institute
Research Triangle Park, NC

George A. Maul
NOAA/AOML
Miami, FL

Estimates of surface divergence, surface vorticity, and terms in the equation for the time rate of change of vorticity at the surface in a Gulf Stream western boundary perturbation were derived using data from satellite track free-drifting buoy and surface temperature patterns from satellite infrared data. In the perturbation study, the curvature acceleration and divergence terms acted to produce cyclonic curvature vorticity at the expense of shear vorticity. It was hypothesized that the banking term, on the other hand, acted in opposition to the curvature acceleration and divergence terms. The growth or dissipation in the wave amplitude of the perturbation, which were judged by the growth or dissipation of the cyclonic curvature vorticity, appeared to depend on the relative magnitude of the curvature acceleration term, the divergence term, and the banking term.

1.0 Introduction

For this study, satellite track, free-drifting buoy data were combined with satellite-derived sea surface temperature data in the western boundary perturbation to estimate the vorticity, divergence, and the time rate of change of vorticity at the surface. The buoy data were obtained from an experiment conducted in 1979. Position of the buoy, which were drogued at the 2-meter level, were obtained by the Tracking and Data Relay Experiment aboard the NIMBUS 6 and 7 satellites. The error in the position associated with this system is about ± 2 km. The buoy was cylindrical in shape, having a diameter of about 0.6 meters and a height of about 0.4 meters. The buoy was ballasted such that only about 0.10 to 0.15 meters of the buoy was exposed above the

surface in order to minimize the effect of wind drag. The winds were from the north, northwest, and northeast for about 80 percent of the period for the case study, and the wind speeds were at most 5 meters per second. The buoy followed the path of the contour of the boundary of the Gulf Stream as defined by the satellite infrared data, suggesting that wind drag did not have an appreciable effect on the path of the buoy. Furthermore, Kirwin et al. (1978) have shown that the satellite track drifters which have lost their drogues, gave reasonable representation of ocean currents in spite of being subjected to large wind speeds. In this case, there is a great deal of assurance that the drogue was not lost.

2.0 Methodology

The vorticity, ζ , and horizontal divergence, D_H , were computed using the following set of equations:

$$\zeta = K_s V - \frac{\partial V}{\partial s} \quad , \quad (1)$$

$$D_H = V \frac{\partial \phi}{\partial n} + \frac{\partial V}{\partial s} \quad ; \quad (2)$$

where K_s is the curvature of the streamlines, V is the current speed, ϕ is the direction of the horizontal streamlines, s is the coordinate along the streamlines, and n is the coordinate normal to the streamline, positive to the left looking downstream (Chew, 1974). The curvature of the streamline was computed using the streamline estimated from the buoy track and satellite infrared data, and by calculating the change in the direction of the streamline along the path. Since the lateral shear could not be calculated directly, an

average value of the lateral shear on the cyclonic side of the Gulf Stream was used and was determined using the distribution of the surface geostrophic currents in similar perturbations presented by Vukovich and Crissman (1980). The directional shear was estimated from the satellite sea surface temperature analysis, and was the difference between the angles made by the intersection of the isotherms which defined the western and eastern boundaries of the Gulf Stream, relative to a fixed coordinate system.

The system of equations derived by Chew (1974) was used to examine the time rate of change of vorticity. The expression for the time rate of change of the curvature of vorticity is:

$$\frac{D(K_s V)}{Dt} = \frac{\partial}{\partial n} \frac{DV}{Dt} - (f + K_s V)D_H - K_s V \frac{\partial V}{\partial s} - \frac{Df}{Dt} \quad , \quad (3)$$

where f is the Coriolis parameter. The last term on the right is the Beta term. The third term on the right is the curvature acceleration term or the product of the curvature vorticity and the speed divergence. The second term on the right is the divergence term, and the first term on the right is the so-called "banking" term. The expression for the time rate of change of shear vorticity is:

$$\frac{D - \frac{\partial V}{\partial n}}{Dt} = - \frac{\partial}{\partial n} \frac{DV}{Dt} + \frac{\partial V}{\partial n} D_H + K_s V \frac{\partial V}{\partial s} + \frac{\partial w}{\partial n} \frac{\partial V}{\partial z} \quad ; \quad (4)$$

where w is the vertical velocity. The Beta term is absent, indicating that it only affects the curvature vorticity. The banking and curvature vorticity terms have opposite signs in Equations (3) and (4). These two terms act to transform curvature vorticity to lateral shear vorticity or, conversely, lateral shear vorticity to curvature vorticity--having no net effect on the

change of the total vorticity. A divergence term is present in Equation (4), but the multiplier is different than that in Equation (3). The last term on the right is the twisting term.

The Gulf Stream western boundary perturbation appears as a wavelike meander. The perturbation possesses shear and curvature vorticity, and the curvature vorticity is present by virtue of the wavelike characteristics. Depending on the curvature vorticity already present in the perturbation, positive and negative changes in the curvature vorticity indicate an intensification and weakening of the wavelike structure of the phenomenon. The available data did not permit calculations of all the terms in Equations (3) and (4). Actually, only two terms could be estimated: the divergence term, and the curvature acceleration term.

3.0 Case Study

Figure 1 gives the sea surface isotherm pattern obtained from the NOAA 6 infrared data for 19 June 1979. There is a Gulf Stream western boundary perturbation centered around 33.6°N and 74.5°W . The perturbation is characterized by a cold core centered, having a temperature around 22.5°C . A warm filament is located on the shoreward side of the cold core center. The region of the filament through which warm Gulf Stream water is being entrained southwestward is located at around 34.5°N and 75°W .

The figure also gives the position of the satellite track, free-drifting buoy (the numbered black dots). The buoy data shown in the figure were collected during the period 3-6 June 1979. After 16 June 1979 (position # 9) no further transmission was received by the satellite from the buoy. It was concluded there was a battery failure on the buoy. The western boundary perturbation was located around 32.5°N on 3 June and moved northward to its

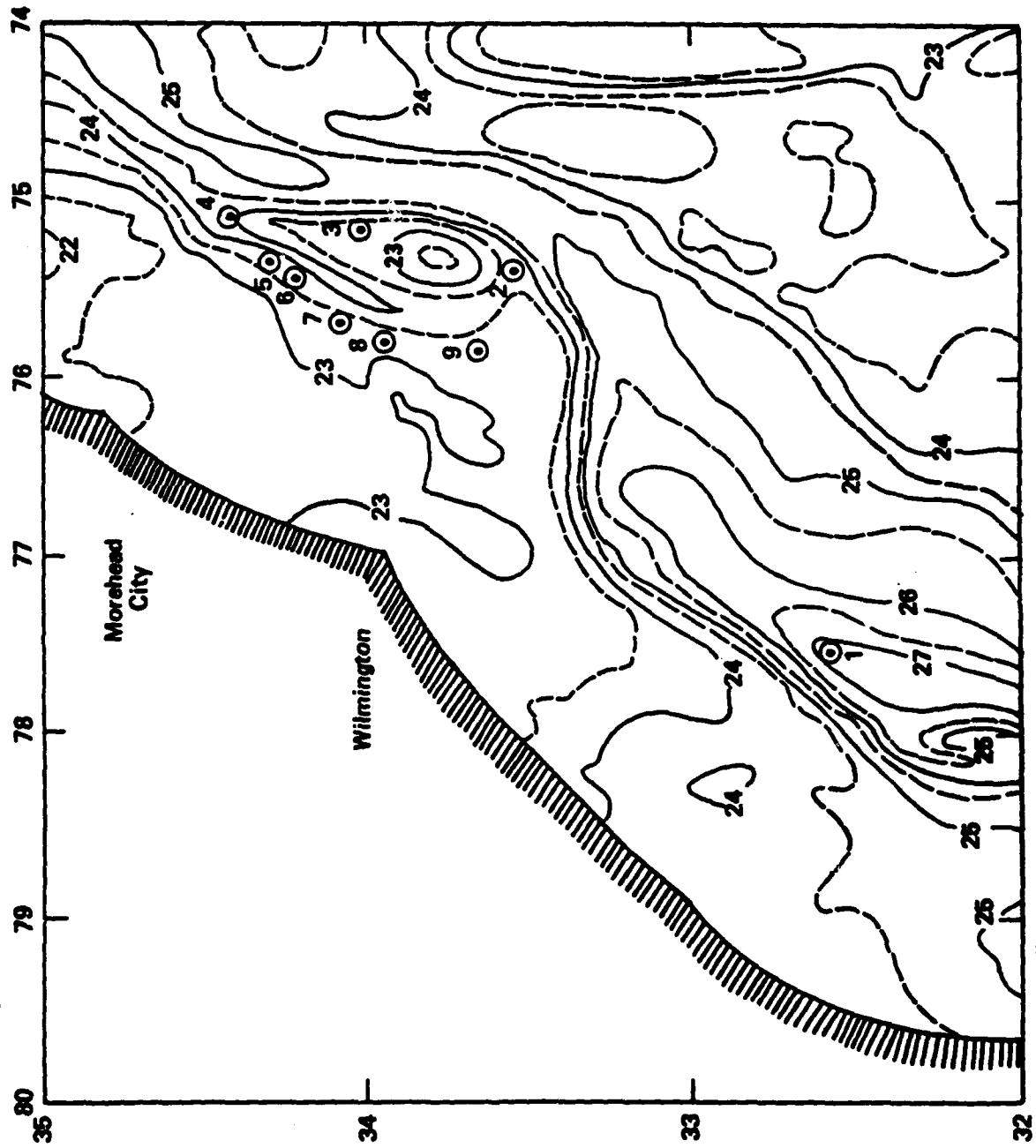


Figure 1. NOAA-6 sea-surface temperature ($^{\circ}\text{C}$) distribution for 19 June 1979. Large black dots represent positions of a satellite-tracked, free-drifting buoy between 3 and 16 June 1979.

position as indicated on 19 June near intervening period. The buoy positions were adjusted by adding an increment of latitude and longitude to their true positions. The increments were determined using the mean speed [36 km per day, a value slightly larger than the mean value found by Vukovich and Crissman (1980)] and direction (northeast) of the perturbation and the time difference between the time of the particular buoy position and the time that the satellite infrared data were obtained. This was done in order to obtain the positions of the buoy relative to the position of the perturbation on 19 June. The speed and direction were based on three satellite views of perturbations between 3 and 19 June.

The continuous pathline of the buoy given in Figure 2 was constructed using the discrete positions of the buoy together with the configuration of the 24° isotherm in Figure 1. There is a reasonable coincidence between the buoy position and the 24°C isotherm in the perturbation. The buoy travelled around the perturbation (Figure 2) and became entrained into the warm filament. As the buoy approached and passed through the perturbation, its speed decreased, reaching a value less than 0.5 meters per second as it approached the cyclonic turn into the filament. In the warm filament the speed of the buoy ranged from 0.2 to 0.4 meters per second in a southwestward direction.

The computation of parameters (see Table 1) were made at the wave crest immediately upstream of the trough, and at the wave trough, and at the downstream position where the Gulf Stream water was being entrained into the warm filament (see Figure 2). As previously mentioned, the lateral shear used in the computation was the average lateral shear determined at the surface on the cyclonic side of the Gulf Stream in a western boundary perturbation using geostrophic current data (Vukovich and Crissman, 1980). The order of magnitude of terms are the same as that previously found by Chew (1974) in the Gulf Stream system.

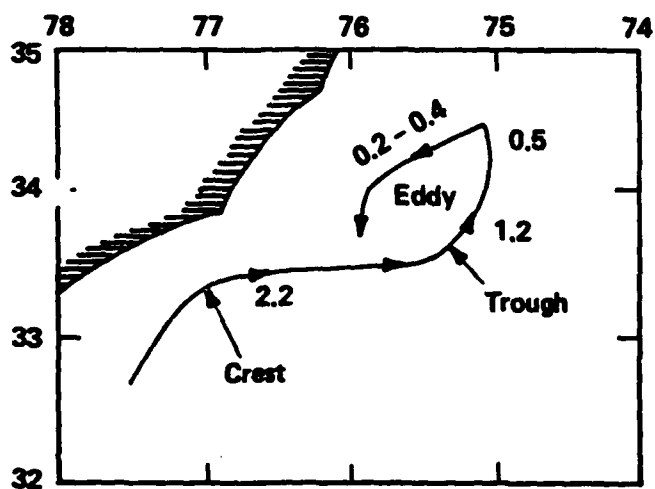


Figure 2. Path of satellite-tracked, free-drifting buoy between 3-16 June 1979 with calculated speeds (m s^{-1}) between positions.

Table 1. Surface dynamic ocean parameters computed for a Gulf Stream western boundary perturbation located south of 34°N using free-drifting buoy data and satellite infrared data.

Location	K_s (m^{-1})	V ($m\ s^{-1}$)	VK_s (s^{-1})	$-\frac{\partial V^*}{\partial n}$ (s^{-1})	ξ (s^{-1})	$\frac{\partial \phi}{\partial n}$ (m^{-1})	$V \frac{\partial \phi}{\partial n}$ (s^{-1})	$\frac{\partial V}{\partial s}$ (s^{-1})	D_H (s^{-1})	$-VK_s \frac{\partial V}{\partial s}$ (s^{-2})	$-(f+VK_s)D_H$ (s^{-2})	$\frac{\partial V}{\partial n} D_H$ (s^{-2})
Upstream [†] Crest	-2×10^{-5}	2.2	-4×10^{-5}	2×10^{-5}	-2×10^{-5}	0	0	6×10^{-6}	6×10^{-6}	2×10^{-10}	-2×10^{-10}	-1×10^{-10}
Trough	2×10^{-5}	1.2	3×10^{-5}	2×10^{-5}	5×10^{-5}	0	0	-1×10^{-6}	-1×10^{-6}	3×10^{-10}	1×10^{-10}	2×10^{-11}
Downstream [†] Mouth of Warm Filament	9×10^{-5}	0.4	4×10^{-5}	2×10^{-5}	6×10^{-5}	4×10^{-6}	2×10^{-6}	-2×10^{-6}	0	8×10^{-10}	0	0

[†]Upstream and downstream are relative to the trough.

*This is the average lateral shear computed at the surface on the cyclonic shear side of the Gulf Stream in a western boundary perturbation south of 34°N using geostrophic current data. (See Vukovich and Crissman, 1980).

The upstream crest is characterized by anticyclonic vorticity primarily as the result of the dominance of the curvature of vorticity terms (Table 1). A positive value of the horizontal divergence was also found at the upstream crest. The divergence was governed by speed divergence. At the trough the cyclonic vorticity was a result of the contribution of the cyclonic vorticity and the lateral shear term which were nearly equal. Convergence characterized the trough, which was a result of the speed divergence term. At the mouth of the warm filament (buoy position 4 in Figure 1), cyclonic vorticity was found and was principally governed by the curvature vorticity term which was twice that of the lateral shear vorticity term, and the horizontal divergence was approximately zero because the lateral direction of the divergence term balanced the speed divergence term.

At the upstream crest (see Figure 2), the divergence term generally balanced the curvature acceleration term so that there was no change in either the lateral shear vorticity or the curvature vorticity as a result of these terms. At the trough, the curvature acceleration and divergence terms have the same sign and the expression for the time rate of change for the curvature vorticity, and they act to create cyclonic curvature vorticity or to increase the amplitude of the perturbation. In the expression for the time rate of change of the lateral shear vorticity, the curvature acceleration term and divergence term have opposite signs, but the curvature acceleration term was an order of magnitude greater than the divergence term and was negative. Therefore, cyclonic curvature vorticity was being created at the expense of the lateral shear vorticity if one accounts for these two terms only. It has been inferred from hydrographic and satellite data that there is upwelling in the central cold core of these perturbations (Vukovich and Crissman, 1980; and Brooks and Bane, 1981). Assuming that the vertical motions in the Gulf Stream

are small compared to those in the cold core center of the perturbation, and that positive vertical motions exist in the cold core perturbation, then positive vertical motions would be greater on the left as the buoy moved through the perturbation. In the presence of cyclonic lateral shear vorticity and positive vertical shear, the banking term would be generally negative and the twisting term generally positive in the western boundary perturbation. Therefore, the banking term would act to produce cyclonic shear vorticity at the expense of curvature vorticity to the cold core regions of these perturbations. The twisting term would also produce cyclonic shear vorticity, but it would not change the curvature vorticity. Therefore, in this case, since the banking term would act in opposition to the curvature acceleration and divergence term, the growth or decline of the wave amplitude depends on the order of magnitude of the terms.

At the mouth of the filament, the divergence term was zero. The curvature acceleration term was positive, indicating that this term contributed to the creation of curvature vorticity at the expense of the lateral shear vorticity.

4.0 References

- Brooks, D. A., and J. M. Bane, 1981: Gulf Stream fluctuations and meanders over the Onslow Bay Upper Continental Slope. J. Phys. Oceanogr., 11, pp. 247-256.
- Chew, F., 1974: The turning process in meandering currents; a case study. J. Phys. Oceanogr., 4:1, pp. 27-57.
- Kirwan, A. D., G. McNally, and S. Pagan, 1978: Wind Drag and Relative Separations of Underground Drifters, J. Phys. Oceanogr., 8:6, pp. 1146-1150.
- Yukovich, F. M., and B. W. Crissman, 1980: Some aspects of Gulf Stream western boundary eddies from satellite and in situ data. J. Phys. Oceanogr., 10, pp. 1792-1813.



OBSERVATIONS ON PROPAGATION AND GROWTH OF GULF STREAM MEANDERS

D. Randolph Watts and William E. Johns (Graduate School of Oceanography, University of Rhode Island, Kingston, R.I. 02881)

ABSTRACT

A new method is presented for continuously tracking the location of the Gulf Stream using a moored array of inverted echo sounders (IES). Time series of lateral displacements of the front, shown accurate to ± 8 km, have been collected along three sections spaced 100, 150 and 200 km downstream (NE) of Cape Hatteras, NC for a period of 12 months. These records are highly coherent at all periodicities longer than 4 days. From the observed phase lags a dispersion relationship is presented for the meanders. As the period and wavelength (T, λ) increase from (4 days, 150 km) to (33 days, 600 km) the phase speed decreases smoothly from 40 km/d to 20 km/d. The meanders exhibited rapid growth at periods longer than 4 days, doubling in variance in each 50 km step downstream. This downstream growth is most appropriately described by a spatial e-folding length $\kappa^{-1} \sim 400$ km for $(T, \lambda) \leq (9 \text{ d}, 250 \text{ km})$, and a temporal e-folding $\sigma^{-1} \sim 6$ days for $(T, \lambda) \geq (14 \text{ d}, 300 \text{ km})$.

INTRODUCTION/OBSERVATIONS

During 1979-1981 we have been observing Gulf Stream meanders using a moored array of inverted echo sounders (IES) and deep current meters deployed 100 to 200 km northeast of Cape Hatteras in 2000-4000 m water depths. These arrays continuously monitored the path of the Gulf Stream and the deep currents under it. This paper presents the IES results, and a companion paper at this workshop by William Johns discusses the current meter measurements.

In this region, where we have chosen to begin our investigation, the Gulf Stream leaves the continental margin and flows into deep water, and the envelope through which the Gulf Stream shifts laterally is known to broaden greatly in the downstream direction. Yet the lateral excursions of the northern edge of the Stream, an ensemble of which

defines a meander envelope, are similar to the width of the Gulf Stream itself (~ 70 km). To monitor the lateral motions of the Stream with IES's under its main baroclinic portions therefore requires relatively fewer instruments in this region.

The IES array is shown in Fig. 1. It consisted of three sections normal to the mean path of the Stream. The technique of determining the Stream position from an IES array is briefly summarized here, but for a detailed discussion one should refer to Watts and Johns (1982). Each IES determines the depth of the main thermocline acoustically. For these deployments Figure 2 compares depths of the 15°C isotherm (Z_{15}) determined from IES measurements against coinciding XBT measurements at the IES sites. The root-mean-square difference is 20 m, which is small compared to the ~ 700 m range over which Z_{15} varies as the Stream meanders. The Z_{15} vertical displacements are not directly proportional to the lateral displacements of the Gulf Stream, but depend upon the local cross-stream slope of the thermocline, i.e. the proximity of the north wall (Z_{15} at ~ 700 m depth) of the Stream to the IES site. The cross-stream sets of Z_{15} time series along the three sections (A,B,C) of Figure 1 are converted to lateral displacement time series, $X(t)$, by using an average cross section of the Gulf Stream, shown in Figure 3. This mean section was produced from 15 XBT sections made in our study region, each of which was normal to the instantaneous path determined immediately prior to the section. To be representative of the instantaneous cross-section, rather than a broadened geographic average, the individual sections were shifted to align their "north wall" positions before averaging. Using the functional form $Z_{15}(X)$, at any one IES site the time series $X(t)$ may be determined, for the distance

of the north wall from that site, and using two or three IES's across the Stream one obtains an improved estimate of the Stream position along the section joining them. The success of this technique has been demonstrated by comparison with several (12) ship surveys of the Stream path through the IES array. The rms difference between ship and IES determinations of X is 8 km. We argue in Watts and Johns (1982), by considering spectra and coherences in the $X(t)$ series, that the rms uncertainty in the IES-determined X is about 5 km.

RESULTS

The time series $X(t)$, indicating where the north wall crosses sections A, B, and C as a function of time, are shown in Figure 4 for May 1979-July 1980 and in Figure 5 for November 1980-July 1981. The zero displacement on each line is taken to be at the northwestern IES site along the line, as identified in Figure 1. A positive X is a displacement offshore toward the Sargasso Sea. The records have been low pass filtered by convolution with a 24 hour Gaussian weighted window.

The Stream's fluctuations have a variety of periodicities, which are evident in Figures 4 and 5. Several events clearly travel downstream, as indicated by the lag between their occurrences in the records, e.g. 5/79, 8/79, 11/79, 2/80, 12/80, 3/81, 6/81 and others. The translation speed for these short period (~ 10 day) features is typically 35 km/day; coherence calculations discussed later develop this subject further.

To illustrate the variety of Stream paths represented by the above time series, a sequence of plan views of the path is presented in Figure 6. In each frame the Stream positions $X(t)$ along each section A,

AD-A128-789

PROCEEDINGS OF THE WORKSHOP ON GULF STREAM STRUCTURE
AND VARIABILITY HELD... (U) NORTH CAROLINA UNIV AT CHAPEL
HILL APR 82 N00014-82-G-0059

55

UNCLASSIFIED

F/G 8/3

NL

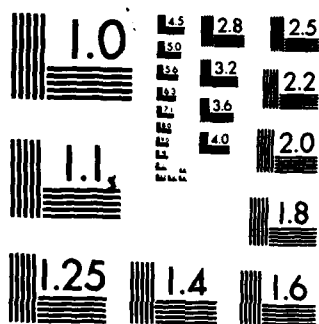


END

DATE

FILED

DTIC



MICROCOPY RESOLUTION TEST CHART
NATIONAL BUREAU OF STANDARDS-1963-A

B, and C have been connected by a smooth curve, and each frame repeats, for visual reference, six IES sites and a rhumb line, which indicates the historical mean north-wall path. The frame interval in this figure, 23 days, is insufficient to smoothly follow the meanders, but was chosen to illustrate that the Stream can flow nearly north (11/9) or east (12/2) through the array; or exhibit significant cyclonic or anticyclonic curvature as large as $0.98 \times 10^{-2} \text{ km}^{-1}$ (12/25) or respectively $-0.91 \times 10^{-2} \text{ km}^{-1}$ (7/15). The corresponding path curvature vorticity associated with near-surface waters moving 2 m/s would be $\sim 25\% f$ in magnitude.

By presenting the path segments at a more frequent time interval (2 days), the wave-like nature of the meanders may be visually emphasized, as in Figure 7. Here the dashed rhumb lines which appeared in each frame in Figure 6 have been aligned horizontally and each path segment offset in time to the left. The distance offset (30 km) and time interval (2 days) correspond to a downstream translation of 15 km/day. The time period, November-December 1979, corresponds to the large perturbations in the $X(t)$ series of Figure 4. Satellite imagery indicates that this large perturbation appears to have been forced by interaction with a warm-core Gulf Stream ring. Cornillon (1982) reports good agreement between tracking of the Stream by satellite and IES during this period.

The path displacement records for 1979-1980 (Fig. 4) and 1980-1981 (Fig. 5) have the corresponding power spectral densities shown respectively in Figures 8 and 9. The spectra for the two time periods and for all three sections are very similar at periods shorter than 100 hours, falling off very rapidly as $\sim f^{-4}$. At periods longer than 100 hours

the slope is -1 to -2. Over 96% of the variance is associated with periods longer than 4 days, and the variance doubles with each 50 km step downstream. During each time period this same pattern of downstream growth obtained: in 1979-1980 the root-mean-square displacements were 15, 20 and 30 km respectively progressing downstream, and in 1980-1981 the corresponding values were about 30% higher (but statistically not different). The 90% confidence limits show the downstream growth to be significant, and a runs-test on the variance confirms that these spectral shapes and the spatial growth are not biased by intermittent bursts of variance.

The averaged cross-spectral coherences and phase delays between section pairs are shown in Figure 10 for the 1979-1980 data set. In all cases the coherences are significant (> 0.32) at the 90% confidence level for periods longer than 4 days. The pairs AB and BC, separated by 50 km, have the greatest coherences and very similar phase relationships for periods greater than 3 days. The downstream pair BC is even more coherent than the upstream pair AB, because the meander signal has grown to overwhelm the "noise" within the extra 50 km distance downstream. ("Noise" here is considered to be both measurement error and any non-propagating fluctuations.) The pair AC, separated by 100 km, is slightly less coherent (but still significant to $T=4$ days), and the phase delays shown in Figure 10 are double those of the pairs 50 km apart.

The sense of the phase lag ϕ is such that the meanders are propagating downstream. The phase speed may be determined as a function of frequency f as $c_T = (2\pi f / \phi) \delta x$, where δx is the downstream spacing between lines. The long period fluctuations propagate more slowly than shorter

periodicities, e.g. $c_r \sim 20$ km/day at $T=800$ h and $c_r \sim 40$ km/day at $T=100$ h. Representing the variability as propagating waves $\propto \exp(i(ky - \omega t))$, downstream spatial growth may be represented in terms of complex wave number $k = k_r - i\kappa$ ($\kappa > 0$), and temporal growth by complex frequency or phase speed $\omega = \omega_r + i\sigma$ or $c = c_r + ic_i$. All these terms may be estimated from the spectra and cross-spectra at the three sections A, B and C. The wave number ($k_r = \phi/\delta x$) is derived from the phase speed and frequency. The spatial growth rate κ may be estimated from the ratio of the smoothed spectral estimates $G_2/G_1 = \exp 2\kappa(x_2 - x_1)$, so $\kappa = \ln(G_2/G_1)/2\delta x$. These are plotted vs f for periods longer than 4 days in the upper half of Figure 11 for each of the deployment periods 1979-1980 and 1980-1981. The lower half of Figure 11 plots the equivalent temporal growth rate $\sigma = \kappa c_r$ in a reference frame moving at speed c_r . The results are consistent for the two data sets: the downward curvature of the k vs ω curve exhibits the systematic decrease of phase speed at low frequencies, and there is significant growth at long periods and also near 4 days with a local minimum near $T \sim 6$ days corresponding to $k \sim 2.5 \times 10^{-2} \text{ km}^{-1}$.

Figure 12 plots the real and imaginary phase speeds (c_r , c_i) as a function of downstream wavenumber k_r , estimated from our 1979-1980 data as described above. The solid symbols are from sections A and C at 100 km spacing, and the open symbols are from sections B and C at 50 km spacing. The phase speed c_r is seen to decrease smoothly from 40 km/day at $k_r \sim 3.5 \times 10^{-2} \text{ km}^{-1}$ ($\lambda \sim 180$ km) to 20 km/day for $k_r \leq 1 \times 10^{-2} \text{ km}^{-1}$ ($\lambda \geq 650$ km). The group speed, also shown in Figure 12 has been estimated by finite difference, from $c_g = c_r + k_r \partial c_r / \partial k_r$; it increases from 45 km/d at $\lambda = 350$ km to 60 km/d at $\lambda = 200$ km. Uncertainty estimates for the

above quantities are as follows: k_r and $c_r \pm 25\%$, $\kappa \pm 30\%$, $\sigma \pm 50\%$, $c_g \pm 35\%$, and c_l nearly $\pm 100\%$.

DISCUSSION/CONCLUSIONS

This observational dispersion relationship for Gulf Stream meanders, indicated in Figures 11 and 12, is statistically the best fit describing propagating, growing waves. The observed high coherence of the path displacement $X(t)$ downstream from sections A to B to C suggests that the downstream path $x(y,t)$ may be predictable from knowledge of the dispersion relationship applied to "inlet" observations such as ours. Work is in progress to test this, however one should note by careful examination of the three sets of $X(t)$ time series that some of the perturbations do not grow as they move downstream, and that fluctuations could develop downstream of these observations, thereby decreasing the downstream coherence and predictive accuracy.

The phase speeds of 20-40 km/day are intermediate between slower speeds which have been reported farther downstream, ~ 5 to 10 km/d (Hansen, 1970; Robinson et al., 1974; Halliwell and Mooers, 1979), and faster speeds farther upstream, ~ 35 -40 km/d (Brooks and Bane, 1981). Growth rates observed by Hansen farther downstream were smaller, $\kappa \sim (2 \pm 1) \times 10^{-3} \text{ km}^{-1}$ (for $\lambda \sim 300 \text{ km}$), and rates predicted theoretically by Tareev (1965) and Orlanski (1969) respectively were $\kappa = 8 \times 10^{-3} \text{ km}^{-1}$ ($\lambda \sim 250 \text{ km}$) and $\kappa = 12 \times 10^{-3} \text{ km}^{-1}$ ($\lambda \sim 360 \text{ km}$). A time dependent thin jet model by Robinson et al. (1975) found for 31 day, 560 km perturbations the corresponding downstream e-folding scale was $\kappa = 5 \times 10^{-3} \text{ km}^{-1}$ in good agreement with these observations.

Our observed spatial growth rates κ indicate that for (T, λ) shorter than (9 days, 300 km) the fluctuations e-fold in a distance long compared to the wavelength. However for (T, λ) longer than (14 days, 400 km) the e-folding growth occurs in less than a wavelength, and consequently the growth has a temporal nature. The temporal growth rate σ^{-1} for these long waves is ~ 6 -14 days, weakly dependent on (T, λ) . We identify growth at wavelengths as short as 180 km and as long as 600 km. The σ values are comparable to Hansen's (1970) estimate of $2 \times 10^{-6} \text{ sec}^{-1}$.

The shape of the $c_r(k)$ curve is remarkably similar to Phillips' (1954) two-layer quasi-geostrophic model of baroclinic instability. Physically only disturbances with wavelengths much longer than the Rossby internal deformation scale, λ_{Ro} , can extract baroclinic energy from the flow and grow, but as wavelengths increase further the β -effect slows and eventually stabilizes the waves (Pedlosky, 1979). A common thread of quasi-geostrophic instability models with temporal growth is a short wavelength cutoff in growth. Hogg (1976) has presented a model in which baroclinically unstable disturbances can grow spatially or temporally, respectively, for shorter or longer (T, λ) . The transition between spatial and temporal growth near $k = 2.4 \times 10^{-2} \text{ km}^{-1}$ as a range of minimal growth, and thus his model closely resembles our observed growth behavior.

Although our measurements cannot indicate a clear distinction between temporal and spatial growth, the similarity with the foregoing theories suggests that the baroclinic instability mechanism is operative in the Gulf Stream and that realistic models should include spatial as well as temporal growth.

REFERENCES

- Brooks, D.A., and J.M. Bane, Jr., Gulf Stream fluctuations and meanders over the Onslow Bay upper continental slope, J. Phys. Oceanogr., 11(2), 247-255, 1981.
- Cornillon, P., The edge of the Gulf Stream: Satellite versus inverted echo sounder determinations, EOS Trans. AGU 63, 363, 1982.
- Halliwel, G.R., Jr., and C.N.K. Mooers, The space-time structure of the Shelf Water-Slope Water and Gulf Stream surface temperature fronts and associated warm-core eddies, J. Geophys. Res., 84, 7707-7725, 1979.
- Hansen, D.V., Gulf Stream meanders between Cape Hatteras and the Grand Banks, Deep-Sea Res., 17, 495-511, 1970.
- Hogg, N.G., On spatially growing baroclinic waves in the ocean, J. Fluid Mech., 78, 217-235, 1976.
- Orlanski, I., The influence of bottom topography on the stability of jets in a baroclinic fluid, J. Atmos. Sci., 26(6), 1216-1232, 1969.
- Pedlosky, J., Geophysical Fluid Dynamics, Springer Verlag, New York, 624 pp., 1979.
- Phillips, N.A., Energy transformations and meridional circulations associated with simple baroclinic waves in a two-level quasi-geostrophic model, Tellus, 6, 273-286, 1954.
- Robinson, A.R., J.R. Luyten, and G. Flierl, On the theory of thin rotating jets: A quasi-geostrophic time-dependent model, Geophysical Fluid Dynamics, 6, 211-244, 1975.
- Robinson, A.R., J.R. Luyten and F.C. Fuglister, Transient Gulf Stream meandering, Part I: An observational experiment, J. Phys. Oceanogr., 4, 237-255, 1974.
- Tareev, B.A., Unstable Rossby waves and the instability of oceanic currents, Atm. and Oceanic Physics Series, 1(4), 426-438, 1965.
- Watts, D.R., and W. E. Johns, Gulf Stream Meanders: Observations on Propagation and Growth, J. Geophys. Res., in press, Nov. 1982.

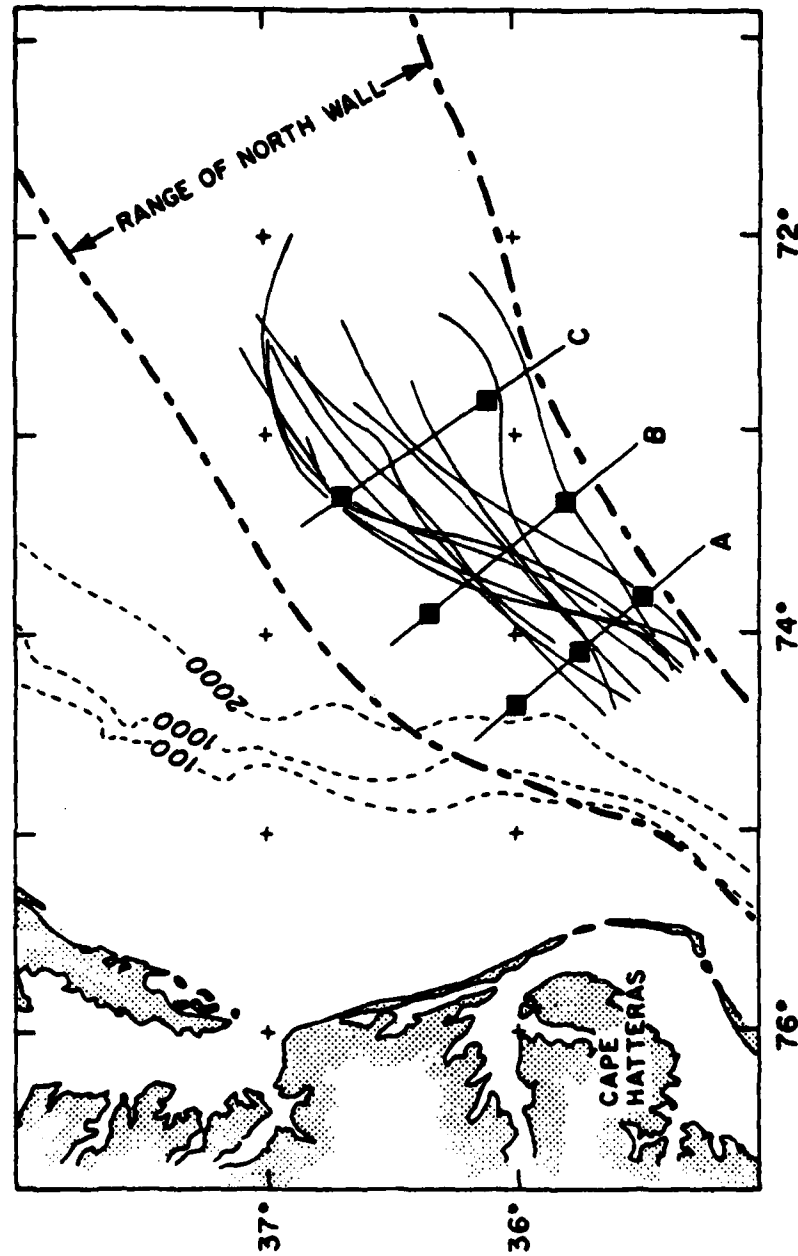


Figure 1. Study area northeast of Cape Hatteras. IES's are at black squares along sections A, B, C. Gulf Stream path surveys from XBT surveys during these deployments are shown as light solid lines. The historical range of the north wall is indicated with dark dashed lines.

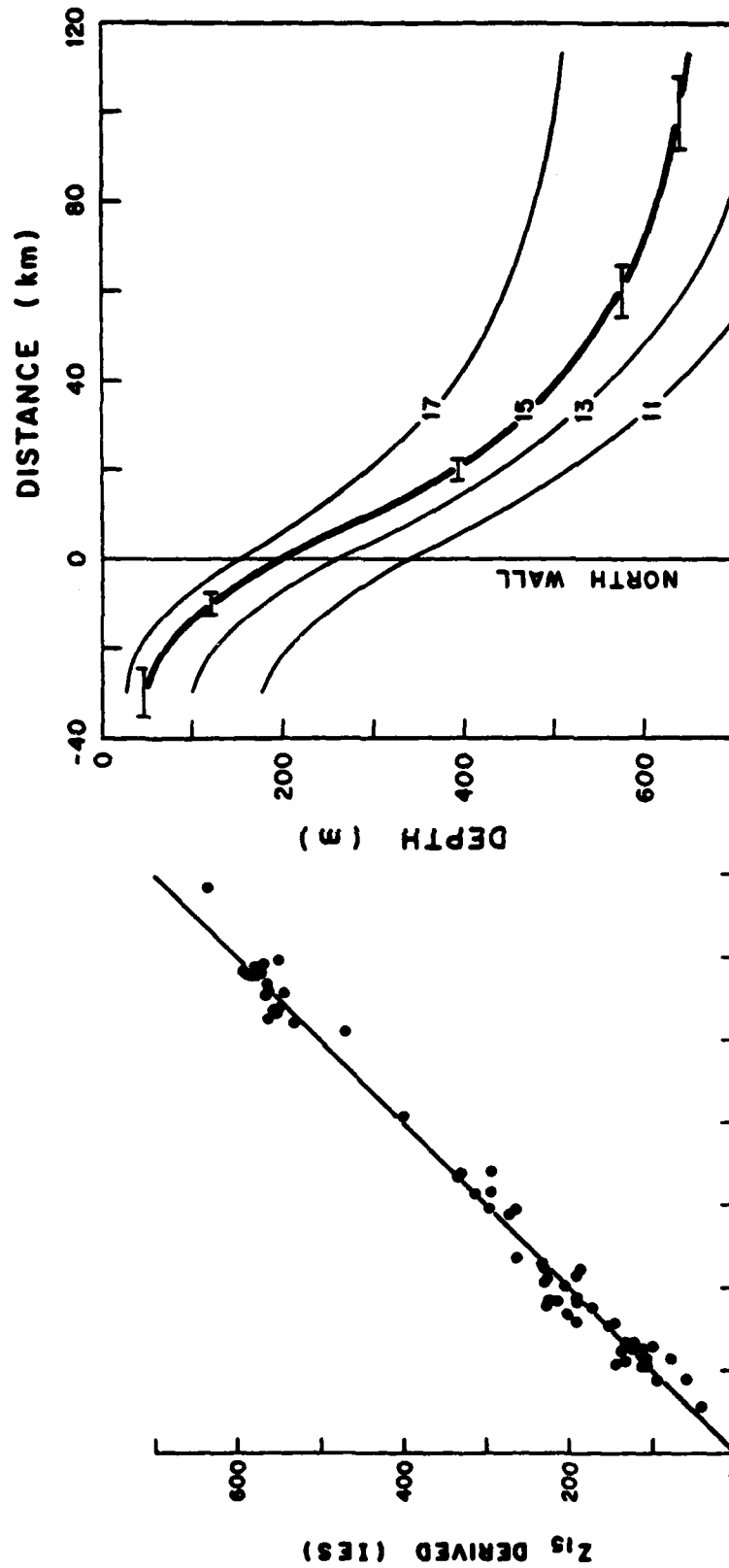


Figure 2. IES derived 15°C depths vs coinciding XBT derived 15°C depths. The rms deviation is 20 m, taken from 61 points in a range greater than 600 m.

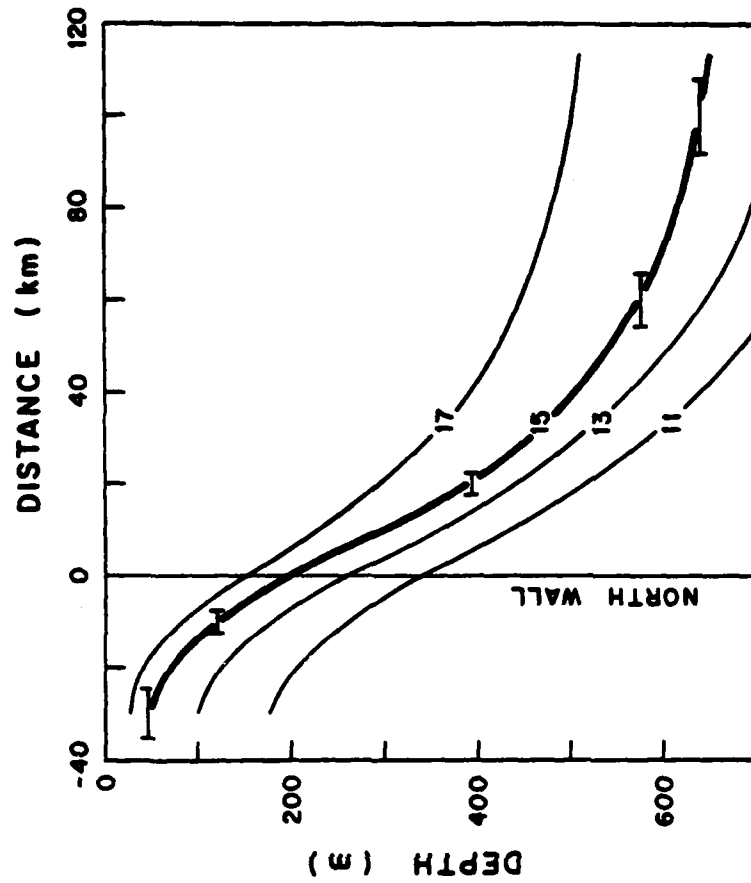


Figure 3. Mean profile of the upper main thermocline constructed from 15 sections normal to the instantaneous path of the Gulf Stream. Sections were shifted to align their north wall (15°C/200 m) positions before averaging, and distances are measured relative to this. The error bars at various points along the 15°C curve represent one standard deviation.

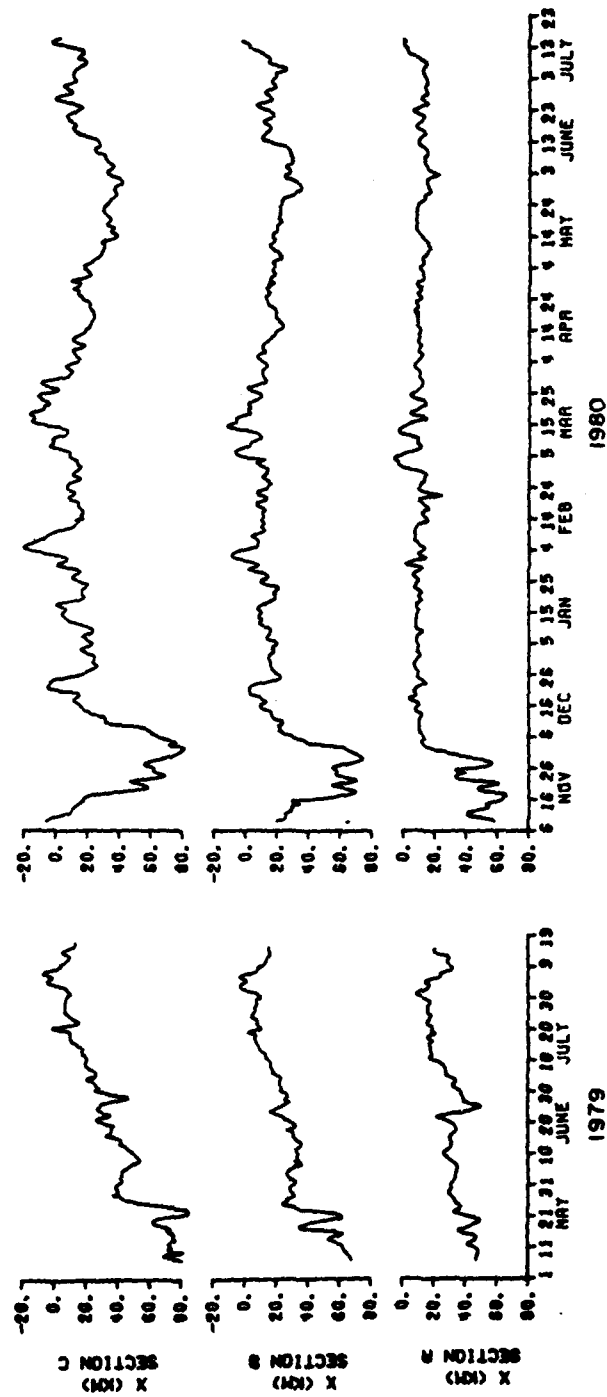


Figure 4. Time series of displacements X at sections A, B, C, in 1979-80. All series have been low-pass filtered by convolution with a 24-hour Gaussian window.

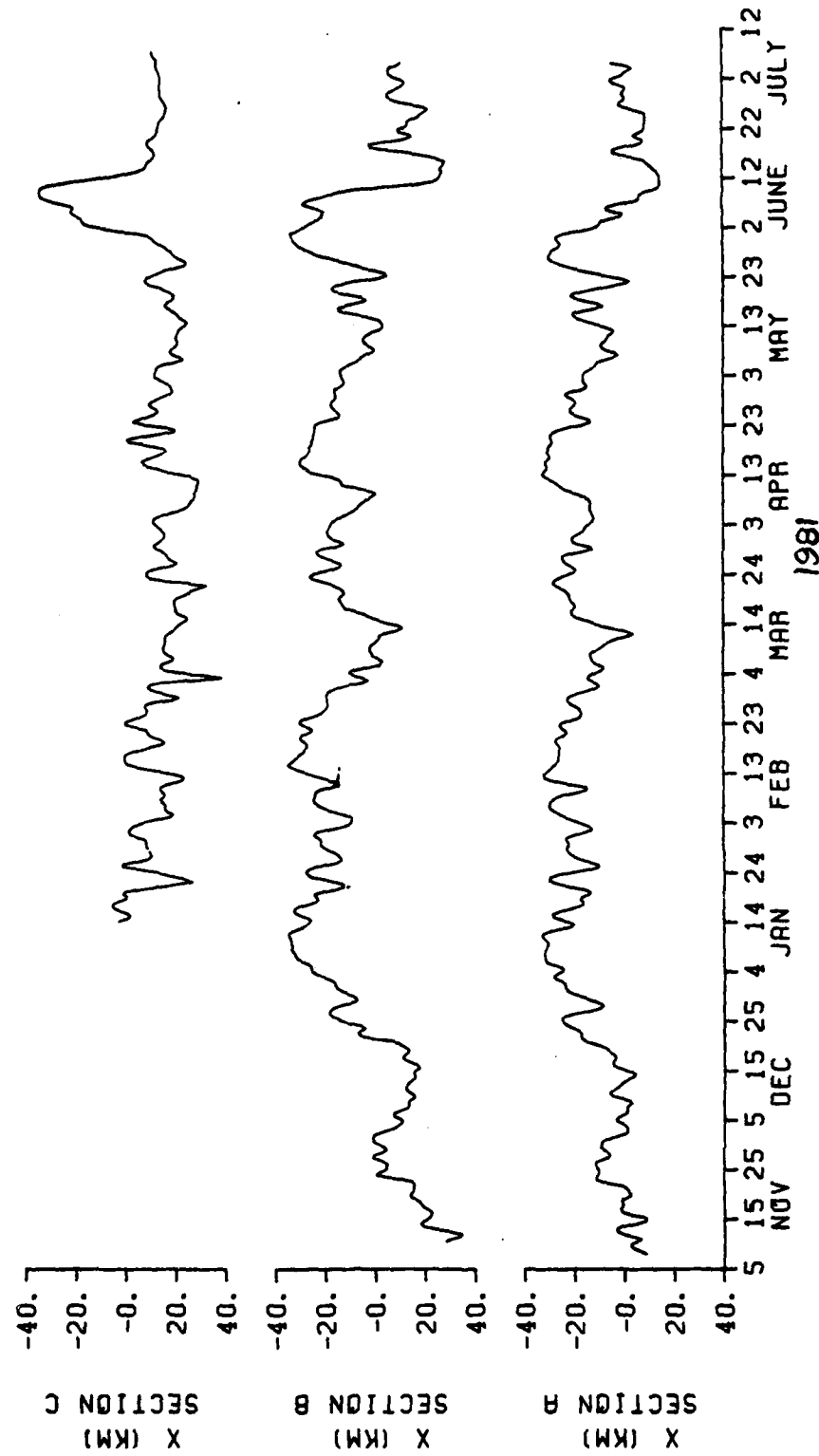


Figure 5. Time series of displacements X at sections A, B, C in 1980-81. All series have been low-pass filtered by convolution with a 24-hour Gaussian window.

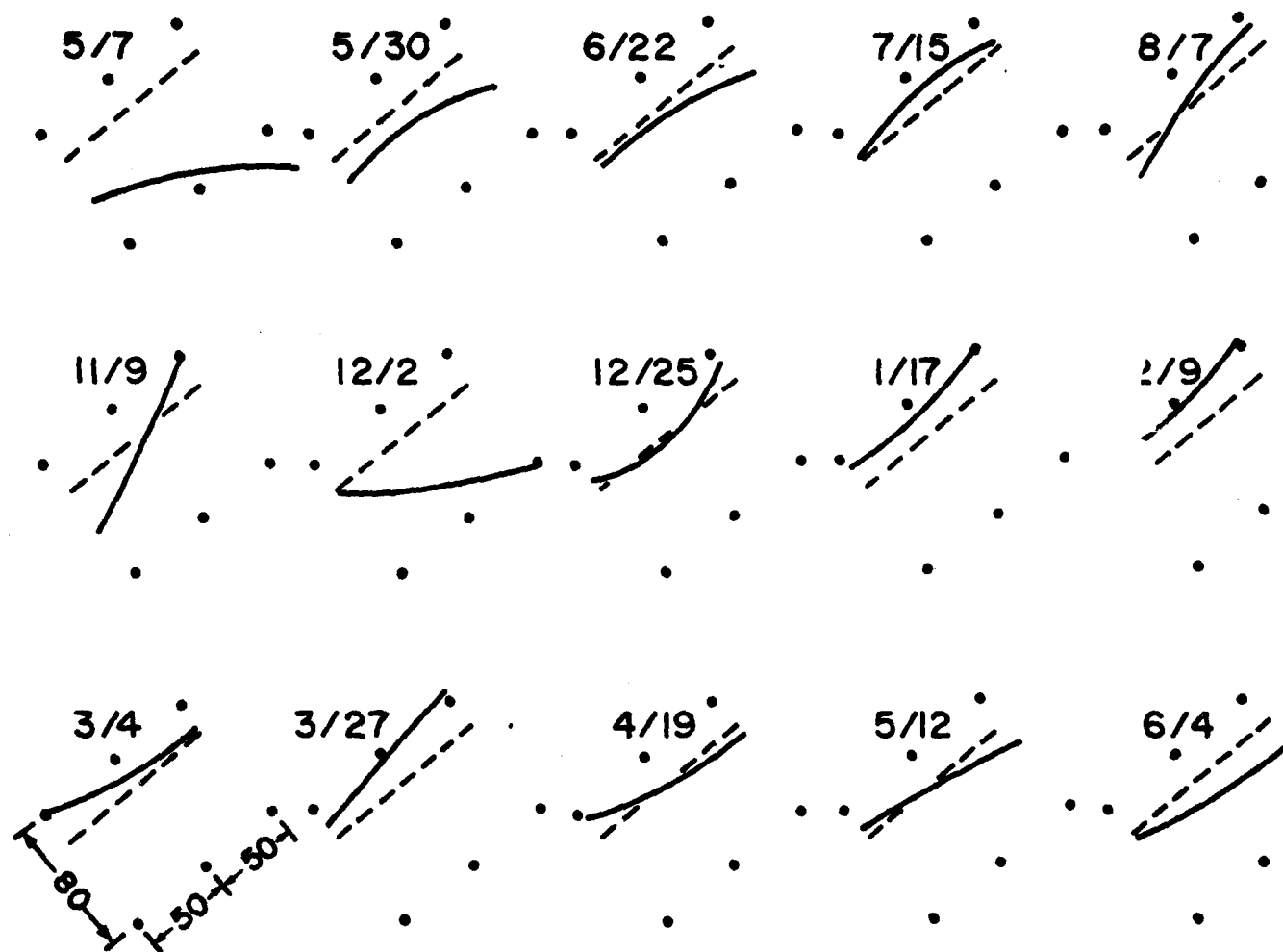


Figure 6. Sequence of Gulf Stream path segments through the IES array (Shown in black circles). For visual reference the dashed rhumb lines indicate the mean location of the north wall. Dates are labeled above each frame, and the instrument spacings (km) are shown at the lower left corner. Paths are drawn as smooth curves through the north wall positions along each of the sections.

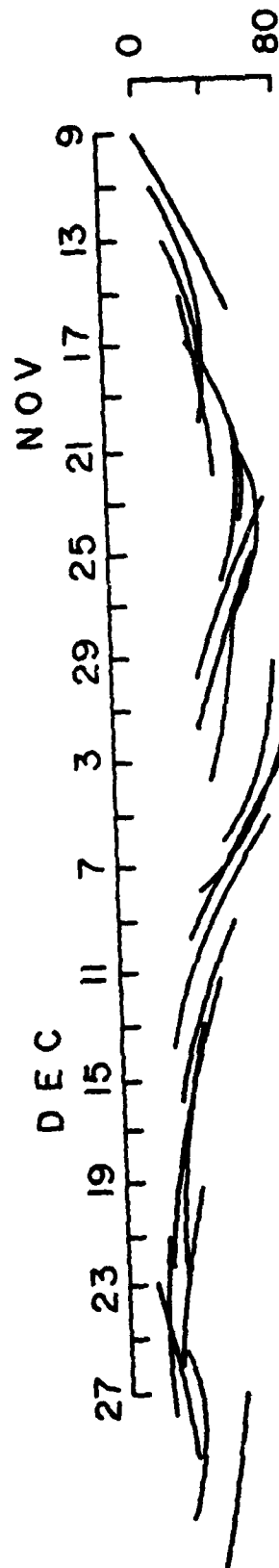


Figure 7. Sequence of Gulf Stream path segments in November-December 1979. Each segment, at two day intervals, is drawn relative to a constant rhumb line through the IES array, but offset 30 km upstream to illustrate the basic wave-like nature of this large meander.

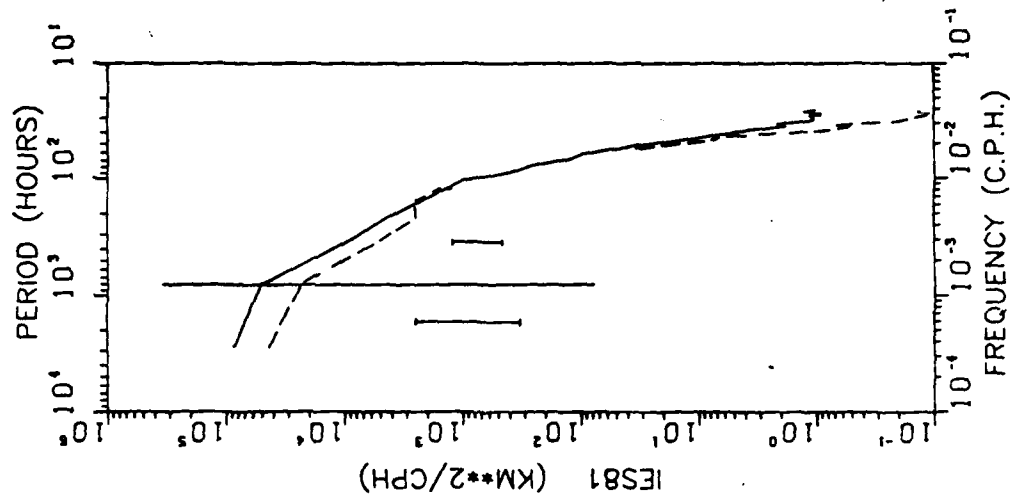


Figure 9. Power spectra of path displacements in 1980-81 at sections A (dashed) and B (solid), incorporating 24 degrees of freedom for $T \leq 800$ h and 8 degrees of freedom for $T > 800$ h. The error bars indicate 90% confidence intervals.

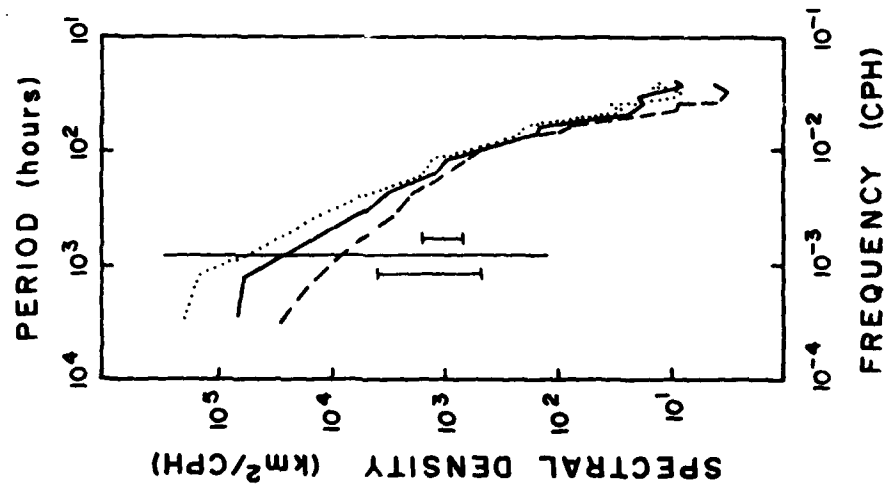


Figure 8. Power spectra of path displacements in 1979-80 at section A (dashed), B (solid), and C (dotted), incorporating 32 degrees of freedom for $T \leq 800$ h and 8 degrees of freedom for $T > 800$ h. The error bars indicate 90% confidence intervals.

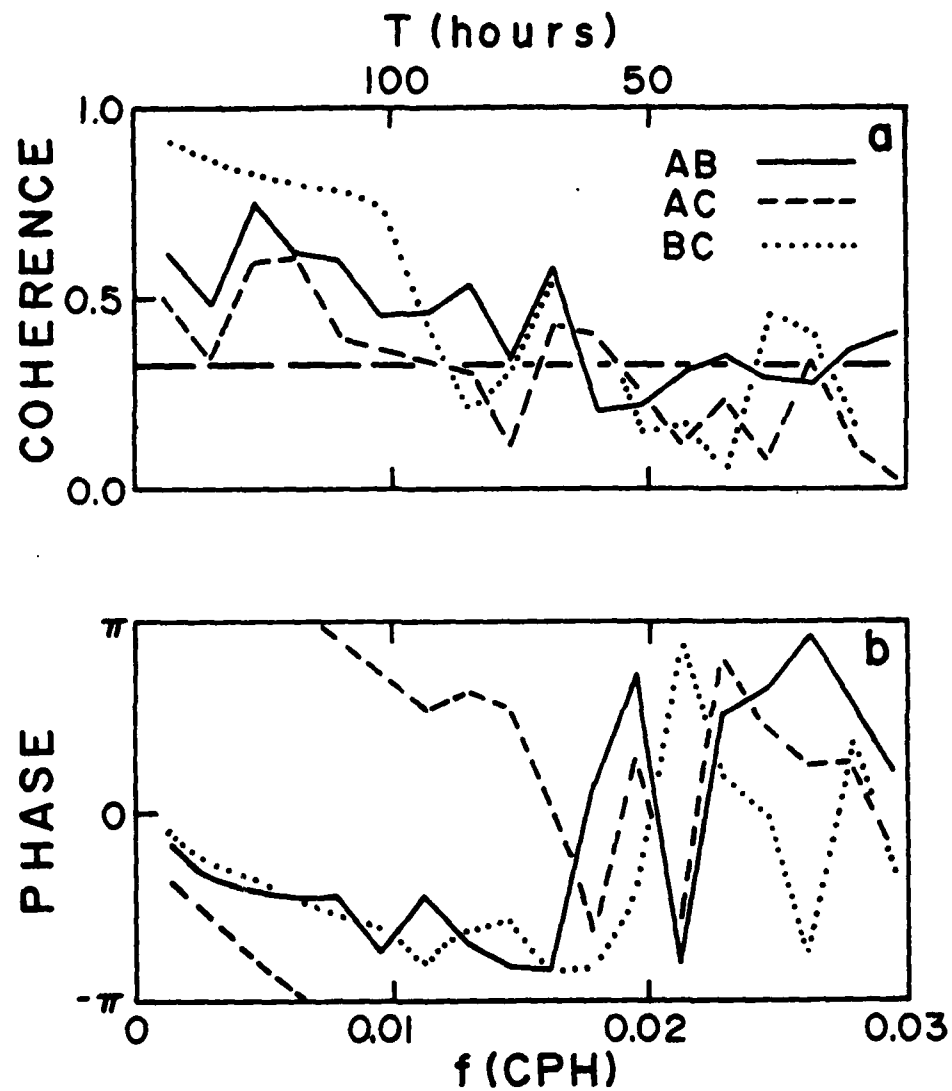


Figure 10. Coherence and phase lag between pairs AB (solid), AC (dashed) and BC (dotted) in 1979-80 records. Heavy dashed line at 0.32 indicates the 90% significance level for a random process.

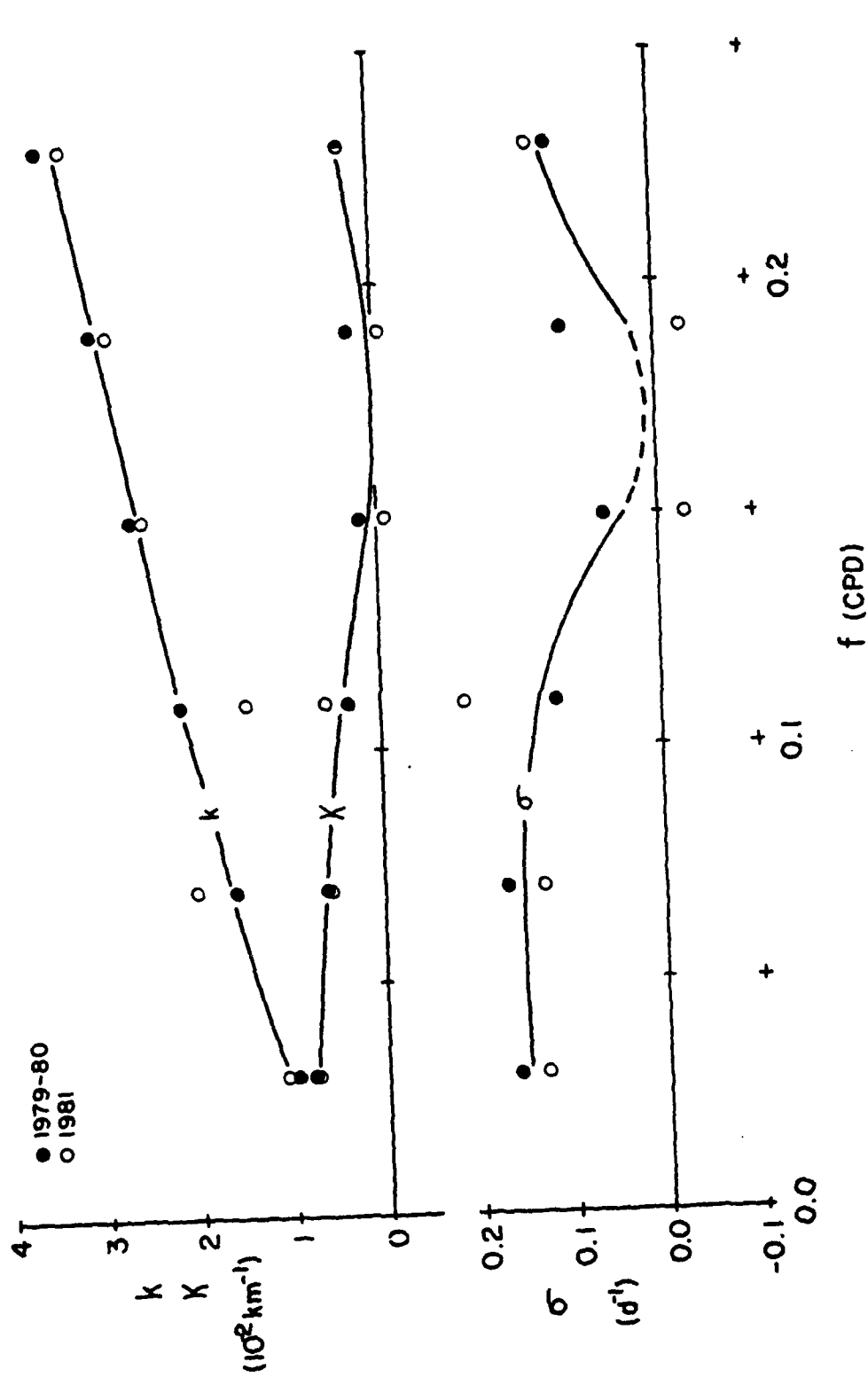


Figure 11. Real part of the wavenumber k , imaginary part κ (spatial growth rate), and imaginary part of the frequency σ (temporal growth rate) plotted vs frequency for the measurement periods 1979-80 (solid symbols) and 1980-81 (open symbols), connected by smooth curves.

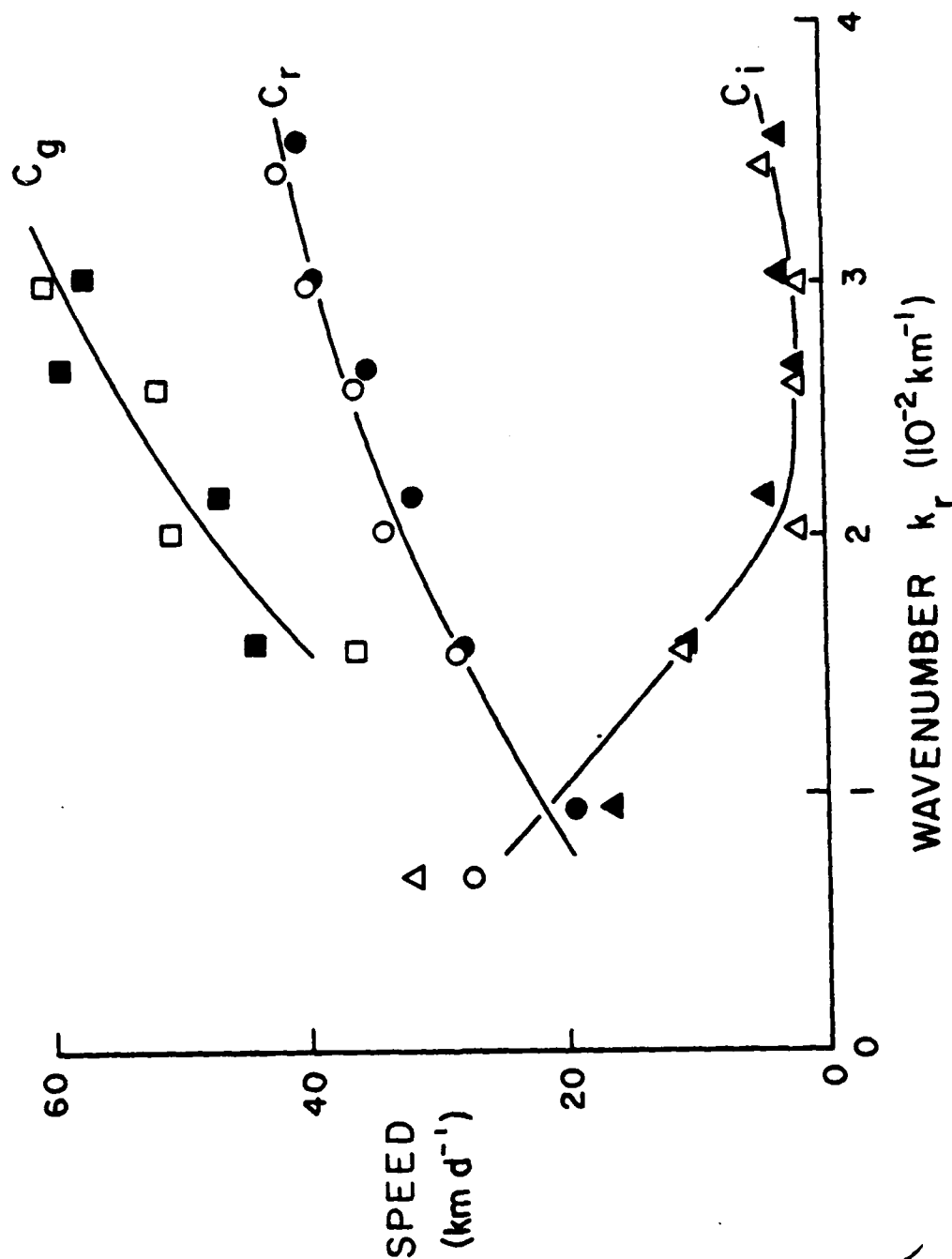


Figure 12. Phase speed components (c_r , c_i) and group speed (c_g) plotted vs wavenumber k_r . Open circles, triangles, and squares represent c_r , c_i and c_g , respectively, calculated from sections B and C separated by 85 km. Solid circles, triangles, and squares represent c_r , c_i and c_g calculated from sections A and C separated by 100 km.

PARTICIPANTSARCO OIL & GAS COMPANY

KENNETH HILDEBRANDT
TOM MITCHELL

THE CATHOLIC UNIVERSITY OF AMERICA

TIMOTHY W. KAO

FLORIDA STATE UNIVERSITY

MARK E. LUTHER

GENERAL OCEANICS

CHRIS CASAGRANDE

GULF OIL COMPANY

IRV BROOKS

JAYCOR

CYNTHIA M. SEAY

JET PROPULSION LABORATORY

JIM MITCHELL

MINERAL MANAGEMENT SERVICES - OCS

WILLIAM LANG

MOBIL OIL COMPANY

JOHN HAUSTEIN

NASA/GSFC

CHARLES R. McCLAIN

NOAA/AOML

FRANK CHEW
GEORGE A. MAUL

NORDA

HARLEY HURLBURT
JOHN McKENDRICK
DANA THOMPSON

NATIONAL CENTER FOR ATMOSPHERIC RESEARCH

WILLIAM R. HOLLAND

NATIONAL SCIENCE FOUNDATION

CURT COLLINS

NAVAL EASTERN OCEANOGRAPHIC CENTER

CHARLES A. WEIGAND

NORTH CAROLINA STATE UNIVERSITY

TOM CURTIN
GERALD JANOWITZ
DAN KAMYKOWSKI
C. E. KNOWLES
LEN PIETRAFESA
ROBERT WEISBERG

NOVA UNIVERSITY

SHENN-YU CHAO

OFFICE OF NAVAL RESEARCH

TOM SPENCE
ROBERT WILLEMS

RESEARCH TRIANGLE INSTITUTE

FRED VUKOVICH

SCIENCE APPLICATIONS, INC.

PETER HAMILTON
JOSEPH KARPEN
JAMES SINGER
EVANS WADDELL

SCRIPPS INSTITUTION OF OCEANOGRAPHY

MEREDITH SESSIONS

SKIDAWAY INSTITUTE OF OCEANOGRAPHY

LARRY ATKINSON
JACK BLANTON

TEXAS A & M UNIVERSITY

DAVID A. BROOKS

UNIVERSITY OF DELAWARE

OWENS WADSWORTH

UNIVERSITY OF MIAMI

OTIS B. BROWN
ROBERT EVANS
THOMAS N. LEE
DONALD B. OLSON
FRIEDRICH SCHOTT

UNIVERSITY OF NORTH CAROLINA

JOHN M. BANE
LEONIDAS CORDOVA

UNIVERSITY OF RHODE ISLAND

AMY BOWER
DAN HALKIN
WILLIAM E. JOHNS
ED LEVIN
KAREN R. LORENSON
ARTHUR MARIANO
ELIZABETH MESSENGER
TOM ROSSBY
PING-TUNG SHAW
JORGE VASQUEZ
D. RANDOLPH WATTS

UNIVERSITY OF WASHINGTON

HARRY BRYDEN

WOODS HOLE OCEANOGRAPHIC INSTITUTION

NICHOLAS FOFONOFF
DALE HAIDVOGEL
W. BRECHNER OWENS
LYNNE D. TALLEY

FILME

7-8